ENGINEERING THE PLANT BIOFACTORY FOR THE PRODUCTION OF BIOLOGICS AND SMALL-MOLECULE MEDICINES - VOLUME 2

EDITED BY: Domenico De Martinis, Eugenio Benvenuto,
Inga Isabel Hitzeroth, Ryo Matsuda and Natacha Soto Pérez

PUBLISHED IN: Frontiers in Plant Science

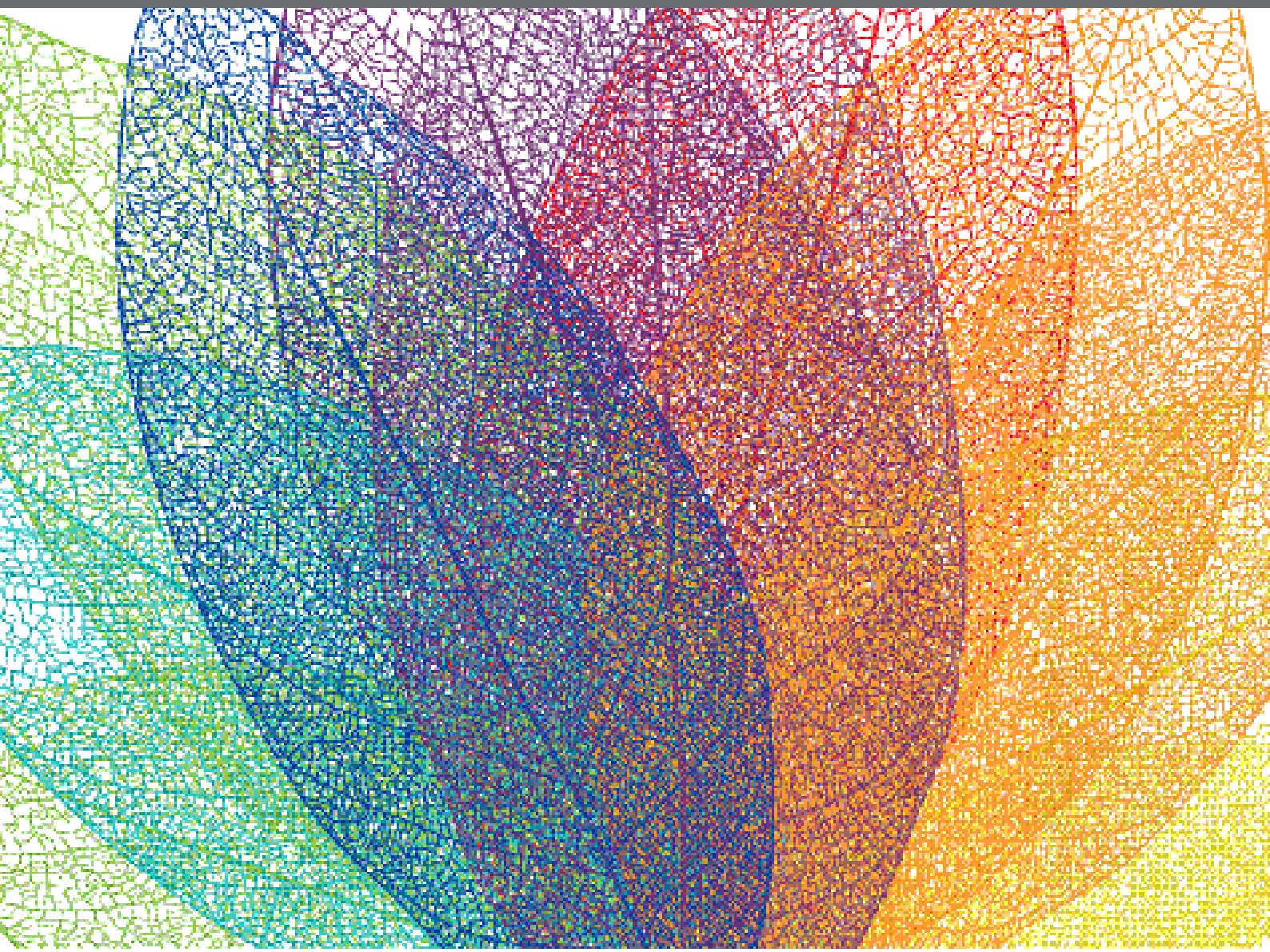

frontiers Research Topics

ISSN 1664-8714
ISBN 978-2-88976-698-7
DOI 10.3389/978-2-88976-698-7

About Frontiers

Frontiers is more than just an open-access publisher of scholarly articles: it is a pioneering approach to the world of academia, radically improving the way scholarly research is managed. The grand vision of Frontiers is a world where all people have an equal opportunity to seek, share and generate knowledge. Frontiers provides immediate and permanent online open access to all its publications, but this alone is not enough to realize our grand goals.

Frontiers Journal Series

The Frontiers Journal Series is a multi-tier and interdisciplinary set of open-access, online journals, promising a paradigm shift from the current review, selection and dissemination processes in academic publishing. All Frontiers journals are driven by researchers for researchers; therefore, they constitute a service to the scholarly community. At the same time, the Frontiers Journal Series operates on a revolutionary invention, the tiered publishing system, initially addressing specific communities of scholars, and gradually climbing up to broader public understanding, thus serving the interests of the lay society, too.

Dedication to Quality

Each Frontiers article is a landmark of the highest quality, thanks to genuinely collaborative interactions between authors and review editors, who include some of the world's best academicians. Research must be certified by peers before entering a stream of knowledge that may eventually reach the public - and shape society; therefore, Frontiers only applies the most rigorous and unbiased reviews.
Frontiers revolutionizes research publishing by freely delivering the most outstanding research, evaluated with no bias from both the academic and social point of view. By applying the most advanced information technologies, Frontiers is catapulting scholarly publishing into a new generation.

What are Frontiers Research Topics?

Frontiers Research Topics are very popular trademarks of the Frontiers Journals Series: they are collections of at least ten articles, all centered on a particular subject. With their unique mix of varied contributions from Original Research to Review Articles, Frontiers Research Topics unify the most influential researchers, the latest key findings and historical advances in a hot research area! Find out more on how to host your own Frontiers Research Topic or contribute to one as an author by contacting the Frontiers Editorial Office: frontiersin.org/about/contact

ENGINEERING THE PLANT BIOFACTORY FOR THE PRODUCTION OF BIOLOGICS AND SMALL-MOLECULE MEDICINES - VOLUME 2

Topic Editors:
Domenico De Martinis, Italian National Agency for New Technologies, Energy and Sustainable Economic Development (ENEA), Italy
Eugenio Benvenuto, Italian National Agency for New Technologies, Energy and Sustainable Economic Development (ENEA), Italy
Inga Isabel Hitzeroth, University of Cape Town, South Africa
Ryo Matsuda, The University of Tokyo, Japan
Natacha Soto Pérez, Center for Genetic Engineering and Biotechnology (CIGB), Cuba

Citation: Martinis, D. D., Benvenuto, E., Hitzeroth, I. I., Matsuda, R., Pérez, N. S., eds. (2022). Engineering the Plant Biofactory for the Production of Biologics and Small-Molecule Medicines - Volume 2. Lausanne: Frontiers Media SA.
doi: 10.3389/978-2-88976-698-7

Table of Contents

frontiers | Frontiers in Plant Science

EDITORIAL
published: 07 July 2022
doi: 10.3389/fpls.2022.942746

Editorial: Engineering the Plant Biofactory for the Production of Biologics and Small-Molecule Medicines—Volume 2

Domenico De Martinis[1*†], *Inga Isabel Hitzeroth*[2†], *Ryo Matsuda*[3†], *Natacha Soto Pérez*[4†] *and Eugenio Benvenuto*[1†]

[1] Italian National Agency for New Technologies, Energy and Sustainable Economic Development (ENEA), Rome, Italy, [2] Biopharming Research Unit, University of Cape Town, Cape Town, South Africa, [3] Graduate School of Agricultural and Life Sciences, The University of Tokyo, Tokyo, Japan, [4] Plant Biotechnology Department, Center for Genetic Engineering and Biotechnology (CIGB), Havana, Cuba

Keywords: biopharmaceuticals, recombinant protein, genetic engineering, transient expression, plant biofactory, antibodies, vaccines

Editorial on the Research Topic

Engineering the Plant Biofactory for the Production of Biologics and Small-Molecule Medicines—Volume 2

OPEN ACCESS

Edited and reviewed by:
Inge Broer,
University of Rostock, Germany

***Correspondence:**
Domenico De Martinis
domenico.demartinis@enea.it

†These authors have contributed equally to this work

Specialty section:
This article was submitted to Plant Biotechnology, a section of the journal Frontiers in Plant Science

Received: *12 May 2022*
Accepted: *23 May 2022*
Published: *07 July 2022*

Citation:
De Martinis D, Hitzeroth II, Matsuda R, Soto Pérez N and Benvenuto E (2022) Editorial: Engineering the Plant Biofactory for the Production of Biologics and Small-Molecule Medicines—Volume 2. Front. Plant Sci. 13:942746. doi: 10.3389/fpls.2022.942746

The transfer of genes into plants, that was achieved in the early 80's, paved the way for the exploitation of the potential of plant genetic engineering, to add novel agronomic traits and/or to design plants as factories for high added value molecules.

"Molecular Farming" was a term coined in reference to such agricultural applications, and major crops like maize and tobacco were originally used for pharma applications. It was since these early studies on plant gene transfer that the scientific community interpreted the technology not only for improving plant performance, as an extension of the plant breeding concept but rather to produce new products, to use the plant as a biofactory for novel designed molecules.

The concept of the "green biofactory" implies different advantages over the typical cell factories based on animal cell or microbial cultures alone when considering the investment and managing costs of fermenters. Although yield, stability, and quality of the molecules may vary among different heterologous systems and plants are competitive on a case-to-case basis, still the "plant biofactory" attracts scientists and technologists for the challenging features of low production cost, product safety, and easy scale-up. The rush to develop a vaccine and the need for fast scale-up production in the years of the COVID-19 pandemic highlighted how a plant biofactory may be useful for global-scale production of large amounts of medicals.

Therefore, in this Research Topic we have tried to gather (again) together the scientific community working on the concept of plant biofactories, as successfully achieved in 2016 (De Martinis et al.). The topic focused on exploring the type of molecules that are currently studied and produced in plants and the approaches to obtain pharmaceutical proteins, medical diagnostics proteins, and vaccine antigens, at an industrial scale. We devoted the work to recent scientific progress in the areas of plant-produced antibodies and vaccines, medicals and diagnostics; protein design for heterologous production in plant biofactories; synthetic biology applied to agriculture; biorefinery, biochemical, and molecular level studies.

The display of studies of this "volume II" gathers together 103 authors from the USA, Canada, Europe, South Africa, South Korea, Thailand, India, and Japan, that approached the complexity

of producing desired molecules in plants and plant cells, covering the topic from engineering, to methods to increase the quality and quantity of the desired molecule.

Several papers in this topic described methods to produce diagnostic or vaccines in plants, including COVID-19 related products; efforts to demonstrate the use of plants to produce effective yet affordable vaccines and fast production of viral antigens, which are required by the industry in high amounts also for serological assays, were made (Schwestka et al.; Siriwattananon et al.); approaches on how to better produce molecules of interest is further explored, with the production of functional antibodies already in the market, such as the Denosumab, used in therapy for osteoporosis (Boonyayothin et al.), and the Pembrolizumab for cancer immunotherapy (Phakham et al.), and the production of chimaeric antibody functional in binding and neutralizing enterohemorrhagic *Escherichia coli* (Chin-Fatt and Menassa).

Plant biofactory, as for others biorefineries, also requires strategies to increase quantity and quality of the molecule of interest; this is the case of a (glyco-) engineered plant line to be used for the production of a functional enzyme β-glucocerebrosidase, for Gaucher disease treatment (Uthailak et al.), and potentially for other pharmaceutical proteins, especially mannose receptor targeted protein (Sariyatun et al.), and the production of heterologous viral glycoproteins in plants with authentic human-like glycosylation (Margolin et al.). Also the use of the B1 domain of Streptococcal protein G (GB1) proved how a multi-functional domain used in recombinant proteins in plants, could both stabilize a chimeric protein and facilitate its detection (Song et al.).

In addition to the quality of a plant produced heterologous molecule, speed of production and yield are important; transgenic plants transformed with a positive cell cycle regulator gene *At-CycD2* resulted in enhanced recombinant protein yield (Kopertekh and Reichardt), cell-free biofactories can be of use for the production of proteins and metabolites within a few hours or days (Buntru et al.), while modifying anthocyanins biosynthesis in plants may represent a strategy to obtain resistance to ionizing radiation and anti-oxidant properties during cultivation in space (Massa et al.). This latest work recalls and binds to the issue of improving the plant biofactory performance to another important aspect, described in the 2020 Front. Plant Science Res. Topic *Next Generation Agriculture: Understanding Plant Life for Food, Health, and Energy*, that is, the necessity to cultivate in non-traditional environments such as indoor urban scenarios, extremely cold or dry areas or even in space, either on orbit around the planet or during space traveling.

The production of any sort of molecules in plants has a great potential, in terms of quality, quantity and economy. This is not restricted to recent approaches to tackle the COVID-19 pandemics, but dates back for decades before and has been suggested to be valuable for rapid production and scale-up already, e.g., in the case of SARS "1" (De Murtas et al.). Once engineered, a plant is among the cheapest and easiest eukaryotic systems to be bred with simple know-how, using nutrients, water and light, and global knowledge of agriculture is well-established for centuries.

"Farming for Pharming" biologics and small-molecule medicines is a challenging area of plant biotechnology that may break the limits of current standard production technologies. The success of fighting Ebola with plant-made antibodies put the spotlight on the enormous potential of next-generation herbal medicines made especially in the name of the guiding principle of reduction of costs, hence reduction of disparities of health rights and as a tool to guarantee adequate health protection in developing countries.

Nevertheless, the recent global sanitary emergency, caused by the COVID-19 pandemic, suggest that the decision makers are not familiar, not at ease, or at least not convinced, by the opportunity of using the plant as easy and scalable biorefinery; the race to the COVID-19 vaccine in most westernized countries ignored the opportunity to work on such platform, neither to promote it as alternative production system to support vaccination campaigns, and/or therapy and diagnostic, in less favorite countries, that would have been helpful during the containment phase when the disease emerged. A similar cold-shoulder has been given to non-EU and non-USA vaccines, as in the case of Russian and Cuban production.

The ability of plants to produce heterologous pharmaceutical proteins has been demonstrated in hundreds of proof-of-principle studies and in a growing number of clinical trials, with a small number of products reaching the market as approved biologics or medical devices (Lobato Gómez et al., 2021), but molecular farming has not overcome the barriers of industry inertia and regulatory restraints. Broad markets and producers as e.g., USA and EU, show disharmony (Case Studies in Agricultural Biosecurity, n.d; European Commission, n.d). The production of biopharmaceutical products through plants lacks specific approved guidelines on the points to consider for the manufacture and application of these products. In this sense, the implementation of new manufacturing processes and quality systems using quality risk management is recognized as something of prime importance in the current pharmaceutical industry. In a thorough review published in Frontiers in 2020 it was discussed how molecular farming could provide practical solutions to address the COVID-19 outbreak in Italy (Lico et al., 2020), that was the first country in Europe to face a large-scale COVID-19 outbreak and it is one of the hardest-hit countries in the EU.

Research carried out in Cuba, showed that the application of the FMEA (Frank et al., 2008) approach to design the manufacturing process of a "plantibody" is necessary for the production of vaccines against hepatitis B, and to guarantee the high quality of the vaccine (Mila et al., 2010). Still in Cuba, several research studies demonstrated the capacity for producing vaccines, antibodies (Hernández-Velázquez et al., 2015), and to purify products to the requested quality and yield for industrial production (Ferro et al., 2015). More generally, the production of transgenic crops in Latin America is increasing. Some countries such as Brazil, Argentina, Mexico, Colombia, Cuba, Honduras, and Uruguay have the necessary practice on the subject of biosafety of transgenic crops.

Regarding biosafety regulation and progress in Latin America, the regulatory powers of the countries in the region are heterogeneous. Again, no consensus exists on the importance and development of molecular farming across the region. In many cases, the necessary background and skills for evaluating aspects of biosafety and the operation of regulatory systems are missing (Barragán-Ocaña et al., 2019).

In Japan, InterBerry α®, a lyophilized powder of transgenic strawberry fruit expressing canine interferon-α to treat canine gingivitis, was approved in 2013. A highly contained factory is used to produce this veterinary pharmaceutical. It comprises the upstream controlled-environment plant production facility with artificial lighting, which follows the domestic law involving the Cartagena Protocol on Biosafety to prevent transgene flow to the outside, and the GMP-compliant downstream processing facility. This type of factory should be a model to manufacture plant-made pharmaceuticals commercially in Japan. On the other hand, biopharmaceuticals for human use have not yet been approved. The requirements are expected to be discussed in detail in the future.

In South Africa, the Biopharming Research Unit (BRU) at the University of Cape Town (UCT), a group at the SA Council for Scientific and Industrial Research (CSIR) and Cape Bio Pharms are the primary three molecular farming research and development teams in the country. There are presently no Good Manufacturing Practice (GMP) facilities in South Africa for plant-produced biopharmaceuticals (Murad et al., 2020) and Cape Bio Pharms, a spin-off company of UCT aimed at commercializing the biotech developed by the BRU, is the only pilot-scale manufacturing facility. In response to the pandemic Cape Bio Pharms expressed antibodies and various regions of the COVID-19 spike protein in plants and some are used in lateral flow devices which have been approved in South Africa by the South African Health Products Regulatory Authority (SAHPRA) for use in South Africa. They plan to build a GMP facility in the near future, which will be a boost for the development of plant-based pharmaceuticals in Africa.

Moreover, one company that has been active in exploiting the plant based platform is *Medicago*, a Canadian biopharmaceutical company, that combined their plant produced COVID-19 vaccine candidate with GSK's pandemic adjuvant and submitted the positive Phase 3 data for regulatory review by Health Canada in December 2021. This vaccine is stable at 4°C and, if authorized, would be the world's first ever plant-based vaccine approved for human use.

Overall, those examples, and the amount of studies developed so far, suggest the great potential for the use of plants, which could be of use for large-scale deployment for plant-produced vaccine and biologics manufacturing. That valuable opportunity happens to be hampered by the heterogeneity of rules and lack of common understanding, and an inability to achieve a proper technological transfer and reach out to the market with continuity, although the first steps of the molecular farming technology were made 40 years ago already.

A possible explanation of such under exploitation of this type of production platform may be the lack of reliability (legislation-wise), as explained, the competitiveness of other well-established systems (bacto-, myco-, animal-based) that hold fast to their market share, and a significant presence of anti- GMO citizen groups, that may ignore how current pharmaceuticals are actually produced. This suggests a failure of the plant science community in communicating such opportunity to the decision makers as well as to the civil society. That leads ultimately to a reflection on how plant science communication should develop, to be able to provide the appropriate information to the society; that would reflect in policy makers to take informed decisions, and citizens to make informed choices.

AUTHOR CONTRIBUTIONS

All authors listed have made a substantial, direct, and intellectual contribution to the work and approved it for publication.

REFERENCES

Barragán-Ocaña, A., Reyes-Ruiz, G., Olmos-Peña, S., and Gómez-Viquez, H. (2019). Production, commercialization, and intellectual property of transgenic crops in Latin America. *J. Agribus. Dev. Emerg. Econ.* 9, 333–351. doi: 10.1108/JADEE-05-2018-0061

Case Studies in Agricultural Biosecurity (n.d.). *U.S. Regulation of Genetically Modified Crops*. Case Studies in Agricultural Biosecurity. Available online at: https://biosecurity.fas.org/education/dualuse-agriculture/2.-agricultural-biotechnology/us-regulation-of-genetically-engineered-crops.html

European Commission (n.d.). *GMO Legislation*. Available online at: https://ec.europa.eu/food/plants/genetically-modified-organisms/gmo-legislation_en

Ferro, W., Álvarez, T., Geada, D., Medina, Y., Guevara, Y., Montero, J., et al. (2015). Two-Step purification of antibody from tobacco plants for vaccine manufacturing: aqueous two-phase extraction and affinity chromatography. *BioProc. J.* 14, 6–14. doi: 10.12665/J141.Valdes

Frank, T., Brooks, S., Creekmore, R., Hasselbalch, B., Murray, K., Obeng, K., et al. (2008). Quality risk management principles and industry case studies. *Pharm. Qual. Res. Inst. Manuf. Technol. Comm*. 1–9.

Hernández-Velázquez, A., López-Quesada, A., Ceballo-Cámara, Y., Cabrera-Herrera, G., Tiel-González, K., Mirabal-Ortega, L., et al. (2015). Tobacco seeds as efficient production platform for a biologically active anti-HBsAg monoclonal antibody. *Transgenic Res.* 24, 897–909 doi: 10.1007/s11248-015-9890-8

Lico, C., Santi, L., Baschieri, S., Noris, E., Marusic, C., Donini, M., et al. (2020). Plant molecular farming as a strategy against COVID-19?the Italian perspective. *Front Plant Sci*. 11:609910. doi: 10.3389/fpls.2020.609910

Lobato Gómez, M., Huang, X., Alvarez, D., He, W., Baysal, C., Zhu, C., et al. (2021). Contributions of the international plant science community to the fight against human infectious diseases—part 1: epidemic and pandemic diseases. *Plant Biotechnol. J.* 19, 1901–1920. doi: 10.1111/pbi.13657

Mila, L., Valdes, R., Padilla, S., Mendoza, O., Gomez, L., García, C., et al. (2010). Using quality risk management in the plantibody HB-01 manufacturing by transgenic tobacco plants for vaccine production. *Lat. Am. J. Pharm*. 29, 383–392.

Murad, S., Fuller, S., Menary, J., Moore, C., Pinneh, E., Szeto, T., et al. (2020). Molecular pharming for low and middle income countries. *Curr. Opin. Biotechnol.* 61, 53–59. doi: 10.1016/j.copbio.2019.10.005

Conflict of Interest: IH declares that she holds shares in Cape Bio Pharms.

The remaining authors declare that the research was conducted in the absence of any commercial or financial relationships that could be construed as a potential conflict of interest.

Publisher's Note: All claims expressed in this article are solely those of the authors and do not necessarily represent those of their affiliated organizations, or those of the publisher, the editors and the reviewers. Any product that may be evaluated in this article, or claim that may be made by its manufacturer, is not guaranteed or endorsed by the publisher.

frontiers in Plant Science

ORIGINAL RESEARCH
published: 13 May 2021
doi: 10.3389/fpls.2021.682953

Plant-Produced Receptor-Binding Domain of SARS-CoV-2 Elicits Potent Neutralizing Responses in Mice and Non-human Primates

*Konlavat Siriwattananon[1,2], Suwimon Manopwisedjaroen[3], Balamurugan Shanmugaraj[4], Kaewta Rattanapisit[4], Supaporn Phumiamorn[5], Sompong Sapsutthipas[5], Sakalin Trisiriwanich[5], Eakachai Prompetchara[6,7], Chutitorn Ketloy[6,7], Supranee Buranapraditkun[6,8], Wassana Wijagkanalan[9], Kittipan Tharakhet[6], Papatsara Kaewpang[6], Kantinan Leetanasaksakul[10], Taratorn Kemthong[11], Nutchanat Suttisan[11], Suchinda Malaivijitnond[11], Kiat Ruxrungtham[6,8], Arunee Thitithanyanont[3] and Waranyoo Phoolcharoen[1,2]**

[1] Research Unit for Plant-produced Pharmaceuticals, Chulalongkorn University, Bangkok, Thailand, [2] Department of Pharmacognosy and Pharmaceutical Botany, Faculty of Pharmaceutical Sciences, Chulalongkorn University, Bangkok, Thailand, [3] Department of Microbiology, Faculty of Science, Mahidol University, Bangkok, Thailand, [4] BaiyaPhytopharm Co., Ltd., Bangkok, Thailand, [5] Department of Medical Sciences, Ministry of Public Health, Institute of Biological Products, Nonthaburi, Thailand, [6] Faculty of Medicine, Center of Excellence in Vaccine Research and Development (Chula Vaccine Research Center, Chula VRC), Chulalongkorn University, Bangkok, Thailand, [7] Department of Laboratory Medicine, Faculty of Medicine, Chulalongkorn University, Bangkok, Thailand, [8] Department of Medicine, Faculty of Medicine, Chulalongkorn University, Bangkok, Thailand, [9] BioNet-Asia Co., Ltd., Bangkok, Thailand, [10] National Center for Genetic Engineering and Biotechnology (BIOTEC), National Science and Technology Development Agency, Pathum Thani, Thailand, [11] National Primate Research Center of Thailand-Chulalongkorn University, Saraburi, Thailand

The emergence of coronavirus disease 2019 (COVID-19) caused by severe acute respiratory syndrome coronavirus 2 (SARS-CoV-2) has affected global public health and economy. Despite the substantial efforts, only few vaccines are currently approved and some are in the different stages of clinical trials. As the disease rapidly spreads, an affordable and effective vaccine is urgently needed. In this study, we investigated the immunogenicity of plant-produced receptor-binding domain (RBD) of SARS-CoV-2 in order to use as a subunit vaccine. In this regard, RBD of SARS-CoV-2 was fused with Fc fragment of human IgG1 and transiently expressed in *Nicotiana benthamiana* by agroinfiltration. The plant-produced RBD-Fc fusion protein was purified from the crude extract by using protein A affinity column chromatography. Two intramuscular administration of plant-produced RBD-Fc protein formulated with alum as an adjuvant have elicited high neutralization titers in immunized mice and cynomolgus monkeys. Further it has induced a mixed Th1/Th2 immune responses and vaccine-specific T-lymphocyte responses which was confirmed by interferon-gamma (IFN-γ) enzyme-linked immunospot assay. Altogether, our results demonstrated that the plant-produced SARS-CoV-2 RBD has the potential to be used as an effective vaccine candidate against SARS-CoV-2. To our knowledge, this is the first report demonstrating the immunogenicity of plant-produced SARS-CoV-2 RBD protein in mice and non-human primates.

Keywords: COVID-19, SARS-CoV-2, receptor-binding domain, *Nicotiana benthamiana*, plant-produced recombinant protein, Fc fusion protein, subunit vaccine

OPEN ACCESS

Edited by:
Ryo Matsuda,
The University of Tokyo, Japan

Reviewed by:
Chiara Lico,
Italian National Agency for New Technologies, Energy and Sustainable Economic Development (ENEA), Italy
Silvana Petruccelli,
National University of La Plata, Argentina

***Correspondence:**
Waranyoo Phoolcharoen
Waranyoo.P@chula.ac.th

Specialty section:
This article was submitted to Plant Biotechnology, a section of the journal Frontiers in Plant Science

Received: *19 March 2021*
Accepted: *15 April 2021*
Published: *13 May 2021*

Citation:
Siriwattananon K, Manopwisedjaroen S, Shanmugaraj B, Rattanapisit K, Phumiamorn S, Sapsutthipas S, Trisiriwanich S, Prompetchara E, Ketloy C, Buranapraditkun S, Wijagkanalan W, Tharakhet K, Kaewpang P, Leetanasaksakul K, Kemthong T, Suttisan N, Malaivijitnond S, Ruxrungtham K, Thitithanyanont A and Phoolcharoen W (2021) Plant-Produced Receptor-Binding Domain of SARS-CoV-2 Elicits Potent Neutralizing Responses in Mice and Non-human Primates. Front. Plant Sci. 12:682953. doi: 10.3389/fpls.2021.682953

INTRODUCTION

In December 2019, the unknown pneumonia cases have been first reported in Wuhan, Hubei Province, China, which were initially reported to be caused by novel coronavirus (nCoV-2019) and later named as SARS-CoV-2. The disease condition associated with it is referred as Coronavirus Disease (COVID-19). The virus was closely related to the severe acute respiratory syndrome coronavirus (SARS-CoV) that cause massive outbreak in 2002–2003 (Amanat and Krammer, 2020; Li Q. et al., 2020; Malik et al., 2020; Quinlan et al., 2020; She et al., 2020; Singhal, 2020). In short time, the virus spreads rapidly to more than 200 countries (Malik et al., 2020; She et al., 2020). As of April 2021, more than 130 million confirmed cases with a toll of more than 2.9 million deaths were globally reported and the number of infected patients has still been exponentially increasing daily (World Health Organization, 2021). Furthermore, only few vaccines are currently approved. Thus, the development of affordable effective vaccine or therapeutics is highly essential to control and prevent the infection.

SARS-CoV-2 belongs to the family Coronaviridae in the genera of *Betacoronavirus*, which are known to infect mammals. Coronaviruses (CoVs) are enveloped and single-stranded positive sense RNA viruses (Banerjee et al., 2019; Amanat and Krammer, 2020; Li H. et al., 2020; Rabi et al., 2020; Yuki et al., 2020). The CoV genome consists of 6–11 open reading frames (ORFs) encoding for non-structural polyproteins and structural proteins. The SARS-CoVs have four major structural proteins such as spike (S) surface glycoprotein, membrane (M) protein, envelope (E) protein, and nucleocapsid (N) protein, which are essential for viral assembly and infection (Bosch et al., 2003; Masters, 2006; Banerjee et al., 2019; Li H. et al., 2020; Malla et al., 2020; Rabi et al., 2020; Yuki et al., 2020). S glycoprotein plays a major role in viral attachment to host cells during the viral infection and cleaved by the host proteases into S1 and S2 subunits. SARS-CoV-2 infection starts with pre-fusion of receptor binding domain (RBD) located on the S1 subunit to host receptor, angiotensin converting enzyme 2 (ACE2 receptor) and followed by S2 subunit post-fusion, leading to viral RNA penetration into host cells (Li et al., 2003; Li, 2016; Yuan et al., 2017; Walls et al., 2019; Rabi et al., 2020; Shanmugaraj et al., 2020c; Yuki et al., 2020; Zhou et al., 2020). In addition, RBD was known to elicit potent immune response and considered as prime target for eliciting of host neutralizing antibodies (Wang et al., 2018; Li H. et al., 2020; Smith et al., 2020). Furthermore, previous studies demonstrated that the sera isolated from animals immunized with inactivated SARS-CoV virus significantly neutralize the virus by inhibiting the binding of RBD with ACE2 receptor which proved that the antibodies targeting the RBD domain could prevent the virus infection (He et al., 2004, 2005a,b; Zhu et al., 2013; Li H. et al., 2020).

Currently, recombinant proteins are produced mainly by bacterial fermentation or mammalian cell cultures, which still have many limitations including high production costs, immunogenicity profile, and pathogen contamination (Kelley, 2009; Phoolcharoen et al., 2011; Gomes et al., 2016; Kodati et al., 2016; Fuenmayor et al., 2017; Kaur et al., 2018; Rattanapisit et al., 2019a). Plant expression system is considered as the cost-effective platform for the production of vaccine antigens, diagnostic reagents, valuable biopharmaceuticals such as therapeutic immunoglobulins, human enzymes, and human growth factors (Gleba et al., 2005; Miao et al., 2008; Phoolcharoen et al., 2011; Ahmad et al., 2019; Rattanapisit et al., 2019a,b, 2021). Plant expression system offers several advantages in terms of rapidity, flexibility, post-translational modification of recombinant proteins, safety due to lack of animal pathogen, toxin contamination and scalability compared to other available conventional systems (Vitale and Denecke, 1999; Ma et al., 2003; Phoolcharoen et al., 2011; Shahid and Daniell, 2016; Bellucci et al., 2017). Hence, plant platform can be considered as an alternative platform for economical production of commercially viable biopharmaceuticals and vaccines especially for developing countries during pandemic situation (Phoolcharoen et al., 2011; Shanmugaraj et al., 2020a).

In this study, we produced SARS-CoV-2 RBD-Fc fusion protein by fusing SARS-CoV-2 RBD to the Fc domain of human IgG1 at the C-terminus and cloned into geminiviral vector for expression in *Nicotiana benthamiana* plants. The plant-produced RBD-Fc showed specific binding with both human embryonic kidney 293 (HEK293) and Chinese hamster ovary (CHO) cells produced ACE2 protein. Further the plant-produced RBD-Fc was shown to be immunogenic and significantly boosted a humoral and cell-mediated immune response in both mice and cynomolgus macaques (*Macaca fascicularis*). Our results demonstrated that this plant-produced protein has the potential for use as a vaccine candidate against SARS-CoV-2.

MATERIALS AND METHODS

Construction of SARS-CoV-2 RBD-Fc Plant Expression Vector

The RBD of SARS-CoV-2 (SARS-CoV-2 RBD) (Genbank accession number: YP_009724390.1; F318-C617) was designed to anneal with Fc region of human immunoglobulin G1 (IgG1) (GenBank accession number: 4CDH_A) by peptide linker 3XGGGGs at the C-terminus (**Figure 1**). The nucleotide sequence of SARS-CoV-2 RBD was codon optimized and commercially synthesized (Genewiz, Suzhou, China) with *Xba*I and *Bam*HI restriction sites for cloning with the Fc region, that contains *Bam*HI and *Sac*I restriction sites at the 5′ and 3′ ends, respectively. The SARS-CoV-2 RBD and human Fc region were ligated into a geminiviral vector (pBYR2eK2Md; pBYR2e) (Chen et al., 2011; Diamos and Mason, 2018) using *Xba*I and *Sac*I restriction sites to construct the plant expression vector pBYR2e-SARS-CoV-2 RBD-Fc. The murine leader sequence (Shanmugaraj et al., 2020b) and ER retention signal peptide (SEKDEL) was included at N-terminus and C-terminus of the gene construct, respectively (**Figure 1**).

Expression of SARS-CoV-2 RBD-Fc in *Nicotiana benthamiana via*., Agroinfiltration

The plant expression vector pBYR2e-SARS-CoV-2 RBD-Fc was transformed into *Agrobacterium tumefaciens* strain GV3101

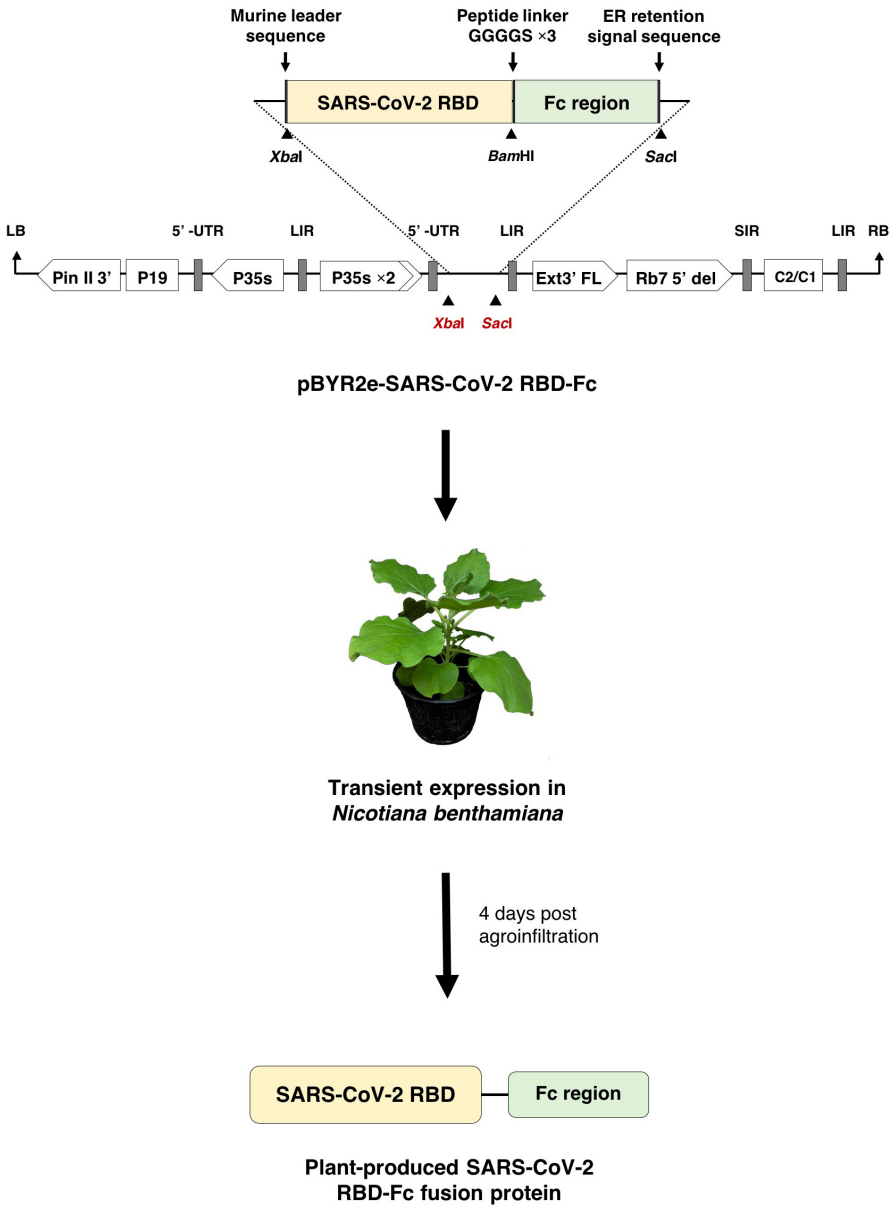

FIGURE 1 | Diagrammatic representation showing the T-DNA of plant expression vector pBYR2e-SARS-CoV-2 RBD-Fc and the overview of transient expression in *N. benthamiana* plants. RB and LB, left and right borders of the T-DNA used in *Agrobacterium* DNA delivery into plant cells; Pin II 3', the terminator from potato proteinase inhibitor II gene; P19, the RNA silencing suppressor from Tomato Bushy Stunt Virus (TBSV); P35s, 35s promoter from Cauliflower Mosaic Virus (CaMV); P35s × 2, 35s promoter from CaMV with duplicated enhancer; Ext3' FL, 3' region of tobacco extension gene; Rb7 5' del, tobacco RB7 promoter; SIR, short intergenic region of Bean Yellow Dwarf Virus (BeYDV); LIR, long intergenic region of BeYDV; C2/C1, Rep/RepA gene from BeYDV encoding for replication initiation protein (Rep) and RepA.

cells by electroporation (MicroPulser, Bio-Rad, United States). The recombinant *Agrobacterium* clones were confirmed by polymerase chain reaction (PCR) using the RBD gene-specific primers. *Agrobacterium* containing pBYR2e-SARS-CoV-2 RBD-Fc was resuspended with 1xinfiltration buffer (10 mM 2-(N-morpholino) etanesulfonic acid (MES), 10 mM MgSO4, at pH 5.5) to get final OD_{600} of 0.2 prior to agroinfiltration. The *Agrobacterium* suspension was injected into the adaxial side of 6-week-old *N. benthamiana* leaves. The infiltrated plants were maintained in an optimal 16-h light/8-h dark condition at 28°C and harvested after 4 days post infiltration (dpi).

Purification of Plant-Produced SARS-CoV-2 RBD-Fc Fusion Protein

The infiltrated leaves were harvested and extracted with 1xPBS (phosphate-buffered saline: 137 mM NaCl, 2.68 mM KCl, 10.1 mM Na_2HPO_4, 1.76 mM KH_2PO_4 pH 7.4) and clarified by

centrifugation at 26,000 *g* for 45 min at 4°C. The supernatant was filtered by using 0.45 μm S-Pak membrane (Merck, Massachusetts, United States). The clarified supernatant was purified by affinity column chromatography with protein-A beads (Expedeon, Cambridge, United Kingdom). The purified column was equilibrated and washed by 1xPBS pH 7.4 followed by elution with 0.1 M glycine buffer pH 3. Subsequently, the pH of the eluted proteins was neutralized by using Tris-HCl pH 8.8. The purified SARS-CoV-2 RBD-Fc was concentrated by using Amicon® ultracentrifugal filter (Merck, Massachusetts, United States) and filtered through 0.22 μm syringe filter (Merck, Massachusetts, United States). The purified plant-produced SARS-CoV-2 RBD-Fc fusion protein was analyzed by using sodium dodecyl sulfate-polyacrylamide gel electrophoresis (SDS-PAGE) and western blotting under reducing and non-reducing conditions. The SARS-CoV-2 RBD-Fc samples were subjected to 8% sodium dodecyl sulfate polyacrylamide gel electrophoresis and stained by Coomassie staining solution for protein visualization. For western blot analysis, the separated proteins were transferred to nitrocellulose membrane (Biorad, United States) and detected with a 1:5,000 sheep anti-human gamma chain-HRP conjugate antibody diluted in 1xPBS (The Binding Site, United Kingdom). The yield of purified plant-produced RBD-Fc fusion protein was estimated by direct ELISA assay using human IgG (Abcam, United Kingdom) as protein standard. The samples were probed by using anti-human gamma chain-HRP fusion (The Binding Site, United Kingdom) at the dilution of 1:1,000 in 1xPBS. A 3,3,5,5′-Tetramethylbenzidine (TMB) solution (Promega, United States) was added into the plate as a colorimetric developer followed by the addition of 1M H_2SO_4. The absorbance at 450 nm was read using a 96-well plate reader (Molecular Devices, United States).

Liquid Chromatography—Mass Spectrometry (LC-MS) of Plant-Produced SARS-CoV-2 RBD-Fc Fusion Protein

The purified proteins were separated on SDS-PAGE. The targeted protein band was excised and sent to National Center for Genetic Engineering and Biotechnology, Pathum Thani, Thailand for LC-MS analysis. The protein was enzymatically digested with trypsin and injected into Hybrid quadrupole Q-Tof impact IITM (Bruker Daltonics Ltd., Hamburg, Germany) equipped with a Nano-captive spray ion source was coupled to a nanoLC system: Ultimate 3000 LC System (Thermo Fisher Scientific, United States). Equipment operation was controlled by Compass 1.9 software (Bruker Daltonics Ltd., Hamburg, Germany). The resulting MS/MS spectra were searched using the Mascot Sever (Matrix Science) against SwissProt database. For Mascot searches, the peptide mass tolerance was set at 0.6 Da and the fragment mass tolerance was set at 1.2 Da.

ACE2 Binding by ELISA

The binding activity of plant-produced SARS-CoV-2 RBD-Fc fusion protein to ACE2 protein was demonstrated by ELISA. Briefly, 96-well ELISA plate was coated by 100 ng of two different ACE2 protein derived either from HEK293-cells (Abcam, United Kingdom) or CHO-cells (InvivoGen, California, United States). For blocking, 5% skim milk in 1xPBS was added into the wells and incubated for 2 h at 37°C. After blocking, the plate was washed three times with 1xPBST (1xPBS plus 0.05% Tween-20) and incubated with various concentrations of plant-produced SARS-CoV-2 RBD-Fc fusion protein in 1xPBS. The SARS-CoV-2 RBD proteins in the wells were detected by addition of 1: 100 dilution of plant-produced anti-SARS-CoV-2 (H4) mAb (Shanmugaraj et al., 2020b) and followed by a 1:1,000 dilution of anti-human Kappa chain-HRP fusion (SouthernBiotech, United States) in 1xPBS for 1 h at 37°C. For colorimetric development, a TMB solution (Promega, United States) was added into the wells followed by addition of 1M H_2SO_4 for terminating the enzymatic reaction. The absorbance at 450 nm was measured using a 96-well microplate reader (Molecular Devices, United States).

Immunization of Mice and Non-human Primates

Mice immunization protocols were approved by the Institutional Animal Care and Use Committee, Faculty of Medicine, Chulalongkorn University (Protocol review No. 012/2563). Seven-week-old female ICR mice (n = 5 per group) were intramuscularly (IM) immunized *via.*, anterior tibialis with 10 μg of plant-produced SARS-CoV-2 RBD-Fc fusion protein without adjuvant or formulated with 0.1 mg alum (InvivoGen, California, United States) on days 0 and 21. Mice sera were collected prior to the first immunization (pre-bleed, day 0) and 14 days post-vaccination to assess the SARS-CoV-2-specific antibody response. The mice were sacrificed on day 35 (14 days after second booster) to collect the spleen for quantitative measurement of SARS-CoV-2 RBD-specific T-cell responses.

For non-human primate immunogenicity studies, all procedures were reviewed and approved by the National Primate Research Center of Thailand-Chulalongkorn University (NPRCT-CU) Animal Care and Use Committee (Protocol review No. 207512) and the facility has been AAALAC International Accredited (1752). Thirteen SPF juvenile cynomolgus macaques (*Macaca fascicularis*), aged between 2.5 and 3.5 years old, and body weight between 2.18 and 3.17 kg, were assigned into three groups in which the control group (n = 3) was immunized by PBS adjuvanted with 0.5 mg alum, and other two groups (n = 5 per group) were administered with 25 and 50 μg of plant-produced SARS-CoV-2 RBD-Fc fusion protein along with 0.5 mg alum adjuvant, respectively. Monkeys were received two intramuscular injections on day 0 and 21. The blood samples were collected on day 0 (pre-immunization) and 14 days after each vaccination (days 14 and 35) to assess SARS-CoV-2 RBD specific IgG, neutralizing antibody and cell-mediated immune responses.

Evaluation of SARS-CoV-2 RBD-Specific Total Antibody Responses by ELISA

96-well plate was coated with 100 ng of SARS-CoV-2 spike protein RBD derived from Sf9 insect cells (GenScript, United States) and incubated overnight at 4°C. Then, the wells were blocked with 5% skim milk powder in 1xPBS for 2

h at 37°C. Subsequently, the animal sera were twofold serially diluted with 1xPBS starting at 1:100 was loaded on the wells and incubated for 2 h at 37°C. Goat anti-mouse IgG HRP conjugate antibody (Jackson ImmunoResearch, Pennsylvania, United States) and goat anti-monkey IgG HRP conjugation (Abcam, United Kingdom) diluted 1:2,000 in 1xPBS were added into the wells for detecting mouse and monkey antibodies, respectively, and the plate was incubated for 2 h at 37°C. TMB substrate (Promega, United States) was added into the plates for colorimetric development. The enzymatic reactions were terminated by adding 1M H_2SO_4. The absorbance was measured at 450 nm using a microplate reader (BMG Labtech, Germany). Between each step, the plates were washed by 1xPBST for three times. For mouse IgG1 and IgG2a analysis, the mice sera were twofold serially diluted with 1xPBS starting 1:100 in the same fashion and detected by 1:2,000 goat anti-mouse IgG1 (HRP) and goat anti-mouse IgG2a heavy chain (HRP) antibody (Abcam, United Kingdom), respectively, diluted in 1xPBS. The endpoint titer of IgG1 and IgG2a were also computed for monitoring Th2 and Th1 lymphocyte responses, respectively. The endpoint titers were determined as the highest dilution of immunized sera, which had A_{450} more than cut off calculated from A_{450} of pre-immunized sera in the dilution of 1:100 in 1xPBS (Frey et al., 1998). All experiments were performed in duplicates and 1xPBS was used as a control. The statistical analyses of immunological data were performed using GraphPad Prism software version 8.0. Statistical significance was calculated by two-way analysis of variance (ANOVA). All data in each group were compared by using Tukey's multiple comparisons test and the values of $p < 0.05$ were considered as statistically significant.

In vitro Microneutralization Assay

Microneutralization assay was performed using Vero E6 cell line and live SARS-CoV-2 virus isolated from a COVID-19 patient and conducted in a certified biosafety level 3 facility of Microbiology department, Faculty of Science, Mahidol University, Bangkok, Thailand. The cells were plated in 96-well plate at 1×10^4 cells/well in DMEM (Dulbecco's Modified Eagle's medium supplemented with 10% heat-inactivated FBS, 100 U/mL of penicillin and 0.1 mg/mL of streptomycin) and incubated for overnight. The immunized sera and positive convalescent serum from COVID-19 patient were heat-inactivated at 56°C for 30 min. The immunized sera were twofold serially diluted in duplicates and incubated with 100 of 50% tissue culture infective dose ($TCID_{50}$) of the SARS-CoV-2 virus in DMEM at 37°C for 1 h. Virus control at 100$TCID_{50}$ and uninfected cell control wells were included in all plates. Subsequently, the mixture of diluted serum and virus was transferred to the cell monolayer and incubated at 37°C with 5% CO_2 for 2 days. After incubation, the cells were washed once with 1xPBS and then fixed and permeabilized with ice-cold 1:1 methanol/acetone fixative solution at 4°C for 20 min. The cells were washed 3 times with 1xPBST and blocked with 2% BSA at room temperature (RT) for 1 h. After washing, the viral nucleocapsid was detected using 1:5,000 of SARS-CoV/SARS-CoV-2 nucleocapsid (N) monoclonal antibody (SinoBiological, United States) and incubated at 37°C for 1 h followed by adding 1:2,000 of HRP-conjugated goat anti-rabbit polyclonal antibody (Dako, Denmark) diluted with 1xPBS and incubated at 37°C for 1h. The KPL Sureblue^{TM} TMB substrate (SeraCare, United States) was added for colorimetric development. Then the reaction was stopped by the addition of 1N HCl. The absorbance at 450 and 620 nm was read by a Sunrise^{TM} microplate reader (Tecan, Switzerland). The absorbance differences between 450 and 620 nm (A_{450}–A_{620}) of diluted samples were compared with the 50% specific signal of the cut point, which was calculated by the following equation to determine the potent neutralization titers of the immunized sera.

$$A_{cutpoint} = \left(\frac{A_{virus\ control} - A_{cell\ control}}{2}\right) + A_{cell\ control}$$

Where $A_{Virus\ control}$ and $A_{cell\ control}$ are the average of A_{450}-A_{620} of virus control wells and cell control wells, respectively. The neutralizing titers were defined as the reciprocal highest dilution providing the average of A_{450}–A_{620} of the diluted serum well more than the cut point. The neutralizing antibody titers of each experimental group were compared by GraphPad Prism 8.0 using Mann-Whitney test. The significant differences were considered when $p < 0.05$.

Mouse IFN-γ ELISPOT Assay

For mouse splenocyte preparation, the spleen cells were aseptically plated in the petri-dish and dissociated into single-cell suspension using needle#21 for 2–3 times. The separated splenocytes were cultured in R5 medium (RPMI1640 with 100 U/mL penicillin, 100 U/mL streptomycin, 5% heat-inactivated fetal bovine serum (FBS, Gibco, United States) and 2-mercaptoethanol) and centrifuged at 1,200 g 4°C for 5 min. Subsequently, splenocytes were lysed with 1xACK lysis buffer, added R5 medium and collected the cell pellet by centrifugation at 1,200 g 4°C for 5 min. Finally, splenocytes were counted and adjusted for using in ELISpot assay. The IFN-γ secreting cells were quantified by using mouse IFN-γ ELISpot assay kit (Mabtech, Stockholm, Sweden). Briefly, splenocytes were resuspended at 5×10^6 cells/mL in R5 medium. The 96-well plates (Millipore, Bedford, MA, United States) were coated with 500 ng of anti-mouse IFN-γ (AN18) monoclonal antibody (mAb) (Mabtech, Stockholm, Sweden) in 1xPBS at 37°C with 5% CO_2 for 3 h. Then, the plates were washed six times with 1xPBS and blocked with R10 medium at RT for 1 h. A quantity of 5×10^5 splenocytes per well were activated by lyophilized SARS-CoV-2 peptide pools (BioNet-Asia, Thailand, and Mimotopes, Australia) at a final concentration of 2 μg/mL at 37°C with 5% CO_2 for 40 h. R5 medium and concanavalin A (ConA) were used as negative and positive controls, respectively. After incubation, the plates were washed six times with 1xPBST followed by three times with 1xPBS. Then, the plates were incubated with anti-mouse IFN-γ-biotinylated mAb (Mabtech, Stockholm, Sweden) diluted in 1xPBS at RT for 3 h. After washing, streptavidin-alkaline phosphatase (ALP: Mabtech, Stockholm, Sweden) was added and incubated at RT for 1 h. The substrate solution (5-bromo-4-chloro-3-indolyl-phosphate/nitro blue tetrazolium; BCIP/NBT) were added into the wells and incubated until distinct spots emerge. Reactions were stopped by washing

extensively in tap water and rinsing the underside of membrane. Inspect and count spots were performed with an ELISpot reader (ImmunoSpot® Analyzer, United States). Results were expressed as spot-forming cells (SFCs)/10^6 splenocytes. The positive responses were defined as $>$ 50 SFCs/10^6 splenocytes over the background signal. The result analyses were conducted using Kruskal-Wallis test in GraphPad Prism 6.0. All p-values < 0.05 were defined as significant.

Non-human Primate IFN-γ ELISpot Assay

For peripheral blood mononuclear cells (PBMCs) preparation, the cells were isolated by density gradient separation using Isoprep (Robbins Scientific Corporation, CA). Briefly, after removal of plasma, EDTA-treated whole blood was diluted (1:1) with RPMI1640 medium containing 2 mM L-Glutamine (Gibco, United States) and layered over Isoprep. Samples were then centrifuged at 1,200 g for 30 min. The PBMC layer was harvested and washed twice with RPMI1640. Then, the cells were resuspended in R10 medium (RPMI1640 supplemented with 100 U/mL of penicillin, 100 U/mL of streptomycin and 10% heat-inactivated fetal bovine serum (FBS, Gibco, United States) for applying in ELISpot assay. The antigen-specific cells secreting monkey IFN-γ were enumerated by using monkey IFN-γ ELISpot assay kit (Mabtech, Stockholm, Sweden). Briefly, PBMCs were stimulated with SARS-CoV-2 spike peptides pools (BioNet-Asia, Thailand, and Mimotopes, Australia) at 37°C with 5% CO_2 for 40 h. R5 medium and phytohemagglutinin (PHA) were served as negative and positive control, respectively. The secreted monkey IFN-γ were detected by anti-monkey IFN-γ-biotinylated mAb (Mabtech, Stockholm, Sweden) and followed by addition of ALP solution (Mabtech, Stockholm, Sweden). For spot development, BCIP/NBT-plus substrate solution was added into the wells and incubated until distinct spots emerge. The spots were inspected and counted by ELISpot reader (ImmunoSpot® Analyzer, Germany). Results were expressed as spot-forming cells (SFCs)/10^6 PBMCs following the subtraction of the negative control. The positive responses were defined $>$ 100 SFCs/10^6 PBMCs over the background. Statistical analyses were presented using GraphPad Prism 8.0. Comparison of frequencies of populations in each group was made using Friedman and Mann-Whitney tests. All p-values < 0.05 were defined as significant.

RESULTS

Transient Expression of SARS-CoV-2 RBD-Fc Fusion Protein in *Nicotiana benthamiana*

The nucleotide sequence of RBD of SARS-CoV-2 was codon-optimized and fused with Fc region of human IgG1 at the C terminus of the RBD gene construct. The codon-optimized SARS-CoV-2 RBD-Fc fusion gene was cloned into the geminiviral plant expression vector pBYR2e. For expression of RBD-Fc fusion protein in plants, *N. benthamiana* plants were infiltrated with *Agrobacterium* containing pBYR2e-SARS-CoV-2 RBD-Fc (**Figure 1**). The leaves infiltrated with *Agrobacterium* containing pBYR2e-SARS-CoV-2 RBD-Fc showed significant phenotypic necrosis compared to the leaves infiltrated by *Agrobacterium* without the plant expression vector (**Figure 2A**).

Purification and Characterization of Plant-Produced RBD-Fc Fusion Protein

Plant-produced SARS-CoV-2 RBD-Fc fusion protein was extracted and purified from crude extract by single-step protein A affinity chromatography. The purified SARS-CoV-2 RBD-Fc fusion protein was concentrated and filtered by using 0.22 μm syringe filter. The purity of the purified plant-produced SARS-CoV-2 RBD-Fc was analyzed by SDS-PAGE gel stained with Coomassie blue staining under reducing and non-reducing condition. The purity of SARS-CoV-2 RBD-Fc fusion protein was found to be higher than 90% based on the visual inspection of a Coomassie-stained SDS gel (**Figure 2B**). The SARS-CoV-2 RBD-Fc fusion protein was further analyzed by western blot probed with anti-human gamma chain-HRP conjugate antibody. The protein band corresponding to the molecular weight of 65 kDa was observed in reducing condition (**Figure 2C**; lane 1). In addition, the plant-produced SARS-CoV-2 RBD-Fc fusion protein under non-reducing condition was observed at approximately 150 kDa (**Figure 2C**; lane 2), which implies that the SARS-CoV-2 RBD-Fc fusion protein could be linked by disulfide bond into dimeric form. The expression level of plant-produced SARS-CoV-2 RBD-Fc was quantified by ELISA and found to be 25 μg/g fresh weight. The authenticity of purified plant-produced SARS-CoV-2 RBD-Fc fusion protein was further confirmed by using a high-resolution LC-TOF MS/MS analysis as shown in **Supplementary Document**.

In vitro Binding Activity of Plant-Produced RBD-Fc Fusion Protein

The binding of plant-produced SARS-CoV-2 RBD-Fc fusion protein was confirmed by ELISA by using commercial HEK293 and CHO-produced ACE2 protein as the capture reagent. The various dilutions of purified plant-produced SARS-CoV-2 RBD-Fc was incubated with commercial ACE2 proteins. For detection of SARS-CoV-2 RBD, anti-SARS-CoV-2 (H4) mAb (Shanmugaraj et al., 2020b) and anti-human kappa chain-HRP conjugate antibody were added into the wells. The results showed that plant-produced SARS-CoV-2 RBD-Fc fusion protein produced saturable binding to both commercial ACE2 proteins with substantially high affinity in comparison to PBS control (**Figure 3**), which confirms the authenticity of plant-produced SARS-CoV-2 RBD-Fc.

Immunogenicity in Mice

Mice immunogenicity was assessed in 7-week-old female Mlac:ICR mice by immunizing intramuscularly on days 0 and 21 with 10 μg of plant-produced SARS-CoV-2 RBD-Fc fusion protein with or without alum adjuvant. Mice sera were collected on days 0, 14, and 35 (**Figure 4A**). SARS-CoV-2 RBD-specific antibodies were evaluated by ELISA using commercial SARS-CoV-2 RBD-His protein produced from Sf9 cells as a capture antigen. The SARS-CoV-2 RBD-specific immune responses were

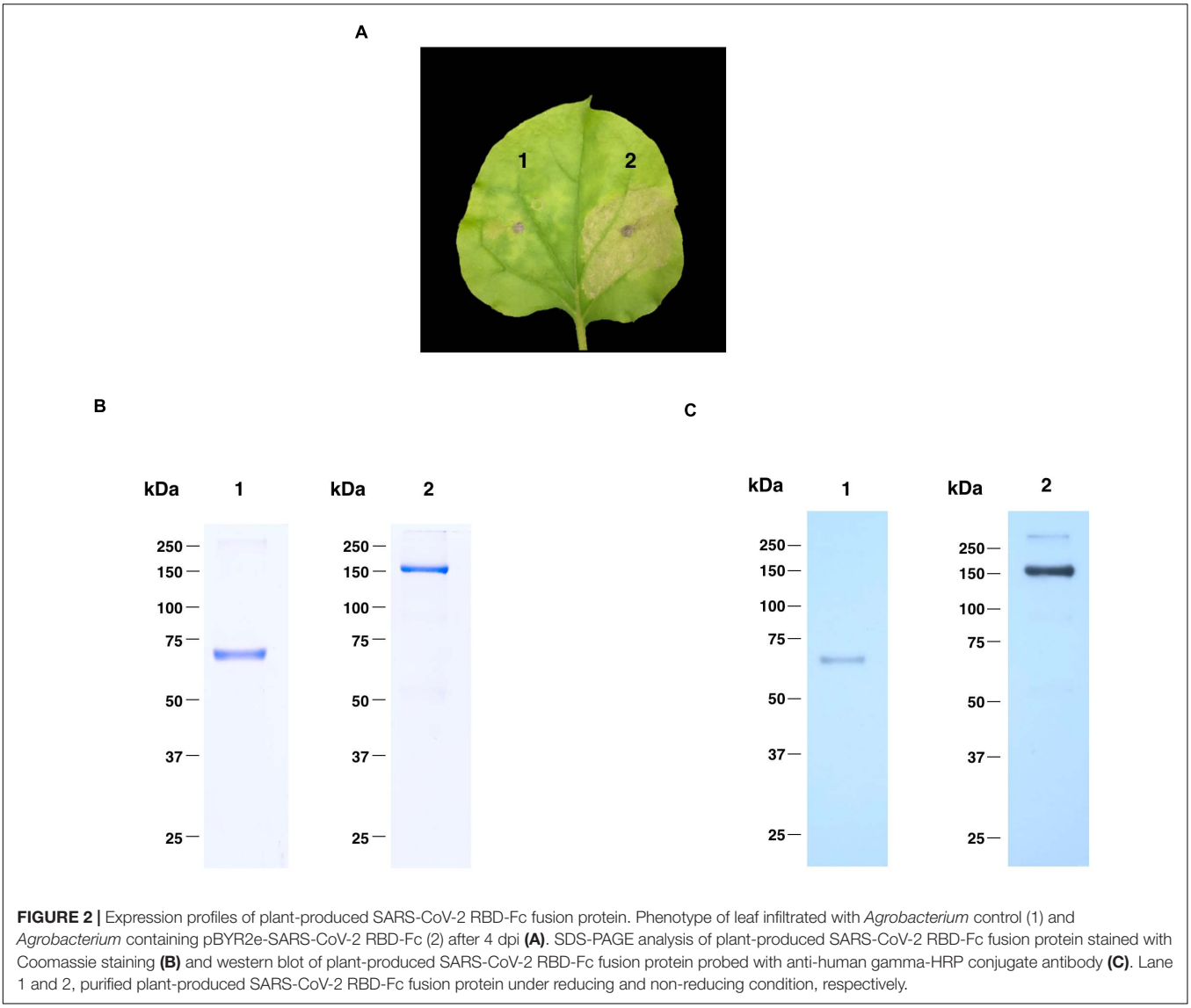

FIGURE 2 | Expression profiles of plant-produced SARS-CoV-2 RBD-Fc fusion protein. Phenotype of leaf infiltrated with *Agrobacterium* control (1) and *Agrobacterium* containing pBYR2e-SARS-CoV-2 RBD-Fc (2) after 4 dpi **(A)**. SDS-PAGE analysis of plant-produced SARS-CoV-2 RBD-Fc fusion protein stained with Coomassie staining **(B)** and western blot of plant-produced SARS-CoV-2 RBD-Fc fusion protein probed with anti-human gamma-HRP conjugate antibody **(C)**. Lane 1 and 2, purified plant-produced SARS-CoV-2 RBD-Fc fusion protein under reducing and non-reducing condition, respectively.

observed after first immunization of plant-produced SARS-CoV-2 RBD-Fc alone, whilst a slightly increased specific-mouse total IgG response was observed in SARS-CoV-2 RBD-Fc immunized with alum. All mice immunized with plant-produced RBD-Fc elicited significantly higher antibody titer after second booster compared with the control group (**Figure 4B**). Plant-produced SARS-CoV-2 RBD-Fc was found to be immunogenic, while the addition of alum adjuvant could significantly improve its immunogenicity. In addition, we appraised the levels of SARS-CoV-2 RBD-specific IgG1 and IgG2a subclasses, which are indicators of Th2 and Th1 lymphocyte responses in mice, respectively. The results demonstrated that plant-produced SARS-CoV-2 RBD-Fc induced both SARS-CoV-2 RBD-specific IgG1 (**Figure 4C**) and IgG2a (**Figure 4D**) with the IgG1 bias. The *in vitro* neutralizing ability of the immunized sera was evaluated. The SARS-CoV-2 RBD-Fc without adjuvant induced neutralizing antibody against SARS-CoV-2 after the second dose at a dilution of 1:1,280 (**Figure 4E**). Interestingly, mice sera immunized by SARS-CoV-2 RBD-Fc adjuvanted with alum displayed maximum SARS-CoV-2 neutralization with a dilution more than 1:10,240 (**Figure 4E**). IFN-γ levels of splenocytes isolated from mice was tested by IFN-γ ELISpot assay. The results showed that plant-produced RBD-Fc elicited IFN-γ secretion which was statistically significant compared with mock control group (**Figure 4F**).

Immunogenicity in Non-human Primates

Cynomolgus macaques (*Macaca fascicularis*) were intramuscularly immunized with 25 and 50 μg of plant-produced SARS-CoV-2 RBD-Fc with the presence of alum on day 0 and 21. Monkey sera were collected on day 0, 14, and 35 (**Figure 5A**). Plant-produced SARS-CoV-2 RBD-Fc protein adjuvanted with alum was capable of inducing dose-independent SARS-CoV-2 RBD-specific IgG antibodies in monkeys after first and second immunization with the dilution 1:800, and 1:51,200, respectively (**Figure 5B**). Specifically, the microneutralization assay was performed by using Vero E6 cell line to evaluate the level of

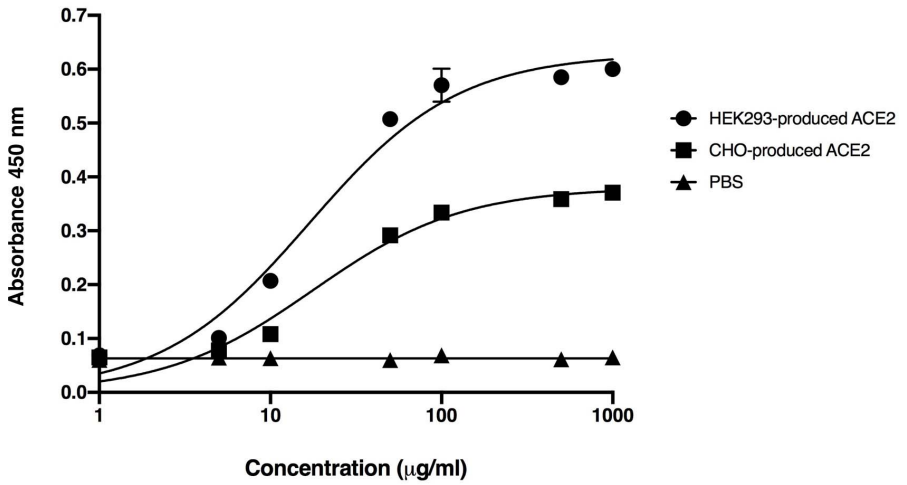

FIGURE 3 | Binding activity of the plant-produced SARS-CoV-2 RBD-Fc with the commercial angiotensin-converting enzyme 2 (ACE2 proteins) derived from HEK293 and CHO cells analyzed by ELISA. PBS was used as negative control. Data are presented as mean ± standard deviation (SD) of triplicates in each sample dilution.

neutralizing antibodies against live SARS-CoV-2. Sera collected 14 days after the first immunization (day 14) showed neutralizing activity against the SARS-CoV-2 and increased at day 35 (14 days after the second immunization) with the neutralization titer approximately 5,120 (**Figure 5C**). In addition, cell-mediated immune responses in cynomolgus monkeys were monitored by IFN-γ ELISpot assay by using peripheral blood mononuclear cells isolated from immunized sera on day 35. The specific IFN-γ expression was detected in monkeys immunized with two doses of plant-produced SARS-CoV-2 RBD-Fc, and a significant difference from the control group was detected compared to immunized monkeys (**Figure 5D**).

DISCUSSION

The recent emergence of coronavirus diseases (COVID-19) in China is responsible for the current global pandemic and public health crisis (Li Q. et al., 2020; Malik et al., 2020; Singhal, 2020; Yuki et al., 2020). Few vaccines are currently approved for human use. Hence, it is highly essential to develop safe, effective vaccines and therapeutics against this infection to prevent its spread. Recently, several groups have predicted and assessed the immunogenicity potential of SARS-CoV-2 related proteins and showed that SARS-CoV-2 S protein is the suitable candidate for recombinant vaccine development as it can elicit potent immune response and is the major target of neutralizing antibodies. The receptor-binding domain (RBD) of SARS-CoV-2 plays a key role in viral attachment and entry into the host cells by interaction with the ACE2 receptor in the host cells (Li et al., 2003; Lei et al., 2020; Quinlan et al., 2020; Rabi et al., 2020; Shanmugaraj et al., 2020c; Sun et al., 2020; Xie et al., 2020; Yuki et al., 2020). Particularly, RBD domain has multiple conformational epitopes, which can induce host immune responses and highly potent neutralizing antibodies (He et al., 2005a,b; Zhu et al., 2013; Wang et al., 2018; Smith et al., 2020). Hence, RBD domain in the S protein is considered as a potential target and could serve as a potent immunogen for developing the possible SARS-CoV-2 vaccines.

Since 1980s, plants have been utilized for the development of highly valuable biopharmaceuticals either for human or veterinary applications. Plant-based expression system offers several key advantages over conventional systems in terms of production speed, cost, and safety (Basaran and Rodríguez-Cerezo, 2008; Paul and Ma, 2011; Krenek et al., 2015; Yao et al., 2015; Burnett and Burnett, 2019; Shanmugaraj et al., 2020a; Daniell et al., 2021). Remarkably, plant-based expression system can produce large amounts of recombinant antigens in a relatively short time period within few weeks after making the gene construct (D'Aoust et al., 2008, 2010; Rybicki, 2009; Vézina et al., 2009; Pillet et al., 2016; Rattanapisit et al., 2020; Ward et al., 2020). The concept of plant-produced biopharmaceuticals and vaccines has been assessed and well explored by number of research groups worldwide. Several plant-produced therapeutics (Kizhner et al., 2015; Ma et al., 2015; Mor, 2015; Prevail Ii Writing Group et al., 2016) and vaccines (Yuki et al., 2013; Hendin et al., 2017; Donini and Marusic, 2019) are currently in pipeline for clinical trials and approval, Notably plant-produced Glucocerebrosidase enzyme (Elelyso^{TM}) for the treatment of type I Gaucher's disease has been approved by US Food and Drug Administration (Fox, 2012) and tobacco-derived seasonal flu VLP vaccine from Medicago Inc., is currently in final stages of clinical trial (Ward et al., 2021). Hence, plant-based expression could be an alternative option for rapid production of emergency vaccines or therapeutic antibodies (Iyappan et al., 2018; Diego-Martin et al., 2020; Rattanapisit et al., 2020; Shanmugaraj and Phoolcharoen, 2021; Siriwattananon et al., 2021).

The geographical distribution of virus is increasing rapidly and global concern on this pandemic demands an affordable and scalable protein production platform that can produce

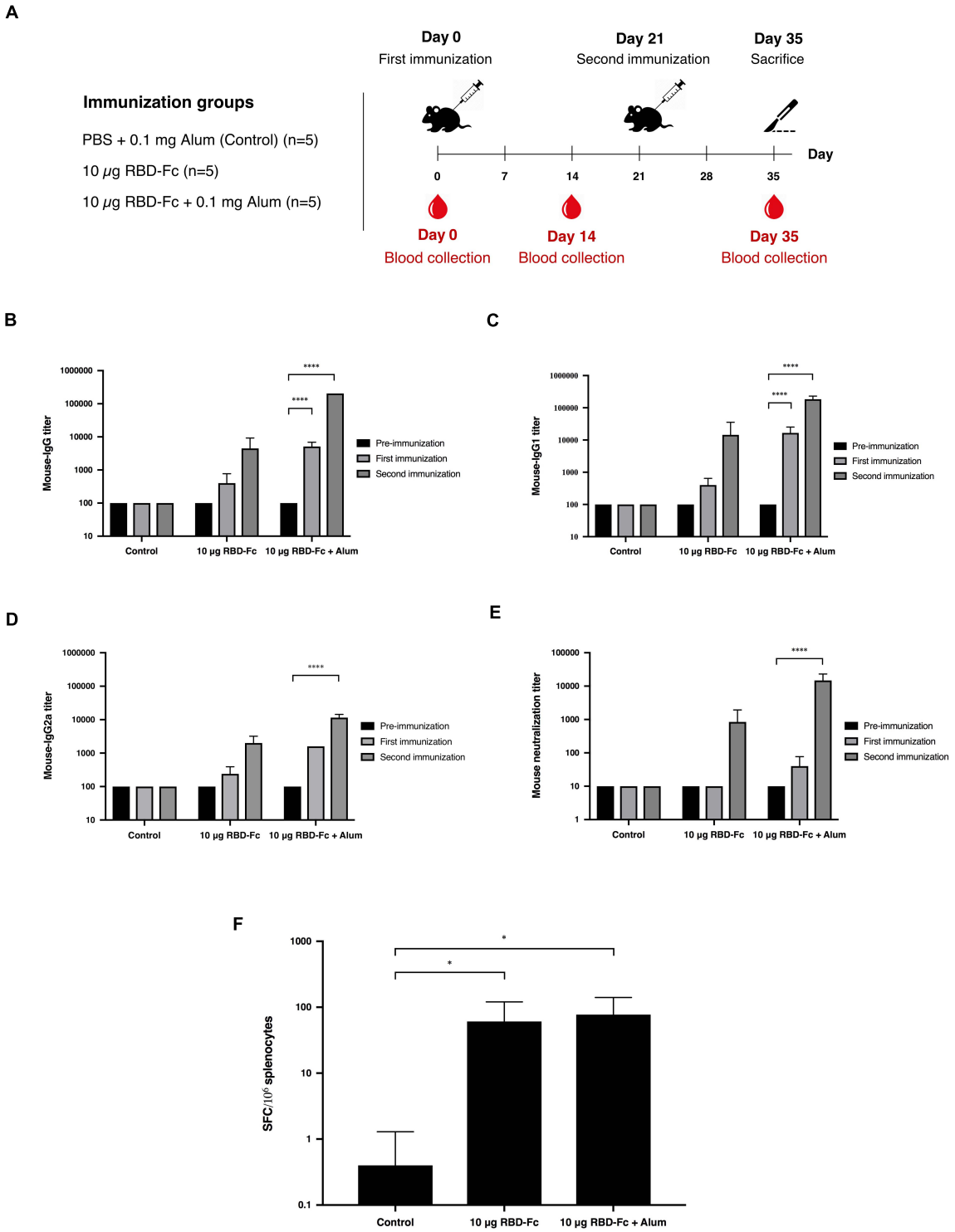

FIGURE 4 | Immunogenic studies in mice. Schematic representation of immunization protocol and sample collection. Groups of mice (five mice per each group) were intramuscularly immunized with 10 μg of SARS-CoV-2 RBD-Fc fusion protein alone or with alum adjuvant, followed by booster dose at 21 days after first immunization. Mice sera were collected on day 0 (pre-bleed) and day 14 post-immunization **(A)**. Titers of SARS-CoV-2 RBD-specific total IgG **(B)**, IgG1 **(C)**, and IgG2a **(D)** in the immunized sera collected on day 0, 14, and 35 were analyzed by indirect ELISA using Sf9-produced SARS-CoV-2 RBD-His as the capture antigen. Potent neutralizing antibody titers in mice sera were tested by *in vitro* microneutralization assay using Vero E6 cell line and live SARS-CoV-2 **(E)**. The functional profiles of SARS-CoV-2 RBD-specific T-cell responses expressing in mouse splenocytes immunized with plant-produced SARS-CoV-2 RBD-Fc adjuvanted with alum were determined by mouse ELISpot assay **(F)**. Data presented as mean ± SD of the endpoint titers in each mice vaccination group ($n = 5$). *$p < 0.05$; **$p < 0.01$; ***$p < 0.001$; ****$p < 0.0001$.

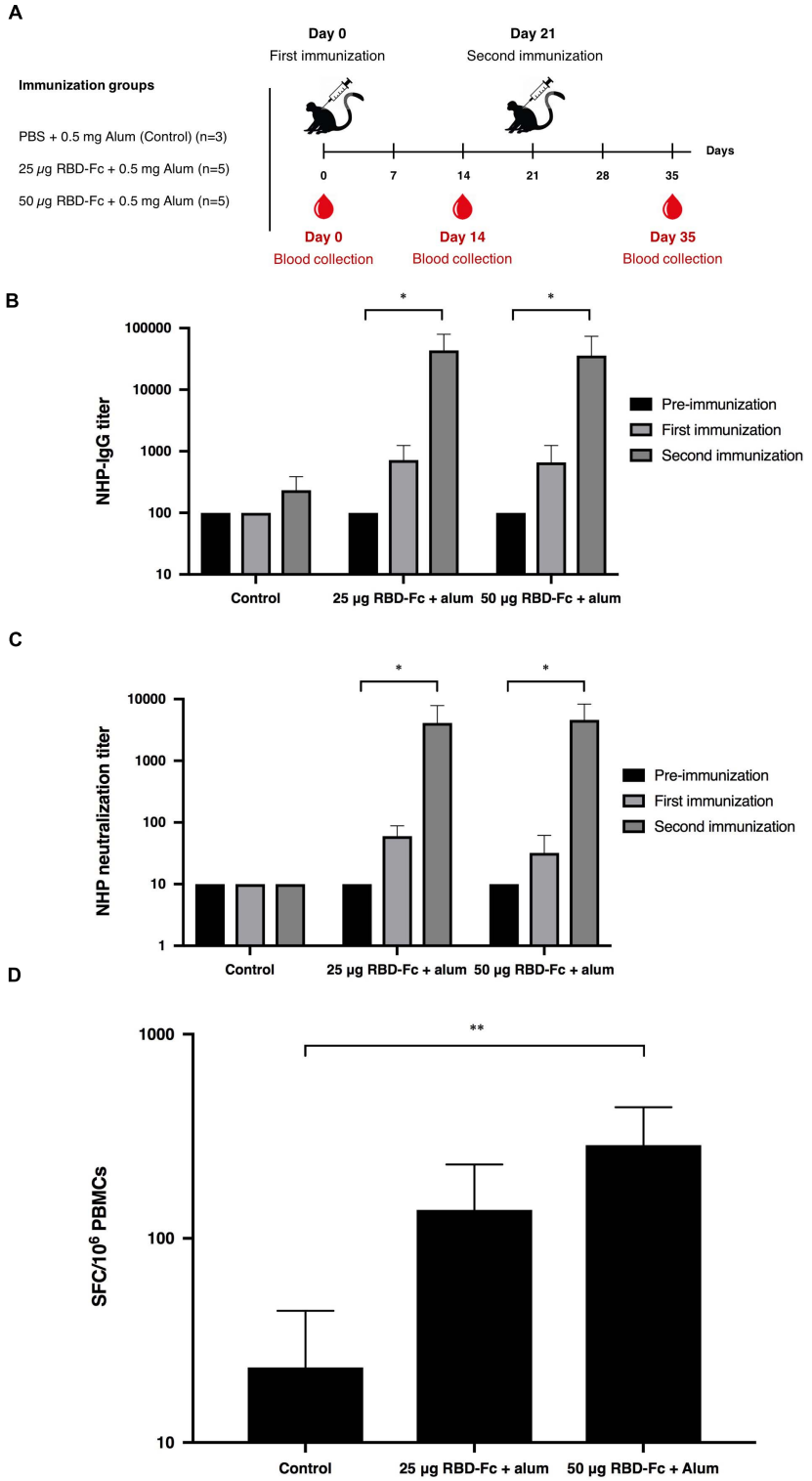

FIGURE 5 | Immunogenic studies in non-human primates (*Macaca fascicularis*). Experimental design of immunogenicity studies in non-human primates. Thirteen juvenile-adult non-human primates were separated into 3 groups; Control group was immunized with PBS adjuvanted by alum (n = 3) and two experimental groups were immunized with 25 and 50 μg SARS-CoV-2 RBD-Fc along with alum adjuvant (n = 5 per group). All non-human primates were intramuscularly injected either with PBS or plant-produced RBD-Fc for 3 weeks interval (on day 0 and 21). The sera were collected on day 0 and 14 after each boost **(A)**. Serum specific IgG response in non-human primates were determined by ELISA **(B)**. Virus neutralizing titer of RBD immunized non-human primate sera against live SARS-CoV-2 were evaluated **(C)**. The functional profiles of SARS-CoV-2 RBD-specific T-cell responses expressing in non-human primate peripheral blood mononuclear cells immunized with plant-produced RBD-Fc adjuvanted with alum on day 14 after second immunization **(D)**. *$p < 0.05$; **$p < 0.01$; ***$p < 0.001$; ****$p < 0.0001$.

recombinant proteins relatively in short time with much reduced cost. Hence in this study, we have demonstrated the rapid production of SARS-CoV-2 RBD-Fc fusion protein in *N. benthamiana* plants that could be used as a potential vaccine candidate for prevention of SARS-CoV-2 infection.

Significant efforts have been made by the scientific community across the world to develop the effective vaccine against SARS-CoV-2. Plant-derived vaccine candidates for other coronaviruses such as SARS and porcine epidemic diarrhea virus are shown to elicit potent immunogenic response in animal studies (Kang et al., 2005; Pogrebnyak et al., 2005). Earlier studies showed that full length S protein-based vaccine could cause liver damage or enhance virus infection. RBD-based vaccines formulated with alum was shown to elicit high level of protective immunity in animal experiments (He et al., 2006; Du et al., 2007; Jiang et al., 2012; Chen et al., 2017, 2020a,b). Hence based on the available data on the immunogenicity of SARS-CoV-2 proteins, we have chosen RBD for plant expression.

The presence of Fc domain in fusion protein offers favorable characteristics such as improving the expression and secretion of the recombinant proteins, improving protein solubility and stability (Huang, 2009; Czajkowsky et al., 2012; Yang et al., 2018). Moreover, Fc domain increases the serum half-life and prolongs therapeutic protein activities due to pH-dependent binding to the neonatal Fc receptor (FcRn) leading to prevention of protein degradation in endosomes as well as reduces renal clearance rate due to larger molecular weight of protein (Jazayeri and Carroll, 2008; Suzuki et al., 2010; Carter, 2011; Rath et al., 2015; Rosales-Mendoza et al., 2017; Yang et al., 2018). Fc region have been used as a fusion protein partner for several recombinant proteins such as receptors, ligands, enzymes, and soluble cytokines for therapeutic applications (Strohl and Knight, 2009; Li and Ravetch, 2011; Czajkowsky et al., 2012; Rattanapisit et al., 2019c; Liu et al., 2020). In addition to the mentioned advantages, Fc region is used as a tagged protein for facilitating the effective purification of recombinant protein by protein A chromatography that can provide high purity of SARS-CoV-2 RBD-Fc which can be visualized on the Coomassie-stained SDS-PAGE compared to crude extract sample as shown in previous studies (Rattanapisit et al., 2019c; Siriwattananon et al., 2021). Hence, we engineered SARS-CoV-2 RBD by fusing with Fc region of human IgG1 in order to use it as a subunit vaccine against SARS-CoV-2.

The SARS-CoV-2 RBD-Fc fusion protein was transiently expressed as a soluble protein in plants. The results showed that the expression of SARS-CoV-2 RBD-Fc was achieved rapidly within 4 days post infiltration with necrosis signal was observed on the infiltrated leaves (**Figure 2A**). The recombinant protein was purified from the plant crude extracts by affinity column chromatography and used for further studies.

The plant-produced SARS-CoV-2 RBD-Fc apparently showed effective binding activity with commercial ACE2 proteins produced from HEK293 and CHO cells (**Figure 3**). This data indicated that the SARS-CoV-2 RBD protein folded correctly in plants and produced authentic antigen. The immunogenicity of plant-produced SARS-CoV-2 RBD-Fc was tested in mice and cynomolgus monkeys using alum as an adjuvant. Alum stimulates the innate immunity, particularly presenting the antigen to major histocompatibility complex (MHC) class II, CD40 and CD86 or inducing the Th2 responses to mediate B-cell differentiation and elicit the antigen specific-IgG1 isotype (Marrack et al., 2009; Exley et al., 2010; Zhang et al., 2016). Furthermore, alum is having good safety profile and has been used as an adjuvant in several currently available licensed vaccines to enhance the immune response of the antigen (HogenEsch et al., 2018).

Mice administered with two doses of plant-derived SARS-CoV-2 RBD-Fc protein formulated with alum as adjuvant developed the neutralizing immune response (**Figure 4E**). The results confirmed the immunogenicity of plant-produced recombinant SARS-CoV-2 RBD protein. Mice immunized with RBD with alum showed the higher titer of neutralizing antibodies compared with the mice immunized with SARS-CoV-2 RBD alone. The analysis of the mouse specific-IgG subtypes suggested that plant-produced SARS-CoV-2 RBD induced a mixed Th1/Th2-specific immune responses. Further the efficacy of plant-produced SARS-CoV-2 RBD-Fc fusion protein was investigated in cynomolgus monkeys by administering the SARS-CoV-2 RBD-Fc with alum as adjuvant. The results confirmed that the plant-produced SARS-CoV-2 RBD-Fc could induce neutralizing antibodies in monkeys (**Figure 5C**). To accomplish the capability of plant-produced SARS-CoV-2 RBD-Fc in induction of cell-mediated immune responses, mouse splenocytes and monkey peripheral blood mononuclear cells were collected 14 days after second immunization (**Figures 4F**, **5D**). The IFN-γ-expressing T cells were analyzed by ELISPOT assay. Plant-produced SARS-CoV-2 RBD-Fc without alum induced SARS-CoV-2-specific T-cell responses, as evidenced by significant IFN-γ expression compared with the control (**Figure 4F**). Addition of alum adjuvant did not significantly increase the number of IFN-γ in the animals. These results suggested that plant-produced SARS-CoV-2 RBD-Fc itself could induce T-cell responses.

These results clearly showed that the plant-expressed SARS-CoV-2 RBD-Fc fusion protein maintains their authentic structure and retains its antigenicity. Our results are consistent with those of previous studies which showed that the vaccine antigens expressed in *N. benthamiana* elicited potent immune responses in animal experiments (Zheng et al., 2009; He et al., 2014). In consistent with earlier reports on the immunogenicity of RBD of SARS-CoV, our study showed that neutralizing antibodies induced by plant produced RBD of SARS-CoV-2 suppress SARS-CoV-2 infection *in vitro* (Bisht et al., 2005; Kapadia et al., 2005; Du et al., 2010). Our data showed the potential of plant-produced subunit vaccine candidate as the effective SARS-CoV-2 vaccine.

CONCLUSION

In conclusion, our study demonstrated that it was feasible to produce SARS-CoV-2 RBD protein in *N. benthamiana* plants by transient expression system. Further plant-produced recombinant protein was shown to be immunogenic in mice and non-human primates. The vaccine elicited both humoral

and cell mediated immune responses suggesting the potential of plant- produced RBD as the effective vaccine against SARS-CoV-2. To our knowledge, this is the first report demonstrating the immunogenicity of plant-produced SARS-CoV-2 RBD protein in mice and non-human primates. Collectively this proof of concept study demonstrated that the plant-produced SARS-CoV-2 proteins could possibly be further developed as candidate vaccines for early stage clinical development.

DATA AVAILABILITY STATEMENT

The original contributions presented in the study are included in the article/**Supplementary Material**, further inquiries can be directed to the corresponding author/s.

ETHICS STATEMENT

The animal study was reviewed and approved by the Institutional Animal Care and Use Committee, Faculty of Medicine and the National Primate Research Center of Thailand-Chulalongkorn University (NPRCT-CU) Animal Care and Use Committee, Chulalongkorn University, Bangkok, Thailand.

AUTHOR CONTRIBUTIONS

KiR, AT, and WP designed all experiments. KS, BS, and KaR performed protein expression, protein purification, ELISA, and protein preparation for animal experiments. KS, SMan, SP, SS, ST, EP, CK, SB, WW, KT, and PK performed vaccination and immunogenic studies in mice. KS, SMan, SP, SS, ST, SB, WW, TK, NS, and SMal performed vaccination and immunogenic studies in non-human primates. KL performed LC-MS analysis. All authors analyzed the data and contributed to manuscript preparation.

FUNDING

This research was funded by Baiya Phytopharm Co., Ltd. and TSRI Fund to SM and WP (CU_FRB640001_01_33_2). The authors declare that Baiya Phytopharm Co., Ltd. was not involved in the study design, collection, analysis, interpretation of data, the writing of this article or the decision to submit it for publication.

ACKNOWLEDGMENTS

We would like to thank the Department of Disease Control, Ministry of Public Health, Thailand for providing clinical specimens for the viral isolate and sera from a COVID-19 survivor. We would like to thank the 100th anniversary Chulalongkorn University (KS) for doctoral scholarship.

SUPPLEMENTARY MATERIAL

The Supplementary Material for this article can be found online at: https://www.frontiersin.org/articles/10.3389/fpls.2021.682953/full#supplementary-material

REFERENCES

Ahmad, A. R., Kaewpungsup, P., Khorattanakulchai, N., Rattanapisit, K., Pavasant, P., and Phoolcharoen, W. (2019). Recombinant human dentin matrix protein 1 (hDMP1) expressed in *Nicotiana benthamiana* potentially induces osteogenic differentiation. *Plants* 8:566. doi: 10.3390/plants8120566

Amanat, F., and Krammer, F. (2020). SARS-CoV-2 vaccines: status report. *Immunity* 52, 583–589. doi: 10.1016/j.immuni.2020.03.007

Banerjee, A., Kulcsar, K., Misra, V., Frieman, M., and Mossman, K. (2019). Bats and Coronaviruses. *Viruses* 11:41. doi: 10.3390/v11010041

Basaran, P., and Rodríguez-Cerezo, E. (2008). Plant molecular farming: opportunities and challenges. *Crit. Rev. Biotechnol.* 28, 153–172. doi: 10.1080/07388550802046624

Bellucci, M., Marchis, F. D., and Pompa, A. (2017). The endoplasmic reticulum is a hub to sort proteins toward unconventional traffic pathways and endosymbiotic organelles. *J. Exp. Bot.* 69, 7–20. doi: 10.1093/jxb/erx286

Bisht, H., Roberts, A., Vogel, L., Subbarao, K., and Moss, B. (2005). Neutralizing antibody and protective immunity to SARS coronavirus infection of mice induced by a soluble recombinant polypeptide containing an N-terminal segment of the spike glycoprotein. *Virology* 334, 160–165. doi: 10.1016/j.virol.2005.01.042

Bosch, B. J., Zee, R. V. D., Haan, C. A. M. D., and Rottier, P. J. M. (2003). The coronavirus spike protein is a class I virus fusion protein: structural and functional characterization of the fusion core complex. *J. Virol.* 77, 8801–8811. doi: 10.1128/JVI.77.16.8801-8811.2003

Burnett, M. J. B., and Burnett, A. C. (2019). Therapeutic recombinant protein production in plants: Challenges and opportunities. *Plants People Planet* 2, 121–132. doi: 10.1002/ppp3.10073

Carter, P. J. (2011). Introduction to current and future protein therapeutics: a protein engineering perspective. *Exp. Cell Res.* 317, 1261–1269. doi: 10.1016/j.yexcr.2011.02.013

Chen, Q., He, J., Phoolcharoen, W., and Mason, H. S. (2011). Geminiviral vectors based on bean yellow dwarf virus for production of vaccine antigens and monoclonal antibodies in plants. *Hum. Vaccin.* 7, 331–338. doi: 10.4161/hv.7.3.14262

Chen, W.-H., Chag, S. M., Poongavanam, M. V., Biter, A. B., Ewere, E. A., Rezende, W., et al. (2017). Optimization of the production process and characterization of the yeast-expressed SARS-CoV recombinant receptor-binding domain (RBD219-N1), a SARS vaccine candidate. *J. Pharm. Sci.* 106, 1961–1970. doi: 10.1016/j.xphs.2017.04.037

Chen, W.-H., Strych, U., Hotez, P. J., and Bottazzi, M. E. (2020a). The SARS-CoV-2 vaccine pipeline: an overview. *Curr. Trop. Med. Rep.* 3, 1–4. doi: 10.1007/s40475-020-00201-6

Chen, W.-H., Tao, X., Agrawal, A., Algaissi, A., Peng, B.-H., Pollet, J., et al. (2020b). Yeast-expressed SARS-CoV recombinant receptor-binding domain (RBD219-N1) formulated with alum induces protective immunity and reduces immune enhancement. *bioRxiv* [preprint] doi: 10.1101/2020.05.15.098079

Czajkowsky, D. M., Hu, J., Shao, Z., and Pleass, R. J. (2012). Fc-fusion proteins: new developments and future perspectives. *EMBO Mol. Med.* 4, 1015–1028. doi: 10.1002/emmm.201201379

D'Aoust, M.-A., Couture, M. M.-J., Charland, N., Trépanier, S., Landry, N., Ors, F., et al. (2010). The production of hemagglutinin-based virus-like particles in plants: a rapid, efficient and safe response to pandemic influenza. *Plant Biotechnol. J.* 8, 607–619. doi: 10.1111/j.1467-7652.2009.00496.x

D'Aoust, M.-A., Lavoie, P.-O., Couture, M. M.-J., Trépanier, S., Guay, J.-M., Dargis, M., et al. (2008). Influenza virus-like particles produced by transient expression

in *Nicotiana benthamiana* induce a protective immune response against a lethal viral challenge in mice. *Plant Biotechnol. J.* 6, 930–940. doi: 10.1111/j.1467-7652.2008.00384.x

Daniell, H., Jin, S., Zhu, X. G., Matthew, A., Gitzendanner, Soltis, D. E., et al. (2021). Green giant—a tiny chloroplast genome with mighty power to produce high−value proteins: history and phylogeny. *Plant Biotechnol. J.* 19, 430–447. doi: 10.1111/pbi.13556

Diamos, A. G., and Mason, H. S. (2018). High-level expression and enrichment of norovirus virus-like particles in T plants using modified geminiviral vectors. *Protein Expr. Purif.* 151, 86–92. doi: 10.1016/j.pep.2018.06.011

Diego-Martin, B., González, B., Vazquez-Vilar, M., Selma, S., Mateos-Fernández, R., Gianoglio, S., et al. (2020). Pilot production of SARS-CoV-2 related proteins in plants: a proof of concept for rapid repurposing of indoor farms into biomanufacturing facilities. *Front. Plant Sci.* 11:612781. doi: 10.3389/fpls.2020.612781

Donini, M., and Marusic, C. (2019). Current state-of-the-art in plant-based antibody production systems. *Biotechnol. Lett.* 41, 335–346. doi: 10.1007/s10529-019-02651-z

Du, L., Zhao, G., Chan, C. C., Li, L., He, Y., Zhou, Y., et al. (2010). A 219-mer CHO-expressing receptor-binding domain of SARS-CoV S protein induces potent immune responses and protective immunity. *Viral. Immunol.* 23, 211–219. doi: 10.1089/vim.2009.0090

Du, L., Zhao, G., He, Y., Guo, Y., Zheng, B.-J., Jiang, S., et al. (2007). Receptor-binding domain of SARS-CoV spike protein induces long-term protective immunity in an animal model. *Vaccine* 25, 2832–2838. doi: 10.1016/j.vaccine.2006.10.031

Exley, C., Siesjö, P., and Eriksson, H. (2010). The immunobiology of aluminium adjuvants: how do they really work? *Trends Immunol.* 31, 103–109. doi: 10.1016/j.it.2009.12.009

Fox, J. L. (2012). First plant-made biologic approved. *Nat. Biotechnol.* 30:472. doi: 10.1038/nbt0612-472

Frey, A., Canzio, J. D., and Zurakowski, D. (1998). A statistically defined endpoint titer determination method for immunoassays. *J. Immunol. Methods* 221, 35–41. doi: 10.1016/s0022-1759(98)00170-7

Fuenmayor, J., Gòdia, F., and Cervera, L. (2017). Production of virus-like particles for vaccines. *N. Biotechnol.* 39, 174–180. doi: 10.1016/j.nbt.2017.07.010

Gleba, Y., Klimyuk, V., and Marillonnet, S. (2005). Magnifection–a new platform for expressing recombinant vaccines in plants. *Vaccine* 23, 2042–2048. doi: 10.1016/j.vaccine.2005.01.006

Gomes, A. R., Munivenkatappa, S., Belamaranahally, B., Veeregowda, M., and Balamurugan, V. (2016). An overview of heterologous expression host systems for the production of recombinant proteins. *Adv. Anim. Vet. Sci.* 4, 346–356. doi: 10.14737/journal.aavs/2016/4.7.346.356

Prevail Ii Writing Group, Multi-National Prevail Ii Study Team, Davey, R. T. Jr., Dodd, L., Proschan, M. A., Neaton, J., et al. (2016). A randomized, controlled trial of ZMapp for ebola virus infection. *N. EngI. J. Med.* 375, 1448–1456. doi: 10.1056/nejmoa1604330

He, J., Peng, L., Lai, H., Hurtado, J., Stahnke, J., and Chen, Q. (2014). A plant-produced antigen elicits potent immune responses against West Nile virus in mice. *Biomed. Res. Int.* 2014:952865. doi: 10.1155/2014/952865

He, Y., Li, J., Li, W., Lustigman, S., Farzan, M., and Jiang, S. (2006). Cross-neutralization of human and palm civet severe acute respiratory syndrome coronaviruses by antibodies targeting the receptor-binding domain of spike protein. *J. Immunol.* 176, 6085–6092. doi: 10.4049/jimmunol.176.10.6085

He, Y., Lu, H., Siddiqui, P., Zhou, Y., and Jiang, S. (2005a). Receptor-binding domain of severe acute respiratory syndrome coronavirus spike protein contains multiple conformation-dependent epitopes that induce highly potent neutralizing antibodies. *J. Immunol.* 174, 4908–4915. doi: 10.4049/jimmunol.174.8.4908

He, Y., Zhou, Y., Siddiqui, P., and Jianga, S. (2004). Inactivated SARS-CoV vaccine elicits high titers of spike protein-specific antibodies that block receptor binding and virus entry. *Biochem. Biophys. Res. Commun.* 325, 445–454. doi: 10.1016/j.bbrc.2004.10.052

He, Y., Zhu, Q., Liu, S., Zhou, Y., Yang, B., Li, J., et al. (2005b). Identification of a critical neutralization determinant of severe acute respiratory syndrome (SARS)-associated coronavirus: importance for designing SARS vaccines. *Virology* 334, 74–82. doi: 10.1016/j.virol.2005.01.034

Hendin, H. E., Pillet, S., Lara, A. N., Wu, C.-Y., Charland, N., Landry, N., et al. (2017). Plant-made virus-like particle vaccines bearing the hemagglutinin of either seasonal (H1) or avian (H5) influenza have distinct patterns of interaction with human immune cells *in vitro*. *Vaccine* 35, 2592–2599. doi: 10.1016/j.vaccine.2017.03.058

HogenEsch, H., O'Hagan, D. T., and Fox, C. B. (2018). Optimizing the utilization of aluminum adjuvants in vaccines: you might just get what you want. *NPJ Vaccines* 3:51. doi: 10.1038/s41541-018-0089-x

Huang, C. (2009). Receptor-Fc fusion therapeutics, traps, and MIMETIBODY technology. *Curr. Opin. Biotechnol.* 20, 692–699. doi: 10.1016/j.copbio.2009.10.010

Iyappan, G., Shanmugaraj, B. M., Inchakalody, V., Ma, J. K. C., and Ramalingam, S. (2018). Potential of plant biologics to tackle the epidemic like situations - case studies involving viral and bacterial candidates. *Int. J. Infect. Dis.* 73:363. doi: 10.1016/j.ijid.2018.04.4236

Jazayeri, J. A., and Carroll, G. J. (2008). Fc-based cytokines: prospects for engineering superior therapeutics. *Biodrugs* 22, 11–26. doi: 10.2165/00063030-200822010-00002

Jiang, S., Bottazzi, M. E., Du, L., Lustigman, S., Tseng, C.-T. K., Curti, E., et al. (2012). Roadmap to developing a recombinant coronavirus S protein receptor-binding domain vaccine for severe acute respiratory syndrome. *Exp. Rev. Vacc.* 11, 1405–1413. doi: 10.1586/erv.12.126

Kang, T.-J., Kim, Y.-S., Jang, Y.-S., and Yang, M.-S. (2005). Expression of the synthetic neutralizing epitope gene of porcine epidemic diarrhea virus in tobacco plants without nicotine. *Vaccine* 23, 2294–2297. doi: 10.1016/j.vaccine.2005.01.027

Kapadia, S. U., Rose, J. K., Lamirande, E., Vogel, L., Subbarao, K., and Robertsc, A. (2005). Long-term protection from SARS coronavirus infection conferred by a single immunization with an attenuated VSV-based vaccine. *Virology* 340, 174–182. doi: 10.1016/j.virol.2005.06.016

Kaur, J., Kumar, A., and Kaur, J. (2018). Strategies for optimization of heterologous protein expression in *E. coli*: roadblocks and reinforcements. *Int. J. Biol. Macromol.* 106, 803–822. doi: 10.1016/j.ijbiomac.2017.08.080

Kelley, B. (2009). Industrialization of mAb production technology: the bioprocessing industry at a crossroads. *MABS* 1, 443–452. doi: 10.4161/mabs.1.5.9448

Kizhner, T., Azulay, Y., Hainrichson, M., Tekoah, Y., Arvatz, G., Shulman, A., et al. (2015). Characterization of a chemically modified plant cell culture expressed human a-Galactosidase-A enzyme for treatment of Fabry disease. *Mol. Genet Metab.* 114, 259–267. doi: 10.1016/j.ymgme.2014.08.002

Kodati, B., Dorbha, S., and Kunaparaju, R. K. (2016). Heterologus protein expression in different host systems. *J. Chem. Pharm. Res.* 8, 1068–1074.

Krenek, P., Samajova, O., Luptovciak, I., Doskocilova, A., Komis, G., and Samaj, J. (2015). Transient plant transformation mediated by *Agrobacterium tumefaciens*: principles, methods and applications. *Biotechnol. Adv.* 33, 1024–1042. doi: 10.1016/j.biotechadv.2015.03.012

Lei, C., Qian, K., Li, T., Zhang, S., Fu, W., Ding, M., et al. (2020). Neutralization of SARS-CoV-2 spike pseudotyped virus by recombinant ACE2-Ig. *Nat. Commun.* 11:2070. doi: 10.1038/s41467-020-16048-4

Li, F. (2016). Structure, function, and evolution of coronavirus spike proteins. *Annu. Rev. Virol.* 3, 237–261. doi: 10.1146/annurev-virology-110615-042301

Li, F., and Ravetch, J. V. (2011). Inhibitory Fcγ receptor engagement drives adjuvant and anti-tumor activities of agonistic CD40 antibodies. *Science* 333, 1030–1034. doi: 10.1126/science.1206954

Li, H., Liu, S.-M., Yu, X.-H., Tang, S.-L., and Tang, C.-K. (2020). Coronavirus disease 2019 (COVID-19): current status and future perspectives. *Int. J. Antimicrob. Agents* 55:105951. doi: 10.1016/j.ijantimicag.2020.105951

Li, Q., Guan, X., Wu, P., Wang, X., Zhou, L., Tong, Y., et al. (2020). Early transmission dynamics in Wuhan, China, of novel coronavirus-infected pneumonia. *N. Engl. J. Med.* 382, 1199–1207. doi: 10.1056/NEJMoa2001316

Li, W., Moore, M. J., Vasilieva, N., Sui, J., Wong, S. K., Berne, M. A., et al. (2003). Angiotensin-converting enzyme 2 is a functional receptor for the SARS coronavirus. *Nature* 426, 450–454. doi: 10.1038/nature02145

Liu, Z., Xu, W., Xia, S., Gu, C., Wang, X., Wang, Q., et al. (2020). RBD-Fc-based COVID-19 vaccine candidate induces highly potent SARS-CoV-2 neutralizing antibody response. *Signal. Transduct. Target. Ther.* 5:282. doi: 10.4172/2167-1079.1000255

Ma, J. K.-C., Drake, P. M. W., and Christou, P. (2003). The production of recombinant pharmaceutical proteins in plants. *Nat. Rev. Genet.* 4, 794–805. doi: 10.1038/nrg1177

Ma, J. K.-C., Drossard, J., Lewis, D., Altmann, F., Boyle, J., Christou, P., et al. (2015). Regulatory approval and a first-in-human phase I clinical trial of a monoclonal antibody produced in transgenic tobacco plants. *Plant Biotechnol. J.* 13, 1106–1120. doi: 10.1111/pbi.12416

Malik, Y. S., Sircar, S., Bhat, S., Sharun, K., Dhama, K., Dadar, M., et al. (2020). Emerging novel coronavirus (2019-nCoV)—current scenario, evolutionary perspective based on genome analysis and recent developments. *Vet. Q.* 40, 68–76. doi: 10.1080/01652176.2020.1727993

Malla, A., Shanmugaraj, B., and Ramalingam, S. (2020). Severe Acute Respiratory Syndrome Coronavirus-2 (SARS-CoV-2): An Emerging Zoonotic Respiratory Pathogen in Humans. *J. Pure. Appl. Microbiol.* 14, 931–936. doi: 10.22207/JPAM.14.SPL1.30

Marrack, P., McKee, A. S., and Munks, M. W. (2009). Towards an understanding of the adjuvant action of aluminium. *Nat. Rev. Immunol.* 9, 287–293. doi: 10.1038/nri2510

Miao, Y., Ding, Y., Sun, Q.-Y., Xu, Z.-F., and Jiang, L. (2008). Plant bioreactors for pharmaceuticals. *Biotechnol. Genet. Eng. Rev.* 25, 363–380. doi: 10.5661/bger-25-363

Mor, T. S. (2015). Molecular pharming's foot in the FDA's door: protalix's trailblazing story. *Biotechnol. Lett.* 37, 2147–2150. doi: 10.1007/s10529-015-1908-z

Paul, M., and Ma, J. K. C. (2011). Plant−made pharmaceuticals: leading products and production platforms. *Biotechnol. Appl. Biochem.* 58, 58–67. doi: 10.1002/bab.6

Phoolcharoen, W., Bhoo, S. H., Lai, H., Ma, J., Arntzen, C. J., Chen, Q., et al. (2011). Expression of an immunogenic Ebola immune complex in *Nicotiana benthamiana*. *Plant Biotechnol. J.* 9, 807–816. doi: 10.1111/j.1467-7652.2011.00593.x

Pillet, S., Aubin, É, Trépanier, S., Bussière, D., Dargis, M., Poulin, J.-F., et al. (2016). A plant- derived quadrivalent virus like particle influenza vaccine induces cross-reactive antibody and T cell response in healthy adults. *Clin. Immunol.* 168, 72–87. doi: 10.1016/j.clim.2016.03.008

Pogrebnyak, N., Golovkin, M., Andrianov, V., Spitsin, S., Smirnov, Y., Egolf, R., et al. (2005). Severe acute respiratory syndrome (SARS) S protein production in plants: development of recombinant vaccine. *Proc. Natl. Acad. Sci. U. S. A.* 102, 9062–9067. doi: 10.1073/pnas.0503760102

Quinlan, B. D., Mou, H., Zhang, L., Guo, Y., He, W., Ojha, A., et al. (2020). The SARS-CoV-2 receptor-binding domain elicits a potent neutralizing response without antibody-dependent enhancement. *bioRxiv* [preprint] doi: 10.1101/2020.04.10.036418

Rabi, F. A., Zoubi, M. S. A., Kasasbeh, G. A., Salameh, D. M., and Al-Nasser, A. D. (2020). SARS-CoV-2 and coronavirus disease 2019: what we know so far. *Pathogens* 9:231. doi: 10.3390/pathogens9030231

Rath, T., Baker, K., Dumont, J. A., Peters, R. T., Jiang, H., Qiao, S.-W., et al. (2015). Fc-fusion proteins and FcRn: structural insights for longer-lasting and more effective therapeutics. *Crit. Rev. Biotechnol.* 35, 235–254. doi: 10.3109/07388551.2013.834293

Rattanapisit, K., Chao, Z., Siriwattananon, K., Huang, Z., and Phoolcharoen, W. (2019a). Plant-produced anti-enterovirus 71 (EV71) monoclonal antibody efficiently protects mice against EV71 infection. *Plants* 8:12. doi: 10.3390/plants8120560

Rattanapisit, K., Phakham, T., Buranapraditkun, S., Siriwattananon, K., Boonkrai, C., Pisitkun, T., et al. (2019b). Structural and *in vitro* functional analyses of novel plant-produced anti-Human PD1 antibody. *Sci. Rep.* 9:15205. doi: 10.1038/s41598-019-51656-1

Rattanapisit, K., Shanmugaraj, B., Manopwisedjaroen, S., Purwono, P. B., Siriwattananon, K., Khorattanakulchai, N., et al. (2020). Rapid and scalable production of functional anti-coronavirus monoclonal antibody CR3022 in plants. *Sci. Rep.* 10:17698. doi: 10.21203/rs.3.rs-27160/v1

Rattanapisit, K., Srifa, S., Kaewpungsup, P., Pavasant, P., and Phoolcharoen, W. (2019c). Plant-produced recombinant Osteopontin-Fc fusion protein enhanced osteogenesis. *Biotechnol. Rep.* 21:e00312. doi: 10.1016/j.btre.2019.e00312

Rattanapisit, K., Yusakul, G., Shanmugaraj, B., Kittirotruji, K., Suwatsrisakul, P., Prompetchara, E., et al. (2021). Plant-produced recombinant SARS-CoV-2 receptor-binding domain; an economical, scalable biomaterial source for COVID-19 diagnosis. *Biomater. Transl.* 2, 43–49. doi: 10.3877/cma.j.issn.2096-112X.2021.01.006

Rosales-Mendoza, S., Nieto-Gómez, R., and Angulo, C. (2017). A perspective on the development of plant-made vaccines in the fight against Ebola virus. *Front. Immunol.* 8:252. doi: 10.3389/fimmu.2017.00252

Rybicki, E. P. (2009). Third international conference on plant-based vaccines and antibodies. *Expert. Rev. Vacc.* 8, 1151–1155. doi: 10.1586/erv.09.85

Masters, S. P. (2006). The molecular biology of coronaviruses. *Adv. Virus Res.* 66, 193–292. doi: 10.1016/s0065-3527(06)66005-3

Shahid, N., and Daniell, H. (2016). Plant-based oral vaccines against zoonotic and non-zoonotic diseases. *Plant Biotechnol. J.* 14, 2079–2099. doi: 10.1111/pbi.12604

Shanmugaraj, B., Bulaon, C. J. I., and Phoolcharoen, W. (2020a). Plant molecular farming: A viable platform for recombinant biopharmaceutical production. *Plants* 9:842. doi: 10.3390/plants9070842

Shanmugaraj, B., and Phoolcharoen, W. (2021). Addressing demand for recombinant biopharmaceuticals in the COVID-19 era. *Asian Pac. J. Trop. Med.* 14, 49–51.

Shanmugaraj, B., Rattanapisit, K., Manopwisedjaroen, S., Thitithanyanont, A., and Phoolcharoen, W. (2020b). Monoclonal antibodies B38 and H4 produced in *Nicotiana benthamiana* neutralize SARS-CoV-2 *in vitro*. *Front. Plant Sci.* 11:589995. doi: 10.3389/fpls.2020.589995

Shanmugaraj, B., Siriwattananon, K., Wangkanont, K., and Phoolcharoen, W. (2020c). Perspectives on monoclonal antibody therapy as potential therapeutic intervention for Coronavirus disease-19 (COVID-19). *Asian Pac. J. Allergy Immunol.* 38, 10–18. doi: 10.12932/ap-200220-0773

She, J., Jiang, J., Ye, L., Hu, L., Bai, C., and Song, Y. (2020). 2019 novel coronavirus of pneumonia in Wuhan, China: emerging attack and management strategies. *Clin. Transl. Med.* 9:19. doi: 10.1186/s40169-020-00271-z

Singhal, T. (2020). A review of coronavirus disease-2019 (COVID-19). *Indian J. Pediatr.* 87, 281–286. doi: 10.1007/s12098-020-03263-6

Siriwattananon, K., Manopwisedjaroen, S., Kanjanasirirat, P., Purwono, P. B., Rattanapisit, K., Shanmugaraj, B., et al. (2021). Development of plant-produced recombinant ACE2-Fc fusion protein as a potential therapeutic agent against SARS-CoV-2. *Front. Plant Sci.* 11:604663. doi: 10.3389/fpls.2020.604663

Smith, T. R. F., Patel, A., Ramos, S., Elwood, D., Zhu, X., Yan, J., et al. (2020). Immunogenicity of a DNA vaccine candidate for COVID-19. *Nat. Commun.* 11:2601. doi: 10.1038/s41467-020-16505-0

Strohl, W. R., and Knight, D. M. (2009). Discovery and development of biopharmaceuticals: current issues. *Curr. Opin. Biotechnol.* 20, 668–672. doi: 10.1016/j.copbio.2009.10.012

Sun, X., Wang, T., Cai, D., Hu, Z., Chen, J. A., Liao, H., et al. (2020). Cytokine storm intervention in the early stages of COVID-19 pneumonia. *Cytokine Growth Factor Rev.* 53, 38–42. doi: 10.1016/j.cytogfr.2020.04.002

Suzuki, T., Ishii-Watabe, A., Tada, M., Kobayashi, T., Kanayasu-Toyoda, T., Kawanishi, T., et al. (2010). Importance of neonatal FcR in regulating the serum half-life of therapeutic proteins containing the Fc domain of human IgG1: a comparative study of the affinity of monoclonal antibodies and Fc-fusion proteins to human neonatal FcR. *J. Immunol.* 184, 1968–1976. doi: 10.4049/jimmunol.0903296

Vézina, L.-P., Faye, L., Lerouge, P., D'Aoust, M.-A., Marquet-Blouin, E., Burel, C., et al. (2009). Transient co-expression for fast and high-yield production of antibodies with human-like N-glycans in plants. *Plant Biotechnol. J.* 7, 442–455. doi: 10.1111/j.1467-7652.2009.00414.x

Vitale, A., and Denecke, J. R. (1999). The endoplasmic reticulum-gateway of the secretory pathway. *Plant Cell* 11, 615–628. doi: 10.1105/tpc.11.4.615

Walls, A. C., Xiong, X., Park, Y.-J., Tortorici, M. A., Snijder, J., Quispe, J., et al. (2019). Unexpected receptor functional mimicry elucidates activation of coronavirus fusion. *Cell* 176, 1026–1039. doi: 10.1016/j.cell.2018.12.028

Wang, L., Shi, W., Chappell, J. D., Joyce, M. G., Zhang, Y., Kanekiyo, M., et al. (2018). Importance of neutralizing monoclonal antibodies targeting multiple antigenic sites on the middle east respiratory syndrome coronavirus spike glycoprotein to avoid neutralization escape. *J. Virol.* 92:10. doi: 10.1128/jvi.02002-17

Ward, B. J., Gobeil, P., Séguin, A., Atkins, J., Boulay, I., Charbonneau, P.-Y., et al. (2020). Phase 1 trial of a candidate recombinant virus-like particle vaccine for COVID-19 disease produced in plants. *medRxiv* [preprint] doi: 10.1101/2020.11.04.20226282

Ward, B. J., Séguin, A., Couillard, J., Trépanier, S., and Landry, N. (2021). Phase III: Randomized observer-blind trial to evaluate lot-to-lot consistency of a new plant-derived quadrivalent virus like particle influenza vaccine in adults 18-49 years of age. *Vaccine* 39, 1528–1533. doi: 10.1016/j.vaccine.2021.01.004

World Health Organization (2021). *Weekly epidemiological update - 6 March 2021* [Online]. Availableonline at: : https://www.who.int/publications/m/item/weekly-epidemiological-update-on-covid-19---6-april-2021 [accessed on Apr 11, 2021]

Xie, P., Ma, W., Tang, H., and Liu, D. (2020). Severe COVID-19: a review of recent progress with a look toward the future. *Front. Publ. Health* 8:189. doi: 10.3389/fpubh.2020.00189

Yang, C., Gao, X., and Gong, R. (2018). Engineering of Fc fragments with optimized physicochemical properties implying improvement of clinical potentials for Fc-based therapeutics. *Front. Immunol.* 8:1860. doi: 10.3389/fimmu.2017.01860

Yao, J., Weng, Y., Dickey, A., and Wang, K. Y. (2015). Plants as factories for human pharmaceuticals: applications and challenges. *Int. J. Mol. Sci.* 16, 28549–28565. doi: 10.3390/ijms161226122

Yuan, Y., Cao, D., Zhang, Y., Ma, J., Qi, J., Wang, Q., et al. (2017). Cryo-EM structures of MERS-CoV and SARS-CoV spike glycoproteins reveal the dynamic receptor binding domains. *Nat. Commun.* 8:15092. doi: 10.1038/ncomms15092

Yuki, K., Fujiogi, M., and Koutsogiannaki, S. (2020). COVID-19 pathophysiology: a review. *Clin. Immunol.* 215:108427. doi: 10.1016/j.clim.2020.108427

Yuki, Y., Mejima, M., Kurokawa, S., Hiroiwa, T., Takahashi, Y., Tokuhara, D., et al. (2013). Induction of toxin-specific neutralizing immunity by molecularly uniform rice-based oral cholera toxin B subunit vaccine without plant-associated sugar modification. *Plant Biotechnol. J.* 11, 799–808.

Zhang, N., Channappanavar, R., Ma, C., Wang, L., Tang, J., Garron, T., et al. (2016). Identification of an ideal adjuvant for receptor-binding domain-based subunit vaccines against Middle East respiratory syndrome coronavirus. *Cell. Mol. Immunol.* 13, 180–190. doi: 10.1038/cmi.2015.03

Zheng, N., Xia, R., Yang, C., Yin, B., Li, Y., Duan, C., et al. (2009). Boosted expression of the SARS-CoV nucleocapsid protein in tobacco and its immunogenicity in mice. *Vaccine* 27, 5001–5007. doi: 10.1016/j.vaccine.2009.05.073

Zhou, P., Yang, X.-L., Wang, X.-G., Hu, B., Zhang, L., Zhang, W., et al. (2020). Discovery of a novel coronavirus associated with the recent pneumonia outbreak in humans and its potential bat origin. *Nature* 579, 270–273. doi: 10.1038/s41586-020-2012-7

Zhu, X., Liu, Q., Du, L., Lu, L., and Jiang, S. (2013). Receptor-binding domain as a target for developing SARS vaccines. *J. Thorac. Dis.* 5, 142–148. doi: 10.3978/j.issn.2072-1439.2013.06.06

Conflict of Interest: WP from Chulalongkorn University is a founder/shareholder of Baiya Phytopharm Co., Ltd. BS and KR are employed by Baiya Phytopharm Co., Ltd., Thailand. WW is employed by BioNet-Asia Co., Ltd., Thailand.

The remaining authors declare that the research was conducted in the absence of any commercial or financial relationships that could be construed as a potential conflict of interest.

frontiers in Plant Science

ORIGINAL RESEARCH
published: 28 May 2021
doi: 10.3389/fpls.2021.686421

A V_HH-Fc Fusion Targeted to the Chloroplast Thylakoid Lumen Assembles and Neutralizes Enterohemorrhagic *E. coli* O157:H7

Adam Chin-Fatt[1,2] *and Rima Menassa*[1,2]*

[1] Agriculture and Agri-Food Canada, London Research and Development Centre, London, ON, Canada, [2] Department of Biology, University of Western Ontario, London, ON, Canada

Chimeric fusion proteins comprising a single domain antibody (V_HH) fused to a crystallizable fragment (Fc) of an immunoglobulin are modular glycoproteins that are becoming increasingly in demand because of their value as diagnostics, research reagents and passive immunization therapeutics. Because ER-associated degradation and misfolding may potentially be limiting factors in the oxidative folding of V_HH-Fc fusion proteins in the ER, we sought to explore oxidative folding in an alternative sub-compartment, the chloroplast thylakoid lumen, and determine its viability in a molecular farming context. We developed a set of in-house expression vectors for transient transformation of *Nicotiana benthamiana* leaves that target a V_HH-Fc to the thylakoid lumen via either secretory (Sec) or twin-arginine translocation (Tat) import pathways. Compared to stromal [6.63 ± 3.41 mg/kg fresh weight (FW)], cytoplasmic (undetectable) and Tat-import pathways (5.43 ± 2.41 mg/kg FW), the Sec-targeted V_HH-Fc showed superior accumulation (30.56 ± 5.19 mg/kg FW), but was less than that of the ER (51.16 ± 9.11 mg/kg FW). Additionally, the introduction of a rationally designed *de novo* disulfide bond enhances *in planta* accumulation when introduced into the Sec-targeted Fc fusion protein from 50.24 ± 4.08 mg/kg FW to 110.90 ± 6.46 mg/kg FW. *In vitro* immunofluorescent labeling assays on V_HH-Fc purified from Sec, Tat, and stromal pathways demonstrate that the antibody still retains V_HH functionality in binding Escherichia *coli* O157:H7 and neutralizing its intimate adherence to human epithelial type 2 cells. These results overall provide a proof of concept that the oxidative folding environment of the thylakoid lumen may be a viable compartment for stably folding disulfide-containing recombinant V_HH-Fc proteins.

Keywords: enterohemorrhagic *E. coli*-EHEC, IgA, single domain antibody, V_HH, Fc fusion, Fc engineering, thylakoid, chloroplast

OPEN ACCESS

Edited by:
Inga Isabel Hitzeroth, University of Cape Town, South Africa

Reviewed by:
Silvana Petruccelli, National University of La Plata, Argentina
Naomichi Fujiuchi, Ehime University, Japan

***Correspondence:**
Rima Menassa
rima.menassa@canada.ca

Specialty section:
This article was submitted to Plant Biotechnology, a section of the journal Frontiers in Plant Science

Received: *26 March 2021*
Accepted: *26 April 2021*
Published: *28 May 2021*

Citation:
Chin-Fatt A and Menassa R (2021) A V_HH-Fc Fusion Targeted to the Chloroplast Thylakoid Lumen Assembles and Neutralizes Enterohemorrhagic E. coli O157:H7. Front. Plant Sci. 12:686421. doi: 10.3389/fpls.2021.686421

INTRODUCTION

Chimeric fusion proteins comprising a single domain antibody (V_HH) fused to a crystallizable fragment (Fc) of an immunoglobulin A (IgA) are modular glycoproteins that are becoming increasingly in demand because of their potential value as passive enteromucosal immunization therapeutics (Harmsen and De Haard, 2007). Structurally, they differ from the native IgA monomer

in that the antigen binding fragment (Fab) has been replaced by a camelid-derived V_HH that is smaller (∼15 kDa), more stable and does not require multi-chain assembly as is the case for Fab heavy and light chains (De Meyer et al., 2014). We have previously produced a V_HH-Fc in *Nicotiana benthamiana* leaf tissue by targeting it to the endoplasmic reticulum (ER) for folding and demonstrated its functionality *in vitro* in binding and neutralizing four serotypes of enterohemorrhagic Escherichia *coli* (EHEC), including O157:H7, the most prevalent serotype in North America (Saberianfar et al., 2019; Chin-Fatt et al., 2021). The national food surveillance programs for foodborne pathogens in the United States and Canada, FoodNet and FoodNet Canada, respectively, reported that the average incidence rate for O157:H7 was most recently estimated at 0.8 per 100,000 persons in the United States (CDC, 2020) and 1.52 per 100,000 persons in Canada (PHAC, 2019). Because the bovine terminal rectum is the primary reservoir of the pathogen, an appealing pre-harvest intervention strategy has been to encapsulate IgA in plant material as part of a feed formulation intended for enteromucosal passive immunization. Seeds of *Arabidopsis thaliana* encapsulating a V_HH-Fc secretory complex have been demonstrated to be effective in passively immunizing weaned piglets against a related *E. coli* strain, enterotoxigenic *E. coli*, and in reducing bacterial shedding to beneath detection levels after 4 days (Virdi et al., 2013). Over the past 20 years, plants have become a platform of choice for producing IgA antibodies and related synthetics in part because of the requirement of disulfide bond formation for proper folding and assembly (Vasilev et al., 2016). In plant cells, the oxidative folding of native proteins with disulfide bonds is localized either in the ER, the mitochondrial intermembrane space or the chloroplast thylakoid lumen (Onda, 2013).

Chloroplasts are structurally complex organelles that consist of a double membrane enclosing a soluble stromal phase (Kirchhoff, 2019). Within the stroma, an independent membrane system known as the thylakoid is embedded with the chlorophyll-containing photosystems responsible for photosynthesis and further encloses an additional luminal phase (Pottosin and Shabala, 2016; Johnson and Wientjes, 2019). Protein transport across these membranes is differentially regulated and each of these compartments can be considered to have different proteomic profiles and contain different folding environments (Lee et al., 2017). Proteins that are encoded by the nucleus, synthesized in the cytosol and localized in the thylakoid lumen require an *N*-terminal bipartite transit peptide consisting of two signals in tandem: a signal to enter the TIC/TOC import system of the outer double membrane followed by a thylakoid targeting signal that uses one of two functionally distinct pathways, known as the secretory (Sec) and twin-arginine translocation (Tat) pathways (Pottosin and Shabala, 2016; Fernandez, 2018; Johnson and Wientjes, 2019; Palmer and Stansfeld, 2020). The Sec pathway bears homology to the bacterial secretory pathway and actively transports the unfolded pre-protein bound to the SecA chaperone through a Sec membrane complex (Ries et al., 2020). On the other hand, protein transport via the Tat pathway uses a transthylakoidal proton gradient as its energy source and can mediate transport of fully folded globular proteins across the thylakoid membrane (Palmer and Stansfeld, 2020). The Tat pathway is also unique in having a protein proofreading ability that targets misfolded proteins for degradation (Robinson et al., 2011). In the thylakoid lumen, a single chimeric protein, lumen thiol oxidoreductase I (LTO1), performs both *de novo* formation and transfer of disulfides to proteins that undergo oxidative folding (Karamoko et al., 2013). Folding of both the Fc and the V_HH requires the formation of intra-chain disulfide bonds as a structure-stabilizing modification to prevent denaturation and reduce susceptibility to proteolysis (Woof and Russell, 2011; Vincke and Muyldermans, 2012). Structurally, the Fc chain consists of two distinct domains, CH2 and CH3, each comprising two anti-parallel beta sheets that are connected at the center by an intra-chain disulfide bond. The Fc also homodimerizes via inter-chain disulfide bonds that cross-link cysteines on the CH2 domain near the hinge. Similarly, the V_HH is predicted to typically contain one to two intra-chain disulfides (Wesolowski et al., 2009), and when produced in bacteria, requires targeting to the periplasm for correct folding (Henry et al., 2017). Because the Sec and Tat pathways differ in trafficking the unfolded and folded protein cargo, respectively, we hypothesized that the inter-chain and intra-chain disulfide formation of the V_HH-Fc would be exclusive to the Sec pathway and may be evident in its dimerization and stable accumulation, respectively.

The oxidizing environment of the thylakoid lumen has conventionally been considered the only site for oxidatively folding chloroplast proteins that require disulfide stabilization because of the control of a *trans*-thylakoid redox pathway (Karamoko et al., 2013). However, a few studies have suggested that proteins requiring disulfide formation may unexpectedly fold and be biologically active in the reducing environment of the stroma (Staub et al., 2000; Daniell et al., 2001; Mayfield et al., 2003; Bally et al., 2008). These discrepancies may possibly be explained by spontaneous disulfide formation in the stroma or activity by the membrane embedded LTO1 even though previous studies have suggested it to be oriented toward the interior of the lumen (Kieselbach and Schroder, 2003; Lu et al., 2013). To differentiate between the ability of the stroma and thylakoid lumen to properly introduce disulfide bonds and fold a V_HH-Fc protein, we targeted it to both compartments.

In this study, we have compared accumulation levels of a V_HH-Fc that was transiently targeted to the chloroplast thylakoid compartment via Sec and Tat pathways or to the chloroplast stroma in *N. benthamiana* leaf cells. We have also demonstrated that the V_HH-Fc targeted to the thylakoid or stromal compartments is functional in binding and neutralizing adherence of *E. coli* O157:H7 to human epithelial cells. This study is notable because it provides a proof of concept that the folding environment of the thylakoid lumen is conducive for accumulating a V_HH-Fc fusion that retains functionality in binding and neutralizing its target, and provides a foundation for producing transplastomic plants targeting such an antibody for folding and accumulation in the thylakoid lumen.

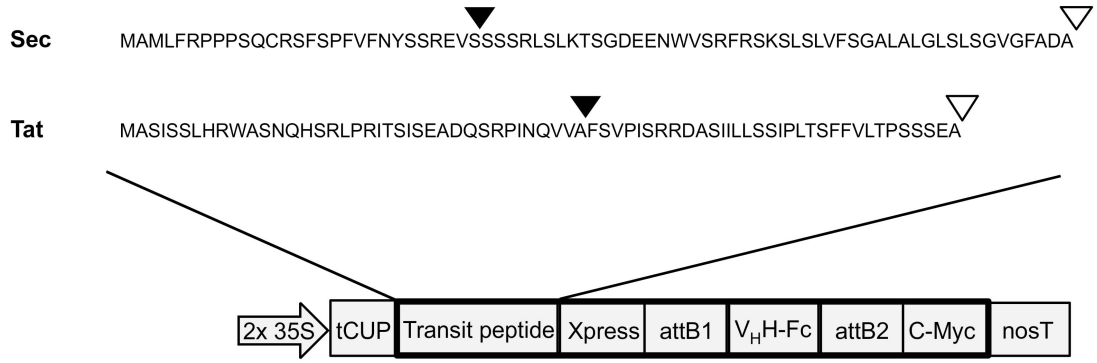

FIGURE 1 | Construction of thylakoid expression vectors. Transit peptide sequences used for thylakoid targeting via either Sec or Tat pathways. Triangles indicate predicted cleavage sites after entry into stromal (black triangles) and thylakoid (white triangles) compartments. 2 × 35S: double-enhanced promoter from Cauliflower Mosaic Virus 35S gene; tCUP, translational enhancer from a tobacco cryptic upstream promoter; attB1/attB2, cloning sites used for Gateway cloning; nosT, nopaline synthase transcription terminator; and Xpress/c-myc, detection/purification tags.

MATERIALS AND METHODS

Cloning and Expression

Both Sec and Tat sequences (Accession #s: NP_001318791 and NP_001321139, respectively) were obtained from a previous proteomics study that isolated and sequenced multiple luminal proteins in *A. thaliana* (Schubert et al., 2002). The Tat targeting sequence corresponds to the *N*-terminal 71 amino acids of a FKBP-type peptidyl-prolyl *cis-trans* isomerase (At1g20810). The Sec targeting sequence corresponds to the *N*-terminal 75 amino acids of a thylakoid luminal 15.0 kDa protein 2 (At5g52970; **Figure 1**). Cleavage sites of the targeting peptides were predicted using the ChloroP and TargetP online tools (Emanuelsson et al., 1999; Almagro Armenteros et al., 2019). Sequences were synthesized by BioBasic Inc. (Mississauga, Canada) and then cloned using a sequence and ligation independent cloning method (SLIC; Li and Elledge, 2007) into an in-house developed cytosolic expression vector, pCaMGate (Pereira et al., 2014). The pCaMGate vector attaches an *N*-terminal Xpress tag for protein stability and a *C*-terminal c-myc tag for detection and purification. The V_HH-Fc construct was developed previously and consists of an anti-EHEC V_HH fused to a bovine Fc (ANN46383; described as V_HH9; Saberianfar et al., 2019). The V_HH-Fc was cloned into this adapted vector by Gateway® cloning and the reading frame was confirmed by sequencing. For stromal and ER expression, we used a set of previously developed in-house expression vectors termed "pCaMGate stroma" and "pCaMGate ER," respectively (Pereira et al., 2014). pCaMgate stroma attaches an *N*-terminal transit peptide derived from the small subunit of RuBisCO. The ER vector attaches an *N*-terminal PR1b tobacco signal peptide for targeting to the secretory pathway and a *C*-terminal KDEL tag for retrieval to the ER. Aside from the signal peptides, the sequences of the stroma and ER expression vectors are identical to the Sec and Tat expression vectors.

For transient expression in plants, expression vectors were transformed by electroporation into *Agrobacterium tumefaciens* (EHA 105) and correct clones selected using 50 μg/ml kanamycin and 10 μg/ml rifampicin antibiotics. Starter cultures of Luria Bertani (LB) medium were inoculated with individual colonies and grown overnight with kanamycin and rifampicin. A starter culture with p19, a suppressor of post-transcriptional silencing (Silhavy et al., 2002), was also grown overnight. The starter culture was then diluted 1:1000 into an infiltration culture consisting of LB medium, 50 μg/ml kanamycin, 10 μg/ml rifampicin, 10 mM 2-(*N*-morpholino)ethanesulfonic acid (MES) at pH 5.6 and 100 μM acetosyringone. Cultures were incubated overnight at 28°C with 250 rpm shaking until an optical density at 600 nm (OD600) of 0.5 was reached using a Nanodrop 2000c spectrophotometer (Thermo-Fisher Scientific, Cat. No. ND-2000c). Cultures were then centrifuged at 4,000 × *g* for 30 min and the pellet resuspended to an OD600 of 1.0 in Gamborg's solution containing 3.2 g/l Gamborg's B5 with vitamins, 20 g/l sucrose, 10 mM MES (pH 5.6), and 100 μM acetosyringone. Cultures were then incubated at room temperature using an end over end rotator for 1 h. Equal volumes of the culture with V_HH-Fc, culture with p19 and Gamborg's solution were then combined and used to infiltrate leaves of 8 to 10 week old *N. benthamiana* plants. Plants were grown in a growth cabinet with a 16 h light/8 h dark cycle, maintained at 21–22°C, with 55% humidity and exposed to 100 μmol/photons m^{-2} s^{-1} of light during day cycles. Agroinfiltration involved puncture of the basal leaf surface using a needle followed by injection of the culture into the leaf using a 3 mL syringe. Following agroinfiltration, plants were returned to the growth cabinet before sampling leaf tissue.

Visualizing Subcellular Compartment Localization

To visualize subcellular compartment localization, GFP was cloned into the 3' end of the V_HH-Fc sequence in a pUC57 vector by SLIC and the reading frame was confirmed by sequencing. The V_HH-Fc-GFP construct was then cloned into Sec, Tat, and chloroplast stroma expression vectors by Gateway cloning and each was agroinfiltrated into leaves of *N. benthamiana*. Tissue was harvested after 2 days, mounted in Aqua-Poly/Mount (Polyscience Inc., Warrington, PA, United States, Cat. No. 18606)

and visualized using a 60 × water immersion objective lens and an Olympus LSM FV 1200 confocal microscope for Sec and stroma samples or a Leica TCS SP2 CLSM confocal microscope for Tat samples. Samples were excited at 488 nm using a multi-argon laser set at 5% and emission was detected at 500–545 nm for GFP and at 630–690 nm for chlorophyll.

Protein Extraction and Western Blot

Pre-weighed leaf samples were frozen in liquid nitrogen and homogenized with silica beads (Bio Spec Products Inc., Bartlesville, OK, United States) for 2 min using a TissueLyser II (Retsch Inc., Newton, PA, United States). One milliliter of a denaturing extraction buffer [1× PBS, pH 7.5, 4% sodium dodecyl sulfate (SDS), 2% polyvinylpolypyrrolidone (PVPP)] was added per approximately one hundred milligrams of sample. All samples were then vortexed on high speed for 30 s and centrifuged at 20,000 × *g* for 10 min to remove cell debris. Extracted protein samples were combined with either a 5 × reducing loading buffer [0.3 M Tris–HCl pH 8.0, 5% SDS, 10% glycerol, 100 mM Dithiothreitol (DTT), 0.05% Phenol Red] or a 5 × non-reducing buffer (0.3 M Tris–HCl pH 8.0, 5% SDS, 10% glycerol, and 0.05% Phenol Red), heated at 90°C for 10 min, then loaded onto Express Plus PAGE 4–20% gradient gels (Genscript Inc., Piscataway, NJ, United States). Gels were run at 100 V for 100 min, then transferred to polyvinylidine difluoride membrane using the *Trans*-Blot Turbo transfer system (Bio-Rad Laboratories Inc., Hercules, CA, United States). Blots were blocked overnight with 5% (w/v) skimmed milk in 1× tris-buffered saline with 0.1% tween-20 (TBS-T), pH 7.5, and proteins of interest were probed with a mouse anti-c-myc antibody (diluted 1:5,000; Genscript Inc., Piscataway, NJ, United States) and the 1-H Basic Western kit for mouse primary antibody (Genscript Inc., Piscataway, NJ, United States). Membranes were washed three times in TBS-T for 10 min each and then incubated for 5 min with either Amersham ECL Western Blot detection reagents (GE Healthcare, Mississauga, ON, Canada) or Enhanced Chemiluminescent detection solution (Biorad Laboratories Inc., Hercules, CA, United States). Membranes were placed into a plastic cover to prevent desiccation and were imaged using a MicroChemi 4.2 imaging system with GelCapture acquisition software (DNA Bio-Imaging Systems Ltd., Jerusalem, Israel). Quantification of accumulation was done using densitometry and a calibrated standard curve based on an in-house developed protein of ∼55 kDa of known concentration using the Totallab TL100 software (Non-linear Dynamics, Durham, United Kingdom). Statistical significance was determined using a two-tailed unpaired *T*-test on 3–5 biological replicates.

Recombinant Protein Purification

Leaf tissue was extracted in approximately one mL of a mild native extraction buffer (1× PBS, pH 7.5, 0.1% Tween-20, 1 mM EDTA, 2% PVPP, 100 mM sodium ascorbate, 8 M sucrose, 1 μg/mL leupeptin, 1 mM PMSF, and 1 μg/mL pepstatin A) per one hundred mg of tissue. Samples were vortexed and the supernatant collected after two rounds of centrifugation at 22,000 × *g* for 20 min each. The recombinant protein in the clarified extract was then purified by affinity chromatography using an anti-c-myc purification kit (MBL International Corp., Woburn, MA, United States) according to the manufacturer's protocol. Briefly, 100 μL anti-c-Myc tag bead suspension was added to 3 mL of clarified extract and incubated in a 4°C room for 1 h using an end-over-end shaker to hybridize the beads to the *C*-terminal c-myc tag on the V_HH-Fc protein. The extract was then transferred to a spin column and centrifuged for 10 s. The beads were then washed three times with the provided washing solution and the protein was eluted by competition using a c-Myc tag peptide in 1x PBS at neutral pH.

E. coli O157:H7 Binding Assay

Escherichia *coli* strain O157:H7 was obtained from Dr. Michael Mulvey (Public Health Agency of Canada, National Microbiology Laboratory, *E. coli* Unit, Enteric Diseases Program, Winnipeg, MB, Canada) and stored at -80°C in a level 2 containment laboratory. Binding assays were performed as previously described (Saberianfar et al., 2019). A summary is as follows. A 3 mL culture of *E. coli* O157:H7 was grown overnight in LB medium at 37°C. The culture was then pelleted, rinsed repeatedly in 1× PBS, then fixed in 4% paraformaldehyde. The fixed cells were incubated with 2 μg purified V_HH-Fc for 1 h at 37°C. The cells were hybridized to a FITC-conjugated secondary antibody (rabbit anti-bovine-FITC; 1:40 dilution, Thermo-Fisher Scientific, Cat. No. SA1-36043) that binds Fc. To stain the bacteria, the cells were briefly incubated with DAPI and then washed with 1x PBS. The cells were then dried onto poly-L-lysine coated coverslips (Millipore Sigma, Cat, No. S1815) and mounted onto glass slides with Aqua-Poly/Mount (Polyscience Inc., Warrington, PA, United States, Cat. No. 18606). FITC and DAPI sequential imaging was performed by confocal microscopy with a 64× water lens and an Olympus LSM FV 1200 confocal microscope. FITC was imaged by excitation with a 480 nm laser and detection at 520–540 nm. DAPI was imaged by excitation at 350 nm and detection at 455–465 nm.

HEp-2 Adherence Inhibition Assay

Inhibition assays were performed as previously described (Saberianfar et al., 2019). A summary is as follows. HEp-2 cells (ATCC) were grown to ∼80% confluency and used to seed eight-well chamber slides overnight with ∼2 × 10^5 cells per well in pre-warmed Dulbecco's Modified Eagle Medium (DMEM; Thermo-Fisher Scientific, Cat. No. 10566016) supplemented with 10% fetal bovine serum (FBS) at 37°C in 5% CO_2. At the start of the assay, the overnight medium was replaced with 225 μL fresh DMEM. *E. coli* strain O157:H7 was grown overnight in LB medium and subcultured to a 1:50 dilution in pre-warmed DMEM with and without 2 μg V_HH-Fc and then incubated with the HEp-2 cells at 37°C in 5% CO_2 for 3 h without shaking. The cultures were washed with 1× PBS to remove non-adherent bacteria, fixed in 4% paraformaldehyde, washed repeatedly again with 1× PBS, and hybridized with Alexa 647 phalloidin (Thermo-Fisher Scientific, Cat. No. A22287) to visualize actin in the HEp-2 cells, and donkey anti-rabbit Alexa 350 (Thermo Fisher Scientific Cat. No.A10039) to visualize O157:H7 cells. To visualize adherence to HEp-2 cells, sequential imaging was

performed using an Olympus LSM FV 1200 confocal microscope with a 64x water objective lens. Alexa 647 phalloidin was imaged by excitation at 650 nm and detection at 660–680 nm. The donkey anti-rabbit Alexa 350 antibody was visualized by excitation at 350 nm and detection at 455–465 nm.

RESULTS

Sub-Compartment Targeting Influences Accumulation and Dimerization Patterns of the V_HH-Fc Fusion

The V_HH-Fc was cloned into five separate plant expression vectors that permit targeting of the protein to the chloroplast thylakoid via Sec or Tat pathways, the chloroplast stroma, the ER or the cytosol. After transiently transforming leaves of *N. benthamiana,* tissue was harvested and crude extract separated by SDS-PAGE in either a reducing buffer or a non-reducing buffer to distinguish disulfide-based dimerization of the V_HH-Fc. We did not observe a difference in chlorosis or necrosis of the areas infiltrated with the various constructs compared to the negative control (p19). Although there are no crystal structures for bovine IgA, X-ray crystal structures for human IgA (Herr et al., 2003; Ramsland et al., 2007), which bears a 70% sequence similarity, suggest that three, or possibly four, cysteines on each CH2 domain of the Fc will form disulfide linkages. Under non-reducing conditions, which retain disulfide bonds in the protein, the V_HH-Fc is detected predominantly as an 88 kDa band matching the predicted size of the V_HH-Fc dimer. Total accumulation is highest in the ER at 51.16 ± 9.11 mg/kg FW, followed by the thylakoid via Sec-targeting at 30.56 ± 5.19 mg/kg FW. Accumulation in the stroma and thylakoid via Tat-targeting are substantially lower at 6.63 ± 3.41 mg/kg FW and 5.43 ± 2.41 mg/kg FW, respectively, and is undetectable in the cytosol. Under reducing conditions, the same samples display an enriched band at 44 kDa matching the predicted size of the V_HH-Fc monomer for the ER, stroma, thylakoid via Sec and via Tat suggesting that the V_HH-Fc dimer in these compartments is stabilized by an inter-chain disulfide bond (**Figures 2A,B**).

Sec- and Tat-Targeted Fc-GFP Localizes in the Thylakoid

To verify that the Tat and Sec transit peptides indeed target the V_HH-Fc to the chloroplast thylakoid sub-compartment, we tracked subcellular localization of the Fc by fusing GFP to the Fc chain in each of the expression vectors. Visualization by confocal microscopy showed the Sec and Tat-targeted GFP-tagged protein to consistently co-localize with chlorophyll, which accumulates in the thylakoid and auto-fluoresces at ∼735 nm (**Figure 3**). On the other hand, the construct targeting the recombinant protein to the stroma showed a very distinct pattern surrounding the thylakoid grana, and into stromules. Therefore, the Sec and Tat transit peptides we used indeed target the recombinant protein to the thylakoid.

Sec-Targeted V_HH-Fc Fusions With an Engineered Disulfide Show Improved Yield

We have previously identified by rational design a residue pair (G196C/R219C) on the Fc that if mutated to cysteines would form a *de novo* disulfide bond that enables a ten-fold improvement in yield of the V_HH-Fc when targeted to the ER (Chin-Fatt et al., 2021). The pair forms an intra-chain disulfide between strand G and strand F on the CH3 domain in oxidative folding conditions (**Figures 4A,B**). To determine if the oxidative folding of the thylakoid can recapitulate the yield-improving effects of an engineered disulfide bond, we targeted the V_HH-Fc fusion carrying the G196C/R219C mutation to the thylakoid lumen via the Sec pathway and measured accumulation by western blotting after agroinfiltration. The engineered V_HH-Fc showed a significant yield improvement at 110.90 ± 6.46 mg/kg FW compared to the native V_HH-Fc at 50.24 ± 4.09 mg/kg FW (**Figure 4C**), suggestive of the ability of the thylakoid lumen to incorporate *de novo* disulfide bonds on a heterologous V_HH-Fc via the Sec pathway.

Sec, Tat, and Stroma-Targeted V_HH-Fc Fusions Bind O157:H7

We previously demonstrated that the ER-targeted V_HH binds to intimin, an integral outer membrane protein of *E. coli* O157:H7 (Saberianfar et al., 2019). To determine if the thylakoid-targeted V_HH-Fc retained the ability to bind *E. coli* O157:H7, purified V_HH-Fc from each compartment was incubated with the pathogen then fixed in paraformaldehyde, washed and probed for immunofluorescence using a FITC labeled anti-c-myc secondary antibody. Visualization by confocal microscopy showed consistent co-localization between DAPI-stained bacterial cells and the FITC-labeled V_HH-Fc for the thylakoid via Sec, thylakoid via Tat, and stromal compartments, indicating that the chloroplast-targeted V_HH-Fc retains the ability to bind intimin on EHEC surfaces (**Figure 5**). As a negative control, O157:H7 cells were also treated with 1x PBS containing 0.1% Tween-20 (PBS-T) instead of the V_HH-Fc and similarly stained but did not show fluorescence under FITC-related imaging conditions (480 nm excitation and 520–540 nm detection). This result suggests that the V_HH is folded properly and recognizes its target when Sec-, Tat-, and stroma-targeted.

Sec-, Tat- and Stroma-Targeted V_HH-Fc Fusions Can Neutralize O157:H7's Adherence to HEp-2 Cells

Given that intimin mediates the attachment of *E. coli* O157:H7 to intestinal epithelial cells, and that V_HH-Fc targeted to the ER neutralizes *E. coli*'s ability to adhere to those cells (Chin-Fatt et al., 2021), we tested if thylakoid targeting of the V_HH-Fc impacted its ability to neutralize the bacterium from adhering to epithelial cells by blocking intimin. HEp-2 cells were incubated with *E. coli* O157:H7 in the presence or absence of purified V_HH-Fc from each of the compartments. Cells were then washed to remove non-adherent bacteria, fixed in paraformaldehyde,

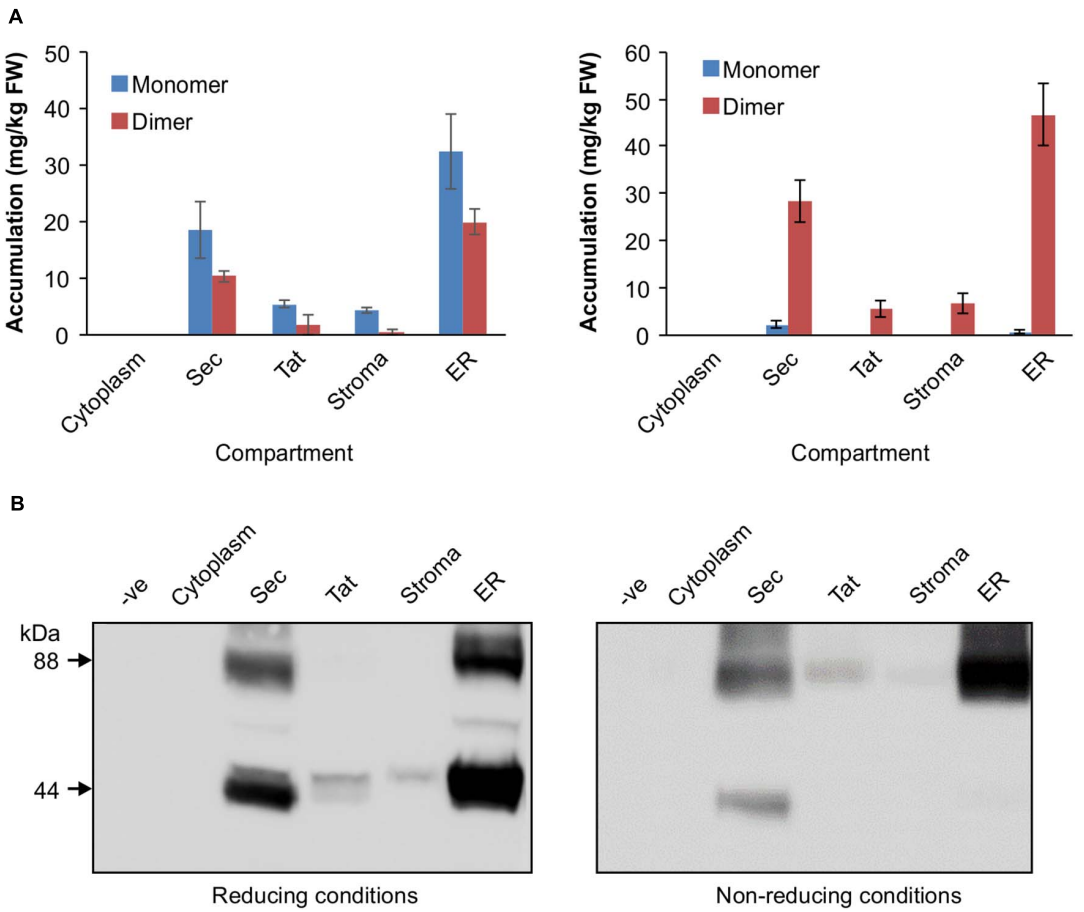

FIGURE 2 | Accumulation profiles of V_HH-Fc targeted with cytoplasm, Sec, Tat, stromal, and ER signals. **(A)** Bar chart comparing V_HH-Fc accumulation levels across cytoplasm, Sec, Tat, stromal, and ER signals extracted in reducing (left) or non-reducing (right) conditions. *N* = 3 biological replicates. Error bars shown are standard error. **(B)** Representative Western blot showing relative accumulation of V_HH-Fc across compartments in reducing (left) and non-reducing (right) conditions.

and incubated with immunofluorescent labels. Human epithelial type-2 (HEp-2) cells were visualized by fluorescent actin staining using rhodamine phalloidin (shown in red) and O157:H7 cells visualized using a donkey anti-rabbit alexa 350 secondary antibody (shown in white; **Figure 6**). Compared to the control lacking V_HH-Fc, and to the control Fc lacking the V_HH, the addition of V_HH-Fc from any of the compartments seems to abrogate adhesion of any labeled *E. coli* O157:H7 to the incubated HEp-2 cells as visualized using confocal microscopy (**Figure 6**). This indicates that the chloroplast-targeted V_HH-Fc retains the ability to neutralize EHEC from colonizing epithelial cells and that the inhibition of adhesion is mediated by the V_HH and not by non-specific interactions of the Fc moiety of the antibody.

DISCUSSION

Utility of a Thylakoid Targeting System for Antibodies

The utility of a plant platform for folding and assembling IgA antibodies and related synthetics in the ER is well established (Ma et al., 1998; Nakanishi et al., 2013; Virdi et al., 2013; Saberianfar et al., 2019). However, in a previous study exploring how recombinant antibodies influence the endogenous proteome, a genome-wide Tiling array suggested that ER-targeted V_HH-IgG Fc fusions in *A. thaliana* seeds generated an unfolded protein response (De Wilde et al., 2013). Because the thylakoid has a different proof-reading system for folding than the ER, there may be value in exploring it as an alternative oxidative folding compartment for antibody folding because of the potential to avoid ER-associated degradation as a limiting factor. In this study, we explored the possibility of producing a V_HH-Fc fusion in the thylakoid lumen as a viable yield-optimization strategy within the context of molecular farming. Overall, the results suggest that the V_HH-Fc fusion seems to fold correctly and assemble with the requisite intra- and inter-chain disulfides as well as retains binding and neutralization efficacy. Although accumulation was not found to be higher than the ER, purified V_HH-Fc protein from both stromal and luminal fractions retained binding and neutralization efficacy. Notably, the Sec-targeted V_HH-Fc fusion accumulated significantly better than stromal and Tat-targeted fusions, albeit at approximately

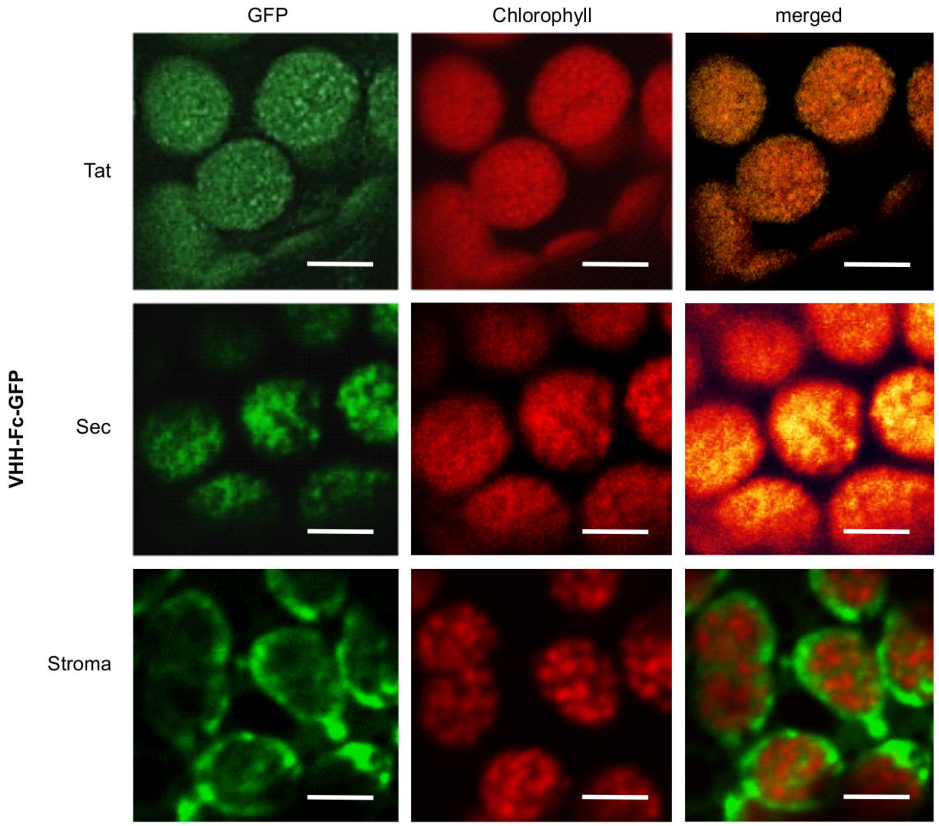

FIGURE 3 | Sec and Tat transit peptides enable localization of the recombinant Fc-GFP to the thylakoid chloroplast sub-compartment. Confocal images visualizing GFP-tagged Fc (green) targeted to the chloroplasts with either Sec, Tat or stromal signals. Chlorophyll (red) indicates the locations of the thylakoid grana. Fluorescence was sequentially captured, and the merged images show co-localization of GFP and chlorophyll (yellow). Size bar = 10 μm.

60% of the ER-targeted V_HH-Fc fusion. Additionally, the Sec-targeted V_HH-Fc was detected as two bands in non-reducing conditions, corresponding to monomeric and dimeric forms, while the ER-targeted V_HH-Fc was detected as a single band corresponding to the dimer (**Figure 2B**). This may indicate either relatively slower or less efficient interchain disulfide formation with Sec-targeted V_HH-Fc compared to the ER, or alternatively, that there is detection of the unfolded preprotein before thylakoid import. Nonetheless, previous experience has suggested that robust accumulation for a transiently expressed, chloroplast targeted recombinant protein is indicative of high yields upon developing a stable transplastomic line for that protein (Kolotilin et al., 2012). Transplastomically-expressed recombinant proteins tend to be of higher yield than when nuclear-expressed due to the polyploidy of the chloroplast genome and the lack of silencing and positional interaction effects (Bock, 2007; Daniell et al., 2009). The use of stably-transformed chloroplasts presents several unique advantages as a molecular farming strategy, notably maternal inheritance of the chloroplast genome which virtually eliminates the prospect of gene escape to the environment by pollen (Kumar et al., 2004). Additionally, the recombinant proteins are encapsulated by chloroplast membranes and are effectively isolated from cellular proteases which are more abundant and diverse than those found in the chloroplast. The proteome and protease profile of the thylakoid lumen in particular is substantially more limited in comparison (Kieselbach and Schroder, 2003). Chloroplast-based expression might also facilitate alternative purification methods because intact chloroplasts can be easily isolated from crude extracts by low-speed centrifugation (Kubis et al., 2008). If yields are high enough, there may be value in scaling up production of biomass that could then be administered orally to animals for enteric protection against EHEC without the need for purification.

Disulfide Formation in the Chloroplast

Under non-reducing conditions, banding corresponding to the V_HH-Fc dimer was unexpectedly detected for the stromal and Tat-targeted compartments. Disulfide formation has conventionally been thought to be exclusive to the oxidative folding environment of the thylakoid. However, a few studies have suggested that disulfide formation is possible in the reducing environment of the stroma for recombinant proteins, though it tends to be at much lower levels and the mechanics of which remain uncertain. For example, human growth hormone (Staub et al., 2000), cholera toxin B (Daniell et al., 2001), a recombinant alkaline phosphatase A (Bally et al., 2008), aprotinin (Tissot et al., 2008), and zeolin (De Marchis et al., 2011) all require

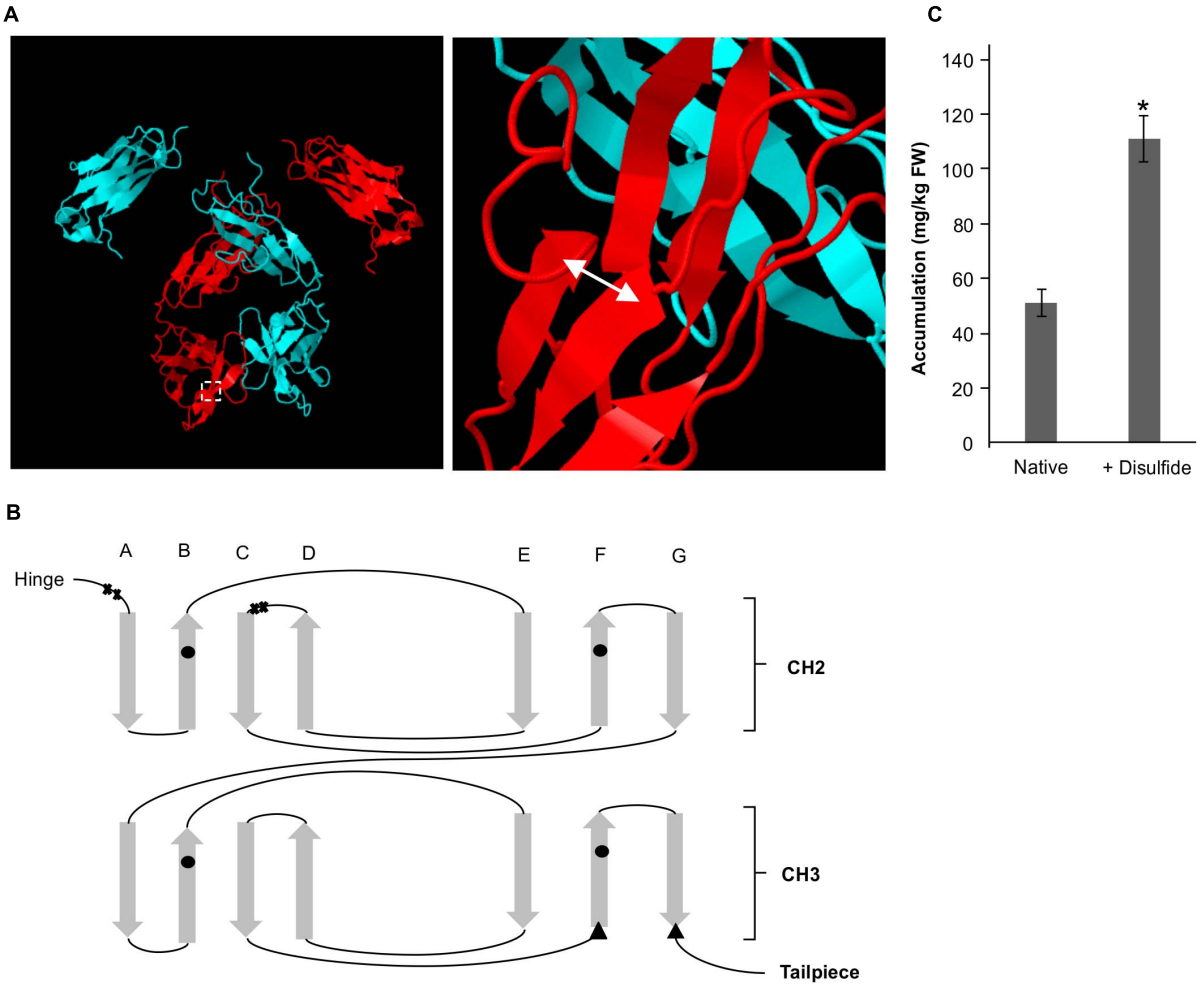

FIGURE 4 | A *de novo* disulfide bond enhances accumulation for a Sec-targeted V_HH-Fc. **(A)** Structural model showing the backbone of two dimerized Fc chains (blue and red). The double headed arrow indicates the position of the introduced disulfide. **(B)** Greek key connectivity schematic showing the relative positions of native disulfides and the introduced disulfide in the Fc. X indicates cysteines involved in interchain disulfide formation, circles indicate cysteines involved in intrachain disulfide formation and triangles indicate introduced cysteines for *de novo* disulfide formation. **(C)** Bar chart showing accumulation of Sec-targeted native V_HH-Fc and a V_HH-Fc with an added disulfide. *indicates statistical significance as determined by a *T*-test with $p < 0.05$, $n = 3$ biological replicates. Error bars shown are standard error of the mean.

disulfide bond formation for folding and are nonetheless biologically active when either expressed in or targeted to the stroma. Notably, Bally et al. (2008) have shown not only that the chloroplast stroma supports the formation of an active alkaline phosphatase A enzyme but also that sorting of the alkaline phosphatase to the thylakoid lumen leads to larger amounts and more active enzyme. If accumulation can be assumed to be a correlative measure of how well folded a protein is, then the higher accumulation observed for the Sec-targeted V_HH-Fc suggests that the oxidative folding environment in the thylakoid lumen is conducive for proper folding of the V_HH-Fc with the requisite disulfide stabilization. In contrast, both the stromal targeted and Tat-targeted V_HH-Fc have low accumulation levels and may be due to the suboptimal folding environment of the stroma. Similarly, the lack of detectable signal in the cytoplasm may be due to the inability of the V_HH-Fc to fold sufficiently, particularly because the intra-chain disulfides are needed to stabilize the characteristic beta sandwich CH domains (Kumar et al., 2020). Several others have reported successfully expressing a V_HH in the chloroplast stroma. A nuclear-expressed and stroma-targeted V_HH was shown to be effective in potato plants in modulating enzyme function endogenously, albeit at a very low accumulation of 0.03% TSP (Jobling et al., 2003). Similarly, a transplastomically produced stromal V_HH in tobacco retained binding efficacy against albumin lysozyme, a causative agent in proteinuria, but was produced at levels too low to be quantified and caused a semi-lethal pale-green seedling phenotype (Magee et al., 2004). Upon exposure to light, the stroma exhibits changes in its pH and redox state and consequently, its capacity for oxidative folding. The stroma has a neutral pH close to 7 under dark conditions but alkalizes to pH 8 upon illumination due to H^+ being actively pumped into the thylakoid lumen

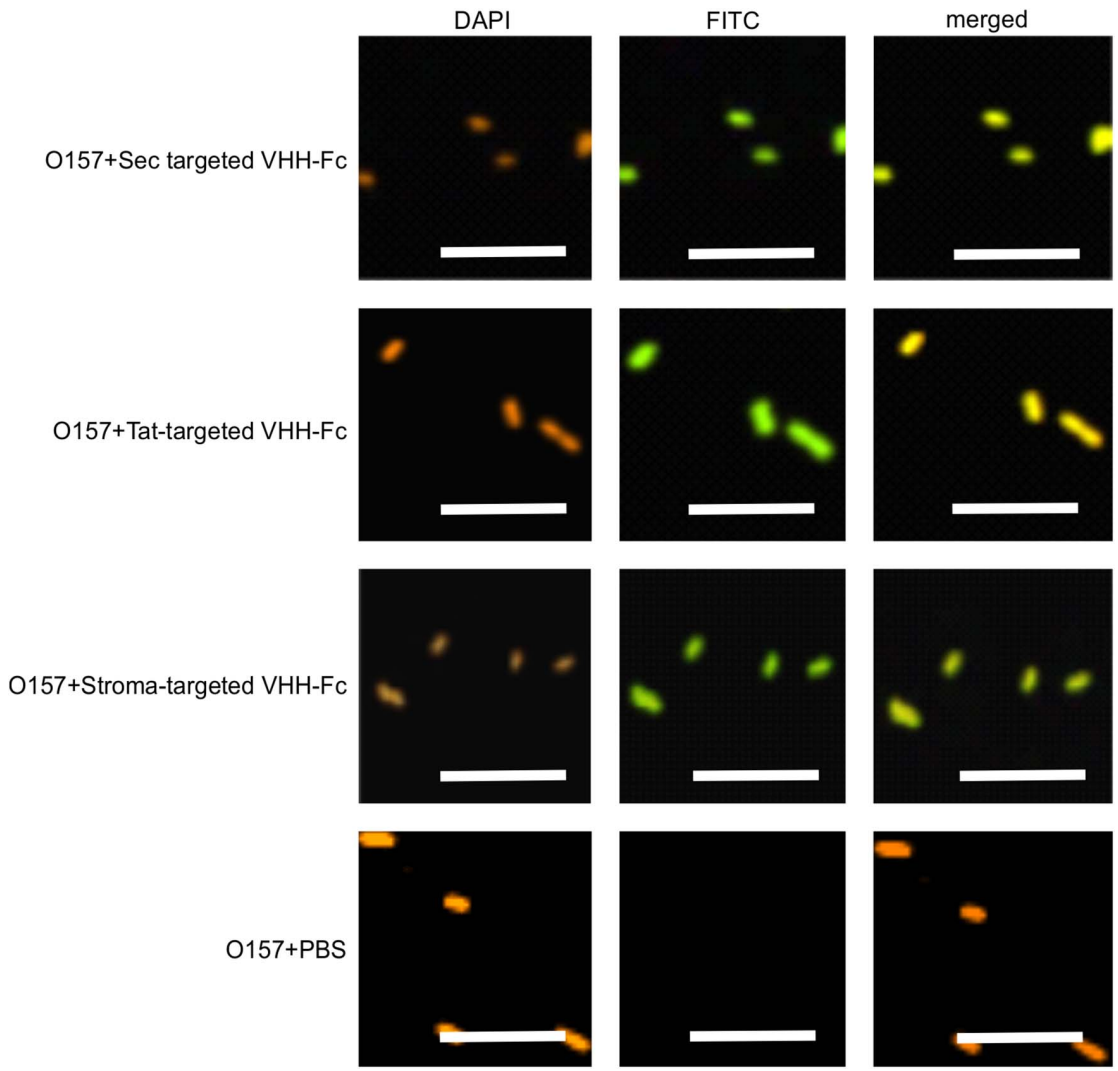

FIGURE 5 | V_HH-Fc targeted with either Sec, Tat or stromal transit peptides can bind O157:H7 cells. Shown are confocal images of V_HH-Fc targeted with either Sec, Tat or stromal signals incubated with EHEC O157:H7. DAPI was used to visualize EHEC cells (orange) and a FITC-conjugated antibody (green) was used to immunolabel the Fc specifically. Size bar = 10 μm.

(Werdan et al., 1975). Additionally, during photosynthesis, the NADPH/$NADP^+$ ratio increases in the stroma causing a more reducing environment (Heineke et al., 1991). Conversely, the thylakoid lumen is acidified upon light exposure with a change in pH from 7.5 under dark conditions to 5.7 under saturating light (Takizawa et al., 2007). Notably, photosynthesis is known to modulate the activity of several enzymes in the stroma by reducing key disulfide bonds via a cascade involving ferredoxin, ferredoxin-thioredoxin reductase, and thioredoxins *m* and *f* (Schürmann and Buchanan, 2008). Prior to triggering of the cascade, the disulfides of these enzymes are at least partially oxidized despite the reducing environment of the stroma. Thus, the relatively low accumulation levels for the stroma- and Tat-targeted V_HH-Fc may potentially be due to an environment made more reducing from photosynthetic activity. Future studies using these sorting signals may want to consider growing infiltrated plants in low light or extended dark conditions for optimal accumulation. On the other hand, V_HHs produced in the chloroplast of the green algae *Chlamydomonas reinhardtii* are competent in binding botulinum neurotoxin and were shown to accumulate to 5% TSP suggesting that there may be key plant-specific physiological factors that limit production in plant chloroplasts versus *C. reinhardtii* chloroplasts (Barrera et al., 2015). Indeed, the protein disulfide isomerase-like RB60 is partitioned between stroma and thylakoids in *C. reinhardtii* chloroplasts and has been suggested to potentially interface bidirectionally (Trebitsh et al., 2001). Conversely, lumen thiol oxidoreductase1 (LTO1), that catalyzes disulfide bond formation, is embedded in the thylakoid membrane of plants and is known to be preferentially oriented toward the thylakoid lumen (Karamoko et al., 2013). It may thus also be possible that aside from spontaneous disulfide formation that the low levels of

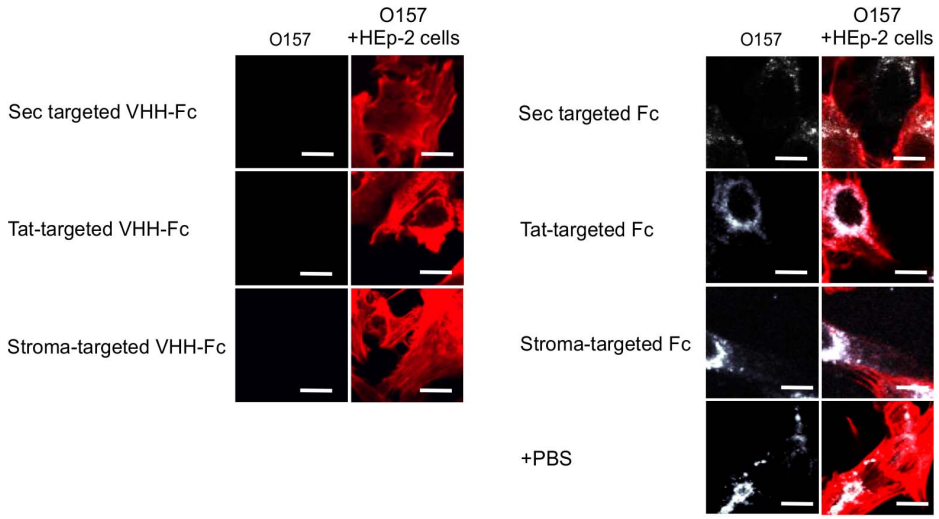

FIGURE 6 | V_HH-Fc targeted with either Sec, Tat or stromal transit peptides can neutralize adherence of O157:H7 to HEp-2 cells. Shown are confocal images of O157:H7 (white) that has been incubated with Hep-2 cells (red) in the presence of either V_HH-Fc targeted to Sec, Tat, and stromal compartments or Fc as a negative control targeted to the same compartments. Size bar = 20 μm.

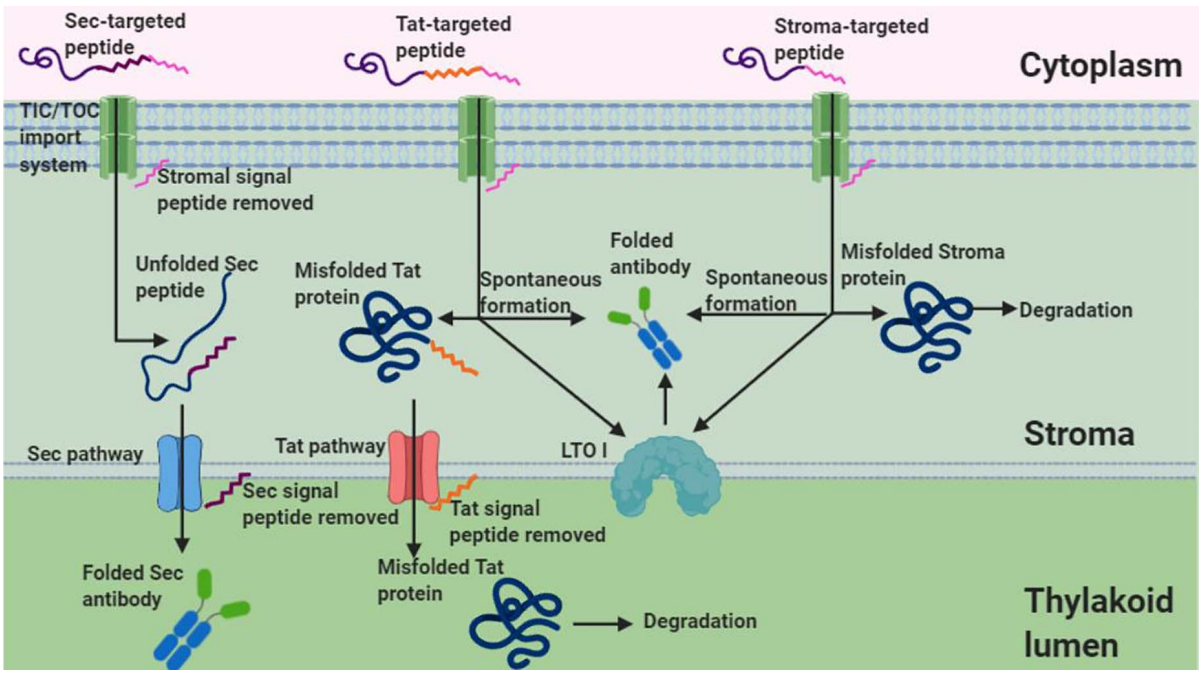

FIGURE 7 | Schematic of Sec, Tat, and stromal import of an antibody. Given that Tat and stromal imported antibodies retain functionality and show dimerized banding under non-reducing conditions, this suggests disulfide formation in the stroma despite its reducing environment. Shown are two possible mechanisms of disulfide formation, interaction with LTOI and spontaneous formation, that may account for disulfide formation of tat and stroma targeted antibodies (Figure created in Biorender.com).

V_HH-Fc when stromal-targeted and Tat-targeted may be due to trace disulfide isomerase activity at this partition. Therefore, this suggests that the stability, and accumulation thereof, of the V_HH-Fc may be a function of its redox potential as it relates to the reactivity of its cysteine residues' thiol groups and/or the availability of disulfide isomerase activity (**Figure 7**).

We also introduced a *de novo* disulfide pair G196C/R219C into the V_HH-Fc targeted with the Sec signal and found a significant yield improvement. Compared to the ten-fold yield improvement observed previously when targeted to the ER (Chin-Fatt et al., 2021), the yield improvement is substantially less at only about a two-fold improvement. This may possibly

be due to the availability of relevant chaperones across the two compartments. The thylakoid lumen is known to contain a unique chaperonin cpn60/cpn10 system distinct from the stromal chaperonin system or the HSP family in the ER (Schlicher and Soll, 1996). Alternatively, the difference in yield improvement may be due to different activities of LTO1 in the thylakoid lumen versus the protein disulfide isomerase (PDI)-mediated folding reactions in the ER.

Structural Considerations for Antibodies Targeted to the Thylakoid Lumen

Although the thylakoid lumen is capable of disulfide formation, it lacks the machinery for glycosylation. Given that V_HHs are not natively glycosylated by their host camelids, and are also competent when produced in *E. coli*, we hypothesized that the V_HH would retain functionality when folded in the thylakoid (Herrmann et al., 2009). Additionally, V_HHs have been shown to be effective in neutralizing a broad array of other enteric pathogens (Vega et al., 2013; Shkoporov et al., 2015; Schmidt et al., 2016; King et al., 2018). Accordingly, the binding and neutralizing assays suggest that efficacy is retained despite the lack of glycosylation. Although the V_HH alone may be sufficient for neutralization, yields are usually low and attaching the Fc has been shown to improve accumulation (Virdi et al., 2019). The Fc also enables improved avidity via its ability to multimerize thereby mediating agglutination. In enteromucosal conditions, neutralization of a pathogen's ability to colonize epithelial cells is predominantly by steric hindrance via agglutination, known as immune exclusion (Li et al., 2020). Although the bovine IgA Fc is natively glycosylated, a recent study that characterized glycosylation on a plant-made ER- and apoplast-targeted Fc fusion protein demonstrated that preventing glycan attachment did not prevent the Fc from correctly folding (Xiong et al., 2019). Therefore, the thylakoid may be a suitable compartment for folding and accumulating functional V_HH-Fc fusion proteins despite the lack of glycosylation.

Overall, this study provides a proof of concept that targeting to the thylakoid lumen via the Sec pathway allows for accumulation of a functional V_HH-Fc fusion and may thus be a strategic way of producing these therapeutics while accruing the benefits of plastidial encapsulation.

DATA AVAILABILITY STATEMENT

The original contributions presented in the study are included in the article/supplementary material, further inquiries can be directed to the corresponding author/s.

AUTHOR CONTRIBUTIONS

AC-F and RM conceived the study. AC-F performed the experiments and wrote the manuscript. AC-F and RM edited the manuscript. Both authors contributed to the article and approved the submitted version.

FUNDING

This research was supported by Agriculture and Agri-Food Canada A-base project 1258 to RM.

ACKNOWLEDGMENTS

We thank Hong Zhu and Angelo Kaldis at Agriculture and Agri-Food Canada for providing technical support, Andrew Scott for help with *E. coli* and HEp-2 cell culture, and Alex Molnar for assistance with preparation of figures.

REFERENCES

Almagro Armenteros, J. J., Salvatore, M., Emanuelsson, O., Winther, O., Von Heijne, G., Elofsson, A., et al. (2019). Detecting sequence signals in targeting peptides using deep learning. *Life Sci. Alliance* 2:e201900429. doi: 10.26508/lsa.201900429

Bally, J., Paget, E., Droux, M., Job, C., Job, D., and Dubald, M. (2008). Both the stroma and thylakoid lumen of tobacco chloroplasts are competent for the formation of disulphide bonds in recombinant proteins. *Plant Biotechnol. J.* 6, 46–61.

Barrera, D. J., Rosenberg, J. N., Chiu, J. G., Chang, Y. N., Debatis, M., Ngoi, S. M., et al. (2015). Algal chloroplast produced camelid VH H antitoxins are capable of neutralizing botulinum neurotoxin. *Plant Biotechnol. J.* 13, 117–124. doi: 10.1111/pbi.12244

Bock, R. (2007). Plastid biotechnology: prospects for herbicide and insect resistance, metabolic engineering and molecular farming. *Curr. Opin. Biotechnol.* 18, 100–106. doi: 10.1016/j.copbio.2006.12.001

CDC. (2020). Preliminary incidence and trends of infections with pathogens transmitted commonly through food — foodborne diseases active surveillance network, 10 U.S. Sites, 2016–2019. *Morb. Mortal. Wkly Rep.* 69, 509–514. doi: 10.15585/mmwr.mm6917a1

Chin-Fatt, A. S., Saberianfar, R., and Menassa, R. (2021). A rationally designed bovine IgA Fc scaffold enhances in planta accumulation of a V_HH-Fc fusion without compromising binding to enterohemorrhagic E. coli. *Front. Plant Sci.* 12:636. doi: 10.3389/fpls.2021.651262

Daniell, H., Lee, S. B., Panchal, T., and Wiebe, P. O. (2001). Expression of the native cholera toxin B subunit gene and assembly as functional oligomers in transgenic tobacco chloroplasts. *J. Mol. Biol.* 311, 1001–1009. doi: 10.1006/jmbi.2001.4921

Daniell, H., Singh, N. D., Mason, H., and Streatfield, S. J. (2009). Plant-made vaccine antigens and biopharmaceuticals. *Trends Plant Sci.* 14, 669–679. doi: 10.1016/j.tplants.2009.09.009

De Marchis, F., Pompa, A., Mannucci, R., Morosinotto, T., and Bellucci, M. (2011). A plant secretory signal peptide targets plastome-encoded recombinant proteins to the thylakoid membrane. *Plant Mol. Biol.* 76, 427–441. doi: 10.1007/s11103-010-9676-6

De Meyer, T., Muyldermans, S., and Depicker, A. (2014). Nanobody-based products as research and diagnostic tools. *Trends Biotechnol.* 32, 263–270. doi: 10.1016/j.tibtech.2014.03.001

De Wilde, K., De Buck, S., Vanneste, K., and Depicker, A. (2013). Recombinant antibody production in arabidopsis seeds triggers an unfolded protein response. *Plant Physiol.* 161, 1021–1033. doi: 10.1104/pp.112.209718

Emanuelsson, O., Nielsen, H., and Von Heijne, G. (1999). ChloroP, a neural network-based method for predicting chloroplast transit peptides and their cleavage sites. *Protein Sci.* 8, 978–984. doi: 10.1110/ps.8.5.978

Fernandez, D. E. (2018). Two paths diverged in the stroma: targeting to dual SEC translocase systems in chloroplasts. *Photosynth. Res.* 138, 277–287. doi: 10.1007/s11120-018-0541-9

Harmsen, M. M., and De Haard, H. J. (2007). Properties, production, and applications of camelid single-domain antibody fragments. *Appl. Microbiol. Biotechnol.* 77, 13–22. doi: 10.1007/s00253-007-1142-2

Heineke, D., Riens, B., Grosse, H., Hoferichter, P., Peter, U., Flügge, U. I., et al. (1991). Redox transfer across the inner chloroplast envelope membrane. *Plant Physiol.* 95, 1131–1137. doi: 10.1104/pp.95.4.1131

Henry, K. A., Kandalaft, H., Lowden, M. J., Rossotti, M. A., Van Faassen, H., Hussack, G., et al. (2017). A disulfide-stabilized human VL single-domain antibody library is a source of soluble and highly thermostable binders. *Mol. Immunol.* 90, 190–196. doi: 10.1016/j.molimm.2017.07.006

Herr, A. B., Ballister, E. R., and Bjorkman, P. J. (2003). Insights into IgA-mediated immune responses from the crystal structures of human FcαRI and its complex with IgA1-Fc. *Nature* 423, 614–620. doi: 10.1038/nature01685

Herrmann, J. M., Kauff, F., and Neuhaus, H. E. (2009). Thiol oxidation in bacteria, mitochondria and chloroplasts: common principles but three unrelated machineries? *Biochim. Biophys. Acta* 1793, 71–77. doi: 10.1016/j.bbamcr.2008.05.001

Jobling, S. A., Jarman, C., Teh, M. M., Holmberg, N., Blake, C., and Verhoeyen, M. E. (2003). Immunomodulation of enzyme function in plants by single-domain antibody fragments. *Nat. Biotechnol.* 21, 77–80. doi: 10.1038/nbt772

Johnson, M. P., and Wientjes, E. (2019). The relevance of dynamic thylakoid organisation to photosynthetic regulation. *Biochim. Biophys. Acta Bioenerg.* 1861:148039. doi: 10.1016/j.bbabio.2019.06.011

Karamoko, M., Gabilly, S. T., and Hamel, P. P. (2013). Operation of trans-thylakoid thiol-metabolizing pathways in photosynthesis. *Front. Plant Sci.* 4:476. doi: 10.3389/fpls.2013.00476

Kieselbach, T., and Schroder, W. P. (2003). The proteome of the chloroplast lumen of higher plants. *Photosynth. Res.* 78, 249–264. doi: 10.1023/b:pres.0000006913.86689.f1

King, M. T., Huh, I., Shenai, A., Brooks, T. M., and Brooks, C. L. (2018). Structural basis of V_HH-mediated neutralization of the food-borne pathogen Listeria monocytogenes. *J. Biol. Chem.* 293, 13626–13635. doi: 10.1074/jbc.ra118.003888

Kirchhoff, H. (2019). Chloroplast ultrastructure in plants. *New Phytol.* 223, 565–574. doi: 10.1111/nph.15730

Kolotilin, I., Kaldis, A., Devriendt, B., Joensuu, J., Cox, E., and Menassa, R. (2012). Production of a subunit vaccine candidate against porcine post-weaning diarrhea in high-biomass transplastomic tobacco. *PLoS One* 7:e42405. doi: 10.1371/journal.pone.0042405

Kubis, S. E., Lilley, K. S., and Jarvis, P. (2008). Isolation and preparation of chloroplasts from arabidopsis thaliana plants. *Methods Mol. Biol.* 425, 171–186. doi: 10.1007/978-1-60327-210-0_16

Kumar, N., Arthur, C. P., Ciferri, C., and Matsumoto, M. L. (2020). Structure of the secretory immunoglobulin a core. *Science* 367, 1008–1014. doi: 10.1126/science.aaz5807

Kumar, S., Dhingra, A., and Daniell, H. (2004). Stable transformation of the cotton plastid genome and maternal inheritance of transgenes. *Plant Mol. Biol.* 56, 203–216. doi: 10.1007/s11103-004-2907-y

Lee, D. W., Lee, J., and Hwang, I. J. (2017). Sorting of nuclear-encoded chloroplast membrane proteins. *Curr. Opin. Plant Biol.* 40, 1–7. doi: 10.1016/j.pbi.2017.06.011

Li, M. Z., and Elledge, S. J. (2007). Harnessing homologous recombination in vitro to generate recombinant DNA via SLIC. *Nat. Methods* 4, 251–256. doi: 10.1038/nmeth1010

Li, Y., Jin, L., and Chen, T. (2020). The effects of secretory IgA in the mucosal immune system. *Biomed. Res. Int.* 2020:2032057.

Lu, Y., Wang, H.-R., Li, H., Cui, H.-R., Feng, Y.-G., and Wang, X.-Y. (2013). A chloroplast membrane protein LTO1/AtVKOR involving in redox regulation and ROS homeostasis. *Plant Cell. Rep.* 32, 1427–1440. doi: 10.1007/s00299-013-1455-9

Ma, J. K. C., Hikmat, B. Y., Wycoff, K., Vine, N. D., Chargelegue, D., Yu, L., et al. (1998). Characterization of a recombinant plant monoclonal secretory antibody and preventive immunotherapy in humans. *Nat. Med.* 4, 601–606. doi: 10.1038/nm0598-601

Magee, A. M., Coyne, S., Murphy, D., Horvath, E. M., Medgyesy, P., and Kavanagh, T. A. (2004). T7 RNA polymerase-directed expression of an antibody fragment transgene in plastids causes a semi-lethal pale-green seedling phenotype. *Transgenic Res.* 13, 325–337. doi: 10.1023/b:trag.0000040019.35147.a4

Mayfield, S. P., Franklin, S. E., and Lerner, R. A. (2003). Expression and assembly of a fully active antibody in algae. *Proc. Natl. Acad. Sci. U S A* 100, 438–442. doi: 10.1073/pnas.0237108100

Nakanishi, K., Narimatsu, S., Ichikawa, S., Tobisawa, Y., Kurohane, K., Niwa, Y., et al. (2013). Production of hybrid-IgG/IgA plantibodies with neutralizing activity against Shiga toxin 1. *PLoS One* 8:e80712. doi: 10.1371/journal.pone.0080712

Onda, Y. (2013). Oxidative protein-folding systems in plant cells. *Int. J. Cell Biol.* 2013:585431.

Palmer, T., and Stansfeld, P. (2020). Targeting of proteins to the twin-arginine translocation pathway. *Mol. Microbiol.* 113, 861–871. doi: 10.1111/mmi.14461

Pereira, E. O., Kolotilin, I., Conley, A. J., and Menassa, R. (2014). Production and characterization of in planta transiently produced polygalacturanase from Aspergillus niger and its fusions with hydrophobin or ELP tags. *BMC Biotechnol* 14:59. doi: 10.1186/1472-6750-14-59

PHAC. (2019). *FoodNet Canada Annual Report 2018*. Available Online at: https://www.canada.ca/en/public-health/services/surveillance/foodnet-canada/publications/foodnet-canada-annual-report-2018.html Accessed 21 Mar 2021

Pottosin, I., and Shabala, S. (2016). Transport across chloroplast membranes: optimizing photosynthesis for adverse environmental conditions. *Mol. Plant* 9, 356–370. doi: 10.1016/j.molp.2015.10.006

Ramsland, P. A., Willoughby, N., Trist, H. M., Farrugia, W., Hogarth, P. M., Fraser, J. D., et al. (2007). Structural basis for evasion of IgA immunity by *Staphylococcus aureus* revealed in the complex of SSL7 with Fc of human IgA1. *Proc. Nat. Acad. Sci.* 104, 15051–15056. doi: 10.1073/pnas.0706028104

Ries, F., Herkt, C., and Willmund, F. (2020). Co-translational protein folding and sorting in chloroplasts. *Plants* 9:214. doi: 10.3390/plants9020214

Robinson, C., Matos, C. F., Beck, D., Ren, C., Lawrence, J., Vasisht, N., et al. (2011). Transport and proofreading of proteins by the twin-arginine translocation (Tat) system in bacteria. *Biochim. Biophys. Acta* 1808, 876–884. doi: 10.1016/j.bbamem.2010.11.023

Saberianfar, R., Chin-Fatt, A., Scott, A., Henry, K. A., Topp, E., and Menassa, R. (2019). Plant-produced chimeric V_HH-sIgA against enterohemorrhagic E. coli Intimin shows cross-serotype inhibition of bacterial adhesion to epithelial cells. *Front. Plant Sci.* 10:270. doi: 10.3389/fpls.2019.00270

Schlicher, T., and Soll, J. (1996). Molecular chaperones are present in the thylakoid lumen of pea chloroplasts. *FEBS Lett.* 379, 302–304. doi: 10.1016/0014-5793(95)01534-5

Schmidt, D. J., Beamer, G., Tremblay, J. M., Steele, J. A., Kim, H. B., Wang, Y., et al. (2016). A tetraspecific V_HH-based neutralizing antibody modifies disease outcome in three animal models of clostridium difficile infection. *Clin. Vaccine Immunol.* 23, 774–784. doi: 10.1128/cvi.00730-15

Schubert, M., Petersson, U. A., Haas, B. J., Funk, C., Schroder, W. P., and Kieselbach, T. (2002). Proteome map of the chloroplast lumen of arabidopsis thaliana. *J. Biol. Chem.* 277, 8354–8365. doi: 10.1074/jbc.m108575200

Schürmann, P., and Buchanan, B. B. (2008). The ferredoxin/thioredoxin system of oxygenic photosynthesis. *Antioxid Redox Signal* 10, 1235–1274. doi: 10.1089/ars.2007.1931

Shkoporov, A., Khokhlova, E., Savochkin, K., Kafarskaia, L., and Efimov, B. (2015). Production of biologically active scFv and V_HH antibody fragments in bifidobacterium longum. *FEMS Microbiol. Lett.* 362:fnv083.

Silhavy, D., Molnar, A., Lucioli, A., Szittya, G., Hornyik, C., Tavazza, M., et al. (2002). A viral protein suppresses RNA silencing and binds silencing-generated, 21- to 25-nucleotide double-stranded RNAs. *Embo J.* 21, 3070–3080. doi: 10.1093/emboj/cdf312

Staub, J. M., Garcia, B., Graves, J., Hajdukiewicz, P. T., Hunter, P., Nehra, N., et al. (2000). High-yield production of a human therapeutic protein in tobacco chloroplasts. *Nat. Biotechnol.* 18, 333–338. doi: 10.1038/73796

Takizawa, K., Cruz, J. A., Kanazawa, A., and Kramer, D. M. (2007). The thylakoid proton motive force in vivo. Quantitative, non-invasive probes, energetics, and regulatory consequences of light-induced pmf. *Biochim. Biophys. Acta* 1767, 1233–1244. doi: 10.1016/j.bbabio.2007.07.006

Tissot, G., Canard, H., Nadai, M., Martone, A., Botterman, J., and Dubald, M. (2008). Translocation of aprotinin, a therapeutic protease inhibitor, into the thylakoid lumen of genetically engineered tobacco chloroplasts. *Plant Biotechnol. J.* 6, 309–320. doi: 10.1111/j.1467-7652.2008.00321.x

Trebitsh, T., Meiri, E., Ostersetzer, O., Adam, Z., and Danon, A. (2001). The protein disulfide isomerase-like RB60 is partitioned between stroma and thylakoids in chlamydomonas reinhardtii chloroplasts. *J. Biol. Chem.* 276, 4564–4569. doi: 10.1074/jbc.m005950200

Vasilev, N., Smales, C. M., Schillberg, S., Fischer, R., and Schiermeyer, A. (2016). Developments in the production of mucosal antibodies in plants. *Biotechnol. Adv.* 34, 77–87. doi: 10.1016/j.biotechadv.2015.11.002

Vega, C. G., Bok, M., Vlasova, A. N., Chattha, K. S., Gómez-Sebastián, S., Nuñez, C., et al. (2013). Recombinant monovalent llama-derived antibody fragments (V_HH) to rotavirus VP6 protect neonatal gnotobiotic piglets against human rotavirus-induced diarrhea. *PLoS Pathog.* 9:e1003334. doi: 10.1371/journal.ppat.1003334

Vincke, C., and Muyldermans, S. (2012). Introduction to heavy chain antibodies and derived nanobodies. *Methods Mol. Biol.* 911, 15–26. doi: 10.1007/978-1-61779-968-6_2

Virdi, V., Coddens, A., De Buck, S., Millet, S., Goddeeris, B. M., Cox, E., et al. (2013). Orally fed seeds producing designer IgAs protect weaned piglets against enterotoxigenic *Escherichia coli* infection. *Proc. Natl. Acad. Sci. U S A* 110, 11809–11814. doi: 10.1073/pnas.1301975110

Virdi, V., Palaci, J., Laukens, B., Ryckaert, S., Cox, E., Vanderbeke, E., et al. (2019). Yeast-secreted, dried and food-admixed monomeric IgA prevents gastrointestinal infection in a piglet model. *Nat. Biotechnol.* 37, 527–530. doi: 10.1038/s41587-019-0070-x

Werdan, K., Heldt, H. W., and Milovancev, M. (1975). The role of pH in the regulation of carbon fixation in the chloroplast stroma. Studies on CO2 fixation in the light and dark. *Biochim. Biophys. Acta.* 396, 276–292. doi: 10.1016/0005-2728(75)90041-9

Wesolowski, J., Alzogaray, V., Reyelt, J., Unger, M., Juarez, K., Urrutia, M., et al. (2009). Single domain antibodies: promising experimental and therapeutic tools in infection and immunity. *Med. Microbiol. Immunol.* 198, 157–174. doi: 10.1007/s00430-009-0116-7

Woof, J., and Russell, M. (2011). Structure and function relationships in IgA. *Mucosal. Immunol.* 4, 590–597. doi: 10.1038/mi.2011.39

Xiong, Y., Karuppanan, K., Bernardi, A., Li, Q., Kommineni, V., Dandekar, A. M., et al. (2019). Effects of N-glycosylation on the structure, function, and stability of a plant-made fc-fusion anthrax decoy protein. *Front. Plant Sci.* 10:768. doi: 10.3389/fpls.2019.00768

Conflict of Interest: The authors declare that the research was conducted in the absence of any commercial or financial relationships that could be construed as a potential conflict of interest.

frontiers in Plant Science

ORIGINAL RESEARCH
published: 07 June 2021
doi: 10.3389/fpls.2021.683762

Transient Production of Human β-Glucocerebrosidase With Mannosidic-Type *N*-Glycan Structure in Glycoengineered *Nicotiana benthamiana* Plants

Naphatsamon Uthailak[1], *Hiroyuki Kajiura*[1,2], *Ryo Misaki*[1,2] *and Kazuhito Fujiyama*[1,2,3]*

[1] International Center for Biotechnology, Osaka University, Osaka, Japan, [2] Industrial Biotechnology Initiative Division, Institute for Open and Transdisciplinary Research Initiatives, Osaka University, Osaka, Japan, [3] Cooperative Research Station in Southeast Asia, International Center for Biotechnology, Osaka University, Mahidol University, Bangkok, Thailand

Gaucher disease is an inherited lysosomal storage disorder caused by a deficiency of functional enzyme β-glucocerebrosidase (GCase). Recombinant GCase has been used in enzyme replacement therapy to treat Gaucher disease. Importantly, the terminal mannose *N*-glycan structure is essential for the uptake of recombinant GCase into macrophages via the mannose receptor. In this research, recombinant GCase was produced using *Agrobacterium*-mediated transient expression in both wild-type (WT) and *N*-acetylglucosaminyltransferase I (GnTI) downregulated *Nicotiana benthamiana* (ΔgntI) plants, the latter of which accumulates mannosidic-type *N*-glycan structures. The successfully produced functional GCase exhibited GCase enzyme activity. The enzyme activity was the same as that of the conventional mammalian-derived GCase. Notably, *N*-glycan analysis revealed that a mannosidic-type *N*-glycan structure lacking plant-specific *N*-glycans (β1,2-xylose and α1,3-fucose residues) was predominant in all glycosylation sites of purified GCase produced from ΔgntI plants. Our research provides a promising alternative plant line as a host for the production of recombinant GCase with a mannosidic-type *N*-glycan structure. This glycoengineered plant might be applicable to the production of other pharmaceutical proteins, especially mannose receptor targeted protein, for therapeutic uses.

Keywords: β-glucocerebrosidase, transient expression, *Nicotiana benthamiana*, *N*-glycosylation, plant-made pharmaceuticals, *N*-acetylglucosaminyltransferase I

OPEN ACCESS

Edited by:
Ryo Matsuda,
The University of Tokyo, Japan

Reviewed by:
Richard Strasser,
University of Natural Resources and Life Sciences Vienna, Austria
Kisung Ko,
Chung-Ang University, South Korea

***Correspondence:**
Kazuhito Fujiyama
fujiyama@icb.osaka-u.ac.jp

Specialty section:
This article was submitted to Plant Biotechnology, a section of the journal Frontiers in Plant Science

Received: *22 March 2021*
Accepted: *07 May 2021*
Published: *07 June 2021*

Citation:
Uthailak N, Kajiura H, Misaki R and Fujiyama K (2021) Transient Production of Human β-Glucocerebrosidase With Mannosidic-Type N-Glycan Structure in Glycoengineered Nicotiana benthamiana Plants. Front. Plant Sci. 12:683762. doi: 10.3389/fpls.2021.683762

INTRODUCTION

Gaucher disease, one of the most common lysosomal storage disorders, is caused by the mutation of the *GBA1* gene, resulting in the defective activity of a lysosomal enzyme called glucocerebrosidase (GCase, β-glucosidase; EC: 3.2.1.45). Enzyme replacement therapy (ERT) is the most effective treatment for Gaucher disease type 1; it involves intravenous infusions of exogenous recombinant GCase to patients (Siebert et al., 2014; Stirnemann et al., 2017; Boer et al., 2020). Three drugs are commercially available: Imiglucerase (Cerezyme®, Genzyme Corporation), Velaglucerase alfa (VPRIV®, Shire Plc), and Taliglucerase alfa (Elelyso®, Pfizer). These drugs are recombinant GCases produced in Chinese hamster ovary (CHO) cells, human fibroblasts, and carrot suspension cells, respectively. Moreover, all are glycoproteins containing different *N*-glycan structures (Bennett and Fellner, 2018).

Glycosylation is the enzymatic transfer and attachment of glycans to specific sites on proteins. It is important for certain protein characteristics, including folding, solubility, stability, functionality, half-life, and quality control (Castilho and Steinkellner, 2012; Loos and Steinkellner, 2014; Schoberer and Strasser, 2018; Zhou and Qiu, 2019). Since recombinant GCase is taken up by macrophage via the mannose receptor, the terminal mannose *N*-glycan structure is essential for the translocation of commercial drugs into macrophages (Friedman et al., 1999). For this reason, the *N*-glycan structures of three commercially available GCases have been modified using different approaches in order to possess terminal mannose residues. First, Imiglucerase has been modified by exoglycosidase digestion during the post-production process, whereas mannosidic-type *N*-glycan of Velaglucerase alfa has been achieved by the addition of kifunensine, a mannosidase I inhibitor, into medium. On the other hand, Taliglucerase alfa has been modified by targeting GCase to the vacuole in order to produce the pauci-mannosidic structure (Van Patten et al., 2007; Tekoah et al., 2013; Kallemeijn et al., 2017). Although Imiglucerase is the leading brand, its manufacturing plants were shut down due to viral contamination in 2009, which resulted in a shortage of drugs for ERT (Hollak et al., 2010). Compared to those two drugs, Taliglucerase alfa is free from contamination by human pathogens and does not require post-production modification (Grabowski et al., 2014; Gupta and Pastores, 2017; Zimran et al., 2018). Even though drugs are commercially available, a large amount of recombinant GCase is required for ERT. Recently, administration of an ERT drug at a dosage of 60 Units/kg body weight every 2 weeks costs ∼$128,000 to $544,000 per patient annually. Thus, Gaucher disease drugs have been reported to be among the most expensive drugs available (Joerg et al., 2007; Burnett and Burnett, 2020).

A plant-based expression platform has many advantages for the production of pharmaceutical recombinant proteins, including low cultivation costs, scale-up possibility, complex protein production ability with post-translational modifications, and a low risk of contamination by human pathogens (Paul and Ma, 2011; Moon et al., 2019; Burnett and Burnett, 2020; Shanmugaraj et al., 2020). After Taliglucerase alfa became the first plant-made pharmaceutical approved by the U.S. Food and Drug Administration in 2012, studies on the use of plants for pharmaceutical and non-pharmaceutical recombinant protein production have been increasing (Van Dussen et al., 2013; Tschofen et al., 2016). Many studies have focused on the production of recombinant GCase in plants including *Arabidopsis thaliana* (He et al., 2012), rice suspension culture (Nam et al., 2017; Jung et al., 2019), and *Nicotiana benthamiana* (Limkul et al., 2015, 2016; Naphatsamon et al., 2018). However, some studies did not report the *N*-glycan structure of recombinant GCase (Limkul et al., 2015; Nam et al., 2017), whereas one study revealed the majority of *N*-glycan structure containing residues of plant-specific glycan (β1,2-xylose and α1,3-fucose) (Naphatsamon et al., 2018). Those nonhuman glycosylations have the potential to induce immunogenic responses in human (Gomord et al., 2005, 2010; Montero-Morales and Steinkellner, 2018). *N*-glycan modification is one of the approaches to overcome this problem. Many plant-based glycoengineering studies have focused on the knockdown or knockout of the *N*-acetyltglucosaminyltransferase I (GnTI) gene, leading to mannosidic-type structures and to the absence of plant-specific glycan residues (Strasser, 2014; Limkul et al., 2016; Montero-Morales and Steinkellner, 2018).

Agrobacterium-mediated transient expression (agroin filtration) is widely used to produce large amounts of protein due to its high expression level. It also has other advantages, including effectiveness, low-cost production, time saving and scalability (Moon et al., 2019). Notably, this system is useful for pandemic responses due to rapid gene introduction (Burnett and Burnett, 2020). For instance, the end product of an influenza vaccine was produced within 3 weeks by the Medicago company using plant transient expression (D'Aoust et al., 2010). Compared to other plants, *N. benthamiana* has been widely used for recombinant protein production because of its high biomass and susceptibility to a wide range of plant pathogens, the latter of which is useful for introducing foreign genes (Goodin et al., 2008).

In this study, we developed an alternative system to produce recombinant GCase with mannosidic-type *N*-glycan structure in WT and glycoengineered *N. benthamiana* plants (NbGNTI-RNAi7; ΔgntI) (Limkul et al., 2016) using *Agrobacterium*-mediated transient expression. After purification using two steps of column chromatography, purified recombinant GCase was analyzed by an enzymatic activity assay. The glycan structure of purified recombinant GCase was analyzed at three glycosylated positions. Our work demonstrated that recombinant GCase was successfully produced as an active glycoprotein with a mannosidic-type glycan structure.

MATERIALS AND METHODS

Plants and Growth Conditions

Stable glycoengineered *gntI*-knockdown *N. benthamiana* plants [NbGNTI-RNAi7; ΔgntI) T7 were generated as described previously (Limkul et al., 2016). Seeds of ΔgntI plants were sterilized using PPM solution (Plant Preservative Mixture; Plant Cell Technology, USA) and selected on a Murashige and Skoog (MS) medium agar plate supplemented with hygromycin (30 mg/L). Germinated seedlings were transferred to soil pots and grown at 25°C under a 16 h light and 8 h dark condition for 4 weeks. Seeds of WT *N. benthamiana* were geminated on soil and grown under same condition as described above.

Agrobacterium Strains and Plant Expression Vectors

Agrobacterium tumefaciens strain LBA4404 harboring GCase expression plasmid (pAt-GC-HSP) was constructed previously (Limkul et al., 2015) (**Figure 1A**). A vector for the expression of RNA silencing suppressor 19 (p19) was kindly provided by Prof. Atsushi Takeda (Ritsumeikan University). The p19 vector was transformed into *A. tumefaciens* by electroporation. An *A. tumefaciens* transformant was selected using kanamycin (50 mg/L), rifampicin (50 mg/L), and streptomycin (50 mg/L).

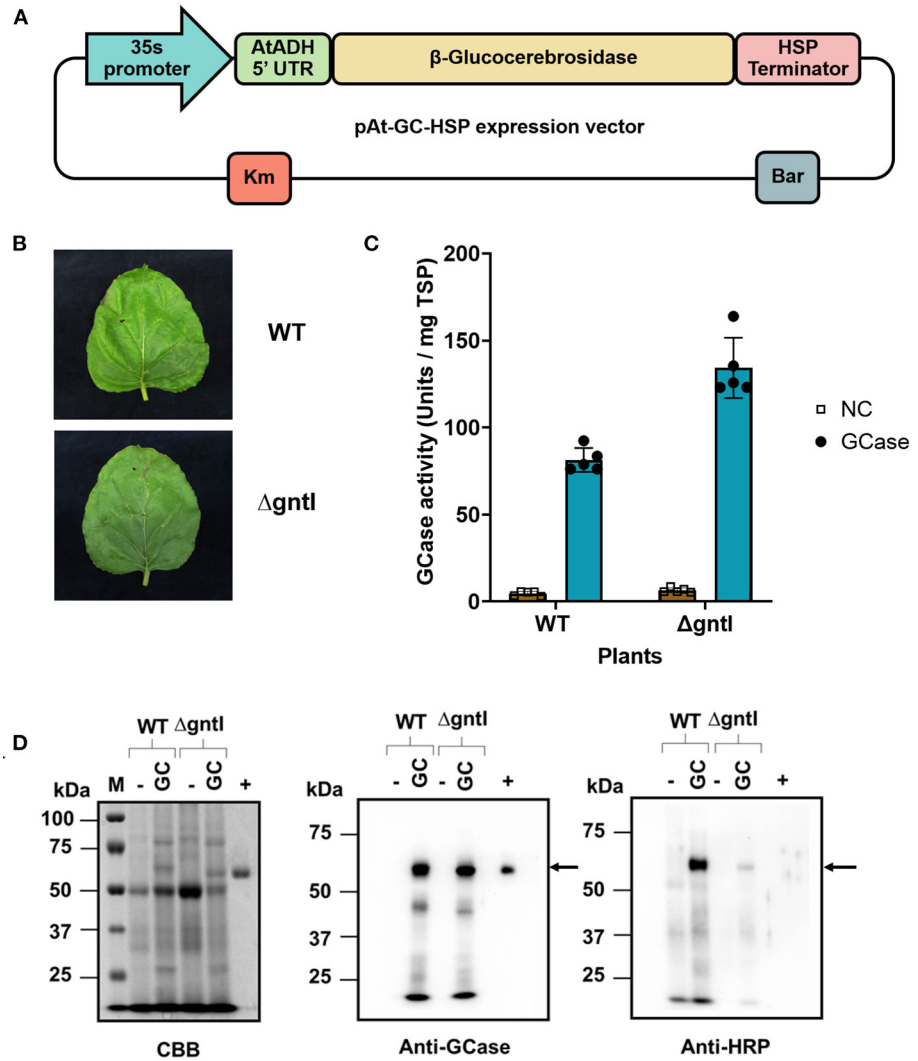

FIGURE 1 | Transient production of recombinant GCase in wild-type (WT) and ΔgntI *N. benthamiana* plants. **(A)** The pAt-GC-HSP expression vector. 35S promoter: Cauliflower mosaic virus 35S RNA promoter; AtADH 5'UTR: 5'-UTR of *Arabidopsis* alcohol dehydrogenase (AtADH) gene; β-Glucocerebrosidase: β-glucocerebrosidase gene; HSP terminator: Transcription terminator from *A. thaliana* heat shock protein; Bar: bialaphos resistance gene; Km: Kanamycin resistance gene. **(B)** Infiltrated leaves and **(C)** GCase activity of crude protein from infiltrated WT and ΔgntI leaves at 7 days post-infiltration. NC: non-infiltrated leaves (negative control). The experiment was performed in five replications. Error bars represent the standard deviation (SD). **(D)** Total soluble protein: 10, 5, and 1 μg were loaded and analyzed by Coomassie Brilliant Blue (CBB) staining, anti-GCase blotting, and anti-HRP blotting, respectively. M, Precision Plus Protein standards marker; WT, wild-type *N. benthamiana*; ΔgntI, *gntI*-knockdown *N. benthamiana*; (-), non-infiltrated leaves (negative control); (+), Cerezyme®, a commercial GCase produced in Chinese Hamster Ovary (CHO) cells. Arrows represent the GCase band.

Agrobacterium-Mediated Transient Expression

A single colony of *Agrobacterium* was inoculated into 2xYT liquid medium supplemented with the appropriate antibiotics and cultivated at 28°C overnight. Two milliliters of culture was inoculated into 2xYT liquid medium (200 ml) supplemented with the same antibiotics and cultivated at 28°C overnight. Cells were collected by centrifugation at 4,000 × *g*. *Agrobacterium* containing different vectors (GCase or p19) was resuspended and mixed at a 1:1 ratio in infiltration buffer (10 mM MES, 10 mM $MgSO_4$, 100 μM acetosyringone, pH 5.5) with OD_{600} of 0.5. The *Agrobacterium* mixture was incubated at room temperature for 2–4 h. Both WT and ΔgntI *N. benthamiana* plants were infiltrated using vacuum infiltration (Chen et al., 2013). Infiltrated plants were grown at 25°C under 16 h light and 8 h dark condition for 1 week.

Optimization of Vacuum Infiltration

Agrobacterium culture and infiltration buffer were prepared as described above. For OD_{600} optimization, 4-week-old *N. benthamiana* plants were infiltrated in the *Agrobacterium* mixture with different OD_{600} values: 0, 0.25, 0.50, 0.75, and 1.0. Infiltrated plants were grown at 25°C under 16 h light and 8 h dark condition. Agroinfiltrated leaves were collected at 7

days post-infiltration (dpi). For the optimization of harvest time, *N. benthamiana* plants were infiltrated with the *Agrobacterium* mixture as described above ($OD_{600} = 0.5$). Agroinfiltrated leaves were collected at 5, 6, 7, and 8 days post-infiltration (dpi).

Protein Extraction From Agroinfiltrated Leaves

The protein extraction method was modified from a previous study (Limkul et al., 2015). Briefly, leaves were homogenized by grinding with liquid nitrogen. Leaf powders were suspended in GCase extraction buffer (20 mM Tris-HCl pH 7.0, 150 mM NaCl, 0.5% taurocholic acid, and ethylenediaminetetraacetic acid (EDTA)-free Protease Inhibitor Cocktail (Roche Diagnostics GmbH, Germany) and centrifuged at 12,000 × *g* for 15 min. The supernatant was collected and analyzed by a GCase activity assay, a Bradford assay, SDS-PAGE, and Western blotting, as described below.

GCase Activity Assay

The enzyme activity assay was performed as described previously (Limkul et al., 2015). Briefly, crude extract was co-incubated with GCase assay buffer (60 mM phosphate-citrate buffer pH 6.0, 4 mM β-mercaptoethanol, 1.3 mM EDTA, 0.15% Triton X-100, 0.125% taurocholic acid) and 0.2 mM of 4-methylumbelliferyl β-D-glucopyranoside (4-MUG; Wako, Japan) at 37°C for 1 h. The enzymatic reaction was terminated using cold glycine stop buffer (0.2 M glycine, 0.125 M sodium carbonate, pH 10.7). The fluorescence of the product, 4-methylumbelliferone (4-MU; Wako), was detected using an F-25000 fluorescence spectrophotometer (Hitachi High-Technologies, Japan) at $\lambda_{ex} =$ 365 nm and $\lambda_{em} = 460$ nm. The amount of reaction product from the GCase activity assay was calculated using the 4-MU standard curve. An enzyme unit was defined as the amount of enzyme used to release 1 nmol of 4-MU/min. GCase enzyme activity was calculated by Units/mg of total soluble protein (TSP).

SDS-PAGE and Western Blot Analysis

Crude extracted protein of agroinfiltrated leaves was separated by 10% sodium dodecyl sulfate-polyacrylamide gel electrophoresis (SDS-PAGE). Proteins were stained using Coomassie Brilliant Blue (CBB) following the manufacturer's instructions (Ready to Use; Nacalai Tesque, Japan). For Western blot analysis, proteins in polyacrylamide gel were transferred to a polyvinylidene difluoride (PVDF) membrane (Millipore, USA). The membrane was incubated with skim milk (5%) in PBS-T (1.47 mM KH_2PO_4, 10 mM Na_2HPO_4, 2.7 mM KCl, 137 mM NaCl, 0.05% Tween-20, pH 7.4) at room temperature for 1 h. Then it was further incubated with 1:5,000 diluted polyclonal anti-glucocerebrosidase (GCase) antibody from rabbit (Sigma-Aldrich, USA) or polyclonal anti-horseradish peroxidase from rabbit (Sigma-Aldrich) with 1:12,500 dilution at 25°C for 1 h. The membrane was washed with PBS-T and further incubated with the 1:5,000 diluted anti-rabbit IgG, HRP-linked whole antibody (GE Healthcare, Japan) at 25°C for 1 h. After washing with PBS-T, proteins were detected by incubation with Luminata™ (Millipore) at room temperature for 5 min using the iBright Imaging System (Invitrogen, USA).

GCase Purification From Agroinfiltrated Leaves

Purification was performed as described previously (Limkul et al., 2016). Agroinfiltrated leaves were homogenized by grinding with liquid nitrogen. Leaf powders were suspended in GCase extraction buffer and incubated on ice for 20 min. Crude extracts were collected using centrifugation (10,000 x *g* for 20 min) and loaded into a Concanavalin (Con A)- Agarose column (Vector Laboratories, USA) using a peristaltic pump (Perista Pump SJ-1211; ATTO, Japan) with a recycling system at 4°C for 12 h. The column was washed with Con A buffer (500 mM NaCl, 1 mM $MgCl_2$, 1 mM $MnCl_2$, 1 mM $CaCl_2$ in 20 mM Tris-HCl pH 7.0). Proteins were eluted with GCase assay buffer containing 300 mM α-methyl-D-mannoside (Nacalai Tesque). Each eluted fraction was analyzed by a GCase enzymatic assay. All eluted fractions with GCase activity were collected and resuspended in 2 M NaCl. Protein solution was loaded onto a Phenyl 650M column (Tosoh, Japan). Proteins were eluted by decreasing the NaCl concentration. Each elution fraction was analyzed using the GCase enzyme assay. Active fractions were dialyzed and concentrated using an Amicon® Ultra centrifugal filter (Millipore). Concentrated protein was analyzed by the GCase activity assay, Bradford assay, SDS-PAGE, and Western blotting.

N-Glycan Analysis of Purified GCase

Purified GCase from agroinfiltrated leaves was used for *N*-glycan analysis as described previously (Limkul et al., 2016). The purified GCase was separated using SDS-PAGE and stained by PageBlue protein stain solution (Thermo Fisher Scientific, USA). In-gel digestion was performed as follows: GCase bands were de-stained using 1:1 v/v of acetonitrile and 50 mM NH_4HCO_3 at room temperature overnight. The proteins were then digested with Trypsin Gold (Promega, USA) in ProteaseMAX™ surfactant solution (Promega) at 50°C for 1 h. The reaction was terminated by 1% trifluoroacetic acid in 60% acetonitrile. Peptides were extracted from gel and evaporated at 30°C for 3 h. Peptides were dissolved in 0.1% formic acid and applied to an ESI-Qq-TOF mass spectrometer (microTOF-Q II, Bruker Daltonics, Germany). The conditions used for *N*-glycan analysis were as described previously (Limkul et al., 2016). Briefly, a nano-LC system (120 series; Agilent Technologies) was used with a trap column (5 μ, 0.3 × 5 mm) and an analytical column (3.5 μ, 0.075 x 150 mm). Both 0.1% formic acid in water and 0.1 % formic acid in acetonitrile were used as the mobile phase. Peptides were trapped in the trapped column and eluted at a flow rate of 0.6 μL/min. The system was completely controlled by microTOF control software (Bruker Daltonics). *N*-Glycan structures were analyzed using DataAnalysis version 4.0 (Bruker Daltonics) with both MS and MS/MS modes.

RESULTS

Transient Production of Recombinant GCase in WT and ΔgntI *N. benthamiana* Plants

To produce recombinant GCase in *N. benthamiana* plants, 4-week-old plants were infiltrated with *Agrobacterium* mixture

harboring GCase and p19 vectors at an OD_{600} of 0.5. At 7 days post-infiltration, leaf samples were collected for protein extraction and crude proteins were further analyzed using an enzymatic assay and protein blotting.

After infiltration, no necrosis was observed from the infiltrated WT or ΔgntI leaves (**Figure 1B**). The enzymatic assay detected GCase activity from crude protein of both plants (**Figure 1C**). The GCase produced in ΔgntI plants showed higher GCase activity (134.3 ± 17.3 U/mg TSP) than that produced in WT plants (81.5 ± 6.9 U/mg TSP). On the other hand, non-infiltrated WT and ΔgntI leaves (negative control) showed low GCase activity (4.7 ± 1.3 and 6.5 ± 1.4 U/mg TSP in WT and ΔgntI plants, respectively). The GCase activity detected in the negative control was considered as an effect of plant-produced β-glucosidase (Seshadri et al., 2009; Pankoke et al., 2013). Crude proteins were further analyzed by CBB staining and Western blotting compared to Cerezyme®, a commercial GCase produced in CHO cells as a positive control (**Figure 1D**). A GCase band was detected using anti-GCase antibody from crude protein extracted from agroinfiltrated WT and ΔgntI leaves with a molecular weight of ∼58 kDa. On the other hand, no GCase band was detected from the negative control. Additionally, plant-specific glycans were determined using anti-HRP antibody blotting. Anti-HRP antibody binds to plant specific *N*-glycan residues, including β1,2-xylose and α1,3-fucose residues (Jin et al., 2008; Iskratsch et al., 2009; Paschinger et al., 2009). In this work, higher-intensity bands were detected from crude protein produced in WT plants than that of ΔgntI plants using anti-HRP antibody. This implies that the GCase produced from ΔgntI plants contains less plant specific glycan residues compared to GCase produced from WT plants. These results indicated that the functional recombinant GCase was successfully produced in both WT and ΔgntI plants. Furthermore, ΔgntI-infiltrated leaves had fewer plant-specific *N*-glycan structures than WT leaves.

Optimization of Infiltration Condition for Transient GCase Production

To obtain a large amount of recombinant GCase, infiltration conditions, including the optical density (OD_{600}) of *Agrobacterium* mixture and the harvest time, were optimized in this study. WT and ΔgntI plants were infiltrated using the *Agrobacterium* mixture with different OD_{600} values: 0.25, 0.50, 0.75, and 1.0. Leaf samples were collected at 7 days post-infiltration.

Crude extracted at an OD_{600} of 0.50 showed the highest GCase activity in both WT and ΔgntI plants (108.5 ± 27.9 and 139.5 ± 19.7 U/mg TSP, respectively), followed by that extracted at an OD_{600} of 0.75 (**Figure 2A**). However, the difference was not significant. Regarding the Western blotting result, OD_{600} values of 0.50 and 0.75 revealed higher intensities of GCase bands compared to OD_{600} values of 0.25 and 1.0 (**Figure 2B**). Because it had the highest GCase activity, OD_{600} of 0.5 was chosen as the optical density for GCase production. At harvest time, infiltrated leaf samples were collected at 5, 6, 7, and 8 days post-infiltration (dpi). The highest GCase activity was observed at 7 dpi in both WT (149.7 ± 14.5 U/mg TSP) and ΔgntI (153.6 ± 17.2 U/mg TSP) plants (**Figure 2C**). Additionally, GCase bands detected in anti-GCase blotting at 5 and 8 dpi showed lower intensities compared to those at 6 and 7 dpi (**Figure 2D**). Therefore, 7 dpi was chosen as the collection day for GCase purification.

GCase Purification From Infiltrated WT and ΔgntI Leaves

Two types of column chromatography were used for GCase purification: Concanavalin (Con A) affinity chromatography and phenyl hydrophobic (P650M) chromatography. The binding between Con A and mannose residues of *N*-glycan structure have been reported (Maupin et al., 2012). After purification, GCases from infiltrated WT and ΔgntI leaves were analyzed using the enzymatic assay and protein blotting.

With the infiltrated WT leaves, purified GCase bands were detected from P650M elution fractions 6 and 7 on CBB staining and Western blotting (**Figure 3A**). The GCase band was ∼58 kDa, which corresponded to the size of the positive control, Cerezyme®. Additionally, no band was detected from the negative control, crude protein extracted from non-infiltrated leaves. The specific enzyme activity was measured using GCase activity assay. Purified GCase hydrolyzed the substrate, 4-MUG to glucose and 4-MU which was detected using a fluorescence spectrophotometer. The 4-MU standard curve was used to calculate the amount of purified GCase. The GCase-specific activities of purified GCase from eluted fractions 6 and 7 were ∼3301.1 ± 48.4 and 1360.7 ± 8.9 U/mg TSP, respectively (**Figure 3B**). As expected, the GCase-specific activities of both eluted fractions were higher than that of crude protein (149.4 ± 18.3 U/mg TSP). The amounts of purified GCase from infiltrated WT leaves were ∼5.4 μg and 2.7 μg in eluted fractions 6 and 7, respectively. The productivity of purified GCase was about 0.45 μg/g of fresh leaves.

On the other hand, purified GCase from infiltrated ΔgntI leaves was detected from P650M eluted fractions 6 and 7. The specific activities of purified GCase from eluted fractions 6 and 7 were 2001.7 ± 7.7 and 1,000.0 ± 13.8 U/mg TSP, respectively (**Figure 3C**). These numbers are much higher than that from the crude protein (84.7 ± 3.2 U/mg TSP). Additionally, a purified GCase band from eluted fraction 6 was detected on CBB staining and Western blotting compared to the positive control (**Figure 3D**). Different amounts of purified GCase from infiltrated ΔgntI leaves were determined from eluted fractions 6 and 7 (9.8 and 17.4 μg, respectively) with an approximate productivity of 2.6 μg/g of fresh leaves.

N-Glycan Analysis of Purified GCase From Infiltrated Leaves

To analyze the *N*-glycan structures of purified GCase from both WT and ΔgntI samples, trypsin-digested glycopeptides were analyzed using nanoLC-MS/MS.

Three *N*-glycosylation sites (N270, N146, and N59) were detected in purified GCase from both WT and ΔgntI plants (**Figure 4**). All possible *N*-glycan structures of each position were analyzed from deconvoluted MS spectra (**Supplementary Figures 1–4**). The composition percentage

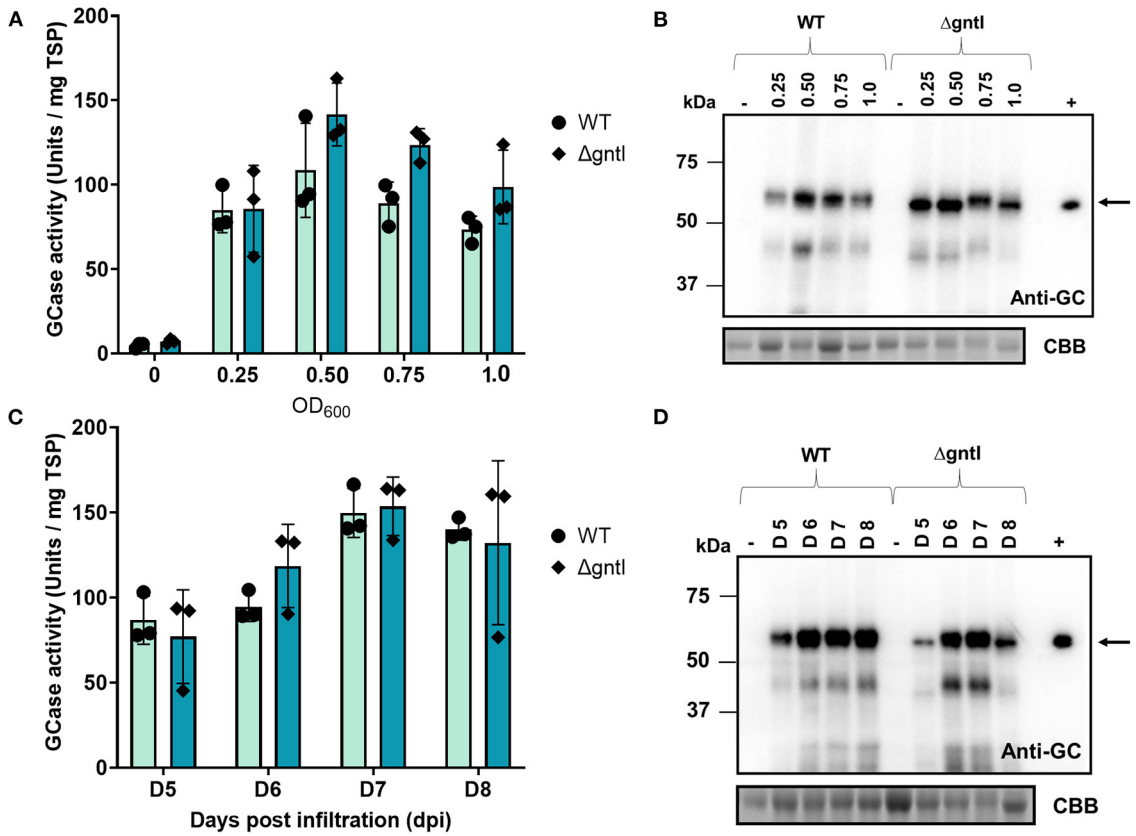

FIGURE 2 | Optimization of GCase transient production. GCase activity of crude protein from wild-type (WT) and ΔgntI leaves infiltrated with **(A)** different OD_{600} values and **(C)** different days post-infiltration. Total soluble proteins: 5 and 10 μg were loaded and analyzed using anti-GCase antibody and CBB staining, respectively **(B,D)**. Error bars represent the standard deviation (SD). The experiment was performed in three replications. (-), negative control from non-infiltrated leaves; (+), Cerezyme®; WT, wild-type *N. benthamiana*; ΔgntI, glycoengineered *N. benthamiana*.

at each *N*-glycosylation site was also summarized (**Table 1**). In the case of WT GCase, GN2M3XF was the predominant structure at positions 59, 146 and 270 with percentages of 29.7%, 63.0%, and 38.2%, respectively. Additionally, GCase at positions N270 (100%), N146 (100%), and N59 (100%) was a *N*-glycosylated with at least one plant-specific *N*-glycans (β1,2-xylose and/or α1,3-fucose residues). On the other hand, Man5 was detected as the predominant structure at the N59 (89.2%), N146 (85%), and N270 (73.0%) positions in ΔgntI GCase. Additionally, the mannosidic-type structure without plant-specific glycan predominated in all positions, including N59 (100%), N146 (100%), and N270 (100%). These results demonstrated that recombinant GCase was successfully produced in ΔgntI plants with mannosidic-type *N*-glycan structures.

DISCUSSION

A large amount of recombinant GCase is required for the ERT treatment of Gaucher disease type 1 (Burnett and Burnett, 2020). Since exogenous GCase is translocated into macrophages via the mannose receptor, the mannose terminal *N*-glycan structure is essential for recombinant GCase (Friedman et al., 1999). In this work, we investigated the impact of *gntI*-downregulated *N. benthamiana* plants (ΔgntI) as a host for the transient expression of recombinant GCase with a mannosidic-type *N*-glycan structure.

Our results demonstrated that recombinant GCase was successfully produced in WT and ΔgntI *N. benthamiana* plants (**Figure 1**). Since *Agrobacterium*-infiltration conditions usually affect the transformation efficiency, resulting in different expression levels of recombinant protein (Hanittinan et al., 2020), two main factors, *Agrobacterium* cell density and harvest time, were optimized to produce a large amount of GCase with biological activity. Previous studies demonstrated that too low cell density might lead to insufficient *Agrobacterium* infection, whereas too high density may cause necrosis (Kagale et al., 2012; Leuzinger et al., 2013; Yan et al., 2019). Additionally, the harvesting time also affects the necrosis and amount of protein production (Kim et al., 2021). Our work revealed that the *Agrobacterium* cell density (OD_{600}) of 0.5 and the harvest time of 7 dpi were the optimal conditions for GCase transient production, as they resulted in the highest GCase enzyme activity in both WT and ΔgntI-infiltrated leaves (**Figure 2**). Notably, the crude GCase activity in our work was higher than in previous

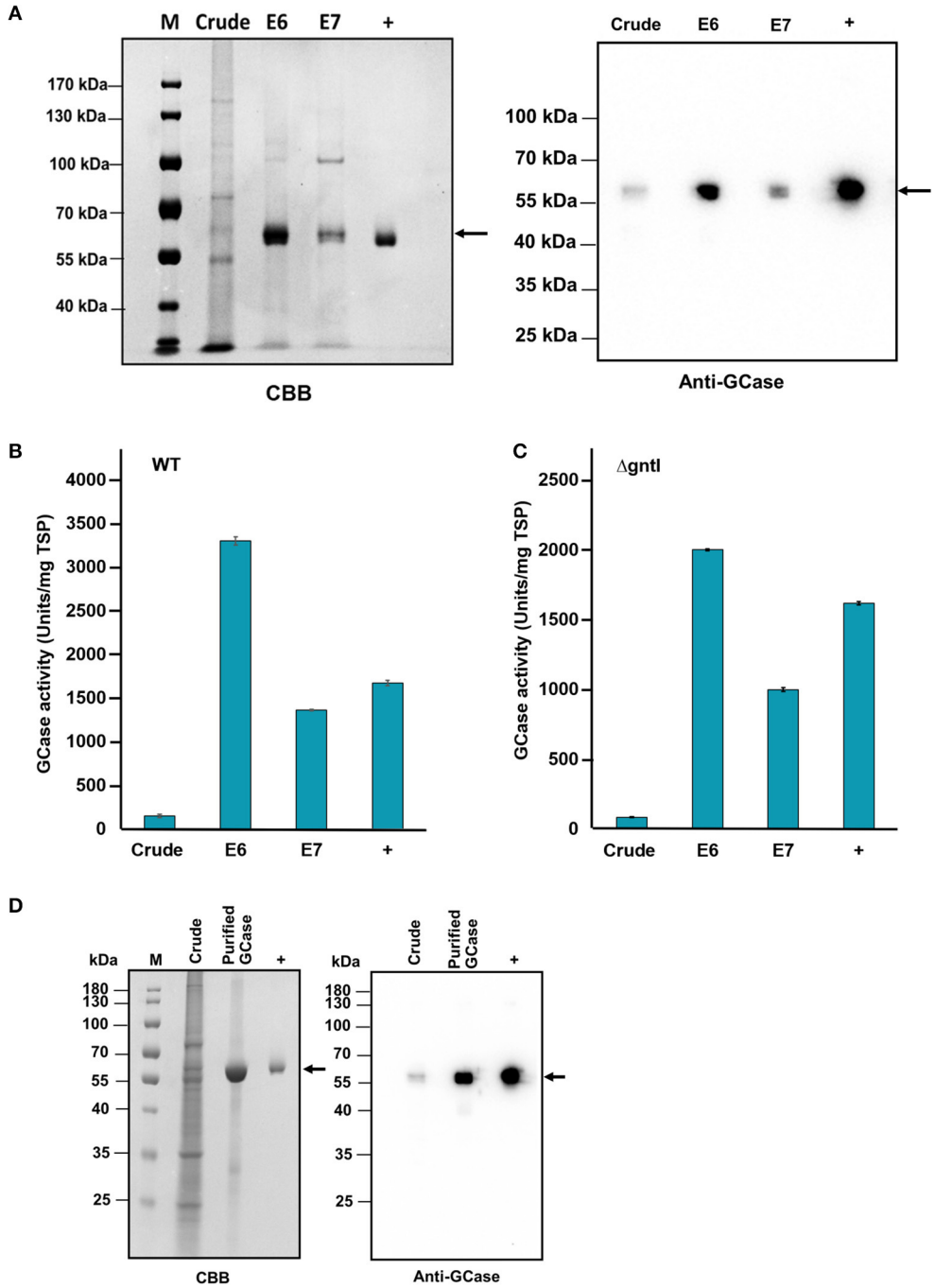

FIGURE 3 | GCase purification from infiltrated wild-type (WT) and ΔgntI *N. benthamiana* leaves. **(A)** Total proteins from infiltrated WT leaves (E6 and E7); 2.5 μg and 100 ng were loaded and analyzed by CBB staining and Western blotting, respectively. **(B)** GCase activity of crude protein and purified GCase from infiltrated WT leaves: elution fractions 6 and 7. Error bars represent the standard deviation (SD) ($N = 3$). **(C)** GCase activity levels of crude protein and purified GCase from infiltrated ΔgntI leaves: elution fractions 6 and 7 (E6 and E7). Error bars represent the standard deviation (SD) ($N = 3$). **(D)** CBB staining and Western blot analysis of crude protein and purified GCase from infiltrated ΔgntI leaves elution fraction 6. M, PageRuler™ protein ladder; Crude, crude protein; Purified GCase, purified GCase from Phenyl 650M elution fractions 6 (E6); +, Cerezyme®.

studies: 65.5 U/mg TSP (Limkul et al., 2016), 24 U/mg TSP (He et al., 2012), 44.5 U/mg TSP (Limkul et al., 2015), and 81.4 U/mg TSP (Naphatsamon et al., 2018). On the other hand, the low GCase activity observed in the negative control was attributed to internal β-glucosidases produced in plants, which plays important roles in plant defense systems. This enzyme is

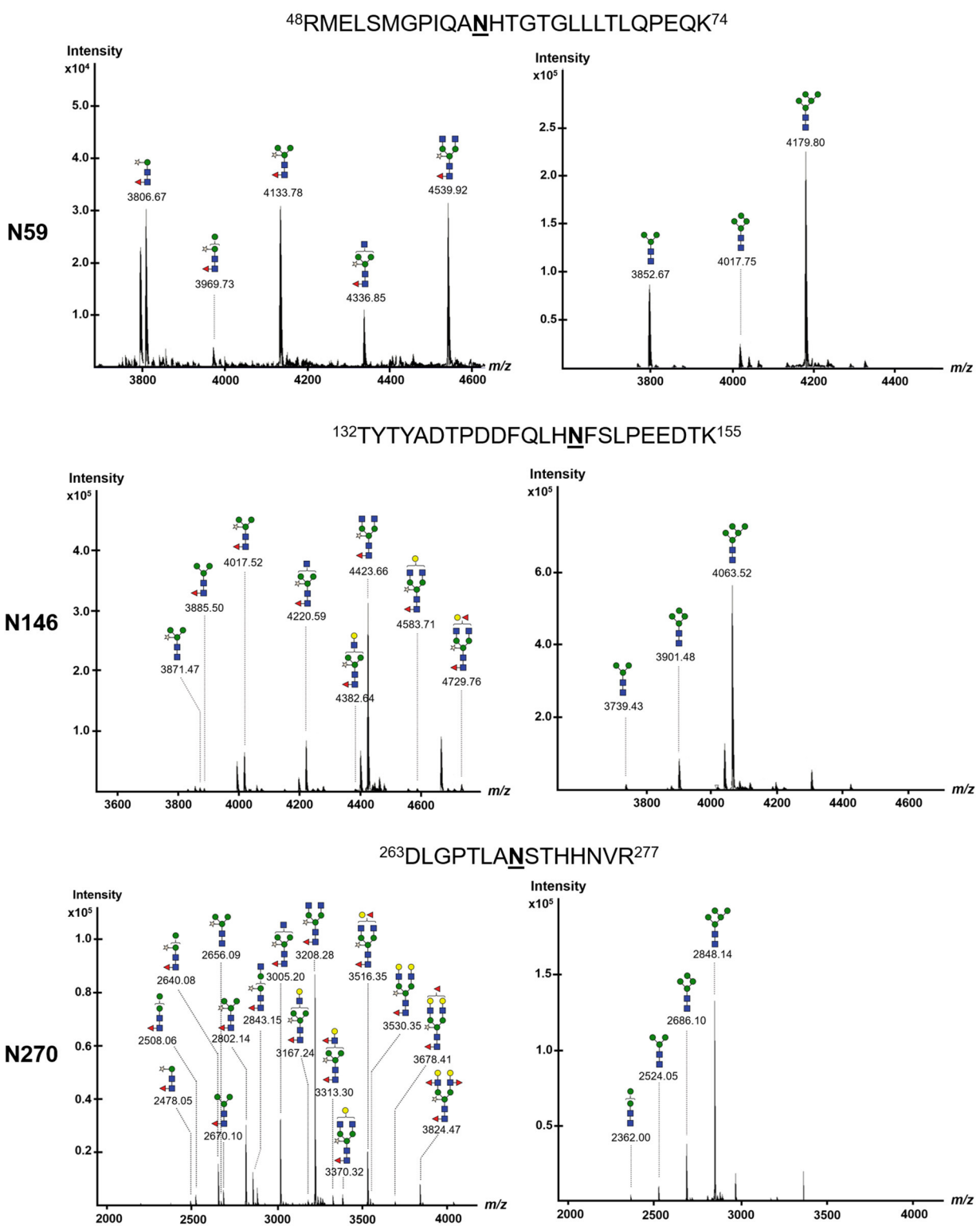

FIGURE 4 | Nano LC–MS spectra of glycopeptides derived from purified GCase produced in wild-type (WT) and ΔgntI-infiltrated leaves. Glycan structures of glycopeptides are shown at different *N*-glycosylation sites (N59, N146, and N270).

TABLE 1 | Composition of *N*-glycan structures on purified GCases from wild type and ΔgntI agroinfiltrated plants at three *N*-glycosylation sites (N59, N146, and N270).

Abbreviation	Structure	Amount of composition (%)					
		N59		N146		N270	
		WT	ΔgntI	WT	ΔgntI	WT	ΔgntI
MXF	ManXylFuc	28.0	0	0	0	0.7	0
M2F	Man2Fuc	0	0	0	0	1.6	0
M2XF	Man2XylFuc	3.6	0	0	0	5.9	0
M3X	Man3Xyl	0	0	1.3	0	0.7	0
M3F	Man3Fuc	0	0	1.0	0	2.4	0
M3XF	Man3XylFuc	28.5	0	13.3	0	13.1	0
GNM2XF	GlcNAcMan2XylFuc	0	0	0	0	5.3	0
GNM3XF	GlcNAcMan3XylFuc	10.2	0	17.3	0	14.0	0
GAGNM3XF	GalGlcNAcMan3XylFuc	0	0	0.8	0	0.9	0
GN2M3XF	GlcNAc2Man3XylFuc	29.7	0	63.0	0	38.2	0
GAFGNM3XF	GalFucGlcNAcMan3XylFuc	0	0	0	0	1.6	0
GAGN2M3XF	GalGlcNAc2Man3XylFuc	0	0	0.9	0	1.8	0
GAFGN2M3XF	GalFucGlcNAc2Man3XylFuc	0	0	2.4	0	8.7	0
GA2GN2M3XF	Gal2GlcNAc2Man3XylFuc	0	0	0	0	1.1	0
GA2FGN2M3XF	Gal2FucGlcNAc2Man3XylFuc	0	0	0	0	0.6	0
GA2F2GN2M3XF	Gal2Fuc2GlcNAc2Man3XylFuc	0	0	0	0	3.4	0
Plant-type structure (%)		**100**	**0**	**100**	**0**	**100**	**0**
M2	Man2	0	0	0	0	0	1.9
M3	Man3	0	1.0	0	2.0	0	4.9
M4	Man4	0	9.8	0	13.0	0	20.2
M5	Man5	0	89.2	0	85.0	0	73.0
Mannosidic-type structure (%)		**0**	**100**	**0**	**100**	**0**	**100**

also related to plant physiology, including cell wall degradation and to the activation of both phytohormones and chemical compounds (Morant et al., 2008; Pankoke et al., 2013). Internal β-glucosidases were also reported previously (Naphatsamon et al., 2018). Our results indicated that this system has the potential to be competitive for recombinant GCase production with high levels of biological activity.

Two different GCase purification strategies have been reported: hexa histidine-tag (His-tag) and a three-step purification method (Nam et al., 2017; Jung et al., 2019). However, the removal of his-tag and the multiple steps required for purification may increase the production cost. In this study, recombinant GCase was successfully purified as a single band using two types of column chromatography (Con A and P650M columns) adapted from our current works (Limkul et al., 2015, 2016; Naphatsamon et al., 2018) (**Figure 3**). The specific activity levels of purified GCase from infiltrated WT and ΔgntI leaves are competitive with those of the recombinant GCase produced in WT transgenic *N. benthamiana* plants (2641 U/mg TSP) and *N. benthamiana* root culture (1618 U/mg TSP) from previous studies (Limkul et al., 2015; Naphatsamon et al., 2018). Although recombinant GCase produced in stable glycoengineered *N. benthamiana* revealed higher specific activity (3063 U/ mg TSP) (Limkul et al., 2016), our recombinant GCase had a higher composition of the mannose terminal *N*-glycan structure, which we discuss below.

Three commercially available recombinant GCases have been approved for the ERT treatment of Gaucher disease type I. The drugs are administered to patients by IV infusions and taken up into macrophages via the mannose receptor (Stirnemann et al., 2017). Moreover, GCase is translocated into lysosome using a lysosomal membrane protein called LIMP-2 (Zhao et al., 2014). It has been demonstrated that the mannose terminal *N*-glycan structure is essential for the macrophage uptake of ERT drugs (Van Patten et al., 2007). Therefore, the present study aimed to produce recombinant GCase with a mannosidic terminal structure and few plant-specific *N*-glycans. Our method relies on the knockdown of the *gntI* gene encoding the key enzyme for the mannose-5 terminal *N*-glycan structure (Strasser, 2014; Montero-Morales and Steinkellner, 2018; Amann et al., 2019). Analysis of the *N*-glycan composition of purified GCase from ΔgntI plants revealed that the mannose-5 terminal (Man5) structure predominated in all glycosylation sites: N59, N146, and N270 (**Figure 4** and **Table 1**). Notably, these percentages of mannosidic-type *N*-glycan structure without plant-specific glycans were higher than those of the purified GCase produced from stable glycoengineered *N. benthamiana* (ranging from 73.3 to 85.5%) and *A. thaliana* complex-glycan-deficient (*cgl*) seeds (85%) in previous studies (He et al., 2012; Limkul et al., 2016). Additionally, the diverse structure and different degree of *N*-glycosylation at N59, N146, and N270 sites were considered to be a microheterogeneity caused by the inefficient enzymatic

pathways of the glycoprotein biosynthesis (Zacchi and Schulz, 2016). These results indicated that our ΔgntI *N. benthamiana* plants have the potential to produce recombinant GCase with a mannosidic-type *N*-glycan structure without plant-specific *N*-glycans.

In our previous study, recombinant GCase was produced in the stable transgenic *N. benthamiana* plant (Limkul et al., 2016). Compared to the stable expression, our transient expression system provided ∼2.3-fold higher crude GCase activity. The increase of crude GCase activity resulted from *Agrobacterium*-mediated transient expression which is more efficient than that of stable expression by the gene integration (Burnett and Burnett, 2020). Additionally, the *N*-glycan structures of purified GCase produced from both stable and transient expression systems were different.

In the case of WT plants, the predominant *N*-glycan structure of purified GCase from stable and transient plants were M3XF and GN2M3XF, respectively. The high amount of GN2M3XF structure may be caused by the rapid production in transient system. In general, two terminal GlcNAc residues of the GN2M3XF structure are cleaved by plant β-hexosaminidases (HEXOs), resulting in the M3XF structure (Altmann et al., 1995; Bosch et al., 2013). In this work, the recombinant GCase was transiently produced in a short time. Therefore, cellular stress may have been induced and HEXOs activity may not have been sufficient to completely convert the GN2M3XF into the M3XF structure. Additionally, the GA2F2GN2M3XF structure was found only in purified GCase produced in transient system, corresponding with previous report on the structures of secreted glycoprotein mostly found in the apoplast (Bosch et al., 2013).

In the case of ΔgntI plants, GCase produced through transient expression had mannosidic structures only (100%). On the other hand, some plant-type structures were remained in the purified GCase from the stable expression (ranging from 14.5 to 26.7%). Therefore, the transient expression in ΔgntI plants has a higher potential to produce recombinant GCase with mannosidic *N*-glycan structures.

Furthermore, this plant can be applied as a host for the production of other pharmaceutical proteins, especially mannose-targeted proteins, for therapeutic uses. The interaction between glycosylated proteins and carbohydrate-binding proteins (lectins) is important for cellular recognition processes, including cellular migration, enzyme trafficking, and immunogenic function (Irache et al., 2008). Several mannosylated structures have been considered as promising devices for drug delivery or vaccination due to their ability to bind the mannose receptor, which is highly expressed on the surfaces of immune cells such as macrophages and dendritic cells (Keler et al., 2004).

CONCLUSION

Our study demonstrated that the ΔgntI *N. benthamiana* plant can be used for the transient production of recombinant GCase with a mannosidic-type *N*-glycan structure. Furthermore, this glycoengineered plant-based transient expression system has potential as an alternative platform for the production of other recombinant therapeutic proteins. This plant is also potentially useful for therapeutic uses during pandemics and outbreaks by virtue of to their rapid response.

DATA AVAILABILITY STATEMENT

The raw data supporting the conclusions of this article will be made available by the authors, without undue reservation.

AUTHOR CONTRIBUTIONS

KF supervised and conceived the original idea of this work. NU designed and performed the experiments with technical support from HK and wrote the manuscript with support from KF, HK, and RM. All authors approved the final manuscript.

FUNDING

The research was supported by the Ministry of Education, Culture, Sports, science, and technology (MEXT).

ACKNOWLEDGMENTS

We gratefully thank Dr. Juthamard Limkul for the generation of stable glycoengineered gntI-knockdown *N. benthamiana* plants (NbGNTI-RNAi7) used in this study. We are grateful to Prof. Atsushi Takeda from Ritsumeikan University for providing the RNA silencing suppressor 19 (p19) vector.

SUPPLEMENTARY MATERIAL

The Supplementary Material for this article can be found online at: https://www.frontiersin.org/articles/10.3389/fpls.2021.683762/full#supplementary-material

REFERENCES

Altmann, F., Schwihla, H., Staudacher, E., Glössl, J., and März, L. (1995). Insect cells contain an unusual, membrane-bound beta-*N*-acetylglucosaminidase probably involved in the processing of protein *N*-glycans. *J. Biol. Chem.* 270, 17344–17349. doi: 10.1074/jbc.270.29.17344

Amann, T., Schmieder, V., Faustrup Kildegaard, H., Borth, N., and Andersen, M. R. (2019). Genetic engineering approaches to improve posttranslational modification of biopharmaceuticals in different production platforms. *Biotechnol. Bioeng.* 116, 2778–2796. doi: 10.1002/bit.27101

Bennett, L. L., and Fellner, C. (2018). Pharmacotherapy of Gaucher disease: current and future options. *Pharmacol. Ther.* 43, 274–309.

Boer, D. E. C., van Smeden, J., Bouwstra, J. A., and Aerts, J. M. F. G. (2020). Glucocerebrosidase: functions in and beyond the lysosome. *J. Clin. Med.* 9:736. doi: 10.3390/jcm9030736

Bosch, D., Castilho, A., Loos, A., Schots, A., and Steinkellner, H. (2013). *N*-glycosylation of plant-produced recombinant proteins.

Curr. Pharm. Des. 19, 5503–5512. doi: 10.2174/13816128113193 10006

Burnett, M. J. B., and Burnett, A. C. (2020). Therapeutic recombinant protein production in plants: challenges and opportunities. *Plants People Planet*. 2, 121–132. doi: 10.1002/ppp3.10073

Castilho, A., and Steinkellner, H. (2012). Glyco-engineering in plants to produce human-like *N*-glycan structures. *Biotechnol. J.* 7, 1088–1098. doi: 10.1002/biot.201200032

Chen, Q., Lai, H., Hurtado, J., Stahnke, J., Leuzinger, K., and Dent, M. (2013). Agroinfiltration as an effective and scalable strategy of gene delivery for production of pharmaceutical proteins. *Adv. Tech. Biol. Med.* 1:103. doi: 10.4172/atbm.1000103

D'Aoust, M. A., Couture, M. M., Charland, N., Trépanier, S., Landry, N., Ors, F., et al. (2010). The production of hemagglutinin-based virus-like particles in plants: a rapid, efficient and safe response to pandemic influenza. *Plant Biotechnol. J.* 8, 607–619. doi: 10.1111/j.1467-7652.2009.00496.x

Friedman, B., Vaddi, K., Preston, C., Mahon, E., Cataldo, J. R., and McPherson, J. M. (1999). A comparison of the pharmacological properties of carbohydrate remodeled recombinant and placental-derived beta-glucocerebrosidase: implications for clinical efficacy in treatment of Gaucher disease. *Blood*. 93, 2807–2816. doi: 10.1182/blood.V93.9.2807.409k08_2807_2816

Gomord, V., Chamberlain, P., Jefferis, R., and Faye, L. (2005). Biopharmaceutical production in plants: problems, solutions and opportunities. *Trends Biotechnol.* 23, 559–565. doi: 10.1016/j.tibtech.2005.09.003

Gomord, V., Fitchette, A. C., Menu-Bouaouiche, L., Saint-Jore-Dupas, C., Plasson, C., Michaud, D., et al. (2010). Plant-specific glycosylation patterns in the context of therapeutic protein production. *Plant Biotechnol. J.* 8, 564–587. doi: 10.1111/j.1467-7652.2009.00497.x

Goodin, M. M., Zaitlin, D., Naidu, R. A., and Lommel, S. A. (2008). *Nicotiana benthamiana*: its history and future as a model for plant-pathogen interactions. *Mol. Plant Microb. Interact.* 21, 1015–1026. doi: 10.1094/MPMI-21-8-1015

Grabowski, G. A., Golembo, M., and Shaaltiel, Y. (2014). Taliglucerase alfa: an enzyme replacement therapy using plant cell expression technology. *Mol. Genet. Metab.* 112, 1–8. doi: 10.1016/j.ymgme.2014.02.011

Gupta, P., and Pastores, G. M. (2017). Spotlight on taliglucerase alfa in the treatment of pediatric patients with type 1 gaucher disease. *Pediatr. Health Med. Ther.* 8, 73–81. doi: 10.2147/PHMT.S93634

Hanittinan, O., Oo, Y., Chaotham, C., Rattanapisit, K., Shanmugaraj, B., and Phoolcharoen, W. (2020). Expression optimization, purification and *in vitro* characterization of human epidermal growth factor produced in *Nicotiana benthamiana*. *Biotechnol. Rep.* 28:e00524. doi: 10.1016/j.btre.2020.e00524

He, X., Galpin, J. D., Tropak, M. B., Mahuran, D., Haselhorst, T., von Itzstein, M., et al. (2012). Production of active human glucocerebrosidase in seeds of *Arabidopsis thaliana* complex-glycan-deficient (*cgl*) plants. *Glycobiology* 22, 492–503. doi: 10.1093/glycob/cwr157

Hollak, C. E., vom Dahl, S., Aerts, J. M., Belmatoug, N., Bembi, B., Cohen, Y., et al. (2010). Force majeure: therapeutic measures in response to restricted supply of imiglucerase (Cerezyme) for patients with gaucher disease. *Blood Cells Mol. Dis.* 44, 41–47. doi: 10.1016/j.bcmd.2009.09.006

Irache, J. M., Salman, H. H., Gamazo, C., and Espuelas, S. (2008). Mannose-targeted systems for the delivery of therapeutics. *Expert Opin. Drug Deliv.* 5, 703–724. doi: 10.1517/17425247.5.6.703

Iskratsch, T., Braun, A., Paschinger, K., and Wilson, I. B. (2009). Specificity analysis of lectins and antibodies using remodeled glycoproteins. *Anal. Biochem.* 386, 133–146. doi: 10.1016/j.ab.2008.12.005

Jin, C., Altmann, F., Strasser, R., Mach, L., Schähs, M., Kunert, R., et al. (2008). A plant-derived human monoclonal antibody induces an anti-carbohydrate immune response in rabbits. *Glycobiology.* 18, 235–241. doi: 10.1093/glycob/cwm137

Joerg, S., Ludger Wilhelm, P., and Stephan vom, D. (2007). Therapy of adult gaucher disease. *Haematologica* 92, 148–152. doi: 10.3324/haematol.11193

Jung, J. W., Choi, H. Y., Huy, N. X., Park, H., Kim, H. H., Yang, M. S., et al. (2019). Production of recombinant human acid β-glucosidase with high mannose-type *N*-glycans in rice *gnt1* mutant for potential treatment of gaucher disease. *Protein Exp. Purif.* 158, 81–88. doi: 10.1016/j.pep.2019.02.014

Kagale, S., Uzuhashi, S., Wigness, M., Bender, T., Yang, W., Borhan, M. H., et al. (2012). TMV-Gate vectors: gateway compatible tobacco mosaic virus based expression vectors for functional analysis of proteins. *Sci. Rep.* 2:874. doi: 10.1038/srep00874

Kallemeijn, W. W., Scheij, S., Hoogendoorn, S., Witte, M. D., Herrera Moro Chao, D., van Roomen, C. P., et al. (2017). Investigations on therapeutic glucocerebrosidases through paired detection with fluorescent activity-based probes. *PLoS ONE* 12:e0170268. doi: 10.1371/journal.pone.0170268

Keler, T., Ramakrishna, V., and Fanger, M. W. (2004). Mannose receptor-targeted vaccines. *Expert Opin. Biol. Ther.* 4, 1953–1962. doi: 10.1517/14712598.4.12.1953

Kim, K., Kang, Y. J., Park, S. R., Kim, D. S., Lee, S. W., Ko, K., et al. (2021). Effect of leaf position and days post-infiltration on transient expression of colorectal cancer vaccine candidate proteins GA733-Fc and GA733-FcK in *Nicotiana benthamiana* plant. *PeerJ.* 9:e10851. doi: 10.7717/peerj.10851

Leuzinger, K., Dent, M., Hurtado, J., Stahnke, J., Lai, H., Zhou, X., et al. (2013). Efficient agroinfiltration of plants for high-level transient expression of recombinant proteins. *J. Vis. Exp.* 77:50521. doi: 10.3791/50521

Limkul, J., Iizuka, S., Sato, Y., Misaki, R., Ohashi, T., Ohashi, T., et al. (2016). The production of human glucocerebrosidase in glyco-engineered *Nicotiana benthamiana* plants. *Plant Biotechnol. J.* 14, 1682–1694. doi: 10.1111/pbi.12529

Limkul, J., Misaki, R., Kato, K., and Fujiyama, K. (2015). The combination of plant translational enhancers and terminator increase the expression of human glucocerebrosidase in *Nicotiana benthamiana* plants. *Plant Sci.* 240, 41–49. doi: 10.1016/j.plantsci.2015.08.018

Loos, A., and Steinkellner, H. (2014). Plant glyco-biotechnology on the way to synthetic biology. *Front. Plant Sci.* 5:523. doi: 10.3389/fpls.2014.00523

Maupin, K. A., Liden, D., and Haab, B. B. (2012). The fine specificity of mannose-binding and galactose-binding lectins revealed using outlier motif analysis of glycan array data. *Glycobiology* 22, 160–169. doi: 10.1093/glycob/cwr128

Montero-Morales, L., and Steinkellner, H. (2018). Advanced plant-based glycan engineering. *Front. Bioeng. Biotechnol.* 6:81. doi: 10.3389/fbioe.2018.00081

Moon, K. B., Park, J. S., Park, Y. I., Song, I. J., Lee, H. J., Cho, H. S., et al. (2019). Development of systems for the production of plant-derived biopharmaceuticals. *Plants* 9:30. doi: 10.3390/plants9010030

Morant, A. V., Jørgensen, K., Jørgensen, C., Paquette, S. M., Sánchez-Pérez, R., Møller, B. L., et al. (2008). Beta-glucosidases as detonators of plant chemical defense. *Phytochemistry* 69, 1795–1813. doi: 10.1016/j.phytochem.2008.03.006

Nam, H. J., Kwon, J. Y., Choi, H. Y., Kang, S. H., Jung, H. S., and Kim, D. I. (2017). Production and purification of recombinant glucocerebrosidase in transgenic rice cell suspension cultures. *Appl. Biochem. Biotechnol.* 181, 1401–1415. doi: 10.1007/s12010-016-2292-4

Naphatsamon, U., Ohashi, T., Misaki, R., and Fujiyama, K. (2018). The production of human β-glucocerebrosidase in *Nicotiana benthamiana* root culture. *Int. J. Mol. Sci.* 19:1972. doi: 10.3390/ijms19071972

Pankoke, H., Buschmann, T., and Müller, C. (2013). Role of plant β-glucosidases in the dual defense system of iridoid glycosides and their hydrolyzing enzymes in *Plantago lanceolata* and *Plantago* major. *Phytochemistry* 94, 99–107. doi: 10.1016/j.phytochem.2013.04.016

Paschinger, K., Rendić, D., and Wilson, I. B. (2009). Revealing the anti-HRP epitope in *Drosophila* and *Caenorhabditis*. *Glycoconj. J.* 26, 385–395. doi: 10.1007/s10719-008-9155-3

Paul, M., and Ma, J. K. (2011). Plant-made pharmaceuticals: leading products and production platforms. *Biotechnol. Appl. Biochem.* 58, 58–67. doi: 10.1002/bab.6

Schoberer, J., and Strasser, R. (2018). Plant glyco-biotechnology. *Semin. Cell Dev. Biol.* 80, 133–141. doi: 10.1016/j.semcdb.2017.07.005

Seshadri, S., Akiyama, T., Opassiri, R., Kuaprasert, B., and Cairns, J. K. (2009). Structural and enzymatic characterization of Os3BGlu6, a rice beta-glucosidase hydrolyzing hydrophobic glycosides and (1->3)- and (1->2)-linked disaccharides. *Plant Physiol.* 151, 47–58. doi: 10.1104/pp.109.139436

Shanmugaraj, B., I., Bulaon, C. J., and Phoolcharoen, W. (2020). Plant molecular farming: a viable platform for recombinant biopharmaceutical production. *Plants* 9:842. doi: 10.3390/plants9070842

Siebert, M., Sidransky, E., and Westbroek, W. (2014). Glucocerebrosidase is shaking up the synucleinopathies. *Brain* 137, 1304–1322. doi: 10.1093/brain/awu002

Stirnemann, J., Belmatoug, N., Camou, F., Serratrice, C., Froissart, R., Caillaud, C., et al. (2017). A review of gaucher disease pathophysiology, clinical presentation and treatments. *Int. J. Mol. Sci.* 18:441. doi: 10.3390/ijms18020441

Strasser, R. (2014). Biological significance of complex *N*-glycans in plants and their impact on plant physiology. *Front. Plant Sci.* 5:363. doi: 10.3389/fpls.2014.00363

Tekoah, Y., Tzaban, S., Kizhner, T., Hainrichson, M., Gantman, A., Golembo, M., et al. (2013). Glycosylation and functionality of recombinant β-glucocerebrosidase from various production systems. *Biosci. Rep.* 33:e00071. doi: 10.1042/BSR20130081

Tschofen, M., Knopp, D., Hood, E., and Stöger, E. (2016). Plant molecular farming: much more than medicines. *Annu. Rev. Anal. Chem.* 9, 271–294. doi: 10.1146/annurev-anchem-071015-041706

Van Dussen, L., Zimran, A., Akkerman, E. M., Aerts, J. M., Petakov, M., Elstein, D., et al. (2013). Taliglucerase alfa leads to favorable bone marrow responses in patients with type I gaucher disease. *Blood Cells Mol. Dis.* 50, 206–211. doi: 10.1016/j.bcmd.2012.11.001

Van Patten, S. M., Hughes, H., Huff, M. R., Piepenhagen, P. A., Waire, J., Qiu, H., et al. (2007). Effect of mannose chain length on targeting of glucocerebrosidase for enzyme replacement therapy of gaucher disease. *Glycobiology* 17, 467–478. doi: 10.1093/glycob/cwm008

Yan, R., Wang, Z., Ren, Y., Li, H., Liu, N., and Sun, H. (2019). Establishment of efficient genetic transformation systems and application of CRISPR/Cas9 genome editing technology in *Lilium pumilum* DC. Fisch. and *Lilium longiflorum* white heaven. *Int. J. Mol. Sci.* 20:2920. doi: 10.3390/ijms20122920

Zacchi, L. F., and Schulz, B. L. (2016). *N*-glycoprotein macroheterogeneity: biological implications and proteomic characterization. *Glycoconj. J.* 33, 359–376. doi: 10.1007/s10719-015-9641-3

Zhao, Y., Ren, J., Padilla-Parra, S., Fry, E. E., and Stuart, D. I. (2014). Lysosome sorting of β-glucocerebrosidase by LIMP-2 is targeted by the mannose 6-phosphate receptor. *Nat. Commun.* 5:4321. doi: 10.1038/ncomms5321

Zhou, Q., and Qiu, H. (2019). The mechanistic impact of *N*-glycosylation on stability, pharmacokinetics, and immunogenicity of therapeutic proteins. *J. Pharm. Sci.* 108, 1366–1377. doi: 10.1016/j.xphs.2018.11.029

Zimran, A., Wajnrajch, M., Hernandez, B., and Pastores, G. M. (2018). Taliglucerase alfa: safety and efficacy across 6 clinical studies in adults and children with gaucher disease. *Orphanet. J. Rare Dis.* 13:36. doi: 10.1186/s13023-018-0776-8

Conflict of Interest: The authors declare that the research was conducted in the absence of any commercial or financial relationships that could be construed as a potential conflict of interest.

frontiers in Plant Science

ORIGINAL RESEARCH
published: 23 June 2021
doi: 10.3389/fpls.2021.683417

Expression and Functional Evaluation of Recombinant Anti-receptor Activator of Nuclear Factor Kappa-B Ligand Monoclonal Antibody Produced in *Nicotiana benthamiana*

*Wanuttha Boonyayothin[1,2], Sirorut Sinnung[3], Balamurugan Shanmugaraj[1,2], Yoshito Abe[4], Richard Strasser[5], Prasit Pavasant[3,6] and Waranyoo Phoolcharoen[1,2]**

[1]Research Unit for Plant-Produced Pharmaceuticals, Chulalongkorn University, Bangkok, Thailand, [2]Department of Pharmacognosy and Pharmaceutical Botany, Faculty of Pharmaceutical Sciences, Chulalongkorn University, Bangkok, Thailand, [3]Center of Excellence in Regenerative Dentistry, Faculty of Dentistry, Chulalongkorn University, Bangkok, Thailand, [4]Department of Pharmaceutical Sciences, School of Pharmacy at Fukuoka, International University of Health and Welfare, Okawa, Japan, [5]Department of Applied Genetics and Cell Biology, University of Natural Resources and Life Sciences, Vienna, Austria, [6]Department of Anatomy, Faculty of Dentistry, Chulalongkorn University, Bangkok, Thailand

OPEN ACCESS

Edited by:
Inga Isabel Hitzeroth, University of Cape Town, South Africa

Reviewed by:
Rolf Fendel, University of Tübingen, Germany
Giacomina Brunetti, University of Bari Aldo Moro, Italy

***Correspondence:**
Waranyoo Phoolcharoen
waranyoo.p@chula.ac.th

Specialty section:
This article was submitted to Plant Biotechnology, a section of the journal Frontiers in Plant Science

Received: *21 March 2021*
Accepted: *31 May 2021*
Published: *23 June 2021*

Citation:
Boonyayothin W, Sinnung S, Shanmugaraj B, Abe Y, Strasser R, Pavasant P and Phoolcharoen W (2021) Expression and Functional Evaluation of Recombinant Anti-receptor Activator of Nuclear Factor Kappa-B Ligand Monoclonal Antibody Produced in Nicotiana benthamiana. Front. Plant Sci. 12:683417. doi: 10.3389/fpls.2021.683417

Denosumab, an anti-receptor activator of nuclear factor-kappa B ligand antibody (anti-RANKL), is a fully human monoclonal antibody (mAb) available for the treatment of osteoporosis. In the present study, an anti-RANKL mAb was transiently expressed using the geminiviral expression system in *Nicotiana benthamiana*, and the functional activity of the plant-produced mAb was determined. The highest expression level of the plant-produced mAb was found at 8 days post-infiltration, and it was estimated to be 0.5 mg/g leaf fresh weight. The recombinant mAb from the plant crude extracts was purified by using Protein A affinity column chromatography. The plant-produced mAb demonstrated good *in vitro* affinity binding with human RANKL, as determined by RANKL-ELISA binding. The function of the plant-produced mAb was evaluated *in vitro*. CD14-positive cells isolated from human peripheral blood mononuclear cells (PBMCs) were cultured *in vitro* in the presence of human RANKL and macrophage-colony-stimulating factor (M-CSF) to stimulate osteoclastogenesis. The results demonstrated that plant-produced mAb could significantly decrease the number of osteoclasts compared to commercial denosumab. These results demonstrated that the plant-produced mAb has the potential to inhibit osteoclast differentiation and that it could be considered for osteoporosis treatment.

Keywords: receptor activator of nuclear factor kappa-B ligand, plant-produced monoclonal antibody, *Nicotiana benthamiana*, transient expression, osteoclastogenesis, denosumab

INTRODUCTION

Osteoporosis is a common skeletal disease caused by an imbalance in the bone remodeling process (or bone metabolism; Lewiecki, 2010b; Cosman et al., 2014). This disease can be characterized by low bone mineral density (BMD) and microarchitectural deterioration, leading to an increase in the risk of fracture (NIH Consensus Development Panel on Osteoporosis Prevention and Therapy, 2001).

Bone remodeling is an essential process that balances bone formation and bone resorption. In brief, osteoclast cells continuously resorb older and damaged bone, while osteoblast cells reconstruct new bone (Hadjidakis and Androulakis, 2006) to maintain a healthy skeleton by preventing microfractures (Sözen et al., 2017). During osteoporosis, the bone resorption rate is greater than the bone formation rate, which increases the risk of osteoporosis-related fractures.

As shown in **Figure 1A**, the main factors regulating the mechanism of bone resorption are receptor activator of nuclear factor kappa B ligand (RANKL) and macrophage-colony-stimulating factor (M-CSF), which are presented by osteoblasts. M-CSF activates the osteoclast precursors. RANKL binds to the receptor activator of nuclear factor kappa-B (RANK) on the cell surface of osteoclast precursors to stimulate active osteoclasts and increases the bone resorption rate (Ono et al., 2020). During the bone remodeling process, osteoprotegerin (OPG) acts as an antagonist of RANKL and is provided by osteoblasts. An imbalance in the RANKL/OPG ratio can cause osteoporosis and metabolic bone diseases.

Currently, there are many treatment agents that are commonly used to decrease osteoclast differentiation, osteoclastic bone resorption and the risk of osteoporotic fracture (Lewiecki, 2010a; Zaheer et al., 2015; Tu et al., 2018). For instance, estrogen replacement therapy (ERT) is commonly used for postmenopausal osteoporosis (Wu et al., 2012). Strontium ranelate (SR) has also

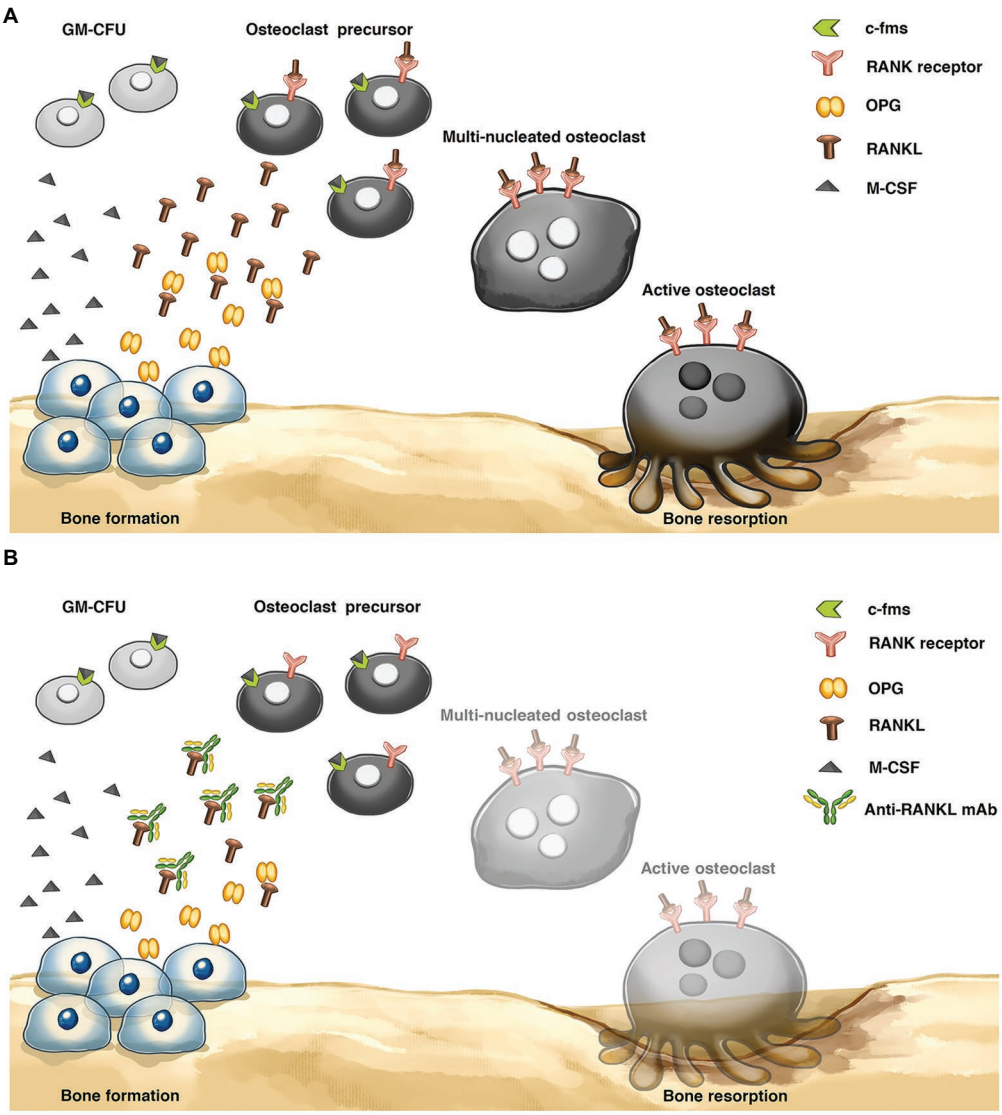

FIGURE 1 | Bone remodeling process **(A)** Osteoclastic bone resorption pathway. Osteoblasts express receptor activator of nuclear factor-κB ligand (RANKL), and RANKL binds to the RANK receptor on the osteoclast precursor surface, inducing active osteoclasts. Osteoprotegerin (OPG) plays an important role in inhibiting the interaction of RANKL and RANK receptors to reduce osteoclast differentiation. **(B)** Mechanism of anti-RANKL mAb. The levels of osteoclast differentiation and activity were decreased *via* an anti-RANKL mAb, preventing the interaction between the RANKL and RANK receptors. Granulocyte-macrophage-colony-forming cell (GM-CFU), macrophage-colony-stimulating factor (M-CSF), and colony-stimulating factor-1 receptor (c-fms).

been reported as a drug that can reduce the risk of fracture (Clarke, 2020). Moreover, the most widely used antiresorptive agent in osteoporosis treatment is bisphosphonates, which can stimulate the apoptosis of osteoclast cells to inhibit bone resorption, but the drug is poorly absorbed and can cause gastrointestinal (GI) side effects and osteonecrosis of the jaw (ONJ) on long-term consumption (Domotor et al., 2020). Currently, one of the biological agents for osteoporosis treatment is denosumab or anti-RANKL monoclonal antibody (mAb). This mAb was approved by the US FDA for treatment of postmenopausal osteoporosis with a high fracture risk, and it can reduce the risk of spine, hip, and nonvertebral fractures (Green, 2010; Deeks, 2018). These mAbs are an alternative for patients who have upper GI problems, and they can prevent upper GI injury from bisphosphonates. Moreover, they are suitable for patients with impaired renal function (Anastasilakis et al., 2018).

Denosumab is a fully human monoclonal antibody that has an approximate molecular weight of 147 kDa. It binds with high affinity to the RANKL, similar to OPG, to prevent the interaction between RANKL and RANK and decrease the rate of bone resorption (Makras et al., 2015; Faienza et al., 2018; **Figure 1B**). Recently, denosumab was produced from Chinese hamster ovary (CHO) cells. Although mammalian cells show beneficial effects in recombinant therapeutic protein production, such as producing properly folded and posttranslationally modified proteins (PTMs; Khan, 2013), this process has a high production cost, a complicated technology, limited scalability, and the possibility of contaminating the product with human and animal pathogens (Yin et al., 2007; Leuzinger et al., 2013).

There are many protein expression systems available, such as mammalian cells, yeast, and bacteria, to produce recombinant therapeutic proteins. There are some drawbacks to each system. For instance, the bacterial expression system is a commonly used platform for producing recombinant proteins. The major drawback associated with the prokaryotic system is the lack of appropriate PTMs that may result in incorrect protein folding (Balamurugan et al., 2006). In contrast, mammalian cells have many beneficial aspects, but the production cost is high (Yin et al., 2007; Leuzinger et al., 2013). For yeast systems, there are many advantages, such as a rapid growth rate, the requirement for a simple growth medium, and the ability to perform PTMs. However, this system has some limitations, such as hyperglycosylation and complicated downstream processes (Gomes et al., 2016). For insect cell systems, there is a possibility of contamination with mammalian viruses, and also, proteases in the host cell might cause protein degradation (Hejnaes and Ransohoff, 2018).

To overcome these limitations, a plant-based production system is an alternative platform for recombinant therapeutic protein production. Plant expression platforms have several advantages over traditional expression platforms. For instance, plants present a lower production cost, an excellent scale-up capacity, and the lack of the chance of contaminating the product with human or animal pathogens (Pogue et al., 2010; Phoolcharoen et al., 2011; Xu et al., 2011; Chen et al., 2013; Leuzinger et al., 2013; D'aoust et al., 2017; Rattanapisit et al., 2017, 2020; Shanmugaraj et al., 2020a). Moreover, plants have the ability to perform PTMs, such as glycosylation, disulfide bond formation, phosphorylation, or proteolytic processing. PTMs play important roles in protein folding, conformational stability, and activity (Xu et al., 2011; Uversky, 2013; Zhang et al., 2017).

Because of its many advantages over other expression systems, the plant expression system could be an alternative platform that is suitable for producing recombinant proteins for therapeutic purposes. Therefore, this study aimed to transiently express anti-RANKL mAb in *Nicotiana benthamiana*. The production time of the plant-produced mAb was optimized to obtain the highest expression level. Moreover, the functional activity of the plant-produced mAb was also examined. The results indicate that the plant-produced mAb has the potential to bind with high affinity to human RANKL, and it can inhibit the differentiation and proliferation of osteoclasts.

MATERIALS AND METHODS

Construction of a Plant Expression Vector for Producing Anti-RANKL mAb

The amino acid sequences of the heavy chain (HC) and light chain (LC) of anti-RANKL (DrugBank accession number: DB06643; **Supplementary Figure S1**) were codon-optimized for *N. benthamiana*, and the gene sequences were synthesized (Bioneer, South Korea). The signal peptide (MGWSCIILFLVATATGVHS) was added to the amino terminus (N-terminus), and SEKDEL was added to the carboxyl terminus (C-terminus) of both the HC and LC. The synthesized gene was digested with *Xba*I and *Sac*I restriction enzymes (New England Biolabs, United Kingdom), and the digested products were gel-extracted and purified. In this study, a geminiviral expression vector (pBYR2eK2 Md; pBYK-2e; Chen et al., 2011) was used as an expression vector that was kindly provided by Prof. Hugh S. Mason, Arizona State University, United States. The gel-extracted product was then ligated into pBYK-2e by using T4 DNA ligase (New England Biolabs, United Kingdom), as shown in **Figure 2A**. The recombinant vector was further transformed into *Escherichia coli* strain DH10B by heat shock (Froger and Hall, 2007) and then transformed into *Agrobacterium tumefaciens* strain GV3101 *via* electroporation. *Agrobacterium* clones were confirmed by PCR using gene-specific forward and reverse primers. The PCR cycling conditions were as follows: an initial denaturation at 94°C for 2 min, followed by 35 cycles of 94°C for 30 s, 55°C for 30 s, and 72°C for 30–60 s, and a final extension at 72°C for 5 min. Taq DNA polymerase (Vivantis Technologies, Malaysia) was used for amplification, and the PCR products were separated on 1% agarose gel. Positive *Agrobacterium* clones were used for further experiments.

Transient Expression of Anti-RANKL mAb in *N. benthamiana*

Agrobacterium tumefaciens harboring the plant expression vector containing either HC or LC was cultured on selective Luria–Bertani (LB) medium containing 50 μg/ml rifampicin, gentamicin, and kanamycin and then incubated at 28°C overnight with continuous shaking at 200 rpm. After incubation, the bacterial

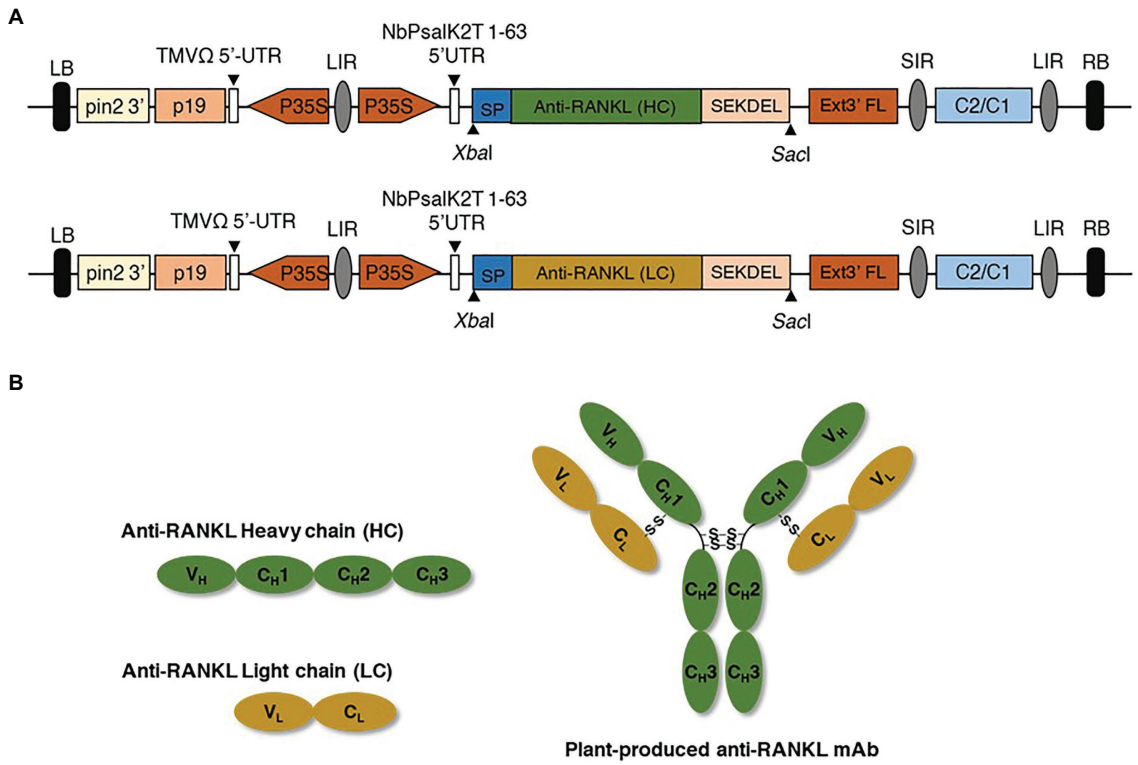

FIGURE 2 | (A) Schematic representation of the geminiviral expression vector. P35S, Cauliflower mosaic virus (CaMV) 35S promoter; TMVΩ 5'-UTR, tobacco mosaic virus Ω 5' untranslated region; anti-RANKL mAb gene, anti-receptor activator of nuclear factor Kappa-B ligand monoclonal antibody; HC and LC, heavy and light chains of the antibody; SP, signal peptide; SEKDEL, C-terminal endoplasmic reticulum (ER) retention signal peptide; Ext3' FL, 3' full length of the tobacco extension gene; C2/C1, C1 and C2 gene of Bean Yellow Dwarf virus (BeYDV) for replication initiation protein (Rep) and RepA; p19, p19 gene from Tomato Bushy Stunt Virus (TBSV); LIR, long intergenic region of BeYDV genome; SIR, short intergenic region of BeYDV genome; LB and RB, left and right borders of the *Agrobacterium*. **(B)** Schematic and structural elements of heavy chain (HC), light chain (LC), and assembled plant-produced anti-RANKL mAb.

suspension was centrifuged at 4,000 *g* for 10 min, and the pellet was resuspended in infiltration buffer [10 mM 2-N-morpholino-ethanesulfonic acid (MES) and 10 mM MgSO4, pH 5.5] to obtain a final optical density (OD_{600}) of 0.4. Then, an *Agrobacterium* suspension containing HC and LC was mixed equally and co-infiltrated into 6- to 8-week-old wild-type *N. benthamiana* by syringe infiltration and incubated at 28°C with a 16-h light/8-h dark cycle. The infiltrated leaves were harvested at 2, 4, 6, 8, and 10 days post-infiltration (dpi), and ELISA was performed for protein quantification. The large-scale production of mAb was performed by using vacuum infiltration.

Anti-RANKL mAb Extraction and Expression-Level Quantification

The infiltrated leaves were harvested at the appropriate dpi and extracted with 1x phosphate-buffered saline (PBS; 137 mM NaCl, 2.68 mM KCl, 10.1 mM Na_2HPO_4, and 1.76 mM KH_2PO_4, pH 7.4). The plant crude extract was centrifuged at 26,000 *g* for 40 min at 4°C to remove the cell debris. Sandwich ELISA was performed to quantify the plant-produced mAb expression level. Briefly, 96-well ELISA plates (Greiner Bio One GmbH, Austria) were coated with 50 µl anti-human IgG-Fc fragment-specific (Abcam, United Kingdom) prepared at 1:1,000 in 1x PBS (pH 7.4) and incubated overnight. Then, the plates were washed with 1x PBST (1xPBS containing 0.05% Tween-20) three times and blocked with 200 µl 5% skim milk in 1x PBS. After washing three times with 1x PBST, the plate was coated with commercial denosumab (AMGEN, United States) or plant-produced mAb at varying dilutions in 1x PBS and incubated at 37°C for 2 h. Each sample was loaded in triplicate wells of an ELISA plate. Then, the plate was washed three times with 1x PBST followed by HRP-conjugated anti-human kappa antibody (Southern Biotech, United States) with a dilution of 1:1,000 in 1x PBS and incubated for 1 h at 37°C. Then, the plate was washed three times with 1x PBST and developed by adding SureBlue™ TMB 1-Component Microwell Peroxidase Substrate (Promega, United States). To stop the reaction, 1 M H_2SO_4 was added, and the absorbance was measured using a microplate reader at an optical density of 450 nm (OD_{450}).

Purification of Anti-RANKL mAb

The crude extract from the infiltrated leaves was clarified by centrifugation, and the supernatant was filtered through a 0.45-micron filter (Millipore Sigma, United States) before loading into a Protein A affinity chromatography column. Amintra® Protein A Resin (Expedeon, United Kingdom) was packed into

the column and equilibrated with 1x PBS (pH 7.4). After equilibration, the filtered crude extract was loaded on the column, and the column was further washed with 1x PBS (pH 7.4). The protein was eluted with elution buffer (0.1 M glycine, pH 2.7) and neutralized with 1.5 M Tris-HCl (pH 8.8). Then, the purified protein was separated by sodium dodecyl sulfate–polyacrylamide gel electrophoresis (SDS–PAGE), followed by either staining with Coomassie Brilliant Blue (AppliChem, Germany) or carrying out western blotting.

SDS–PAGE and Western Blotting

Sodium dodecyl sulfate–polyacrylamide gel electrophoresis and western blotting were performed to determine the purity of the plant-produced mAb. Commercial denosumab (AMGEN, United States) was used as a positive control. The samples were analyzed under reducing and nonreducing conditions. For nonreducing conditions, loading buffer [125 mM Tris-HCl pH 6.8, 12% (w/v) SDS, 10% (v/v) glycerol, and 0.001% (w/v) bromophenol blue] was added, and the sample was denatured at 95°C for 5 min. The denatured samples were separated on 6–10% polyacrylamide gels. For reducing conditions, the sample was mixed with a loading buffer containing 22% β-mercaptoethanol, denatured at 95°C for 5 min, and then separated on 15% polyacrylamide gels. The polyacrylamide gels were stained with Coomassie Brilliant Blue (AppliChem, Germany), and the bands were visualized. For western blot analysis, the separated protein in the polyacrylamide gel was transferred to a nitrocellulose membrane (Bio-Rad, United States). The membrane was blocked with 5% skim milk in 1x PBS (pH 7.4) and then incubated either with HRP-conjugated anti-human gamma antibody (The Binding Site, United Kingdom) or with HRP-conjugated anti-human kappa antibody (Southern Biotech, United States) at a 1:5,000 dilution in 3% skim milk prepared in 1x PBS (pH 7.4). After incubation, the membrane was washed three times with 1x PBST, and the membrane was developed with Amersham ECL prime western blotting detection reagent (GE Healthcare, United Kingdom).

N-Glycan Analysis of the Plant-Produced mAb

The purified plant-produced mAb was separated on 15% polyacrylamide gels under reducing conditions and stained with Coomassie Brilliant Blue (AppliChem, Germany), and the bands were visualized. The HC was excised from the gel, S-alkylated, and digested with trypsin. The tryptic glycopeptides were analyzed by using liquid chromatography–electrospray ionization–mass spectrometry (LC–ESI–MS) as described previously in a study by Strasser et al. (2008).

Antibody Structure Characterization

Structure characterizations were performed using CD and NMR spectroscopic techniques. For CD spectroscopy, plant-produced mAb (10 μM) was dissolved in PBS buffer (pH 7.4). The CD spectra were recorded at room temperature using a quartz cell with a 1 mm optical path length on a J-720 W CD spectropolarimeter (JASCO, Tokyo, Japan). For NMR spectroscopy, NMR samples (100 μM) of plant-produced mAb were dissolved in a PBS buffer (pH 7.4) containing 10% v/v D_2O. NMR spectra were recorded on a Varian Unity INOVA 600 spectrometer (Varian, Palo Alto, CA, United States).

Binding Efficiency of Plant-Produced mAb to Human RANKL Protein

To investigate the binding activity of plant-produced mAb, a 96-well ELISA plate (Greiner Bio One GmbH, Austria) was coated with 3 μg/ml human RANKL protein (ProSpec-Tany TechnoGene Ltd., Israel) and incubated at 37°C for 4 h. Then, the plate was blocked with 200 μl of 5% skim milk (BD, Franklin Lakes, NJ, United States) in 1x PBS at 37°C for 2 h and washed three times with 1x PBST. Serial dilutions of plant-produced mAb, commercial denosumab (as a positive control), and human IgG1 kappa isotype antibody (Abcam, United Kingdom) were added to triplicate wells and incubated at 37°C for 2 h. After washing three times with 1x PBST, the plate was coated with HRP-conjugated anti-human gamma antibody (The Binding Site, United Kingdom) in 1x PBS at 1:1,000 and incubated at 37°C for 1 h. Then, the plate was developed by adding SureBlue™ TMB 1-Component Microwell Peroxidase Substrate (Promega, the United States), and the reaction was stopped by 1 M H_2SO_4. Then, the absorbance was measured using a microplate reader at an optical density of 450 nm (OD_{450}).

Functional Evaluation of the Plant-Produced mAb

Isolation of $CD14^+$ Monocytes

Human peripheral blood mononuclear cells (PBMCs) were isolated from buffy coats obtained from The Thai Red Cross Institute. Briefly, the buffy coats were diluted with equal amounts of Dulbecco's phosphate-buffered saline (DPBS) containing 2% fetal bovine serum (FBS; Thermo Fisher Scientific, United States). The diluted buffy coats were gently overlaid onto Ficoll-Paque PLUS (GE Healthcare, United Kingdom) and centrifuged at 400 *g* for 30 min without braking. After centrifugation, PBMCs at the interface between the plasma and the Ficoll-Paque PLUS were collected and washed with ice-cold DPBS containing 2% FBS. $CD14^+$ monocytes were isolated from the PBMCs by incubation with MACS $CD14^+$ microbeads (Miltenyi Biotec, Germany) for 15 min at 4°C. The cells were washed with buffer (DPBS containing 0.5% BSA and 2 mM EDTA) and passed through a MACS cell separator. The $CD14^+$ monocytes were collected for further experiments.

Induction of Osteoclast and Inhibition

To induce osteoclasts, $CD14^+$ monocytes were seeded at a density of 1×10^6 cells/well in 24-well plates and cultured in 1 ml of α-minimal essential medium (α-MEM; Thermo Fisher Scientific, United States) containing 50 ng/ml M-CSF and 100 ng/ml human RANKL protein (ProSpec-Tany TechnoGene Ltd., Israel). The inhibitory experiments were performed by the addition of either plant-produced mAb or commercial denosumab (AMGEN, United States) to obtain a final

concentration of 500 ng/ml. The anti-SARS-CoV mAb CR3022 (500 ng/ml; Rattanapisit et al., 2020) was used as a control. Fifty percent of the medium was replaced every 3 days with fresh medium containing 50 ng/ml M-CSF, 100 ng/ml human RANKL protein, and 500 ng/ml each of plant-produced mAb, denosumab, or CR3022 mAb, and the cultures were then maintained for 15 days. The experiment was performed in triplicate.

Tartrate-Resistant Acid Phosphatase Staining

Tartrate-resistant acid phosphatase staining (TRAP) was carried out using a commercial kit (Takara Bio, Japan). TRAP-positive multinucleated cells containing more than three nuclei were identified as osteoclasts and were counted under a microscope. Four fields were randomly selected, and pictures were taken by using Axio Observer Z1 and ZEN pro (ZEISS International, Oberkochen, Germany).

Statistical Analysis

The data are presented as the mean ± SEM. To assess the statistical significance of the differences, an unpaired two-sample t-test was performed, with values of $p \leq 0.0001$ considered statistically significant.

RESULTS

Transient Expression of Anti-RANKL mAb in *N. benthamiana* Leaves

To produce an anti-RANKL mAb, the nucleotide sequences of the HC and LC were modified with *N. benthamiana*-optimized codons. The genes were cloned into a geminiviral expression vector (pBYR2eK2 Md; pBYK-2e) using *Xba*I and *Sac*I restriction sites and subsequently electroporated into *A. tumefaciens* strain GV3101. Wild-type *N. benthamiana* leaves were co-infiltrated with *A. tumefaciens* harboring pBYK-2e-anti-RANKL HC and LC to produce assembled antibodies, including 2HC and 2 LC (**Figure 2B**). After agroinfiltration, strong leaf necrosis was observed, which was related to days post-infiltration (dpi; **Figure 3A**). The plant-produced mAb was expressed at the highest level at 8 dpi, up to 0.5 mg/g leaf fresh weight (**Figure 3B**).

Purification of Anti-RANKL mAb From *N. benthamiana* Leaves

The plants were vacuum-infiltrated, and then the infiltrated leaves were harvested at the appropriate time point. The plant-produced mAb was purified from the plant crude extract using Protein A affinity column chromatography. SDS–PAGE and western blotting

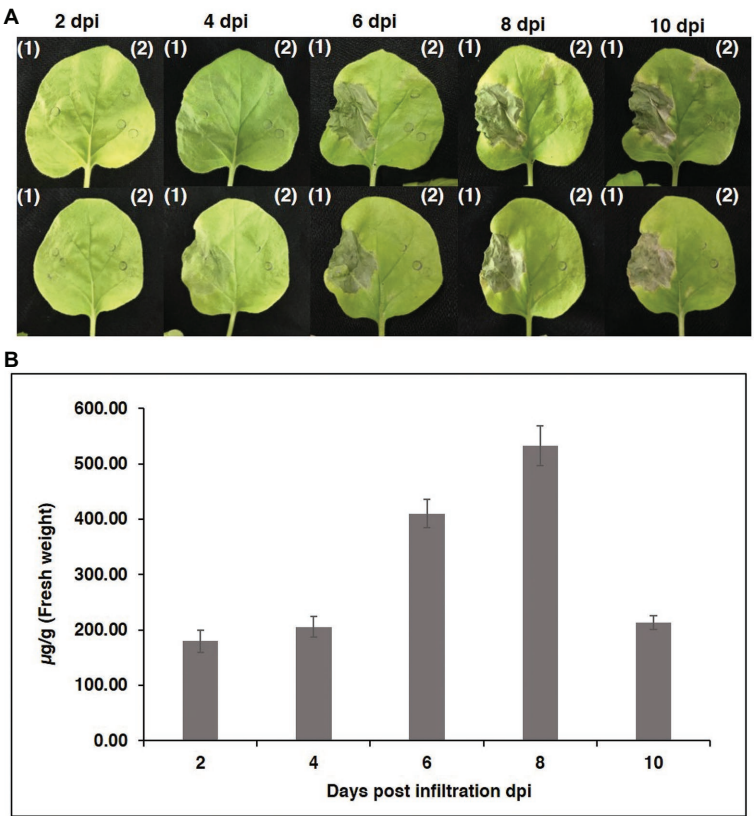

FIGURE 3 | Transient expression of anti-RANKL mAb in *Nicotiana benthamiana* leaves. **(A)** Phenotype of leaves on days 2, 4, 6, 8, and 10 after agroinfiltration. (1) *N. benthamiana* leaves were co-infiltrated with *Agrobacterium tumefaciens* harboring pBYK-2e-anti-RANKL HC + LC and (2) *A. tumefaciens* without an expression vector. **(B)** Infiltrated leaves were harvested on days 2, 4, 6, 8, and 10 from three individual plants each day post-infiltration and quantified by ELISA. The data are shown as the mean ± standard deviation (SD) of triplicate.

were performed to verify the purified plant-produced mAb. The SDS–PAGE gel was stained with Coomassie Brilliant Blue stain to visualize the separated protein bands. Western blotting was performed with anti-human gamma-HRP and anti-human kappa-HRP antibodies. For nonreducing conditions, the assembled antibody was confirmed to be in a tetrameric form with a molecular size of approximately 150 kDa, similar to the commercial denosumab (**Figures 4A–C**, Lanes 1 and 2).

Thus, the HC and LC of anti-RANKL mAb can be produced in *N. benthamiana* leaves. In reducing conditions, the protein bands were detected at molecular sizes of approximately 50 and 25 kDa, which correspond to the HC and LC of the antibody, similar to the commercial denosumab (**Figures 4D–F**, Lanes 1 and 2). No protein band was observed in the wild-type control leaf extract as expected [**Figures 4A–F**, Lane (–)]. These results indicated that the co-infiltration of genes encoding HC and LC produced the assembled anti-RANKL mAb in *N. benthamiana* leaves.

N-Glycan Analysis of Plant-Produced mAb

Liquid chromatography–electrospray ionization–mass spectrometry was performed for the analysis of the glycopeptides from the plant-produced mAb. The results indicated that the mAb displays mainly oligomannosidic N-glycans (Man5-Man9) and small amounts of complex-type and truncated N-glycans (e.g., GnGnXF), as shown in **Figure 5**.

Antibody Structure Characterization

The secondary and tertiary structures of the plant-produced mAb were examined by using CD and NMR spectroscopy techniques. CD spectrum analysis indicated a negative absorbance at 218 nm, which represents the typical β-sheet structure. In ^{1}H-NMR spectroscopy, since the signals of up-field methyl and dispersed aromatic protons were observed, the tertiary structures were retained. Consequently, the plant-produced mAb has a β-sheet-rich structure similar to the immunoglobulin-fold (**Figure 6**).

Binding Properties of Plant-Produced mAb to Human RANKL

Receptor Activator of Nuclear Factor Kappa-B Ligand (RANKL)-ELISA binding analysis was performed to examine the specific binding between the plant-produced mAb and human RANKL. Serial dilutions of purified plant-produced mAb, standard human IgG1 (as a negative control), and commercial denosumab (as

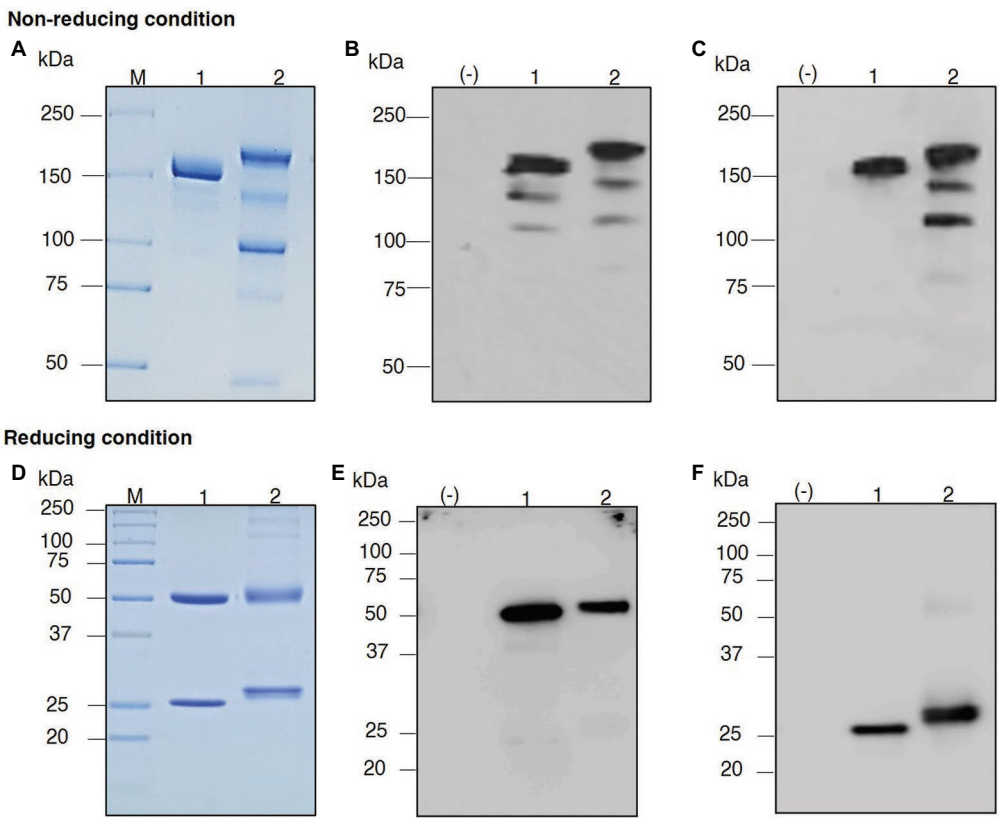

FIGURE 4 | Sodium dodecyl sulfate–polyacrylamide gel electrophoresis (SDS–PAGE) of purified plant-produced anti-RANKL mAb under nonreducing conditions and reducing conditions. Crude extracts from the infiltrated leaves were purified by a Protein A affinity chromatography column. The purified product was analyzed by SDS–PAGE staining with Coomassie Blue **(A,D)**. For western blot analysis, the separated proteins in the polyacrylamide gel were transferred to a nitrocellulose membrane, and the membrane was detected with either HRP-conjugated anti-human gamma chain antibody **(B,E)** or anti-human kappa chain antibody **(C,F)**. Lane M, Protein ladder; Lane (–), Wild-type crude extract; Lane 1, Commercial denosumab; Lane 2, Purified plant-produced anti-RANKL mAb.

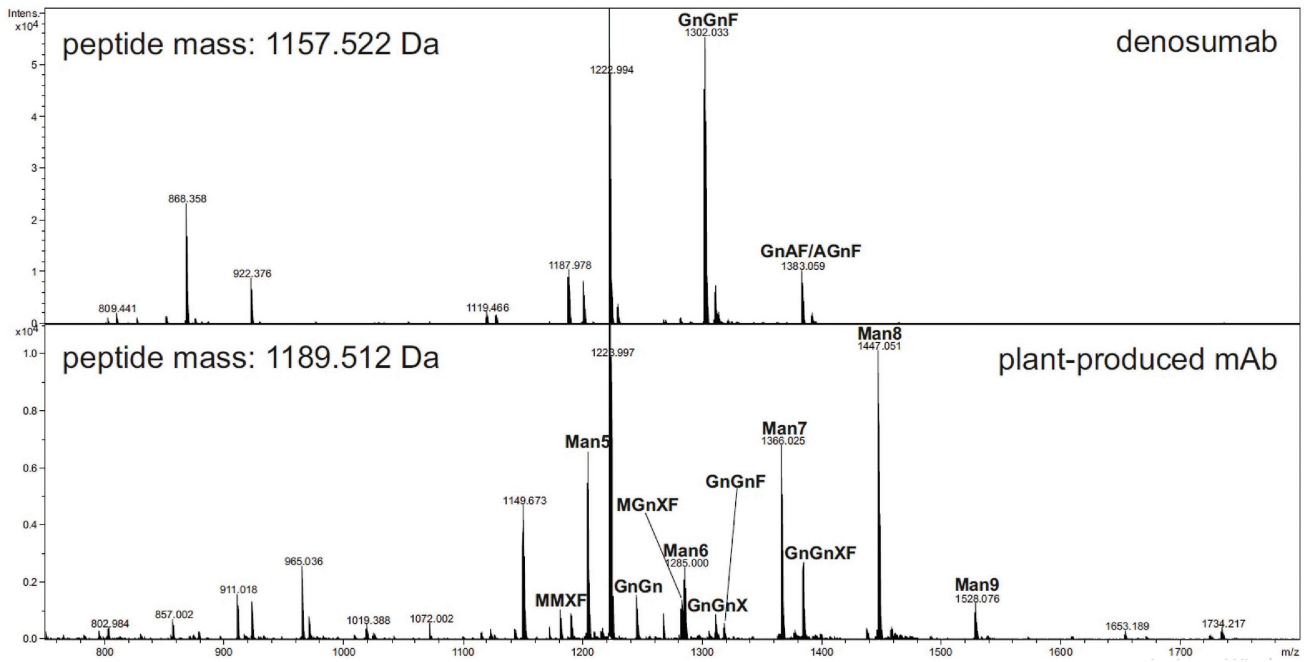

FIGURE 5 | Liquid chromatography–electrospray ionization–mass spectrometry (LC–ESI–MS) of tryptic glycopeptides from anti-RANKL monoclonal antibody (mAb) produced in wild-type *N. benthamiana* plants (see www.proglycan.com for a detailed explanation of the glycan structure abbreviations.)

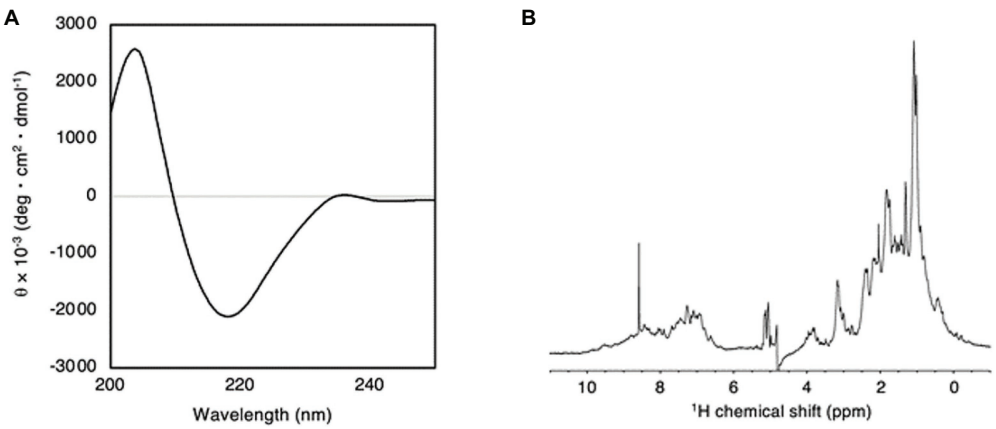

FIGURE 6 | (A) Far-UV CD spectrum of plant-produced anti-RANKL mAb at 25°C. **(B)** ^{1}H NMR spectrum of plant-produced anti-RANKL mAb at pH 7.5 and 25°C.

a positive control) were incubated with captured human RANKL in a 96-well plate. Commercial denosumab and plant-produced mAb presented signals when detected with anti-human gamma-HRP. These results demonstrated that both the commercial denosumab and the plant-produced mAb had the potential to bind to human RANKL, while human IgG1 did not show binding properties (**Figure** 7).

In vitro Functional Analysis

To examine the effect of plant-produced mAb on osteoclastogenesis, CD14^{+} monocytes were cultured with essential factors, including M-CSF (50 ng/ml) and human RANKL protein (ProSpec-Tany TechnoGene Ltd., Israel; 100 ng/ml). As shown in **Figure 8A**, CD14^{+} cells differentiated into osteoclasts as judged by their multinucleated appearance and positive staining of TRAP. The addition of both plant-produced mAb and commercial denosumab significantly reduced osteoclast differentiation at a dose of 500 ng/ml ($p \leq 0.0001$) compared with the control condition of adding M-CSF and RANKL. Comparable effects of both antibodies were found. In contrast, the addition of the plant-produced mAb CR3022 did not affect osteoclast formation (**Figure 8B**).

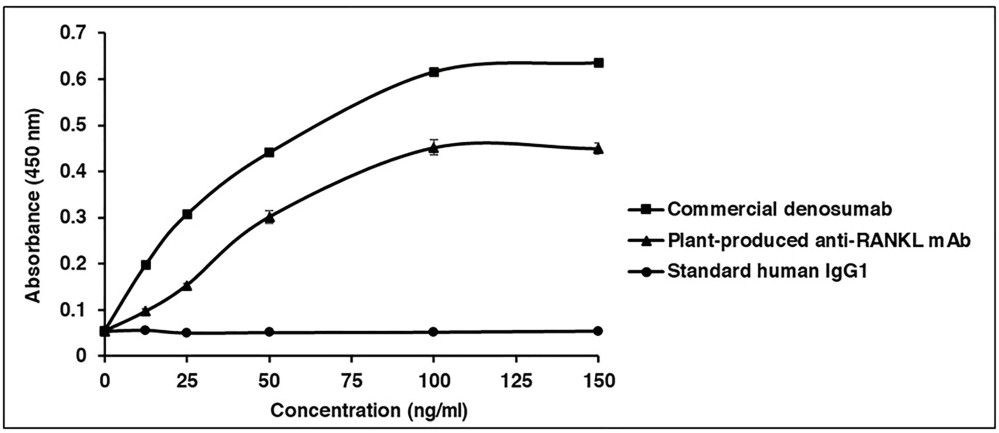

FIGURE 7 | Binding properties of plant-produced anti-RANKL mAb to human RANKL. ELISA was used to investigate the specific binding. The purified plant-produced mAb, standard human immunoglobulin G (IgG)1 (as a negative control), and commercial denosumab (as a positive control) were added to the plates coated with commercial human RANKL. The binding activity of antibody was detected with HRP-conjugated anti-human gamma chain antibody. The data are shown as the mean ± SD of triplicates.

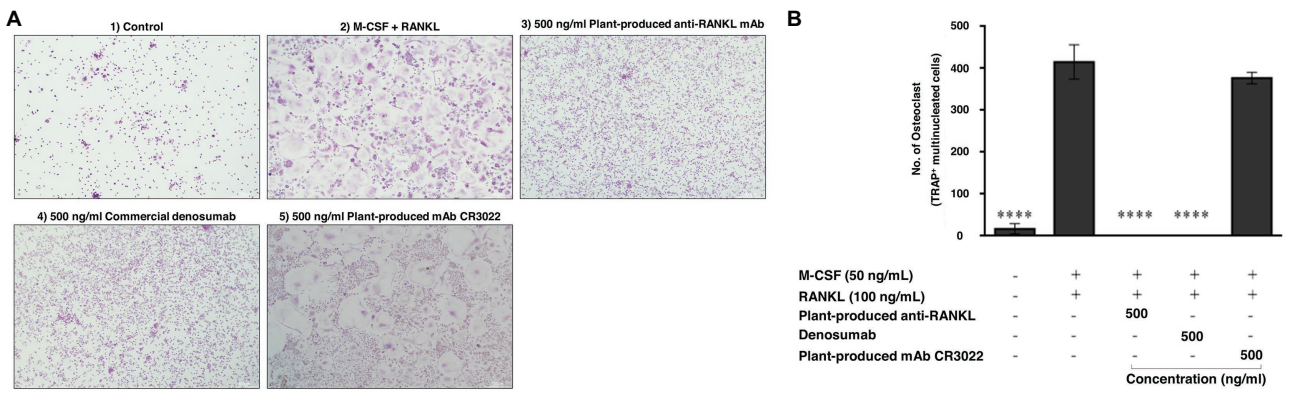

FIGURE 8 | Plant-produced anti-RANKL mAb suppresses osteoclast differentiation. CD14$^+$ monocytes were cultured under different conditions for 15 days following (1) control, (2) M-CSF and RANKL, (3) 500 ng/ml plant-produced anti-RANKL mAb, (4) 500 ng/ml commercial denosumab, and (5) 500 ng/ml plant-produced mAb CR3022. **(A)** Representative images of TRAP staining. **(B)** Quantification of TRAP$^+$ osteoclasts is shown as the mean and SEM of triplicate $^{****}p \leq 0.0001$.

DISCUSSION

Currently, the majority of therapeutic proteins, including vaccines, antibodies, and biologics, are produced from mammalian and microbial platforms. However, there are some drawbacks of these technology platforms, such as a lack of PTMs, high production cost, and scalability limitations. Recently, plants have been considered as bioreactors that can overcome this problem because they can efficiently produce large volumes of recombinant proteins, can perform PTMs, and can increase production cost-effectiveness (Uversky, 2013; Tusé et al., 2014; Chen and Davis, 2016; Chen, 2018; Shanmugaraj and Phoolcharoen, 2021).

There are many plant-produced proteins that are at different stages in clinical trials, and a few have been approved by the FDA. For instance, alpha-galactosidase-A (moss-aGal) has been used for Fabry disease (phase 1; Veen et al., 2020), HIV-neutralizing human mAb 2G12 (phase 1; Tremouillaux-Guiller et al., 2020), HA VLP influenza vaccine (phase 2; Pillet et al., 2019), anti-Ebola IgG cocktail (ZMApp) for the treatment of Ebola infection (phase 2/3; Davey et al., 2016) and glucocerebrosidase enzyme (ELELYSO) for Gaucher's disease (Fox, 2012). *N. benthamiana* is the preferred plant system for recombinant protein expression. This plant is genetically well known and easily manipulated, is a nonfood/nonfeed crop, and produces high biomass (Xu et al., 2012).

In this study, an anti-RANKL mAb was produced in *N. benthamiana* and its biological activity was investigated. The results showed that the mAb can be transiently expressed in *N. benthamiana* by using a geminiviral replicon vector. The geminiviral expression system was modified from the genome structure of the bean yellow dwarf virus to improve

the protein expression level (Chen et al., 2011). Previous studies have shown that many recombinant proteins can be transiently expressed from geminiviral replicon systems. For instance, enterotoxin B and the Ebola immune complex (EIC; including additional antigens or mAbs produced by using a geminiviral vector) were successfully expressed in *N. benthamiana* by using a geminiviral vector (Hefferon and Fan, 2004; Phoolcharoen et al., 2011). Rattanapisit et al. (2017) reported that the geminiviral expression system could be used to produce human osteopontin and showed the potential of recombinant osteopontin to induce periodontal ligament differentiation. Recently, the receptor-binding domain (RBD) of SARS-CoV-2 and the anti-SARS-CoV mAbs, CR3022, H4, and B38, were rapidly produced in *N. benthamiana* during the COVID-19 pandemic (Rattanapisit et al., 2020; Shanmugaraj et al., 2020b).

The nucleotide sequences of the anti-RANKL mAb were optimized with *N. benthamiana* codon usage to enhance recombinant protein expression, and the Ser-Glu-Lys-Asp-Glu-Leu (SEKDEL) sequences were added to the C-terminus to retain the plant-produced mAb in the endoplasmic reticulum (ER). The ER could ensure its proper folding and the assembly structure of antibodies with correct disulfide bond formation and glycosylation (Kleizen and Braakman, 2004; Braakman and Bulleid, 2011; Aebi, 2013). Furthermore, the expression level of the antibody was improved by adding SEKDEL to the amino acid sequence (Petruccelli et al., 2006) because the ER compartment is appropriate for protein retention due to a lack of proteases that can degrade the recombinant protein.

As shown in the results, the plant-produced mAb was expressed with the highest expression level of up to 0.5 mg/g fresh weight at 8 dpi (**Figure 3B**). Previously, some studies demonstrated that the production time of recombinant protein in plants was different and dependent on many factors, including the protein expression system and the specific protein molecules. Sheludko et al. (2007) indicated that the maximum rGFP expression level in plants obtained from the CaMV 35S promoter system with co-expression of TBSV P19 at 3 dpi remained constant until 8 dpi. Furthermore, transient expression of the recombinant EIC in *N. benthamiana* using a geminiviral vector was found to attain a maximum level at 4 dpi (Phoolcharoen et al., 2011).

In this study, N-glycan analysis of the mAb produced from wild-type *N. benthamiana* showed that it mainly had oligomannosidic N-glycans and minor amounts of complex-type N-glycans (**Figure 5**). The oligomannosidic structures are derived from limited processing of the N-glycans due to the retention of the mAb in the ER. The minor amounts of processed complex N-glycans are likely caused by incomplete retention and overload of the KDEL-mediated Golgi-to-ER retrieval pathway. The commercial denosumab produced in CHO cells displays complex N-glycans with a core α1,6-fucose that are typically found on secreted recombinant mAbs produced in mammalian cells. The N-glycan processing pathway in the Golgi apparatus differs between plants and mammals, which results in the presence of different N-glycan modifications on secreted recombinant glycoproteins (Gomord et al., 2004; Saint-Jore-Dupas et al., 2007; Schähs et al., 2007; Strasser, 2016; Montero-Morales and Steinkellner, 2018; Schoberer and Strasser, 2018). β1,2-Xylose of the conserved core complex N-glycan is not present in mammalian N-glycans. In addition, plant N-glycans also attach plant-specific α1,3-fucose residues to the complex core N-glycan instead of the core α1,6-fucose found in mammals. It is well established that the absence of the core α1,6-fucose reduces the affinity of the Fc domain of mAbs to bind to distinct Fc receptors that modulate the immune response (Wang and Ravetch, 2019). According to Stelter et al. (2020), a recombinant mAb with plant-specific N-glycans displayed reduced binding to Fcγ receptors, indicating that the plant-specific core α1,3-fucose has a similar effect. To prevent the attachment of these plant-specific complex N-glycan modifications, the plant-produced anti-RANKL mAb was designed to be retained in the ER.

In this study, we did not investigate the role of different N-glycans in the function of plant-produced anti-RANKL mAb. However, the proof-of-concept study shows that the plant-produced anti-RANKL mAb with primarily oligomannosidic N-glycans has comparable bioactivity to the commercial denosumab produced in a mammalian cell. In future studies, the role of different N-glycan modifications on osteoclast inhibition will be investigated using well-established glycoengineering approaches (Montero-Morales and Steinkellner, 2018; Schoberer and Strasser, 2018; Stelter et al., 2020).

A previous study showed that commercial denosumab provided the ability to bind specifically to human RANKL but not murine RANKL, human TRAIL, or other human TNF family members. In this study, a RANKL-ELISA binding assay, conducted according to Kostenuik et al. (2009), was performed to investigate the *in vitro* binding of the plant-produced mAb in comparison with commercial denosumab. The results showed that plant-produced anti-RANKL mAb demonstrated good binding potential to human RANKL, while the commercial antibody presented a higher binding signal and the standard human IgG1 (as a negative control) did not show any binding signal (**Figure 7**). As shown in **Supplementary Figure S1**, the anti-RANKL mAb amino acid sequences obtained from DrugBank (accession number: DB06643) were different from the commercialized antibody in the patent (Robblee et al., 2017). Therefore, the difference in amino acid sequences might have an impact on its binding affinity.

The bioactivity of plant-produced mAb on osteoclast inhibition was investigated. Human PBMCs were isolated and induced to differentiate into osteoclasts by M-CSF and RANKL. The cultures were treated with each plant-produced mAb, commercial denosumab, and mAb CR3022 (negative control). Our results indicated that plant-produced mAb and commercial denosumab both had the potential to inhibit osteoclast differentiation at the same concentration when tested on the $CD14^+$ cells *in vitro*, whereas no inhibition potential was shown with mAb CR3022 (**Figures 8A,B**). This result was consistent with an earlier study that demonstrated that commercial denosumab could inhibit osteoclast

differentiation *in vitro* at concentrations up to 3 nM (approximately 500 ng/ml; Kostenuik et al., 2009).

In summary, the results showed that plant-based expression systems can rapidly produce an assembled anti-RANKL mAb in *N. benthamiana*. The optimal production period was 8 dpi, with the highest expression level reaching 0.5 mg/g leaf fresh weight. There was good binding efficacy between plant-produced mAb and human RANKL. The functional *in vitro* study demonstrated that the plant-produced mAb reduced osteoclast differentiation. Therefore, these results may support the concept of a cost-effective and rapid production platform for anti-RANKL mAb and other biopharmaceutical products. However, an *in vivo* study should be performed to further confirm the efficacy and safety of the plant-produced mAb.

DATA AVAILABILITY STATEMENT

The original contributions presented in the study are included in the article/supplementary material, further inquiries can be directed to the corresponding author.

ETHICS STATEMENT

The studies involving human participants were reviewed and approved by the human subject ethics board of the Faculty of Dentistry, Chulalongkorn University. The patients/participants provided their written informed consent to participate in this study.

AUTHOR CONTRIBUTIONS

WP and PP designed all of the experiments. WB, SS, BS, YA and RS performed all of the experiments. All authors analyzed the data and contributed to the manuscript preparation.

FUNDING

The financial support was provided by the Second Century Fund (C2F; BS), Chulalongkorn University. SS and PP were supported by the Chulalongkorn Academic Advancement through its Second Century Project.

ACKNOWLEDGMENTS

We would like to thank Hugh Mason (Arizona State University) for providing the geminiviral vector. We also like to thank Clemens Grünwald-Gruber (Department of Chemistry, University of Natural Resources and Life Sciences, Vienna, Austria) for assisting with the LC–ESI–MS analysis. We would also like to thank the 100th Anniversary Chulalongkorn University Fund for Doctoral Scholarship and the 90th Anniversary of Chulalongkorn University Fund (Ratchadaphisek Somphot Endowment Fund), Chulalongkorn University (WB), for providing financial support.

SUPPLEMENTARY MATERIAL

The Supplementary Material for this article can be found online at: https://www.frontiersin.org/articles/10.3389/fpls.2021.683417/full#supplementary-material

REFERENCES

Aebi, M. (2013). N-linked protein glycosylation in the ER. *Biochim. Biophys. Acta Mol. Cell Res.* 1833, 2430–2437. doi: 10.1016/j.bbamcr.2013.04.001

Anastasilakis, A. D., Polyzos, S. A., and Makras, P. (2018). THERAPY OF ENDOCRINE DISEASE: Denosumab vs bisphosphonates for the treatment of postmenopausal osteoporosis. *Eur. J. Endocrinol.* 179, R31–R45. doi: 10.1530/EJE-18-0056

Balamurugan, V., Sen, A., Saravanan, P., and Singh, R. K. (2006). Biotechnology in the production of recombinant vaccine or antigen for animal health. *J. Anim. Vet. Adv.* 5, 487–495.

Braakman, I., and Bulleid, N. J. (2011). Protein folding and modification in the mammalian endoplasmic reticulum. *Annu. Rev. Biochem.* 80, 71–99. doi: 10.1146/annurev-biochem-062209-093836

Chen, Q. (2018). "Chapter seven - recombinant therapeutic molecules produced in plants," in *Advances in Botanical Research*. ed. M. Kuntz (United States: Academic Press Inc), 207–244.

Chen, Q., and Davis, K. R. (2016). The potential of plants as a system for the development and production of human biologics. *F1000Res.* 5:912. doi: 10.12688/f1000research.8010.1

Chen, Q., He, J., Phoolcharoen, W., and Mason, H. S. (2011). Geminiviral vectors based on bean yellow dwarf virus for production of vaccine antigens and monoclonal antibodies in plants. *Hum. Vaccin.* 7, 331–338. doi: 10.4161/hv.7.3.14262

Chen, Q., Lai, H., Hurtado, J., Stahnke, J., Leuzinger, K., and Dent, M. (2013). Agroinfiltration as an effective and scalable strategy of gene delivery for production of pharmaceutical proteins. *Adv. Tech. Biol. Med.* 1:103. doi: 10.4172/atbm.1000103

Clarke, B. L. (2020). "Strontium," in *Encyclopedia of Bone Biology*. ed. M. Zaidi, 652–665.

Cosman, F., De Beur, S. J., Leboff, M. S., Lewiecki, E. M., Tanner, B., Randall, S., et al. (2014). Clinician's guide to prevention and treatment of Osteoporosis. *Osteoporos. Int.* 25, 2359–2381. doi: 10.1007/s00198-014-2794-2

D'aoust, M.-A., Couture, M., Ors, F., Trepanier, S., Lavoie, P.-O., Dargis, M., et al (2017). Recombinant Influenza Virus-Like Particles (VLPs) Produced in Transgenic Plants Expressing Hemagglutinin. United States patent application.

Davey, R. T. Jr., Dodd, L., Proschan, M. A., Neaton, J., Neuhaus Nordwall, J., Koopmeiners, J. S., et al. (2016). A randomized, controlled trial of ZMapp for Ebola virus infection. *N. Engl. J. Med.* 375, 1448–1456. doi: 10.1056/NEJMoa1604330

Deeks, E. D. (2018). Denosumab: a review in postmenopausal Osteoporosis. *Drugs Aging* 35, 163–173. doi: 10.1007/s40266-018-0525-7

Domotor, Z. R., Vorhendi, N., Hanak, L., Hegyi, P., Kiss, S., Csiki, E., et al. (2020). Oral treatment with bisphosphonates of Osteoporosis does not increase the risk of severe gastrointestinal side effects: a meta-analysis of randomized controlled trials. *Front. Endocrinol.* 11:573976. doi: 10.3389/fendo.2020.573976

Faienza, M. F., Chiarito, M., D'amato, G., Colaianni, G., Colucci, S., Grano, M., et al. (2018). Monoclonal antibodies for treating osteoporosis. *Expert. Opin. Biol. Ther.* 18, 149–157. doi: 10.1080/14712598.2018.1401607

Fox, J. L. (2012). First plant-made biologic approved. *Nat. Biotechnol.* 30, 472–472. doi: 10.1038/nbt0612-472

Froger, A., and Hall, J. E. (2007). Transformation of plasmid DNA into *E. coli* using the heat shock method. *J. Vis. Exp.* 6:253. doi: 10.3791/253

Gomes, A., Byregowda, S., Veeregowda, B., and Vinayagamurthy, B. (2016). An overview of heterologous expression host systems for the production of recombinant proteins. *Adv. Anim. Vet. Sci.* 4, 346–356. doi: 10.14737/journal.aavs/2016/4.7.346.356

Gomord, V., Sourrouille, C., Fitchette, A. C., Bardor, M., Pagny, S., Lerouge, P., et al. (2004). Production and glycosylation of plant-made pharmaceuticals: the antibodies as a challenge. *Plant Biotechnol. J.* 2, 83–100. doi: 10.1111/j.1467-7652.2004.00062.x

Green, W. (2010). Denosumab (Prolia) injection: a new approach to the treatment of women with postmenopausal Osteoporosis. *Pharm. Ther.* 35, 553–559.

Hadjidakis, D. J., and Androulakis, I. I. (2006). Bone Remodeling. *Ann. N. Y. Acad. Sci.* 1092, 385–396. doi: 10.1196/annals.1365.035

Hefferon, K. L., and Fan, Y. (2004). Expression of a vaccine protein in a plant cell line using a geminivirus-based replicon system. *Vaccine* 23, 404–410. doi: 10.1016/j.vaccine.2004.04.038

Hejnaes, K. R., and Ransohoff, T. C. (2018). "Chemistry, manufacture and control," in *Biopharmaceutical Processing*. eds. G. Jagschies, E. Lindskog, K. Łącki and P. Galliher, 1105–1136.

Khan, K. H. (2013). Gene expression in mammalian cells and its applications. *Adv. Pharm. Bull.* 3, 257–263. doi: 10.5681/apb.2013.042

Kleizen, B., and Braakman, I. (2004). Protein folding and quality control in the endoplasmic reticulum. *Curr. Opin. Cell Biol.* 16, 343–349. doi: 10.1016/j.ceb.2004.06.012

Kostenuik, P. J., Nguyen, H. Q., McCabe, J., Warmington, K. S., Kurahara, C., Sun, N., et al. (2009). Denosumab, a fully human monoclonal antibody to RANKL, inhibits bone resorption and increases BMD in knock-in mice that express chimeric (murine/human) RANKL. *J. Bone Miner. Res.* 24, 182–195. doi: 10.1359/jbmr.081112

Leuzinger, K., Dent, M., Hurtado, J., Stahnke, J., Lai, H., Zhou, X., et al. (2013). Efficient agroinfiltration of plants for high-level transient expression of recombinant proteins. *J. Vis. Exp.* 77:50521. doi: 10.3791/50521

Lewiecki, E. M. (2010a). Bisphosphonates for the treatment of osteoporosis: insights for clinicians. *Ther. Adv. Chronic Dis.* 1, 115–128. doi: 10.1177/2040622310374783

Lewiecki, E. M. (2010b). Treatment of osteoporosis with denosumab. *Maturitas* 66, 182–186. doi: 10.1016/j.maturitas.2010.02.008

Makras, P., Delaroudis, S., and Anastasilakis, A. D. (2015). Novel therapies for osteoporosis. *Metabolism* 64, 1199–1214. doi: 10.1016/j.metabol.2015.07.011

Montero-Morales, L., and Steinkellner, H. (2018). Advanced plant-based glycan engineering. *Front. Bioeng. Biotechnol.* 6:81. doi: 10.3389/fbioe.2018.00081

NIH Consensus Development Panel on Osteoporosis Prevention and Therapy (2001). Osteoporosis prevention, diagnosis, and therapy. *JAMA* 285, 785–795. doi: 10.1001/jama.285.6.785

Ono, T., Hayashi, M., Sasaki, F., and Nakashima, T. (2020). RANKL biology: bone metabolism, the immune system, and beyond. *Inflamm. Regen.* 40:2. doi: 10.1186/s41232-019-0111-3

Petruccelli, S., Otegui, M. S., Lareu, F., Tran Dinh, O., Fitchette, A.-C., Circosta, A., et al. (2006). A KDEL-tagged monoclonal antibody is efficiently retained in the endoplasmic reticulum in leaves, but is both partially secreted and sorted to protein storage vacuoles in seeds. *Plant Biotechnol. J.* 4, 511–527. doi: 10.1111/j.1467-7652.2006.00200.x

Phoolcharoen, W., Bhoo, S. H., Lai, H., Ma, J., Arntzen, C. J., Chen, Q., et al. (2011). Expression of an immunogenic Ebola immune complex in *Nicotiana benthamiana*. *Plant Biotechnol. J.* 9, 807–816. doi: 10.1111/j.1467-7652.2011.00593.x

Pillet, S., Couillard, J., Trépanier, S., Poulin, J. F., Yassine-Diab, B., Guy, B., et al. (2019). Immunogenicity and safety of a quadrivalent plant-derived virus like particle influenza vaccine candidate-two randomized phase II clinical trials in 18 to 49 and ≥50 years old adults. *PLoS One* 14:e216533. doi: 10.1371/journal.pone.0216533

Pogue, G. P., Vojdani, F., Palmer, K. E., Hiatt, E., Hume, S., Phelps, J., et al. (2010). Production of pharmaceutical-grade recombinant aprotinin and a monoclonal antibody product using plant-based transient expression systems. *Plant Biotechnol. J.* 8, 638–654. doi: 10.1111/j.1467-7652.2009.00495.x

Rattanapisit, K., Abdulheem, S., Chaikeawkaew, D., Kubera, A., Mason, H. S., Ma, J. K., et al. (2017). Recombinant human osteopontin expressed in *Nicotiana benthamiana* stimulates osteogenesis related genes in human periodontal ligament cells. *Sci. Rep.* 7:17358. doi: 10.1038/s41598-017-17666-7

Rattanapisit, K., Shanmugaraj, B., Manopwisedjaroen, S., Purwono, P. B., Siriwattananon, K., Khorattanakulchai, N., et al. (2020). Rapid production of SARS-CoV-2 receptor binding domain (RBD) and spike specific monoclonal antibody CR3022 in *Nicotiana benthamiana*. *Sci. Rep.* 10:17698. doi: 10.1038/s41598-020-74904-1

Robblee, J., Collins, B. E., Kaundinya, G., and Bosques, C. J. (2017). Methods Related To Denosumab. U.S. Patent Application.

Saint-Jore-Dupas, C., Faye, L., and Gomord, V. (2007). From planta to pharma with glycosylation in the toolbox. *Trends Biotechnol.* 25, 317–323. doi: 10.1016/j.tibtech.2007.04.008

Schähs, M., Strasser, R., Stadlmann, J., Kunert, R., Rademacher, T., and Steinkellner, H. (2007). Production of a monoclonal antibody in plants with a humanized N-glycosylation pattern. *Plant Biotechnol. J.* 5, 657–663. doi: 10.1111/j.1467-7652.2007.00273.x

Schoberer, J., and Strasser, R. (2018). Plant glyco-biotechnology. *Semin. Cell Dev. Biol.* 80, 133–141. doi: 10.1016/j.semcdb.2017.07.005

Shanmugaraj, B., Bulaon, C. J. I., and Phoolcharoen, W. (2020a). Plant molecular farming: a viable platform for recombinant biopharmaceutical production. *Plan. Theory* 9:842. doi: 10.3390/plants9070842

Shanmugaraj, B., and Phoolcharoen, W. (2021). Addressing demand for recombinant biopharmaceuticals in the COVID-19 era. *Asian Pac. J. Trop. Med.* 14, 49–51. doi: 10.4103/1995-7645.306736

Shanmugaraj, B., Rattanapisit, K., Manopwisedjaroen, S., Thitithanyanont, A., and Phoolcharoen, W. (2020b). Monoclonal antibodies B38 and H4 produced in *Nicotiana benthamiana* neutralize SARS-CoV-2 *in vitro*. *Front. Plant Sci.* 11:589995. doi: 10.3389/fpls.2020.589995

Sheludko, Y. V., Sindarovska, Y. R., Gerasymenko, I. M., Bannikova, M. A., and Kuchuk, N. V. (2007). Comparison of several Nicotiana species as hosts for high-scale agrobacterium-mediated transient expression. *Biotechnol. Bioeng.* 96, 608–614. doi: 10.1002/bit.21075

Sözen, T., Özışık, L., and Başaran, N. Ç. (2017). An overview and management of osteoporosis. *Eur. J. Rheumatol.* 4, 46–56. doi: 10.5152/eurjrheum.2016.048

Stelter, S., Paul, M. J., Teh, A. Y. H., Grandits, M., Altmann, F., Vanier, J., et al. (2020). Engineering the interactions between a plant-produced HIV antibody and human Fc receptors. *Plant Biotechnol. J.* 18, 402–414. doi: 10.1111/pbi.13207

Strasser, R. (2016). Plant protein glycosylation. *Glycobiology* 26, 926–939. doi: 10.1093/glycob/cww023

Strasser, R., Stadlmann, J., Schahs, M., Stiegler, G., Quendler, H., Mach, L., et al. (2008). Generation of glyco-engineered *Nicotiana benthamiana* for the production of monoclonal antibodies with a homogeneous human-like N-glycan structure. *Plant Biotechnol. J.* 6, 392–402. doi: 10.1111/j.1467-7652.2008.00330.x

Tremouillaux-Guiller, J., Moustafa, K., Hefferon, K., Gaobotse, G., and Makhzoum, A. (2020). Plant-made HIV vaccines and potential candidates. *Curr. Opin. Biotechnol.* 61, 209–216. doi: 10.1016/j.copbio.2020.01.004

Tu, K. N., Lie, J. D., Wan, C. K. V., Cameron, M., Austel, A. G., Nguyen, J. K., et al. (2018). Osteoporosis: a review of treatment options. *Phys. Ther.* 43, 92–104.

Tusé, D., Tu, T., and McDonald, K. A. (2014). Manufacturing economics of plant-made biologics: case studies in therapeutic and industrial enzymes. *Biomed. Res. Int.* 2014:256135. doi: 10.1155/2014/256135

Uversky, V. N. (2013). "Posttranslational Modification," in *Brenner's Encyclopedia of Genetics*. eds. S. Maloy and K. Hughes, 425–430.

Veen, S. J., Hollak, C. E. M., Kuilenburg, A. B. P., and Langeveld, M. (2020). Developments in the treatment of Fabry disease. *J. Inherit. Metab. Dis.* 43, 908–921. doi: 10.1002/jimd.12228

Wang, T. T., and Ravetch, J. V. (2019). Functional diversification of IgGs through Fc glycosylation. *J. Clin. Invest.* 129, 3492–3498. doi: 10.1172/JCI130029

Wu, X., Li, Z., Yang, Z., Zheng, C., Jing, J., Chen, Y., et al. (2012). Caffeic acid 3,4-dihydroxy-phenethyl ester suppresses receptor activator of NF-kappaB ligand-induced osteoclastogenesis and prevents ovariectomy-induced bone loss through inhibition of mitogen-activated protein kinase/activator protein 1 and Ca^{2+}-nuclear factor of activated T-cells cytoplasmic 1 signaling pathways. *J. Bone Miner. Res.* 27, 1298–1308. doi: 10.1002/jbmr.1576

Xu, J., Dolan, M. C., Medrano, G., Cramer, C. L., and Weathers, P. J. (2012). Green factory: plants as bioproduction platforms for recombinant proteins. *Biotechnol. Adv.* 30, 1171–1184. doi: 10.1016/j.biotechadv.2011.08.020

Xu, J., Ge, X., and Dolan, M. C. (2011). Towards high-yield production of pharmaceutical proteins with plant cell suspension cultures. *Biotechnol. Adv.* 29, 278–299. doi: 10.1016/j.biotechadv.2011.01.002

Yin, J., Li, G., Ren, X., and Herrler, G. (2007). Select what you need: a comparative evaluation of the advantages and limitations of frequently used expression systems for foreign genes. *J. Biotechnol.* 127, 335–347. doi: 10.1016/j.jbiotec.2006.07.012

Zaheer, S., Leboff, M., and Lewiecki, E. M. (2015). Denosumab for the treatment of osteoporosis. *Expert Opin. Drug Metab. Toxicol.* 11, 461–470. doi: 10.1517/17425255.2015.1000860

Zhang, B., Shanmugaraj, B., and Daniell, H. (2017). Expression and functional evaluation of biopharmaceuticals made in plant chloroplasts. *Curr. Opin. Chem. Biol.* 38, 17–23. doi: 10.1016/j.cbpa.2017.02.007

Conflict of Interest: The authors declare that the research was conducted in the absence of any commercial or financial relationships that could be construed as a potential conflict of interest.

frontiers in Plant Science

ORIGINAL RESEARCH
published: 14 July 2021
doi: 10.3389/fpls.2021.703020

Production of Human Acid-Alpha Glucosidase With a Paucimannose Structure by Glycoengineered *Arabidopsis* Cell Culture

*Ratna Sariyatun[1], Florence[1], Hiroyuki Kajiura[1,2], Takao Ohashi[1†], Ryo Misaki[1,2] and Kazuhito Fujiyama[1,2,3]**

[1]*Laboratory of Applied Microbiology, International Center for Biotechnology, Osaka University, Suita, Japan,* [2]*Institute for Open and Transdisciplinary Research Initiatives (OTRI), Osaka University, Suita, Japan,* [3]*Cooperative Research Station in Southeast Asia (OU:CRS), Faculty of Science, Mahidol University, Bangkok, Thailand*

OPEN ACCESS

Edited by:
Domenico De Martinis, Energy and Sustainable Economic Development (ENEA), Italy

Reviewed by:
Adam Barb, University of Georgia, United States
Hisashi Koiwa, Texas A&M University, United States

***Correspondence:**
Kazuhito Fujiyama
fujiyama@icb.osaka-u.ac.jp

†Present address:
Takao Ohashi, Department of Life Science, Faculty of Science and Engineering, Setsunan University, Neyagawa, Japan

Specialty section:
This article was submitted to Plant Biotechnology, a section of the journal Frontiers in Plant Science

Received: *30 April 2021*
Accepted: *15 June 2021*
Published: *14 July 2021*

Citation:
Sariyatun R, Florence, Kajiura H, Ohashi T, Misaki R and Fujiyama K (2021) Production of Human Acid-Alpha Glucosidase With a Paucimannose Structure by Glycoengineered Arabidopsis *Cell Culture. Front. Plant Sci. 12:703020. doi: 10.3389/fpls.2021.703020*

Plant cell cultures have emerged as a promising platform for the production of biopharmaceutics due to their cost-effectiveness, safety, ability to control the cultivation, and secrete products into culture medium. However, the use of this platform is hindered by the generation of plant-specific *N*-glycans, the inability to produce essential *N*-glycans for cellular delivery of biopharmaceutics, and low productivity. In this study, an alternative acid-alpha glucosidase (GAA) for enzyme replacement therapy of Pompe disease was produced in a glycoengineered *Arabidopsis alg3* cell culture. The *N*-glycan composition of the GAA consisted of a predominantly paucimannosidic structure, $Man_3GlcNAc_2$ (M3), without the plant-specific *N*-glycans. Supplementing the culture medium with NaCl to a final concentration of 50 mM successfully increased GAA production by 3.8-fold. GAA from an NaCl-supplemented culture showed a similar *N*-glycan profile, indicating that the NaCl supplementation did not affect *N*-glycosylation. The results of this study highlight the feasibility of using a glycoengineered plant cell culture to produce recombinant proteins for which M3 or mannose receptor-mediated delivery is desired.

Keywords: acid-alpha glucosidase, α1,3 mannosyltransferase, *alg3*, GAA, paucimannose, Pompe disease

INTRODUCTION

The market of biopharmaceutical proteins has been a rapidly developing area of economics. Accordingly, large biotechnological and pharmaceutical companies, such as Medicago, Ventria, Pfizer, Greenovation, and Epicyte, have a strong interest and large investment in the development of novel platforms for producing pharmaceutical proteins (Zagorskaya and Deineko, 2017). In this environment, plant cell cultures have emerged as a potential bioproduction system for recombinant pharmaceuticals due to their greater cost-effectiveness and safety over other eukaryotic platforms (Hellwig et al., 2004; Xu et al., 2011; Santos et al., 2016). Plant cells can grow in simple medium, do not harbor any known human pathogens or bacterial endotoxins, and can conduct post-translational modifications similar to those in mammals (Moustafa et al., 2016; Zhang et al., 2016). Plant culture systems also share many similarities to microbial and mammalian cells, such as enabling a contained, controlled, and sterile production environment

meeting the criteria of good manufacturing practice for producing biopharmaceutical proteins (Santos et al., 2016). Plant cell cultures have also shown a good track record for production of biopharmaceutics as shown by the commercialization and the US Food and Drugs Administration approval to carrot cell-produced β-glucocerebrosidase (Elelyso) for the treatment of Gaucher disease. Notably, plant media do not contain animal-derived products, and thus, they can be used for the development of halal pharmaceutics for Islamic people, which is emerging as a prominent global market with an industry worth USD 2.3 trillion (Yusuf and Yajid, 2016). Another advantage of using plant culture is that the product can be secreted into the plant culture medium, which generally contains mainly sucrose and salts and no macromolecules (Kwon et al., 2003), thereby simplifying the downstream purification step. Due to these features, plant cell cultures have attracted enormous attention as a next-generation platform for producing biopharmaceutics, with the potential to challenge other well-established production systems (e.g., microbial and mammalian cells).

N-Glycosylation is crucial for manufacturing biopharmaceutical glycoproteins, as it greatly affects the stability, activity, and pharmacodynamics of glycoproteins in the human body (Seeberger and Cummings, 2015). Therefore, it is not surprising that control over the *N*-glycan profile is a regulatory prerequisite for recombinant protein therapeutics prior to use in patients (Rudge and Nims, 2018). For this reason, differences between human and plant *N*-glycosylation have become a limiting factor in the use of plants for the production of pharmaceutics. Plants lack core α1,6-fucose, β1,4-galactose, and sialic acid residues on *N*-glycans. Instead, plants generate β1,2-xylose and core α1,3-fucose residues on *N*-glycans, which are absent in humans, thus raising a concern of potential immunogenic reaction upon parenteral administration of the plant-made pharmaceuticals to humans (Gomord et al., 2010). Moreover, the production of pharmaceutics with minimal glycan heterogeneity is highly desirable in order to obtain consistent efficacy, which remains a bottleneck even in the well-established mammalian cell expression system (Goochee et al., 1991; Sethuraman and Stadheim, 2006). Thus, it is essential to generate human-type and homogenous *N*-glycosylation in the plant expression system.

A number of glycoengineering strategies have been done to optimize the use of plant cells for producing biopharmaceutical glycoproteins for human therapy. The main approaches consist of (1) elimination of the potentially immunogenic plant-specific *N*-glycans and (2) introduction of human-type glycosyltransferases into the plant cell system (Strasser et al., 2014; Montero-Morales and Steinkellner, 2018). The former can be done by cellular targeting of recombinant proteins into the ER by fusion with KDEL/SEKDEL ER retention signal or by knocking-out/down the plant β1,2-xylosyltransferases, α1,3-fucosyltransferases, and *N*-acetylglucosaminyltransferase-I enzymes. On the other hand, the introduction of human-type glycosyltransferases has been done by co-expressions of the human *N*-acetylglucosaminyltransferases-IV and V, galactosyltransferase, and sialic-acid synthesizing enzymes (Strasser et al., 2014; Montero-Morales and Steinkellner, 2018; Rozov et al., 2018). Surprisingly, introductions of these genes do not affect the plant phenotype, indicating that plant cells harbor high plasticity to tolerate multiple human-type glycosyltransferase enzymes (Strasser et al., 2014).

Certain *N*-glycan structures are often required to mediate delivery of biopharmaceutics to the target cells. Mannose-terminal *N*-glycans are capable of directing cellular delivery of biopharmaceutics *via* binding with mannose receptor (MR) expressed on the cell surface. Notably, the number of exposed terminal mannose residues has been shown to affect the efficacy of MR-mediated delivery. The paucimannosidic structure $Man_3GlcNAc_2$ (M3; Man: mannose; and GlcNAc: *N*-acetylglucosamine) exhibits a higher level of binding with MR than other *N*-glycans bearing more mannose-terminal residues/high-mannose structures (e.g., M5-M9; Van Patten et al., 2007; Shen et al., 2016). Moreover, M3 also has a clearance rate in mammalian hosts that is lower than those of high-mannose structures due to its lower affinity for binding with mannose-binding lectin (Van Patten et al., 2007). Unfortunately, the M3 structure is scarcely found in plant glycoproteins (Kajiura et al., 2010). Thus, a glycoengineering strategy is required in order to optimize the use of plant cells for producing biopharmaceutics bearing the M3 structure for MR-mediated delivery.

Our previous study showed that a glycoengineered *Arabidopsis* plant lacking the activity of α1,3-mannosyltransferase (ALG3), a so called *alg3* mutant, resulted in the generation of a predominantly M3 structure and a lower amount of plant-specific *N*-glycans (Kajiura et al., 2010). These characteristics imply that this glycoengineered plant line would be of great benefit for producing biopharmaceutics with the M3 structure to mediate delivery through the MR pathway and lacking plant-specific *N*-glycans. To date, however, there have been no studies exploring the use of *Arabidopsis alg3* suspension cell culture for the production of biopharmaceutics.

In this study, an *Arabidopsis alg3* cell culture was developed and used for producing acid-alpha glucosidase (GAA). GAA is an enzyme that catalyzes the breakdown of glycogen into glucoses in the acidic milieu of the lysosome. In human cells, GAA is produced as 110 kDa precursor, 95 kDa intermediate, and 76/70 kDa mature glycoproteins (Moreland et al., 2005). Deficiency of this enzyme results in Pompe disease, which is characterized by lysosomal accumulation of glycogen leading to severe metabolic myopathy (Kohler et al., 2018). The advent of enzyme replacement therapy (ERT) by injection with recombinant human GAA has prolonged the life span of patients with Pompe disease by restoring the function of cardiac muscles. However, the ability of ERT to improve the manifestations related to skeletal muscle (e.g., motor weakness, speech difficulties, dysphagia, osteopenia, and macroglossia) and smooth muscle damages (e.g., respiratory, vascular, gastrointestinal, genitourinary, ocular, and dermatologic smooth muscle pathologies) has not fully met expectations (Kohler et al., 2018; McCall et al., 2018). The latter ability is critical because smooth muscle damages in the lower respiratory tract could contribute to respiratory failure, which is the main cause of death in patients with late-onset Pompe disease despite use of ERT (Meena and Raben, 2020). This failure of ERT to fully restore the functions of skeletal and smooth muscle cells is due to the low number

of mannose-6-phosphate receptors on the cell surface of these cells, which results in insufficient enzyme delivery to the lysosome (Wenk et al., 1991). Importantly, MR is known to be expressed on smooth muscle cells (Lew et al., 1994; Taylor et al., 2005). By using an *Arabidopsis alg3* cell culture, it would be possible to produce an alternative GAA that bears the M3 structure and allows cellular delivery through MR, thereby outperforming the efficacy of the commercial GAA for targeting smooth muscle cells.

A common limitation of plant cultures is their low productivity (Su and Lee, 2007; Xu and Zhang, 2014). In plant cell cultures, medium or nutrient engineering is considered as important as the expression construct and cell line development for increasing the protein productivity (Holland et al., 2010; Xu et al., 2011; Fischer et al., 2015). However, because plant cultures are still relatively new platform compared to other well-established approaches for the production of biopharmaceutics, such as mammalian and microbial cells, there have been few investigations into methods for enhancing protein secretion into the plant culture media. Previous studies have demonstrated the effects of protein stabilizers [e.g., polyvinylpyrrolidone (PVP), polyethylene glycol (PEG), bovine serum albumin (BSA), NaCl, gelatin, and dimethyl sulfoxide (DMSO)] to improve recombinant protein production in plant cell cultures (LaCount et al., 1997; James et al., 2000; Sharp and Doran, 2001; Lee et al., 2002). Others have also shown enhanced recombinant protein production by using mannitol to induce osmotic stress (Tsoi and Doran, 2002) or modifying nitrogen content of the medium (Zhang et al., 2016). However, none has been tested in *Arabidopsis* or for GAA production.

In the present study, we develop an *Arabidopsis alg3* cell culture for the production of GAA bearing the M3 structure. The effects of medium engineering on the GAA production in *Arabidopsis* cell culture are also examined. The results of this study will contribute to optimization of plant cell cultures to produce recombinant proteins.

MATERIALS AND METHODS

Plasmid Construction

A modified pGPTV-BAR binary plasmid containing the pAt-GC-HSP cassette was previously constructed in our laboratory (Limkul et al., 2015). To prepare it for use in GAA expression, this plasmid was amplified using the primers pFK1-Fw (5'-GCT ACT AGT TAT CAA CAT GAA GAA CTT GCT TTT G-3') and pFK1-Rv (5'-GGT ACC GAG CTC ATA TGA AGA TGA AG-3'; the underlined letters indicate the *Spe*I restriction site) to generate a linear fragment without the GC sequence and containing a *Spe*I site near the 5'-end. Another *Spe*I restriction enzyme site was added by using the primers Mut*Spe*I_Fw (5'-TCA TAT GAG CTC GGT ACC AGT CGA CTA GT-3') and Mut*Spe*I_Rv (5'-CGG TAC CAG TCG ACT AGT TAT CAA CAT GA-3'), generating the linear fragment pFK1-BAR. On the other hand, an insert of GAA cDNA (NCBI NM_000152.3) was amplified from human liver cDNA along with addition of *Spe*I sites using the primers GAA-*Spe*I-Fw (5'-GTC ACT AGT ACC ATG GGA GTG AGG CAC CCG CC-3') and GAA-*Spe*I-Rv (5'-GAT ACA CTA GTC TAA CAC CAG CTG ACG AGA AAC TGC TCT CCC A-3'). Both the GAA and pFK1-BAR fragments were digested by *Spe*I restriction enzyme (New England Biolabs) and subsequently ligated using Ligation High Ver. 2.0 (Toyobo). This resulted in a circular binary plasmid containing the GAA expression cassette, which was designated pFK1-BAR-GAA.

Plant Cell Culture and Generation of GAA-Producing *Arabidopsis alg3* Cell Culture

The *Arabidopsis alg3* cell culture was developed from leaves of our *Arabidopsis alg3* plant (Kajiura et al., 2010) using a standard protocol (Sanchez-Serrano and Salinas, 2014). Briefly, the leaves were sterilized, sectioned, and transferred into sterile Murashige and Skoog (MS) medium (Murashige and Skoog, 1962) containing 0.3% gellan gum for callus induction. After about a month in the dark at 25°C, calli were transferred into sterile liquid MS medium and incubated in the dark at 25°C on a rotary shaker at 120 rpm until becoming a suspension cell culture. The culture was maintained in MS medium on a rotary shaker at 120 rpm in the dark at 25°C. About 10 ml of fresh cells was inoculated into 100 ml of fresh MS medium weekly for maintenance.

The *Arabidopsis alg3* cell culture was transformed by the *Agrobacterium*-mediated transformation as follows. First, the binary plant expression vector pFK1-BAR-GAA was introduced into *Agrobacterium tumefaciens* LBA4404 cells by electroporation. The transformed *Agrobacterium* cells were cultivated in 2 × YT liquid medium containing kanamycin (50 μg/ml), streptomycin (100 μg/ml), and rifampicin (10 μg/ml) until an OD_{600} of 0.8. About 5 ml of 4-day-old *Arabidopsis* cells was mixed with 200 μl of *Agrobacterium* solution on a petri dish and incubated in the dark at 25°C for 2–3 days. Subsequently, cells were washed with MS liquid medium containing 250 mg/l carbenicillin before being selected on MS medium containing bialaphos (10 μg/ml). Successfully transformed *Arabidopsis* calli were checked by Western blot to confirm the GAA production. Calli were grown in one whole petri dish and subsequently propagated in 100 ml of MS liquid medium in the dark at 25°C on a rotary shaker at 120 rpm speed until becoming a suspension cell culture. For maintenance, about 10 ml of fresh cells was transferred into 100 ml of fresh MS liquid medium weekly.

Protein Extraction and Western Blot Analysis

Harvested cells were dissolved in lysis buffer (20 mM Tris-HCl pH 7.5, 10 mM EDTA, and 1 ml/mg of cells). The mixture was sonicated for 1 min and centrifuged at 12,000 × *g* for 20 min at 4°C, and then the supernatant was collected as the intracellular protein extract. Meanwhile, analysis of secreted proteins was conducted using the harvested culture media directly. Protein concentration of samples was determined by Bradford assay.

The extracted intracellular and extracellular proteins were separated *via* sodium dodecyl sulfate-polyacrylamide gel

electrophoresis (SDS-PAGE). The separated proteins were transferred into a nitrocellulose membrane in transfer buffer (50 mM Tris, 40 mM glycine, and 20% methanol) using a mini-trans blot apparatus (Bio-Rad) for 90 min. To prevent non-specific binding, membranes were blocked with 5% non-fat milk powder in phosphate-buffered saline containing 0.05% Tween 20 buffer with gentle agitation on a rotary shaker at 20 rpm for 1 h. The membrane was incubated with a 1:5,000 dilution of anti-GAA monoclonal antibody produced in rabbit (Abcam) or 1:10,000 dilution of anti-horseradish peroxidase (HRP) polyclonal antibody produced in rabbit (Sigma-Aldrich) for 1 h, followed by a 1:5,000 dilution of anti-rabbit IgG conjugated to alkaline phosphatase (Sigma-Aldrich) for 1 h. For detection, Luminata™ Forte Western HRP substrate (Merck Millipore) was added to the membrane, and luminescent signals on the membrane were detected using the Invitrogen iBright Imaging System 1,500 Series (Thermo Fisher Scientific).

GAA Enzyme Activity Assay

GAA activity was measured by hydrolysis of the synthetic substrate *p*-nitrophenyl α-D-glucopyranoside (Santa Cruz Biotechnologies) in 50 mM sodium acetate pH 4.3 containing 0.1% BSA. The assay was performed at 37°C for 30–60 min and stopped by the addition of 0.87 M sodium bicarbonate pH 11.0. Hydrolysis of the substrate was monitored by release of the reaction product, *p*-nitrophenol, which can be measured at an absorbance of 405 nm by using iMark™ Microplate Reader (Bio-Rad). One unit (U) of activity was defined as the amount of activity that resulted in the hydrolysis of 1 μmol of substrate per minute at 37°C under the assay condition.

GAA Purification

The medium of GAA-producing *Arabidopsis alg3* culture was filtered through a Glass Econo-Column (Bio-Rad). NaCl was subsequently added to the medium until reaching a final concentration of 4 M. Then, the NaCl-containing medium was loaded into a hydrophobic interaction chromatography column (Toyopearl Phenyl-650 M, Tosoh Corporation) pre-equilibrated in 20 mM Tris-HCl pH 7.5 with 4 M NaCl. After washing the column using 4 M NaCl in 20 mM Tris-HCl pH 7.5 buffer, GAA was eluted by decreasing NaCl concentration. GAA-containing fractions were dialyzed to exchange the buffer into 20 mM sodium acetate pH 4.3. The dialyzed sample was applied to a cation exchange chromatography column (Toyopearl SP 550C, Tosoh Corporation) pre-equilibrated in 20 mM sodium acetate pH 4.3 buffer. After washing the column, GAA was eluted with 20 mM sodium acetate pH 4.3 containing 0.1–0.5 M NaCl. GAA-containing fractions were concentrated using a Vivaspin 20 with a 10 kDa cutoff (Sartorius Stedim Biotech GmbH).

Manipulation of Medium Composition

Polyvinylpyrrolidone (MW 360,000, 0.125 g/ml), PEG (MW 8,000, 0.2 g/ml), and BSA (10%) stock solutions were prepared and filter-sterilized using a Millex-GP syringe filter unit, 0.22 μm (Merck Millipore) before use, while 5 M NaCl, 0.5 M EDTA, and 1.0 M ammonium nitrate (NH_4NO_3) stock solutions were sterilized by autoclaving. Then, appropriate amounts of PVP, PEG, BSA, EDTA, and DMSO stock solutions were added to 100 ml of MS medium to final concentrations of 0.75 g/l, 2 g/l, 0.1%, 1 mM, and 4%, respectively, while NaCl was added to final concentrations of 25 mM, 50 mM, 100 mM, and 150 mM. Meanwhile, supplementation of gelatin 5% (w/v) and mannitol 34 g/l (186.6 mM) was conducted by inputting appropriate amounts of stock powders before autoclaving the MS medium. While the MS medium already contains NH_4NO_3 (165 mg/100 ml), in some experiments an additional 330 mg of NH_4NO_3 was added to the 100 ml of MS medium from the stock solution resulting in final NH_4NO_3 concentration of 495 mg/100 ml (61.8 mM).

In all experiments, 10 ml of fresh cells was inoculated into 100 ml of MS medium in 300 ml flasks. All of the tested compounds were added on the day of cell cultivation (day 0), and then, the cultures were grown for 14 days. One ml of cell culture was taken on each of days 0, 4, 7, 11, and 14 of treatment. The cells were separated from the medium for the determination of fresh cell weight and the analysis of intracellular proteins. The medium was also collected for the analysis of secreted proteins. All samples were stored at −20°C until analysis.

Analysis of *N*-Glycan Structures Attached to GAA Produced in *Arabidopsis alg3* Cell Culture

Purified GAA was separated on SDS-PAGE and stained with Coomassie Brilliant Blue (CBB). The 95 and 76 kDa GAA bands were excised from the gel. The GAA-containing gels were sliced and destained with methanol:50 mM NH_4HCO_3 (1:1 v/v) for 2 min with intermittent vortex mixing followed by overnight destaining in acetonitrile:50 mM NH_4HCO_3 (1:1 v/v) with intermittent vortex mixing. Then, the GAAs were digested in the gel using Trypsin Gold (Promega) in ProteaseMAX™ Surfactant (Promega) at 50°C for 1 h. The reaction was terminated by addition of trifluoroacetic acid to a final concentration of 0.5%. Digested glycopeptides were extracted from the gel, dried, and dissolved in 0.1% formic acid prior to injection into a nanoLC-MS/MS system. The nanoLC-MS/MS analysis was performed on an ESI-Qq-TOF mass spectrometer (micrOTOF-Q II; Bruker Daltonics) using a nanoLC system (1,200 series; Agilent Technologies) incorporating a trap column (5 μm, 0.3 × 5 mm) and analytical column (3.5 μm, 0.075 × 150 mm), both packed with Zorbax 300SB C-18 (Agilent Technologies). For the nanoLC system, the mobile phase consisted of 0.1% formic acid in water (solvent A) and 0.1% formic acid in acetonitrile (solvent B). The tryptic peptides were trapped in the column at a flow rate of 10 μl/min for 5 min. Elution was performed at a flow rate of 0.6 μl/min using a 2 to 8% gradient of solvent B over 5 min followed by a linear increase of solvent B to 50% for 40 min at 35°C. After elution, the column was washed with 95% solvent B for 5 min before returning to the initial conditions. For MS and MS/MS analyses, the system was operated with automatic switching between MS and MS/MS modes. The operating parameters were set

as follows: positive-ion mode, mass range 50–4,500 *m/z*, nebulizer flow 1.0 psi, dry gas flow rate 5.0 l/min, dry temperature 180°C, and ISCID energy 5.0 eV. The three most abundant signals (absolute threshold >20 counts/s) were selected on each MS spectrum for further isolation and fragmentation. The complete system was fully controlled by micrOTOF control software (Bruker Daltonics). Bruker Compass DataAnalysis (version 4.0) was used for deconvolution of MS spectra and glycan analysis, and BioTools (version 3.2) was used for *de novo* sequencing.

RESULTS

GAA Production in the Transformed *Arabidopsis alg3* Cell Culture

A GAA expression cassette was successfully constructed within pFK1-BAR-GAA. The cassette had a GAA sequence downstream of the *Cauliflower mosaic virus* (CaMV) CaMV 35S promoter and 5'-UTR AtADH enhancer, followed by an HSP terminator (**Figure 1A**). The binary plasmid was successfully inserted into *A. tumefaciens* LBA4404 cells, and then, the *Agrobacterium* was used for *Agrobacterium*-mediated transformation to generate GAA-producing *Arabidopsis alg3* cells. Putative transformants were selected with bialaphos. The GAA-producing calli were selected and used to establish a suspension cell culture. GAA production in the culture was confirmed by Western blot (**Figures 1B,C**). In human cells, GAA polypeptide is processed through sequential protease cleavages in the *N*- and *C*-termini generating 110 kDa GAA precursor, 95 kDa GAA intermediate, and 76 and 70 kDa GAA mature forms (Moreland et al., 2005). In *Arabidopsis alg3* cell culture, GAA was produced in the intracellular fraction as three forms corresponding to the 110, 95, and 76 kDa GAAs. The latter seemed to have slightly lower size than 76 kDa, which could be due to the different *N*-glycosylation from that in humans. Moreover, the 95 and 76 kDa GAAs were also secreted into the plant culture medium. Detection of these proteins indicated that the plant cells were capable of conducting a GAA processing mechanism similar to that in humans.

The GAA-producing *Arabidopsis* culture showed higher GAA-specific activity compared to an untransformed culture both intracellularly (9.1 ± 0.7 mU/mg in the *alg3* culture and 35.1 ± 5.2 mU/mg in the GAA-producing culture; **Figure 1D**) and extracellularly (35.4 ± 1.0 mU/mg in the *alg3* culture and 1,420 ± 37 mU/mg in the GAA-producing culture; **Figure 1E**). These results indicated that the *Arabidopsis*-produced GAA was functional. Notably, the extracellular fraction showed higher activity than the intracellular fraction, suggesting that most of the GAAs were secreted to the medium.

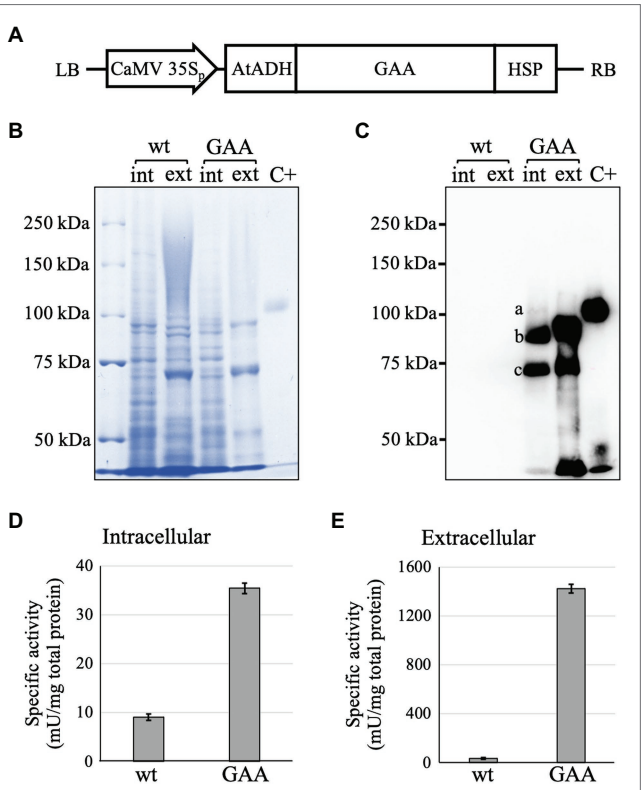

FIGURE 1 | Expression cassette and confirmation of acid-alpha glucosidase (GAA) production in the transformed *Arabidopsis alg3* cell culture. **(A)** Schematic representation of pFK1-BAR-GAA. *Cauliflower mosaic virus* (CaMV) 35S$_p$: CaMV 35S promoter; AtADH 5'-UTR: 5'-untranslated region of *Arabidopsis alcohol dehydrogenase* gene which acts as an enhancer; GAA: cDNA of human GAA; HSP: *Arabidopsis* heat shock protein terminator; and LB and RB: left and right borders of T-DNA, respectively. **(B,C)** CBB staining and Western blot analysis of untransformed (wt) and transformed (GAA) 7-day-old *Arabidopsis alg3* cell culture to confirm GAA production intra (int)- and extracellularly (ext). Marks a, b, and c indicate the 110, 95, and 76 kDa GAAs, respectively. C+ is human embryonic kidney/HEK293-derived recombinant human GAA used as a positive control. **(D,E)** GAA-specific activities in crude intracellular and extracellular proteins of untransformed (wt) and transformed (GAA) *Arabidopsis alg3* cell culture.

GAA Purification

GAA was successfully purified from the plant culture medium using two-step chromatography columns. GAA was purified as 95 and 76 kDa forms (**Figures 2A,B**). The 95 kDa GAA contains seven *N*-glycosylation sites (N140, N233, N390, N470, N652, N882, and N925), whereas the 76 kDa GAA contains five *N*-glycosylation sites (N140, N233, N390, N470, and N652). Therefore, it was expected that some bands would be observed around these sizes due to the different glycoforms on each of these sites. A faint band between the 95 and 76 kDa GAAs in the CBB staining was absent in the Western blot. This band was a degraded GAA as indicated by detection of the same GAA *N*-glycosylation sites from this band (**Supplementary Figure 1**; **Supplementary Table 1**). The degradation should have occurred near the *N*-terminus, thereby causing failed detection by the monoclonal anti-GAA antibody which binds an epitope near the *N*-terminus of GAA (within aa 150–250). After purification, the GAA-specific activity in the purified sample (10,600 ± 250 mU/mg) increased up to 26 times compared to that in the crude sample (409 ± 8.0 mU/mg; **Figure 2C**). The yield of GAA purified from the medium of the *Arabidopsis alg3* cell culture was 2.5% of the initial sample, or 60.9 ± 12.4 μg/l (**Supplementary Table 2**).

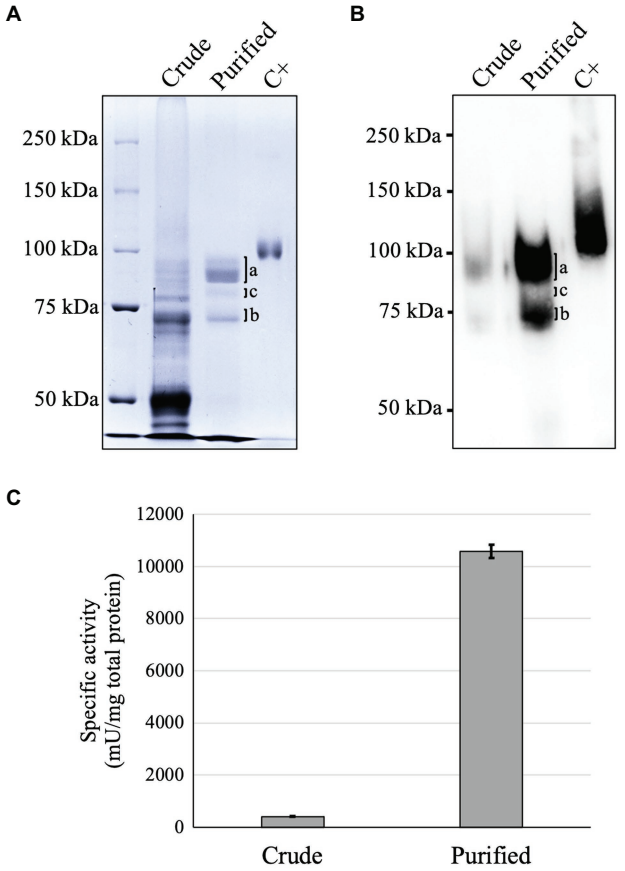

FIGURE 2 | Analysis of GAA purified from GAA-producing *Arabidopsis alg3* cell culture by Coomassie Brilliant Blue (CBB) staining **(A)**, Western blot **(B)**, and GAA activity assay **(C)**. Marks a and b indicate the 95 and 76 kDa GAAs, respectively, whereas mark c indicates a degraded GAA (**Supplementary Figure 1** and **Supplementary Table 1**). C+ is human embryonic kidney/HEK293-derived recombinant human GAA used as a positive control.

Effects of PEG, PVP, BSA, EDTA, DMSO, Gelatin, Mannitol, NH_4NO_3, and NaCl Supplementations to the *Arabidopsis alg3* Cell Growth and GAA Production

The following nine compounds were examined for their effects on the *Arabidopsis alg3* cell growth and GAA production: PVP, PEG, BSA, EDTA, DMSO, NH_4NO_3, mannitol, gelatin, and NaCl. These compounds have been reported to increase the production of some recombinant proteins in plant cell cultures. In the present study, the presence of 0.1% BSA, 4% DMSO, 34 g/l (186.6 mM) mannitol, 100 mM NaCl, 1 mM EDTA, or 5% gelatin in the MS medium severely inhibited the *Arabidopsis* cell growth. Conversely, addition of 0.75 g/l PVP or 2 g/l PEG increased the cell growth. Meanwhile, supplementing the MS medium with an additional 330 mg of NH_4NO_3 (61.8 mM) slightly decreased the cell growth, but lengthened the exponential growth phase (**Figure 3A**).

In comparison with the control, samples from the media supplemented with 0.75 g/l PVP, 2 g/l PEG, additional 330 mg (61.8 mM) NH_4NO_3, 34 g/l (186.6 mM) mannitol, or 100 mM NaCl showed higher GAA activities both at 7 and 11 days of culture. Those supplemented with 0.1% BSA or 5% gelatin showed higher activities than the control only at 11 days of culture. The highest GAA activity was observed at 11 days of culture supplemented with 100 mM NaCl (**Figure 3B**). These results were confirmed by Western blot analysis, which revealed GAA bands for the 11-day-old culture media (**Figure 3C**), except in the case of the gelatin-supplemented culture. Western blot analysis of the gelatin-supplemented culture showed thick band, indicating that gelatin helped stabilize the secreted GAA and prevent it from degradation. However, the activity assay showed low activity indicating that the presence of gelatin might hinder the assay. In addition, because gelatin supplementation severely inhibited the cell growth, caused medium solution to become viscous, and would be an additional contaminant protein in the purification step, we did not continue using it for further optimization. Instead, NaCl was chosen for further optimization to obtain the highest GAA production in the medium.

Selection of an NaCl Concentration for Optimum GAA Production

Supplementing the MS medium with 100 mM NaCl highly increased GAA accumulation in the medium, but also severely reduced the growth of GAA-producing *Arabidopsis* cells. Thus, further investigation was performed to determine the optimum NaCl concentration to obtain high GAA yield while maintaining cell growth. For this purpose, the GAA-producing *Arabidopsis alg3* cell culture was grown in MS media containing 0 mM (control), 25 mM, 50 mM, 100 mM, and 150 mM NaCl. The results showed that cell growth was severely inhibited under NaCl concentrations of 100 mM or more. The *Arabidopsis* cell culture maintained cell growth in the presence of 25 mM or 50 mM NaCl (**Figure 4A**). Among the tested groups, the highest GAA activity was observed in the medium sample from 11-day-old culture grown in MS containing 50 mM NaCl (**Figure 4B**). This result was confirmed by Western blot data showing the thickest band on this sample (**Figure 4C**).

To elucidate the reason for the higher GAA accumulation in the medium of NaCl-supplemented culture, the intracellular GAA production and activity were also tested. Interestingly, the intracellular GAA-specific activity and production were also increased with each increment of NaCl concentration (**Figure 5**). This suggested that the enhanced GAA accumulation in the medium was a result of increased intracellular GAA production. However, because the *Arabidopsis* cell growth was severely inhibited in the presence of 100 or 150 mM NaCl, the total GAA accumulation in the media of cultures supplemented with 100 or 150 mM NaCl was also low.

After purification, the NaCl-supplemented culture resulted in 3.8-times higher yield of GAA production (228 ± 21.1 μg/l) than the control (60.9 ± 12.4 μg/l; **Figure 6A**). The GAA purity from NaCl-supplemented culture was also similar to that in the control (**Figures 6B,C**). Of note, the degraded GAA band that appeared between the 95 and 76 kDa GAAs was less visible

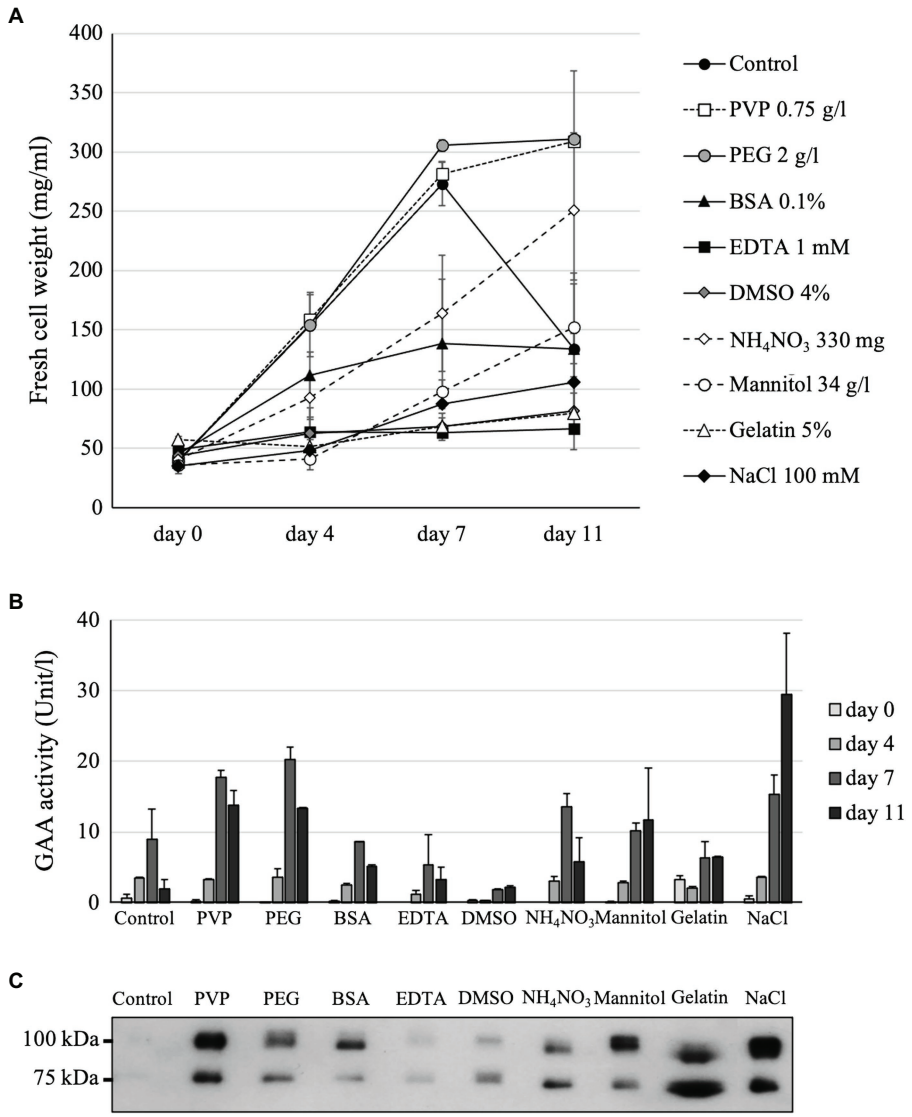

FIGURE 3 | Effects of chemical additives on the cell growth of GAA-producing *Arabidopsis alg3* cell culture **(A)** as well as on GAA production as evaluated by a GAA activity assay **(B)**, and Western blotting **(C)**. Data of **(A)** are average of three independent replications. The media of 11-day-old cultures are used for the Western blot.

in the purified GAA from the NaCl-supplemented culture. This indicated that NaCl helped protect GAA from degradation.

N-Glycan Profiles of GAA Produced in *Arabidopsis alg3* Cell Culture With and Without NaCl Supplementation

To identify the presence of plant-specific *N*-glycans, we performed Western blot analysis of crude and purified GAAs by using an anti-HRP antibody known to bind the plant-specific α1,3-fucose and β1,2-xylose residues (Laurière et al., 1989). The result showed that *Arabidopsis alg3* cell culture contained a small amount of plant-specific *N*-glycans (**Figure 7**). Notably, the Western blot data showed no signal in the sizes of GAA, suggesting that the GAA lacked the plant-specific *N*-glycans.

Constituent *N*-glycans of each *N*-glycosylation site in GAA were further determined by *de novo* sequencing of the tryptic GAA peptides using nanoLC-MS/MS analysis. The glycopeptides bearing the sequence of N390 (^{386}QVVENMTR^{393}), N470 (^{465}GVFITNETGQPLIGK^{479}), and N882 (^{882}NNTIVNELVR^{891}) were successfully detected. As expected, the majority of the *N*-glycans in both 95 and 76 kDa GAAs from *Arabidopsis alg3* cell culture was composed of the M3 structure which accounted for 51.1–80.1% of total *N*-glycan variants (**Figure 8**; **Table 1**; **Supplementary Tables 3–6**). Plant-specific *N*-glycans were not detected in any of the sites. Moreover, the GAA produced in the NaCl-supplemented culture also showed a

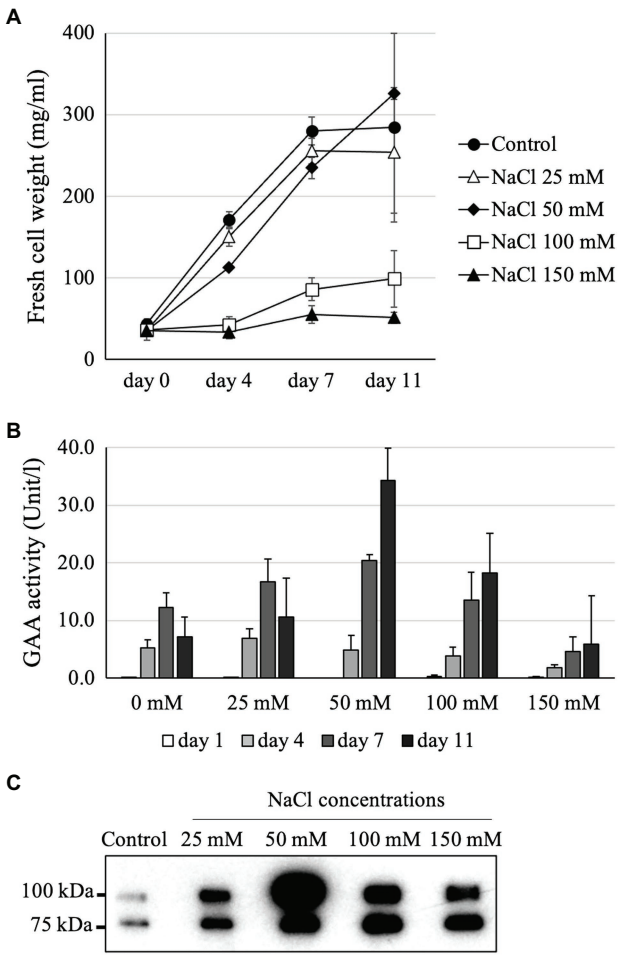

FIGURE 4 | Optimization of the NaCl concentration for yielding the highest GAA production while maintaining *Arabidopsis alg3* cell growth. **(A)** Effects of addition of 0–150 mM NaCl on the cell growth of a GAA-producing *Arabidopsis alg3* cell culture. Data are average of three independent replications. **(B,C)** Evaluation of GAA accumulation in the NaCl-supplemented culture medium by GAA activity assay and Western blot, respectively. The media of 11-day-old cultures are used for the Western blot.

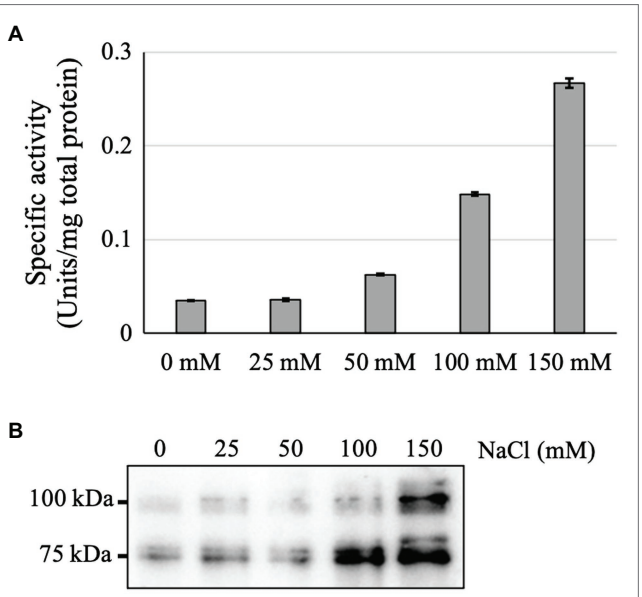

FIGURE 5 | Effects of NaCl supplementation on intracellular GAA production. **(A)** Intracellular GAA-specific activity in cultures supplemented with various amounts of NaCl (0–150 mM). **(B)** Western blot of crude intracellular proteins of NaCl-supplemented 11-day-old culture cells. The result of CBB staining as a loading control is shown in **Supplementary Figure 2**.

similar composition, indicating that increasing the GAA production by NaCl supplementation at a concentration of 50 mM did not affect GAA *N*-glycosylation.

DISCUSSION

The first study using an *Arabidopsis alg3* mutant to produce a recombinant protein was reported a decade ago. In this study, a single chain Fv-Fc antibody MBP10 was produced in an *Arabidopsis alg3* mutant plant (Henquet et al., 2011). However, the antibody carried a KDEL ER retention signal so that the antibody accumulated in the ER and consequently bore mostly the aberrant M5 structure, which is unique to the *alg3* mutant, rather than the M3 structure. Since then, no other study has been done using the *alg3* mutant line. In the present study, human recombinant GAA without any ER retention signal was produced in an *Arabidopsis alg3* cell culture, and thereby, the fate of the recombinant protein in the *alg3* mutant cells could be better understood.

GAA is a lysosomal enzyme known to undergo sequential proteolytic processing and *N*-glycosylation for enzyme maturation (Moreland et al., 2012). In humans, GAA is initially synthesized as a polypeptide of 952 amino acids containing an *N*-terminal signal peptide for co-translational transport into the lumen of the ER. The signal peptide is cleaved by the host signal peptidase, generating a 110 kDa GAA precursor. Then, the precursor is cleaved in the *N*-terminus to generate a 95 kDa GAA intermediate. Subsequently, another protease cleaves the *C*-terminus, resulting in a 76 kDa mature GAA. Finally, a protease cleaves the *N*-terminus to generate the final mature GAA of 70 kDa (Moreland et al., 2005). These sequential proteolytic processes are critical for the enzyme activity, as the 76/70 kDa mature forms show 7–10 times greater affinity to the substrate compared to the 110 kDa precursor (Wisselaar et al., 1993; Bijvoet et al., 1998). Yet, the proteases responsible for these processes are still unidentified. In this study, we found that *Arabidopsis alg3* cells were capable of recognizing and cleaving the native human GAA signal peptide in addition to conducting the multiple proteolytic processing, as indicated by the presence of 110, 95, and 76 kDa forms in the GAA-producing cells. However, the 70 kDa form could not be detected, indicating that the essential protease is absent in *Arabidopsis* cells. Moreover, the proportion of the 95 kDa GAA seemed to be higher than that of the 76 kDa GAA. Therefore, to optimize the GAA

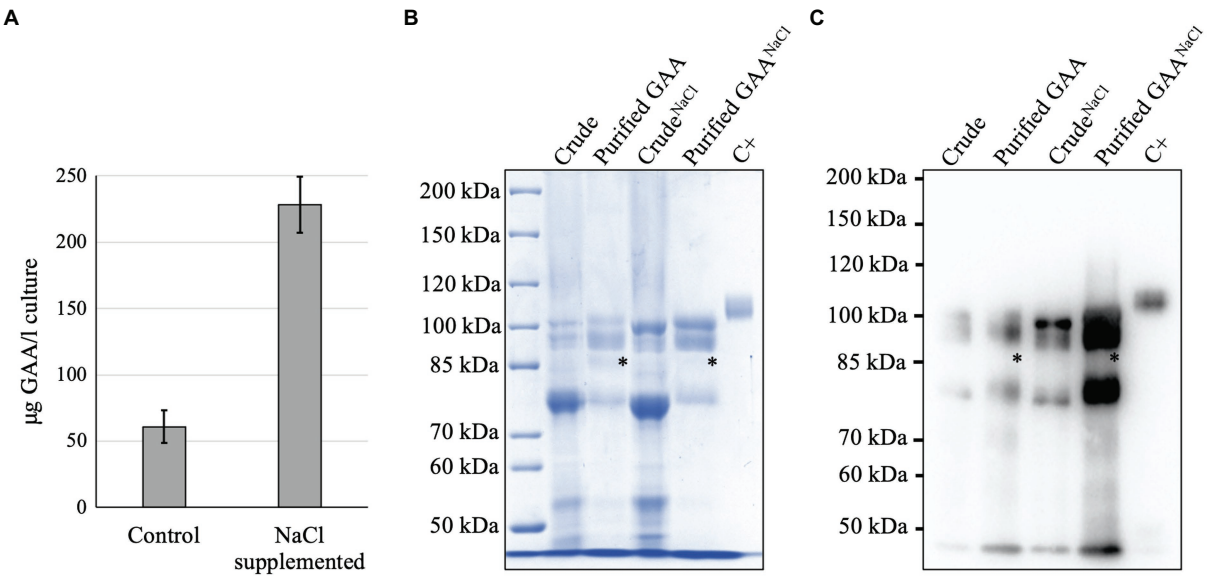

FIGURE 6 | Analysis of GAA purification from NaCl-supplemented culture. **(A)** Yield of GAA production from cultures with and without NaCl supplementation. **(B,C)** CBB staining and Western blot of purified GAAs from cultures with and without NaCl supplementation. An asterisk (*) indicates degraded GAA.

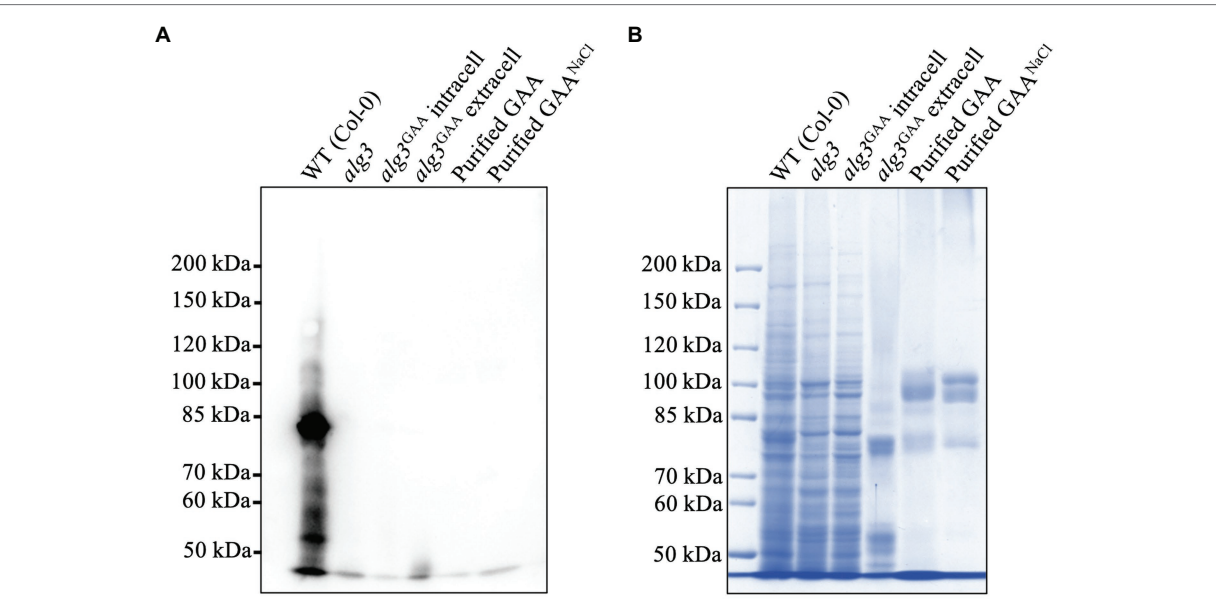

FIGURE 7 | Detection of plant-specific *N*-glycans in an *Arabidopsis alg3* cell culture and purified GAA from the cultures with and without NaCl supplementation. **(A)** Western blot analysis using anti-HRP to detect plant specific *N*-glycans. **(B)** CBB staining as a loading control.

production in plant culture, it will be necessary to identify the proteases responsible for the cleavages. With this knowledge in hand, it will become possible to increase the production of mature GAA by co-expressing the human protease(s) *in vivo* or by performing the protease cleavage *in vitro*.

Studies on the production of recombinant human GAA in plant cells have been done in tobacco plant (Martiniuk et al., 2013), rice culture (Jung et al., 2016, 2017), and moss culture (Hintze et al., 2020). In all of these studies, GAAs were constructed under plant-derived signal peptides to drive plant organ-specific localization or secretion into the culture medium. In the present study, the native human GAA signal peptide was used. Interestingly, our results showed that *Arabidopsis* cells were capable of recognizing and processing the human GAA signal peptide, as indicated by the detection of a cleaved GAA polypeptide generating the 110 kDa GAA (**Figure 1C**). This indicates that the human GAA signal peptide was capable of facilitating GAA entrance into the ER, followed by further

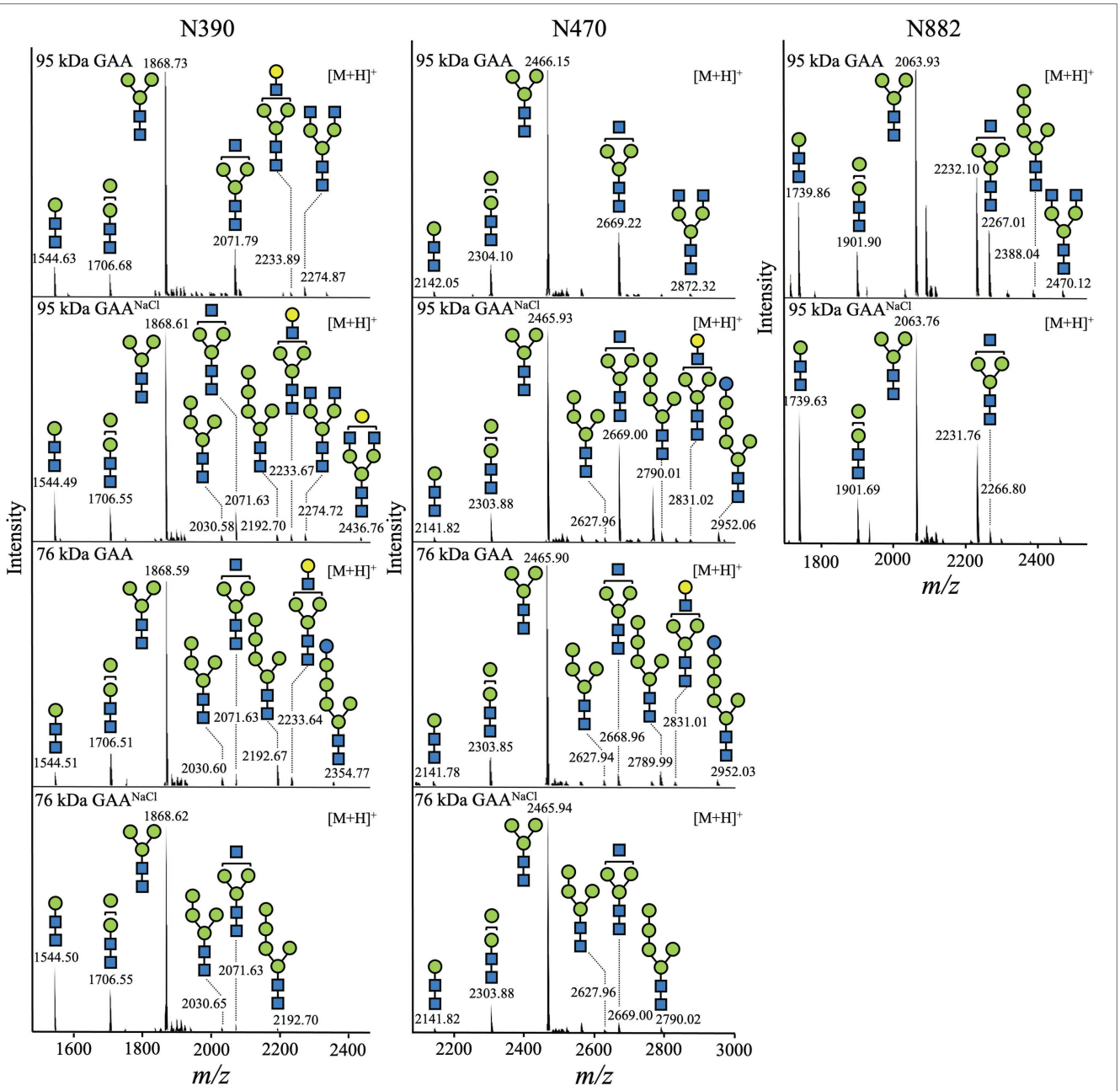

FIGURE 8 | *N*-glycan profile of GAA produced in *Arabidopsis alg3* cell cultures with and without NaCl supplementation. In the shown deconvoluted MS spectra, the mass $[M + H]^+$ of the tryptic glycopeptides carrying *N*-glycosylation sites (N390, N470, and N882) is depicted.

transport into the Golgi apparatus and, finally, secretion into the plant culture medium.

GAA is known to be extensively *N*-glycosylated—the 95 and 76 kDa forms contain seven and five *N*-glycosylation sites, respectively (Moreland et al., 2005). As expected, the *Arabidopsis alg3*-produced GAAs have a predominantly M3 structure (51.1–80.1%). Moreover, anti-HRP antibody could not detect any plant-specific *N*-glycans in GAA, although a low amount of plant-specific *N*-glycans were detected in the culture (**Figure 7**). This suggests that the ruling of *N*-glycosylation may be protein specific. The lack of plant-specific *N*-glycans in our GAA would eliminate the concern of potential allergic reaction upon administration to patients with Pompe disease. For further work, it will be preferable to also knock-out the *gnt-I* and *gnt-II* genes in the *Arabidopsis alg3* cell line to increase *N*-glycan homogeneity and ensure the safety of the product. In addition, galactose-terminal *N*-glycans were also detected. This residue is a component of the Lewis a structure commonly found in the *trans* Golgi apparatus and extracellular proteins and is generated by the β1,3-galactosyltransferase

TABLE 1 | Composition of the *N*-glycan structures in GAA produced in *Arabidopsis alg3* cell cultures with and without NaCl supplementation.

Abbreviation	Structure	Relative amount (%)									
		95 kDa GAA			76 kDa GAA			95 kDa GAA^{NaCl}		76 kDa GAA^{NaCl}	
		N390	N470	N882	N390	N470	N390	N470	N882	N390	N470
M1	$ManGlcNAc_2$	8.7	1.5	21.2	4.4	1.4	14.7	1.2	33.0	30.1	1.6
M2	$Man_2GlcNAc_2$	6.4	9.5	10.1	11.4	9.5	10.2	7.6	11.3	13.2	11.2
M3	$Man_3GlcNAc_2$	68.0	68.2	51.1	67.5	75.5	56.6	57.8	51.8	54.0	80.1
$M4^{ER}$	$Man_4GlcNAc_2$	–	–	–	2.6	1.8	1.6	1.1	–	0.9	1.1
$M5^{ER}$	$Man_5GlcNAc_2$	–	–	1.5	6.6	4.5	1.4	3.1	–	0.6	2.3
$GlcM5^{ER}$	$GlcMan_5GlcNAc_2$	–	–	–	1.2	2.0	–	2.6	–	–	–
GnM3	$GlcNAcMan_3GlcNAc_2$	12.6	20.0	14.3	3.4	4.0	10.6	25.7	3.9	1.2	3.7
Gn2M3	$GlcNAc_2Man_3GlcNAc_2$	2.7	0.8	1.8	–	–	2.2	–	–	–	–
GalGnM3	$GalGlcNAcMan_3GlcNAc_2$	1.6	–	–	2.9	1.3	2.0	0.9	–	–	–
GalGn2M3	$GalGlcNAc_2Man_3GlcNAc_2$	–	–	–	–	–	0.7	–	–	–	–
	Total	100	100	100	100	100	100	100	100	100	100

enzyme resident in the Golgi apparatus (Fitchette et al., 1999; Strasser et al., 2007). Detection of this structure in GAA confirms that GAA is properly transported to the Golgi apparatus prior to secretion into the plant culture medium.

Previous studies have demonstrated the potentials of some chemicals to improve the production of recombinant proteins in plant culture; however, these effects seem to be dependent on the target protein and plant species. For instance, PVP was reported to enhance the secreted recombinant heavy-chain monoclonal antibody in *Nicotiana tabacum* NT-1 suspension culture (LaCount et al., 1997). On the other hand, Lee et al. did not find any effect of PVP in the production of human granulocyte-macrophage colony-stimulating factor in *N. tabacum* cv. Havana SR1 suspension culture (Lee et al., 2002). Therefore, medium optimization needs to be done for each product and cell line on a case-by-case basis. In this study, a number of chemicals were shown to increase GAA production, including PVP, PEG, NH_4NO_3, mannitol, and NaCl. Supplementation with 50 mM NaCl achieved the highest production while maintaining cell growth, resulting in 3.8-fold higher yield than the control.

The increment of GAA production in intra- and extracellular fractions of NaCl-supplemented culture can be attributed to the stabilizing effect of NaCl, which protects GAA from degradation, as indicated by the relative absence of a degraded GAA band as compared to the control (**Figure 6B**). Moreover, the increased GAA accumulation in the medium of NaCl-supplemented culture might have been the result of enhanced GAA secretion. This hypothesis is based on the previous reports showing that salt (e.g., NaCl) induces the generation of reactive oxygen species which subsequently attacks membrane lipoproteins and causes impaired membrane permeability (Mansour, 2013), thereby facilitating the secretion of intracellular proteins. However, whether this mechanism occurs in our case and contributes to increased GAA secretion is still unknown. Notably, the *N*-glycan profiles of GAAs produced in NaCl-supplemented culture were similar to those in the control, indicating that NaCl supplementation to a final concentration of 50 mM does not affect *N*-glycosylation in the *Arabidopsis* cells. These findings indicate that NaCl supplementation can be an economic, easy, and effective strategy to increase GAA production in the *Arabidopsis* cell culture.

Despite the improved GAA production by NaCl supplementation, the yield was relatively low as compared to the previous studies of GAA production in tobacco seed (40 μg/g; Martiniuk et al., 2013) and rice cell culture (up to 45 mg/l; Jung et al., 2016, 2017). The low level of production could be the result of ER stress as previously observed in *Arabidopsis alg3* plant (Henquet et al., 2008, 2011; Kajiura et al., 2010). For future work, it may be possible to increase GAA production by co-expressing chaperon proteins to alleviate the ER stress (Margolin et al., 2020). Moreover, the GAA production may be improved by combining with other enhanced production of recombinant proteins in plant cells, such as suppression of gene silencing (Papp et al., 2003; Butaye et al., 2004; Jeong et al., 2018), use of more robust expression system (e.g., use of geminiviral replication, double promoter and terminator; Yamamoto et al., 2018), and transient expression strategy (e.g., plant-cell pack technology; Rademacher et al., 2019).

Finally, we succeeded in producing GAA bearing predominantly the M3 structure. Previous studies have highlighted the merit of using M3 for MR-mediated cellular delivery (Van Patten et al., 2007; Shen et al., 2016). Our success in producing GAA with the M3 structure in the *Arabidopsis alg3* cell culture emphasizes the potential of our glycoengineered *Arabidopsis* cell culture for producing other recombinant proteins in which M3 and/or cellular delivery through MR is desired, such as in the enzyme replacement therapies for Gaucher disease, Fabry disease, Wolman disease, and cholesteryl ester storage disease (Du et al., 2005; Limkul et al., 2016; Shen et al., 2016).

DATA AVAILABILITY STATEMENT

The raw data supporting the conclusions of this article will be made available by the authors, without undue reservation.

AUTHOR CONTRIBUTIONS

RS, Florence, HK, and KF conceived and designed the experiments. RS and Florence conducted laboratory experiments and analyses. HK, TO, RM, and KF conducted data analyses as well. RS wrote the manuscript and all authors provided editorial advice and revised manuscript. All authors contributed to the article and approved the submitted version.

FUNDING

This work was supported by the Ministry of Education, Culture, Sports, Science and Technology (MEXT).

ACKNOWLEDGMENTS

This research was conducted by RS in partial fulfillment of the requirements for a Ph.D. We are also grateful to Dr. Juthamard Limkul for developing the *Arabidopsis alg3* suspension cell culture used in this research.

SUPPLEMENTARY MATERIAL

The Supplementary Material for this article can be found online at https://www.frontiersin.org/articles/10.3389/fpls.2021.703020/full#supplementary-material

REFERENCES

Bijvoet, A. G. A., Kroos, M. A., Pieper, F. R., Van der Vliet, M., De Boer, H. A., Van der Ploeg, A. T., et al. (1998). Recombinant human acid-glucosidase: high level production in mouse milk, biochemical characteristics, correction of enzyme deficiency in GSDII KO mice. *Hum. Mol. Genet.* 7, 1815–1824. doi: 10.1093/hmg/7.11.1815

Butaye, K. M. J., Goderis, I. J. W. M., Wouters, P. F. J., Pues, J. M.-T. G., Delauré, S. L., Broekaert, W. F., et al. (2004). Stable high-level transgene expression in *Arabidopsis thaliana* using gene silencing mutants and matrix attachment regions. *Plant J.* 39, 440–449. doi: 10.1111/j.1365-313X.2004.02144.x

Du, H., Levine, M., Ganesa, C., Witte, D. P., Cole, E. S., and Grabowski, G. A. (2005). The role of mannosylated enzyme and the mannose receptor in enzyme replacement therapy. *Am. J. Hum. Genet.* 77, 1061–1074. doi: 10.1086/498652

Fischer, R., Vasilev, N., Twyman, R. M., and Schillberg, S. (2015). High-value products from plants: the challenges of process optimization. *Curr. Opin. Biotechnol.* 32, 156–162. doi: 10.1016/j.copbio.2014.12.018

Fitchette, A. C., Cabanes-Macheteau, M., Marvin, L., Martin, B., Satiat-Jeunemaitre, B., Gomord, V., et al. (1999). Biosynthesis and immunolocalization of Lewis a-containing N-glycans in the plant cell. *Plant Physiol.* 121, 333–344. doi: 10.1104/pp.121.2.333

Gomord, V., Fitchette, A.-C., Menu-Bouaouiche, L., Saint-Jore-Dupas, C., Plasson, C., Michaud, D., et al. (2010). Plant-specific glycosylation patterns in the context of therapeutic protein production: pmp-specific glycosylation patterns. *Plant Biotechnol. J.* 8, 564–587. doi: 10.1111/j.1467-7652.2009.00497.x

Goochee, C. F., Gramer, M. J., Andersen, D. C., Bahr, J. B., and Rasmussen, J. R. (1991). The oligosaccharides of glycoproteins: bioprocess factors affecting oligosaccharide structure and their effect on glycoprotein properties. *Nat. Biotechnol.* 9, 1347–1355. doi: 10.1038/nbt1291-1347

Hellwig, S., Drossard, J., Twyman, R. M., and Fischer, R. (2004). Plant cell cultures for the production of recombinant proteins. *Nat. Biotechnol.* 22, 1415–1422. doi: 10.1038/nbt1027

Henquet, M., Eigenhuijsen, J., Hesselink, T., Spiegel, H., Schreuder, M., van Duijn, E., et al. (2011). Characterization of the single-chain Fv-Fc antibody MBP10 produced in *Arabidopsis* alg3 mutant seeds. *Transgenic Res.* 20, 1033–1042. doi: 10.1007/s11248-010-9475-5

Henquet, M., Lehle, L., Schreuder, M., Rouwendal, G., Molthoff, J., Helsper, J., et al. (2008). Identification of the gene encoding the α1,3-mannosyltransferase (ALG3) in *Arabidopsis* and characterization of downstream N-glycan processing. *Plant Cell* 20, 1652–1664. doi: 10.1105/tpc.108.060731

Hintze, S., Limmer, S., Dabrowska-Schlepp, P., Berg, B., Krieghoff, N., Busch, A., et al. (2020). Moss-derived human recombinant GAA provides an optimized enzyme uptake in differentiated human muscle cells of Pompe disease. *Int. J. Mol. Sci.* 21:2642. doi: 10.3390/ijms21072642

Holland, T., Sack, M., Rademacher, T., Schmale, K., Altmann, F., Stadlmann, J., et al. (2010). Optimal nitrogen supply as a key to increased and sustained production of a monoclonal full-size antibody in BY-2 suspension culture. *Biotechnol. Bioeng.* 107, 278–289. doi: 10.1002/bit.22800

James, E. A., Wang, C., Wang, Z., Reeves, R., Shin, J. H., Magnuson, N. S., et al. (2000). Production and characterization of biologically active human GM-CSF secreted by genetically modified plant cells. *Protein Expr. Purif.* 19, 131–138. doi: 10.1006/prep.2000.1232

Jeong, I. S., Lee, S., Bonkhofer, F., Tolley, J., Fukudome, A., Nagashima, Y., et al. (2018). Purification and characterization of *Arabidopsis thaliana* oligosaccharyltransferase complexes from the native host: a protein super-expression system for structural studies. *Plant J.* 94, 131–145. doi: 10.1111/tpj.13847

Jung, J.-W., Huy, N.-X., Kim, H.-B., Kim, N.-S., Van Giap, D., and Yang, M.-S. (2017). Production of recombinant human acid α-glucosidase with high-mannose glycans in gnt1 rice for the treatment of Pompe disease. *J. Biotechnol.* 249, 42–50. doi: 10.1016/j.jbiotec.2017.03.033

Jung, J.-W., Kim, N.-S., Jang, S.-H., Shin, Y.-J., and Yang, M.-S. (2016). Production and characterization of recombinant human acid α-glucosidase in transgenic rice cell suspension culture. *J. Biotechnol.* 226, 44–53. doi: 10.1016/j.jbiotec.2016.03.031

Kajiura, H., Seki, T., and Fujiyama, K. (2010). *Arabidopsis thaliana* ALG3 mutant synthesizes immature oligosaccharides in the ER and accumulates unique N-glycans. *Glycobiology* 20, 736–751. doi: 10.1093/glycob/cwq028

Kohler, L., Puertollano, R., and Raben, N. (2018). Pompe disease: from basic science to therapy. *Neurotherapeutics* 15, 928–942. doi: 10.1007/s13311-018-0655-y

Kwon, T. H., Seo, J. E., Kim, J., Lee, J. H., Jang, Y. S., and Yang, M. S. (2003). Expression and secretion of the heterodimeric protein interleukin-12 in plant cell suspension culture. *Biotechnol. Bioeng.* 81, 870–875. doi: 10.1002/bit.10528

LaCount, W., An, G., and Lee, J. M. (1997). The effect of polyvinylpyrrolidone (PVP) on the heavy chain monoclonal antibody production from plant suspension cultures. *Biotechnol. Lett.* 19, 93–96. doi: 10.1023/A:1018383524389

Laurière, M., Laurière, C., Chrispeels, M. J., Johnson, K. D., and Sturm, A. (1989). Characterization of a xylose-specific antiserum that reacts with the

complex asparagine-linked glycans of extracellular and vacuolar glycoproteins. *Plant Physiol.* 90, 1182–1188. doi: 10.1104/pp.90.3.1182

Lee, J.-H., Kim, N.-S., Kwon, T.-H., Jang, Y.-S., and Yang, M.-S. (2002). Increased production of human granulocyte-macrophage colony stimulating factor (hGM-CSF) by the addition of stabilizing polymer in plant suspension cultures. *J. Biotechnol.* 96, 205–211. doi: 10.1016/S0168-1656(02)00044-5

Lew, D. B., Songu-Mize, E., Pontow, S. E., Stahl, P. D., and Rattazzi, M. C. (1994). A mannose receptor mediates mannosyl-rich glycoprotein-induced mitogenesis in bovine airway smooth muscle cells. *J. Clin. Invest.* 94, 1855–1863. doi: 10.1172/JCI117535

Limkul, J., Iizuka, S., Sato, Y., Misaki, R., Ohashi, T., Ohashi, T., et al. (2016). The production of human glucocerebrosidase in glyco-engineered *Nicotiana benthamiana* plants. *Plant Biotechnol. J.* 14, 1682–1694. doi: 10.1111/pbi.12529

Limkul, J., Misaki, R., Kato, K., and Fujiyama, K. (2015). The combination of plant translational enhancers and terminator increase the expression of human glucocerebrosidase in *Nicotiana benthamiana* plants. *Plant Sci.* 240, 41–49. doi: 10.1016/j.plantsci.2015.08.018

Mansour, M. M. F. (2013). Plasma membrane permeability as an indicator of salt tolerance in plants. *Biol. Plant.* 57, 1–10. doi: 10.1007/s10535-012-0144-9

Margolin, E., Oh, Y. J., Verbeek, M., Naude, J., Ponndorf, D., Meshcheriakova, Y. A., et al. (2020). Co-expression of human calreticulin significantly improves the production of HIV gp140 and other viral glycoproteins in plants. *Plant Biotechnol. J.* 18, 2109–2117. doi: 10.1111/pbi.13369

Martiniuk, F., Reggi, S., Tchou-Wong, K.-M., Rom, W. N., Busconi, M., and Fogher, C. (2013). Production of a functional human acid maltase in tobacco seeds: biochemical analysis, uptake by human GSDII cells, and *in vivo* studies in GAA knockout mice. *Appl. Biochem. Biotechnol.* 171, 916–926. doi: 10.1007/s12010-013-0367-z

McCall, A. L., Salemi, J., Bhanap, P., Strickland, L. M., and Elmallah, M. K. (2018). The impact of Pompe disease on smooth muscle: a review. *J. Smooth Muscle Res.* 54, 100–118. doi: 10.1540/jsmr.54.100

Meena, N. K., and Raben, N. (2020). Pompe disease: new developments in an old lysosomal storage disorder. *Biomol. Ther.* 10:1339. doi: 10.3390/biom10091339

Montero-Morales, L., and Steinkellner, H. (2018). Advanced plant-based glycan engineering. *Front. Bioeng. Biotechnol.* 6:81. doi: 10.3389/fbioe.2018.00081

Moreland, R. J., Higgins, S., Zhou, A., VanStraten, P., Cauthron, R. D., Brem, M., et al. (2012). Species-specific differences in the processing of acid α-glucosidase are due to the amino acid identity at position 201. *Gene* 491, 25–30. doi: 10.1016/j.gene.2011.09.011

Moreland, R. J., Jin, X., Zhang, X. K., Decker, R. W., Albee, K. L., Lee, K. L., et al. (2005). Lysosomal acid α-glucosidase consists of four different peptides processed from a single chain precursor. *J. Biol. Chem.* 280, 6780–6791. doi: 10.1074/jbc.M404008200

Moustafa, K., Makhzoum, A., and Trémouillaux-Guiller, J. (2016). Molecular farming on rescue of pharma industry for next generations. *Crit. Rev. Biotechnol.* 36, 840–850. doi: 10.3109/07388551.2015.1049934

Murashige, T., and Skoog, F. (1962). A revised medium for rapid growth and bio assays with tobacco tissue cultures. *Physiol. Plant.* 15, 473–497. doi: 10.1111/j.1399-3054.1962.tb08052.x

Papp, I., Mette, M. F., Aufsatz, W., Daxinger, L., Schauer, S. E., Ray, A., et al. (2003). Evidence for nuclear processing of plant micro RNA and short interfering RNA precursors. *Plant Physiol.* 132, 1382–1390. doi: 10.1104/pp.103.021980

Rademacher, T., Sack, M., Blessing, D., Fischer, R., Holland, T., and Buyel, J. (2019). Plant cell packs: a scalable platform for recombinant protein production and metabolic engineering. *Plant Biotechnol. J.* 17, 1560–1566. doi: 10.1111/pbi.13081

Rozov, S. M., Permyakova, N. V., and Deineko, E. V. (2018). Main strategies of plant expression system glycoengineering for producing humanized recombinant pharmaceutical proteins. *Biochemistry* 83, 215–232. doi: 10.1134/S0006297918030033

Rudge, S., and Nims, R. (2018). ICH topic Q 6 B specifications: test procedures and acceptance criteria for biotechnological/biological products. Available at: https://www.ema.europa.eu/en/documents/scientific-guideline/ich-q-6-b-test-procedures-acceptance-criteria-biotechnological/biological-products-step-5_en.pdf (Accessed December 4, 2020).

Sanchez-Serrano, J. J., and Salinas, J. (Eds.) (2014). *Arabidopsis Protocols*. Totowa, NJ: Humana Press.

Santos, R. B., Abranches, R., Fischer, R., Sack, M., and Holland, T. (2016). Putting the spotlight back on plant suspension cultures. *Front. Plant Sci.* 7:297. doi: 10.3389/fpls.2016.00297

Seeberger, P., and Cummings, R. (2015). "Glycans in biotechnology and the pharmaceutical industry" in *Essentials of Glycobiology. 3rd Edn*. eds. A. Varki, R. D. Cummings, J. D. Esko, P. Stanley, G. W. Hart, M. Aebi, et al. (Cold Spring Harbor, NY: Cold Spring Harbor Laboratory Press), 729–741.

Sethuraman, N., and Stadheim, T. A. (2006). Challenges in therapeutic glycoprotein production. *Curr. Opin. Biotechnol.* 17, 341–346. doi: 10.1016/j.copbio.2006.06.010

Sharp, J. M., and Doran, P. M. (2001). Strategies for enhancing monoclonal antibody accumulation in plant cell and organ cultures. *Biotechnol. Prog.* 17, 979–992. doi: 10.1021/bp010104t

Shen, J.-S., Busch, A., Day, T. S., Meng, X.-L., Yu, C. I., Dabrowska-Schlepp, P., et al. (2016). Mannose receptor-mediated delivery of moss-made α-galactosidase a efficiently corrects enzyme deficiency in Fabry mice. *J. Inherit. Metab. Dis.* 39, 293–303. doi: 10.1007/s10545-015-9886-9

Strasser, R., Altmann, F., and Steinkellner, H. (2014). Controlled glycosylation of plant-produced recombinant proteins. *Curr. Opin. Biotechnol.* 30, 95–100. doi: 10.1016/j.copbio.2014.06.008

Strasser, R., Bondili, J. S., Vavra, U., Schoberer, J., Svoboda, B., Glössl, J., et al. (2007). A unique β1,3-galactosyltransferase is indispensable for the biosynthesis of *N*-glycans containing Lewis a structures in *Arabidopsis thaliana*. *Plant Cell* 19, 2278–2292. doi: 10.1105/tpc.107.052985

Su, W. W., and Lee, K.-T. (2007). "Plant cell and hairy root cultures – process characteristics, products, and applications" in *Bioprocessing for Value-Added Products from Renewable Resources*. ed. S.-T. Yang (Amsterdam, Netherlands: Elsevier), 263–292.

Taylor, P., Gordon, S., and Martinez-Pomares, L. (2005). The mannose receptor: linking homeostasis and immunity through sugar recognition. *Trends Immunol.* 26, 104–110. doi: 10.1016/j.it.2004.12.001

Tsoi, B. M.-Y., and Doran, P. M. (2002). Effect of medium properties and additives on antibody stability and accumulation in suspended plant cell cultures. *Biotechnol. Appl. Biochem.* 35, 171–180. doi: 10.1042/BA20010105

Van Patten, S. M., Hughes, H., Huff, M. R., Piepenhagen, P. A., Waire, J., Qiu, H., et al. (2007). Effect of mannose chain length on targeting of glucocerebrosidase for enzyme replacement therapy of Gaucher disease. *Glycobiology* 17, 467–478. doi: 10.1093/glycob/cwm008

Wenk, J., Hille, A., and von Figura, K. (1991). Quantitation of Mr 46000 and Mr 300000 mannose 6-phosphate receptors in human cells and tissues. *Biochem. Int.* 23, 723–731.

Wisselaar, H. A., Kroos, M. A., Hermans, M. M., van Beeumen, J., and Reuser, A. J. (1993). Structural and functional changes of lysosomal acid alpha-glucosidase during intracellular transport and maturation. *J. Biol. Chem.* 268, 2223–2231. doi: 10.1016/S0021-9258(18)53985-5

Xu, J., Ge, X., and Dolan, M. C. (2011). Towards high-yield production of pharmaceutical proteins with plant cell suspension cultures. *Biotechnol. Adv.* 29, 278–299. doi: 10.1016/j.biotechadv.2011.01.002

Xu, J., and Zhang, N. (2014). On the way to commercializing plant cell culture platform for biopharmaceuticals: present status and prospect. *Pharm. Bioprocess.* 2, 499–518. doi: 10.4155/pbp.14.32

Yamamoto, T., Hoshikawa, K., Ezura, K., Okazawa, R., Fujita, S., Takaoka, M., et al. (2018). Improvement of the transient expression system for production of recombinant proteins in plants. *Sci. Rep.* 8:4755. doi: 10.1038/s41598-018-23024-y

Yusuf, E., and Yajid, M. S. A. (2016). Halal pharmaceuticals and cosmeceuticals from the perspective of higher education. *Asian. J. Pharm. Sci.* 11, 18–19. doi: 10.1016/j.ajps.2015.10.013

Zagorskaya, A. A., and Deineko, E. V. (2017). Suspension-cultured plant cells as a platform for obtaining recombinant proteins. *Russ. J. Plant Physiol.* 64, 795–807. doi: 10.1134/S102144371705017X

Zhang, N., Dolan, M., Wu, D., Phillips, G. C., and Xu, J. (2016). Dramatic secretion of recombinant protein expressed in tobacco cells with a designer glycopeptide tag is highly impacted by medium composition. *Plant Cell Rep.* 35, 2513–2522. doi: 10.1007/s00299-016-2051-6

Conflict of Interest: The authors declare that the research was conducted in the absence of any commercial or financial relationships that could be construed as a potential conflict of interest.

frontiers in Plant Science

ORIGINAL RESEARCH
published: 22 July 2021
doi: 10.3389/fpls.2021.709344

Site-Specific Glycosylation of Recombinant Viral Glycoproteins Produced in *Nicotiana benthamiana*

Emmanuel Margolin[1,2,3,4†], Joel D. Allen[5†], Matthew Verbeek[4], Michiel van Diepen[1,3], Phindile Ximba[1,3], Rosamund Chapman[1,3], Ann Meyers[4], Anna-Lise Williamson[1,2,3], Max Crispin[5*] and Edward Rybicki[3,4]*

[1] Division of Medical Virology, Department of Pathology, Faculty of Health Sciences, University of Cape Town, Cape Town, South Africa, [2] Wellcome Trust Centre for Infectious Disease Research in Africa, University of Cape Town, Cape Town, South Africa, [3] Institute of Infectious Disease and Molecular Medicine, Faculty of Health Sciences, University of Cape Town, Cape Town, South Africa, [4] Biopharming Research Unit, Department of Molecular and Cell Biology, University of Cape Town, Cape Town, South Africa, [5] School of Biological Sciences, University of Southampton, Southampton, United Kingdom

OPEN ACCESS

Edited by:
Natacha Soto Pérez,
Center for Genetic Engineering and Biotechnology (CIGB), Cuba

Reviewed by:
Marina Clemente,
CONICET Institute of Biotechnological Research (IIB-INTECH), Argentina
Somen Nandi,
University of California, Davis, United States

***Correspondence:**
Emmanuel Margolin
Emmanuel.margolin@uct.ac.za
Max Crispin
max.crispin@soton.ac.uk

[†] These authors share first authorship

Specialty section:
This article was submitted to Plant Biotechnology, a section of the journal Frontiers in Plant Science

Received: 13 May 2021
Accepted: 24 June 2021
Published: 22 July 2021

Citation:
Margolin E, Allen JD, Verbeek M, van Diepen M, Ximba P, Chapman R, Meyers A, Williamson A-L, Crispin M and Rybicki E (2021) Site-Specific Glycosylation of Recombinant Viral Glycoproteins Produced in Nicotiana benthamiana. Front. Plant Sci. 12:709344. doi: 10.3389/fpls.2021.709344

There is an urgent need to establish large scale biopharmaceutical manufacturing capacity in Africa where the infrastructure for biologics production is severely limited. Molecular farming, whereby pharmaceuticals are produced in plants, offers a cheaper alternative to mainstream expression platforms, and is amenable to rapid large-scale production. However, there are several differences along the plant protein secretory pathway compared to mammalian systems, which constrain the production of complex pharmaceuticals. Viral envelope glycoproteins are important targets for immunization, yet in some cases they accumulate poorly in plants and may not be properly processed. Whilst the co-expression of human chaperones and furin proteases has shown promise, it is presently unclear how plant-specific differences in glycosylation impact the production of these proteins. In many cases it may be necessary to reproduce features of their native glycosylation to produce immunologically relevant vaccines, given that glycosylation is central to the folding and immunogenicity of these antigens. Building on previous work, we transiently expressed model glycoproteins from HIV and Marburg virus in *Nicotiana benthamiana* and mammalian cells. The proteins were purified and their site-specific glycosylation was determined by mass-spectrometry. Both glycoproteins yielded increased amounts of protein aggregates when produced in plants compared to the equivalent mammalian cell-derived proteins. The glycosylation profiles of the plant-produced glycoproteins were distinct from the mammalian cell produced proteins: they displayed lower levels of glycan occupancy, reduced complex glycans and large amounts of paucimannosidic structures. The elucidation of the site-specific glycosylation of viral glycoproteins produced in *N. benthamiana* is an important step toward producing heterologous viral glycoproteins in plants with authentic human-like glycosylation.

Keywords: glycoprotein, glycosylation, occupancy, folding, processing, molecular pharming

INTRODUCTION

Plant-based expression systems are gaining increased attention for the production of recombinant proteins, including subunit vaccines and therapeutic monoclonal antibodies (Sack et al., 2015; Group et al., 2016). This is largely driven by the potential for more rapid implementation timelines and capacity for rapid production scale-up when compared to established expression systems. The upfront capital investment for a plant-based manufacturing facility is also considerably lower than for mammalian cell production, and the production costs for the raw material are similarly reduced (Nandi et al., 2016). These features are appealing to low-and middle-income countries where biomanufacturing capacity is urgently needed, but is mostly absent (Margolin et al., 2020a). The inherent ease of biomass production also offers the prospect of rapid vaccine production in response to pandemic viral outbreaks (Margolin et al., 2018), as has recently been demonstrated by Medicago Inc., in Canada for a SARS-CoV-2 virus-like particle (VLP) vaccine candidate (Ward et al., 2020a). However, products from plant-based expression systems may not always display desired critical quality attributes: for example, when a biologic requires extensive post-translational modifications, that are not performed in plants as in other cell types, there is consequently a need to further develop plant-based expression technologies to better support the production of complex pharmaceutical products such as glycosylated biologics (Margolin et al., 2020b).

Ideally, a plant-based manufacturing platform should support high yields of recombinant proteins that are appropriately post-translationally processed and biologically active. Encouraging findings have been described for many targets, including the clinical development of influenza and SARS-CoV-2 VLP-based vaccines, and the emergency use of plant-made antibody cocktails for treatment of Ebola virus infection (Landry et al., 2010; Ward et al., 2014; Group et al., 2016; Pillet et al., 2016). However, in many other cases expression yields remain a challenge, and the plant cellular machinery may also not support extensive post-translational modifications for complex biopharmaceutical targets (Margolin et al., 2020c). Virion envelope glycoproteins are amongst the most challenging targets to produce in plants, and the inability to consistently produce native-like glycoproteins from diverse targets constrains the use of the platform for vaccine development against more complex pathogens.

The requirement for "native-like" glycosylation for appropriate immunogenicity is dictated by the antigen of interest rather than being an absolute, and it is worth noting that many targets do not require native glycosylation to elicit appropriate immunogenicity. It is also noteworthy that oligomannose-type glycans are often enriched in viral glycoproteins, such as reported for HIV-1 (Doores et al., 2010; Bonomelli et al., 2011) and SARS-CoV-2 (Watanabe et al., 2020), but are generally less abundant in plants and mammalian systems. Plant-produced influenza hemagglutinin (HA)-based VLP vaccines, for example, have been reported to be efficacious and well tolerated in phase 3 clinical trials despite the presence of typical plant-derived glycans (Ward et al., 2020b). Similarly, an insect-cell produced SARS-CoV-2 spike nanoparticle vaccine has recently been reported to be protective against COVID-19 (Keech et al., 2020), and the presence of species-specific glycosylation does not appear to negatively impact the folding or immunogenicity of this antigen. In contrast, native-like glycosylation is widely regarded as an essential requirement for an HIV envelope-based vaccine, and subtle differences in glycosylation can dictate the quality of the immune response (Behrens and Crispin, 2017). Additionally, glycosylation is intrinsically linked to protein folding, and aberrant glycosylation and particularly under-glycosylation could compromise the efficient production of viral glycoproteins in a heterologous system (Margolin et al., 2020b).

Remodeling the secretory pathway has been proposed as a strategy to improve the production of complex biologics in plants, by providing a tailor-made environment to support their maturation (Margolin et al., 2020b,e). In the case of viral glycoproteins this would involve eliminating undesired plant-specific glycosylation and expressing the required heterologous cellular machinery to support appropriate glycosylation, folding and processing of the proteins as dictated by the antigen of interest (Meyers et al., 2018; Margolin et al., 2020c,e). Accordingly, the co-expression of human chaperone proteins was reported to improve the yields of several viral glycoproteins in plants and supported the production of antigens that could not previously be produced in the system (Meyers et al., 2018; Margolin et al., 2020c,d). Proteolytic processing of a viral glycoprotein has also been achieved–this time by the co-expression of human furin (Margolin et al., 2020c). However, similar strategies to produce viral glycoproteins with "human-like" glycosylation in plants have not been reported, although considerable progress has been made in this regard for antibodies and other biologics (Montero-Morales and Steinkellner, 2018).

The expression of glycoproteins in plants leads to the formation of three major glycoforms–namely complex, paucimannosidic and Lewis A structures–which are a feature of the expression system and distinguish plant-produced proteins from those made in conventional expression platforms (Montero-Morales and Steinkellner, 2018). Complex-type glycans containing α1,3-fucose and β1,2-xylose are the most abundant glycan species, and are generated in the Golgi apparatus by α1,3-fucosyltransferase and β1,2-xylosyltransferase, respectively (Wilson et al., 2001). Although these extensions do not occur in mammalian cells and might therefore be expected to appear foreign to mammalian immune systems, they do not seem to impair the immunogenicity of plant-produced influenza vaccines in humans, nor is there any evidence that they pose safety concerns in individuals with pre-existing plant allergies (Ward et al., 2014). However, the observation that these vaccines induced transient IgG and IgE responses to glyco-epitopes cannot be discounted (Ward et al., 2014) and some concerns remain, especially in the context of more heavily glycosylated proteins or where repeated administration may be necessary (Margolin et al., 2020b). Paucimannosidic glycans, comprising truncated structures where the terminal N-acetylglucosamines have been removed from the glycan core, also occur in plants (Liebminger et al., 2011). These are observed in vacuolar and extracellular glycoproteins due to processing by β-hexosaminidases that are localized to these sites (Shin et al., 2017). These modifications

are generally undesirable for human pharmaceuticals as they may promote rapid protein clearance following immunization if they are recognized as foreign (Yang et al., 2015). The final plant glycan structure is the Lewis A epitope which is defined by the presence of β1,3-galactose and α1,4-fucose extensions of the terminal N-acetylglucosamines of the glycan (Fitchette-Laine et al., 1997; Wilson et al., 2001).

Recent studies have also suggested that certain proteins may have lower levels of glycan occupancy when produced in plants, but is presently unclear how widespread this phenomenon is (Jarczowski et al., 2016; Castilho et al., 2018; Göritzer et al., 2020; Singh et al., 2020). Encouragingly, a recent study reported similar glycan occupancy for recombinant human cytomegalovirus glycoprotein B when produced in *Nicotiana tabacum* BY-2 and CHO cells. However, under-glycosylation could account for the poor yields of other glycoproteins in the system, given that inadequate glycan occupancy could impair protein folding and result in the degradation of aberrantly folded protein (Wormald and Dwek, 1999; Margolin et al., 2020b). This could also result in suboptimal immunogenicity, or the induction of antibodies against epitopes that are not accessible on the wild type virus if glycosylation occludes these regions (Zhou et al., 2017; Margolin et al., 2020b).

It is presently unclear to what extent these different plant-specific glycan structures decorate plant-produced viral glycoproteins, or if under-glycosylation occurs in this context. Therefore, in this study we aimed to define the site-specific glycan occupancy of cleavage-independent heavily glycosylated envelope glycoproteins from HIV and Marburg virus (MARV) that were produced in *Nicotiana benthamiana* plants. These examples were chosen as challenging test cases for the development of plant expression systems capable of producing humanized mimetics of these extensively post-translationally modified viral glycoproteins. A head-to-head comparison of the site-specific glycan occupancy of the proteins was performed with the equivalent mammalian cell-produced proteins. We also determined the glycosylation of plant-produced Epstein-Barr virus (EBV) gp350 and a cleaved HIV Env SOSIP.664 antigen from a previous study (Margolin et al., 2020c), to determine whether the structures observed were common to heavily glycosylated glycoproteins produced in the system.

MATERIALS AND METHODS

Design of Genes for Heterologous Expression in Plants and Mammalian Cells

The design and codon optimization of the synthetic gene sequences for HIV-1 CAP256 SU gp140 NFL, HIV-1 CAP256 SU SOSIP.664, EBV gp350, furin and calreticulin have been previously described (van Diepen et al., 2018; Margolin et al., 2019, 2020c). The MARV glycoprotein antigen (GP) generated in this study was based on the sequence of the Lake Victoria isolate (strain Musoke-80, UniProt accession #P35253). A soluble derivative of the antigen gene was constructed by truncating the ORF after amino acid 648 to remove the transmembrane and cytoplasmic domains. The gene sequence was further modified by replacing the native leader sequence with the heterologous leader peptide heavy chain (LPH) leader peptide (Margolin et al., 2019) or the tissue plasminogen activator (TPA) leader sequence, and replacing the furin cleavage site with a $(GGGGS)_2$ linker (van Diepen et al., 2018). A synthetic Kozak sequence (CCACC) was included at the 5' end of the gene. The MARV glycoprotein coding sequence was synthesized to reflect the preferred human codon usage.

Construction of Expression Plasmids for Heterologous Glycoprotein Production

Recombinant protein expression was done using the pEAQ-*HT* and pTHpCapR plasmid systems for glycoprotein expression in plants and mammalian cells, respectively (Sainsbury et al., 2009; Tanzer et al., 2011; van Diepen et al., 2018; Margolin et al., 2019). A stably transfected HEK293 cell line was previously generated for production of the cleavage-independent soluble HIV Env gp140 antigen from the CAP256 SU virus (van Diepen et al., 2018). Similarly, recombinant *Agrobacterium tumefaciens* strains encoding the matched HIV Env antigen, the EBV gp350 antigen and the CAP256 SU SOSIP.664 gp140 were previously generated as part of independent studies (Margolin et al., 2019, 2020c). The MARV GPΔTM sequence was assembled in pEAQ-*HT*. The LPH leader was replaced with the TPA leader sequence for expression in mammalian cells and the fusion gene cloned into the pTHpCapR expression plasmid. The recombinant pEAQ-*HT* expression plasmid was electroporated into *A. tumefaciens* AGL1 as described previously (Margolin et al., 2019).

Recombinant Viral Glycoprotein Production in Plants and Mammalian Cells

All recombinant viral glycoproteins were produced in plants by agroinfiltration of *N. benthamiana* with recombinant *A. tumefaciens* bacteria as described previously (Margolin et al., 2020c). The HIV Env gp140 NFL protein was produced using a stably transfected cell line that was developed as part of an independent study (van Diepen et al., 2019). MARV GPΔTM was expressed by transient transfection of HEK293T cells, under serum-free conditions as previously described (van Diepen et al., 2018). Expression of the MARV GPΔTM protein was verified by western blotting of crude cell lysates using a polyclonal rabbit antibody raised against a synthetic peptide (CDQIKKDEQKEGTGW) in immunized rabbits. The recombinant proteins were purified from either cell culture media or leaf lysate following homogenization. The HIV and MARV glycoproteins were purified by sequential *Galanthus nivalis* lectin (GNL) affinity chromatography and gel filtration, as previously described, whereas the EBV gp350ΔTM protein was purified directly by GNL-affinity chromatography (Margolin et al., 2019; van Diepen et al., 2019). Size exclusion chromatography profiles were normalized by dividing each datapoint by the peak signal and then represented as a proportion of 1. The data was presented as overlayed elution profiles using GraphPad Prism 5 software. The purified proteins were quantified using the Bio-Rad protein *DC* assay. The recombinant antigens were also

resolved on 4–12% NativePAGE Bis-Tris gels and stained with Bio-Safe™ Coomassie.

Site-Specific N-Glycan Analysis of Recombinant Viral Glycoproteins

In order for each glycoprotein to be analyzed by liquid-chromatography-mass spectrometry (LC-MS), three aliquots of purified protein were denatured for 1 h in 50 mM Tris/HCl [pH 8.0], containing 6 M of urea and 5 mM of dithiothreitol (DTT). Next, the proteins were reduced and alkylated by adding 20 mM iodoacetic acid (IAA) and incubating the samples for 1 h in the dark. The samples were then incubated with DTT to remove residual IAA. The alkylated glycoproteins were buffer exchanged into 50 mM Tris/HCl [pH 8.0] and digested separately using trypsin, chymotrypsin (Mass Spectrometry Grade, Promega) and alpha-lytic protease (Sigma-Aldrich) at a ratio of 1:30 (w/w). Following overnight digestion, the resulting peptide/glycopeptides were dried and extracted using C18 Zip-tip (Merck Millipore). After elution, the peptide/glycopeptides were dried again, resuspended in 0.1% formic acid and then analyzed by nanoLC-ESI MS with an Easy-nLC 1200 (Thermo Fisher Scientific) system coupled to a Fusion mass spectrometer (Thermo Fisher Scientific) using higher energy collision-induced dissociation (HCD) fragmentation. Peptides were separated using an EasySpray PepMap RSLC C18 column (75 μm × 75 cm). A trapping column (PepMap 100 C18, 3 μm particle size, 75 μm × 2 cm) was used in line with the LC prior to separation with the analytical column. The LC conditions were as follows: 275 min linear gradient consisting of 0-32% acetonitrile in 0.1% formic acid over 240 min, followed by 35 min of 80% acetonitrile in 0.1% formic acid. The flow rate was set to 300 nl/min. The spray voltage was set to 2.7 kV and the temperature of the heated capillary was set to 40°C. The ion transfer tube temperature was set to 275°C. The scan range was 400-1600 m/z. The HCD collision energy was set to 50%, appropriate for fragmentation of glycopeptide ions. Precursor and fragment detection were performed using an Orbitrap at a resolution MS1 = 100,000. MS2 = 30,000. The automatic gain control (AGC) target for MS1 = 4e5 and MS2 = 5e4 and injection time: MS1 = 50 ms MS2 = 54 ms.

Glycopeptide fragmentation data were extracted from the raw file using Byonic™ and Byologic™ software (Version 3.5; Protein Metrics Inc.). The glycopeptide fragmentation data were evaluated manually for each glycopeptide; the peptide was scored as true-positive when the correct b and y fragment ions were observed along with oxonium ions corresponding to the glycan identified. The MS data was searched using the Protein Metrics' N-glycan libraries: for mammalian expression the 309 N-glycan library was used and for material produced in plants the 52 plant library was used. The relative amounts of glycan at each site, as well as the unoccupied proportion, were determined by comparing the extracted chromatographic areas for different glycotypes with an identical peptide sequence. All charge states for a single glycopeptide were summed. The precursor mass tolerance was set at 4 ppm and 10 ppm for fragments. A 1% false discovery rate (FDR) was applied. The relative amounts of each glycoform at each site, as well as the unoccupied proportion, were determined by comparing the extracted ion chromatographic areas for different glycopeptides with an identical peptide sequence. Glycans are categorized according to the detected compositions by LC-MS. Compositions containing Hex(10-12) HexNAc(2) were categorized as M9Glc1-3 and Hex(9-5) HexNAc(2) as M9-M5. These are classified as oligomannose-type glycans and are colored green. Hybrid-type glycans contain compositions consisting of Hex(5)HexNAc(3)X or Hex(6)HexNAc(4)X. Remaining glycan compositions were assigned as complex-type. Any composition Hex(3) HexNAc(2) or smaller is classified as truncated. The proportion of unoccupied N-linked glycan sites at each site are colored gray.

RESULTS

Viral Glycoprotein Selection and Antigen Design

Viral envelope glycoproteins from HIV-1, EBV, and MARV were selected for this study as they are all extensively glycosylated and are therefore ideal models to interrogate the impact of the plant cellular machinery on glycosylation. Both HIV gp140 and EBV gp350ΔTM were successfully expressed in plants as part of a previous study exploring the impact of co-expressing human chaperones on viral glycoprotein production in *N. benthamiana* (Margolin et al., 2020c). MARV is a re-emerging virus with a high probability of causing disease outbreaks in humans, prompting the suitability of plant-based expression to be explored for the development of a vaccine against a prototype emerging filovirus (Letko et al., 2020). MARV and HIV glycoproteins were both expressed as soluble cleavage-independent antigens for ease of production and recovery (**Figure 1A**) using previously described approaches (Margolin et al., 2019, 2020c; van Diepen et al., 2019).

Transient Expression of MARV GPΔTM in Plants and Mammalian Cells

Marburg virus GPΔTM was transiently expressed in plants and mammalian cells by agroinfiltration and transfection, respectively. Western blotting of crude extract from agroinfiltrated leaves yielded a product of ∼115-125 kDa and some diffuse higher molecular weight products which were not well resolved by SDS-PAGE (**Figure 1B**). Western blotting of lysate from transfected HEK293 cells produced a similar product, although the protein appeared slightly larger and the signal was fairly diffuse (**Figure 1C**). An additional product of <100 kDa was observed for the mammalian cell-produced protein which may have arisen from intracellular processing. Expression of the recombinant HIV Env gp140 antigens and EBV g350ΔTM were both previously described (Margolin et al., 2019, 2020c; van Diepen et al., 2019).

Purification of Soluble MARV and HIV Glycoproteins

The soluble glycoproteins (HIV Env gp140 and MARV GPΔTM) were captured by GNL affinity chromatography and then fractionated by gel filtration, to recover trimeric glycoproteins

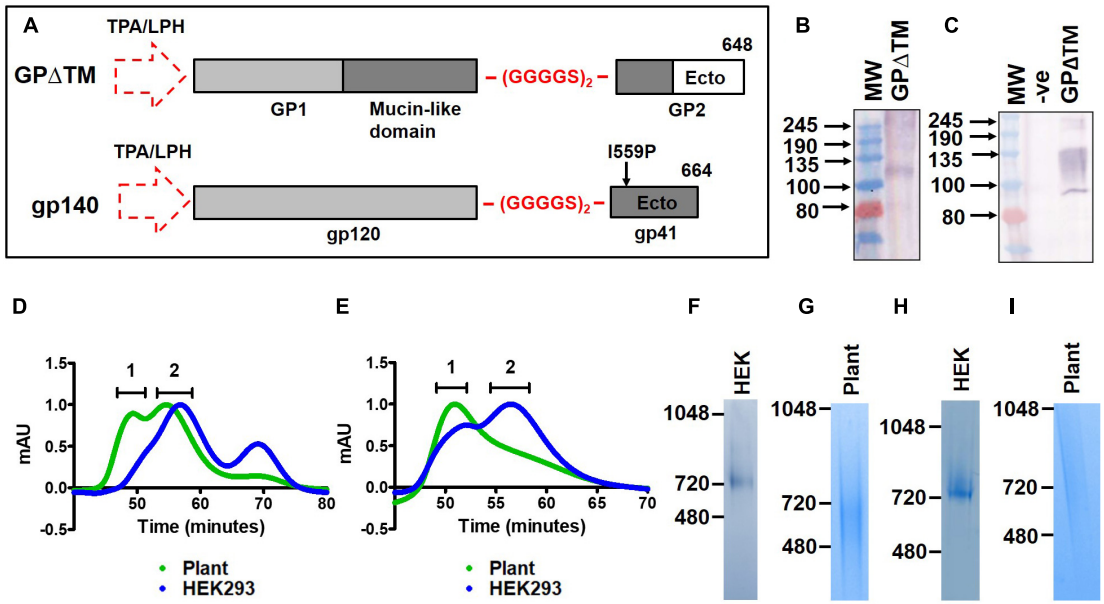

FIGURE 1 | Design and purification of recombinant viral glycoproteins in plants. **(A)** Schematic of the synthetic MARV GPΔTM (top) and HIV Env gp140 (bottom) antigen sequences. The natural signal peptide was replaced with the LPH or TPA leader peptides (dotted arrow) for expression in plants and mammalian cells respectively. A flexible linker peptide, $(GGGGS)_2$, was inserted in place of the furin cleavage site and the transmembrane and cytoplasmic domains of the proteins were removed. The location of the GP_1 and GP_2 subunits, and the mucin-like domain are indicated for MARV GPΔTM. The gp120 and gp41 subunits are similarly shown for HIV Env gp140. A stabilizing isoleucine to proline mutation was also included in the HIV Env gp140 antigen (I559P). The amino acids where the proteins were truncated are indicated as 648 and 664 for MARV and HIV, respectively. **(B)** Western blotting of plant homogenate to detect expression of recombinant MARV GPΔTM. **(C)** Western blotting to detect expression of MARV GPΔTM in transfected mammalian cell lysate. In both panels **(B,C)**, the recombinant protein was detected using a polyclonal rabbit antibody raised against a synthetic peptide from the glycoprotein. **(D,E)** Overlayed S200 elution profiles of recombinant plant-produced and mammalian cell-derived HIV Env gp140 NFL and MARV GPΔTM, respectively. The plant-produced protein is shown in green whereas the mammalian cell-derived protein is indicated in blue. 1 = aggregate peak, 2 = putative trimer peak. Coomassie-stained BN-PAGE gels for the pooled trimer fractions are shown in panels **(F–I)** for mammalian cell-produced HIV Env gp140 (HEK), plant-plant produced gp140 (plant), mammalian cell-derived MARV GPΔTM and plant-produced MARV GPΔTM, respectively. (-ve = untransfected cell lysate, Ecto = Ectodomain, TM = transmembrane region, CT = cytoplasmic tail).

and to exclude non-trimeric protein species (**Figures 1D,E**). The size exclusion chromatography elution profiles for the plant-produced and mammalian cell-derived glycoproteins were overlayed to compare the relative abundance of the different protein species in both systems. Both glycoproteins exhibited a marked increase in higher molecular weight aggregates when produced in plants as reflected in the profile shifting toward the left (**Figures 1D,E**). While the plant-produced HIV Env gp140 exhibited a peak of the expected size for trimers (**Figure 1D**), the plant-produced MARV GPΔTM did not yield a defined peak as expected (**Figure 1E**). Instead, a diffuse shoulder was observed suggesting that the purified protein was highly heterogenous, even after purification.

Coomassie-stained BN-PAGE gels mirrored the observations from size exclusion chromatography. The pooled trimer peak derived from mammalian cells yielded a defined band of ∼720 kDa for both HIV Env gp140 (**Figure 1F**) and MARV GPΔTM (**Figure 1H**), which is consistent with our previous observations for HIV (van Diepen et al., 2019) and published accounts for filovirus glycoprotein trimers (Rutten et al., 2020). In contrast, Coomassie staining of the pooled fractions corresponding to the plant-derived glycoprotein trimers yielded a diffuse signal (**Figures 1G,I**).

Aberrant Glycosylation of HIV Env Using *N. benthamiana* as a Production System

To determine the site-specific changes in glycosylation of HIV-1 Env when using *N. benthamiana* as the expression system we applied LC-MS to the purified proteins (**Figure 2**). The data is displayed as the percentage point change in site-specific glycosylation when the protein is expressed using *N. benthamiana*, so a positive value represents a category which is more abundant in *N. benthamiana* compared to mammalian produced protein. This methodology has been used previously to compare and contrast the glycosylation of the viral glycoprotein from BG505 and other HIV strains (Behrens et al., 2016; Struwe et al., 2018). There are distinct glycan processing states on HIV Env which form key epitopes for broadly neutralizing antibodies. The early glycan processing pathway in both mammals and plants is conserved and involves the attachment and subsequent trimming of oligomannose-type glycans in the ER and early Golgi apparatus (Montero-Morales and Steinkellner, 2018). The density of N-linked glycans on HIV Env perturb this process, and the resultant mature protein contains remnants of these under-processed glycans. These oligomannose-type glycans can form epitopes for broadly neutralizing antibodies that target several regions of the Env spike. Two key regions for antibody

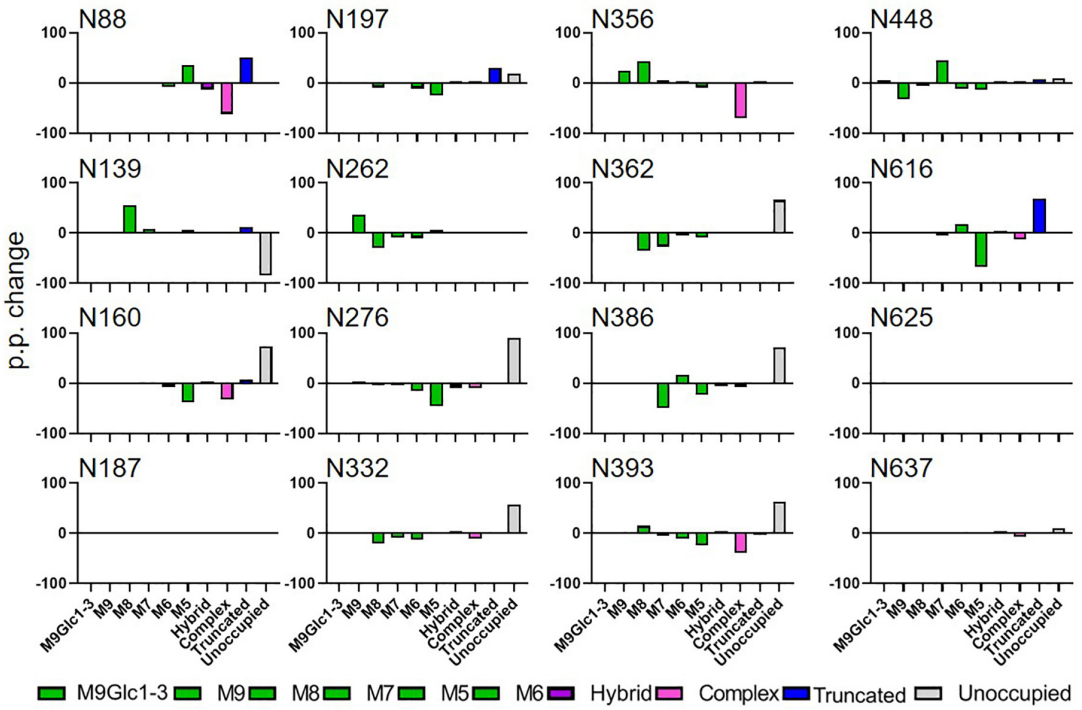

FIGURE 2 | Comparison of site-specific glycosylation of HIV Env gp140 NFL when produce in plants or mammalian cells. The data represent the percentage point change in glycosylation when the protein was expressed in *N. benthamiana* compared to HEK293, so a positive value represents a category of glycan that is enriched on material produced in *N. benthamiana*. Glycans are categorized according to the detected compositions by LC-MS. Compositions containing Hex(10-12) HexNAc(2) were categorized as M9Glc1-3 and Hex(9-5) HexNAc(2) as M9-M5. These are classified as oligomannose-type glycans and are colored green. Hybrid-type glycans contain compositions consisting of Hex(5)HexNAc(3)X or Hex(6)HexNAc(4)X. Remaining glycan compositions were assigned as complex-type. Any composition Hex(3) HexNAc(2) or smaller is classified as truncated. The proportion of potential N-linked glycans which are classified as unocupied are coloured grey.

recognition are the intrinsic mannose patch (IMP), focused around the N332 supersite of vulnerability, and the trimer-associated patch (TAMP), with the N160 glycans of the V1/V2 region forming a key part of several antibody epitopes (Behrens and Crispin, 2017). The TAMP is only present when correctly processed and cleaved Env is analyzed, and forms at the trimer interface and the apex of the protein (Behrens et al., 2017). These two key regions of oligomannose-type glycans are key for immunogen design efforts (Haynes et al., 2019).

When comparing the glycosylation of CAP256 SU gp140 expressed in mammalian and plant cells the distribution and processing of these oligomannose-type glycans is affected. Sites that form the IMP such as N332 and N386 show a decrease in oligomannose-type glycans (40 and 55 percentage points, respectively) when *N. benthamiana* is used as the expression system (**Supplementary Table 1**). The TAMP is also disrupted with a similar reduction in oligomannose-type glycans at N160 and N197. Oligomannose-type glycans increase in abundance at N356, however this site appears more fully processed in HEK293 cells.

The reason for the decrease in oligomannose-type glycans at key bnAb recognition sites is the near universal increase in potential N-linked glycosylation sites that lack post-translational modifications. Sites N160, N197, N276, N332, N362, N386, N393, N447, and N637 all show an increase in the proportion of unoccupied glycan sites. This represents an asparagine of an NxS/T sequon which has the capacity for the addition of an N-linked glycan, but where the glycosylation machinery has not attached a glycan. Recombinant expression systems are suboptimal for recapitulating the high occupancy of viral-derived Env, especially on gp41, and this has also been observed in mammalian expression systems, albeit to a lesser extent (Derking et al., 2021).

This can be seen on CAP256 SU gp140 expressed in both HEK293 and *N. benthamiana*, for example at N625 (**Supplementary Table 1**). The presence of these so-called glycan holes has been shown to induce non-neutralizing antibody responses during immunizations which do not protect from HIV acquisition (Crooks et al., 2015; Zhou et al., 2017). The CAP256 SU gp140 expressed using *N. benthamiana* contains the same glycan holes as with HEK293 cells, however, the presence of additional holes at sites such as N332 will likely generate detrimental antibody responses when used in immunizations. Finally, at three sites on CAP256 SU gp140 from *N. benthamiana*, N88, N197 and N616, a substantial increase in smaller glycan structures were observed (ranging from a single hexosamine to $Man_3GlcNAc_2$) which were not observed on mammalian proteins.

TABLE 1 | Site-specific glycosylation of plant produced CAP256 SU gp140 SOSIP.664 and EBV gp350ΔTM.

CAP256 SU SOSIP.664

	85	130	139	160	187	197	230	234	241	262	276	289	295	301	332	356	362	386	393	406	411	448	462	611	616	625	637	Average
M9GlC1-3	0	0	0	0	0	0				0	0				0	8	0	0	0			0	33		0	0	0	2
M9	42	0	26	0	0	0				35	0				50	2	0	0	8			1	0		0	0	0	9
M8	12	18	42	16	0	0				44	0				28	61	26	31	12			23	0		0	0	1	17
M7	26	7	0	2	0	0				14	0				7	12	6	24	10			18	0		0	0	0	7
M6	0	0	0	0	0	0				2	0				6	2	2	0	3			6	0		0	0	0	1
M5	2	0	0	2	0	0				2	0				3	6	1	6	1			5	0		0	0	0	2
Hybrid	0	0	0	0	0	0				0	0				0	0	0	0	0			0	0		0	0	0	0
Complex	0	0	0	0	0	1				0	0				0	2	1	0	0			1	0		0	0	0	0
Truncated	0	3	18	3	0	25				0	0				3	0	0	0	1			5	65		0	0	0	7
Unoccupied	0	71	14	76	100	75				0	99				2	0	60	39	65			42	2		0	99	99	47

EBV gp350ΔTM

	66	106	133	185	188	214	248	196	337	347	364	375	397	405	430	454	462	476	516	538	552	566	587	608	629	643	646	664	675	702	720	754	765	774	799	834	Average
M9GlC1-3	0	0	0	0	0	0	1	0	0		0	0	0	0	83	2	6	3		0	0	0	3	2	0		0	0	0	0	0	0	0	1		23	4
M9	28	6	5	7	0	0	29	13	55		3	3	0	15	9	4	14	13		4	0	0	5	3	0		7	0	0	0	0	0	0	9		48	9
M8	65	50	31	42	21	2	32	55	29		64	16	0	42	5	19	29	30		27	37	2	13	8	28		32	51	36	43	0	0	0	14		23	27
M7	7	11	18	11	19	1	9	18	5		0	7	0	13	1	11	10	24		0	15	2	10	8	13		13	49	11	12	0	86	0	10		6	12
M6	0	1	15	5	2	0	7	4	5		0	2	0	7	1	0	3	7		0	0	0	2	2	0		4	0	0	0	0	1	0	2		0	2
M5	0	5	18	6	10	0	16	5	6		21	4	0	13	0	1	0	12		0	0	0	3	3	0		5	0	0	0	0	0	0	3		0	4
Hybrid	0	0	0	0	0	0	0	0	0		0	0	0	0	0	0	0	0		0	0	29	0	0	0		0	0	0	0	55	0	0	0		0	3
Complex	0	3	4	7	5	0	2	1	0		0	2	0	4	0	4	4	11		1	0	48	3	2	13		2	0	13	0	42	0	0	1		0	5
Truncated	0	14	3	11	42	0	4	2	0		1	30	0	2	0	45	35	0		62	48	1	38	48	46		37	0	40	44	2	8	6	59		0	20
Unoccupied	0	10	6	12	0	96	1	1	0		11	36	99	4	1	15	0	0		6	0	0	23	24	0		1	0	0	0	0	5	94	0		0	14

Different tints of blue, from dark through to light, indicate the highest through to the lowest numbers in the table.

Incomplete Processing of Complex Glycans on MARV GPΔTM Expressed in *N. benthamiana* Compared to Mammalian Cells

To investigate whether the observed changes in glycosylation were specific to HIV Env, we performed a comparative analysis of MARV GPΔTM produced in HEK293 and *N benthamiana*. Data of sufficient quality could only be obtained for 8 sites with the full list of sites shown in **Supplementary Table 2**. As with HIV Env, the site-specific glycosylation of MARV GPΔTM varied extensively between HEK293 and *N. benthamiana* (**Figure 3**). For the HEK293 cell-produced protein, several sites displayed extensive glycan processing typical of mammalian glycoproteins. Interestingly, a high proportions of hybrid-type glycans were observed, which are named as such because they contain one arm which is fully processed and one arm presenting terminal mannose residues. Importantly, both the hybrid and complex-type glycans observed on HEK293 MARV GP were not present on material produced in *N. benthamiana*. This includes mature glycans modified with xylose which were included in the library used to search the LC-MS data. Instead, there was a global increase of oligomannose-type glycans, for example at N96 in mammalian cells where 41% of the glycans were oligomannose-type. In contrast this increased to 71% when produced in plants, at 30 percentage point increase (**Figure 3** and **Supplementary Table 2**). The presence of elevated amounts of pauciglycan structures was also observed at five sites, with pauciglycans consisting of 20% of the averaged compositions of all sites obtained by LC-MS. Sites N173 and N572 also lacked glycans on 70 and 100% of the sites, whereas for HEK293 these sites were fully occupied. The higher levels of oligomannose-type glycans observed for MARV GPΔTM is likely due to the cell line used for protein production. In the case of HIV Env, the presence of oligomannose-type glycans is due to steric clashes inhibiting the ability of glycan processing enzymes whereas the lack of oligomannose-type glycans on MARV GPΔTM suggests a differential mechanism. The glycan processing machinery in plants may be unable to process such extensive glycosylation to the same extent as HEK293 cells.

In order to determine if this glycosylation signature was specific to the proteins in question, or rather a feature of producing heavily glycosylated glycoproteins in plants, the site-specific glycosylation of previously produced EBV gp350 and CAP256 SU gp140 SOSIP.664 (Margolin et al., 2020c) were also determined (**Table 1**). Both antigens displayed a similar glycosylation profile comprising of large amounts of oligomannose-type glycans, low levels of complex glycans and considerable amounts of paucimannosidic glycans. Similar to the plant-produced MARV GPΔTM and HIV Env gp140 antigens, a large amount of under-glycosylation was observed. Interestingly for EBV gp350 and CAP256 SU gp140 SOSIP produced in plants, sites displayed glucosylated $Man_9GlcNAc_2$ (categorized as M9Glc1-3 in **Table 1**). This precursor oligosaccharide is present during the early ER folding stages and the removal of the glucose monosaccharides acts as a checkpoint to signal that the protein is correctly folded. The presence of these glycans in the resultant purified protein is unusual, given that 0% of the glycans from both CAP256 SU gp140 and MARV GPΔTM produced in HEK293 cells contained these moeities. These observations are consistent with the increase in oligomannose-type glycans observed on MARV GPΔTM suggesting that immaturely processed glycoproteins are being released from the ER during homogenization of plant material and purified.

DISCUSSION

Viral glycoprotein-based subunit vaccines are amongst the most complex recombinant proteins that are being pursued in plant expression systems (Margolin et al., 2018). These proteins have intricate architectures with extensive post-translational modifications, and are heavily reliant on the host cellular machinery to support their maturation. However, some of these maturation events may not occur optimally in plants, necessitating molecular engineering of the host machinery to support the synthesis of these proteins (Margolin et al., 2020b,e). Approaches that have been successfully implemented to increase glycoprotein yields are co-expression of human chaperones, and ectopic expression of the protease furin to support proteolytic processing in plants (Margolin et al., 2020c). Considerable success in this regard has been reported for the production of antibodies and other less complex glycoproteins (Montero-Morales and Steinkellner, 2018), but it is apparent that continued development of plant-based expression systems will be required for the production of complex viral glycoproteins that recapitulate the post-translational processing of mammalian production systems.

Host-derived glycosylation is central to glycoprotein folding and regulates the interaction of the proteins with ER-resident chaperones (Watanabe et al., 2019). In addition, these glycans also determine the immunogenicity of the glycoprotein in natural infection or following vaccination (Dalziel et al., 2014; Watanabe et al., 2019). Therefore, it may be necessary to reproduce the native glycosylation of many viral glycoproteins to elicit appropriate immune responses in the context of vaccination. As a starting point to develop approaches to produce natively glycosylated viral glycoproteins in plants, we interrogated the site-specific glycosylation of recombinant plant-produced MARV and HIV Env glycoproteins and compared them to the equivalent proteins produced in mammalian cells. We also determined the glycosylation of EBV gp350ΔTM and HIV Env gp140 SOSIP.664 produced in plants in a previous study (Margolin et al., 2020c).

Building on previous work to express HIV Env gp140 in plants and mammalian cells (van Diepen et al., 2018, 2019; Margolin et al., 2019, 2020c), we produced a soluble MARV glycoprotein in both systems. This is to our knowledge the first report describing the expression of this filoviral glycoprotein in a plant expression system, and adds to an increasing number of viral glycoproteins that have been expressed in plants. The HIV and MARV glycoproteins were purified by sequential affinity chromatography and gel filtration steps, and the size exclusion elution profiles were overlayed with the equivalent mammalian cell-produced proteins for comparison. Whilst the HIV Env gp140 antigen produced a peak that is consistent with the

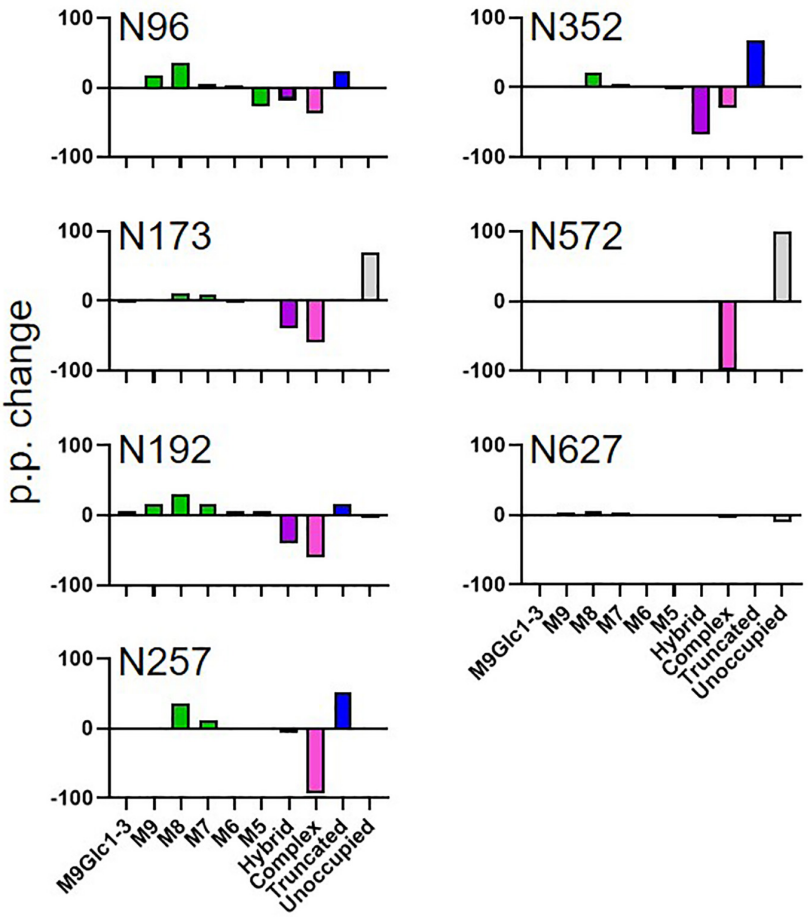

FIGURE 3 | Comparison of MARV GPΔTM glycosylation when the protein was expressed in plants and mammalian cells. The data represent the percentage point change in glycosylation when the protein was expressed in *N. benthamiana* compared to HEK293, so a positive value represents a category of glycan that is enriched on material produced in *N. benthamiana*. Glycans are categorized according to the detected compositions by LC-MS. Compositions containing Hex(10-12) HexNAc(2) were categorized as M9Glc1-3 and Hex(9-5) HexNAc(2) as M9-M5. These are classified as oligomannose-type glycans and are colored green. Hybrid-type glycans contain compositions consisting of Hex(5)HexNAc(3)X or Hex(6)HexNAc(4)X. Remaining glycan compositions were assigned as complex-type. Any composition Hex(3) HexNAc(2) or smaller is classified as truncated. The proportion of potential N-linked glycans which are classified as unocupied are coloured grey.

expected size for trimeric Env, the MARV GPΔTM protein yielded a diffuse shoulder, suggesting high levels of heterogeneity for the recombinant protein. In both cases, there was a striking shift of the plant-produced protein toward the left of the profile indicating an increase in size. This corresponds to increased aggregation in the system, which is consistent with previous reports describing unresolved higher molecular weight products following the expression of HIV Env gp140 antigens in plants (Rosenberg et al., 2013; Margolin et al., 2019).

Given the extensive under-glycosylation of the protein observed in this study it is likely that these aggregates comprise of aberrantly folded protein species. This is also supported by the presence of glucosylated mannose species that were observed. Whilst several studies have reported under-glycosylation in a range of plant-produced proteins (Jarczowski et al., 2016; Castilho et al., 2018; Singh et al., 2020), this is the most extensive under-glycosylation that has been reported to date. This observation may account for the inferior immunogenicity of the plant-produced HIV gp140 antigen compared to the mammalian cell-produced protein that was observed in a previous study, where the trimer elicited high titers of binding antibodies in immunized rabbits but did not induce any appreciable autologous neutralizing antibodies (Margolin et al., 2019). If these antibodies were raised against epitopes that were shielded by glycans on the wild type virus, it would explain why they failed to neutralize. It is well established that antibodies targeting holes in the glycan shield are readily induced against the HIV Env glycoprotein, and therefore reproducing the glycan shield on trimer immunogens is critical to prevent undesired off-target immune responses (Zhou et al., 2017; Crispin et al., 2018; Ringe et al., 2019). Glycans can also constitute important epitopes targeted by neutralizing antibodies, and in the absence of glycosylation these epitopes would not be reproduced (Crispin et al., 2018). The N160 glycan at the apex of the trimer,

for example, is almost completely unoccupied in the plant-produced antigen, and therefore the protein is not expected to exhibit appreciable binding by PG-9 and other related antibodies that recognize this epitope (McLellan et al., 2011). Under-glycosylation was similarly observed at the N332 glycan site which is commonly targeted by broadly neutralizing antibodies during natural infection (Sok et al., 2016). Future work should compare the reactivity of plant-produced and mammalian cell-derived proteins with prototype monoclonal antibodies from natural infection. These antibodies could serve as useful tools to further investigate how closely these plant-produced antigens resemble their mammalian cell-produced counterparts, and will help establish if host engineering approaches improve their folding and antigenicity.

Based on the work described here, and in other recent studies of plant-produced enzymes and antibodies, it seems likely that under-glycosylation of heterologous proteins may be more common than was previously appreciated (Castilho et al., 2018; Göritzer et al., 2020). Given the central role of glycosylation in protein folding, this could be an important contributory factor to inefficient production of certain viral glycoproteins in the system, and could be expected to pose a similar challenge for other similarly glycosylated target proteins (Margolin et al., 2018). The molecular basis for under-glycosylation in the system is not well understood but it has been suggested that this is related to the distinct recognition preferences of the plant oligosaccaryltransferase complex (Margolin et al., 2020e). It is also probably a consequence of the purification process where homogenization of plant tissue will liberate proteins from all stages of the secretory pathway, including those that have not yet been properly glycosylated. Encouragingly, it has recently been shown that the co-expression of *Leishmania major* LmSTT3D increased the glycan occupancy of several model proteins in *N. benthamiana* (Castilho et al., 2018; Göritzer et al., 2020).

The almost complete absence of plant-specific complex glycans in the purified proteins is an unexpected observation, and contrasts with other reports describing plant-produced viral glycoproteins from influenza virus and HIV-1 (Rosenberg et al., 2013; Le Mauff et al., 2015). However, it is difficult to compare these to the current study due to differences in glycoprotein complexity and different antigen design strategies: both glycoproteins produced in this study contain considerably more N-glycan sequons than influenza HA which only contains six N-glycan sites, and therefore the burden on the host cellular machinery is expected to be commensurately greater (Le Mauff et al., 2015). The HIV-1 Env trimer described in this study was also engineered to preserve the structure, whereas the previously described glycoprotein was modified to remove the cleavage site, fusion peptide and immunodominant region of gp41 (Rosenberg et al., 2013). These alterations are expected to have impacted protein folding, and based on subsequent insights into the protein structure, would be likely to have compromised the folding of the glycoprotein (Ringe et al., 2013). It is also plausible that the processing by host mannosidases could be less efficient in plants resulting in poor formation of complex glycans. These enzymes may be less abundant in plants than mammalian cells as the requirement for glycosylation is often considerably less.

Although the levels of truncated and paucimannose-type glycans following expression in plants is surprising, it is not unprecedented. Similar observations have been reported for other heterologous plant-produced proteins, such as α1-antitrypsin (Castilho et al., 2014), IgA (Dicker et al., 2016), and bovine follicle stimulation hormone (Dirnberger et al., 2001). These truncated glycans arise from the removal of *N*-acetylglucosamines from the non-reducing end by β-hexosaminidases (HEXOs) (Liebminger et al., 2011). The responsible enzymes are localized to vacuoles and the plasma membrane in *N. benthamiana*, and previous work has shown that their downregulation by RNA interference increased the levels of intact complex-type glycans (Shin et al., 2017). These structures do not naturally occur on viral glycoproteins and therefore this approach will be necessary to eliminate this undesirable processing *in planta*.

In conclusion, we have delineated the site-specific glycosylation of several model human viral glycoproteins that were produced in *N. benthamiana*, and identified key constraints in the host glycosylation machinery. This work adds to a growing body of evidence suggesting that remodeling the secretory pathway may be necessary to support the production of complex pharmaceutical targets in the plant expression system, and provides a rational starting point to produce recombinant glycoproteins with humanized glycosylation in plants (Margolin et al., 2020e). The data presented here has important implications for plant molecular farming of viral glycoproteins and suggests that under-glycosylation may be more widespread than previously realized.

DATA AVAILABILITY STATEMENT

The original contributions presented in the study are included in the article/**Supplementary Material**, further inquiries can be directed to the corresponding author/s.

AUTHOR CONTRIBUTIONS

EM, JA, and MC conceptualized the study. EM and RC designed the gene sequences and conceived the cloning strategy. EM and MV conducted protein expression in plants. EM, MD, and PX conducted protein expression in mammalian cells. JA carried out the site-specific glycosylation. A-LW and RC supervised mammalian cell culture aspects of the project. ER and AM supervised plant-based protein expression component of the project. EM and JA drafted the manuscript. Funding for the project in Cape Town was obtained by EM, A-LW and ER. All authors contributed to data analysis and reviewed the manuscript.

FUNDING

This work is based upon research supported by the South African Medical Research Council with funds received from the South African Department of Science and Technology, the

South African Research Chairs Initiative of the Department of Science and Technology, and the National Research Foundation (Grant number: 64819). Further funding support was provided by core funding from the Wellcome Trust (203135/Z/16/Z). The work in the laboratory of MC was supported by the International AIDS Vaccine Initiative (IAVI) through grant OPP1153692/INV-008352 funded by the Bill & Melinda Gates Foundation.

SUPPLEMENTARY MATERIAL

The Supplementary Material for this article can be found online at: https://www.frontiersin.org/articles/10.3389/fpls.2021.709344/full#supplementary-material

Supplementary Table 1 | Comparison of site-specific glycosylation of HIV Env gp140 NFL when produce in plants or mammalian cells. The glycosylation profile of the recombinant protein is shown when the protein was expressed in *N. benthamiana* **(A)** and HEK293 cells **(B)**. The change in glycosylation that occurs when the protein is produced in plants is shown in **(C)**.

Supplementary Table 2 | Comparison of MARV GPΔTM glycosylation when the protein was expressed in plants and mammalian cells. The glycosylation of the glycoprotein is shown when the protein was expressed in *N. benthamiana* **(A)** and in HEK293 cells **(B)**. The change in glycosylation that occurs when the protein was produced in *N. benthamiana* is shown in **(C)**. (m5-m12 = high-mannose, pauci = paucimannosidic). In each cases the numbers on *X* axis of the Figure indicate the position of a putative N-glycan sequon. (m5-m12 = high-mannose, pauci = paucimannosidic). In each case the number above the tables indicates the position of a putative N-glycan sequon. Numbers in the table indicate the relative proportion of each glycoforms at this site. The table to the right summarizes the relative abundance of each glycan species considering all the individual sites together.

REFERENCES

Behrens, A. J., and Crispin, M. (2017). Structural principles controlling HIV envelope glycosylation. *Curr. Opin. Struct. Biol.* 44, 125–133. doi: 10.1016/j.sbi.2017.03.008

Behrens, A. J., Harvey, D. J., Milne, E., Cupo, A., Kumar, A., Zitzmann, N., et al. (2017). Molecular architecture of the cleavage-dependent mannose patch on a soluble HIV-1 envelope glycoprotein trimer. *J. Virol.* 91:e1894-16.

Behrens, A. J., Vasiljevic, S., Pritchard, L. K., Harvey, D. J., Andev, R. S., Krumm, S. A., et al. (2016). Composition and antigenic effects of individual glycan sites of a trimeric HIV-1 envelope glycoprotein. *Cell Rep.* 14, 2695–2706. doi: 10.1016/j.celrep.2016.02.058

Bonomelli, C., Doores, K. J., Dunlop, D. C., Thaney, V., Dwek, R. A., Burton, D. R., et al. (2011). The glycan shield of HIV is predominantly oligomannose independently of production system or viral clade. *PLoS One* 6:e23521. doi: 10.1371/journal.pone.0023521

Castilho, A., Beihammer, G., Pfeiffer, C., Goritzer, K., Montero-Morales, L., Vavra, U., et al. (2018). An oligosaccharyltransferase from Leishmania major increases the N-glycan occupancy on recombinant glycoproteins produced in *Nicotiana benthamiana*. *Plant Biotechnol. J.* 16, 1700–1709. doi: 10.1111/pbi.12906

Castilho, A., Windwarder, M., Gattinger, P., Mach, L., Strasser, R., Altmann, F., et al. (2014). Proteolytic and N-glycan processing of human alpha1-antitrypsin expressed in *Nicotiana benthamiana*. *Plant Physiol.* 166, 1839–1851. doi: 10.1104/pp.114.250720

Crispin, M., Ward, A. B., and Wilson, I. A. (2018). Structure and immune recognition of the HIV glycan shield. *Annu. Rev. Biophys.* 47, 499–523. doi: 10.1146/annurev-biophys-060414-034156

Crooks, E. T., Tong, T., Chakrabarti, B., Narayan, K., Georgiev, I. S., Menis, S., et al. (2015). Vaccine-elicited Tier 2 HIV-1 neutralizing antibodies bind to quaternary epitopes involving glycan-deficient patches proximal to the CD4 binding site. *PLoS Pathog.* 11:e1004932. doi: 10.1371/journal.ppat.1004932

Dalziel, M., Crispin, M., Scanlan, C. N., Zitzmann, N., and Dwek, R. A. (2014). Emerging principles for the therapeutic exploitation of glycosylation. *Science* 343:1235681. doi: 10.1126/science.1235681

Derking, R., Allen, J. D., Cottrell, C. A., Sliepen, K., Seabright, G. E., Lee, W. H., et al. (2021). Enhancing glycan occupancy of soluble HIV-1 envelope trimers to mimic the native viral spike. *Cell Rep.* 35:108933. doi: 10.1016/j.celrep.2021.108933

Dicker, M., Tschofen, M., Maresch, D., Konig, J., Juarez, P., Orzaez, D., et al. (2016). Transient glyco-engineering to produce recombinant IgA1 with defined N- and O-glycans in plants. *Front. Plant Sci.* 7:18. doi: 10.3389/fpls.2016.00018

Dirnberger, D., Steinkellner, H., Abdennebi, L., Remy, J. J., and van de Wiel, D. (2001). Secretion of biologically active glycoforms of bovine follicle stimulating hormone in plants. *Eur. J. Biochem.* 268, 4570–4579. doi: 10.1046/j.1432-1327.2001.02384.x

Doores, K. J., Bonomelli, C., Harvey, D. J., Vasiljevic, S., Dwek, R. A., Burton, D. R., et al. (2010). Envelope glycans of immunodeficiency virions are almost entirely oligomannose antigens. *Proc. Natl. Acad. Sci. U.S.A.* 107, 13800–13805. doi: 10.1073/pnas.1006498107

Fitchette-Laine, A. C., Gomord, V., Cabanes, M., Michalski, J. C., Saint Macary, M., Foucher, B., et al. (1997). N-glycans harboring the Lewis a epitope are expressed at the surface of plant cells. *Plant J.* 12, 1411–1417. doi: 10.1046/j.1365-313x.1997.12061411.x

Göritzer, K., Goet, I., Duric, S., Maresch, D., Altmann, F., Obinger, C., et al. (2020). Efficient N-glycosylation of the heavy chain tailpiece promotes the formation of plant-produced dimeric IgA. *Front. Chem.* 8:346. doi: 10.3389/fchem.2020.00346

Group, P. I. W., Multi-National, P. I. I. S. T., Davey, R. T. Jr., Dodd, L., Proschan, M. A., Neaton, J., et al. (2016). A randomized, controlled trial of ZMapp for ebola virus infection. *N. Engl. J. Med.* 375, 1448–1456. doi: 10.1056/nejmoa1604330

Haynes, B. F., Burton, D. R., and Mascola, J. R. (2019). Multiple roles for HIV broadly neutralizing antibodies. *Sci. Transl. Med.* 11:eaaz2686. doi: 10.1126/scitranslmed.aaz2686

Jarczowski, F., Kandzia, R., Thieme, F., Klimyuk, V., and Gleba, Y. (2016). *Methods of Modulating N-Glycosylation site Occupancy of Plant-Produced Glycoproteins and Recombinant Glycoproteins*. US Patent 2016/0115498 A1. Washington, DC: U.S. Patent and Trademark Office.

Keech, C., Albert, G., Cho, I., Robertson, A., Reed, P., Neal, S., et al. (2020). Phase 1-2 trial of a SARS-CoV-2 recombinant spike protein nanoparticle vaccine. *N. Engl. J. Med.* 383, 2320–2332.

Landry, N., Ward, B. J., Trepanier, S., Montomoli, E., Dargis, M., Lapini, G., et al. (2010). Preclinical and clinical development of plant-made virus-like particle vaccine against avian H5N1 influenza. *PLoS One* 5:e15559. doi: 10.1371/journal.pone.0015559

Le Mauff, F., Mercier, G., Chan, P., Burel, C., Vaudry, D., Bardor, M., et al. (2015). Biochemical composition of haemagglutinin-based influenza virus-like particle vaccine produced by transient expression in tobacco plants. *Plant Biotechnol. J.* 13, 717–725. doi: 10.1111/pbi.12301

Letko, M., Seifert, S. N., Olival, K. J., Plowright, R. K., and Munster, V. J. (2020). Bat-borne virus diversity, spillover and emergence. *Nat. Rev. Microbiol.* 18, 461–471. doi: 10.1038/s41579-020-0394-z

Liebminger, E., Veit, C., Pabst, M., Batoux, M., Zipfel, C., Altmann, F., et al. (2011). Beta-N-acetylhexosaminidases HEXO1 and HEXO3 are responsible for the formation of paucimannosidic N-glycans in Arabidopsis thaliana. *J. Biol. Chem.* 286, 10793–10802. doi: 10.1074/jbc.m110.178020

Margolin, E., Burgers, W. A., Sturrock, Mendelson, M., Chapman, R., Douglass, N., et al. (2020a). Prospects for SARS-CoV-2 diagnostics, therapeutics and vaccines in Africa. *Nat. Rev. Microbiol.* 18, 690–704. doi: 10.1038/s41579-020-00441-3

Margolin, E., Chapman, R., Meyers, A. E., van Diepen, M. T., Ximba, P., Hermanus, T., et al. (2019). production and immunogenicity of soluble plant-produced HIV-1 Subtype C Envelope gp140 Immunogens. *Front. Plant Sci.* 10:1378. doi: 10.3389/fpls.2019.01378

Margolin, E., Chapman, R., Williamson, A. L., Rybicki, E. P., and Meyers, A. E. (2018). Production of complex viral glycoproteins in plants as vaccine immunogens. *Plant Biotechnol. J.* 19, 1531–1545. doi: 10.1111/pbi.12963

Margolin, E., Crispin, M., Meyers, A., Chapman, R., and Rybicki, E. P. (2020b). A roadmap for the molecular farming of viral glycoprotein vaccines: engineering glycosylation and glycosylation-directed folding. *Front. Plant Sci.* 11:609207. doi: 10.3389/fpls.2020.609207

Margolin, E., Oh, Y. J., Verbeek, M., Naude, J., Ponndorf, D., Meshcheriakova, Y. A., et al. (2020c). Co-expression of human calreticulin significantly improves the production of HIV gp140 and other viral glycoproteins in plants. *Plant Biotechnol. J.* 18, 2109–2117. doi: 10.1111/pbi.13369

Margolin, E., Verbeek, M., Meyers, A., Chapman, R., Williamson, A.-L., and Rybicki, E. P. (2020d). Calreticulin co-expression supports high level production of a recombinant SARS-CoV-2 spike mimetic in *Nicotiana benthamiana*. *bioRxiv [Preprint]* doi: 10.1101/2020.06.14.150458:2020.06.14.150458

Margolin, E. A., Strasser, R., Chapman, R., Williamson, A. L., Rybicki, E. P., and Meyers, A. E. (2020e). Engineering the plant secretory pathway for the production of next-generation pharmaceuticals. *Trends Biotechnol.* 38, 1034–1044. doi: 10.1016/j.tibtech.2020.03.004

McLellan, J. S., Pancera, M., Carrico, C., Gorman, J., Julien, J. P., Khayat, R., et al. (2011). Structure of HIV-1 gp120 V1/V2 domain with broadly neutralizing antibody PG9. *Nature* 480, 336–343.

Meyers, A. E., Peter, R. E., and Margolin, E. A. (2018). *Co-Expression of Human Chaperone Proteins in Plants for Increased Expression of Heterologous Polypeptides*.

Montero-Morales, L., and Steinkellner, H. (2018). Advanced plant-based glycan engineering. *Front. Bioeng. Biotechnol.* 6:81. doi: 10.3389/fbioe.2018.00081

Nandi, S., Kwong, A. T., Holtz, B. R., Erwin, R. L., Marcel, S., and McDonald, K. A. (2016). Techno-economic analysis of a transient plant-based platform for monoclonal antibody production. *MAbs* 8, 1456–1466. doi: 10.1080/19420862.2016.1227901

Pillet, S., Aubin, E., Trepanier, S., Bussiere, D., Dargis, M., Poulin, J. F., et al. (2016). A plant-derived quadrivalent virus like particle influenza vaccine induces cross-reactive antibody and T cell response in healthy adults. *Clin. Immunol.* 168, 72–87. doi: 10.1016/j.clim.2016.03.008

Ringe, R. P., Pugach, P., Cottrell, C. A., LaBranche, C. C., Seabright, G. E., Ketas, T. J., et al. (2019). Closing and opening holes in the glycan shield of HIV-1 envelope glycoprotein SOSIP trimers can redirect the neutralizing antibody response to the newly unmasked epitopes. *J. Virol.* 93:e1656-18.

Ringe, R. P., Sanders, R. W., Yasmeen, A., Kim, H. J., Lee, J. H., Cupo, A., et al. (2013). Cleavage strongly influences whether soluble HIV-1 envelope glycoprotein trimers adopt a native-like conformation. *Proc. Natl. Acad. Sci. U.S.A.* 110, 18256–18261. doi: 10.1073/pnas.1314351110

Rosenberg, Y., Sack, M., Montefiori, D., Forthal, D., Mao, L., Hernandez-Abanto, S., et al. (2013). Rapid high-level production of functional HIV broadly neutralizing monoclonal antibodies in transient plant expression systems. *PLoS One* 8:e58724. doi: 10.1371/journal.pone.0058724

Rutten, L., Gilman, M. S. A., Blokland, S., Juraszek, J., McLellan, J. S., and Langedijk, J. P. M. (2020). Structure-based design of prefusion-stabilized filovirus glycoprotein trimers. *Cell Rep.* 30, 4540.e3–4550.e3.

Sack, M., Hofbauer, A., Fischer, R., and Stoger, E. (2015). The increasing value of plant-made proteins. *Curr. Opin. Biotechnol.* 32, 163–170. doi: 10.1016/j.copbio.2014.12.008

Sainsbury, F., Thuenemann, E. C., and Lomonossoff, G. P. (2009). pEAQ: versatile expression vectors for easy and quick transient expression of heterologous proteins in plants. *Plant Biotechnol. J.* 7, 682–693. doi: 10.1111/j.1467-7652.2009.00434.x

Shin, Y. J., Castilho, A., Dicker, M., Sadio, F., Vavra, U., Grunwald-Gruber, C., et al. (2017). Reduced paucimannosidic N-glycan formation by suppression of a specific beta-hexosaminidase from *Nicotiana benthamiana*. *Plant Biotechnol. J.* 15, 197–206. doi: 10.1111/pbi.12602

Singh, A. A., Pooe, O., Kwezi, L., Lotter-Stark, T., Stoychev, S. H., Alexandra, K., et al. (2020). Plant-based production of highly potent anti-HIV antibodies with engineered posttranslational modifications. *Sci. Rep.* 10:6201.

Sok, D., Pauthner, M., Briney, B., Lee, J. H., Saye-Francisco, K. L., Hsueh, J., et al. (2016). A prominent site of antibody vulnerability on HIV Envelope incorporates a motif associated with CCR5 binding and its camouflaging glycans. *Immunity* 45, 31–45. doi: 10.1016/j.immuni.2016.06.026

Struwe, W. B., Chertova, E., Allen, J. D., Seabright, G. E., Watanabe, Y., Harvey, D. J., et al. (2018). Site-specific glycosylation of virion-derived HIV-1 Env is mimicked by a soluble trimeric immunogen. *Cell Rep.* 24, 1958.e5–1966.e5.

Tanzer, F. L., Shephard, E. G., Palmer, K. E., Burger, M., Williamson, A. L., and Rybicki, E. P. (2011). The porcine circovirus type 1 capsid gene promoter improves antigen expression and immunogenicity in a HIV-1 plasmid vaccine. *Virol. J.* 8:51. doi: 10.1186/1743-422x-8-51

van Diepen, M. T., Chapman, R., Douglass, N., Galant, S., Moore, P. L., Margolin, E., et al. (2019). Prime-boost immunizations with DNA, modified vaccinia virus ankara, and protein-based vaccines elicit robust HIV-1 Tier 2 neutralizing antibodies against the CAP256 superinfecting virus. *J .Virol.* 93:e2155-18.

van Diepen, M. T., Chapman, R., Moore, P. L., Margolin, E., Hermanus, T., Morris, L., et al. (2018). The adjuvant AlhydroGel elicits higher antibody titres than AddaVax when combined with HIV-1 subtype C gp140 from CAP256. *PLoS One* 13:e0208310. doi: 10.1371/journal.pone.0208310

Ward, B. J., Gobeil, P., Séguin, A., Atkins, J., Boulay, I., Charbonneau, P.-Y., et al. (2020a). Phase 1 trial of a candidate recombinant virus-like particle vaccine for Covid-19 disease produced in plants. *medRxiv [Preprint]* doi: 10.1101/2020.11.04.20226282:2020.11.04.20226282

Ward, B. J., Landry, N., Trepanier, S., Mercier, G., Dargis, M., Couture, M., et al. (2014). Human antibody response to N-glycans present on plant-made influenza virus-like particle (VLP) vaccines. *Vaccine* 32, 6098–6106. doi: 10.1016/j.vaccine.2014.08.079

Ward, B. J., Makarkov, A., Seguin, A., Pillet, S., Trepanier, S., Dhaliwall, J., et al. (2020b). Efficacy, immunogenicity, and safety of a plant-derived, quadrivalent, virus-like particle influenza vaccine in adults (18-64 years) and older adults (>/=65 years): two multicentre, randomised phase 3 trials. *Lancet* 396, 1491–1503. doi: 10.1016/S0140-6736(20)32014-6

Watanabe, Y., Allen, J. D., Wrapp, D., McLellan, J. S., and Crispin, M. (2020). Site-specific glycan analysis of the SARS-CoV-2 spike. *Science* 369, 330–333. doi: 10.1126/science.abb9983

Watanabe, Y., Bowden, T. A., Wilson, I. A., and Crispin, M. (2019). Exploitation of glycosylation in enveloped virus pathobiology. *Biochim. Biophys. Acta* 1863, 1480–1497. doi: 10.1016/j.bbagen.2019.05.012

Wilson, I. B., Zeleny, R., Kolarich, D., Staudacher, E., Stroop, C. J., Kamerling, J. P., et al. (2001). Analysis of Asn-linked glycans from vegetable foodstuffs: widespread occurrence of Lewis a, core alpha1,3-linked fucose and xylose substitutions. *Glycobiology* 11, 261–274. doi: 10.1093/glycob/11.4.261

Wormald, M. R., and Dwek, R. A. (1999). Glycoproteins: glycan presentation and protein-fold stability. *Structure* 7, R155–R160.

Yang, W. H., Aziz, P. V., Heithoff, D. M., Mahan, M. J., Smith, J. W., and Marth, J. D. (2015). An intrinsic mechanism of secreted protein aging and turnover. *Proc. Natl. Acad. Sci. U.S.A.* 112, 13657–13662. doi: 10.1073/pnas.1515464112

Zhou, T., Doria-Rose, N. A., Cheng, C., Stewart-Jones, G. B. E., Chuang, G. Y., Chambers, M., et al. (2017). Quantification of the impact of the HIV-1-glycan shield on antibody elicitation. *Cell Rep.* 19, 719–732.

Conflict of Interest: EM, RC, AM, AL-W, and ER have filed patent applications describing the development of approaches to support production of glycoproteins in plants including US 2019/0337994 A1, WO 2018 220595 A1, PA174002_PCT, and PA2106659.4.

The remaining author declares that the research was conducted in the absence of any commercial or financial relationships that could be construed as a potential conflict of interest.

frontiers in Plant Science

ORIGINAL RESEARCH
published: 09 September 2021
doi: 10.3389/fpls.2021.736299

Functional Characterization of Pembrolizumab Produced in *Nicotiana benthamiana* Using a Rapid Transient Expression System

Tanapati Phakham[1,2], Christine Joy I. Bulaon[3,4], Narach Khorattanakulchai[3,4], Balamurugan Shanmugaraj[5], Supranee Buranapraditkun[6,7], Chatikorn Boonkrai[1,2], Sarintip Sooksai[8], Nattiya Hirankarn[6], Yoshito Abe[9], Richard Strasser[10], Kaewta Rattanapisit[5] and Waranyoo Phoolcharoen[3,4]**

[1] Interdisciplinary Program of Biomedical Sciences, Graduate School, Chulalongkorn University, Bangkok, Thailand, [2] Center of Excellence in Systems Biology, Faculty of Medicine, Chulalongkorn University, Bangkok, Thailand, [3] Department of Pharmacognosy and Pharmaceutical Botany, Faculty of Pharmaceutical Sciences, Chulalongkorn University, Bangkok, Thailand, [4] Plant-Produced Pharmaceutical Research Unit, Chulalongkorn University, Bangkok, Thailand, [5] Baiya Phytopharm Co., Ltd., Bangkok, Thailand, [6] Department of Microbiology, Faculty of Medicine, Center of Excellence in Immunology and Immune-Mediated Diseases, Chulalongkorn University, Bangkok, Thailand, [7] Center of Excellence in Vaccine Research and Development (Chula Vaccine Research Center-Chula VRC), Faculty of Medicine, Chulalongkorn University, Bangkok, Thailand, [8] The Institute of Biotechnology and Genetic Engineering, Chulalongkorn University, Bangkok, Thailand, [9] Department of Pharmaceutical Sciences, School of Pharmacy at Fukuoka, International University of Health and Welfare, Okawa, Japan, [10] Department of Applied Genetics and Cell Biology, University of Natural Resources and Life Sciences, Vienna, Austria

OPEN ACCESS

Edited by:
Ryo Matsuda,
The University of Tokyo, Japan

Reviewed by:
Julia Jansing,
Maastricht University, Netherlands
Mainak Das Gupta,
LenioBio, Germany

***Correspondence:**
Kaewta Rattanapisit
kaewta.r@baiyaphytopharm.com
Waranyoo Phoolcharoen
Waranyoo.P@chula.ac.th

Specialty section:
This article was submitted to Plant Biotechnology, a section of the journal Frontiers in Plant Science

Received: 05 July 2021
Accepted: 18 August 2021
Published: 09 September 2021

Citation:
Phakham T, Bulaon CJI, Khorattanakulchai N, Shanmugaraj B, Buranapraditkun S, Boonkrai C, Sooksai S, Hirankarn N, Abe Y, Strasser R, Rattanapisit K and Phoolcharoen W (2021) Functional Characterization of Pembrolizumab Produced in Nicotiana benthamiana Using a Rapid Transient Expression System. Front. Plant Sci. 12:736299. doi: 10.3389/fpls.2021.736299

The striking innovation and clinical success of immune checkpoint inhibitors (ICIs) have undoubtedly contributed to a breakthrough in cancer immunotherapy. Generally, ICIs produced in mammalian cells requires high investment, production costs, and involves time consuming procedures. Recently, the plants are considered as an emerging protein production platform due to its cost-effectiveness and rapidity for the production of recombinant biopharmaceuticals. This study explored the potential of plant-based system to produce an anti-human PD-1 monoclonal antibody (mAb), Pembrolizumab, in *Nicotiana benthamiana*. The transient expression of this mAb in wild-type *N. benthamiana* accumulated up to 344.12 ± 98.23 μg/g fresh leaf weight after 4 days of agroinfiltration. The physicochemical and functional characteristics of plant-produced Pembrolizumab were compared to mammalian cell-produced commercial Pembrolizumab (Keytruda®). Sodium dodecyl sulfate polyacrylamide gel electrophoresis (SDS-PAGE) and western blot analysis results demonstrated that the plant-produced Pembrolizumab has the expected molecular weight and is comparable with the Keytruda®. Structural characterization also confirmed that both antibodies have no protein aggregation and similar secondary and tertiary structures. Furthermore, the plant-produced Pembrolizumab displayed no differences in its binding efficacy to PD-1 protein and inhibitory activity between programmed cell death 1 (PD-1) and programmed cell death ligand 1 (PD-L1) interaction with the Keytruda®. *In vitro* efficacy

for T cell activation demonstrated that the plant-produced Pembrolizumab could induce IL-2 and IFN-γ production. Hence, this proof-of-concept study showed that the plant-production platform can be utilized for the rapid production of functional mAbs for immunotherapy.

Keywords: *Nicotiana benthamiana*, molecular farming, transient expression, cancer immunotherapy, anti-PD-1 antibody, Pembrolizumab, plant-produced Pembrolizumab

INTRODUCTION

Immunotherapy is a form of cancer treatment that utilizes the immune system of a patient to target cancer cells (Pardoll, 2012). Among the types of immunotherapies, immune checkpoint inhibitors (ICIs) therapy is based on monoclonal antibody (mAb) to target immune checkpoint molecules on immune cells or cancer cells. These ICIs act by blocking and inhibiting co-stimulatory molecules between tumor cells and immune cells resulting in the enhanced T-cells activation and revival of anergic tumor-reactive T cells mounted effective antitumor responses (Marin-Acevedo et al., 2018; Wei et al., 2018). In 2018, the market value of these ICIs was more than US $34.6 billion and increasing annually (Lu et al., 2020). One of the most effective ICIs used for the cancer treatment is Pembrolizumab (Keytruda®) which targets human programmed cell death protein 1 (PD-1). Pembrolizumab was approved by the US Food and Drug Administration (FDA) for more than 15 cancer indications (Paul et al., 2013).

Generally, the therapeutic antibodies are mostly produced in mammalian cell cultures (Chartrain and Chu, 2008; Chames et al., 2009). The mammalian expression system is currently favorable for recombinant protein production due to the optimized manufacturing conditions and regulatory approval. However, the mammalian expression system still has some concerns, such as safety, risk of contamination, expensive raw materials, high initial investment, extensive demands, and time-consuming for the upstream process development (Li et al., 2010; Moussavou et al., 2015).

In recent days, plants are widely used for pharmaceutical and industrial protein production, such as human growth factors, cytokines, enzymes, anti-microbial peptides, vaccines, antibodies, and diagnostic reagents (Obembe et al., 2011; Donini and Marusic, 2019; Diego-Martin et al., 2020; Porngarm et al., 2020; Rattanapisit et al., 2020; Shanmugaraj et al., 2020a, 2021; Siriwattananon et al., 2020). The plant-based platforms can reduce the investment costs for upstream processing and manufacturing while addressing simple, rapid, and versatile technology for protein production in a short period of time (Buyel and Fischer, 2012; Mir-Artigues et al., 2019). Furthermore, the plants offer no limitations on scalability and flexibility because of low-cost planting and well-established transformation protocols as well as human viral safety and low risk of contamination (Buyel and Fischer, 2012; Moussavou et al., 2015; Zhang et al., 2017). Recently, *Nicotiana benthamiana* has been widely used as a model organism in basic research on the plant biology and utilized for plant molecular farming for several biopharmaceutical productions, such as mAbs (Whaley et al., 2011; Moustafa et al., 2016). The development of plant-produced mAb has achieved similar GMP requirements as those produced in mammalian cells in terms of safety, quality, lifespan, and immunogenicity (Fischer et al., 2012; Klimyuk et al., 2014; Ma et al., 2015). Therefore, the plant expression system represents a cutting-edge platform that extends potential clinical benefits for mAbs-based therapy (Fischer et al., 2012).

The present study aimed to utilize plant-based technology to produce an anti-human PD-1 antibody, Pembrolizumab, in *N. benthamiana*. The plant-produced Pembrolizumab was characterized for both physicochemical and functional properties *in vitro*. The results revealed that plant-produced Pembrolizumab displayed a similar binding affinity and PD-1/PD-L1 neutralizing activity compared with the commercial Pembrolizumab (Keytruda®). In addition, it stimulates T cell responses *in vitro*. Hence, this plant-produced Pembrolizumab has the potential to use as ICI for cancer immunotherapy.

MATERIALS AND METHODS

Expression Vector Construction

The gene fragments encoding Pembrolizumab (Drug bank accession number DB09037) heavy chain (HC) and light chain (LC) were codon-optimized *in silico* using GeneArt™ GeneOptimizer™ software (Invitrogen, Thermo Fisher Scientific, MA, United States) for the expression in *N. benthamiana*. The plant-optimized codon sequences (as shown in **Supplementary Figure 1**) were synthesized (Bioneer, South Korea). Both the full-length HC and LC sequences were flanked with a murine leader sequence (Shanmugaraj et al., 2020b) at the N-terminus and a Ser-Glu-Lys-Asp-Glu-Leu (SEKDEL) sequence at the C-terminus of HC. The Pembrolizumab HC and LC constructs were double digested with *Xba*I and *Sac*I. The antibody gene fragments were purified and cloned into a geminiviral vector pBYR2eK2Md (pBYR2e) (Chen et al., 2011; Diamos and Mason, 2019). The pBYR2e-Pem-HC and pBYR2e-Pem-LC expression vectors were transformed into *Agrobacterium tumefaciens* GV3101 by electroporation. The *A. tumefaciens* cells harboring expression vectors were used for infiltration into plant leaves for recombinant antibody production.

Plant Transformation and Protein Quantification

In this study, 6–8 weeks-old wild-type *N. benthamiana* were grown in a greenhouse under controlled conditions with 16 h light/8 h dark cycle at 28°C. *A. tumefaciens* GV3101 harboring pBYR2e-Pem-HC and pBYR2e-Pem-LC were cultivated in Luria

Bertani broth supplemented with 50 mg/l kanamycin, 50 mg/l gentamicin, and 50 mg/l rifampicin at 28°C for overnight. The overnight grown *Agrobacterium* cells were used for small-scale agroinfiltration by mixing the cell suspensions at a 1:1 ratio and diluting with infiltration buffer (10 mM 2-N-morpholino-ethanesulfonic acid (MES) and 10 mM $MgSO_4$, pH 5.5) to get a final OD_{600} 0.2. The plants were subjected to spot infiltration using a syringe without a needle. The infiltrated leaves were harvested on day 2, 4, 6, and 8 post-infiltration to monitor the expression of Pembrolizumab. The samples were pooled by combining three infiltrated leaf spots to reach an average of 30 mg leaf fresh weight (FW). The pooled leaf samples were extracted with 100 μl PBS buffer (137 mM NaCl, 2.7 mM KCl, 4.3 mM Na_2HPO_4, 1.47 mM KH_2PO_4, and pH 7.4) using a pestle and centrifuged at 20,000 × *g* for 5 min. The supernatant was used to quantify the plant-produced antibody by enzyme-linked immuno-absorbent assay (ELISA). Briefly, ELISA plate was coated with 50 μl of anti-human IgG-Fc fragment (ab97221, Abcam, United Kingdom) diluted (1:1,000) in PBS and incubated at 4°C overnight. The plate was washed with phosphate-buffered saline-Tween (PBST) (0.05% Tween-20 in PBS buffer) and blocked with 5% skim milk in PBS at 37°C for 2 h. Then, the plate was washed and incubated with diluted IgG1 kappa isotype antibody (ab206198, Abcam, United Kingdom) and antibody crude extracts (50 μl/well) at 37°C for 2 h. The plate was washed and incubated with 50 μl/well of HRP-conjugated anti-human kappa antibody (AP015, The Binding Site, United Kingdom) diluted (1:1,000) in PBST at 37°C for 1 h. After washing, the plate was developed using 3,3′,5,5′ tetramethylbenzidine (TMB) substrate (SurModics, MN, United States), and 50 μl/well of 1 M H_2SO_4 was added to stop the reaction. The absorbance was measured at 450 nm.

Purification of Plant-Produced Pembrolizumab

About 100 g of infiltrated leaves were harvested 4 days after agroinfiltration and the leaves were homogenized with 200 ml PBS buffer. The plant crude extract was centrifuged at 26,000 × *g* at 4°C for 40 min and clarified with a 0.45-μm membrane filter. The resulting supernatant was purified by protein A affinity resin (Expedeon, United Kingdom) packed in a polypropylene column (Qiagen, Germany) with 15 mm column diameter. The proteins were washed with PBS buffer and the recombinant antibody was eluted using 0.1 M glycine at pH 2.7 and neutralized with 1.5 M Tris-HCl pH 8.8 to final pH 7.4. Purified plant-produced antibody was buffer exchanged and concentrated using Amicon® Ultra (30 K) centrifugal filter (Merck, Germany) according to the instructions from the manufacturer. Purified plant-produced antibody was quantified by ELISA and used for further experiments.

Sodium Dodecyl Sulfate Polyacrylamide Gel Electrophoresis (SDS-PAGE) and Western Blot Analysis

The sodium dodecyl sulfate polyacrylamide gel electrophoresis (SDS-PAGE) and western blot analysis of the purified plant-produced Pembrolizumab was performed under both the reducing and non-reducing conditions as described previously (Rattanapisit et al., 2019b). For the SDS-PAGE analysis, the bands (2 μg) were visualized by InstantBlue staining (Expedeon, United Kingdom). For western blot, approximately 0.05–0.5 μg of antibodies were transferred onto nitrocellulose membrane (Bio-Rad, CA, United States). The membrane was blocked with 5% skim milk in PBS and then washed with PBST. Proteins were detected either with HRP-conjugated anti-human gamma antibody (The Binding Site, United Kingdom) or HRP-conjugated anti-human kappa antibody (The Binding Site, United Kingdom) diluted (1:5,000) in PBS. The membranes were washed with PBST, developed using enhanced chemiluminescence (ECL) plus detection reagent (Abcam, United Kingdom), and recorded in a medical X-ray green (MXG) film (Carestream, GA, United States).

Size Exclusion Chromatography

The ÄKTA Pure fast protein liquid chromatography (FPLC) purification system was used to assess protein purity and protein aggregations. In brief, antibody samples (0.5 mg/ml, 100 μl) were injected into the Superdex® 200 Increase 10/300 GL column (Cytiva, MA, United States). A PBS buffer was used as a running buffer with a flow rate of 0.5 ml/min. The absorbance monitored the chromatogram of each antibody sampled at 280 nm.

Circular Dichroism (CD) Spectroscopy

Before measurements, the plant-produced and commercial Pembrolizumab antibodies were concentrated by Amicon® Ultra (30 K) (Merck, Germany). Their concentrations were determined using their extinction coefficients at 280 nm that were calculated by their amino acid sequence. Then, their concentrations were adjusted to 10 μM using PBS buffer at pH 7.4. The CD spectra were recorded at room temperature using a quartz cell with a 1-mm optical path length on a J-720W CD spectropolarimeter (JASCO, Japan). The molar ellipticity expressed in degrees × cm^2/dmol was calculated based on a mean residue molecular weight of 110.

NMR Spectroscopy

NMR spectra were recorded on a Varian Unity INOVA 600 spectrometer (Varian, CA, United States). For NMR measurements, the antibody concentrations were adjusted to 100 μM using PBS buffer at pH 7.4 containing 10% v/v D_2O. Topspin 4.1.1 software (Bruker Corporation, MA, United States) was used to process the data.

N-Glycan Analysis

Purified plant-produced antibody was subjected to SDS-PAGE under non-reducing conditions. The target protein band was excised from the gel, S-alkylated, and digested with trypsin. Liquid chromatography-electrospray ionization-mass spectrometry (LC-ESI-MS) of tryptic glycopeptides was performed as described previously (Strasser et al., 2008).

PD-1 Binding Profile by ELISA

The PD-1 binding activity of plant-produced Pembrolizumab was determined by ELISA. Briefly, the ELISA plate was coated with 100 μl/well of recombinant human PD-1 His tag protein at 0.1 μg/ml (8986-PD, R&D Systems, MN, United States) at 4°C for overnight. The plate was washed and blocked with PBST. The two-fold serial dilutions of anti-PD-1 antibodies or human IgG4 isotype control (403701, BioLegend, CA, United States) starting from 2 μg/ml (100 μl/well) were added and the plate was incubated at 37°C for 1 h. Then, the HRP-conjugated goat anti-human IgG antibody (109035088, Jackson ImmunoResearch, PA, United States) diluted (1:10,000) in PBST was added and incubated at 37°C for 1 h. The plate was washed and developed with 100 μl/well of SigmaFast™ OPD substrate solution in the dark at room temperature for 20 min. The reaction was stopped by adding 50 μl/well of 1 M H_2SO_4 and the absorbance was measured at 492 nm using a Cytation™ five cell imaging multi-mode reader.

PD-1 Binding Kinetics by Surface Plasmon Resonance (SPR)

The Biacore T200 equipped with a protein G sensor chip (chip ID. 10258853, GE Healthcare, IL, United States) was used to determine the binding kinetics of anti-PD-1 antibodies. In the protein-capturing step, anti-PD-1 antibodies in HBS-EP running buffer at 3 μg/ml were injected into an individual flow cell of the protein G sensor chip. A single-cycle kinetic was performed to determine the binding kinetics by injecting five different concentrations (10, 20, 40, 80, and 160 nM) of human PD-1 His tag (8986-PD, R&D Systems, MN, United States) at a flow rate of 30 μl/min with association time for 60 s and dissociation time for 120 s. The signal of an uncoated reference cell was subtracted from the sensor grams, and the HBS-EP buffer blank was also included as a negative control for double referencing. The Biacore T200 evaluation software version 3.1 was used for the calculation of association rate constant (k_{on}), dissociation rate constant (k_{off}), and equilibrium dissociation constant (K_D) by curve fitting the data with a Langmuir 1:1 binding model.

PD-1/PD-L1 Blockade Assay

The PD-1/PD-L1 neutralizing activity was determined by cell-based luciferase reporter assay (PD-1/PD-L1 blockade bioassays, Promega, WI, United States). Briefly, PD-L1 aAPC/CHO-K1 cells were seeded into a white flat-bottom 96-well plate and incubated in a 5% CO_2 humidified incubator at 37°C for 16 h. Three-fold serial dilutions of anti-PD-1 antibodies and the PD-1 effector cells were added to the plate and incubated in 5% CO_2 humidified incubator at 37°C for 6 h. After co-culture, the Bio-Glo™ substrate reagent was added to the plate and incubated at room temperature for 5 min. The luminescence signal was measured using a Cytation™ 5 cell imaging multi-mode reader and reported as relative light units (RLUs).

Production of Cytokines

The peripheral blood mononuclear cells (PBMCs) were separated from healthy blood donors by density gradient centrifugation with Isoprep (Robbins Scientific Corporation, CA, United States). The isolated PBMCs were resuspended in fetal bovine serum (FBS) with 10% dimethyl sulfoxide (DMSO) and kept frozen until assay time. On day 0, frozen PBMCs ($n = 4$) were thawed and seeded at 1×10^5 cells/well in the assay plate. The cells were stimulated with the Staphylococcal enterotoxin B (SEB) (Rattanapisit et al., 2019b) at 1 ng/ml in the presence of antibodies at 0.01 and 0.1 μg/ml. Keytruda® and human IgG4 antibody (BioLegend, CA, United States) were used as positive and negative control, respectively. On day 3, the secretion levels of IL-2 and IFN-γ in culture supernatant were determined by ELISA (BioLegend).

Statistical Analysis

All the experiments in the study were performed three times. A statistical analysis was performed using GraphPad Prism 8.0 (GraphPad Software, CA, United States). A multiple *t*-test was utilized to determine statistically significant differences between each group using the Holm–Sidak method, with alpha equal to 0.05. A P value less than 0.05 ($P \leq 0.05$) was considered as statistically significant.

RESULTS

Rapid Transient Expression of Pembrolizumab *in N. benthamiana*

To evaluate the expression of Pembrolizumab, *Agrobacterium* harboring the heavy chain (Pem-HC) and light chain (Pem-LC) expression vectors (**Figure 1A**) were co-infiltrated into the plant leaves. An 8-day expression time-course experiment was performed and infiltrated leaves were harvested every 2 days after agroinfiltration. The expression levels of Pembrolizumab were quantified by ELISA and were reported as microgram per gram (μg/g) leaf FW. The results showed that the maximum expression level of antibody was observed 4 days after agroinfiltration reaching up to 344.12 ± 98.23 μg/g FW as shown in **Figure 1B** and **Supplementary Table 1**. However, the expression level of Pembrolizumab was 4-fold declined from day 6 to 8 post-infiltration. All infiltrated leaf samples that showed a significant reduction in antibody expression also displayed rapid wilting and apparent necrosis at the infiltrated site (data not shown), potentially affecting the antibody levels obtained from the leaves harvested on day 6 and 8. We also demonstrated that this rapid transient expression platform could be used for recombinant antibody production within 4 days after infiltration when compared with other expression platforms, as indicated in **Figure 1C** and **Supplementary Table 2**.

Physicochemical Characteristics of Purified Plant-Produced Pembrolizumab

As we have successfully obtained plant-produced Pembrolizumab, the characterization of its molecular features was subsequently performed. A gradient 4–15% SDS-PAGE (reducing and non-reducing conditions) and western blot

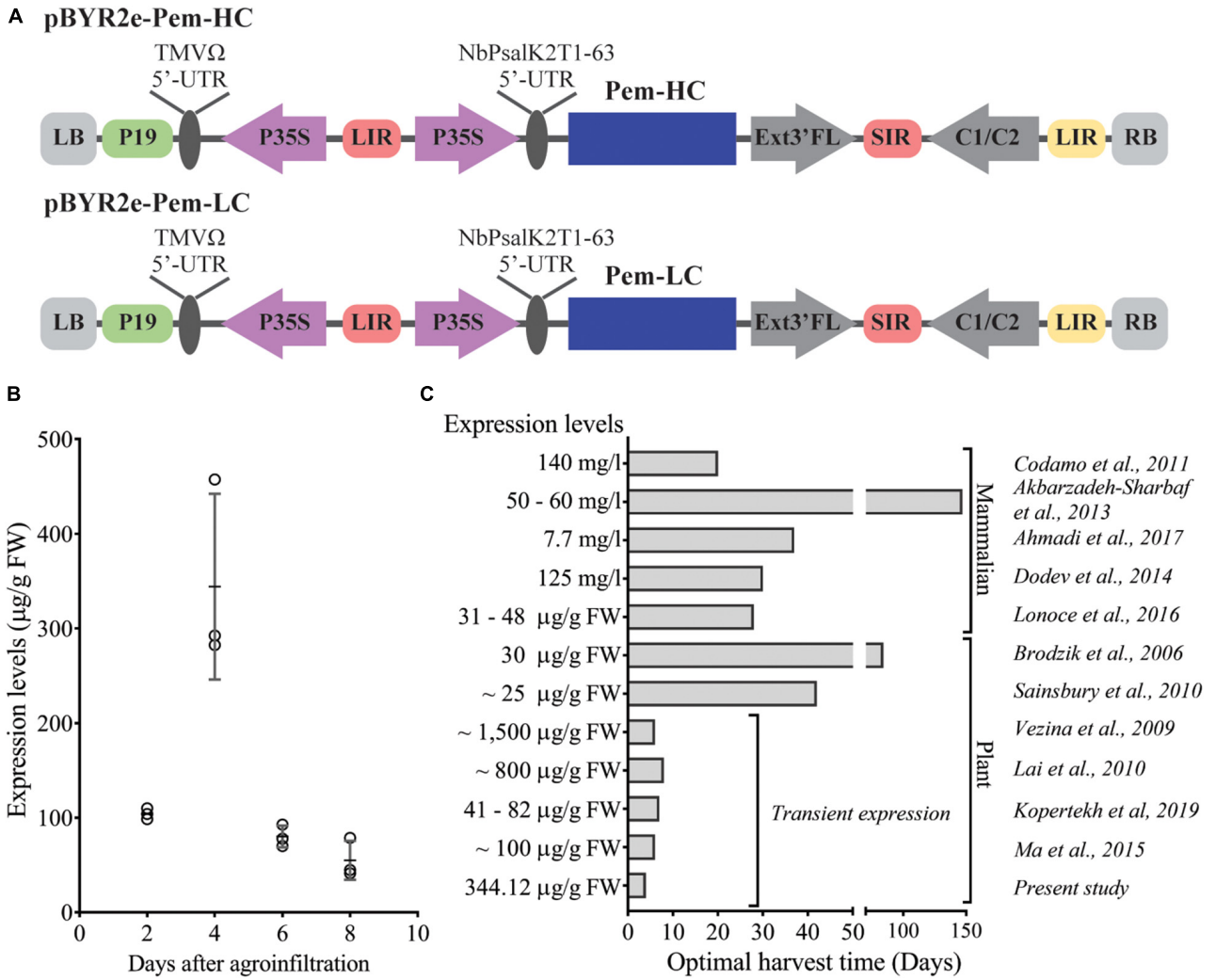

FIGURE 1 | Rapid transient expression of Pembrolizumab in *N. benthamiana*. **(A)** Schematic representation of the T-DNA regions of the expression vectors used for the transient expression of Pembrolizumab in *N. benthamiana*. P19: the RNA silencing suppressor gene derived from tobacco bushy stunt virus (TBSV); P35S: Cauliflower Mosaic Virus (CaMV) 35S promoter; TMVΩ 5′-UTR: 5′ untranslated region (UTR) of tobacco mosaic virus Ω; NbPsalK2T1-63 5′UTR: 5′ UTR of *Nicotiana* photosystem I reaction center subunit *psaK*; Pem-HC: heavy chain of Pembrolizumab; Pem-LC: light chain of Pembrolizumab; Ext3′FL: 3′ region of tobacco extension gene; C1/C2: Bean Yellow Dwarf Virus (BeYDV) ORFs C1 and C2 encoding for replication initiation protein (Rep) and RepA; SIR and LIR: short and long intergenic regions of the BeYDV genome; LB and RB: left and right borders of the *Agrobacterium* T-DNA region. **(B)** The antibody expression levels in wild-type *N. benthamiana* on day 2, 4, 6, and 8 after agroinfiltration were quantified by ELISA. Data are presented as mean ± SD. **(C)** Comparison between the optimal harvest time and the recombinant antibody expression levels with previous reports. Cost comparison of these mAbs production in plants and mammalian system was not performed.

analysis were performed with plant-produced Pembrolizumab. Under the reducing condition, HC and LC were observed at approximately 50 and 25 kDa, respectively. A western blot analysis with anti-human kappa antibody and anti-human gamma antibody also confirmed the expression of both HC and LC with the expected molecular size comparable to Keytruda® (**Figure 2A**). Meanwhile, the results under the non-reducing condition revealed that plant-produced antibody exhibited assembly into its tetrameric form, which was found at 150 kDa, as shown in **Figure 2B**. However, minor amounts of antibody fragments were also observed, as indicated by the additional bands in the SDS-PAGE gels.

Size exclusion chromatography was performed to assess the antibody aggregation. The results demonstrated that plant-produced Pembrolizumab assembled as full IgG molecule (major peak) as shown in **Figure 2C** with a relatively low-level of antibody aggregates (small minor peaks). No fragmented forms of the antibodies were observed in the chromatogram. Furthermore, the secondary structure of plant-produced Pembrolizumab was compared with Keytruda® using CD spectroscopy. The CD results demonstrated that the secondary structure of plant-produced Pembrolizumab was comparable to that of the Keytruda® (**Figure 2D**). Both the spectra denote negative absorbance at 218 nm, which infers

a β-sheet-rich structure. Further, the tertiary structure of plant-produced Pembrolizumab was compared with Keytruda® using NMR spectroscopy. The up-fielded methyl protons were observed in both spectra, indicating that the tertiary structures are retained (**Figure 2E**). The peaks at the same chemical shifts in NMR spectra also confirmed that the tertiary structures are similar for plant-produced Pembrolizumab and Keytruda®.

N-Glycosylation Profile

Generally, the early stages of N-glycosylation are similar between plant and mammalian cells whereas the maturation steps responsible for the complex glycan differs between these systems. To evaluate the *N*-glycan profile of plant-produced Pembrolizumab, LC-ESI-MS was used (**Figure 3**). Based on the results, the *N*-glycan profile of Keytruda® revealed the presence of mammalian-type *N*-glycan species, such as GlcNAc2Man3FucGlcNAc2 (GnGnF) and GalGlcNAc2Man3FucGlcNAc2 (AGnF) as expected for a mammalian-cell produced mAb. By contrast, the plant-produced Pembrolizumab displayed oligomannosidic *N*-glycans, i.e., Man7GlcNAc2, Man8GlcNAc2, and Man9GlcNAc2 which are typical for endoplasmic reticulum (ER)-retained glycoproteins. However, the *N*-glycans in plant-produced Pembrolizumab did not affect the binding properties or binding affinity of the antibody with its target.

Functional Characterization of Plant-Produced Pembrolizumab

It is known that plants have different molecular machinery for protein production and post-translational modifications in comparison with the mammalian system (Gomord and Faye, 2004). Thus, we focused on the analysis of functional characteristics of plant-produced Pembrolizumab.

To determine the functional characteristics of plant-produced Pembrolizumab, ELISA was performed to evaluate the binding activity to human PD-1, while the PD-1/PD-L1 cell-based blockade bioassay was used to assess the inhibitory action. Serial dilutions of each antibody sample were added to the PD-1-coated ELISA plate, and the goat anti-human IgG-HRP antibody was used to detect the antibody that was specifically bound to the PD-1 protein. The specific binding results demonstrated that the plant-produced Pembrolizumab showed similar dose-dependent binding activity with human PD-1 protein compared with Keytruda® (**Figure 4A**), while the negative control human IgG4 antibody did not exhibit any binding to human PD-1 protein. Furthermore, the inhibitory activity of plant-produced Pembrolizumab was assessed. Serial dilutions of each antibody sample and Jurkat/PD-1 effector cell were added to the assay plate containing pre-cultured CHO-K1/PD-L1 cells, and the plate was incubated for 6 h. The presence of anti-human PD-1 antibody inhibits the interaction between PD-1 and PD-L1 resulting in the activation of luciferase reporter gene. The results indicated that plant-produced Pembrolizumab inhibited the interaction between PD-1 and PD-L1 in a dose-dependent manner (**Figure 4B**) with a half-maximal effective concentration (EC_{50}) of 147.2 ng/ml compared with Keytruda® (EC_{50} = 146.7 ng/ml). These results confirmed that the plant-produced Pembrolizumab displayed functional binding to human PD-1 and inhibits PD-1 and PD-L1 interaction *in vitro* at a comparable level with Keytruda®.

Since plant-produced Pembrolizumab has exhibited both binding and inhibitory functions, we then, determined the binding kinetics of plant-produced Pembrolizumab with human PD-1 protein. A single-cycle binding kinetics was performed using surface plasmon resonance (SPR). Data showed that the equilibrium dissociation constant (K_D) of plant-produced Pembrolizumab was 8.51 nM, while the K_D of Keytruda® was 8.26 nM, as shown in **Figure 5A** and **Supplementary Table 3**. Both antibodies exhibited subnanomolar binding affinity with its target. These data confirmed that the plant-produced Pembrolizumab has high binding affinity with human PD-1 protein.

This study successfully confirmed that plant-produced Pembrolizumab has binding and inhibition activities with its target. So, we further examined the potency of the antibody on T cell activation *in vitro*. The SEB stimulation of PBMCs in the presence of either anti-PD-1 antibodies or human IgG4 antibody control at 0.01 and 0.1 μg/ml was performed. Antigen-presenting cell and effector T cells were co-cultured in the presence of SEB toxin. The SEB toxin stimulates T cell response *in vitro*. However, when T cells are activated for a while, regulatory mechanisms break the over-induction signals in PD-1/PD-L1 pathway. The presence of anti-PD-1 antibody inhibits the regulatory mechanism. Hence, T cell becomes activated and secrets activating cytokines, such as IFN-gamma and IL-2. On the other hand, without anti-PD-1 antibody in the assay plate, antigen-presenting cell and effector T cells maintain a balance between stimulatory and regulatory mechanism. The results showed that the plant-produced Pembrolizumab and Keytruda® (at 0.1 μg/ml) were significantly able to stimulate T cell responses *via* IL-2 (**Figure 5B**) and IFN-γ (**Figure 5C**) secretion compared with the human IgG4 antibody control. Noticeably, plant-produced Pembrolizumab even at a low dose (0.01 μg/ml) significantly induced both IL-2 and IFN-γ production. At the same time, Keytruda® displayed no significant in IFN-γ production compared with human IgG4 control. These findings revealed that plant-produced Pembrolizumab promoted T cells responses *in vitro*.

DISCUSSION

Immunotherapy represents an innovative approach for the treatment of multiple types of cancer. Several immune checkpoint molecules have been discovered and explored over the years, such as programmed cell death 1 (PD-1), programmed cell death ligand 1 (PD-L1), and cytotoxic T-lymphocyte antigen 4 (CTLA-4) (He and Xu, 2020). The development of ICIs against these inhibitory immunoreceptors has potential benefits and shaped the therapeutic ways of several cancer types. Ever since, these drugs have translated to a great deal of success in cancer immunotherapy (Robert et al., 2014; Weber et al., 2015; Kasamon et al., 2017; Liu and Cho, 2017).

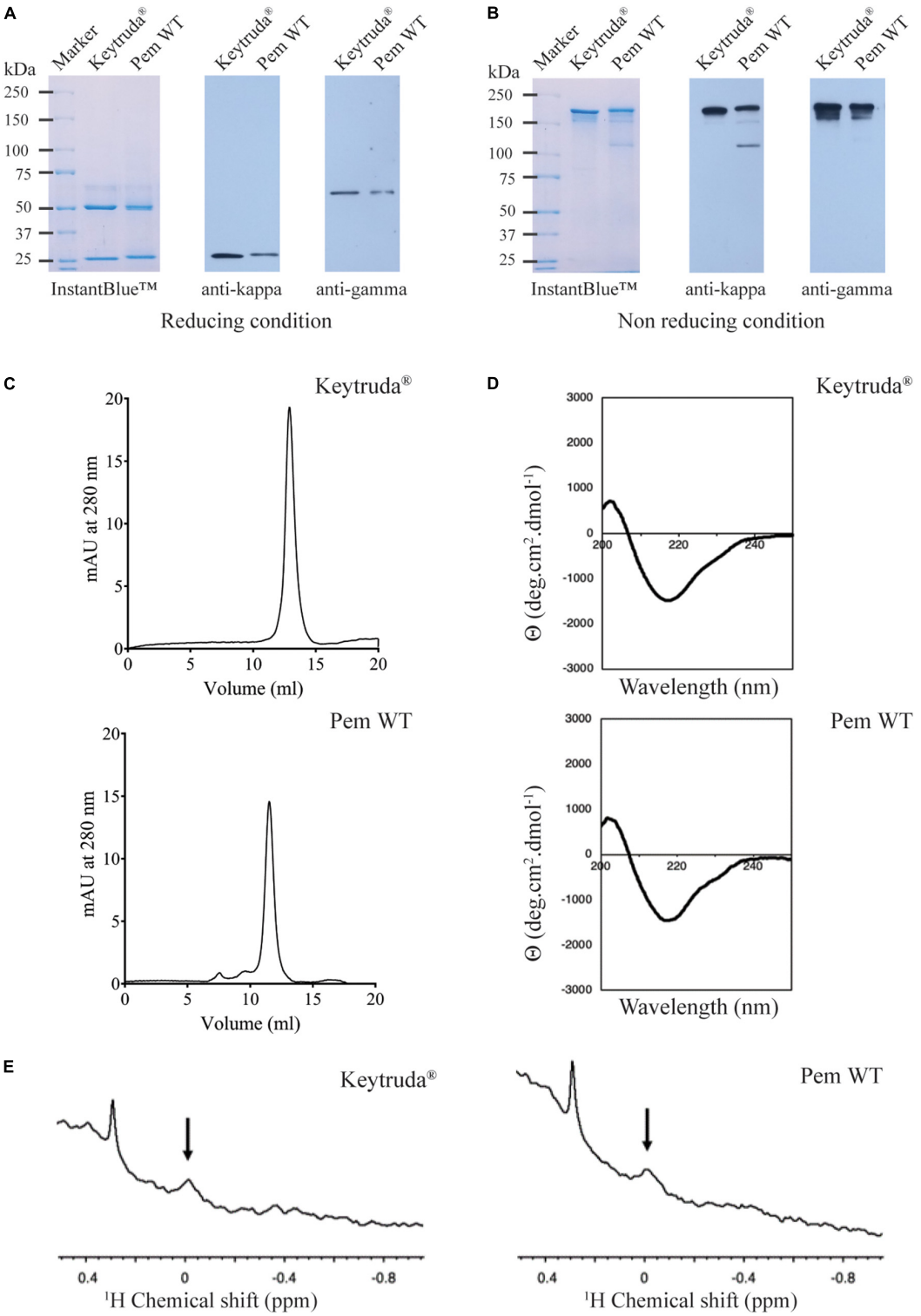

FIGURE 2 | Physicochemical characteristics of purified plant-produced Pembrolizumab. Sodium dodecyl sulfate polyacrylamide gel electrophoresis (SDS-PAGE) (4–15%) and western blot analysis of plant-produced Pembrolizumab (Pem WT) under **(A)** reducing condition and **(B)** non-reducing condition. For the SDS-PAGE, proteins were stained with InstantBlue™ staining solution. For the western blot analysis, proteins were probed with either HRP-conjugated anti-human kappa or anti-human gamma and detected with enhanced chemiluminescence (ECL) substrate solution. **(C)** Chromatogram of Keytruda® (top) and Pem WT (bottom) analyzed by size-exclusion chromatography. **(D)** Circular dichroism spectrum of Keytruda® (top) and Pem WT (bottom) in PBS at pH 7.4. **(E)** NMR spectra in methyl region of Keytruda® (left) and Pem WT (right) in PBS buffer at pH 7.4 containing 10% v/v D_2O at 25°C.

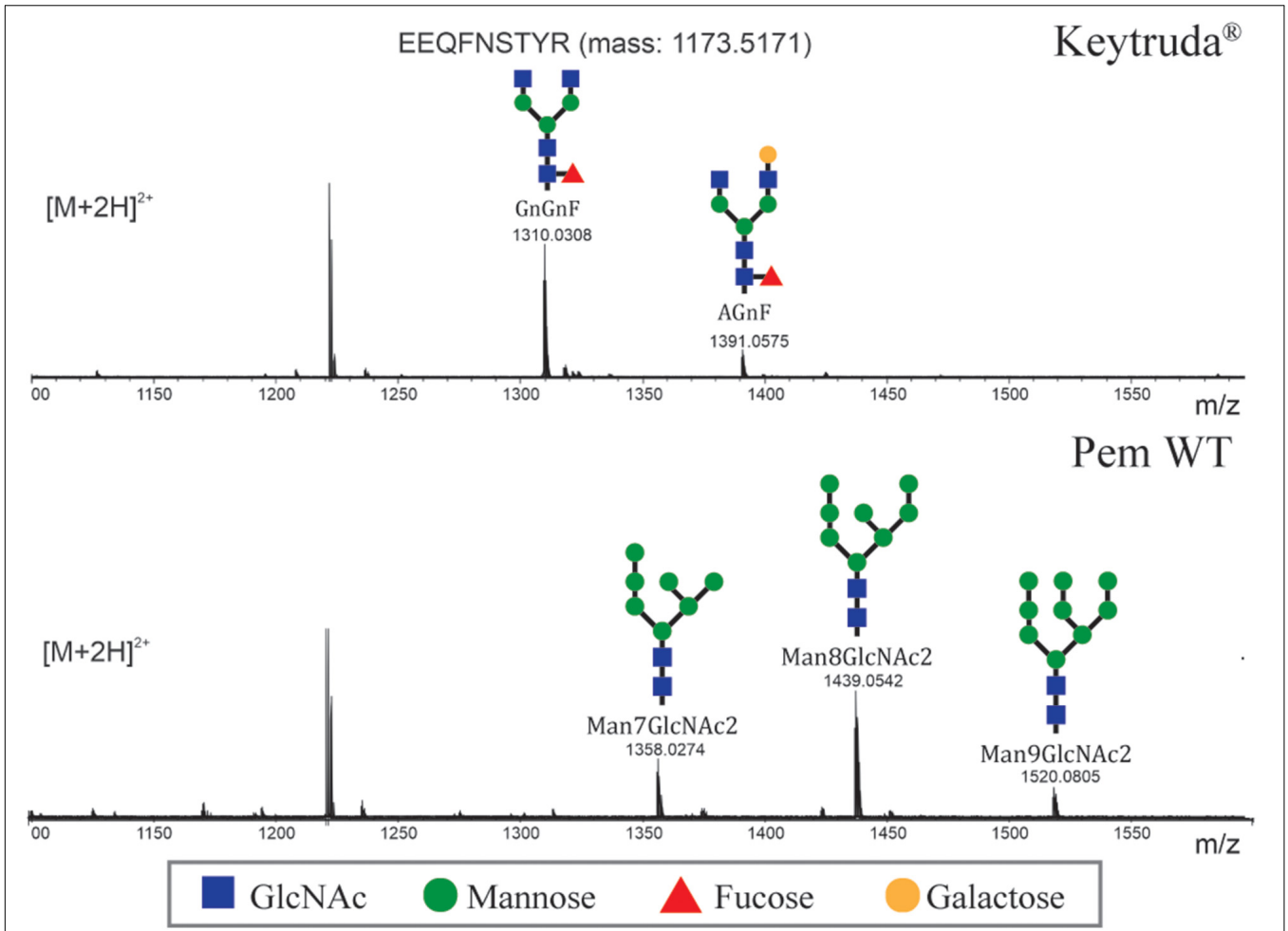

FIGURE 3 | N-glycosylation profile of plant-produced Pembrolizumab. The N-glycosylation profile of the glycopeptide EEQFNSTYR is shown, and the major glycosylated peaks $[M + 2H]^{2+}$ are depicted. For a detailed explanation of glycan structure abbreviations, see www.proglycan.com.

Generally, ICIs used for cancer treatment were produced in mammalian cells. However, the investment costs and production process of ICIs produced from mammalian-based are varied and took longer time. Because the investment cost and time for phase 1 cGMP manufacturing of plant expression system are comparatively cost-effective (7.5- to 10-fold) and faster (<6 months) than mammalian expression system, the plant-production platform might be an alternative platform for the production of many biopharmaceutical products. The use of plant expression systems for the production of pharmaceutically important proteins (Bulaon et al., 2020; Hanittinan et al., 2020), vaccines (Marsian et al., 2017; Rosales-Mendoza et al., 2017), diagnostic reagents (Rattanapisit et al., 2021), and antibodies (Kopertekh et al., 2019; Hurtado et al., 2020; Rattanapisit et al., 2020) were documented. In addition, the prior studies reported that the generation of plant-made protective immunogen and therapeutic antibodies (Dent et al., 2016; Rattanapisit et al., 2019a,b; Nessa et al., 2020; Yiemchavee et al., 2021).

Herein, we successfully produced Pembrolizumab using a rapid transient expression system in *N. benthamiana*. This study utilized the benefits of plant viral vectors in terms of speed and yield to produce a recombinant anti-human PD-1 antibody for effective cancer immunotherapy. In particular, a geminiviral vector pBYR2e based on the bean yellow dwarf virus (BeYDV) was used (Diamos and Mason, 2019). It contains the self-rolling circle replication elements, which can produce a high copy number of the expression cassette eventually resulting in a high accumulation of recombinant proteins in plants (Huang et al., 2010; Chen, 2018). More so, the use of viral vectors for transient expression in *N. benthamiana* has proven its efficiency as a suitable host for viral infectivity (Goodin et al., 2008). In particular, mAbs against enterovirus infection (Rattanapisit et al., 2019a), porcine epidemic diarrhea virus infection (Rattanapisit et al., 2017), and even the recent coronavirus infection (Shanmugaraj et al., 2020b) were transiently expressed in *N. benthamiana* using this geminiviral vector. The optimal yields obtained vary from 4 to 130 μg/g leaf fresh weight within 3–6 days after infiltration. Due to these advantages, geminiviral vectors have been utilized for transient production of therapeutically important mAbs in plants. Intriguingly, other

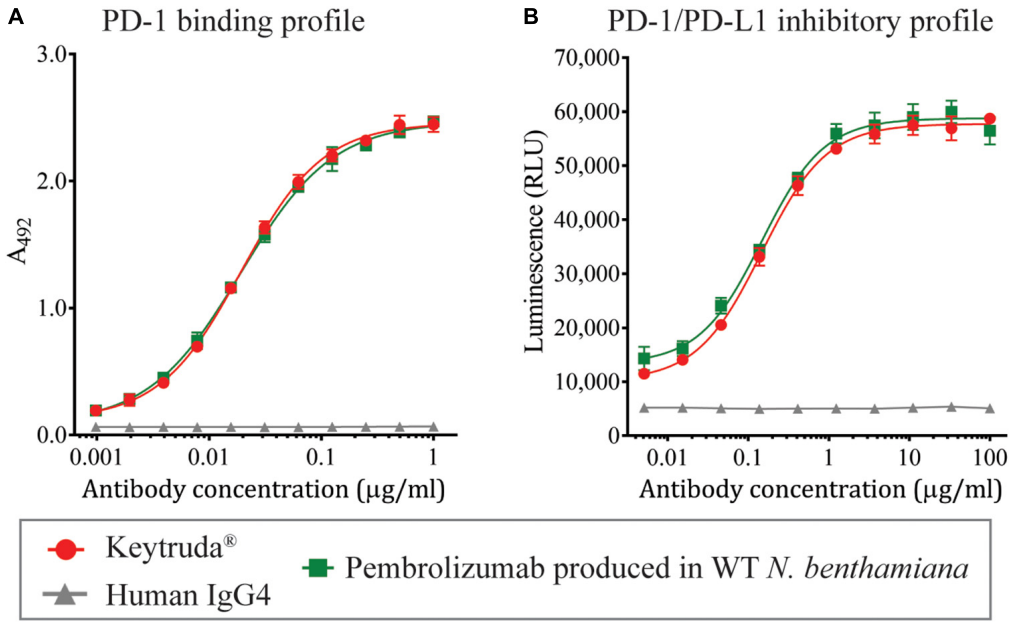

FIGURE 4 | Binding and inhibition profiles of plant-produced Pembrolizumab. Purified plant-produced Pembrolizumab was assessed for the **(A)** binding activity with human PD-1 by ELISA and **(B)** PD-1/PD-L1 inhibition activity by PD-1/PD-L1 blockade bioassay. The Keytruda® and human IgG4 were used as positive and negative control, respectively. Data are presented as mean ± SD.

studies utilized the plant expression system for the production of anti-human immunodeficiency virus (HIV) mAb (Sainsbury et al., 2010), tumor-targeting mAb (Vaquero et al., 1999; Villani et al., 2009), HCG-specific mAb (Kathuria et al., 2002), murine anti-human IgG C5-1 (Vézina et al., 2009), anti-West Nile virus mAb (Lai et al., 2010), and reported varying levels of antibody accumulation.

The SEKDEL motif at the C-terminus of the HC was added for ER retention to improve protein accumulation in the ER (Petruccelli et al., 2006). The folding and assembly of newly synthesized proteins to form mature complex protein in the ER begins prior complete translation of polypeptide (Farràs et al., 2020) and final transport to cellular destination (Yamamoto et al., 2001). In this work, we adapted this principle and hypothesize that SEKDEL-tagged HC could stabilize initially by forming disulfide-bonded dimers, to which LC can be assembled by forming disulfide bond between constant domains (C_L and C_H1) (Feige et al., 2010; Weiner, 2015), eventually the fully assembled antibody can be retrieved from cis-Golgi back to the ER for retention and subsequent protein accumulation.

The results demonstrated that Pembrolizumab was expressed rapidly in *N. benthamiana* at the highest level of expression obtained within 4 days post-infiltration providing essential advantages of speed over transgenic plant expression system (Brodzik et al., 2006; Ma et al., 2015; Lonoce et al., 2016), mammalian expression system (Codamo et al., 2011; Akbarzadeh-Sharbaf et al., 2013; Dodev et al., 2014; Ahmadi et al., 2017), and in some transient expression systems (Sainsbury et al., 2010; Kopertekh et al., 2019). The maximum expression level of Pembrolizumab reached up to 344.12 ± 98.23 µg/g FW after 4 days of post-infection followed by a marked decrease after 6 days. The significant drop in antibody expression might be due to the progressive development of necrosis on the infiltrated leaves observed from day 6 to 8 post-infiltration. The high-level of necrosis, eventually resulting in cell death, is considered a critical factor for reduced protein yield (Mathew et al., 2014; Hamorsky et al., 2015).

The results from size-exclusion chromatography revealed that plant-produced Pembrolizumab efficiently assembled into the whole IgG molecule and displayed the tetrameric isoform. The protein impurities and IgG aggregates were observed at small amounts, supporting the intrinsic aggregation propensity of all therapeutic proteins, such as antibodies (Roberts, 2014). Aggregation is considered either process or product-related impurities that must be monitored and controlled to a minimum extent (Cleland et al., 1993). Moreover, antibody fragments were not observed in the size exclusion chromatogram prospectively due to the low concentration of fragments in the sample solution (Adawy and Groves, 2017). Likewise, the results from CD confirmed similar secondary structures of the Pembrolizumab produced in a plant and a mammalian cell. This study findings from NMR spectroscopy also presented similarities on the tertiary structures of the plant-derived Pembrolizumab and mammalian cell-derived Pembrolizumab.

The earlier stages of *N*-glycan processing in the ER are highly conserved across the species but differ significantly during the late stages in the Golgi apparatus. In particular, the plant-produced recombinant proteins contain plant-specific glycans, such as β1,2-xylose and core α1,3-fucose (Strasser, 2016), which are of concern for human applications. Nonetheless,

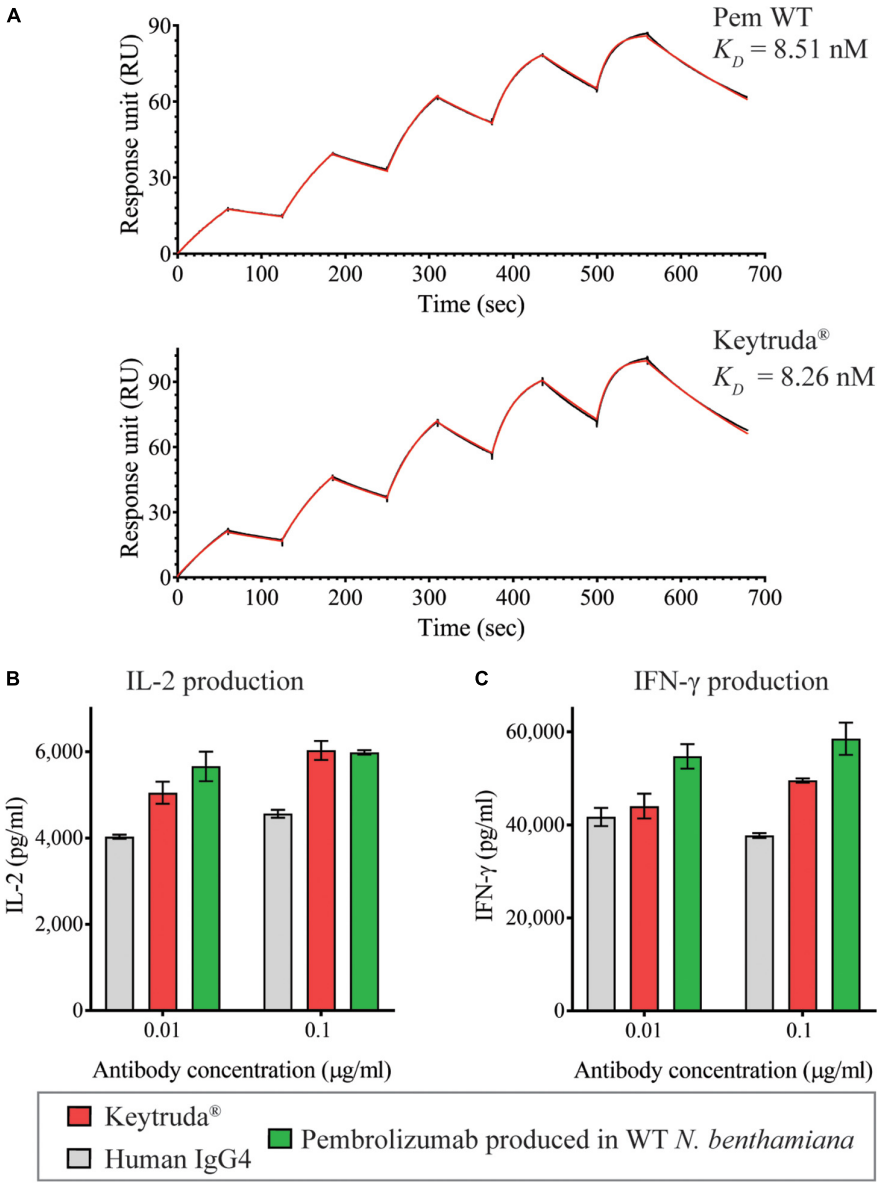

FIGURE 5 | Functional characterization of plant-produced Pembrolizumab. **(A)** Binding kinetics data of plant-produced Pembrolizumab and Keytruda® with human PD-1 analyzed by SPR. PBMCs from healthy donors were stimulated with 1 ng/ml SEB in the presence of antibodies at 0.01 and 0.1 μg/ml. The secretion levels of **(B)** IL-2 and **(C)** IFN-γ in culture supernatant after co-culture for 3 days were measured by ELISA. Data are presented as mean ± SD.

no severe allergic reactions or hypersensitive indications were previously documented from such plant-specific *N*-glycans (Ma et al., 2015; Pillet et al., 2019). The glycan profile data confirmed that the plant-produced Pembrolizumab displayed oligomannosidic *N*-glycans attributed to targeted retention in the ER due to SEKDEL sequence. Similar to the prior reports, SEKDEL-tagged antibodies displayed non-immunogenic high-mannose *N*-glycans (Sriraman et al., 2004). However, high-mannose *N*-glycans in the plant-produced antibodies contributes for increase in the antibody clearance rate from circulation (Reusch and Tejada, 2015). Hence, glycan-engineered plants could be used instead to obtain more mammalian-like *N*-glycans that have more potentially favorable properties for therapeutic applications.

Furthermore, the functional characteristics of plant-produced Pembrolizumab were evaluated. The binding activity and binding kinetics data confirmed that the mAb effectively binds to human PD-1 protein with a high affinity similar to Keytruda®. It also inhibits the interaction between PD-1 and PD-L1 with equivalent EC_{50} values compared to the commercial mAb. The different RU in SPR was noted between both the antibodies which might be due to the difference in the antibody concentration captured on a protein G sensor chip. The results of the SEB stimulated PBMCs confirmed that the plant-produced Pembrolizumab could induce

and promote T cells responses *in vitro*. These findings are similar to the previous report (Rattanapisit et al., 2019b).

CONCLUSION

We have demonstrated the feasibility of rapid transient expression of Pembrolizumab in *N. benthamiana*. The plant-produced Pembrolizumab has *in vitro* physicochemical and functional characteristics quite similar to mammalian cell-produced Pembrolizumab. Future studies will focus on analyzing the *in vivo* efficacy of plant-produced Pembrolizumab in animal models. Altogether, this proof-of-concept study proved the robustness of the plant expression system for the production of anti-PD-1 Pembrolizumab, which could be used as employed for cancer immunotherapy.

DATA AVAILABILITY STATEMENT

The original contributions presented in the study are included in the article/**Supplementary Material**, further inquiries can be directed to the corresponding author/s.

AUTHOR CONTRIBUTIONS

KR and WP designed all the experiments. CJIB, NK, BS, and KR performed antibody gene synthesis, antibody expression, purification, and quantification. YA performed structural characterization. RS performed *N*-glycan analysis. TP, SB, CB, SS, and NH performed the binding, binding kinetics, blockade bioassay, and *in vitro* functional assays. All authors analyzed the data and contributed to manuscript preparation.

FUNDING

This study was supported by the National Research Council of Thailand, 100th Anniversary Chulalongkorn University Fund for Doctoral Scholarship and Scholarship Program for ASEAN and Non-ASEAN Countries.

ACKNOWLEDGMENTS

We would like to thank Clemens Grünwald-Gruber (BOKU Core Mass Spectrometry Facility, University of Natural Resources and Life Sciences, Vienna, Austria) for assisting with LC-ESI-MS analysis.

SUPPLEMENTARY MATERIAL

The Supplementary Material for this article can be found online at: https://www.frontiersin.org/articles/10.3389/fpls.2021.736299/full#supplementary-material

REFERENCES

Adawy, A., and Groves, M. R. (2017). The use of size exclusion chromatography to monitor protein self-assembly. *Crystals* 7:331.

Ahmadi, S., Davami, F., Davoudi, N., Nematpour, F., Ahmadi, M., Ebadat, S., et al. (2017). Monoclonal antibodies expression improvement in CHO cells by PiggyBac transposition regarding vectors ratios and design. *PLoS One* 12:e0179902. doi: 10.1371/journal.pone.0179902

Akbarzadeh-Sharbaf, S., Yakhchali, B., Minuchehr, Z., Shokrgozar, M. A., and Zeinali, S. (2013). Expression enhancement in trastuzumab therapeutic monoclonal antibody production using genomic amplification with methotrexate. *Avicenna J. Med. Biotechnol.* 5, 87–95.

Brodzik, R., Glogowska, M., Bandurska, K., Okulicz, M., Deka, D., Ko, K., et al. (2006). Plant-derived anti-Lewis Y mAb exhibits biological activities for efficient immunotherapy against human cancer cells. *Proc. Natl. Acad. Sci. U. S. A.* 103, 8804–8809. doi: 10.1073/pnas.0603043103

Bulaon, C. J. I., Shanmugaraj, B., Oo, Y., Rattanapisit, K., Chuanasa, T., Chaotham, C., et al. (2020). Rapid transient expression of functional human vascular endothelial growth factor in *Nicotiana benthamiana* and characterization of its biological activity. *Biotechnol. Rep.* 27:e00514. doi: 10.1016/j.btre.2020.e00514

Buyel, J. F., and Fischer, R. (2012). Predictive models for transient protein expression in tobacco (*Nicotiana tabacum* L.) can optimize process time, yield, and downstream costs. *Biotechnol. Bioeng.* 109, 2575–2588. doi: 10.1002/bit.24523

Chames, P., Van Regenmortel, M., Weiss, E., and Baty, D. (2009). Therapeutic antibodies: successes, limitations and hopes for the future. *Br. J. Pharmacol.* 157, 220–233. doi: 10.1111/j.1476-5381.2009.00190.x

Chartrain, M., and Chu, L. (2008). Development and production of commercial therapeutic monoclonal antibodies in Mammalian cell expression systems: an overview of the current upstream technologies. *Curr. Pharm. Biotechnol.* 9, 447–467. doi: 10.2174/138920108786786367

Chen, Q. (2018). "Chapter seven - recombinant therapeutic molecules produced in plants," in *Advances in Botanical Research*, ed. M. Kuntz (United States: Academic Press), 207–244.

Chen, Q., He, J., Phoolcharoen, W., and Mason, H. S. (2011). Geminiviral vectors based on bean yellow dwarf virus for production of vaccine antigens and monoclonal antibodies in plants. *Hum. Vaccin.* 7, 331–338. doi: 10.4161/hv.7.3.14262

Cleland, J., Powell, M., and Shire, S. (1993). The development of stable protein formulations: a close look at protein aggregation, deamidation, and oxidation. *Crit. Rev. Ther. Drug Carr. Syst.* 10, 307–377.

Codamo, J., Munro, T. P., Hughes, B. S., Song, M., and Gray, P. P. (2011). Enhanced CHO cell-based transient gene expression with the epi-CHO expression system. *Mol. Biotechnol.* 48, 109–115. doi: 10.1007/s12033-010-9351-9

Dent, M., Hurtado, J., Paul, A. M., Sun, H., Lai, H., Yang, M., et al. (2016). Plant-produced anti-dengue virus monoclonal antibodies exhibit reduced antibody-dependent enhancement of infection activity. *J. Gen. Virol.* 97, 3280–3290. doi: 10.1099/jgv.0.000635

Diamos, A. G., and Mason, H. S. (2019). Modifying the replication of geminiviral vectors reduces cell death and enhances expression of biopharmaceutical proteins in *nicotiana benthamiana* leaves. *Front. Plant Sci.* 9:1974. doi: 10.3389/fpls.2018.01974

Diego-Martin, B., González, B., Vazquez-Vilar, M., Selma, S., Mateos-Fernández, R., Gianoglio, S., et al. (2020). Pilot production of SARS-CoV-2 related proteins in plants: a proof of concept for rapid repurposing of indoor farms into biomanufacturing facilities. *Front. Plant Sci.* 11:612781. doi: 10.3389/fpls.2020.612781

Dodev, T. S., Karagiannis, P., Gilbert, A. E., Josephs, D. H., Bowen, H., James, L. K., et al. (2014). A tool kit for rapid cloning and expression of recombinant antibodies. *Sci. Rep.* 4:5885. doi: 10.1038/srep05885

Donini, M., and Marusic, C. (2019). Current state-of-the-art in plant-based antibody production systems. *Biotechnol. Lett.* 41, 335–346. doi: 10.1007/s10529-019-02651-z

Farràs, M., Román, R., Camps, M., Miret, J., Martínez, Ó, Pujol, X., et al. (2020). Heavy chain dimers stabilized by disulfide bonds are required to promote in vitro assembly of trastuzumab. *BMC Mol. Biol.* 21:2. doi: 10.1186/s12860-019-0244-x

Feige, M. J., Hendershot, L. M., and Buchner, J. (2010). How antibodies fold. *Trends Biochem. Sci.* 35, 189–198. doi: 10.1016/j.tibs.2009.11.005

Fischer, R., Schillberg, S., Hellwig, S., Twyman, R. M., and Drossard, J. (2012). GMP issues for recombinant plant-derived pharmaceutical proteins. *Biotechnol. Adv.* 30, 434–439. doi: 10.1016/j.biotechadv.2011.08.007

Gomord, V., and Faye, L. (2004). Posttranslational modification of therapeutic proteins in plants. *Curr. Opin. Plant Biol.* 7, 171–181. doi: 10.1016/j.pbi.2004.01.015

Goodin, M. M., Zaitlin, D., Naidu, R. A., and Lommel, S. A. (2008). *Nicotiana benthamiana*: its history and future as a model for plant-pathogen interactions. *Mol. Plant Microbe Interact.* 21, 1015–1026. doi: 10.1094/mpmi-21-8-1015

Hamorsky, K. T., Kouokam, J. C., Jurkiewicz, J. M., Nelson, B., Moore, L. J., Husk, A. S., et al. (2015). N-Glycosylation of cholera toxin B subunit in *Nicotiana benthamiana*: impacts on host stress response, production yield and vaccine potential. *Sci. Rep.* 5:8003. doi: 10.1038/srep08003

Hanittinan, O., Oo, Y., Chaotham, C., Rattanapisit, K., Shanmugaraj, B., and Phoolcharoen, W. (2020). Expression optimization, purification and in vitro characterization of human epidermal growth factor produced in *Nicotiana benthamiana*. *Biotechnol. Rep.* 28:e00524. doi: 10.1016/j.btre.2020.e00524

He, X., and Xu, C. (2020). Immune checkpoint signaling and cancer immunotherapy. *Cell Res.* 30, 660–669. doi: 10.1038/s41422-020-0343-4

Huang, Z., Phoolcharoen, W., Lai, H., Piensook, K., Cardineau, G., Zeitlin, L., et al. (2010). High-level rapid production of full-size monoclonal antibodies in plants by a single-vector DNA replicon system. *Biotechnol. Bioeng.* 106, 9–17. doi: 10.1002/bit.22652

Hurtado, J., Acharya, D., Lai, H., Sun, H., Kallolimath, S., Steinkellner, H., et al. (2020). *In vitro* and *in vivo* efficacy of anti-chikungunya virus monoclonal antibodies produced in wild-type and glycoengineered *Nicotiana benthamiana* plants. *Plant Biotechnol. J.* 18, 266–273. doi: 10.1111/pbi.13194

Kasamon, Y. L., de Claro, R. A., Wang, Y., Shen, Y. L., Farrell, A. T., and Pazdur, R. (2017). FDA approval summary: nivolumab for the treatment of relapsed or progressive classical Hodgkin lymphoma. *Oncologist* 22, 585–591. doi: 10.1634/theoncologist.2017-0004

Kathuria, S., Sriraman, R., Nath, R., Sack, M., Pal, R., Artsaenko, O., et al. (2002). Efficacy of plant-produced recombinant antibodies against HCG. *Hum. Reprod.* 17, 2054–2061. doi: 10.1093/humrep/17.8.2054

Klimyuk, V., Pogue, G., Herz, S., Butler, J., and Haydon, H. (2014). Production of recombinant antigens and antibodies in *Nicotiana benthamiana* using 'magnifection' technology: GMP-compliant facilities for small- and large-scale manufacturing. *Curr. Top. Microbiol. Immunol.* 375, 127–154. doi: 10.1007/82_2012_212

Kopertekh, L., Meyer, T., Freyer, C., and Hust, M. (2019). Transient plant production of *Salmonella* Typhimurium diagnostic antibodies. *Biotechnol. Rep.* 21:e00314. doi: 10.1016/j.btre.2019.e00314

Lai, H., Engle, M., Fuchs, A., Keller, T., Johnson, S., Gorlatov, S., et al. (2010). Monoclonal antibody produced in plants efficiently treats West Nile virus infection in mice. *Proc. Natl. Acad. Sci. U. S. A.* 107, 2419–2424. doi: 10.1073/pnas.0914503107

Li, F., Vijayasankaran, N., Shen, A. Y., Kiss, R., and Amanullah, A. (2010). Cell culture processes for monoclonal antibody production. *mAbs* 2, 466–479. doi: 10.4161/mabs.2.5.12720

Liu, X., and Cho, W. C. (2017). Precision medicine in immune checkpoint blockade therapy for non-small cell lung cancer. *Clin. Transl. Med.* 6:7. doi: 10.1186/s40169-017-0136-7

Lonoce, C., Salem, R., Marusic, C., Jutras, P. V., Scaloni, A., Salzano, A. M., et al. (2016). Production of a tumour-targeting antibody with a human-compatible glycosylation profile in *N. benthamiana* hairy root cultures. *Biotechnol. J.* 11, 1209–1220. doi: 10.1002/biot.201500628

Lu, R.-M., Hwang, Y.-C., Liu, I. J., Lee, C.-C., Tsai, H.-Z., Li, H.-J., et al. (2020). Development of therapeutic antibodies for the treatment of diseases. *J. Biomed. Sci.* 27:1. doi: 10.1186/s12929-019-0592-z

Ma, J. K., Drossard, J., Lewis, D., Altmann, F., Boyle, J., Christou, P., et al. (2015). Regulatory approval and a first-in-human phase I clinical trial of a monoclonal antibody produced in transgenic tobacco plants. *Plant Biotechnol. J.* 13, 1106–1120. doi: 10.1111/pbi.12416

Marin-Acevedo, J. A., Soyano, A. E., Dholaria, B., Knutson, K. L., and Lou, Y. (2018). Cancer immunotherapy beyond immune checkpoint inhibitors. *J. Hematol. Oncol.* 11:8. doi: 10.1186/s13045-017-0552-6

Marsian, J., Fox, H., Bahar, M. W., Kotecha, A., Fry, E. E., Stuart, D. I., et al. (2017). Plant-made polio type 3 stabilized VLPs—a candidate synthetic polio vaccine. *Nat. Commun.* 8:245. doi: 10.1038/s41467-017-00090-w

Mathew, L. G., Herbst-Kralovetz, M. M., and Mason, H. S. (2014). Norovirus Narita 104 virus-like particles expressed in *Nicotiana benthamiana* induce serum and mucosal immune responses. *Biomed Res. Int.* 2014:807539. doi: 10.1155/2014/807539

Mir-Artigues, P., Twyman, R. M., Alvarez, D., Cerda Bennasser, P., Balcells, M., Christou, P., et al. (2019). A simplified techno-economic model for the molecular pharming of antibodies. *Biotechnol. Bioeng.* 116, 2526–2539. doi: 10.1002/bit.27093

Moussavou, G., Ko, K., Lee, J. H., and Choo, Y. K. (2015). Production of monoclonal antibodies in plants for cancer immunotherapy. *Biomed Res. Int.* 2015:306164. doi: 10.1155/2015/306164

Moustafa, K., Makhzoum, A., and Trémouillaux-Guiller, J. (2016). Molecular farming on rescue of pharma industry for next generations. *Crit. Rev. Biotechnol.* 36, 840–850. doi: 10.3109/07388551.2015.1049934

Nessa, M. U., Rahman, M. A., and Kabir, Y. (2020). Plant-produced monoclonal antibody as immunotherapy for cancer. *Biomed Res. Int.* 2020:3038564. doi: 10.1155/2020/3038564

Obembe, O. O., Popoola, J. O., Leelavathi, S., and Reddy, S. V. (2011). Advances in plant molecular farming. *Biotechnol. Adv.* 29, 210–222. doi: 10.1016/j.biotechadv.2010.11.004

Pardoll, D. M. (2012). The blockade of immune checkpoints in cancer immunotherapy. *Nat. Rev. Cancer* 12, 252–264. doi: 10.1038/nrc3239

Paul, M. J., Teh, A. Y. H., Twyman, R. M., and Ma, J. K.-C. (2013). Target product selection - where can molecular pharming make the difference? *Curr. Pharm. Des.* 19, 5478–5485.

Petruccelli, S., Otegui, M. S., Lareu, F., Tran Dinh, O., Fitchette, A. C., Circosta, A., et al. (2006). A KDEL-tagged monoclonal antibody is efficiently retained in the endoplasmic reticulum in leaves, but is both partially secreted and sorted to protein storage vacuoles in seeds. *Plant Biotechnol. J.* 4, 511–527. doi: 10.1111/j.1467-7652.2006.00200.x

Pillet, S., Couillard, J., Trépanier, S., Poulin, J. F., Yassine-Diab, B., Guy, B., et al. (2019). Immunogenicity and safety of a quadrivalent plant-derived virus like particle influenza vaccine candidate-Two randomized Phase II clinical trials in 18 to 49 and ≥ 50 years old adults. *PLoS One* 14:e0216533. doi: 10.1371/journal.pone.0216533

Porngarm, B., Ahmad, A., Neelasawee, K., Joiphaeng, P., Hoonsuwan, T., Rattanapisit, K., et al. (2020). Expression of porcine reproductive and respiratory syndrome virus nucleocapsid protein in *nicotiana benthamiana* for diagnostic applications. *Adv. Anim. Vet. Sci.* 9, 576–580. doi: 10.17582/journal.aavs/2021/9.4.581.587

Rattanapisit, K., Chao, Z., Siriwattananon, K., Huang, Z., and Phoolcharoen, W. (2019a). Plant-produced anti-enterovirus 71 (EV71) monoclonal antibody efficiently protects mice against EV71 infection. *Plants* 8:560.

Rattanapisit, K., Phakham, T., Buranapraditkun, S., Siriwattananon, K., Boonkrai, C., Pisitkun, T., et al. (2019b). Structural and *in vitro* functional analyses of novel plant-produced anti-human PD1 antibody. *Sci. Rep.* 9:15205. doi: 10.1038/s41598-019-51656-1

Rattanapisit, K., Shanmugaraj, B., Manopwisedjaroen, S., Purwono, P. B., Siriwattananon, K., Khorattanakulchai, N., et al. (2020). Rapid production of SARS-CoV-2 receptor binding domain (RBD) and spike specific monoclonal antibody CR3022 in *Nicotiana benthamiana*. *Sci. Rep.* 10:17698. doi: 10.1038/s41598-020-74904-1

Rattanapisit, K., Srijangwad, A., Chuanasa, T., Sukrong, S., Tantituvanont, A., Mason, H. S., et al. (2017). Rapid Transient Production of a Monoclonal Antibody Neutralizing the Porcine Epidemic Diarrhea Virus (PEDV) in *Nicotiana benthamiana* and Lactuca sativa. *Planta Med.* 83, 1412–1419. doi: 10.1055/s-0043-112344

Rattanapisit, K., Yusakul, G., Shanmugaraj, B., Kittirotruji, K., Suwatsrisakul, P., Prompetchara, E., et al. (2021). Plant-produced recombinant SARS-CoV-2 receptor-binding domain; an economical, scalable biomaterial source for

COVID-19 diagnosis. *Biomaterials Translational* 2, 43–49. doi: 10.3877/cma.j.issn.2096-112X.2021.01.006

Reusch, D., and Tejada, M. L. (2015). Fc glycans of therapeutic antibodies as critical quality attributes. *Glycobiology* 25, 1325–1334. doi: 10.1093/glycob/cwv065

Robert, C., Ribas, A., Wolchok, J. D., Hodi, F. S., Hamid, O., Kefford, R., et al. (2014). Anti-programmed-death-receptor-1 treatment with pembrolizumab in ipilimumab-refractory advanced melanoma: a randomised dose-comparison cohort of a phase 1 trial. *Lancet* 384, 1109–1117. doi: 10.1016/S0140-6736(14)60958-2

Roberts, C. J. (2014). Therapeutic protein aggregation: mechanisms, design, and control. *Trends Biotechnol.* 32, 372–380. doi: 10.1016/j.tibtech.2014.05.005

Rosales-Mendoza, S., Nieto-Gómez, R., and Angulo, C. (2017). A perspective on the development of plant-made vaccines in the fight against Ebola virus. *Front. Immunol.* 8:252. doi: 10.3389/fimmu.2017.00252

Sainsbury, F., Sack, M., Stadlmann, J., Quendler, H., Fischer, R., and Lomonossoff, G. P. (2010). Rapid transient production in plants by replicating and non-replicating vectors yields high quality functional anti-HIV antibody. *PLoS One* 5:e13976. doi: 10.1371/journal.pone.0013976

Shanmugaraj, B., Bulaon, C. J. I., and Phoolcharoen, W. (2020a). Plant molecular farming: a viable platform for recombinant biopharmaceutical production. *Plants* 9:842. doi: 10.3390/plants9070842

Shanmugaraj, B., Bulaon, C. J. I., Malla, A., and Phoolcharoen, W. (2021). Biotechnological insights on the expression and production of antimicrobial peptides in plants. *Molecules* 26:4032.

Shanmugaraj, B., Rattanapisit, K., Manopwisedjaroen, S., Thitithanyanont, A., and Phoolcharoen, W. (2020b). Monoclonal Antibodies B38 and H4 Produced in *Nicotiana benthamiana* Neutralize SARS-CoV-2 *in vitro*. *Front. Plant Sci.* 11:589995. doi: 10.3389/fpls.2020.589995

Siriwattananon, K., Manopwisedjaroen, S., Kanjanasirirat, P., Budi Purwono, P., Rattanapisit, K., Shanmugaraj, B., et al. (2020). Development of plant-produced recombinant ACE2-Fc fusion protein as a potential therapeutic agent against SARS-CoV-2. *Front. Plant Sci.* 11:604663. doi: 10.3389/fpls.2020.604663

Sriraman, R., Bardor, M., Sack, M., Vaquero, C., Faye, L., Fischer, R., et al. (2004). Recombinant anti-hCG antibodies retained in the endoplasmic reticulum of transformed plants lack core-xylose and core-alpha(1,3)-fucose residues. *Plant Biotechnol. J.* 2, 279–287. doi: 10.1111/j.1467-7652.2004.00078.x

Strasser, R. (2016). Plant protein glycosylation. *Glycobiology* 26, 926–939. doi: 10.1093/glycob/cww023

Strasser, R., Stadlmann, J., Schähs, M., Stiegler, G., Quendler, H., Mach, L., et al. (2008). Generation of glyco-engineered *Nicotiana benthamiana* for the production of monoclonal antibodies with a homogeneous human-like N-glycan structure. *Plant Biotechnol. J.* 6, 392–402. doi: 10.1111/j.1467-7652.2008.00330.x

Vaquero, C., Sack, M., Chandler, J., Drossard, J., Schuster, F., Monecke, M., et al. (1999). Transient expression of a tumor-specific single-chain fragment and a chimeric antibody in tobacco leaves. *Proc. Natl. Acad. Sci. U.S.A.* 96:11128. doi: 10.1073/pnas.96.20.11128

Vézina, L.-P., Faye, L., Lerouge, P., D'Aoust, M.-A., Marquet-Blouin, E., Burel, C., et al. (2009). Transient co-expression for fast and high-yield production of antibodies with human-like N-glycans in plants. *Plant Biotechnol. J.* 7, 442–455. doi: 10.1111/j.1467-7652.2009.00414.x

Villani, M. E., Morgun, B., Brunetti, P., Marusic, C., Lombardi, R., Pisoni, I., et al. (2009). Plant pharming of a full-sized, tumour-targeting antibody using different expression strategies. *Plant Biotechnol. J.* 7, 59–72. doi: 10.1111/j.1467-7652.2008.00371.x

Weber, J. S., D'Angelo, S. P., Minor, D., Hodi, F. S., Gutzmer, R., Neyns, B., et al. (2015). Nivolumab versus chemotherapy in patients with advanced melanoma who progressed after anti-CTLA-4 treatment (CheckMate 037): a randomised, controlled, open-label, phase 3 trial. *Lancet Oncol.* 16, 375–384. doi: 10.1016/S1470-2045(15)70076-8

Wei, S. C., Duffy, C. R., and Allison, J. P. (2018). Fundamental mechanisms of immune checkpoint blockade therapy. *Cancer Discov.* 8, 1069–1086. doi: 10.1158/2159-8290.Cd-18-0367

Weiner, G. J. (2015). Building better monoclonal antibody-based therapeutics. *Nat. Rev. Cancer* 15, 361–370. doi: 10.1038/nrc3930

Whaley, K. J., Hiatt, A., and Zeitlin, L. (2011). Emerging antibody products and *Nicotiana* manufacturing. *Hum. Vaccin.* 7, 349–356. doi: 10.4161/hv.7.3.14266

Yamamoto, K., Fujii, R., Toyofuku, Y., Saito, T., Koseki, H., Hsu, V. W., et al. (2001). The KDEL receptor mediates a retrieval mechanism that contributes to quality control at the endoplasmic reticulum. *EMBO J.* 20, 3082–3091. doi: 10.1093/emboj/20.12.3082

Yiemchavee, S., Wong-Arce, A., Romero-Maldonado, A., Shanmugaraj, B., Monsivais-Urenda, A. E., Phoolcharoen, W., et al. (2021). Expression and immunogenicity assessment of a plant-made immunogen targeting the cytotoxic T-lymphocyte associated antigen-4: a possible approach for cancer immunotherapy. *J. Biotechnol.* 329, 29–37. doi: 10.1016/j.jbiotec.2021.01.016

Zhang, B., Shanmugaraj, B., and Daniell, H. (2017). Expression and functional evaluation of biopharmaceuticals made in plant chloroplasts. *Curr. Opin. Chem. Biol.* 38, 17–23. doi: 10.1016/j.cbpa.2017.02.007

Conflict of Interest: KR and BS are employed by Baiya Phytopharm Co., Ltd. WP is a co-founder/shareholder of Baiya Phytopharm Co., Ltd.

The remaining authors declare that the research was conducted in the absence of any commercial or financial relationships that could be construed as a potential conflict of interest.

Publisher's Note: All claims expressed in this article are solely those of the authors and do not necessarily represent those of their affiliated organizations, or those of the publisher, the editors and the reviewers. Any product that may be evaluated in this article, or claim that may be made by its manufacturer, is not guaranteed or endorsed by the publisher.

frontiers in Plant Science

ORIGINAL RESEARCH
published: 10 September 2021
doi: 10.3389/fpls.2021.712438

At-CycD2 Enhances Accumulation of Above-Ground Biomass and Recombinant Proteins in Transgenic *Nicotiana benthamiana* Plants

Lilya Kopertekh and Sven Reichardt*

Institute for Biosafety in Plant Biotechnology, Julius Kühn-Institut (JKI) - Federal Research Centre for Cultivated Plants, Quedlinburg, Germany

Transient expression in *Nicotiana benthamiana* holds great potential for recombinant protein manufacturing due to its advantages in terms of speed and yield compared to stably transformed plants. To continue improving the quantity of recombinant proteins the plant host will need to be modified at both plant and cellular levels. In attempt to increase leaf mass fraction, we transformed *N. benthamiana* with the *At-CycD2* gene, a positive regulator of the cell cycle. Phenotypic characterization of the T_1 progeny plants revealed their accelerated above-ground biomass accumulation and enhanced rate of leaf initiation. In comparison to non-transgenic control the best performing line At-CycD2-15 provided 143 and 140% higher leaf and stem biomass fractions, respectively. The leaf area enlargement of the At-CycD2-15 genotype was associated with the increase of epidermal cell number compensated by slightly reduced cell size. The production capacity of the At-CycD2-15 transgenic line was superior to that of the non-transgenic *N. benthamiana*. The accumulation of transiently expressed GFP and scFv-TM43-E10 proteins per unit biomass was increased by 138.5 and 156.7%, respectively, compared to the wild type. With these results we demonstrate the potential of cell cycle regulator gene *At-CycD2* to modulate both plant phenotype and intracellular environment of *N. benthamiana* for enhanced recombinant protein yield.

Keywords: *At-CycD2*, *Nicotiana benthamiana*, plant architecture, recombinant proteins, transient expression

OPEN ACCESS

Edited by:
Eugenio Benvenuto, Energy and Sustainable Economic Development (ENEA), Italy

Reviewed by:
Hugh S. Mason, Arizona State University, United States
Henrik Nausch, Fraunhofer Fraunhofer Society (FHG), Germany

****Correspondence:***
Lilya Kopertekh
lilya.kopertekh@julius-kuehn.de

Specialty section:
This article was submitted to Plant Biotechnology, a section of the journal Frontiers in Plant Science

Received: *20 May 2021*
Accepted: *11 August 2021*
Published: *10 September 2021*

Citation:
Kopertekh L and Reichardt S (2021) At-CycD2 Enhances Accumulation of Above-Ground Biomass and Recombinant Proteins in Transgenic Nicotiana benthamiana Plants. Front. Plant Sci. 12:712438. doi: 10.3389/fpls.2021.712438

INTRODUCTION

The growing market for recombinant proteins requires effective and safe production platforms. Currently most of the recombinant proteins are manufactured in bacterial and mammalian cells, which are complex to handle and susceptible to contamination with human pathogens. The advances in molecular biology and plant biotechnology opened an avenue for using plants as bioreactors. Despite several advantages such as reduced upstream complexity, animal-free production, improved protein quality and speed in case of transient expression, improvements in protein yield, purification costs, and development of regulatory framework are essential to enable commercial utilization of plant-based production platform (Schillberg et al., 2019).

Two main approaches, namely stable transformation and transient expression, are currently used to manufacture foreign proteins in plant cells. Transient expression technology has made rapid and impressive progress in recent years and reached the status of established platform for commercial application (Lomonossoff and D'Aoust, 2016). This technique holds great potential for the production of rapid-response and emergency vaccines or biologics that was particularly shown for Ebola (The PREVAIL II Writing Group, for the Multi-National PREVAIL II Study Team, 2016), seasonal influenza (Ward et al., 2020), and COVID-19 (Capell et al., 2020; Diego-Martin et al., 2020) diseases.

Transient expression is a two-component system including expression vector and plant host. Among the expression vectors, virus vectors are very attractive for recombinant protein production due to the time efficiency, scalability and high yield of the target product. The majority of plant viral vectors used to date are based on RNA viruses, such as tobacco mosaic virus (TMV), potato virus X (PVX), and cowpea mosaic virus (CPMV; Hefferon, 2012). Two strategies, full virus strategy and deconstructed virus strategy, have been exploited for the construction of virus expression vectors. In the first strategy a wild type virus carries and expresses a gene of interest. In the second approach the limiting or undesirable for recombinant protein production viral functions are eliminated (Gleba et al., 2004; Peyret and Lomonossoff, 2015). Currently three deconstructed versions of TMV, which are deficient for the systemic virus movement, are available. These are magnICON® (Gleba et al., 2014), TRBO (Lindbo, 2007), and TMV launch vector (Musiychuk et al., 2007). In comparison to the three-component magnICON® system, one-component TRBO and TMV launch expression vectors may simplify the application. *Nicotiana benthamiana* is the plant of choice for transient expression of recombinant proteins (Powell, 2015). This plant belongs to *Solanaceae* family and originates from Australia. Its allotetraploid genome, which most probably results from hybridization of *Nicotiana sylvestris* and *Nicotiana tomentosiformis*, comprises 19 chromosomes (Goodin et al., 2008). A naturally occurring mutation in an RNA dependent RNA polymerase gene (Nb-RDR1) is, at least partly, responsible for *N. benthamiana*'s susceptibility to *Agrobacterium tumefaciens* and virus infection (Yang et al., 2004). Additional to this key trait further factors including its non-food status and easy cultivation make this species a dominant plant host for molecular farming. To date a number of biotechnology companies such as Medicago (Quebec, Canada), Kentucky Bioprocessing (Owensboro, KY, United States), iBio (Bryan, TX, United States), PlantForm (Ontario, Canada) and Leaf Expression Systems (Norwich, United Kingdom) use *N. benthamiana* as a plant host in their production systems (Bally et al., 2018). During the last decade significant efforts have been made in engineering *N. benthamiana* host including designing a supportive cell environment to improve the quality and quantity of recombinant proteins and modification of plant habitus to increase the space–time yield (Buyel et al., 2021). Diverse plant cell engineering approaches such as suppression of gene silencing (Arzola et al., 2011; Garabagi et al., 2012; Matsuo and Matsumura, 2017; Matsuo and Atsumi, 2019), reduction of unintended proteolysis (Jutras et al., 2020) and leaf proteome rebalancing (Robert et al., 2015) have proved to be effective in increasing foreign protein accumulation. Alteration of the plant habitus to increase biomass accumulation and subsequent recombinant protein yield can be established using two strategies, modulation of cultural practices (Fujiuchi et al., 2016) and modification of the host plant. In the first approach, optimization of light quality and planting density affected the accumulation of hemagglutinin (HA) in agroinfiltrated *N. benthamiana* (Fujiuchi et al., 2017; Shang et al., 2018). Low plant density provided 15–49% and 10–15% higher recombinant protein yield per unit harvested biomass and unit area-time, respectively (Fujiuchi et al., 2017). Another study demonstrated the impact of growth promoting hormone 6-Benzylaminopurine (6-BAP) and tip pruning on H1 vaccine antigen yield (Goulet et al., 2019). The apex pruning had negative effect on the total H1 yield, whereas treatment of plants with 6-BAP caused a 65–75% increase in the H1 accumulation. In the second strategy the genetic background of the host plant is modified using crossing or genetic engineering. For instance, the hybrid host *Nicotiana excelsiana*, which was developed by crossing *N. benthamiana* with *Nicotiana excelsior*, produces two times more biomass than *N. benthamiana* (Fitzmaurice, 2002). In the transgenic methodological approach, several classes of genes including those involved in photosynthetic pathways, hormone metabolism, transcription, signalling, secondary wall biosynthesis and cell cycle regulation may be useful in an attempt to increase the plant biomass production (Busov et al., 2008; Rojas et al., 2010; Lima et al., 2017). Among these genes, cell cycle regulators have already attracted considerable attention in order to alter the plant architecture.

The basic components of the plant cell cycle are G1 (postmitotic interphase), S-phase (DNA synthesis phase), G2 (premitotic interphase), and mitosis/cytokinesis. The cell cycle machinery is strongly regulated at two major checkpoints, G2/M and G1/S (Francis, 2007). The G2/M and G1/S transitions require the activity of cyclin dependent kinases (CDKs). CDK activity is orchestrated at multiple levels involving association with cyclins, interaction with inhibitory proteins and targeted proteolysis (Inze and De Veylder, 2006; Scofield et al., 2014). Down-regulation of multiple inhibitors of CDK activity, ICK genes (*ick1*/*ick2*/*ick6*/*ick7* and *ick1*/*ick2*/*ick5*/*ick6*/*ick7*) stimulated cell proliferation and resulted in larger organs and seeds in *Arabidopsis thaliana* (Cheng et al., 2013). In *Nicotiana tabacum* overexpression of the At-APC10 and At-CDC27a subunits of the anaphase–promoting complex (APC) controlling the transition of cell cycle phases in *A. thaliana* increased the plant biomass production (Rojas et al., 2009; Lima et al., 2013). In addition, combination of the *At-APC10* and *At-CDC27a* genes in *N. tabacum* by crossing resulted in synergistic effect compared to the parental lines containing individual subunits (Lima et al., 2013). Transformation of *N. tabacum* plants with the *CycD2* gene from *A. thaliana*, which is involved in controlling the transition of G1/S phase, promoted cell division and cell proliferation in leaf and cell meristem. The modified tobacco plants displayed normal cell and meristem

size, but enhanced growth, increased rates of leaf initiation and accelerated development in all stages from seedlings to maturity (Cockcroft et al., 2000).

Here we demonstrate that stable expression of the *At-CycD2* gene in *N. benthamiana* resulted in the increased leaf and stem biomass accumulation in line At-CycD2-15 by 143 and 140%, respectively. The overall plant morphology of these transgenic plants was not affected. We also observed the enhanced transiently expressed foreign protein accumulation in the *At-CycD2* plants in comparison to non-transgenic *N. benthamiana*. The concentration of recombinant proteins increased from 2,496 ± 689 to 3,457 ± 401 μg/g fresh leaf weight for GFP and from 620 ± 195 to 971 ± 308 μg/g fresh leaf weight for scFv-TM43-E10 when wild type and At-CycD2-15 transgenic plants were compared. These results are relevant for the improvement of recombinant protein production per unit of biomass under contained conditions.

MATERIALS AND METHODS

Plasmid Constructs

The pLH-*35S-At-CycD2* (Kopertekh and Schiemann, 2019) plant transformation vector and pJL-*TRBO-G* (TRBO-*gfp*) construct have been described previously (Lindbo, 2007). To generate TRBO-*scFv-TM43-E10* construct the *Not*I restricted pJL-*TRBO-G* plasmid was treated with T4 DNA polymerase, digested with *Pac*I and ligated with the scFv-TM43-E10 PCR product cut with *Pac*I-*Eco*RV. The PCR product was amplified from the pOPE101-*TM43-E10* template (Meyer et al., 2011) using the PacI-TM43-E10-forw and TM43-E10-EcoRV-rev primers and checked by sequence analysis. The PacI-TM43-E10-forw and TM43-E10-EcoRV primers are presented in **Supplementary Table S1**.

Plant Transformation

The binary pLH-*35S-At-CycD2* vector was introduced into *A. tumefaciens* (recently renamed to *Rhizobium radiobacter*) strain LBA4404 by the freeze–thaw method (Holsters et al., 1978). Transformed colonies were selected on solid LB medium supplemented with 300 mg/L streptomycin (Duchefa, Haarlem, Netherland), 100 mg/L spectinomycin (Duchefa, Haarlem, Netherland), 50 mg/L rifampicin (Duchefa, Haarlem, Netherland) and checked by PCR analysis. *A. tumefaciens*-mediated transformation of *N. benthamiana* leaf explants was performed as described previously (Kopertekh et al., 2004). Briefly, *N. benthamiana* leaves were removed from the 6 weeks old plants and cut into 1 cm squares. *A. tumefaciens* containing the pLH-*35S-At-CycD2* plasmid was cultured overnight at 28°C in LB medium with appropriate antibiotics. The cells were harvested by centrifugation and then resuspended in liquid MS medium (Duchefa, Haarlem, Netherland) to give an absorbency of 0.6 at 600 nm. Leaf segments were immersed in the *A. tumefaciens* suspension for 20 min, blotted dry on sterile paper, and placed on MS medium supplemented with 1 mg/L 6-BAP (Duchefa, Haarlem, Netherland) and 0,1 mg/L 1-naphthaleneacetic acid (NAA; Duchefa, Haarlem, Netherland). After 2 days, explants were transferred to similar medium to which 500 mg/L ticarcillin (Duchefa, Haarlem, Netherland) and 5 mg/L phosphinothricin (PPT; Duchefa, Haarlem, Netherland) were added. Two weeks after cocultivation with *Agrobacterium*, the concentration of ticarcillin in the medium was decreased to 300 mg/L. Shoots were excised and rooted on MS medium without plant growth regulators containing 300 mg/L ticarcillin and 5 mg/L PPT. Rooted plants were transferred to soil to set seeds.

For seed germination, T_1 progeny seeds were surface-sterilised for 5 min with 70% ethanol, rinsed 5 times with sterile water and germinated on solid MS medium supplemented with 20 g/L sucrose, 0.5 g/L 2-(N-morpholino)ethanesulfonic acid (MES; Roth, Karlsruhe, Germany) and 5 mg/L PPT. After 2 weeks, the number of PPT-resistant to PPT-sensitive plants was calculated to evaluate the segregation ratio. PPT resistant plants containing T-DNA of the pLH-*35S-At-CycD2* were transferred into the greenhouse and used in subsequent experiments. Plants and germinated seeds were kept in the controlled environment chamber or greenhouse at 24°C with 16 day/8 night photoperiod.

Molecular Analysis of Transgenic Plants

To confirm the transgenic nature of the regenerated plants the genomic DNA was prepared from leaf material by the CTAB method and used as a template for the PCR reaction. PCR was performed with primer pairs that are specific to the *At-CycD2* and *bar* genes (**Supplementary Table S1**). Thermal cycling was done at 94°C for 5 min followed by 30 cycles at 94°C for 1 min, 60°C for 1 min, 72°C for 1 min and 10 min of a final elongation at 72°C. Reactions were performed using the PTC-200 Peltier Thermal Cycler (Bio-Rad, Feldkirchen, Germany).

To determine the number of T-DNA inserts, genomic DNA was extracted from leaf tissue of transgenic and non-transformed plants by DNeasy Plant Maxi Kit (Qiagen, Hilden, Germany). Southern blot analysis was performed with 16 μg of DNA after restriction with *Eco*RI and *Hind*III. The restricted DNA was separated by 0.8% agarose gel and UV coupled to a Hybond N^+ nylon membrane. Blots were hybridized with a *bar* probe, labelled with a PCR DIG Probe Synthesis Kit (Merck, Darmstadt, Germany). **Supplementary Table S1** presents the *bar* primers used for generation of the DIG labelled *bar* probe. The membranes were developed and detected with a DIG Detection system (Merck, Darmstadt, Germany) using conditions suggested by the supplier.

RNA for the reverse transcription RT-PCR analysis was extracted using RNeasy Plant Mini Kit (Qiagen, Hilden, Germany). Total RNA (2 μg) was reverse transcribed using the Maxima Reverse Transcriptase and random hexamer primer following manufacturer's specifications (Thermo Scientific, Waltham, United States). RT-PCR was performed by the At-CycD2-349-forw, At-CycD2-rev and GAPDH-238-forw, GAPDH-238-rev primers specific to the *At-CycD2* and glyceraldehyde 3-phosphate dehydrogenase (*GAPDH*) genes, respectively (**Supplementary Table S1**).

Phenotypic Evaluation of Transgenic Lines

To evaluate the phenotype of transgenic lines harbouring the *At-CycD2* gene T_1 seeds were germinated on solid MS medium containing 5 mg/L PPT, whereas wild type *N. benthamiana* seeds were germinated on non-selective medium. Non-transgenic and PPT resistant transgenic *N. benthamiana* seedlings were transferred to the greenhouse at 2 weeks after sowing. Morphological data (plant height, number of leaves per plant, plant and stem biomass) were collected at 4 weeks after planting. The experiment was repeated three times. Each replication included 15 plants per transgenic line or wild type non-transformed control. The unpaired T-test using SigmaStat software was used to determine differences among the mean values.

For the leaf area analysis, the second, third, fourth, fifth leaves from eight transgenic and eight wild type *N. benthamiana* plants were harvested at 4 weeks after planting. Leaves were numbered from bottom to top. Leaf area was measured by ImageJ software[1] after scanning. The data were statistically analysed with Mann–Whitney test using SigmaStat statistic software.

Analysis of Cell Size and Cell Number

The cell size and number of cells for third leaf were compared in wild type and At-CycD2-15 transgenic plants. Only abaxial epidermal cells were considered in this study and they are referred to hereafter as epidermal cells throughout the text. The epidermal cells were first visualized using the GFP protein. To this end, fully expanded third leaves were agroinfiltrated with the pLH-*35S-gfp* construct at 4 weeks after planting as described previously (Kopertekh and Schiemann, 2019). Three plants for each genotype were involved in this experiment. The leaves were collected 3 days after agroinfiltration and scanned to calculate the leaf area as described in previous section. After this, the base, middle and tip zones of each leaf were randomly selected, investigated and photographed by a fluorescence microscope (Nikon Eclipse equipped with FITC filters). A total of 739 and 668 epidermal cells for the At-CycD2 and wild type genotypes, respectively, were drawn manually to calculate the cell area with ImageJ software. The distribution of the cell area per genotype was obtained by pooling data from all cells drawn for wild type and transgenic line. The mean epidermal cell number per leaf was calculated as the ratio of leaf area to mean of leaf epidermal cell area.

Plant Agroinfiltration

A. tumefaciens strain AGL0 cultures containing the TRBO-*gfp* and TRBO-*scFv-TM43-E10* expression constructs were grown overnight at 28°C in LB medium supplemented with 50 mg/L kanamycin (Duchefa, Haarlem, Netherland), pelleted by centrifugation and resuspended in MMA solution (10 mM MES, pH 5.6, 10 mM $MgCl_2$, 150 µM acetosyringone) to OD_{600} of 0.1. Middle leaves of 6 weeks old *N. benthamiana* plants were infiltrated using a syringe without a needle.

[1]http://rsb.info.nih.gov/ij/

For vacuum agroinfiltration the bacterial suspensions were prepared as described above. The *N. benthamiana* plants were immersed into the MMA infiltration solution and vacuum was applied for 1 min at a vacuum pressure of 100–120 mBar and then slowly released. The vacuum system LVS 601 Tp (ILMVAC, Ilmenau, Germany) was used for the experiments.

The agroinfiltration experiments were repeated two times with 3–4 plants per replication. The probes for ELISA were harvested at 9 days after agroinoculation (dpi). Each sample is a pooled sample from three middle leaves of one plant. The data were statistically analysed with Mann–Whitney test using SigmaStat statistic software.

Quantitative ELISA

ELISA was used to quantify the amount of recombinant proteins (GFP, scFv-TM43-E10) in the protein extracts from the agroinfiltrated transgenic (line At-CycD2-15) and wild type *N. benthamiana* plants. Leaf material (200 mg) was harvested, homogenized with motor and pestle in 2 volumes (w/v) of phosphate buffer (137 mM NaCI, 2.7 mM KCI, 10 mM Na_2HPO_4, 1.8 mM KH_2PO_4, pH 7.2) and clarified by centrifugation for 10 min at 4°C. ELISA plates were coated overnight at 4°C with 100 µl of fresh prepared plant extract. After incubation the plates were washed three 3 with PBS and blocked with PBS-B (PBS supplemented with 2% BSA) at room temperature for 2 h. Following 3 washes with PBS the plates were probed with the anti-Myc (Sigma-Aldrich, Taufkirchen, Germany) and anti-GFP (Roche, Penzberg, Germany) antibody for scFv-TM43-E10 and GFP, respectively. Subsequently, the washing step was repeated and a goat anti-mouse IgG alkaline phosphatase conjugate (Sigma-Aldrich, Taufkirchen, Germany) in PBS-B was added and incubated at room temperature for 1 h. Finally, the plates were developed for 30 min at 37°C with the p-nitrophenyl phosphate as substrate after washing. Optical density was measured at 405 nm in a SUNRISE ™ microplate reader (Tecan, Männedorf, Switzerland). All plates contained control proteins for a standard curve, which were diluted with PBS and processed as above.

RESULTS

Generation and Verification of Transgenic Plants

To investigate the effect of the *At-CycD2* gene on *N. benthamiana* phenotype the pLH-*35S-At-CycD2* (**Figure 1A**) transformation vector containing *bar* and *At-CycD2* expression cassettes was introduced in the plant genome by *A. tumefacines*-mediated transformation. In the *At-CycD2* expression unit the *At-CycD2* gene is controlled by the 35S promoter and 35S terminator providing its constitutive expression.

A total of 21 regenerants were initially screened on selective medium containing 5 mg/L PPT and subjected to PCR analysis using primers specific to *bar* and *At-CycD2* genes. The Bar-forw/Bar-rev primers produce a 503 bp fragment of the *bar* gene, whereas the At-CycD2-forw/At-CycD2-rev primers amplify a

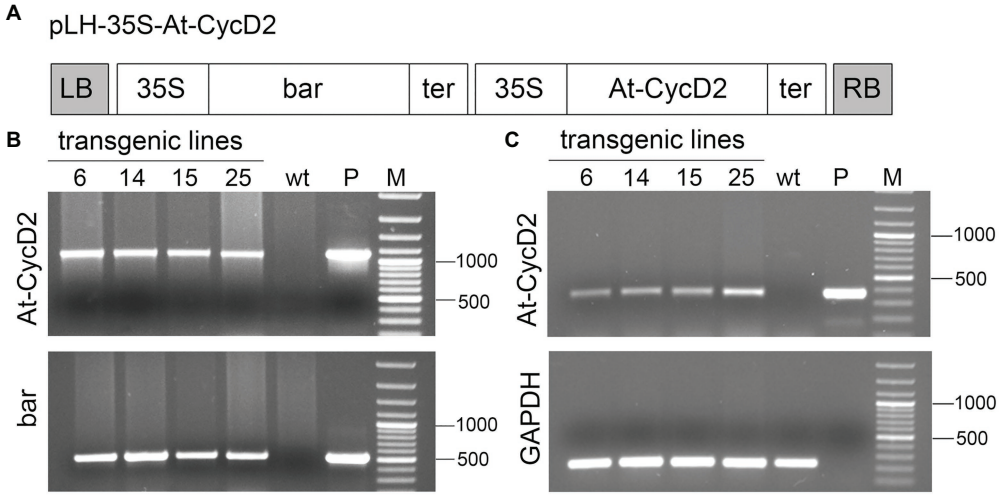

FIGURE 1 | Molecular characterization of the *At-CycD2* transgenic lines. **(A)** Schematic representation of the pLH-*35S-At-CycD2* construct. The pLH-*35S-At-CycD2* plant transformation vector harbors *bar* and *At-CycD2* expression cassettes. In both expression units the constitutive expression of the *bar* and *At-CycD2* genes is regulated by the CaMV 35S promoter and terminator. Open boxes indicate the following genes: *bar*, *At-CycD2*, *bar* and *At-CycD2* genes, respectively; 35S, 35S promoter; ter, terminator. LB, RB, left and right border of T-DNA, respectively. **(B)** Verification of transgenic plants by PCR analysis. Genomic DNA from the PPT resistant regenerants (At-CycD2-6, At-CycD2-14, At-CycD2-15, and At-CycD2-25) was probed with primers specific to *bar* and *At-CycD2* genes. DNAs of wild type *N. benthamiana* plant (wt) and plasmid pLH-*35S-At-CycD2* (P) were included as negative and positive controls, respectively. GeneRuler 100 bp Plus DNA marker (Thermo Scientific, Waltham, United States; M). **(C)** Expression analysis of the *At-CycD2* gene in transgenic lines. RNA isolated form the PCR-positive primary transgenic plants (At-CycD2-6, At-CycD2-14, At-CycD2-15, and At-CycD2-25) was subjected to RT-PCR analysis using *At-CycD2* and *GAPDH* specific primers. Non-transgenic *N. benthamiana* cDNA (wt) and plasmid pLH-*35S-At-CycD2* DNA (P) served as negative and positive controls, respectively. GeneRuler 100 bp Plus DNA marker (Thermo Scientific, Waltham, United States; M).

1,070 bp fragment of the *At-CycD2* gene. For negative and positive controls, genomic DNAs from wild type plant and pLH-*35S-At-CycD2* plasmid, respectively, were taken as a template. The predicted PCR fragments were observed for 19 regenerants confirming the presence of the *bar* and *At-CycD2* sequences in investigated DNA samples. The results of the PCR analysis are shown in **Figure 1B** and **Supplementary Figure S1**.

The expression of the *At-CycD2* gene in PCR-positive T_0 plants was investigated by the RT-PCR. CDNA synthesised from RNA of these plants was probed with the At-CycD2-349-forw/ At-CycD2-rev primers amplifying a 349 bp PCR product of the *At-CycD2* gene and the GAPDH-238-forw and GAPDH-238-rev primers amplifying a 238 bp fragment of endogenous gene GAPDH. **Figure 1C** presents RT-PCR data for At-CycD2-6, At-CycD2-14, At-CycD2-15 and At-CycD2-25 lines. This analysis showed that the *At-CycD2* gene was expressed in the investigated *N. benthamiana* lines.

N. benthamiana lines confirmed as transgenic at DNA and RNA level were transferred to the soil and allowed to set seeds. One regenerant did not grow in the soil. T_1 progeny of At-CycD2 transgenic lines was subjected to segregation test. The observed ratio of PPT resistant to PPT sensitive seedlings suggests that all investigated lines are heterozygous transgenic events (**Supplementary Table S2**). Additionally, most of the investigated lines harbour multiple T-DNA insertion loci.

Seven transgenic lines, At-CycD2-1, At-CycD2-3, At-CycD2-4, At-CycD2-5, At-CycD2-10, At-CycD2-13, and CycD2-19 showed rare small chlorotic spots on some leaves and were excluded from the further analysis.

Phenotypic Evaluation of the *At-CycD2* Transgenic Lines

T_1 seeds of 11 *N. benthamiana* transgenic lines expressing *At-CycD2* gene were germinated on selective MS medium, transferred to soil and grown in the greenhouse for 4 weeks. Several morphological measurements such as plant height, number of leaves, leaf and stem biomass were conducted to evaluate the phenotype of these lines (**Supplementary Table S3**). Across the 11 investigated transgenic lines, we did not observe any phenotypic abnormalities. Transgenic events At-CycD2-6, At-CycD2-14, At-CycD2-15, and At-CycD2-25 showed an enhanced above ground biomass accumulation compared to wild type plants (**Figure 2A**; **Supplementary Table S4**). The relative leaf biomass accumulation varied from 122% (line At-CycD2-25) to 143% (line At-CycD2-15) and the differences between the control and transgenic genotypes were statistically significant. A statistical significant difference in relative stem biomass accumulation could be also observed for all 4 assessed lines. In comparison to wild type *N. benthamiana* plants the means for this parameter increased by 125, 120, 140 and 136% for the At-CycD2-6, At-CycD2-14, At-CycD2-15, and At-CycD2-25 transgenic lines, respectively. In terms of plant height lines At-CycD2-6 and At-CycD2-25 were similar to the non-transgenic control, whereas plants of lines At-CycD2-14 and At-CycD2-15 were 10–12% shorter than the wild type counterpart. Moreover, the enhanced leaf biomass accumulation for the At-CycD2-15 transgenic event was accompanied by an increased number of leaves by 123%.

It should be mentioned that an enhanced initiation of secondary stem leaves also contributed to this phenotypic characteristic (**Supplementary Figure S2**).

The largest increase in biomass accumulation was observed for the At-CycD2-15 transgenic line. When compared to non-transgenic *N. benthamiana* the At-CycD2-15 line exhibited an enhanced growth of young seedlings *in vitro* and it was sustained during vegetative growth in soil (**Figures 2B,C**). Segregation test of T_1 generation of this transgenic line showed a Mendelian ratio 3:1 of PPT resistant to PPT sensitive seedlings indicating the integration of the pLH-*35S-At-CycD2* T-DNA (T-DNAs) at a single locus (**Supplementary Table S2**). To further investigate the integration pattern of the At-CycD2-15 transgenic event, the genomic DNA from T_1 progeny plants was digested with either *Eco*RI or *Hind*III and hybridized with the digoxigenin-labelled *bar* probe. Southern blot hybridization confirmed that one T-DNA insertion was integrated in a single locus in the At-CycD2-15 line (**Supplementary Figure S3**). We selected the At-CycD2-15 line for further investigation based on its genotypic and phenotypic characterization.

Leaf Area and Cellular Size-Related Traits of the At-CycD2-15 Line

Phenotypic analysis of the At-CycD2-15 transgenic line revealed positive effect of the *At-CycD2* gene on leaf biomass production. Next, we asked whether this greater biomass accumulation is associated with the increased leaf size. To answer this question, the leaf area of the second, third, fourth, and fifth leaves from the greenhouse-grown plants of line At-CycD2-15 was measured at 4 weeks after planting. In general, a beneficial impact of the At-CycD2 overexpression on leaf size was observed. The total leaf area for the second, third, fourth, and fifth leaves of the transgenic plants ($64.5 \pm 3.6\,cm^2$) was significantly larger than that of the non-transgenic *N. benthamiana* plants ($53.5 \pm 8.9\,cm^2$; **Figure 3A**). There was significant difference in the leaf area of the second leaf between the At-CycD2-15 transgenic line ($59.8 \pm 5.7\,cm^2$) and the wild type ($40.2 \pm 6.6\,cm^2$; **Figure 3B**). The leaf area of the third leaf was also significantly larger in the At-CycD2-15 transgenic line ($81.1 \pm 3.3\,cm^2$) in comparison to the non-transgenic control ($56.1 \pm 9.7\,cm^2$). The leaf area of the At-CycD2-15 fourth and fifth leaves

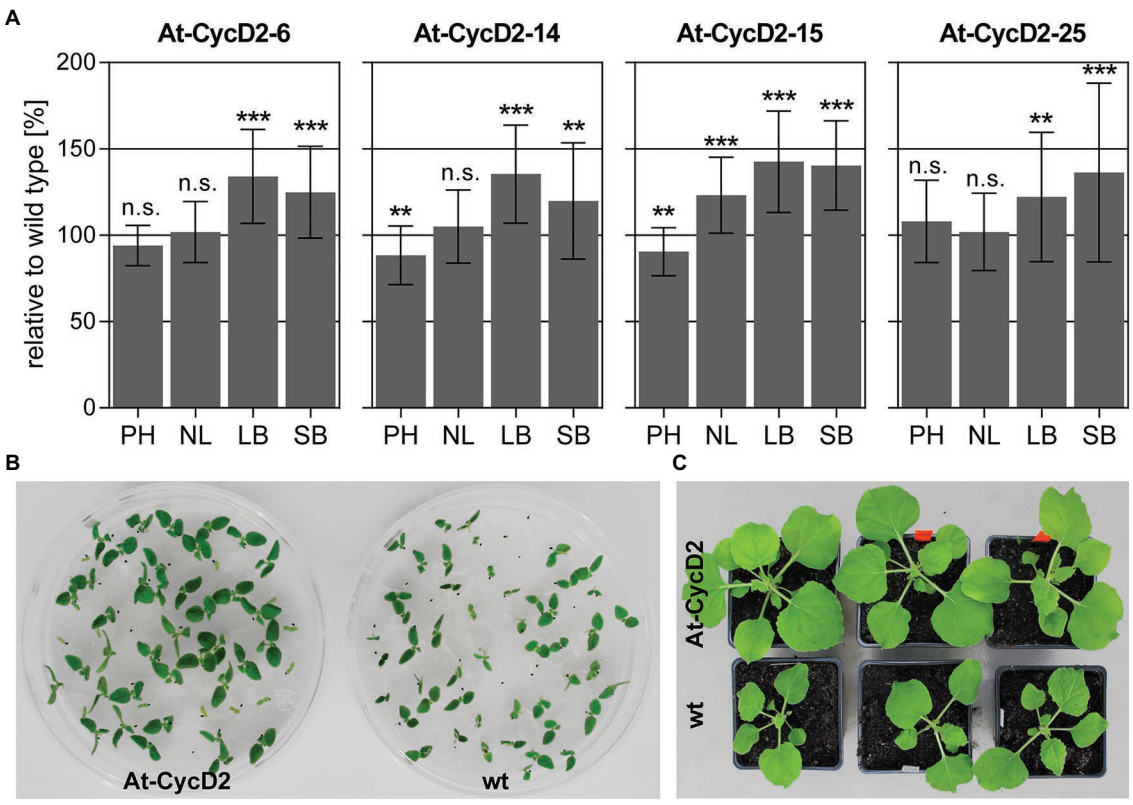

FIGURE 2 | Phenotypic characterization of transgenic *N. benthamiana* lines expressing the *At-CycD2* gene. **(A)** Evaluation of plant height (PH), number of leaves (NL), leaf biomass (LB) and stem biomass (SB). Non-transgenic and T_1 progeny of At-CycD2-6, At-CycD2-14, At-CycD2-15, and At-CycD2-25 transgenic plants were grown in greenhouse for 4 weeks and assayed for the plant height, number of leaves and above ground biomass characteristics. The phenotypic parameters are expressed as a percent relative to the wild type. Values represent the means with standard deviation ($n = 45$). Asterisks indicate significance as determined by the unpaired T-test, with ** and *** denoting $p < 0.01$ and $p < 0.001$, respectively. Not significant values are determined as ns. Non-transgenic and transgenic At-CycD2-15 plants grown *in vitro* **(B)** and in soil **(C)**. At-CycD2-15 and wild type *N. benthamiana* seeds were germinated *in vitro* on selective (5 mg/L PPT) and non-selective MS medium, respectively, and photographed at 12 days after sowing. The soil-grown plants were photographed at 21 days after planting.

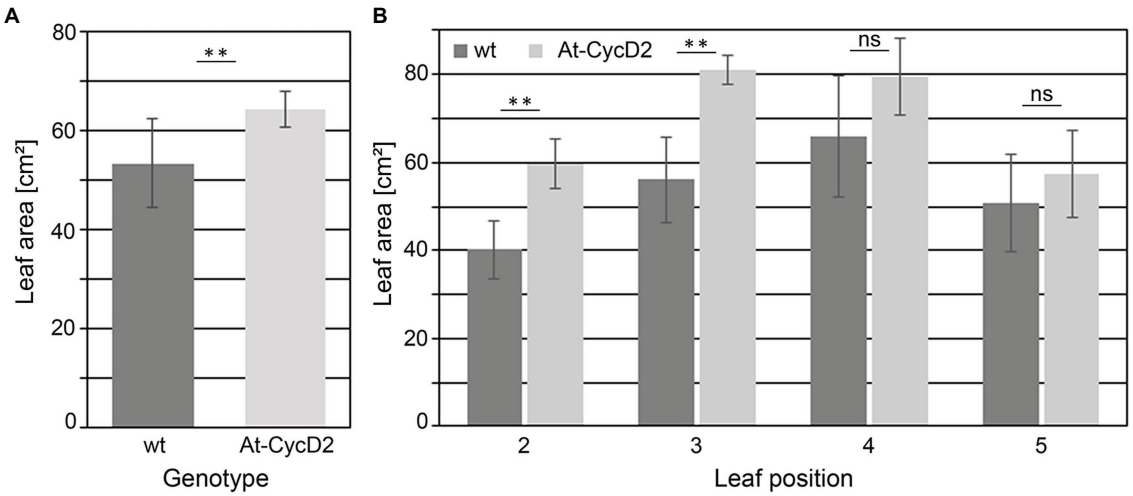

FIGURE 3 | Leaf area of the At-CycD2-15 and wild type (wt) *N. benthamiana* plants. Leaves 2, 3, 4, and 5 from the soil-grown transgenic At-CycD2-15 and non-transgenic plants were harvested at 4 weeks after planting to measure the leaf area. **(A)** Total leaf area. The leaf area for leaves 2, 3, 4, and 5 was measured and summarized for each plant. **(B)** Area of leaves at different positions. Values represent the means with standard deviation ($n = 8$). Asterisks indicate significance as determined by the Mann–Whitney test, with ** denoting $p < 0.01$. Not significant values are determined as ns.

was higher than that of the control, but the difference did not reach a significant level (**Figure 3B**).

The final size of plant leaves is determined by a combination of cell proliferation and cell expansion. To analyse the extent to which cell expansion and/or cell proliferation contribute to increased leaf size, we compared the area und number of epidermal cells in the At-CycD2-15 line and wild type *N. benthamiana*. We selected the third leaf for cellular analysis. The size of epidermal cells in the At-CycD2-15 transgene reached $3{,}384 \pm 71\,\mu m^2$ and was significantly smaller than the same parameter of the non-transgenic control ($3{,}623 \pm 80\,\mu m^2$) at 4 weeks after planting (**Figure 4A**). When the distribution of epidermal cell areas was considered, a larger proportion of expanding cells was found in the third leaf of wild type plants compared to the At-CycD2-15 transgene (**Figure 4B**). The calculation of the cell number revealed that overexpression of the *At-CycD2* gene in *N. benthamiana* led to a significant increase of the cell number (**Figure 4C**). The third leaves of the At-CycD2 transgenic line contained 2.44×10^6 cells, whereas in wild type 1.54×10^6 cells have been counted.

Taken together, our data indicate that the ectopic expression of the *At-CycD2* gene in *N. benthamiana* resulted in larger leaves primarily due to an increased cell number.

Production of Recombinant Proteins in At-CycD2-15 Transgenic Plants

To investigate the production capacity of the At-CycD2-15 transgenic line wild type and At-CycD2-15 transgenic plants were inoculated with the TMV-based deconstructed TRBO expression vector carrying the *gfp* and *scFv-TM43-E10* genes (**Figure 5A**) and evaluated for the recombinant protein yield at 9 dpi. In the first set of experiments the efficiency of syringe and vacuum infiltration methods in the At-CycD2-15 transgenic plants was compared. The accumulation of the GFP and scFv-TM43-E10 proteins was estimated by ELISA. As shown in **Figure 5B** no significant differences between the vacuum and syringe infiltrated samples were observed for both the GFP and scFv-TM43-E10 proteins. In order to assess the production capacity of the At-CycD2-15 genotype, the accumulation of the GFP and scFv-TM43-E10 proteins was quantified in non-transgenic and At-CycD2-15 transgenic plants following a vacuum infiltration procedure (**Figure 5C**). Infiltration of wild type and At-CycD2-15 transgenic plants with the TRBO-GFP expression vector led to the production of $2{,}496 \pm 689\,\mu g/g$ fresh leaf weight (FW) and $3{,}457 \pm 401\,\mu g$ GFP /g fresh weight (FW), respectively. The scFv-TM43-E10 accumulation levels reached $620 \pm 195\,\mu g/g$ FW and $971 \pm 308\,\mu g/g$ FW in non-transgenic and At-CycD2-15 transgenic plants, respectively. Therefore, the presence of the *At-CycD2* gene enhanced the accumulation of both recombinant proteins.

DISCUSSION

In this study, the stable genetic transformation with the *At-CycD2* gene from *A. thaliana* was used to enhance the *N. benthamiana* biomass accumulation. The *At-CycD2* gene is a member of the D-type cyclin family, which is involved in the signal transduction pathway mediating cell cycle progression (Soni et al., 1995). This pathway involves the activation of the CDKs by association with cyclin(s), CDK-mediated inhibition of the retinoblastoma-related protein (RBR) which regulates the transcription factor E2F promoting expression of the S-phase genes (Inze and De Veylder, 2006). In the CDK complex, the cyclin determines the choice of substrate protein whereas the catalytic CDK subunit phosphorylates protein (Wittenberg, 2005). Immunoprecipitation experiments carried

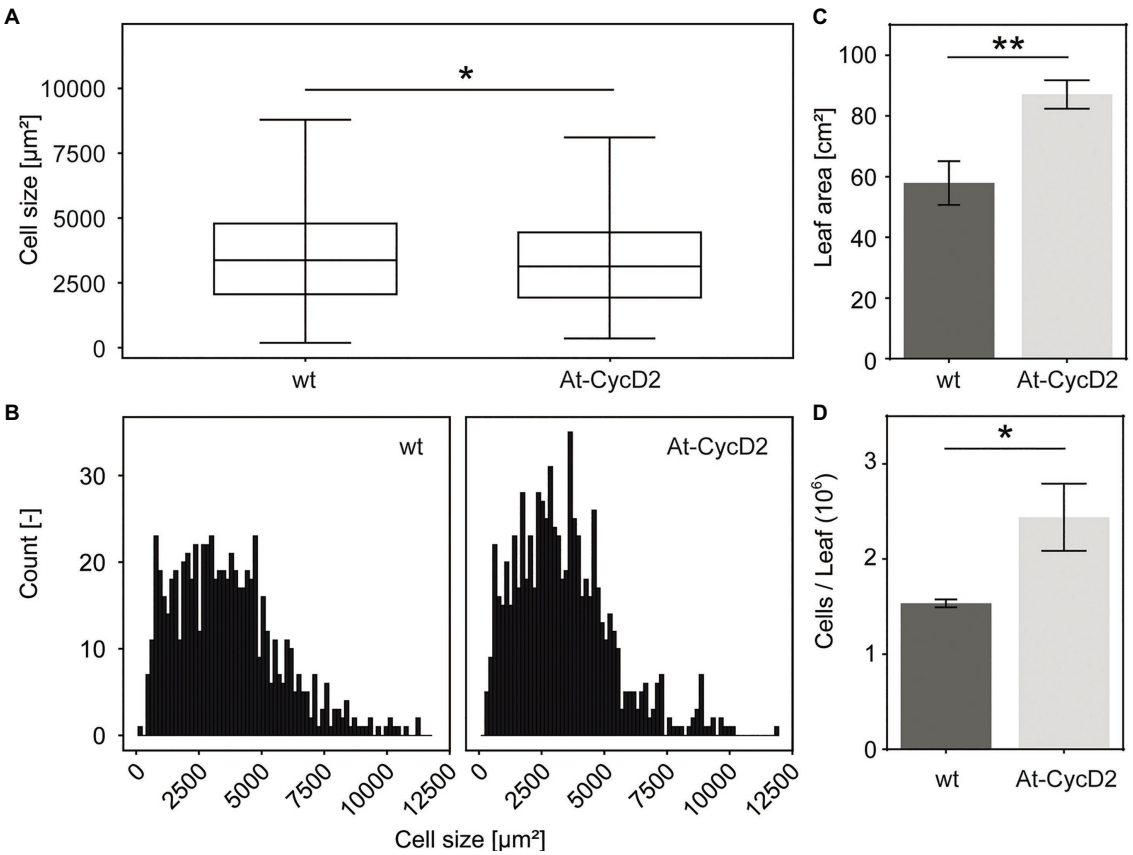

FIGURE 4 | Comparison of leaf size-related characteristics for the At-CycD2-15 line and non-transgenic *N. benthamiana* plants. The third leaves for measurements were harvested from the wild type and At-CycD2-15 plants grown in soil at 4 weeks after planting. The following parameters were evaluated: epidermal cell area **(A)**, cell distribution **(B)**, leaf area **(C)** and number of cells per leaf **(D)**. The number of total cells per leaf was calculated from **(C)** and **(A)**. The single cell distribution was obtained by pooling cell distributions observed for 3 plants. Values represent the means with standard error. Asterisks indicate significance as determined by the unpaired *T*-test, with * and ** denoting $p < 0.05$ and $p < 0.01$, respectively.

out by Cockcroft et al. (2000) demonstrated that the At-CycD2 interacted with the *N. tabacum* CDC2a protein to form functional CDK complex.

We established 19 At-CycD2 lines, verified as transgenic by PCR and segregation analysis. Ectopic expression of the *At-CycD2* gene led to enhanced stem and leaf biomass accumulation in four transgenic lines (At-CycD2-6, At-CycD2-14, At-CycD2-15, and At-CycD2-25). These transgenic lines exhibited normal morphology at all stages of the development. Our results are in agreement with those reported previously. Overexpression of the *At-CycD2* gene in *N. tabacum* resulted in lines with accelerated growth rate, observed as an increased rate of the above-ground biomass accumulation, when compared with the non-transgenic control (Cockcroft et al., 2000). This faster growth is a consequence of both shorter cell cycles and a higher growth fraction in meristematic cells, whereas the meristem size was unaffected (Boucheron et al., 2005). In another study, which investigated the regulation of cell division in stem tissue of the At-CycD2 expressing tobacco plants, enhanced cell division rates in vascular cambium and increased secondary xylem differentiation have been observed (Fujii et al., 2012). In contrast to our study an adverse effect of the *At-CycD2* gene on *N. tabacum* phenotype has not been reported by Cockcroft et al. (2000).

Two mechanisms may be proposed to explain the effect of the At-CycD2 on the plant phenotype. First, the At-CycD2-CDK complex could accelerate G1 phase resulting in an increased rate of cell division in meristematic tissue. A further hypothesis could be the involvement of the At-CycD2-CDK in cellular growth within the meristem due to the effect on general biosynthesis. As a consequence of this shorter time could be required to reach a critical cell size during G1 phase leading to cell division (Cockcroft et al., 2000; Boucheron et al., 2005).

We selected the At-CycD2-15 line due to its genotypic (single locus T-DNA integration pattern) and phenotypic (increased biomass accumulation) characteristics. The modified phenotype of the At-CycD2-15 line was associated with a total larger leaf area. Leaf area is affected by both genetic and environmental factors (Cookson et al., 2005). When plants are grown in stable environmental conditions final leaf area at a given rank on the plant is related to the epidermal cell number (Tisné et al., 2008). In accordance to this view of leaf development we observed the increased cell number in the third leaf of the At-CycD2-15 transgenic

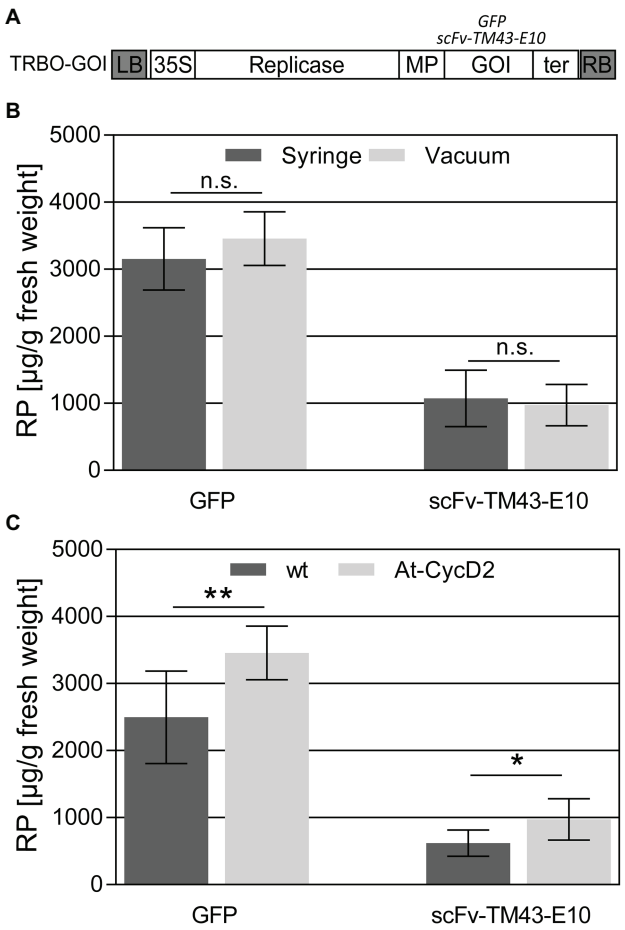

FIGURE 5 | Accumulation of recombinant proteins in leaves of *N. benthamiana*. **(A)** Schematic representation of the TRBO expression vector. Open boxes indicate the following genes: Rep, viral replicase; MP, movement protein; GOI, gene of interest; 35S, 35S promoter. LB, RB, left and right border of T-DNA, respectively. Wild type (wt) and At-CycD2 transgenic plants were agroinfiltrated with the TRBO-*gfp* and TRBO-*scFv-TM43-E10*. **(B)** Comparison of the agroinfiltration methods (vacuum and syringe) in the At-CycD2-15 transgenic plants. **(C)** Comparison of the GFP and scFv-TM43-E10 accumulation in vacuum infiltrated wild type (wt) and At-CycD2-15 transgenic plants. Recombinant protein concentration is expressed in µg/g leaf fresh weight. Y-axis, RP is a recombinant protein. Values represent the means with standard deviation ($n = 7$). Asterisks indicate significance as determined by the Mann–Whitney test, with * and ** denoting $p < 0.05$ and $p < 0.01$, respectively. Not significant values are determined as ns.

line in comparison to the wild type control. This increase in the cell number was accompanied by a decrease in the cell area. This compensatory effect between cell number and cell area has been reported for several cell cycle regulator genes. For example, for the *At-CycD3*gene an increased number of smaller cells have been observed in leaves of transgenic *A. thaliana* in comparison to the non-transgenic plants (Dewitte et al., 2003). In contrast in transgenic *A. thaliana* lines overexpressing Kip-related proteins (KRPs), which inhibit cell cycle progression *via* downregulation of the CDK activity, a reduced cell number was escorted by an increase in cell area (De Veylder et al., 2001).

The At-CycD2-15 transgenic line developed in this study is of particular interest for molecular farming due to its increased leaf mass fraction and genetic background supporting enhanced recombinant protein production. The combination of stably integrated *At-CycD2* gene with the transiently provided *gfp* and *scFv-TM43-E10* genes resulted in enhanced accumulation of the GFP and scFv-TM43-E10 proteins. In our previous study we demonstrated the beneficial effect of the At-CycD2 on the expression of the recombinant proteins expressed by the full TMV-based vector in a transient assay (Kopertekh and Schiemann, 2019). Co-infiltration of TMV-gfp, TMV-scFv-TM43-E10, and pLH-*35S-At-CycD2* vectors resulted in 3 and 2 fold increase in the accumulation of GFP and scFv-TM43-E10 recombinant proteins, respectively. The present investigation extends this finding and shows the influence of the *At-CycD2* cell cycle regulator gene, which was stably integrated in the *N. benthamiana* genome, on the production of foreign proteins expressed by the deconstructed TMV-based vector TRBO. Another study showed that virus-derived cell cycle regulators, the *RepA* genes from tobacco yellow dwarf virus and maize streak virus, the *Clink* gene from banana bunchy top virus, and the *REn* gene from tomato leaf curl virus, co-expressed with the pEAQ-GUS vector significantly increased the GUS accumulation levels about 2 to 3 fold (Norkunas et al., 2018). Both investigations provide data indicating that plant and virus derived cell cycle regulator genes have a positive impact on foreign protein accumulation in *N. benthamiana*.

In contrast to DNA viruses, there are only few publications, which are devoted to the interaction of TMV and host cell cycle machinery. For instance, early investigations of the TMV accumulation in *N. sylvestris* protoplasts revealed that the host cell position in the cell cycle impact the attachment efficiency of TMV (Gould et al., 1981). Investigating the function of the cell division cycle protein 48 (CDC48) from *A. thaliana* during TMV infection Niehl *et al.* proposed a model in which CDC48 participates in the regulation of TMV replication and cell-to-cell transport *via* interaction with the TMV movement protein (Niehl et al., 2012, 2013). In the At-CycD2/TMV combination transient application of the *At-CycD2* cell cycle regulator gene increased the virus RNA accumulation (Kopertekh and Schiemann, 2019). Although the mechanism of this phenomenon remains to be investigated the modulation of virus replication and/or cell-to-cell movement in the presence of the *At-CycD2* may be proposed.

The efficiency of transient expression in *N. benthamiana* depends on 2 yield-related quantities, recombinant protein accumulation per unit harvested biomass and leaf biomass per plant before agroinfiltration (Schillberg et al., 2019). The modified phenotype of the At-CycD2-15 transgenic line characterized by a significant increase in the leaf mass fraction contributes to the recombinant protein yield per unit of biomass. Application of this line can reduce the plant density during upstream production. The positive impact of reduced plant density during upstream production has been reported for the recombinant HA. The whole shoots from the plants, which were grown at low plant density, provided 15–49% higher yield per unit harvested biomass and 10–15% higher yield per unit area-time

(Fujiuchi et al., 2017). The second phenotypic trait of the At-CycD2-15 genotype, enhanced initiation of secondary stem leaves, can be also favourable for recombinant protein production in closed facilities. Recent study demonstrated that axillary stem leaves contributed more than 50% of the recombinant HA H1 yield despite representing only one-third of the total biomass (Goulet et al., 2019).

In this study we showed the potential of the cell cycle regulator gene *At-CycD2* to modulate the host plant for enhanced recombinant protein yield. The At-CycD2-15 transgenic line displayed several features such as improved phenotype and intracellular environment that are relevant to the plant molecular farming application. We used the *Agrobacterium*-mediated transformation technology to modify the *N. benthamiana* genotype. With the availability of the *N. benthamiana* genome assembly (Bombarely et al., 2012) and development of genome editing technologies (TALENs, CRISPR/Cas9) more precise modification of intracellular environment and plant habitus is possible in order to improve *N. benthamiana* as a manufacturing platform for recombinant proteins (Buyel et al., 2021).

DATA AVAILABILITY STATEMENT

The original contributions presented in the study are included in the article/**Supplementary Material**, further inquiries can be directed to the corresponding author.

AUTHOR CONTRIBUTIONS

LK designed the study, analysed the results, and wrote the manuscript. SR performed statistical analysis of data and created figures. All authors contributed to the article and approved the submitted version.

FUNDING

This research was financed in frame of the self-funded JKI project by the German Federal Ministry of Food and Agriculture (BMEL).

ACKNOWLEDGMENTS

We thank J. Lindbo for providing pJL-TRBO-G plasmid (Addgene plasmid # 80083; http://n2t.net/addgene:80083; RRID: Addgene_80083). We also thank Cornelia Freyer, Nadja Engelhardt and Bärbel Apel for their technical support.

SUPPLEMENTARY MATERIAL

The Supplementary Material for this article can be found online at: https://www.frontiersin.org/articles/10.3389/fpls.2021.712438/full#supplementary-material

REFERENCES

Arzola, L., Chen, J. X., Rattanaporn, K., Maclean, J. M., and McDonald, K. A. (2011). Transient co-expression of post-transcriptional gene silencing suppressors for increased in planta expression of a recombinant anthrax receptor fusion protein. *Int. J. Mol. Sci.* 12, 4975–4990. doi: 10.3390/ijms12084975

Bally, J., Jung, H., Mortimer, C., Naim, F., Philips, J. G., Roger Hellens, R., et al. (2018). Waterhouse PM, The rise and rise of *Nicotiana benthamiana*: a Plant for all reasons. *Annu. Rev. Phytopathol.* 56, 405–426. doi: 10.1146/annurev-phyto-080417-050141

Bombarely, A., Rosli, H. G., Vrebalov, J., Moffett, P., Mueller, L. A., and Martin, G. B. (2012). A draft genome sequence of *Nicotiana benthamiana* to enhance molecular plant-microbe biology research. *Mol. Plant-Microbe Interact.* 25, 1523–1530. doi: 10.1094/MPMI-06-12-0148-TA

Boucheron, E., Healy, J. H., Bajon, C., Sauvanet, A., Rembur, J., Noin, M., et al. (2005). Ectopic expression of *Arabidopsis* CYCD2 and CYCD3 in tobacco has distinct effects on the structural organization of the shoot apical meristem. *J. Exp. Bot.* 56, 123–134. doi: 10.1093/jxb/eri001

Busov, V. B., Brunner, A. M., and Strauss, S. H. (2008). Genes for control of plant stature and form. *New Phytol.* 177, 589–607. doi: 10.1111/j.1469-8137.2007.02324.x

Buyel, J. F., Stöger, E., and Bortesi, L. (2021). Targeted genome editing of plants and plant cells for biomanufacturing. *Transgenic Res.* 30, 401–426. doi: 10.1007/s11248-021-00236-z

Capell, T., Twyman, R. M., Armario-Najera, V., Ma, J. K.-C., Schillberg, S., and Christou, P. (2020). Potential applications of plant biotechnology against SARS-CoV-2. *Trends Plant Sci.* 25, 635–643. doi: 10.1016/j.tplants.2020.04.009

Cheng, Y., Cao, L., Wang, S., Li, Y. P., Shi, X. Z., Liu, H., et al. (2013). Downregulation of multiple CDK inhibitor ICK/KRP genes upregulates the E2F pathway and increases cell proliferation and organ and seed sizes in *Arabidopsis*. *Plant J.* 75, 642–655. doi: 10.1111/tpj.12228

Cockcroft, C. E., den Boer, B. G. W., Healy, J. M. S., and Murray, J. A. H. (2000). Cyclin D control of growth rate in plants. *Nature* 405, 575–579. doi: 10.1038/35014621

Cookson, S. J., Van Lijsebettens, M., and Granier, C. (2005). Correlation between leaf growth variables suggest intrinsic and early controls of leaf size in *Arabidopsis thaliana*. *Plant Cell Environ.* 28, 1355–1366. doi: 10.1111/j.1365-3040.2005.01368.x

De Veylder, L., Beeckman, T., Beemster, G. T. S., Krols, L., Terras, F., Landrieu, I., et al. (2001). Functional analysis of cyclin-dependent kinase inhibitors of *Arabidopsis*. *Plant Cell* 13, 1653–1667. doi: 10.1105/TPC.010087

Dewitte, W., Riou-Khamlichi, C., Scofield, S., Healy, J. M. S., Jacqmard, A., Kilby, N. J., et al. (2003). Altered cell cycle distribution, hyperplasia, and inhibited differentiation in *Arabidopsis* caused by the D-type cyclin CYCD3. *Plant Cell* 15, 79–92. doi: 10.1105/tpc.004838

Diego-Martin, B., González, B., Vazquez-Vilar, M., Selma, S., Mateos-Fernández, R., Gianoglio, S., et al. (2020). Pilot production of SARS-CoV-2 related proteins in plants: a proof of concept for rapid repurposing of indoor farms into biomanufacturing facilities. *Front. Plant Sci.* 11:612781. doi: 10.3389/fpls.2020.612781

Fitzmaurice, W. P. (2002). Interspecific Nicotianahybrids and their progeny. US Patent 6344597B1.

Francis, D. (2007). The plant cell cycle – 15 years on. *New Phytol.* 174, 261–278. doi: 10.1111/j.1469-8137.2007.02038.x

Fujii, T., Sato, K., Matsui, N., Furuichi, T., Takenouchi, S., Nishikubo, N., et al. (2012). Enhancement of secondary xylem cell proliferation by *Arabidopsis* cyclin D overexpression in tobacco plants. *Plant Cell Rep.* 31, 1573–1580. doi: 10.1007/s00299-012-1271-7

Fujiuchi, N., Matoba, N., and Matsuda, R. (2016). Environment control to improve recombinant protein yields in plants based on *Agrobacterium*-mediated transient gene expression. *Front. Bioeng. Biotechnol.* 4:23. doi: 10.3389/fbioe.2016.00023

Fujiuchi, N., Matsuda, R., Matoba, N., and Fujiwara, K. (2017). Effects of plant density on recombinant protein hemagglutinin yields in an *Agrobacterium*

-mediated transient gene expression system using *Nicotiana benthamiana* plants. *Biotechnol. Bioeng.* 114, 1762–1770. doi: 10.1002/bit.26303

Garabagi, F., Gilbert, E., Loos, A., McLean, M. D., and Hall, J. C. (2012). Utility of the P19 suppressor of gene-silencing protein for production of therapeutic antibodies in Nicotiana expression hosts. *Plant Biotechnol. J.* 10, 1118–1128. doi: 10.1111/j.1467-7652.2012.00742.x

Gleba, Y., Marillonnet, S., and Klimyuk, V. (2004). Engineering viral expression vectors for plants: the 'full virus' and the 'deconstructed virus' strategies. *Curr. Opin. Plant Biol.* 7, 182–188. doi: 10.1016/j.pbi.2004.01.003

Gleba, Y. Y., Tusé, D., and Giritch, A. (2014). "Plant viral vectors for delivery by agrobacterium," in *Plant Viral Vectors*. *Vol.* 375. eds. K. Palmer and Y. Gleba (Berlin-Heidelberg: Springer), 155–192.

Goodin, M. M., Zaitlin, D., Naidu, R. A., and Lommel, S. A. (2008). *Nicotiana benthamiana*: its history and future as a model for plant-pathogen interactions. *Mol. Plant-Microbe Interact.* 21, 1015–1026. doi: 10.1094/MPMI-21-8-1015

Gould, A. R., Ashmore, S. E., and Gibbs, A. J. (1981). Cell cycle related changes in the quantity of TMV virions bound to protoplasts of *Nicotiana sylvestris*. *Protoplasma* 108, 211–223. doi: 10.1007/BF02224420

Goulet, M. C., Gaudreau, L., Gagné, M., Maltais, A. M., Laliberté, A. C., Éthier, G., et al. (2019). Production of biopharmaceuticals in *Nicotiana benthamiana*-axillary stem growth as a key determinant of total protein yield. *Front. Plant Sci.* 10:735. doi: 10.3389/fpls.2019.00735

Hefferon, K. L. (2012). Plant virus expression vectors set the stage as production platforms for biopharmaceutical proteins. *Virology* 433, 1–6. doi: 10.1016/j.virol.2012.06.012

Holsters, M., de Waele, D., Depicker, A., Messens, E., van Montagu, M., and Schell, J. (1978). Transfection and transformation of *A. tumefaciens*. *Mol. Gen. Genet.* 163, 181–187. doi: 10.1007/BF00267408

Inze, D., and De Veylder, L. (2006). Cell cycle regulation in plant development. *Annu. Rev. Genet.* 40, 77–105. doi: 10.1146/annurev.genet.40.110405.090431

Jutras, P. V., Dodds, I., and van der Hoorn, A. L. R. (2020). Proteases of *Nicotiana benthamiana*: an emerging battle for molecular farming. *Curr. Opin. Biotechnol.* 61, 60–65. doi: 10.1016/j.copbio.2019.10.006

Kopertekh, L., Jüttner, G., and Schiemann, J. (2004). PVX-Cre-mediated marker gene elimination from transgenic plants. *Plant Mol. Biol.* 55, 491–500. doi: 10.1007/s11103-004-0237-8

Kopertekh, L., and Schiemann, J. (2019). Enhanced foreign protein accumulation in *Nicotiana benthamiana* leaves co-infiltrated with a TMV vector and plant cell cycle regulator genes. *Transgenic Res.* 28, 411–417. doi: 10.1007/s11248-019-00128-3

Lima, M. F., Eloy, N. B., Bottino, M. C., Hemerly, A. S., and Ferreira, P. C. (2013). Overexpression of the anaphase-promoting complex (APC) genes in *Nicotiana tabacum* promotes increasing biomass accumulation. *Mol. Biol. Rep.* 40, 7093–7102. doi: 10.1007/s11033-013-2832-8

Lima, M. F., Eloy, N. B., Siqueira, J. A. B., Inzé, D., Hemerly, A. D., and Ferreira, P. C. G. (2017). Molecular mechanisms of biomass increase in plants. *Biotechnol. Res. Innov.* 1, 14–25. doi: 10.1016/j.biori.2017.08.001

Lindbo, J. A. (2007). TRBO: a high-efficiency tobacco mosaic virus RNA-based overexpression vector. *Plant Physiol.* 145, 1232–1240. doi: 10.1104/pp.107.106377

Lomonossoff, G. P., and D'Aoust, M. A. (2016). Plant-produced biopharmaceuticals: a case of technical developments driving clinical deployment. *Science* 353, 1237–1240. doi: 10.1126/science.aaf6638

Matsuo, K., and Atsumi, G. (2019). CRISPR/Cas9-mediated knockout of the RDR6 gene in *Nicotiana benthamiana* for efficient transient expression of recombinant proteins. *Planta* 250, 463–473. doi: 10.1007/s00425-019-03180-9

Matsuo, K., and Matsumura, T. (2017). Repression of the DCL2 and DCL4 genes in *Nicotiana benthamiana* plants for the transient expression of recombinant proteins. *J. Biosci. Bioeng.* 124, 215–220. doi: 10.1016/j.jbiosc.2017.02.019

Meyer, T., Stratmann-Selke, J., Meens, J., Schirrmann, T., Gerlach, G. F., Frank, R., et al. (2011). Hust M, Isolation of scFv fragments specific to OmpD of Salmonella Typhimurium. *Vet. Microbiol.* 147, 162–169. doi: 10.1016/j.vetmic.2010.06.023

Musiychuk, K., Stephenson, N., Bi, H., Farrance, C. E., Orozovic, G., Brodelius, M., et al. (2007). A launch vector for the production of vaccine antigens in plants. *Influenza Other Respir. Viruses* 1, 19–25. doi: 10.1111/j.1750-2659.2006.00005.x

Niehl, A., Amari, K., Gereige, D., Brandner, K., Me'ly, Y., and Heinlein, M. (2012). Control of tobacco mosaic virus movement protein fate by cell-division-cycle protein 48 (CDC48). *Plant Physiol.* 160, 2093–2108. doi: 10.1104/pp.112.207399

Niehl, A., Amari, K., and Heinlein, M. (2013). CDC48 function during TMV infection: regulation of virus movement and replication by degradation? *Plant Signal. Behav.* 8:e22865. doi: 10.4161/psb.22865

Norkunas, K., Harding, R., Dale, J., and Dugdale, B. (2018). Improving agroinfiltration-based transient gene expression in *Nicotiana benthamiana*. *Plant Methods* 14:71. doi: 10.1186/s13007-018-0343-2

Peyret, H., and Lomonossoff, G. P. (2015). When plant virology met *Agrobacterium*: the rise of the deconstructed clones. *Plant Biotechnol. J.* 13, 1121–1135. doi: 10.1111/pbi.12412

Powell, J. D. (2015). From pandemic preparedness to biofuel production: tobacco finds its biotechnology niche in North America. *Agriculture* 5, 901–917. doi: 10.3390/agriculture5040901

Robert, S., Goulet, M.-C., D'Aoust, M.-A., Sainsbury, F., and Michaud, D. (2015). Leaf proteome rebalancing in *Nicotiana benthamiana* for upstream enrichment of a transiently expressed recombinant protein. *Plant Biotechnol. J.* 13, 1169–1179. doi: 10.1111/pbi.12452

Rojas, C. A., Eloy, N. B., Lima Mde, F., Rodrigues, R. L., Franco, L. O., Himanen, K., et al. (2009). Overexpression of the *Arabidopsis* anaphase promoting complex subunit CDC27a increases growth rate and organ size. *Plant Mol. Biol.* 71, 307–318. doi: 10.1007/s11103-009-9525-7

Rojas, C. A., Hemerly, A. S., and Ferreira, P. C. (2010). Genetically modified crops for biomass increase. Genes and strategies. *GM Crops* 1, 137–142. doi: 10.4161/gmcr.1.3.12615

Schillberg, S., Raven, N., Spiegel, H., Rasche, S., and Buntru, M. (2019). Critical analysis of the commercial potential of plants for the production of recombinant proteins. *Front. Plant Sci.* 10:720. doi: 10.3389/fpls.2019.00720

Scofield, S., Jones, A., and Murray, J. A. (2014). The plant cell cycle in context preface. *J. Exp. Bot.* 65, 2557–2562. doi: 10.1093/jxb/eru188

Shang, L., Gaudreau, L., Martel, M., Michaud, D., Pepin, S., and Gosselin, A. (2018). Effects of CO_2 enrichment, LED inter-lighting, and high plant density on growth of *Nicotiana benthamiana* used as a host to express influenza virus hemagglutinin H1. *Hortic. Environ. Biotechnol.* 59, 637–648. doi: 10.1007/s13580-018-0085-0

Soni, R., Carmichael, J. P., Shah, Z. H., and Murray, J. A. (1995). A family of cyclin D homologs from plants differentially controlled by growth regulators and containing the conserved retinoblastoma protein interaction motif. *Plant Cell* 7, 85–103. doi: 10.1105/tpc.7.1.85

The PREVAIL II Writing Group, for the Multi-National PREVAIL II Study Team (2016). A randomized, controlled trial of ZMapp for ebola virus infection. *N. Engl. J. Med.* 375, 1448–1456. doi: 10.1056/NEJMoa1604330

Tisné, S., Reymond, M., Vile, D., Fabre, J., Dauzat, M., and Koornneef, M. (2008). Granier C, Combined genetic and modeling approaches reveal that epidermal cell area and number in leaves are controlled by leaf and plant developmental processes in *Arabidopsis*. *Plant Physiol.* 148, 1117–1127. doi: 10.1104/pp.108.124271

Ward, J. B., Makarkov, A., Séguin, A., Pillet, S., Trépanier, S., Dhaliwall, J., et al. (2020). Efficacy, immunogenicity, and safety of a plant-derived, quadrivalent, virus-like particle influenza vaccine in adults (18–64 years) and older adults (≥65 years): two multicentre, randomised phase 3 trials. *Lancet* 396, 1491–1503. doi: 10.1016/S0140-6736(20)32014-6

Wittenberg, C. (2005). Cyclin guides the way. *Nature* 434, 34–35. doi: 10.1038/434034a

Yang, S. J., Carter, S. A., Cole, A. B., Cheng, N. H., and Nelson, R. S. (2004). A natural variant of a host RNA-dependent RNA polymerase is associated with increased susceptibility to viruses by *Nicotiana benthamiana*. *Proc. Natl. Acad. Sci. U. S. A.* 101, 6297–6302. doi: 10.1073/pnas.0304346101

Conflict of Interest: The authors declare that the research was conducted in the absence of any commercial or financial relationships that could be construed as a potential conflict of interest.

Publisher's Note: All claims expressed in this article are solely those of the authors and do not necessarily represent those of their affiliated organizations, or those of the publisher, the editors and the reviewers. Any product that may

be evaluated in this article, or claim that may be made by its manufacturer, is not guaranteed or endorsed by the publisher.

frontiers in Plant Science

ORIGINAL RESEARCH
published: 27 September 2021
doi: 10.3389/fpls.2021.747500

Impact of Specific *N*-Glycan Modifications on the Use of Plant-Produced SARS-CoV-2 Antigens in Serological Assays

*Jennifer Schwestka[1], Julia König-Beihammer[1], Yun-Ji Shin[1], Ulrike Vavra[1], Nikolaus F. Kienzl[1], Clemens Grünwald-Gruber[2], Daniel Maresch[2], Miriam Klausberger[3], Elisabeth Laurent[4,5], Maria Stadler[6], Gabriele Manhart[7], Jasmin Huber[8], Manuela Hofner[8], Klemens Vierlinger[8], Andreas Weinhäusel[8], Ines Swoboda[9], Christoph J. Binder[10], Wilhelm Gerner[6†], Florian Grebien[7], Friedrich Altmann[2], Lukas Mach[1], Eva Stöger[1] and Richard Strasser[1]**

[1] Department of Applied Genetics and Cell Biology, Institute of Plant Biotechnology and Cell Biology, University of Natural Resources and Life Sciences, Vienna, Austria, [2] Department of Chemistry, Institute of Biochemistry, University of Natural Resources and Life Sciences, Vienna, Austria, [3] Department of Biotechnology, University of Natural Resources and Life Sciences, Vienna, Austria, [4] Department of Biotechnology, University of Natural Resources and Life Sciences, Vienna, Austria, [5] Core Facility Biomolecular & Cellular Analysis, University of Natural Resources and Life Sciences, Vienna, Austria, [6] Institute of Immunology, University of Veterinary Medicine, Vienna, Austria, [7] Institute for Medical Biochemistry, University of Veterinary Medicine, Vienna, Austria, [8] Competence Unit Molecular Diagnostics, Center for Health and Bioresources, AIT Austrian Institute of Technology GmbH, Vienna, Austria, [9] Biotechnology Section, FH Campus Wien, University of Applied Sciences, Vienna, Austria, [10] Department of Laboratory Medicine, Medical University of Vienna, Vienna, Austria*

The receptor binding domain (RBD) of the SARS-CoV-2 spike protein plays a key role in the virus-host cell interaction, and viral infection. The RBD is a major target for neutralizing antibodies, whilst recombinant RBD is commonly used as an antigen in serological assays. Such assays are essential tools to gain control over the pandemic and detect the extent and durability of an immune response in infected or vaccinated populations. Transient expression in plants can contribute to the fast production of viral antigens, which are required by industry in high amounts. Whilst plant-produced RBDs are glycosylated, *N*-glycan modifications in plants differ from humans. This can give rise to the formation of carbohydrate epitopes that can be recognized by anti-carbohydrate antibodies present in human sera. For the performance of serological tests using plant-produced recombinant viral antigens, such cross-reactive carbohydrate determinants (CCDs) could result in false positives. Here, we transiently expressed an RBD variant in wild-type and glycoengineered *Nicotiana benthamiana* leaves and characterized the impact of different plant-specific *N*-glycans on RBD reactivity in serological assays. While the overall performance of the different RBD glycoforms was comparable to each other and to a human cell line produced RBD, there was a higher tendency toward false positive results with sera containing allergy-related CCD-antibodies when an RBD carrying β1,2-xylose and core α1,3-fucose was used. These rare events could be further minimized by pre-incubating sera from allergic individuals with a CCD-inhibitor. Thereby, false positive signals obtained from anti-CCD antibodies, could be reduced by 90%, on average.

Keywords: allergen, cross-reactive carbohydrate determinant, COVID-19, glycosylation, posttranslational modification, SARS-CoV-2, virus

OPEN ACCESS

Edited by:
Domenico De Martinis, Italian National Agency for New Technologies, Energy and Sustainable Economic Development (ENEA), Italy

Reviewed by:
Stephanie Archer-Hartmann, University of Georgia, United States
Linda Avesani, University of Verona, Italy

****Correspondence:***
Richard Strasser
richard.strasser@boku.ac.at

†Present address:
Wilhelm Gerner, The Pirbright Institute, Woking, United Kingdom

Specialty section:
This article was submitted to Plant Biotechnology, a section of the journal Frontiers in Plant Science

Received: *26 July 2021*
Accepted: *08 September 2021*
Published: *27 September 2021*

Citation:
Schwestka J, König-Beihammer J, Shin Y-J, Vavra U, Kienzl NF, Grünwald-Gruber C, Maresch D, Klausberger M, Laurent E, Stadler M, Manhart G, Huber J, Hofner M, Vierlinger K, Weinhäusel A, Swoboda I, Binder CJ, Gerner W, Grebien F, Altmann F, Mach L, Stöger E and Strasser R (2021) Impact of Specific N-Glycan Modifications on the Use of Plant-Produced SARS-CoV-2 Antigens in Serological Assays. Front. Plant Sci. 12:747500. doi: 10.3389/fpls.2021.747500

INTRODUCTION

The worldwide deployment of vaccination programs against coronavirus disease 2019 (COVID-19) is one of the key measures in the fight against the current pandemic. Immunization of the population in a fast and controlled manner can protect individuals from severe COVID-19 and simultaneously limit the possibility of spreading the virus. To test the success of vaccination campaigns and monitor the immune response of vaccinated and naturally infected people, it is essential to measure the antibody titers against SARS-CoV-2 over time (Amanat et al., 2020). Serological assays using recombinant SARS-CoV-2 antigens are used to quantify the extent and durability of specific antibodies in the blood (Amanat et al., 2020; Klausberger et al., 2021). Subsequently, in order to monitor the levels of immunity in whole populations, billions of reliable antibody tests are needed.

Subunits of the SARS-CoV-2 spike protein are frequently used in serological assays to detect a specific immune response against the virus. As many neutralizing antibodies target the receptor binding domain (RBD) of the spike protein (Kreer et al., 2020; Liu et al., 2020; Pinto et al., 2020), the RBD is commonly used as an antigen in serological assays. Recombinant, soluble RBD variants have been purified from different expression systems including: mammalian cells, insect cells and plants (Diego-Martin et al., 2020; Li et al., 2020; Rattanapisit et al., 2020; Castro et al., 2021; Klausberger et al., 2021). Transient expression in plants such as *Nicotiana benthamiana* provides an attractive alternative to mammalian cell culture-based systems for cheap, fast and scalable production of diagnostic reagents and vaccine candidates (Stoger et al., 2014; Capell et al., 2020).

The monomeric SARS-CoV-2 spike protein is heavily glycosylated, featuring 22 *N*-glycosylation sites and numerous potential sites for *O*-glycosylation (Shajahan et al., 2020; Watanabe et al., 2020; Zhao et al., 2020; Sanda et al., 2021; Zhang et al., 2021). Within the RBD sequence, two *N*-glycosylation sites are typically *N*-glycosylated with complex *N*-glycans (Allen et al., 2021). While the overall role of the *N*-glycans for SARS-CoV-2 receptor binding and infection have been studied (Yang et al., 2020; Wang et al., 2021), the function of distinct *N*-glycans is less understood. Recent reports suggested that *N*-glycosylation at the two sites in the RBD is critical for binding to the cellular ACE2 receptor (Azad et al., 2021) and stabilization of the RBD in the "up" state that is required for ACE2 binding and cell entry (Sztain et al., 2021). Moreover, *N*-glycosylation of both sites is crucial for efficient expression of soluble RBD in *N. benthamiana,* indicating a role of the *N*-glycans in protein folding (Shin et al., 2021).

In comparison to mammalian cells, the *N*-glycan-processing pathway in the Golgi apparatus of plants is much simpler. Consequently, plant-produced recombinant glycoproteins carry quite homogenous complex *N*-glycans (Dicker and Strasser, 2015). Glycoengineering by knockdown of β1,2-xylosyltransferase (XT) and core α1,3-fucosyltransferase (FT) in *N. benthamiana* (ΔXT/FT) resulted in the production of recombinant glycoproteins carrying mainly the $GlcNAc_2Man_3GlcNAc_2$ (GnGn) complex *N*-glycan (Strasser et al., 2008). As this Golgi-processed oligosaccharide structure serves as the basis for further modifications that are frequently found in humans, glycoengineering can be used to modulate the function of glycoproteins, such as immunoglobulins (Montero-Morales and Steinkellner, 2018). Wild-type plants, on the other hand, mainly produce complex and truncated *N*-glycans carrying β1,2-xylose and core α1,3-fucose residues. These sugar residues are part of carbohydrate epitopes present on plant, insect or helminth proteins which can be recognized by IgE antibodies and are considered as cross-reactive carbohydrate determinants (CCDs) (Platts-Mills et al., 2021). Approximately one fifth of patients with allergies develop IgE antibodies against such *N*-glycans (Altmann, 2007; Holzweber et al., 2013). Furthermore, production of high-affinity IgGs against these carbohydrate epitopes have also been observed (Bardor et al., 2003; Jin et al., 2006). While the clinical relevance of these epitopes is low and they do not appear to affect the safety and efficacy of recombinant biotherapeutics (Rup et al., 2017), these CCDs are a constant problem in allergy diagnosis where they are the frequent cause of false positives (Altmann, 2016; Aberer et al., 2017).

Here, we generated glycoforms of a truncated recombinant RBD variant called RBD-215 by transient expression in *N. benthamiana* and investigated their recognition by virus-specific antibodies in convalescent sera from SARS-CoV-2 exposed individuals. Our data show that all RBD glycoforms are highly suitable to detect IgG and IgM antibodies in convalescent sera and unspecific binding by pre-COVID-19 sera was generally low. However, the results obtained with a selected group of sera from allergic individuals producing anti-CCD antibodies indicated some risk of false positives caused by binding of anti-carbohydrate antibodies. In these cases, the production of recombinant viral antigens in glycoengineered ΔXT/FT plants, or the inhibition of CCDs, reduces the risk of false positives.

RESULTS

RBD-215 Glycoforms With Different Types of Complex *N*-Glycans Can Be Efficiently Produced in *N. benthamiana*

In a previous study we observed that the most frequently used recombinant RBD variant (R319-F541) is poorly expressed in *N. benthamiana* and tends to form homodimers or aggregates (Klausberger et al., 2021). Therefore, we expressed a slightly shorter variant called RBD-215 (amino acids R319-L533). This variant lacks an unpaired cysteine at position 538 that is responsible for aberrant disulfide bridge formation (**Figure 1A**). This variant shows much lower amounts of homodimers/aggregates and higher yields than RBD R319-F541 upon transient expression in *N. benthamiana* leaves (Shin et al., 2021). To generate alternative RBD-215 glycoforms we infiltrated wild-type (WT) and ΔXT/FT plants, which have very low levels of β1,2-xylose and core α1,3-fucose (Strasser et al., 2008). Recombinant RBD-215 from WT (RBD-215 WT) and ΔXT/FT (RBD-215 ΔXF) are expected to differ in the presence or absence of β1,2-xylose and core α1,3-fucose residues (**Figure 1B**). Plant complex *N*-glycans can be further elongated by the incorporation

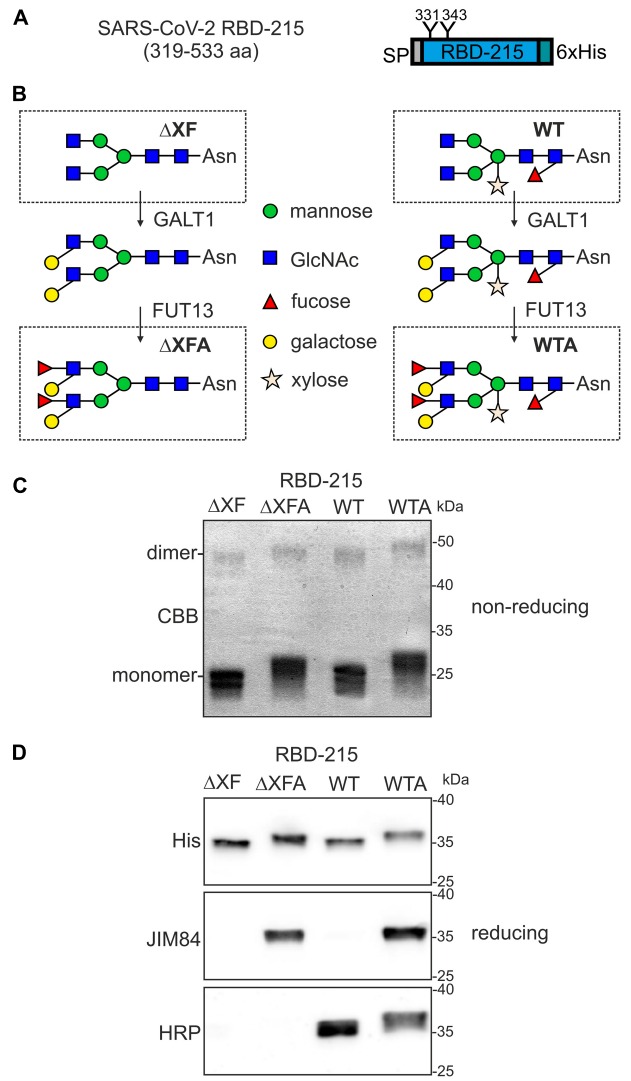

FIGURE 1 | Production of RBD-215 glycoforms in *Nicotiana benthamiana*. **(A)** Schematic illustration of the expressed RBD-215 protein. The signal peptide (SP), *N*-glycosylation sites (N331 and N343) and the polyhistidine (6xHis) tag are indicated. **(B)** Cartoon illustration of the glycoengineering approach to produce the RBD-215 glycoforms. RBD-215 is expressed in wild-type (WT) or ΔXT/FT (ΔXF) plants. The Lewis A epitope is further attached by co-expression of β1,3-galactosyltransferase (GALT1) and α1,4-fucosyltransferase (FUT13). RBD-215 ΔXFA and RBD-215 WTA are RBD-215 variants carrying *N*-glycans with the Lewis A epitope. **(C)** RBD-215 glycoforms purified from the apoplastic fluid of infiltrated wild-type (WT) or ΔXT/FT (ΔXF) *N. benthamiana* leaves were subjected to SDS-PAGE under non-reducing conditions and stained with Coomassie Brilliant Blue (CBB). **(D)** Immunoblot analysis of purified RBD-215 glycoforms with anti-His (His), anti-Lewis A (JIM84) and anti-β1,2-xylose and core α1,3-fucose (HRP) antibodies.

of β1,3-galactose and α1,4-fucose, which results in the generation of Lewis A containing *N*-glycans (Strasser et al., 2007). While this complex *N*-glycan modification is only found on a small number of native plant glycoproteins (Beihammer et al., 2021), substantial amounts of Lewis A structures can be present on moss- or plant-produced recombinant glycoproteins such as human erythropoietin or β-glucocerebrosidase (Parsons et al., 2012; Castilho et al., 2013; Uthailak et al., 2021). To examine whether human sera harbor antibodies directed against Lewis A containing *N*-glycans, we generated recombinant RBD-215 modified with Lewis A structures on both *N*-glycans. The two enzymes responsible for Lewis A synthesis in *Arabidopsis*, β1,3-galactosyltransferase (GALT1) and α1,4-fucosyltransferase (FUT13) were transiently co-expressed with RBD-215 in WT and ΔXT/FT plants to generate the RBD-215 glycoforms RBD-215 WTA and RBD-215 ΔXFA (**Figure 1B**).

All four RBD-215 glycoforms were purified using immobilized metal affinity chromatography (IMAC) from apoplastic fluid isolated from infiltrated leaves and the overall yield was in a similar range (approximately 20 μg/g fresh weight). SDS-PAGE under non-reducing conditions revealed the presence of mainly monomeric RBD-215 with minor amounts of RBD dimers (**Figure 1C**). Differences in electrophoretic mobility indicated the presence of complex *N*-glycans with or without Lewis A containing *N*-glycans. The presence of Lewis A structures on RBD-215 WTA and RBD-215 ΔXFA was further confirmed using the Lewis A-specific monoclonal antibody JIM84 (Fitchette et al., 1999) (**Figure 1D**). RBD-215 WT did not give a signal with JIM84 showing the absence of Lewis A structures on wild-type produced RBD-215. RBD-215 WT and RBD-215 WTA reacted with antibodies against horseradish peroxidase (HRP), indicating the presence of *N*-glycans with β1,2-xylose and core α1,3-fucose residues (Strasser et al., 2004).

To analyze the *N*-glycan patterns in more detail, purified RBD-215 glycoforms were subjected to proteolytic digestion with LysC and GluC and the resulting glycopeptides SIVRFPNITNLCPFGE and VFNATRFASVYAWNRK analyzed by mass spectrometry. RBD-215 ΔXF carried mainly GnGn structures on both *N*-glycosylation sites with low amounts of truncated $GlcNAc_1Man_3GlcNAc_2$ and $Man_3GlcNAc_2$ structures (**Figure 2**). On RBD-215 WT, the main structure was GnGnXF carrying β1,2-xylose and core α1,3-fucose. Co-expression of the glycosyltransferases required for Lewis A biosynthesis efficiently converted GnGn and GnGnXF to (FA)(FA) and (FA)(FA)XF, respectively. In addition, several peaks corresponding to processing intermediates or truncated complex *N*-glycans were present on RBD-215 WTA and RBD-215 ΔXFA.

RBD-215 Glycoforms Display Comparable Functionality in ACE-2 Binding Assays

To examine whether differences in *N*-glycan processing affect RBD binding to the SARS-CoV-2 host cell receptor angiotensin-converting enzyme 2 (ACE2) an ELISA was carried out. ACE2-Fc was coated on the ELISA plate and the binding of RBD-215 glycoforms and a HEK293-produced truncated RBD (tRBD, R319-K537) to ACE2 was measured. Overall, the binding to ACE2-Fc was comparable between all glycoforms tested and to HEK293-expressed tRBD (**Figure 3A**). For in-depth characterization of ACE2 binding, we used biolayer interferometry using SEC-purified monomeric variants of

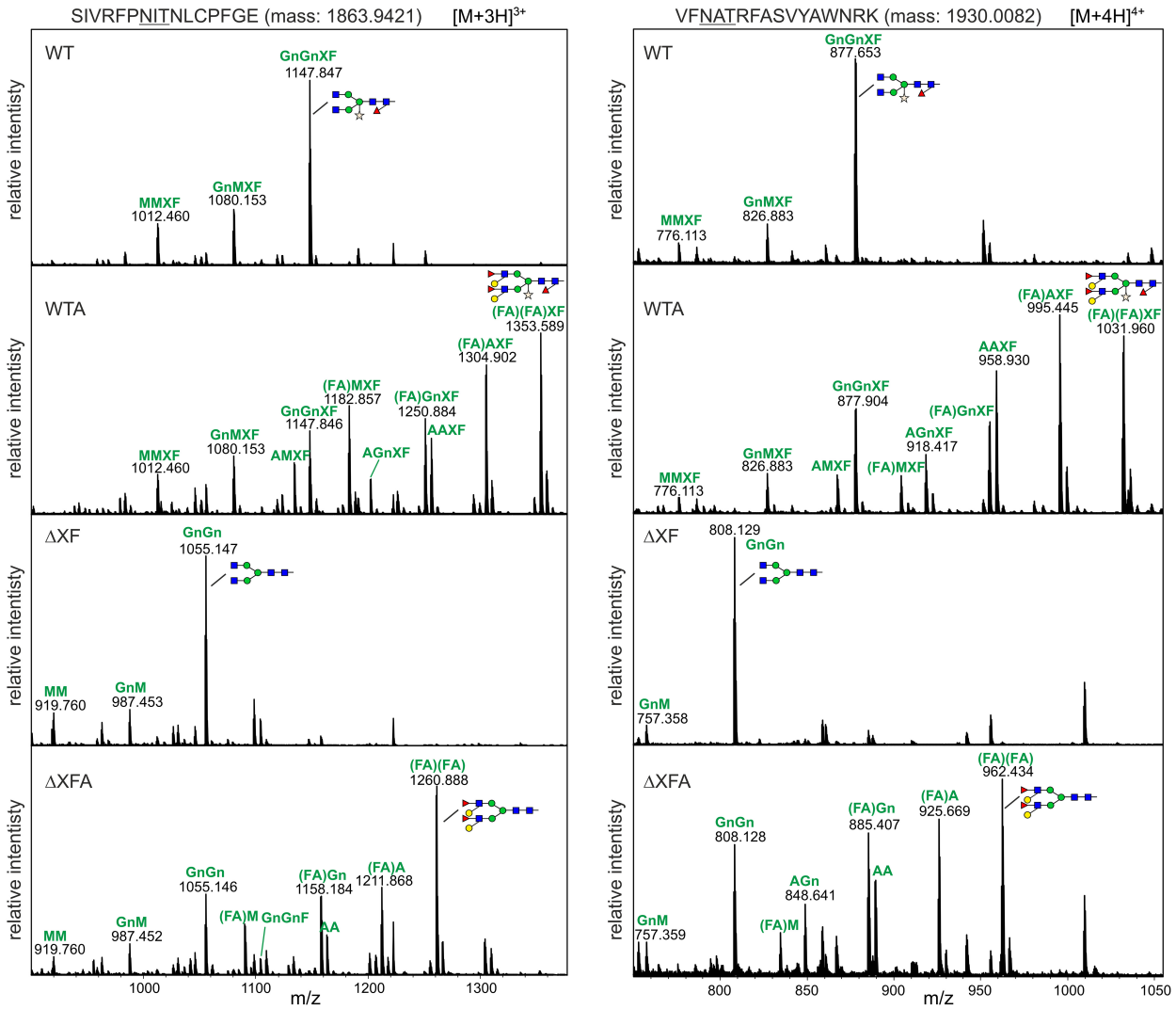

FIGURE 2 | The MS spectra of the RBD-215 glycopeptides carrying the *N*-glycosylation site N331 and N343. RBD-215 glycoforms were purified by IMAC from the apoplastic fluid 3 days after infiltration, LysC and GluC digested and analyzed by MS. Major *N*-glycan peaks are illustrated with a cartoon presentation. Nomenclature of *N*-glycans is according to the ProGlycAn system (http://www.proglycan.com/). Only one *N*-glycan isoform is indicated per peak.

RBD-215 glycoforms (**Figure 3B**). Kinetic analysis revealed that all RBD-215 glycoforms have comparable affinities for the ACE2-Fc receptor fusion protein (13–20 nM; n = 3) (**Figure 3C** and **Supplementary Table 1**), which is in the same range as observed for tRBD (18.1 ± 0.6 nM; n = 3). Taken together, our data show that glycoengineering can be used to produce functional recombinant RBD-215 variants carrying different types of complex *N*-glycans.

RBD-215 Glycoforms Specifically React With Convalescent Sera From COVID-19 Patients

Next, we aimed to investigate the recognition of plant-produced RBD-215 glycoforms by SARS-CoV-2-specific antibodies in serological assays. In ELISA assays using sera from SARS-CoV-2 exposed (n = 30) and non-exposed (n = 12) individuals, we found that the RBD-215 glycoforms and HEK293-derived tRBD displayed similar IgG binding patterns (**Figure 4A**).

Using a bead-based multiplexed binding assay, SARS-CoV-2 specific IgG and IgM antibodies were quantified in sera from a larger cohort of SARS-CoV-2 exposed (n = 124) and non-exposed (n = 210) individuals (**Figures 4B,C**). The performance of the glycoengineered RBD-215 antigens in diagnostic tests was assessed through comparing receiver operating characteristic (ROC) curves and the analysis of the area under the respective ROC curve (AUC). Area under the ROC curves are performance metrics that indicate the capability of a diagnostic test to discriminate between two populations (Klausberger et al., 2021). All four RBD-215 glycoforms demonstrated AUC values of >0.98 for IgG, demonstrating their high suitability as diagnostic antigens to detect a specific immune response

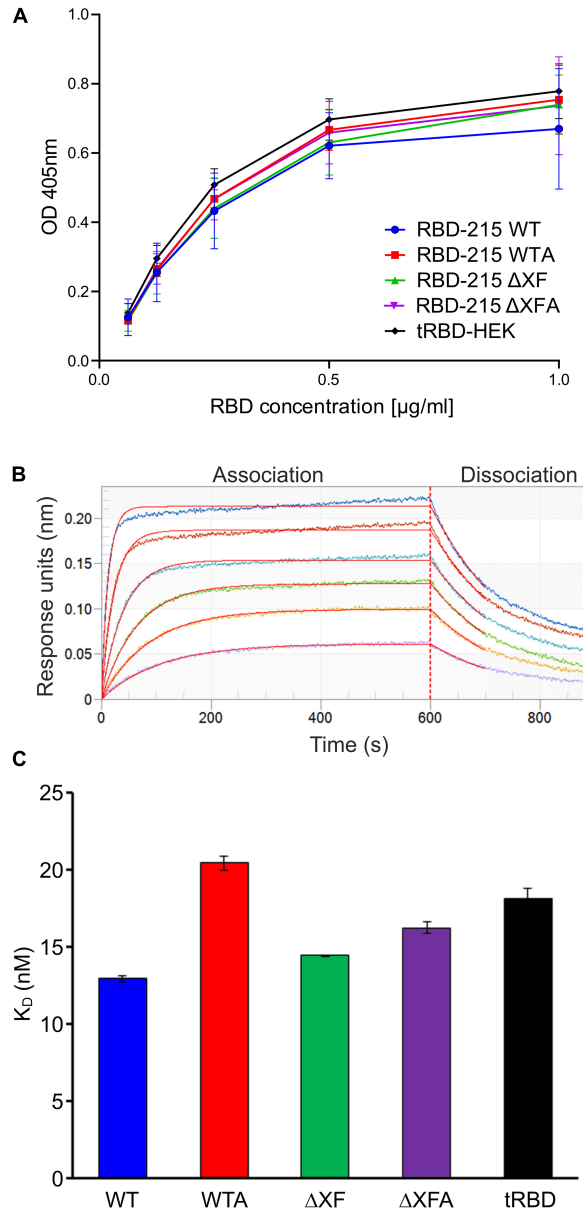

FIGURE 3 | RBD-215 glycoforms display binding to ACE2-Fc. **(A)** ACE2-Fc ELISA. Binding curves of different concentrations of purified RBD-215 glycoforms and HEK293-derived tRBD (tRBD-HEK, positive control, Klausberger et al., 2021) to plates coated with ACE2-Fc. Values represent the mean ± SD (n = 3). **(B)** BLI analysis. Binding kinetics of the interaction between biotinylated ACE2-Fc loaded on SAX biosensors and SEC-purified monomeric RBD-215 glycoforms at a concentration range of 6.25–200 nM were determined. Representative real-time association and dissociation curves for RBD-215 ΔXF are shown. The individual curves show the association/dissociation at different concentrations of RBD-215 ΔXF. **(C)** K_D values for the interactions between ACE2-Fc and the RBD-215 glycoforms. tRBD-HEK is included for comparison. Values represent the mean ± SEM (n = 3).

against SARS-CoV-2 (**Figure 4D** and **Supplementary Table 2**). Comparable AUC values for IgG were recently reported for tRBD produced in HEK293 cells using the same experimental

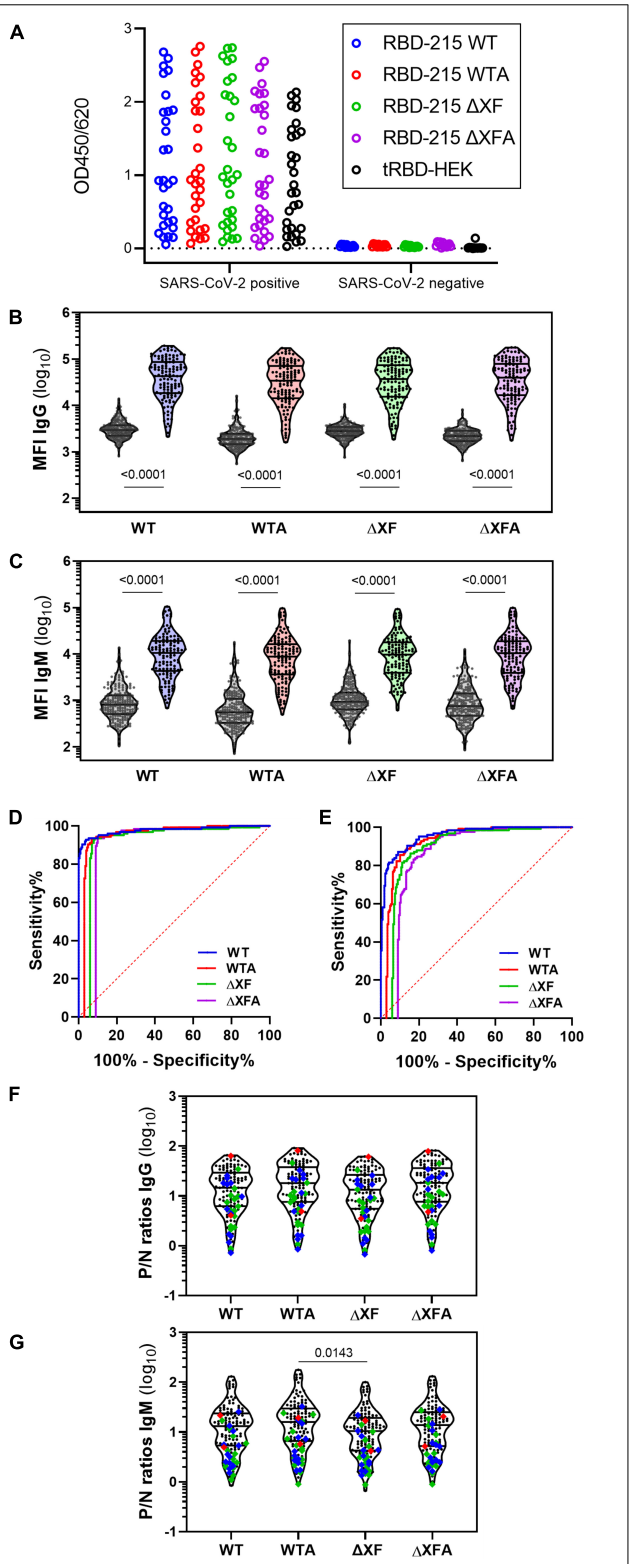

FIGURE 4 | IgG and IgM antibody binding to the RBD-215 variants. **(A)** Reactivity with convalescent sera (SARS-CoV-2 positive, n = 30) and pre-COVID controls (SARS-CoV-2 negative, n = 12) with RBD-215 glycoforms and HEK293-produced tRBD. Data give the mean of three blank-corrected

(Continued)

FIGURE 4 | (Continued)
replicates. **(B,C)** A bead-based multiplexed seroassay using 124 convalescent sera from individuals with previous SARS-CoV-2 infection and 210 pre-pandemic sera. Violin plots give the IgG **(B)** and IgM **(C)** immunoreactivity of individual sera as median fluorescence intensity (MFI). Lines indicate the median and quartiles. A non-parametric two-tailed Mann–Whitney *U*-test was used to compare group medians of pre-pandemic and convalescent sera. **(D,E)** An overlay of the areas under the receiver-operating characteristic curve (AUC-ROC) is given for the IgG **(D)** and IgM **(E)** seroreactivity of all RBD-215 glycoforms. To ease visualization, ROC curves were horizontally nudged in respect to the ROC curve of RBD-215 WT. **(F,G)** The positive/negative (*P*/*N*) ratio of the MFI readout of each convalescent serum compared to the median of the pre-pandemic group is given for IgG and IgM. Data on the courses of disease (as per self-assessment) were color-coded (green: asymptomatic-mild, blue-moderate, red-severe; $n = 28$). Mean ranks of all groups were compared using the non-parametric Kruskal–Wallis test, followed by a Dunn's *post hoc* test.

setup (Klausberger et al., 2021). For IgM the AUC levels were slightly lower (approximately 0.95) but comparable for all four RBD-215 antigens (**Figure 4E** and **Supplementary Table 2**). The positive/negative (*P*/*N*) ratios of convalescent sera were also similar, when compared to the median of the pre-pandemic group (**Figures 4F,G**).

Effect of Anti-carbohydrate Antibodies on the Antibody Reactivity to Plant-Produced RBD-215 Glycoforms in Serological Assays

To gain more information on the potential role of the β1,2-xylose and core α1,3-fucose and the contribution of the Lewis A structure to seroreactivity to the RBD-215 glycoforms, we analyzed a smaller cohort of sera from SARS-CoV-2 exposed ($n = 30$) and sera from non-exposed ($n = 12$) individuals for the presence of IgG antibodies to CCDs by ELISA (**Figure 5A**). One serum from a SARS-CoV-2 exposed individual (P1 in **Supplementary Table 3**) displayed high CCD reactivity to the MUXF3-HSA, in a range that was comparable to the reactivity of the control sera from the two CCD-sensitized allergic individuals. In addition, a few other sera of the SARS-CoV-2 exposed individuals displayed moderately increased reactivity indicating that CCD reactivity of CCD-sensitized individuals might contribute to the signals obtained in SARS-CoV-2 assays when using RBD-215 WT (**Figure 5A** and **Supplementary Table 3**). However, a closer look at the IgG reactivity of the MUXF3-HSA positive serum P1 to the RBD-215 glycoforms did not reveal major differences between the plant-specific RBD-215 glycoforms and tRBD produced in HEK293 cells (**Supplementary Figure 1**). The number of individuals with anti-CCD antibodies against β1,2-xylose and core α1,3-fucose was quite low in our cohort of SARS-CoV-2 exposed and non-exposed patients.

To assess how much of the antibody reactivity to RBD-215 glycoforms was directed against CCDs, we therefore concentrated on a selected group of sera that had been collected in the pre-COVID-19 era from fifteen allergic individuals with known CCD-reactivity. The majority of these sera displayed increased

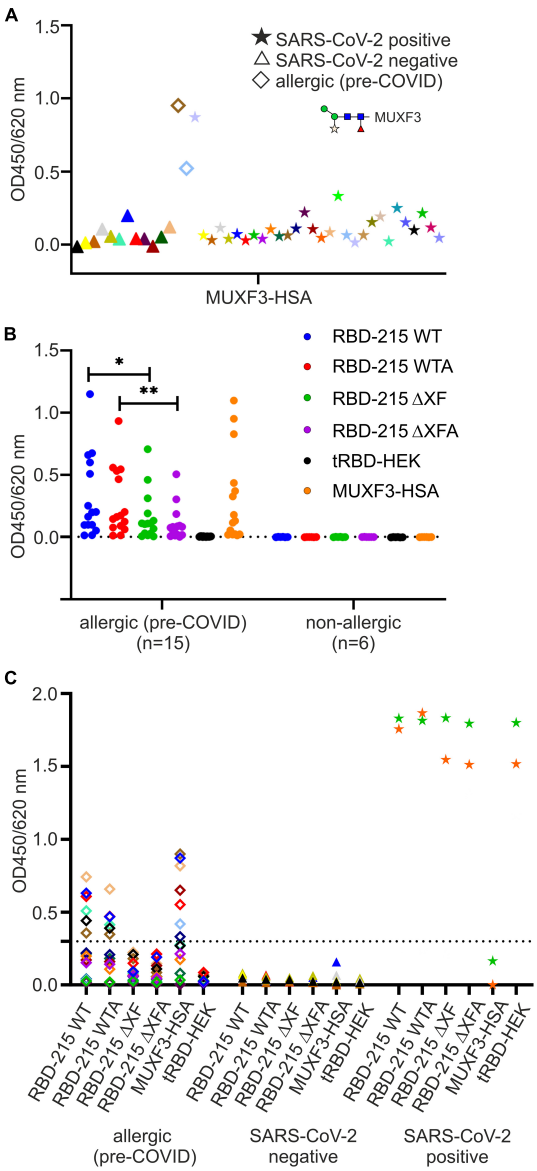

FIGURE 5 | Detection of anti-carbohydrate antibodies binding to the RBD glycoforms. **(A)** Screening for anti-carbohydrate IgG antibodies in sera of SARS-CoV-2 positive ($n = 30$) and negative ($n = 12$) individuals. As antigen we used the *N*-glycan MUXF3 coupled to human serum albumin (MUXF3-HSA), because it represents a well-characterized model CCD, recognized by the vast majority of sera from CCD positive patients. Two (non-exposed) sera of allergic individuals sensitized to CCDs (allergic) served as positive controls. **(B)** Screening (IgE antibody reactivity) of a panel of sera from allergic individuals (CCD-positive, $n = 15$) to RBD-215 glycoforms, tRBD and MUXF-HSA. Sera from non-exposed non-allergic individuals ($n = 6$) served as negative controls. Data are presented as the mean of three replicates. Differences between seroreactivity to RBD-215 WT and RBD-215 ΔXF as well as for RBD-215 WTA and RBD-215 ΔXFA were tested for significance using a Student's *t*-test (*$p < 0.05$, **$p < 0.01$). The dashed line represents the mean from non-allergic sera plus three times the standard deviation. **(C)** IgG reactivity of allergic ($n = 15$), SARS-CoV-2 negative ($n = 7$) and of SARS-CoV-2 positive patients ($n = 2$) to the RBD-215 glycoforms, to MUXF-HSA and to tRBD. Data represent the mean of three blank-corrected replicates. The dashed line represents the mean from allergic sera to RBD-215 ΔXF/A plus three times the standard deviation.

IgE levels, not only to MUXF3-HSA, but also to RBD-215 WT and RBD-215 WTA (**Figure 5B** and **Supplementary Table 4**). While the reactivity to RBD-215 ΔXF and RBD-215 ΔXFA was significantly reduced (RBD-215 WT $p < 0.05$, RBD-215 WTA $p < 0.01$), IgE binding in most sera was still higher than that obtained for tRBD produced in HEK293 cells. Next, we determined the binding of IgG antibodies present in sera from the selected allergic individuals to the RBD-215 glycoforms. Six out of fifteen individuals displayed increased IgG levels to RBD-215 WT and RBD-215 WTA, but strongly reduced reactivity to RBD-215 ΔXF and RBD-215 ΔXFA, respectively (**Figure 5C** and **Supplementary Table 5**). Despite overall reduced antibody binding capacity, the variants without plant-specific *N*-glycans showed higher antibody reactivity than the HEK293-produced tRBD. This might be due to the residual occurrence of small amounts of β1,2-xylose and core α1,3-fucose in material produced in the ΔXT/FT line, as these *N*-glycans are completely absent in HEK293 cells. The presence of the Lewis A epitope, on the other hand, had no apparent impact on antibody reactivity, suggesting that for the selected cases, it is not an immunogenic epitope. Our data show that in rare cases the presence of plant-specific modifications on viral glycoproteins could lead to false positive results in diagnostic SARS-CoV-2 antibody tests. To overcome this shortcoming, we tested the use of a CCD-inhibitor for samples which showed an increased reactivity to RBD-215 WT, but were taken in the pre-COVID era. By pre-incubating the selected sera with the model CCD, MUXF3-HSA, the IgG antibody binding capacity in all sera from allergic individuals was – on average – reduced by 90%, to a similar level as observed with HEK293 derived recombinant tRBD, which is completely devoid of β1,2-xylose and/or core α1,3-fucose residue containing *N*-glycans (**Figure 6** and **Supplementary Table 6**).

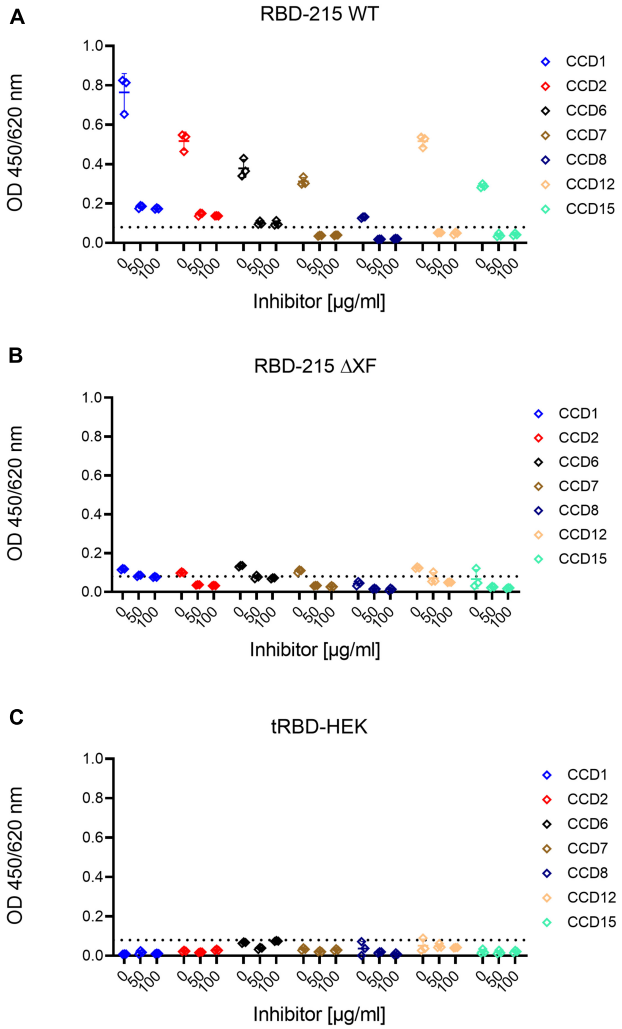

FIGURE 6 | Inhibition of anti-carbohydrate IgG antibody binding by pre-incubation with MUXF3-HSA. Highly reactive sera were pre-incubated with different concentrations of MUXF3-HSA to block the binding to core α1,3-fucose and β1,2-xylose present on RBD-215 glycoforms produced in **(A)** wild-type and **(B)** ΔXT/FT plants and **(C)** HEK293 cells. The base line (dashed line) was defined as the highest signal obtained with HEK293-derived tRBD.

DISCUSSION

A limitation of wild-type plant-produced recombinant viral antigens for serological assays is the possibility of false positives in allergic persons with antibodies against CCDs. Here, we confirm that recombinant RBD glycovariants transiently produced in *N. benthamiana* can be used as antigens in serological assays to monitor the specific antibody response against SARS-CoV-2 (Makatsa et al., 2021). Using the same set of convalescent and pre-COVID-19 sera, the antibody reactivity to *N. benthamiana* produced RBD variants was overall comparable to the antibody reactivity to RBD variants produced in other expression systems (Klausberger et al., 2021). The plant-produced RBD variants can also be used in assays with sera from individuals vaccinated with vaccines based on the SARS-CoV-2 spike glycoprotein. The different *N*-glycans attached to the plant-produced RBD variants do not alter the binding kinetics to ACE2-Fc. In fact, their affinities are comparable to tRBD produced in mammalian cells. Owing to these similar performance characteristics with ACE2-Fc, plant-produced RBD can be employed for SARS-CoV-2 surrogate virus neutralization tests (Tan et al., 2020).

Interference by carbohydrates in immunological tests is still often ignored. Yet, recombinant RBDs from different expression systems may contain carbohydrate epitopes that can be recognized by anti-carbohydrate antibodies that are commonly found in humans. Glycosylation of viral antigens depends on the host glycosylation machinery. For instance, the alpha-Gal epitope is another well-characterized carbohydrate moiety that is common in many non-human mammalian cell lines, but not present in plants (Butler and Spearman, 2014; Dicker and Strasser, 2015; Román-Carrasco et al., 2020). Furthermore, mammalian cell-based production systems, like CHO cells, can produce low levels of *N*-glycans carrying the sialic acid *N*-glycolylneuraminic acid (Neu5Gc). Neu5Gc is absent in humans due to a specific gene defect and humans have high levels of circulating anti-Neu5Gc antibodies (Yehuda and Padler-Karavani, 2020). Insect cells, on the other hand, produce

recombinant glycoproteins with core α1,3-fucose that is also found in plants (Altmann, 1997). In a recent study, these specific protein modifications are thought to have caused an increased tendency toward false-positives than RBD variants derived from other non-human or human expression systems (Klausberger et al., 2021). Except for human cell lines such as HEK293, all these expression systems can potentially lead to the production of viral antigens with non-human and thus, potentially immunogenic glycan epitopes.

Therefore, the controlled modification of glycosylation pathways in expression systems, generally known as glycoengineering, is one way to circumvent given issues. Here, we show that the expression of RBD-215 in *N. benthamiana* ΔXT/FT plants, which have silenced α1,2-xylosyltransferase and core α1,3-fucosyltransferase gene expression, can reduce the seroreactivity of anti-CCD antibody bearing sera. Additionally, the use of 100 μg/ml of the described CCD blocker led to an average 90% inhibition of anti-CCD IgG antibodies in the serum of a set of selected CCD-positive patients. The inhibitor constitutes one way to circumvent given issues and can be used to avoid false positives with sera from allergic individuals sensitized to CCDs (Aberer et al., 2017). Moreover, it is now possible to produce viral antigens such as RBD in genome edited plants or plant cells that are completely devoid of β1,2-xylose and α1,3-fucose (Hanania et al., 2017; Mercx et al., 2017; Jansing et al., 2019; Herman et al., 2021). Alternatively, RBD and other glycosylated viral antigens can be manufactured in the presence of a pharmacological glycosylation inhibitor such as kifunensine which blocks α-mannose trimming from oligomannosidic *N*-glycans and thus the formation of processed complex *N*-glycans (Xiong et al., 2018; Kommineni et al., 2019; Shin et al., 2021). The retention of recombinant glycoproteins in the ER by attachment of a C-terminal HDEL/KDEL tetrapeptide is another frequently used strategy to avoid potential limitations associated with processing into complex *N*-glycans, which requires delivery of the respective glycoprotein to the Golgi apparatus (Ko et al., 2003; Petruccelli et al., 2006; Diego-Martin et al., 2020).

In contrast to *N*-glycans carrying β1,2-xylose and core α1,3-fucose, we provide an indication that *N*-glycans containing Lewis A epitopes are apparently not associated with elevated unspecific seroreactivity. Hence, plant-derived Lewis A appears not to be immunogenic suggesting that humans do not carry considerable amounts of anti-carbohydrate IgG and IgM antibodies directed against plant complex *N*-glycans with Lewis A structures. Lewis A structures are abundant on human glycolipids and are therefore not likely to be recognized as foreign, when presented on recombinant proteins (Gagneux and Varki, 1999). When produced in wild type plants overexpressing GALT1 and FUT13, the seroreactivity of CCD-positive individuals was reduced, suggesting that the Lewis A epitope masks CCD epitopes. This is in line with other studies showing altered immunoreactivity with β1,2-xylose and core α1,3-fucose when untrimmed mannoses are present on the α1,6-arm of *N*-glycans (Kaulfürst-Soboll et al., 2011) or trimming of GlcNAc residues is blocked (Liebminger et al., 2011). The reduced reactivity could be caused by the presence of decreased amounts of MMXF structures that are mainly recognized by anti-CCD antibodies (Jin et al., 2008).

In summary, the data shown here are relevant for the plant-based production of glycosylated viral antigens and demonstrate the suitability of all plant-produced glycoforms investigated in this study for SARS-CoV-2 serological assays, using 124 convalescent sera from individuals with previous SARS-CoV-2 infection and 210 pre-pandemic sera. Only when using a pre-selected cohort of sera from allergic persons with antibodies against CCDs, our data also point to a limitation of wild-type plant-produced recombinant viral antigens for serological assays. In these rare cases, the anti-CCD signals measured may be interpreted as false positive SARS-CoV-2 signals; however, this is easily reduced through the use of glycoengineered production plants and/or CCD-inhibitors. Plants therefore offer a valuable contribution to the production of recombinant viral antigens, which are needed worldwide in large amounts for serological assays to monitor the quality and longevity of the antibody response or in surrogate assays to determine titers of neutralizing antibodies (Tan et al., 2020), which represents a key indicator of protection against viruses. Furthermore, the fast transient expression of viral antigens in *N. benthamiana* allows to quickly respond to the evolution of viruses during a pandemic, for example to produce RBDs corresponding to SARS-CoV-2 variants of concerns.

MATERIALS AND METHODS

Protein Expression and Purification

The generation of the pEAQ-*HT* expression vectors for RBD-215 was described previously (Shin et al., 2021). Syringe-mediated agroinfiltration of leaves from 5-week-old *N. benthamiana* wild-type or ΔXT/FT was used for transient expression of RBD-215 variants (Strasser et al., 2008). For the generation of the Lewis A structures, p43-GALT1 (*A. thaliana* β1,3-galactosyltransferase fused to an HA-tag) and p47-FUT13 (expression of *A. thaliana* β1,4-fucosyltransferase fused to GFP) were co-expressed by mixing of the agrobacteria prior to agroinfiltration. In both vectors, expression is under the control of the *A. thaliana ubiquitin 10* promoter.

For RBD purification, leaves were harvested 3 days after infiltration and intracellular fluid was collected by low-speed centrifugation as described in detail previously (Castilho et al., 2011). His-tagged RBD-215 was purified from collected intracellular fluid using a 5-ml HisTrap HP column (Sigma-Aldrich). Elution with imidazole, dialysis against phosphate-buffered saline solution (PBS) and concentration by ultracentrifugation was carried out as described in detail previously (Göritzer et al., 2019; Shin et al., 2021). Expression and purification of truncated RBD-His (tRBD) and ACE2-Fc in HEK293 cells has been described recently (Castilho et al., 2021; Klausberger et al., 2021).

Immunoblot Analysis

Purified proteins were subjected to SDS-PAGE under reducing or non-reducing conditions. Samples to be analyzed under

non-reducing conditions were not boiled prior to loading. Separated proteins were either stained with Coomassie Brilliant Blue (Sigma-Aldrich) or transferred to a nitrocellulose membrane (Cytiva) and detected using anti-His (Thermo Fisher Scientific), anti-HRP (Sigma-Aldrich), or JIM84 (Strasser et al., 2007) antibodies.

Liquid Chromatography-Electrospray Ionization-Mass Spectrometry (LC-ESI-MS)

Purified RBD-215 proteins were *S*-alkylated with iodoacetamide and digested in solution with endoproteinases LysC (Roche) and GluC (Promega). Digested samples were analyzed using a maXis 4G QTOF mass spectrometer (Bruker) as described (Klausberger et al., 2021).

ACE2-Fc Binding ELISA

ELISA was carried out according to standard protocols. Briefly, 96-well plates (Nunc MaxiSorp^{TM}, Thermo Fisher) were coated overnight at 4°C with 250 ng/well of in-house produced ACE2-Fc in PBS. Plates were washed three times with PBS containing 0.1% (v/v) Tween-20 (PBS-T) using an automated plate washer. All subsequent steps were carried out at room temperature (RT). Wells were blocked for 1 h with PBS-T containing 3% (w/v) milk powder (MP-PBS-T). From an initial concentration of 1 μg/ml, a twofold serial dilution of the antigen samples was performed in blocking solution. After washing the plates three times with PBS-T, antigen samples were incubated for 2 h. Next, plates were washed three times and incubated for 2 h with mouse-anti-His-6 (1:2,000; Invitrogen) diluted in 3% (w/v) MP-PBS-T. Plates were washed again and incubated for 1 h with anti-mouse-HRP (1:2,500; Promega). After washing plates three times with PBS-T, 100 μl of 0.2 mM 2,2′-azino-bis(3-ethylbenzothiazoline-6-sulfonic acid) (ABTS; Sigma-Aldrich) in 50 mM phosphate-citrate buffer pH 5 was added and the reaction was stopped with 100 μl of 1% (w/v) SDS. The optical density (OD) of the ABTS oxidation reaction was measured at 405 nm. Background resulting from unspecific binding of detection antibodies was subtracted from the obtained values. Three technical replicates were performed. Data was analyzed using GraphPad Prism Version 9.0.0.

Biolayer Interferometry Measurements

Interaction studies of RBD-215 with in-house produced biotinylated ACE2-Fc (Klausberger et al., 2021) was performed on an Octet RED96e system using high precision streptavidin biosensors (FortéBio). All assays were conducted in PBS supplemented with 0.05% (v/v) Tween 20 and 0.1% (w/v) BSA (PBST-BSA) at 25°C with the plate shaking at 1,000 rpm. The biosensors were equilibrated in PBST-BSA followed by dipping into a 34 nM solution of the respective biotinylated ACE2-Fc molecule. To determine dissociation constant (K_d) values, titration of RBD-215 was performed to cover a broad concentration range around the respective K_d value. To record association rates, ACE2-loaded biosensors were submerged into twofold (6.25–200 nM) serial dilutions of RBD variants for 600 s. For dissociation, the biosensors were dipped into PBST-BSA for 100 s. Each experiment was performed in triplicates. Data were evaluated using the Octet data analysis software version 11.1.1.39 as previously described (Klausberger et al., 2021).

Luminex Assays

The four RBD-215 glycoforms were separately coupled to MagPlex carboxylated polystyrene microspheres (Luminex Corporation) according to the manufacturer's instructions, with the following minor modifications: 5 μg of each RBD-215 antigen was used for coupling per one million microspheres. Coupling was performed in a total volume of 500 μl in 96-Well Protein LoBind Deepwell plates (Eppendorf) and plates were incubated at 600 rpm on a Heidolph Titramax 1000 plate shaker (Heidolph). The coupled glycoforms were assayed in parallel with pre-COVID19 sera and sera from SARS-CoV-2 infected individuals (AIT cohorts). The source of the sera and the assay were described in detail recently (Klausberger et al., 2021).

Measurement of IgG Antibody Responses to Receptor Binding Domains and MUXF3-HSA

ELISAs with convalescent and pre-COVID sera were carried out as described (Klausberger et al., 2021). Briefly, the respective MaxiSorp^{TM} 96-well plates were coated with 0.3 μg/well SARS-CoV-2 antigen or MUXF3-HSA (ProGlycAn) and incubated overnight at 4°C. Plates were washed 3 times with PBS-T and blocked for 1 h at RT with 3% (w/v) MP-PBS-T. Serum samples were diluted 1:200 in 1% (w/v) MP-PBS-T, 100 μl/well applied to assay plates and incubated for 2 h at RT while shaking. For inhibition of anti-CCD antibodies, 50–100 μg/ml of MUXF3-HSA was added to sera and pre-incubated for 30 min at RT. Plates were washed 4 times and incubated with anti-human IgG-HRP [Fc-specific, Sigma, 1:50000 in 1% (w/v) MP-PBS-T, 50 μl/well] for 1 h at RT while shaking. After washing for 4 times, freshly prepared substrate solution [substrate buffer (10 mM sodium acetate, pH 5 + 1:60 diluted TMB-stock solution (0.4% (w/v) tetramethylbenzidine (Fluka) in DMSO) + 1:300 diluted H_2O_2 (0.6% (v/v) in H_2O))] was applied (150 μl/well) and incubated for 25 min at RT while shaking. Reactions were stopped with 25 μl/well sulfuric acid (1M, VWR) and their absorbance measured at 450 nm (reference wavelength: 620 nm) on a Tecan Sunrise reader using Magellan V 7.2 SP1 software. Data are presented as the mean of three replicates. For data analysis and visualization GraphPad Prism 9.0.0 was used.

Detection of Anti-CCD IgE Antibodies

The source of sera from allergic individuals was described in a previous study (Román-Carrasco et al., 2020). MaxiSorp^{TM} 96-well plates were coated o/n at 4°C with 0.25 μg/well of SARS-CoV-2 antigens and MUXF3-HSA. MUXF3 is a well characterized model CCD, recognized by the vast majority of CCD positive

individuals, because it contains the *N*-glycan structures known to be involved in IgE binding to CCDs: α1,3-fucose and β1,2-xylose (Holzweber et al., 2013). For blocking of the ELISA plates and for dilution of the sera and of the antibodies 0.1% HSA in PBS-T was used. Plates were blocked for 2.5 h at 37°C. After washing the plates with PBS-T, sera (diluted 1:20) were incubated o/n at 4°C while shaking. After washing of the plates, IgE binding was detected with an HRP-labeled monoclonal anti-human IgE antibody (1:5000; 2 h; SouthernBiotech, Birmingham, AL, United States). After washing the plates three times with PBS-T, freshly prepared TMB substrate solution was applied (150 µl/well) and samples were analyzed as described above. Data are presented as the mean of three replicates. For data analysis and visualization GraphPad Prism 9.0.0 was used. Student's *t*-test was used to identify differences between RBD-215 WT and RBD-215 ΔXF, as well as between RBD-215 WTA and RBD-215 ΔXFA.

DATA AVAILABILITY STATEMENT

The raw data supporting the conclusions of this article will be made available by the authors, without undue reservation.

ETHICS STATEMENT

The studies involving human participants were reviewed and approved by Ethics Committee Medical University of Vienna, Borschkegasse 8b/E06, 1090 Vienna; Ethics Committee City of Vienna, Thomas-Klestil-Platz 8, 1030 Vienna. Written informed consent for participation was not required for this study in accordance with the national legislation and the institutional requirements.

AUTHOR CONTRIBUTIONS

JS, JK-B, Y-JS, UV, NK, CG-G, DM, EL, MS, GM, JH, MH, and KV conducted the experiments. JS, MK, EL, CG-G, AW, IS, WG, FG, FA, LM, ES, and RS analyzed the results. JS, FG, FA, LM, ES, and RS supervised and designed the experiments. IS, AW, and CB provided material. JS and RS conceptualized the study and wrote the manuscript with support from MK, FG, IS, LM, and ES. All authors have made a substantial and intellectual contribution to the work and approved it for publication.

FUNDING

This work was supported by the Austrian Science Fund (FWF) Project P31920-B32 and the Doctoral Program BioToP–Biomolecular Technology of Proteins (W1224-B09). This project was supported by the BOKU COVID-19 Initiative and the BOKU Core Facilities Biomolecular & Cellular Analysis and Mass Spectrometry. This study received funding from Equipment-BOKU Vienna Institute of Biotechnology (EQ-BOKU VIBT) GmbH. The EQ-BOKU VIBT was not involved in the study design, collection, analysis, interpretation of data, the writing of this article or the decision to submit it for publication. All authors declare no other competing interests.

ACKNOWLEDGMENTS

We thank George Lomonossoff (John Innes Centre, Norwich, United Kingdom) and Plant Bioscience Limited (PBL) (Norwich, United Kingdom) for supplying the pEAQ-*HT* expression vector and Rudolf Figl for assisting in the preparation of CCD inhibitor. HEK293 cell-derived tRBD protein was kindly provided through the BOKU COVID-19 platform (https://portal.boku-covid19.at/), which enables researcher easy access to COVID-related protein reagents.

SUPPLEMENTARY MATERIAL

The Supplementary Material for this article can be found online at: https://www.frontiersin.org/articles/10.3389/fpls.2021.747500/full#supplementary-material

REFERENCES

Aberer, W., Holzweber, F., Hemmer, W., Koch, L., Bokanovic, D., Fellner, W., et al. (2017). Inhibition of cross-reactive carbohydrate determinants (CCDs) enhances the accuracy of in vitro allergy diagnosis. *Allergol. Select.* 1, 141–149. doi: 10.5414/ALX01638E

Allen, J. D., Chawla, H., Samsudin, F., Zuzic, L., Shivgan, A. T., Watanabe, Y., et al. (2021). Site-specific steric control of SARS-CoV-2 spike glycosylation. *Biochemistry* 60, 2153–2169. doi: 10.1021/acs.biochem.1c00279

Altmann, F. (1997). More than silk and honey–or, can insect cells serve in the production of therapeutic glycoproteins? *Glycoconj. J.* 14, 643–646.

Altmann, F. (2007).). The role of protein glycosylation in allergy. *Int. Arch. Allergy Immunol.* 142, 99–115.

Altmann, F. (2016). Coping with cross-reactive carbohydrate determinants in allergy diagnosis. *Allergo J. Int.* 25, 98–105. doi: 10.1007/s40629-016-0115-3

Amanat, F., Stadlbauer, D., Strohmeier, S., Nguyen, T. H. O., Chromikova, V., McMahon, M., et al. (2020). A serological assay to detect SARS-CoV-2 seroconversion in humans. *Nat. Med.* 26, 1033–1036. doi: 10.1038/s41591-020-0913-5

Azad, T., Singaravelu, R., Taha, Z., Jamieson, T. R., Boulton, S., Crupi, M. J. F., et al. (2021). Nanoluciferase complementation-based bioreporter reveals the importance of N-linked glycosylation of SARS-CoV-2 S for viral entry. *Mol. Ther.* 29, 1984–2000. doi: 10.1016/j.ymthe.2021.02.007

Bardor, M., Faveeuw, C., Fitchette, A., Gilbert, D., Galas, L., Trottein, F., et al. (2003). Immunoreactivity in mammals of two typical plant glyco-epitopes, core alpha(1,3)-fucose and core xylose. *Glycobiology* 13, 427–434.

Beihammer, G., Maresch, D., Altmann, F., Van Damme, E. J. M., and Strasser, R. (2021). Lewis A glycans are present on proteins involved in cell wall biosynthesis and appear evolutionarily conserved among natural. *Front. Plant Sci.* 12:630891. doi: 10.3389/fpls.2021.630891

Butler, M., and Spearman, M. (2014). The choice of mammalian cell host and possibilities for glycosylation engineering. *Curr. Opin. Biotechnol.* 30, 107–112. doi: 10.1016/j.copbio.2014.06.010

Capell, T., Twyman, R. M., Armario-Najera, V., Ma, J. K., Schillberg, S., and Christou, P. (2020). Potential applications of plant biotechnology against

SARS-CoV-2. *Trends Plant Sci.* 25, 635–643. doi: 10.1016/j.tplants.2020.04.009

Castilho, A., Gattinger, P., Grass, J., Jez, J., Pabst, M., Altmann, F., et al. (2011). N-glycosylation engineering of plants for the biosynthesis of glycoproteins with bisected and branched complex N-glycans. *Glycobiology* 21, 813–823.

Castilho, A., Neumann, L., Gattinger, P., Strasser, R., Vorauer-Uhl, K., Sterovsky, T., et al. (2013). Generation of biologically active multi-sialylated recombinant human EPOFc in plants. *PLoS One* 8:e54836. doi: 10.1371/journal.pone.0054836

Castilho, A., Schwestka, J., Kienzl, N. F., Vavra, U., Grünwald-Gruber, C., Izadi, S., et al. (2021). Generation of enzymatically competent SARS-CoV-2 decoy receptor ACE2-Fc in glycoengineered Nicotiana benthamiana. *Biotechnol. J.* 16:e2000566. doi: 10.1002/biot.202000566

Castro, R., Nobre, L. S., Eleutério, R. P., Thomaz, M., Pires, A., Monteiro, S. M., et al. (2021). Production of high-quality SARS-CoV-2 antigens: impact of bioprocess and storage on glycosylation, biophysical attributes, and ELISA serologic tests performance. *Biotechnol. Bioeng.* 118, 2202–2219. doi: 10.1002/bit.27725

Dicker, M., and Strasser, R. (2015). Using glyco-engineering to produce therapeutic proteins. *Expert Opin. Biol. Ther.* 15, 1501–1516. doi: 10.1517/14712598.2015.1069271

Diego-Martin, B., González, B., Vazquez-Vilar, M., Selma, S., Mateos-Fernández, R., Gianoglio, S., et al. (2020). Pilot production of SARS-CoV-2 related proteins in plants: a proof of concept for rapid repurposing of indoor farms into biomanufacturing facilities. *Front. Plant Sci.* 11:612781. doi: 10.3389/fpls.2020.612781

Fitchette, A., Cabanes-Macheteau, M., Marvin, L., Martin, B., Satiat-Jeunemaitre, B., Gomord, V., et al. (1999). Biosynthesis and immunolocalization of Lewis a-containing N-glycans in the plant cell. *Plant Physiol.* 121, 333–344.

Gagneux, P., and Varki, A. (1999). Evolutionary considerations in relating oligosaccharide diversity to biological function. *Glycobiology* 9, 747–755. doi: 10.1093/glycob/9.8.747

Göritzer, K., Turupcu, A., Maresch, D., Novak, J., Altmann, F., Oostenbrink, C., et al. (2019). Distinct Fcα receptor N-glycans modulate the binding affinity to immunoglobulin A (IgA) antibodies. *J. Biol. Chem.* 294, 13995–14008. doi: 10.1074/jbc.RA119.009954

Hanania, U., Ariel, T., Tekoah, Y., Fux, L., Sheva, M., Gubbay, Y., et al. (2017). Establishment of a tobacco BY2 cell line devoid of plant-specific xylose and fucose as a platform for the production of biotherapeutic proteins. *Plant Biotechnol. J.* 15, 1120–1129. doi: 10.1111/pbi.12702

Herman, X., Far, J., Courtoy, A., Bouhon, L., Quinton, L., De Pauw, E., et al. (2021). Inactivation of N-Acetylglucosaminyltransferase I and α1,3-Fucosyltransferase genes in *Nicotiana tabacum* BY-2 Cells results in glycoproteins with highly homogeneous. High-Mannose N-Glycans. *Front. Plant Sci.* 12:634023. doi: 10.3389/fpls.2021.634023

Holzweber, F., Svehla, E., Fellner, W., Dalik, T., Stubler, S., Hemmer, W., et al. (2013). Inhibition of IgE binding to cross-reactive carbohydrate determinants enhances diagnostic selectivity. *Allergy* 68, 1269–1277. doi: 10.1111/all.12229

Jansing, J., Sack, M., Augustine, S. M., Fischer, R., and Bortesi, L. (2019). CRISPR/Cas9-mediated knockout of six glycosyltransferase genes in *Nicotiana benthamiana* for the production of recombinant proteins lacking β-1,2-xylose and core α-1,3-fucose. *Plant Biotechnol. J.* 17, 350–361. doi: 10.1111/pbi.12981

Jin, C., Altmann, F., Strasser, R., Mach, L., Schähs, M., Kunert, R., et al. (2008). A plant-derived human monoclonal antibody induces an anti-carbohydrate immune response in rabbits. *Glycobiology* 18, 235–241. doi: 10.1093/glycob/cwm137

Jin, C., Bencúrová, M., Borth, N., Ferko, B., Jensen-Jarolim, E., Altmann, F., et al. (2006). Immunoglobulin G specifically binding plant N-glycans with high affinity could be generated in rabbits but not in mice. *Glycobiology* 16, 349–357.

Kaulfürst-Soboll, H., Rips, S., Koiwa, H., Kajiura, H., Fujiyama, K., and von Schaewen, A. (2011). Reduced immunogenicity of *Arabidopsis* hgl1 mutant N-glycans caused by altered accessibility of xylose and core fucose epitopes. *J. Biol. Chem.* 286, 22955–22964. doi: 10.1074/jbc.M110.196097

Klausberger, M., Dürkop, M., Haslacher, H., Wozniak-Knopp, G., Cserjan-Puschmann, M., Perkmann, T., et al. (2021). A comprehensive antigen production and characterisation study for easy-to-implement, specific and quantitative SARS-CoV-2 serotests. *EBioMedicine* 67:103348. doi: 10.1016/j.ebiom.2021.103348

Ko, K., Tekoah, Y., Rudd, P. M., Harvey, D. J., Dwek, R. A., Spitsin, S., et al. (2003). Function and glycosylation of plant-derived antiviral monoclonal antibody. *Proc. Natl. Acad. Sci. U.S.A.* 100, 8013–8018. doi: 10.1073/pnas.0832472100

Kommineni, V., Markert, M., Ren, Z., Palle, S., Carrillo, B., Deng, J., et al. (2019). In Vivo Glycan engineering via the mannosidase I inhibitor (Kifunensine) improves efficacy of rituximab manufactured in *Nicotiana benthamiana* Plants. *Int. J. Mol. Sci.* 20:194. doi: 10.3390/ijms20010194

Kreer, C., Zehner, M., Weber, T., Ercanoglu, M. S., Gieselmann, L., Rohde, C., et al. (2020). Longitudinal isolation of potent near-germline SARS-CoV-2-Neutralizing antibodies from COVID-19 patients. *Cell* 182, 843–854. doi: 10.1016/j.cell.2020.06.044

Li, T., Zheng, Q., Yu, H., Wu, D., Xue, W., Xiong, H., et al. (2020). SARS-CoV-2 spike produced in insect cells elicits high neutralization titres in non-human primates. *Emerg. Microbes Infect.* 9, 2076–2090. doi: 10.1080/22221751.2020.1821583

Liebminger, E., Veit, C., Pabst, M., Batoux, M., Zipfel, C., Altmann, F., et al. (2011). {beta}-N-Acetylhexosaminidases HEXO1 and hexo3 are responsible for the formation of paucimannosidic N-Glycans in *Arabidopsis thaliana*. *J. Biol. Chem.* 286, 10793–10802.

Liu, L., Wang, P., Nair, M. S., Yu, J., Rapp, M., Wang, Q., et al. (2020). Potent neutralizing antibodies against multiple epitopes on SARS-CoV-2 spike. *Nature* 584, 450–456. doi: 10.1038/s41586-020-2571-7

Makatsa, M. S., Tincho, M. B., Wendoh, J. M., Ismail, S. D., Nesamari, R., Pera, F., et al. (2021). SARS-CoV-2 antigens expressed in plants detect antibody responses in COVID-19 patients. *Front. Plant Sci.* 12:589940. doi: 10.3389/fpls.2021.589940

Mercx, S., Smargiasso, N., Chaumont, F., De Pauw, E., Boutry, M., and Navarre, C. (2017). Inactivation of the β(1,2)-xylosyltransferase and the α(1,3)-fucosyltransferase genes in *Nicotiana tabacum* BY-2 cells by a multiplex CRISPR/Cas9 strategy results in glycoproteins without plant-specific glycans. *Front. Plant Sci.* 8:403. doi: 10.3389/fpls.2017.00403

Montero-Morales, L., and Steinkellner, H. (2018). Advanced plant-based glycan engineering. *Front. Bioeng. Biotechnol.* 6:81. doi: 10.3389/fbioe.2018.00081

Parsons, J., Altmann, F., Arrenberg, C. K., Koprivova, A., Beike, A. K., Stemmer, C., et al. (2012). Moss-based production of asialo-erythropoietin devoid of Lewis A and other plant-typical carbohydrate determinants. *Plant Biotechnol. J.* 10, 851–861. doi: 10.1111/j.1467-7652.2012.00704.x

Petruccelli, S., Otegui, M. S., Lareu, F., Tran Dinh, O., Fitchette, A. C., Circosta, A., et al. (2006). A KDEL-tagged monoclonal antibody is efficiently retained in the endoplasmic reticulum in leaves, but is both partially secreted and sorted to protein storage vacuoles in seeds. *Plant Biotechnol. J.* 4, 511–527. doi: 10.1111/j.1467-7652.2006.00200.x

Pinto, D., Park, Y. J., Beltramello, M., Walls, A. C., Tortorici, M. A., Bianchi, S., et al. (2020). Cross-neutralization of SARS-CoV-2 by a human monoclonal SARS-CoV antibody. *Nature* 583, 290–295. doi: 10.1038/s41586-020-2349-y

Platts-Mills, T. A., Hilger, C., Jappe, U., Hage, M., Gadermaier, G., Spillner, E., et al. (2021). Carbohydrate epitopes currently recognized as targets for IgE antibodies. *Allergy* 76, 2383–2394. doi: 10.1111/all.14802

Rattanapisit, K., Shanmugaraj, B., Manopwisedjaroen, S., Purwono, P. B., Siriwattananon, K., Khorattanakulchai, N., et al. (2020). Rapid production of SARS-CoV-2 receptor binding domain (RBD) and spike specific monoclonal antibody CR3022 in *Nicotiana benthamiana*. *Sci. Rep.* 10:17698. doi: 10.1038/s41598-020-74904-1

Román-Carrasco, P., Hemmer, W., Klug, C., Friedrich, A., Stoll, P., Focke-Tejkl, M., et al. (2020). Individuals with IgE antibodies to α-Gal and CCD show specific IgG subclass responses different from subjects non-sensitized to oligosaccharides. *Clin. Exp. Allergy* 50, 1107–1110. doi: 10.1111/cea.13695

Rup, B., Alon, S., Amit-Cohen, B. C., Brill Almon, E., Chertkoff, R., Tekoah, Y., et al. (2017). Immunogenicity of glycans on biotherapeutic drugs produced in plant expression systems-The taliglucerase alfa story. *PLoS One* 12:e0186211. doi: 10.1371/journal.pone.0186211

Sanda, M., Morrison, L., and Goldman, R. (2021). N- and O-Glycosylation of the SARS-CoV-2 Spike Protein. *Anal. Chem.* 93, 2003–2009. doi: 10.1021/acs.analchem.0c03173

Shajahan, A., Supekar, N. T., Gleinich, A. S., and Azadi, P. (2020). Deducing the N- and O- glycosylation profile of the spike protein of novel coronavirus SARS-CoV-2. *Glycobiology* 30, 981–988. doi: 10.1093/glycob/cwaa042

Shin, Y.-J., König-Beihammer, J., Vavra, U., Schwestka, J., Kienzl, N. K., Klausberger, M., et al. (2021). N-glycosylation of the SARS-CoV-2 receptor binding domain is important for plant-based expression. *Front. Plant Sci.* 12:689104. doi: 10.3389/fpls.2021.689104

Stoger, E., Fischer, R., Moloney, M., and Ma, J. K. (2014). Plant molecular pharming for the treatment of chronic and infectious diseases. *Annu. Rev. Plant Biol.* 65, 743–768. doi: 10.1146/annurev-arplant-050213-035850

Strasser, R., Altmann, F., Mach, L., Glössl, J., and Steinkellner, H. (2004). Generation of *Arabidopsis thaliana* plants with complex N-glycans lacking beta1,2-linked xylose and core alpha1,3-linked fucose. *FEBS Lett.* 561, 132–136.

Strasser, R., Bondili, J., Vavra, U., Schoberer, J., Svoboda, B., Glössl, J., et al. (2007). A unique beta1,3-galactosyltransferase is indispensable for the biosynthesis of N-glycans containing Lewis a structures in *Arabidopsis thaliana*. *Plant Cell* 19, 2278–2292.

Strasser, R., Stadlmann, J., Schähs, M., Stiegler, G., Quendler, H., Mach, L., et al. (2008). Generation of glyco-engineered *Nicotiana benthamiana* for the production of monoclonal antibodies with a homogeneous human-like N-glycan structure. *Plant Biotechnol. J.* 6, 392–402.

Sztain, T., Ahn, S. H., Bogetti, A. T., Casalino, L., Goldsmith, J. A., McCool, R. S., et al. (2021). A glycan gate controls opening of the SARS-CoV-2 spike protein. *bioRxiv* [Preprint]. doi: 10.1101/2021.02.15.431212

Tan, C. W., Chia, W. N., Qin, X., Liu, P., Chen, M. I., Tiu, C., et al. (2020). A SARS-CoV-2 surrogate virus neutralization test based on antibody-mediated blockage of ACE2-spike protein-protein interaction. *Nat. Biotechnol.* 38, 1073–1078. doi: 10.1038/s41587-020-0631-z

Uthailak, N., Kajiura, H., Misaki, R., and Fujiyama, K. (2021). Transient production of human β-glucocerebrosidase with mannosidic-type N-Glycan structure in glycoengineered *Nicotiana benthamiana* plants. *Front. Plant Sci.* 12:683762. doi: 10.3389/fpls.2021.683762

Wang, P., Ye, F., Zhao, J., Xu, P., Liu, X., Yu, J., et al. (2021). Synthetic homogeneous glycoforms of the SARS-CoV-2 spike receptor-binding domain reveals different binding profiles of monoclonal antibodies. *Angew. Chem. Int. Ed. Engl.* 60, 12904–12910. doi: 10.1002/anie.202100543

Watanabe, Y., Allen, J. D., Wrapp, D., McLellan, J. S., and Crispin, M. (2020). Site-specific glycan analysis of the SARS-CoV-2 spike. *Science* 369, 330–333. doi: 10.1126/science.abb9983

Xiong, X., Tortorici, M. A., Snijder, J., Yoshioka, C., Walls, A. C., Li, W., et al. (2018). Glycan shield and fusion activation of a deltacoronavirus spike glycoprotein fine-tuned for enteric infections. *J. Virol.* 92:e01628-17. doi: 10.1128/JVI.01628-17

Yang, J., Wang, W., Chen, Z., Lu, S., Yang, F., Bi, Z., et al. (2020). A vaccine targeting the RBD of the S protein of SARS-CoV-2 induces protective immunity. *Nature* 586, 572–577. doi: 10.1038/s41586-020-2599-8

Yehuda, S., and Padler-Karavani, V. (2020). Glycosylated biotherapeutics: immunological effects of N-Glycolylneuraminic acid. *Front. Immunol.* 11:21. doi: 10.3389/fimmu.2020.00021

Zhang, Y., Zhao, W., Mao, Y., Chen, Y., Wang, S., Zhong, Y., et al. (2021). Site-specific N-glycosylation characterization of recombinant SARS-CoV-2 spike proteins. *Mol. Cell Proteomics.* 20:100058. doi: 10.1074/mcp.RA120.002295

Zhao, P., Praissman, J. L., Grant, O. C., Cai, Y., Xiao, T., Rosenbalm, K. E., et al. (2020). Virus-receptor interactions of glycosylated SARS-CoV-2 spike and human ACE2 receptor. *Cell Host Microbe* 28, 586.e6–601.e6. doi: 10.1016/j.chom.2020.08.004

Conflict of Interest: JH, MH, KV, and AW were employed by AIT Austrian Institute of Technology GmbH. FA who developed the CCD inhibitor is in a commercial relationship with companies who sell the inhibitor.

The remaining authors declare that the research was conducted in the absence of any commercial or financial relationships that could be construed as a potential conflict of interest.

Publisher's Note: All claims expressed in this article are solely those of the authors and do not necessarily represent those of their affiliated organizations, or those of the publisher, the editors and the reviewers. Any product that may be evaluated in this article, or claim that may be made by its manufacturer, is not guaranteed or endorsed by the publisher.

frontiers in Plant Science

ORIGINAL RESEARCH
published: 28 January 2022
doi: 10.3389/fpls.2021.794999

Plant-Derived Cell-Free Biofactories for the Production of Secondary Metabolites

*Matthias Buntru[1], Nils Hahnengress[1], Alexander Croon[1] and Stefan Schillberg[1,2]**

[1] Fraunhofer Institute for Molecular Biology and Applied Ecology IME, Aachen, Germany, [2] Institute of Phytopathology, Justus Liebig University, Giessen, Germany

Cell-free expression systems enable the production of proteins and metabolites within a few hours or days. Removing the cellular context while maintaining the protein biosynthesis apparatus provides an open system that allows metabolic pathways to be installed and optimized by expressing different numbers and combinations of enzymes. This facilitates the synthesis of secondary metabolites that are difficult to produce in cell-based systems because they are toxic to the host cell or immediately converted into downstream products. Recently, we developed a cell-free lysate derived from tobacco BY-2 cell suspension cultures for the production of recombinant proteins. This system is remarkably productive, achieving yields of up to 3 mg/mL in a one-pot *in vitro* transcription–translation reaction and contains highly active energy and cofactor regeneration pathways. Here, we demonstrate for the first time that the BY-2 cell-free lysate also allows the efficient production of several classes of secondary metabolites. As case studies, we synthesized lycopene, indigoidine, betanin, and betaxanthins, which are useful in the food, cosmetic, textile, and pharmaceutical industries. Production was achieved by the co-expression of up to three metabolic enzymes. For all four products, we achieved medium to high yields. However, the yield of betanin (555 μg/mL) was outstanding, exceeding the level reported in yeast cells by a factor of more than 30. Our results show that the BY-2 cell-free lysate is suitable not only for the verification and optimization of metabolic pathways, but also for the efficient production of small to medium quantities of secondary metabolites.

Keywords: betanin, BYL, cell-free lysate, indigoidine, lycopene, metabolic enzymes

OPEN ACCESS

Edited by:
Domenico De Martinis, Italian National Agency for New Technologies, Energy and Sustainable Economic Development (ENEA), Italy

Reviewed by:
Dong-Myung Kim, Chungnam National University, South Korea
Mitchel J. Doktycz, Oak Ridge National Laboratory (DOE), United States

***Correspondence:**
Stefan Schillberg
stefan.schillberg@ime.fraunhofer.de

Specialty section:
This article was submitted to Plant Biotechnology, a section of the journal Frontiers in Plant Science

Received: *14 October 2021*
Accepted: *17 December 2021*
Published: *28 January 2022*

Citation:
Buntru M, Hahnengress N, Croon A and Schillberg S (2022) Plant-Derived Cell-Free Biofactories for the Production of Secondary Metabolites. Front. Plant Sci. 12:794999. doi: 10.3389/fpls.2021.794999

INTRODUCTION

Secondary metabolites are organic natural products synthesized by plants, microbes, or animals *via* enzymatic cascades. They are generally not required for normal growth and development and instead facilitate ecological interactions, although the benefit to the producer is not always clear. However, many secondary metabolites, including alkaloids, terpenoids, polyketides, antibiotics, peptides, and growth hormones, have structures or biological activities that make them useful for applications in the chemical, agri-food, cosmetic, and pharmaceutical industries. Traditionally, secondary metabolites are extracted from their natural sources using solvents or are produced by chemical synthesis. However, both methods tend to be inefficient and harmful to the environment, making them costly and unsustainable. Furthermore, many natural products are too complex for

chemical synthesis. To overcome these drawbacks, the industrial-scale production of secondary metabolites is often achieved by the metabolic engineering of microbial cells. However, the preparation of production strains is laborious and the heterologous production of some secondary metabolites can be difficult or even impossible due to the lack of precursors, the low activity of the introduced enzymes, or the inhibition of cell growth by the product (Pyne et al., 2019; Zhang and Too, 2020).

Cell-free systems avoid many of the limitations of cell-based expression and are now widely used to optimize metabolic pathways and produce secondary metabolites (Li et al., 2018; Bogart et al., 2021). For example, diketopiperazine, limonene and various indole alkaloids have been produced in *Escherichia coli* lysates or the commercial *E. coli*-based PURExpress system (Goering et al., 2017; Dudley et al., 2020; Khatri et al., 2020). These open cell-free systems facilitate manipulation, monitoring, optimization, and sampling, providing the following advantages over cell-based systems: (i) simplified processes for the introduction and optimization of complex pathways, including complex multi-domain enzymes; (ii) simple adjustment of suitable reaction conditions; (iii) fast reaction rates; and (iv) tolerance of otherwise toxic products. The combination of these advantages can lead to a significant increase in product yields.

We recently developed a new cell-free expression platform based on tobacco BY-2 cells. With the exception of the vacuole and the nucleus, the cell-free BY-2 lysate contains the entire contents of the cell, including functional mitochondria, which provide the energy for protein biosynthesis and produces recombinant proteins with yields of up to 3 mg/mL in a coupled transcription–translation batch process (Buntru et al., 2015; Madduri et al., 2018; Schillberg et al., 2019). The productivity of the BY-2 lysate (BYL) is therefore in the same range as prokaryotic cell-free systems and about 15-fold higher than any commercial eukaryotic cell-free batch process. Numerous proteins that are difficult to produce in intact cells, including membrane proteins, plant antigens and transcription factors, have been produced successfully in the BYL system (Buntru et al., 2015; Havenith et al., 2017; Wu et al., 2019). Here, we describe for the first time the use of the BYL system for the production of secondary metabolites, using lycopene, indigoidine, and betalains as case studies.

Lycopene is a bright red carotenoid found in tomatoes and other red fruits and vegetables. It is widely used as a natural food coloring, and its antioxidant activity has led to tests as a cancer therapeutic (Saini et al., 2020; Nowroozi et al., 2021). Lycopene is synthesized from the precursor isopentenyl diphosphate (IPP) and its isomer dimethylallyl diphosphate (DMAPP). DMAPP is then converted in three enzymatic steps to geranylgeranyl pyrophosphate (GGPP), phytoene, and finally lycopene (**Figure 1A**).

Indigoidine is a non-ribosomal peptide (NRP) produced and excreted by some species of bacteria. It is a blue pigment that has been considered as a more sustainable alternative for industrial dyes (Wehrs et al., 2019), but it has also been evaluated for its antimicrobial activity (Cude et al., 2012; Gromek et al., 2016). Indigoidine is synthesized by the condensation of two molecules of L-glutamine in a reaction catalyzed by an NRP synthetase, which is activated by an Sfp-type phosphopantetheinyl transferase (Kim et al., 2018; **Figure 2A**).

Betalains are pigments found in the flowers, fruits, and/or vegetative organs of many plants in the order Caryophyllales, as well as leaf fungi and bacteria (Contreras-Llano et al., 2019). They are structurally related to alkaloids and can be divided into the red-violet betacyanins (e.g., betanin) and the yellow-orange betaxanthins. Betalain biosynthesis in plants begins with the conversion of tyrosine into L-3,4-dihydroxyphenylalanine (L-DOPA) by a cytochrome P450 hydroxylase and then to betalamic acid by a DOPA 4,5-dioxygenase (DOD) enzyme. Betalamic acid then reacts with various amino acids or amines to form diverse yellow-orange betaxanthins. Alternatively, L-DOPA is oxidized by the diphenolase activity of a cytochrome P450 to dopaquinone, which spontaneously cyclizes into *cyclo*-DOPA. The latter is converted to *cyclo*-DOPA-5-O-glucoside by a glucosyltransferase and reacts with betalamic acid to form the red pigment betanin (Polturak and Aharoni, 2018; **Figure 3A**). Alternatively, the order of glucosylation and condensation can be reversed. The glucosylated betanin is dramatically more stable than the unstable intermediate betanidin. Betalains are used as food colorants, but also possess antimicrobial, antimalarial and antidiabetic properties leading to their assessment as drug candidates (Madadi et al., 2020). For example, betanin (the most common betacyanin) from red beet has been approved for use as a natural colorant in food and cosmetic products, and is also being evaluated for its anti-inflammatory and hepatoprotective activity *in vitro* (Vieira Teixeira da Silva et al., 2019).

Here, we report the successful expression of metabolic enzymes in the BYL system leading to the formation of three different classes of secondary metabolites: terpenes (lycopene), NRPs (indigoidine), and alkaloid-like betalains (betanin and betaxanthins). Given the inherent color of the products, their accumulation in the cell-free system can easily be monitored using non-invasive methods and the performance of individual enzymes can be determined by separate expression and step-by-step construction of the pathway. In addition, precursors can be added to the cell-free system to maximize product accumulation. This is the first step toward the wider use of the BYL platform for the engineering of metabolic pathways to produce valuable secondary metabolites.

MATERIALS AND METHODS

Construction of Expression Vectors

All cDNAs were transferred to the expression vector pLenEx (**Supplementary Figure S1A**), which was fully synthesized by BioCat (Heidelberg, Germany). The vector backbone is based on the plasmid pIVEX_GAA_Omega (Buntru et al., 2015) with some modifications. The transcriptional start site GAAAGA upstream of the tobacco mosaic virus 5′ omega leader sequence was replaced with GGGAGA (Buntru et al., 2017). The partial *lacZ* sequence and the F1 origin of replication were removed. To construct the control vector pLenEx_Strep-eYFP, expressing the fluorescent protein eYFP including an N-terminal streptavidin affinity tag, the Strep-eYFP sequence

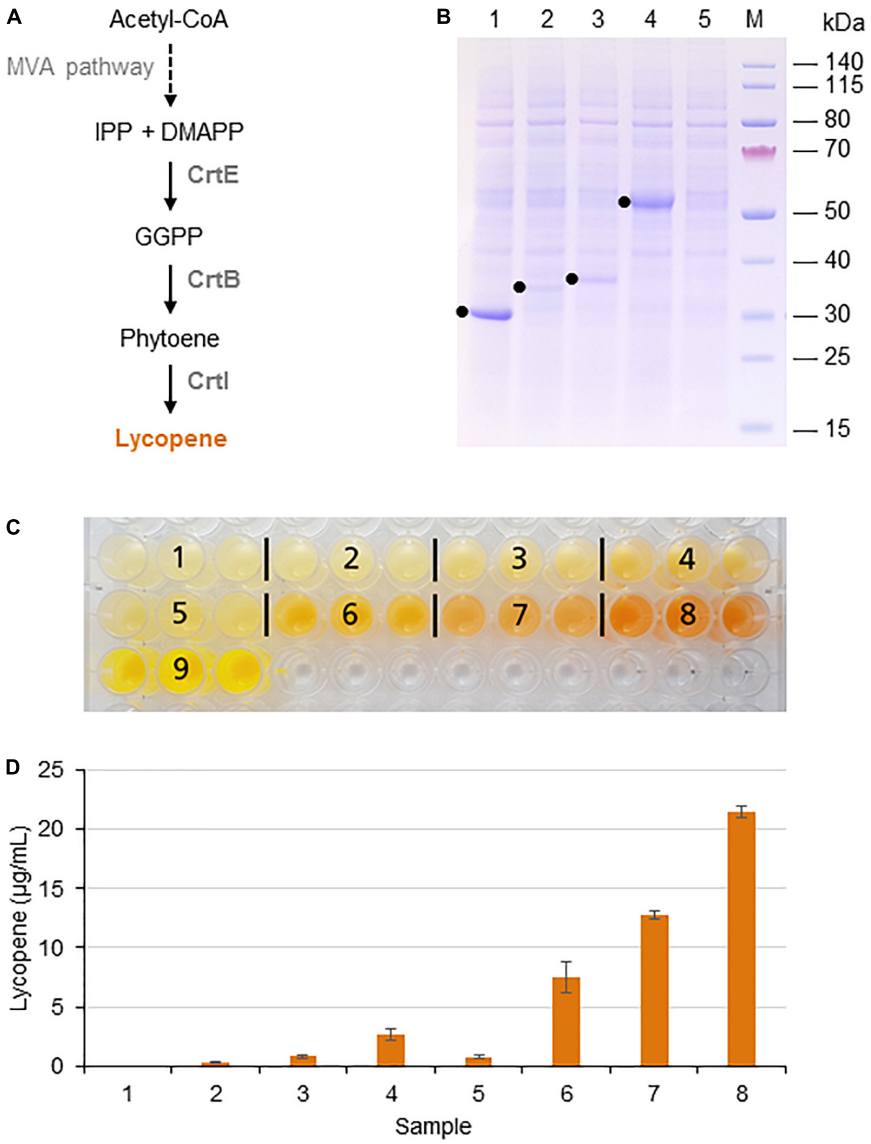

FIGURE 1 | Lycopene biosynthesis in the BY-2 cell-free system. **(A)** Schematic overview of the endogenous mevalonate (MVA) pathway and the engineered carotenoid biosynthesis pathway in the BYL system. These pathways are localized in the cytosol or the cytosolic fraction of BYLs. Solid arrows represent single enzymatic steps and dashed arrows represent multiple enzymatic steps. The reactions catalyzed by *P. ananatis* CrtE, CrtB, and CrtI are indicated. IPP, isopentenyl diphosphate; DMAPP, dimethylallyl diphosphate; GGPP, geranylgeranyl diphosphate; CrtE, GGPP synthase; CrtB, phytoene synthase; and CrtI, phytoene desaturase. **(B)** SDS-PAGE analysis of BYL transcription–translation reactions after 44 h at 25°C and 70% humidity, shaking at 500 rpm. In each case, 0.5 µL of the reaction mix was loaded onto a 4–12% (w/v) gradient gel. Lane 1: Strep-eYFP (29 kDa), lane 2: CrtE-Strep (34 kDa), lane 3: CrtB-Strep (36 kDa), lane 4: CrtI-Strep (56 kDa), and lane 5: no template control. **(C)** Image of the *in vitro* reactions after incubation for 21 h: (1) no-template control, (2) CrtE, (3) CrtB, (4) CrtI, (5) CrtE + CrtB, (6) CrtB + CrtI, (7) CrtE + CrtI, (8) CrtE + CrtB + CrtI, and (9) Strep-eYFP. **(D)** Lycopene produced in BYL transcription–translation reactions after incubation for 21 h: (1) no-template control, (2) CrtE, (3) CrtB, (4) CrtI, (5) CrtE + CrtB, (6) CrtB + CrtI, (7) CrtE + CrtI, and (8) CrtE + CrtB + CrtI. After lycopene extraction, the concentration was determined by absorbance spectrophotometry at 472 nm and was compared to a standard curve prepared using commercial lycopene. Data represent the means and standard deviations of three independent transcription–translation experiments.

was amplified by PCR using primers 5′-GGT AGT CCA TGG CTT GGT CTC ATC CGC AAT TC-3′ and 5′-GAC ACG GGT ACC TTA TTA CTT GTA CAG CTC GTC CAT GC-3′, with pIVEX_GAA_Omega_Strep-eYFP as the template (Buntru et al., 2015). The PCR product was digested with *Nco*I and *Kpn*I (underlined in the primer sequences) and inserted at the *Nco*I and *Kpn*I sites of pLenEx.

The DNA fragments encoding the full−length *Pantoea ananatis* CrtE, CrtB, and CrtI proteins (GenBank accession numbers WP_176017233, WP_013027995, and WP_176017230, respectively) for lycopene synthesis, the *Streptomyces lavendulae* BpsA and *Bacillus subtilis* Sfp proteins (GenBank accession numbers QYB25025 and WP_015715234, respectively) for indigoidine synthesis, and the *Beta vulgaris* CYP76AD1_W13L,

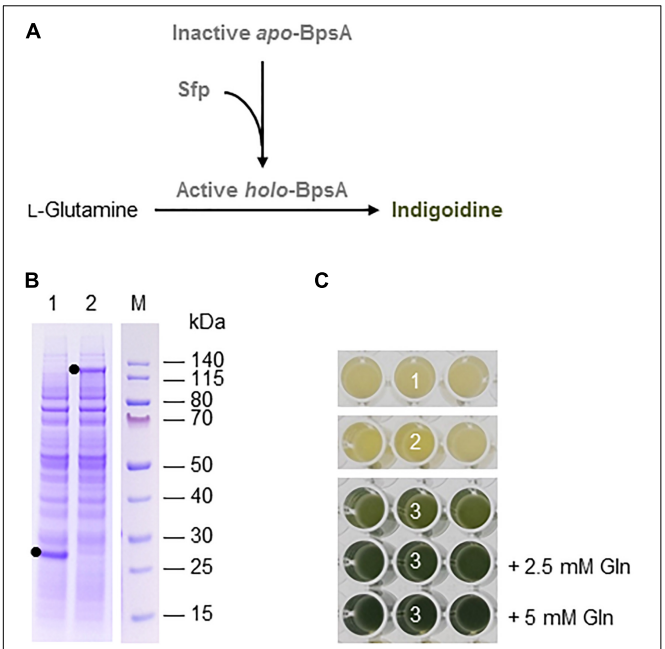

FIGURE 2 | Indigoidine biosynthesis in the BY-2 cell-free system. **(A)** Schematic overview of the engineered indigoidine biosynthesis pathway. The inactive *apo*-form of blue pigment synthetase A (BpsA) from *S. lavendulae* is activated by the 4′-phosphopantetheinyl transferase Sfp from *B. subtilis* in a reaction requiring coenzyme A. The active *holo*-form of BpsA then catalyzes the conversion of two L-glutamine molecules to indigoidine. **(B)** SDS-PAGE analysis of BYL transcription–translation reactions after incubation for 44 h at 25°C and 70% humidity, shaking at 500 rpm. In each case, 0.5 μL of the reaction mix was loaded onto a 4–12% (w/v) gradient gel. Lane 1: Sfp (26 kDa), lane 2: BpsA (141 kDa). **(C)** Image of the *in vitro* reactions after incubation for 18 h: (1) Sfp, (2) BpsA, and (3) Sfp + BpsA. Reactions were supplemented with L-glutamine (Gln) as indicated.

Mirabilis jalapa DOD, *M. jalapa* cDOPA5GT and *B. vulgaris* CYP76AD5 proteins (GenBank accession numbers AET43290, BAG80686, BAD91803, and AJD87473, respectively) for betalain synthesis, were synthesized as double-stranded DNA fragments (Integrated DNA Technologies, Coralville, IA, United States) including overhangs suitable for Gibson assembly (Gibson et al., 2009). The double-stranded DNA fragments were introduced into pLenEx_Strep-eYFP at the *Nco*I and *Kpn*I sites by Gibson DNA assembly using NEBuilder HiFi DNA Assembly Master Mix (New England Biolabs, Frankfurt, Germany), replacing the Strep-eYFP cDNA with the sequence encoding the enzyme of interest (**Supplementary Figure S1B**). For CrtE, CrtB, and CrtI, a C-terminal streptavidin affinity tag sequence (StrepII tag) was included, and an additional alanine residue was introduced after the start codon to create an *Nco*I restriction site. The *bpsA* and *sfp* sequences were codon optimized for tobacco (*Nicotiana tabacum*) using the codon optimization tool provided by Integrated DNA Technologies, and the first codon after the start codon was replaced with glycine to create an *Nco*I restriction site as previously described (Wehrs et al., 2019). The activity of CYP76AD1 was increased by introducing a W13L mutation (DeLoache et al., 2015). For MjDOD and MjcDOPA5GT, an additional alanine was introduced after the start codon to create an *Nco*I restriction site. The integrity of all 10 final expression vectors (**Table 1**) was verified by DNA sequencing, confirming the coding sequence of each expression cassette and the connection to the untranslated regions.

Preparation of Tobacco Cell-Free Lysate and Reaction Mix

The tobacco cell-free lysate (BYL) was prepared as previously described (Madduri et al., 2018) with minor modifications. Tobacco BY-2 cells were cultivated batch-wise in shake flasks and were harvested during the exponential growth phase at a packed cell volume of 20–25% (v/v). They were treated with 3% (v/v) Rohament CL and 0.2% (v/v) Rohapect UF (AB Enzymes, Darmstadt, Germany) directly in the fermentation medium. The osmolarity was adjusted by adding 360 mM mannitol. The resulting protoplasts were layered onto a discontinuous Percoll gradient containing (from bottom to top) 70% (v/v, 3 mL), 40% (v/v, 5 mL), 30% (v/v, 3 mL), 15% (v/v, 3 mL), and 0% (3 mL) Percoll (GE Healthcare, Munich, Germany) in 0.7 M mannitol, 20 mM $MgCl_2$, and 5 mM PIPES-KOH (pH 7.0) in a 50-mL polypropylene tube (Greiner Bio-One, Frickenhausen, Germany). After centrifugation at 6,800 × *g* for 1 h at 25°C in a swing-bucket rotor, evacuolated protoplasts were recovered from the 40–70% (v/v) Percoll solution interface and suspended in three volumes of TR buffer (30 mM HEPES-KOH (pH 7.4), 60 mM potassium glutamate, 0.5 mM magnesium glutamate, 2 mM DTT) supplemented with one tablet per 50 mL of Complete EDTA-free Protease Inhibitor Mixture (Roche Diagnostics, Mannheim, Germany). The protoplasts were disrupted on ice using 15 strokes of a Dounce homogenizer (Braun, Melsungen, Germany), and the nuclei and non-disrupted cells were removed by centrifugation at 500 × *g* for 10 min at 4°C. Standard cell-free reactions contained 40% (v/v) BYL, 20 mM HEPES-KOH (pH 7.8), 9 mM magnesium glutamate, 20 mM potassium glutamate, 4 mM ATP, 1.6 mM GTP, 1.6 mM CTP, 1.6 mM UTP, 100 μg/mL chloramphenicol, and 30 ng/μL in-house T7 RNA polymerase. The reaction mix was supplemented with 2.5% (w/v) trehalose as a cryoprotectant and then frozen in 1-mL aliquots at −80°C.

Coupled Transcription–Translation Cell-Free Reaction

Coupled transcription–translation reactions were carried out in aliquots of 50, 150, or 500 μL at 25°C and 70% humidity, shaking at 500 rpm (12.5 mm amplitude) in a Lab-Therm LT-X incubator shaker (Kuhner, Herzogenrath, Germany). Ten to 30 ng/μL (5–10 nM) plasmid DNA was added to the cell-free reaction mix. BYL mixtures for betanin and indigoidine production were optionally supplemented at the start of the reaction with 5 mM tyrosine and 2.5 or 5 mM glutamine, respectively, as precursors.

SDS-PAGE Analysis

Samples were separated by SDS-PAGE in precast NuPAGE 4–12% (w/v) polyacrylamide Bis-Tris gels (Thermo Fisher Scientific, Waltham, MA, United States) alongside PageRuler

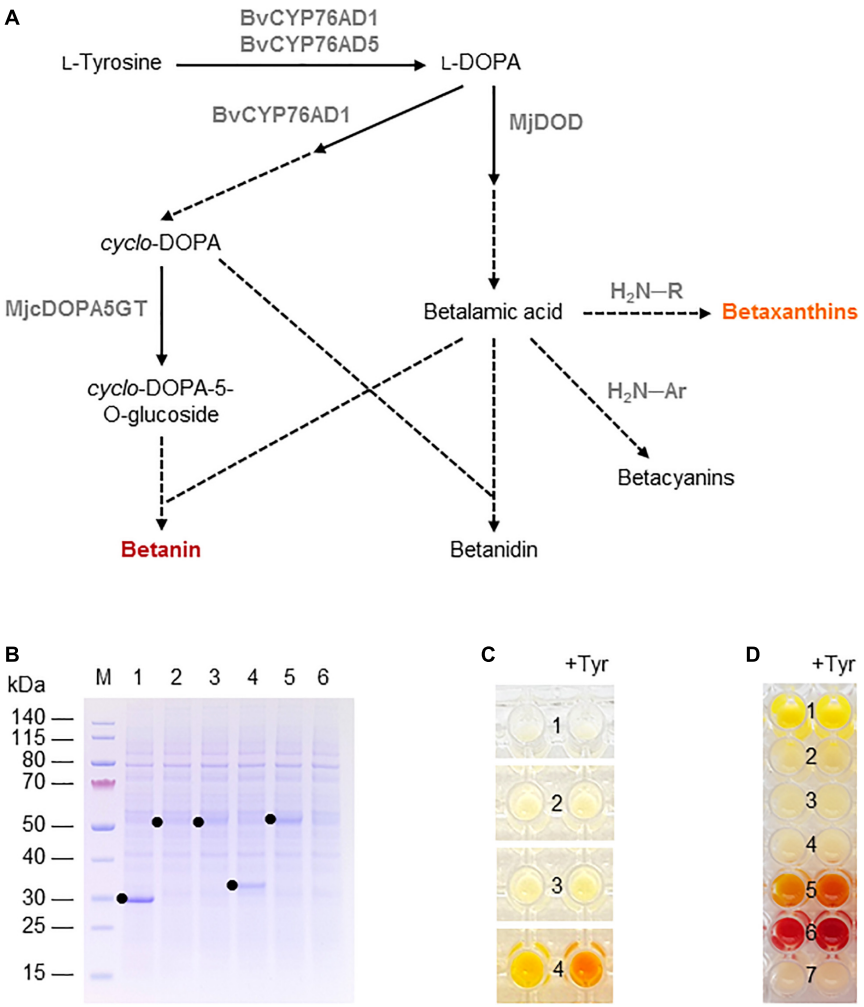

FIGURE 3 | Betalain biosynthesis in the BY-2 cell-free system. **(A)** Schematic overview of the betalain biosynthesis pathway. Solid lines are enzymatic reactions and dashed lines are spontaneous reactions. R = any organic group; Ar = any organic aromatic group. **(B)** SDS-PAGE analysis of BYL transcription–translation reactions after incubation for 44 h at 25°C and 70% humidity, shaking at 500 rpm. In each case, 0.5 μL of the reaction mix was loaded onto a 4–12% (w/v) gradient gel. Lane 1: Strep-eYFP (29 kDa), lane 2: BvCYP76AD1_W13L (56 kDa), lane 3: BvCYP76AD5 (57 kDa), lane 4: MjDOD (30 kDa), lane 5: MjcDOPA5GT (57 kDa). **(C)** Image of the *in vitro* reactions for betaxanthin biosynthesis after incubation for 24 h: (1) no-template control, (2) BvCYP76AD5, (3) MjDOD, and (4) BvCYP76AD5 + MjDOD. Reactions were supplemented with 5 mM L-tyrosine (Tyr) as indicated. **(D)** Image of the *in vitro* reactions for betacyanin biosynthesis after incubation for 24 h: (1) Strep-eYFP, (2) BvCYP76AD1_W13L, (3) MjDOD, (4) MjcOPA5GT, (5) BvCYP76AD1_W13L + MjDOD, (6) BvCYP76AD1_W13L + MjDOD + MjcOPA5GT, and (7) no-template control. Reactions were supplemented with 5 mM L-tyrosine (Tyr) as indicated.

Prestained Protein Ladder markers (Thermo Fisher Scientific). The gels were stained with Coomassie Brilliant Blue R-250.

Metabolite Detection

Lycopene was extracted as described by Dzakovich et al. (2019) with modifications. Briefly, 150 μL of the BYL sample was mixed sequentially with 200 μL methanol and 600 μL hexane/acetone (1:1) by vortexing. We then added 300 μL water to induce phase separation, vortexed the mixture briefly and centrifuged at 5,000 × *g* for 30 s. The upper organic phase was transferred to a fresh microcentrifuge tube and the absorbance was measured at 472 nm (Shi and Le Maguer, 2000) using quartz cuvettes and an Infinite M200 reader (Tecan, Männedorf, Switzerland). The quantity of lycopene was determined by generating a standard curve based on different concentrations of a commercial lycopene standard (Sigma-Aldrich, Seelze, Hanover, Germany) in the organic phase prepared from BYL reactions without a DNA template.

Indigoidine was detected by optical verification of a color change in the BYL reaction samples from pale yellow to blue-green.

For betanin detection, insoluble compounds were removed by passing the samples through a regenerated cellulose 0.2-μm filter (Sartorius, Göttingen, Germany). The samples were then analyzed by chromatography using an Ultimate3000 UHPLC system (Thermo Fisher Scientific) including a quaternary pump, autosampler, column oven and UV-detector. The sampler temperature was set to 10°C and the column compartment to

TABLE 1 | List of plasmids used in this work.

Expression vector	Target protein/enzyme and cDNA source	Pathway
pLenEx_Strep-eYFP	Enhanced yellow fluorescent protein from *Aequorea victoria*	–
pLenEx_crtE-Strep	Geranylgeranyl diphosphate synthase from *Pantoea ananatis*	Lycopene
pLenEx_crtB-Strep	Phytoene synthase from *P. ananatis*	Lycopene
pLenEx_crtI-Strep	Phytoene desaturase from *P. ananatis*	Lycopene
pLenEx_bpsA	Blue pigment synthetase A from *Streptomyces lavendulae*	Indigoidine
pLenEx_sfp	4′-Phosphopantetheinyl transferase from *Bacillus subtilis*	Indigoidine
pLenEx_CYP76AD1_W13L	Monophenolase/diphenolase from *Beta vulgaris*	Betalains
pLenEx_MjDOD	DOPA-4,5-dioxygenase from *Mirabilis jalapa*	Betalains
pLenEx_MjcDOPA5GT	*cyclo*-DOPA glucosyltransferase from *M. jalapa*	Betalains
pLenEx_CYP76AD5	Monophenolase from *Beta vulgaris*	Betalains

25°C. Compounds of interest were analyzed in reversed phase mode on a LiChrosorb RP-18 column (250 × 4.6 mm, 5 μm) (Merck, Darmstadt, Germany). We separated 5.0-μL samples at a flow rate of 0.5 mL/min using 5.0% (v/v) methanol plus 94.9% (v/v) water with 0.1% (v/v) trifluoroacetic acid as eluent A and 95.0% (v/v) methanol plus 4.9% (v/v) water with 0.1% (v/v) trifluoroacetic acid as eluent B. The program began with an isocratic segment at 100% eluent A for 5 min, followed by a linear gradient to 60.0% eluent B (5–17 min), a linear gradient to 100% eluent B (17–19 min), an isocratic segment at 100% eluent B (19–23 min) and finally a linear gradient to 100% eluent A (23–24 min). The column was re-equilibrated for 6 min in 100% eluent A. Betanin was detected at 536 nm and was compared to a commercial betanin standard (Sigma-Aldrich). The formation of betaxanthins was detected by optical verification of a color change in the BYL reaction samples from pale yellow to bright yellow to orange.

RESULTS

Expression Constructs

All target cDNAs were cloned separately into the expression vector pLenEx for the cell-free production of lycopene (three genes), indigoidine (two genes), and betalains (four genes) (**Supplementary Figure S1B**). Codon optimization of the target cDNA is usually not required to improve production in the cell-free BYL lysate. However, the bacterial *bpsA* and *sfp* sequences were codon optimized for tobacco to facilitate comparison with a previous study in which codon-optimized sequences were used for cell-based production in *Rhodosporidium toruloides* (Wehrs et al., 2019). In the case of *bpsA*, we also removed sequence repeats, hairpins and regions with a high GC content (>70%) to ensure efficient cDNA synthesis. For similar reasons, a C-terminal StrepII tag sequence was introduced into the CrtE, CrtB, and CrtI constructs since Matthäus et al. (2014) have shown that this tag did not interfere with the catalytic activity of the heterologous enzymes. We also expressed the fluorescent marker eYFP, which usually accumulates to levels of 3 mg per mL cell-free reaction (Schillberg et al., 2019), as a positive control to ensure cell-free protein synthesis was working as anticipated.

All 10 target genes were expressed under the control of the T7 promoter in the pLenEx expression vector. The T7 polymerase and all other factors necessary for *in vitro* transcription and translation, such as nucleoside triphosphates (NTPs), amino acids and salts, are already provided in the lysate. Accordingly, only vectors carrying the appropriate cDNAs need to be added to the cell-free lysate to facilitate rapid protein biosynthesis, enzyme analysis and the accumulation of secondary metabolites in a single reaction vessel.

Lycopene Biosynthesis

Lycopene biosynthesis was achieved by expressing the enzymes CrtE, CrtB, and CrtI from the bacterium *P. ananatis*. These enzymes convert IPP and its isomer DMAPP to lycopene in three steps (**Figure 1A**). First, the three target proteins were produced separately in batch reactions, using the same molar concentration (5 nM) in each case to account for differences in cDNA size. The plasmid concentration of 5 nM was selected based on the optimal concentration of the template plasmid pLenEx_Strep-eYFP for Strep-eYFP production in the BYL system. After 44 h, BYL aliquots were analyzed by SDS-PAGE. CrtI accumulated to high levels, similar to the control protein eYFP (**Figure 1B**). In contrast, the levels of CrtE and CrtB were significantly lower, as shown by the weak bands barely visible against the background of tobacco host proteins. Nevertheless, the bands representing all three proteins were of the correct size: 34 kDa (CrtE), 36 kDa (CrtB), and 56 kDa (CrtI).

Next, we expressed the three enzymes individually, in pairs and also all three simultaneously in a single batch reaction. As above, we accounted for differences in cDNA size by using the same molar concentration of each construct (5 nM) in the individual reactions. In the combinatorial reactions we used equimolar concentrations of each construct and a total molar concentration of 5 nM. After 21 h, the reaction with three plasmids producing the full complement of enzymes (CrtE, CrtB, and CrtI) showed the most intense orange color, indicating the accumulation of large amounts of lycopene (**Figure 1C**). In contrast, there was no significant color in any of the single or double reactions lacking CrtI, which is understandable because this enzyme catalyzes the final step in the pathway. However, an orange color was observed in the reactions containing CrtI alone or paired with one of the other enzymes, although it was not as intense as the reaction with all three enzymes. The visual observations were confirmed by extracting the lycopene and measuring its absorbance at 472 nm. As expected, the highest level of 21 μg per mL cell-free reaction was detected when expressing all three enzymes (**Figure 1D**). However, significant levels were also detected when expressing CrtI alone (3 μg/mL) or in combination with CrtB (7 μg/mL) or CrtE (13 μg/mL), indicating that the precursors IPP/DMAPP, GGPP, and/or phytoene are present in the cell-free lysate. Carotenoids

are found in all higher plants and related enzymes are also present in the proplastids of tobacco BY-2 cells (Baginsky et al., 2004).

Indigoidine Biosynthesis

Indigoidine biosynthesis was achieved by expressing the *S. lavendulae* blue pigment synthetase A (*bpsA*) and *B. subtilis* 4′-phosphopantetheinyl transferase (*sfp*) genes. Following the activation of BpsA by the Sfp transferase, BpsA catalyzes the condensation of two molecules of L-glutamine to form indigoidine (**Figure 2A**). As above, we initially expressed the enzymes separately for 44 h using the same molar concentration of each construct (5 nM). SDS-PAGE analysis confirmed the presence of each protein, with anticipated band sizes of 141 and 26 kDa for BpsA and Sfp, respectively (**Figure 2B**).

Next we produced BpsA and Sfp alone using 5 nM of each construct and simultaneously using equimolar concentrations of each construct (2.5 nM). Indigoidine formation was detected optically based on a color change from pale yellow to blue-green. As expected, the expression of Sfp alone did not change the color of the lysate (number 1 in **Figure 2C**). The expression of BpsA alone led to a very slight color change of the BYL reaction samples (number 2 in **Figure 2C**). BpsA was probably activated by endogenous phosphopantetheinyl transferases with broad substrate spectrum (Yalpani et al., 2001), albeit with very low efficiency. The co-expression of both enzymes confirmed that the NRP synthetase BpsA was efficiently activated by the phosphopantetheinyl transferase Sfp, leading to the accumulation of the blue-green pigment (number 3 in **Figure 2C**). The yield of indigoidine could be increased by adding 2.5 mM glutamine as precursor to the reaction, as indicated by the darker blue-green color. However, the addition of 5 mM glutamine did not increase the color intensity significantly, indicating that higher indigoidine levels may interfere with the components of the cell-free lysate.

Betalain Biosynthesis

Finally, we used the BYL system to produce betalains from the amino acid tyrosine. We investigated two overlapping pathways for the biosynthesis of (1) yellow-orange betaxanthins, which requires the monophenolase activity of the cytochrome P450 BvCYP76AD5 from *B. vulgaris* and the dioxygenase MjDOD from *M. jalapa*; and (2) the red-violet betacyanin betanin, which requires the monophenolase as well the diphenolase activity of the cytochrome P450 BvCYP76AD1_W13L from *B. vulgaris*, MjDOD, and the glucosyltransferase MjcDOPA5GT from *M. jalapa* (**Figure 3A**). As above, all four enzymes were first produced separately, allowing us to verify the correct size of the proteins by SDS-PAGE (**Figure 3B**). As anticipated, we detected bands of 56 kDa (BvCYP76AD1_W13L), 57 kDa (BvCYP76AD5), 30 kDa (MjDOD) and 57 kDa (MjcDOPA5GT). The yields of all four proteins were lower than the 29 kDa eYFP control, with particularly weak bands representing BvCYP76AD1_W13L and BvCYP76AD5 barely visible against the background of host cell proteins in the BYL.

For the synthesis of betaxanthins, BvCYP76AD5, and MjDOD were expressed alone or together using the same molar concentration of template DNA (5 nM or 2.5 nm each). The exclusive monophenolase activity of BvCYP76AD5 ensured that the L-DOPA was channeled toward the synthesis of betalamic acid and subsequently betaxanthins (Grewal et al., 2018). The reactions containing BvCYP76AD5 alone remained the same color as the non-template control (number 1 and 2 in **Figure 3C**). The reactions containing MjDOD alone turned slightly more yellow (number 3 in **Figure 3C**), indicating that the precursor L-DOPA is present in the cell-free lysate. In plants, L-DOPA is a precursor of many alkaloids, catecholamines, and melanin, which is present in many tissues (Soares et al., 2014). The co-expression of both enzymes led to the high accumulation of yellow-orange betaxanthins (number 4 in **Figure 3C**). Adding the precursor tyrosine (5 mM) at the beginning of the reaction increased the product levels as indicated by the significantly higher color intensity and change from yellow-orange to orange.

Similarly, the cell-free production of betanin was demonstrated by expressing BvCYP76AD1_W13L, MjDOD, and MjcDOPA5GT alone or in all possible combinations using the same molar concentrations of template DNA (5 nM). In this reaction, the monophenolase activity of BvCYP76AD1_W13L produced L-DOPA but the additional diphenolase activity converted it into *cyclo*-DOPA (Grewal et al., 2018). When all three enzymes were present, the color of the cell-free lysate turned from pale yellow to red-violet after 24 h (**Figure 3D**). Adding the precursor tyrosine (5 mM) at the beginning of the reaction increased the yield of betanin, as shown by the greater intensity of the red-violet color. No color development (and thus no betanin accumulation) was detected when any of the enzymes were produced alone, but the co-expression of the first two enzymes of the pathway (BvCYP76AD1_W13L and MjDOD) resulted in a yellow-orange color, indicating the formation of various betaxanthins resulting from the spontaneous reaction of betalamic acid with amino acids and the unstable, red-violet betacyanin betanidin (**Figure 3A**). Once again, adding the precursor tyrosine increased product yields resulting in a more intense color.

To determine the betanin content, the cell-free reactions were repeated at the 500-μL scale using the same molar concentrations of template DNA (1.73 nm each) with and without 5 mM tyrosine. The betanin concentration was determined after 24 h by UHPLC. The yield in the absence of tyrosine was 125 μg betanin per mL cell-free reaction, whereas the provision of 5 mM tyrosine increased the yield to 470 μg per mL. Higher molar concentrations of template DNA (3.33 nm each) increased the betanin yield even further to 555 μg per mL cell-free reaction. These remarkable yields demonstrate that the cell-free BYL system is not only suitable for the analysis of metabolic pathways but also for the rapid production of target molecules.

DISCUSSION

We have demonstrated for the first time the successful production of secondary metabolites in the cell-free BYL system. Thus far, cell-free lysates prepared from tobacco BY-2 cells have been used as a powerful screening platform for recombinant proteins in small-scale reactions of 50–100 μL and for the

production of recombinant proteins that are difficult to express in living cells due to their toxicity (Havenith et al., 2017; Huck et al., 2017; unpublished data). Notably, the BYL contains active mitochondria that deliver energy for protein synthesis and can synthesize recombinant proteins with yields of up to 3 mg per mL by *in vitro* transcription–translation in batch reactions, which is ∼15 times more productive than other eukaryotic cell-free systems in batch mode (Madduri et al., 2018; Schillberg et al., 2019). Glutamate supplied to the BYL in the form of magnesium glutamate and potassium glutamate can enter the citrate cycle within the mitochondria *via* α-ketoglutarate, leading to the formation of the reducing equivalents NADH and FADH. Electrons enter the electron transport chain *via* NADH and FADH to generate ATP through oxidative phosphorylation consuming molecular oxygen (Madduri et al., 2018). Consequently, the BYL system can also be used to produce larger quantities of metabolic enzymes for analysis or for the synthesis of specific metabolites. We clearly demonstrated this application by the successful production of lycopene, indigoidine, and betalains.

Importantly, the preparation of cell-free lysates can be decoupled from recombinant protein expression and metabolite biosynthesis. Following lysate preparation, ready-to-use reaction samples can be stored at −80°C for up to 1 year. If necessary, the template DNA (plasmids or PCR products carrying the expression cassettes for the target proteins) can be added to the thawed lysate to initiate biosynthesis. The cell-free platform thus provides a flexible, on-demand tool for the analysis and optimization of metabolic pathways, and can provide sufficient quantities of secondary metabolites for various assays without the costly infrastructure required for cell-based protein production. It is therefore unsurprising that cell-free expression has already been exploited for such approaches, although these systems are typically derived from microbial cells (for review see Bogart et al., 2021). Cell-free systems have been used, for example, to characterize and optimize specific enzymes (Körfer et al., 2016; Kightlinger et al., 2018), and to mix and match combinations of enzymes to rapidly prototype and optimize metabolic pathways (Kightlinger et al., 2019; Jaroentomeechai et al., 2020; Karim et al., 2020). We selected lycopene, indigoidine and betalains as case studies for the BYL platform because they are industrially relevant molecules that can be detected and quantified using simple colorimetric methods, and there is already a large amount of appropriate comparative data from cell-based and cell-free production systems.

The major commercial source of lycopene is currently tomato fruits, although the extraction of lycopene from plants is expensive and environmentally harmful. This has prompted the transfer of the metabolic pathway to microbial production platforms such as *E. coli*, *Saccharomyces cerevisiae* and *Yarrowia lipolytica* (Li et al., 2020; Wang et al., 2020). During the last year, the productivity of these engineered biofactories has been improved significantly, mainly by engineering gene expression, improving lycopene storage capacity, optimizing fermentation processes, and combinatorial pathway engineering (Li et al., 2020). The highest lycopene titer achieved thus far is 4.2 g per L culture medium in the yeast *Y. lipolytica*, which was achieved by a combination of pathway engineering and improved fermentation strategies (Luo et al., 2020). The yield in the BYL system was significantly lower (21 μg/mL) but this is, to our knowledge, the first time lycopene has been produced in a cell-free expression system and thus provides a versatile platform for the production optimization of carotenoids and other high-value isoprenoids.

In a similar effort to improve the synthesis of indogoidine, the *S. lavendulae bpsA* gene has been transferred to the industrial production strains *Corynebacterium glutamicum* and *Rhodosporidium toruloides*. When combined with metabolic engineering and the optimization of fermentation strategies, this achieved indigoidine yields of 49 and 86 g per L, respectively (Wehrs et al., 2019; Ghiffary et al., 2021). Indigoidine has also been produced by cell-free biosynthesis in the commercial *E. coli*-based PURExpress system (Siebels et al., 2020). This system contains all necessary components of the *E. coli* transcription and translation machinery, which have been produced as recombinant proteins and combined in defined concentrations (Shimizu et al., 2001). In contrast to our study, the cell-free synthesis of indogoidine in the PURExpress system was achieved by expressing *S. lavendulae* BpsA but not *B. subtilis* Sfp, which was instead added to the reaction along with coenzyme A to enable the post-translational phosphopantetheinylation of the BpsA thiolation domain (as required for substrate shuffling). The reported yield was up to 250 μM (62 mg/L). More precise quantitative analysis was not possible due to the lack of suitable standards, which is also why we did not determine the concentration of indigoidine in our study. Nevertheless, the colorimetric assay confirmed the accumulation of large amounts of indigoidine, indicating that the BYL system can be harnessed for the rapid engineering and optimization of indigoidine biosynthesis.

The production of betalains has also been transferred to microbes by metabolic engineering. Various betaxanthins and betacyanins have been produced in *E. coli*, with yields of up to 288 mg per L (Guerrero-Rubio et al., 2019; Hou et al., 2020). Grewal et al. (2018) reported the production of betalains in the yeast *S. cerevisiae*, achieving a titer of 17 μg per mL for betanin, the most industrially relevant betalain. To our knowledge, the cell-free biosynthesis of betalains has not been reported thus far. The successful production of betaxanthins and betacyanins in the BYL system is therefore the first step toward the engineering and optimization of betalain biosynthesis in this platform. Notably, we achieved yields of up to 555 μg betanin per mL BYL solution, which is 32 times higher than previously achieved by cell-based expression in *S. cerevisiae* (Grewal et al., 2018) and thus the highest yield thus far achieved by metabolic engineering.

We have shown that the cell-free BYL system can support the production of secondary metabolites, using representatives from the carotenoids, NRPs and betalains as case studies. In the future, we will optimize the BYL system to improve the accumulation of lycopene, indigoidine and betalains by testing enzymes from alternative organisms and/or by optimizing enzyme sequences and improving reaction conditions before transferring optimized pathways to cell-based production platforms. In addition, metabolic pathways can be modified and augmented to synthesize products with improved or new properties, including

xenobiotics that are not found in nature because they are unstable and/or quickly metabolized in living cells. This could provide a new source of novel active substances as drug leads. The cell-free BYL system can be scaled up inexpensively by using more BY-2 cell biomass for lysate preparation, with work underway to reach scales of 1 L and even 10 L per reaction (Schillberg and Finnern, 2021). This would facilitate the production of gram quantities of secondary metabolites, making cell-based systems ultimately unnecessary for challenging products.

DATA AVAILABILITY STATEMENT

The original contributions presented in the study are included in the article/**Supplementary Material**, further inquiries can be directed to the corresponding author/s.

AUTHOR CONTRIBUTIONS

MB and SS conceived the study and wrote the manuscript. MB, NH, and AC conducted the experiments and collected the data. All authors interpreted data, proofread, and approved the manuscript.

FUNDING

This research was supported by the Fraunhofer-Gesellschaft.

ACKNOWLEDGMENTS

We thank Richard M. Twyman (Twyman Research Management Ltd., Scarborough, United Kingdom) for editorial assistance.

SUPPLEMENTARY MATERIAL

The Supplementary Material for this article can be found online at: https://www.frontiersin.org/articles/10.3389/fpls.2021.794999/full#supplementary-material

REFERENCES

Baginsky, S., Siddique, A., and Gruissem, W. (2004). Proteome analysis of tobacco bright yellow-2 (BY-2) cell culture plastids as a model for undifferentiated heterotrophic plastids. *J. Proteome Res.* 3, 1128–1137. doi: 10.1021/pr0499186

Bogart, J. W., Cabezas, M. D., Vögeli, B., Wong, D. A., Karim, A. S., and Jewett, M. C. (2021). Cell-Free exploration of the natural product chemical space. *ChemBioChem* 22, 84–91. doi: 10.1002/cbic.202000452

Buntru, M., Vogel, S., and Schillberg, S. (2017). *Promoter construct for cell-free protein synthesis*. Geneva: WIPO.

Buntru, M., Vogel, S., Stoff, K., Spiegel, H., and Schillberg, S. (2015). A versatile coupled cell-free transcription-translation system based on tobacco BY-2 cell lysates. *Biotechnol. Bioengine.* 112, 867–878. doi: 10.1002/bit.25502

Contreras-Llano, L. E., Guerrero-Rubio, M. A., Lozada-Ramírez, J. D., García-Carmona, F., and Gandía-Herrero, F. (2019). First betalain-producing bacteria break the exclusive presence of the pigments in the plant kingdom. *mBio* 10, e345–e319. doi: 10.1128/mBio.00345-19

Cude, W. N., Mooney, J., Tavanaei, A. A., Hadden, M. K., Frank, A. M., Gulvik, C. A., et al. (2012). Production of the antimicrobial secondary metabolite indigoidine contributes to competitive surface colonization by the marine roseobacter Phaeobacter sp. strain Y4I. *Appl. Environ. Microbiol.* 78, 4771–4780. doi: 10.1128/AEM.00297-12

DeLoache, W. C., Russ, Z. N., Narcross, L., Gonzales, A. M., Martin, V. J. J., and Dueber, J. E. (2015). An enzyme-coupled biosensor enables (S)-reticuline production in yeast from glucose. *Nat. Chem. Biol.* 11, 465–471. doi: 10.1038/nchembio.1816

Dudley, Q. M., Karim, A. S., Nash, C. J., and Jewett, M. C. (2020). In vitro prototyping of limonene biosynthesis using cell-free protein synthesis. *Metab. Engine.* 61, 251–260. doi: 10.1016/j.ymben.2020.05.006

Dzakovich, M. P., Gas-Pascual, E., Orchard, C. J., Sari, E. N., Riedl, K. M., Schwartz, S. J., et al. (2019). Analysis of tomato carotenoids: Comparing extraction and chromatographic methods. *J. AOAC Int.* 102, 1069–1079. doi: 10.5740/jaoacint.19-0017

Ghiffary, M. R., Prabowa, C. P. S., Sharma, K., Yan, Y., Lee, S. Y., and Kim, H. U. (2021). High-level production of the natural blue pigment indigoidine from metabolically engineered Corynebacterium glutamicum for sustainable fabric dyes. *ACS Sustainable Chem. Eng.* 9, 6613–6622. doi: 10.1021/acssuschemeng.0c09341

Gibson, D. G., Young, L., Chuang, R. Y., Venter, J. C., Hutchison, C. A. III, and Smith, H. O. (2009). Enzymatic assembly of DNA molecules up to several hundred kilobases. *Nat. Methods* 6, 343–345. doi: 10.1038/nmeth.1318

Goering, A. W., Li, J., McClure, R. A., Thomson, R. J., Jewett, M. C., and Kelleher, N. L. (2017). In vitro reconstruction of nonribosomal peptide biosynthesis directly from DNA using cell-free protein synthesis. *ACS Synthetic Biol.* 6, 39–44. doi: 10.1021/acssynbio.6b00160

Grewal, P. S., Modavi, C., Russ, Z. N., Harris, N. C., and Dueber, J. E. (2018). Bioproduction of a betalain color palette in Saccharomyces cerevisiae. *Metab. Engine.* 45, 180–188. doi: 10.1016/j.ymben.2017.12.008

Gromek, S. M., Suria, A. M., Fullmer, M. S., Garcia, J. L., Gogarten, J. P., Nyholm, S. V., et al. (2016). Leisingera sp. JC1, a bacterial isolate from Hawaiian bobtail squid eggs, produces indigoidine and differentially inhibits Vibrios. *Front. Microbiol.* 7:1342. doi: 10.3389/fmicb.2016.01342

Guerrero-Rubio, M. A., López-Llorca, R., Henarejos-Escudero, P., García-Carmona, F., and Gandía-Herrero, F. (2019). Scaled-up biotechnological production of individual betalains in a microbial system. *Microb. Biotechnol.* 12, 993–1002. doi: 10.1111/1751-7915.13452

Havenith, H., Kern, K., Rautenberger, P., Spiegel, H., Szardenings, M., Ueberham, E., et al. (2017). Combination of two epitope identification techniques enables the rational design of soy allergen Gly m 4 mutants. *Biotechnol. J.* 12:201600441. doi: 10.1002/biot.201600441

Hou, Y., Liu, X., Li, S., Zhang, X., Yu, S., and Zhao, G. R. (2020). Metabolic Engineering of *Escherichia coli* for de Novo Production of Betaxanthins. *J. Agricult. Food Chem.* 68, 8370–8380. doi: 10.1021/acs.jafc.0c02949

Huck, N. V., Leissing, F., Majovsky, P., Buntru, M., Aretz, C., Flecken, M., et al. (2017). Combined ^{15}N-labeling and tandemMOAC quantifies phosphorylation of MAP kinase substrates downstream of MKK7 in *Arabidopsis*. *Front. Plant Sci.* 8:2050. doi: 10.3389/fpls.2017.02050

Jaroentomeechai, T., Taw, M. N., Li, M., Aquino, A., Agashe, N., Chung, S., et al. (2020). Cell-free fynthetic glycobiology: Designing and engineering glycomolecules outside of living cells. *Front. Chem.* 8:645. doi: 10.3389/fchem.2020.00645

Karim, A. S., Dudley, Q. M., Juminaga, A., Yuan, Y., Crowe, S. A., Heggestad, J. T., et al. (2020). In vitro prototyping and rapid optimization of biosynthetic enzymes for cell design. *Nat. Chem. Biol.* 16, 912–919. doi: 10.1038/s41589-020-0559-0

Khatri, Y., Hohlman, R. M., Mendoza, J., Li, S., Lowell, A. N., Asahara, H., et al. (2020). Multicomponent microscale biosynthesis of unnatural cyanobacterial indole alkaloids. *ACS Synth. Biol.* 9, 1349–1360. doi: 10.1021/acssynbio.0c00038

Kightlinger, W., Duncker, K. E., Ramesh, A., Thames, A. H., Natarajan, A., Stark, J. C., et al. (2019). A cell-free biosynthesis platform for modular construction of protein glycosylation pathways. *Nat. Commun.* 10:5404. doi: 10.1038/s41467-019-12024-9

Kightlinger, W., Lin, L., Rosztoczy, M., Li, W., DeLisa, M. P., Mrksich, M., et al. (2018). Design of glycosylation sites by rapid synthesis and analysis of glycosyltransferases. *Nat. Chem. Biol.* 14, 627–635. doi: 10.1038/s41589-018-0051-2

Kim, J. H., Komatsu, M., Shin-Ya, K., Omura, S., and Ikeda, H. (2018). Distribution and functional analysis of the phosphopantetheinyl transferase superfamily in *Actinomycetales* microorganisms. *Proc. Nat. Acad. Sci. U S A.* 115, 6828–6833. doi: 10.1073/pnas.1800715115

Körfer, G., Pitzler, C., Vojcic, L., Martinez, R., and Schwaneberg, U. (2016). In vitro flow cytometry-based screening platform for cellulase engineering. *Sci. Rep.* 6:26128. doi: 10.1038/srep26128

Li, J., Zhang, L., and Liu, W. (2018). Cell-free synthetic biology for *in vitro* biosynthesis of pharmaceutical natural products. *Synth. Syst. Biotechnol.* 3, 83–89. doi: 10.1016/j.synbio.2018.02.002

Li, L., Liu, Z., Jiang, H., and Mao, X. (2020). Biotechnological production of lycopene by microorganisms. *Appl. Microbiol. Biotechnol.* 104, 10307–10324. doi: 10.1007/s00253-020-10967-4

Luo, Z., Liu, N., Lazar, Z., Chatzivasileiou, A., Ward, V., Chen, J., et al. (2020). Enhancing isoprenoid synthesis in Yarrowia lipolytica by expressing the isopentenol utilization pathway and modulating intracellular hydrophobicity. *Metab. Engine.* 61, 344–351. doi: 10.1016/j.ymben.2020.07.010

Madadi, E., Mazloum-Ravasan, S., Yu, J. S., Ha, J. W., Hamishehkar, H., and Kim, K. H. (2020). Therapeutic application of betalains: A review. *Plants* 9:1219. doi: 10.3390/plants9091219

Madduri, K., Armstrong, J., Etter, A., Buntru, M., Vogel, S., Schillberg, S., et al. (2018). *Novel eukaryotic cell-free protein expression system that does not require an artificial energy regeneration system*. Alexandria, VA: USPTO.

Matthäus, F., Ketelhot, M., Gatter, M., and Barth, G. (2014). Production of lycopene in the non-carotenoid-producing yeast Yarrowia lipolytica. *Appl. Environ. Microbiol.* 80, 1660–1669. doi: 10.1128/AEM.03167-13

Nowroozi, M. R., Ghaedi, E., Behnamfar, A., Amini, E., Momeni, S. A., Mahmoudi, M., et al. (2021). The role of nutritional interventions in prostate cancer: A review. *J. Res. Med. Sci.* 26:29. doi: 10.4103/jrms.JRMS_975_20

Polturak, G., and Aharoni, A. (2018). "La Vie en Rose": Biosynthesis, sources, and applications of betalain pigments. *Mol. Plant* 11, 7–22. doi: 10.1016/j.molp.2017.10.008

Pyne, M. E., Narcross, L., and Martin, V. (2019). Engineering plant secondary metabolism in microbial systems. *Plant Physiol.* 179, 844–861. doi: 10.1104/pp.18.01291

Saini, R. K., Keum, Y. S., Daglia, M., and Rengasamy, K. R. (2020). Dietary carotenoids in cancer chemoprevention and chemotherapy: A review of emerging evidence. *Pharmacol. Res.* 157:104830. doi: 10.1016/j.phrs.2020.104830

Schillberg, S., and Finnern, R. (2021). Plant molecular farming for the production of valuable proteins - Critical evaluation of achievements and future challenges. *J. Plant Physiol.* 258-259:153359. doi: 10.1016/j.jplph.2020.153359

Schillberg, S., Raven, N., Spiegel, H., Rasche, S., and Buntru, M. (2019). Critical analysis of the commercial potential of plants for the production of recombinant proteins. *Front. Plant Sci.* 10:720. doi: 10.3389/fpls.2019.00720

Shi, J., and Le Maguer, M. (2000). Lycopene in tomatoes: chemical and physical properties affected by food processing. *Crit. Rev. Food Sci. Nutrit.* 40, 1–42. doi: 10.1080/10408690091189275

Shimizu, Y., Inoue, A., Tomari, Y., Suzuki, T., Yokogawa, T., Nishikawa, K., et al. (2001). Cell-free translation reconstituted with purified components. *Nat. Biotechnol.* 19, 751–755. doi: 10.1038/90802

Siebels, I., Nowak, S., Heil, C. S., Tufar, P., Cortina, N. S., Bode, H. B., et al. (2020). Cell-free synthesis of natural compounds from genomic DNA of biosynthetic gene clusters. *ACS Synth. Biol.* 9, 2418–2426. doi: 10.1021/acssynbio.0c00186

Soares, A. R., Marchiosi, R., Siqueira-Soares, R., Barbosa, de Lima, R., Dantas, et al. (2014). The role of L-DOPA in plants. *Plant Signal. Behav.* 9:e28275. doi: 10.4161/psb.28275

Vieira Teixeira da Silva, D., Dos Santos Baião, D., de Oliveira Silva, F., Alves, G., Perrone, D., and Mere Del Aguila, E. (2019). Betanin, a natural food additive: Stability, bioavailability, antioxidant and preservative ability assessments. *Molecules* 24:458. doi: 10.3390/molecules24030458

Wang, Z., Sun, J., Yang, Q., and Yang, J. (2020). Metabolic engineering *Escherichia coli* for the production of lycopene. *Molecules* 25:3136. doi: 10.3390/molecules25143136

Wehrs, M., Gladden, J. M., Liu, Y., Platz, L., Prahl, J. P., Moon, J., et al. (2019). Sustainable bioproduction of the blue pigment indigoidine: Expanding the range of heterologous products in R. toruloides to include non-ribosomal peptides. *Green Chem.* 21, 3394–3406. doi: 10.1039/C9GC00920E

Wu, D., von Roepenack-Lahaye, E., Buntru, M., de Lange, O., Schandry, N., Pérez-Quintero, A. L., et al. (2019). A plant pathogen type III effector protein subverts translational regulation to boost host polyamine levels. *Cell Host Microbe.* 13, 638–649.e5. doi: 10.1016/j.chom.2019.09.014

Yalpani, N., Altier, D. J., Barbour, E., Cigan, A. L., and Scelonge, C. J. (2001). Production of 6-methylsalicylic acid by expression of a fungal polyketide synthase activates disease resistance in tobacco. *Plant Cell* 13, 1401–1409. doi: 10.1105/tpc.13.6.1401

Zhang, C., and Too, H. P. (2020). Strategies for the biosynthesis of pharmaceuticals and nutraceuticals in microbes from renewable feedstock. *Curr. Med. Chem.* 27, 4613–4621. doi: 10.2174/0929867327666200212121047

Conflict of Interest: SS is member of the Scientific Advisory Board of LenioBio GmbH, which distributes the BY-2 cell-free lysate developed by Fraunhofer IME and Dow AgroSciences.

The remaining authors declare that the research was conducted in the absence of any commercial or financial relationships that could be construed as a potential conflict of interest.

Publisher's Note: All claims expressed in this article are solely those of the authors and do not necessarily represent those of their affiliated organizations, or those of the publisher, the editors and the reviewers. Any product that may be evaluated in this article, or claim that may be made by its manufacturer, is not guaranteed or endorsed by the publisher.

frontiers in Plant Science

ORIGINAL RESEARCH
published: 24 February 2022
doi: 10.3389/fpls.2022.830931

Modifying Anthocyanins Biosynthesis in Tomato Hairy Roots: A Test Bed for Plant Resistance to Ionizing Radiation and Antioxidant Properties in Space

Silvia Massa[1], Riccardo Pagliarello[1,2], Alessia Cemmi[3], Ilaria Di Sarcina[3], Aureliano Bombarely[4], Olivia Costantina Demurtas[1], Gianfranco Diretto[1], Francesca Paolini[5], H. Earl Petzold[6], Mattijs Bliek[7], Elisabetta Bennici[1], Antonella Del Fiore[8], Patrizia De Rossi[9], Cornelis Spelt[7], Ronald Koes[7], Francesca Quattrocchio[7] and Eugenio Benvenuto[1]*

[1] Department for Sustainability, Biotechnology and Agro-Industry Division – Biotec Laboratory, Italian National Agency for New Technologies, Energy and Sustainable Economic Development, Rome, Italy, [2] Department of Agriculture and Forest Sciences, University of Tuscia, Viterbo, Italy, [3] Fusion and Nuclear Safety Technologies Department, Italian National Agency for New Technologies, Energy and Sustainable Economic Development, Rome, Italy, [4] Department of Biosciences, University of Milan, Milan, Italy, [5] 'Regina Elena' National Cancer Institute, HPV-UNIT, Department of Research, Advanced Diagnostic and Technological Innovation, Translational Research Functional Departmental Area, Rome, Italy, [6] School of Plants and Environmental Sciences, Virginia Tech, Blacksburg, VA, United States, [7] Department of Plant Development and (Epi)Genetics, Swammerdam Institute for Life Sciences, University of Amsterdam, Amsterdam, Netherlands, [8] Department for Sustainability, Biotechnology and Agro-Industry Division – Agrifood Sustainability, Quality, and Safety Laboratory, Italian National Agency for New Technologies, Energy and Sustainable Economic Development, Rome, Italy, [9] Energy Efficiency Unit Department – Northern Area Regions Laboratory, Casaccia Research Center, Italian National Agency for New Technologies, Energy and Sustainable Economic Development, Rome, Italy

OPEN ACCESS

Edited by:
Henrik Toft Simonsen, Technical University of Denmark, Denmark

Reviewed by:
Concetta Licciardello, CREA Research Centre for Olive, Fruit and Citrus Crops, Italy
Zhengkun Qiu, South China Agricultural University, China

***Correspondence:**
Silvia Massa
silvia.massa@enea.it

Specialty section:
This article was submitted to Plant Biotechnology, a section of the journal Frontiers in Plant Science

Received: *07 December 2021*
Accepted: *07 January 2022*
Published: *24 February 2022*

Citation:
Massa S, Pagliarello R, Cemmi A, Di Sarcina I, Bombarely A, Demurtas OC, Diretto G, Paolini F, Petzold HE, Bliek M, Bennici E, Del Fiore A, De Rossi P, Spelt C, Koes R, Quattrocchio F and Benvenuto E (2022) Modifying Anthocyanins Biosynthesis in Tomato Hairy Roots: A Test Bed for Plant Resistance to Ionizing Radiation and Antioxidant Properties in Space. Front. Plant Sci. 13:830931. doi: 10.3389/fpls.2022.830931

Gene expression manipulation of specific metabolic pathways can be used to obtain bioaccumulation of valuable molecules and desired quality traits in plants. A single-gene approach to impact different traits would be greatly desirable in agrospace applications, where several aspects of plant physiology can be affected, influencing growth. In this work, MicroTom hairy root cultures expressing a MYB-like transcription factor that regulates the biosynthesis of anthocyanins in *Petunia hybrida* (*PhAN4*), were considered as a testbed for bio-fortified tomato whole plants aimed at agrospace applications. Ectopic expression of *PhAN4* promoted biosynthesis of anthocyanins, allowing to profile 5 major derivatives of delphinidin and petunidin together with pelargonidin and malvidin-based anthocyanins, unusual in tomato. Consistent with *PhAN4* features, transcriptomic profiling indicated upregulation of genes correlated to anthocyanin biosynthesis. Interestingly, a transcriptome reprogramming oriented to positive regulation of cell response to biotic, abiotic, and redox stimuli was evidenced. *PhAN4* hairy root cultures showed the significant capability to counteract reactive oxygen species (ROS) accumulation and protein misfolding upon high-dose gamma irradiation, which is among the most potent pro-oxidant stress that can be encountered in space. These results may have significance in the engineering of whole tomato plants that can benefit space agriculture.

Keywords: MicroTom, hairy root cultures, agrospace, biofortification, anthocyanins, gamma radiation

INTRODUCTION

Anthocyanins are valuable water-soluble plant pigments. They accumulate in the vacuole of specialized cells and play a crucial role in pigmentation of flowers and fruits, pollinators attraction, plant-pathogen interaction, protection against ultraviolet (UV) light, and modulation of reactive oxygen species (ROS)-signaling both in reproductive and in vegetative tissues (Brunetti et al., 2013). As plant-derived molecules, anthocyanins are naturally present in the human diet where they are predominantly represented as glycosides, in a multitude of fruits and vegetables, among which berries and grapes have the highest content (Bognar et al., 2013). Anthocyanins act as health-promoting and chronic-diseases-preventing molecules, due to antioxidant, anti-inflammatory, anti-proliferative and anti-neurodegenerative functions (Blesso, 2019; Krga and Milenkovic, 2019; Tian et al., 2019; Bendokas et al., 2020; Kalt et al., 2020). Due to these properties, anthocyanins have increasing applications in the food sector and there is also growing interested in the design of food crops with improved levels and composition of these antioxidant nutraceuticals. In particular, the research involved in the definition of plants intended for 'agrospace' applications, will have to tackle the issue to provide fresh and healthy food for space crews in the context of a harmful ionizing irradiated environment, and to cope with cultivation areas subjected to possible biotic contaminations, as well (Amalfitano et al., 2020; Bijlani et al., 2021). Agrospace crops are, therefore, candidates for the application of technologies aiming to improve both their content in antioxidant nutraceuticals and resistance to biotic and abiotic stresses (Zabel et al., 2015, 2016; Massa et al., 2016; Khodadad et al., 2020).

Tomato (*Solanum lycopersicum* L.) is a rich source of bioactive molecules such as carotenoids (in particular, lycopene), polyphenols and flavonoids, ascorbic acid, and other vitamins (Gerszberg et al., 2015; Martí et al., 2016). However, anthocyanins are poorly accumulated in cultivated tomatoes and even the fruits of cultivar harboring natural mutants for the *Abg* (*Aubergine*), *Aft* (*Anthocyanin fruit*), and *Atv* (*Atroviolaceum*) loci, only contain these molecules in the peel (Mes et al., 2008; Gonzali et al., 2009; Povero et al., 2011). Accumulation in fruit flesh and other organs upon genetic engineering indicates that tomatoes can be manipulated to this end (Zhang et al., 2014; Lloyd et al., 2017). By breeding, tomato lines were generated that combine the dominant *Atv* allele with *Aft* or *Abg*. These lines accumulated up to 0.1% (in fresh weight) of the anthocyanin petunidin-3-(p-coumaryl)-rutinoside-5-glucoside in the fruit epidermis (Mes et al., 2008; Povero et al., 2011). Gene and pathway engineering are powerful approaches to enhance the biosynthesis of anthocyanins in plants, and they have been successfully applied in food staples (Garg et al., 2018). Transcription factors, regulating the expression of structural biosynthetic genes, control the activity of the anthocyanin pathway in all plant species (Gonzalez et al., 2008). In particular, proteins belonging to specific clades of R2R3-MYB, bHLH, WDR, and WRKY have been shown to regulate anthocyanins biosynthesis combined in the MBWW transcription complex, as shown for a multitude of plant species among which tomato (Ramsay and Glover, 2005; Zhang et al., 2014; Gao et al., 2018). The combined expression of a MYB and bHLH regulators of the anthocyanin pathway from *Antirrhinum majus* (*Delila* and *Rosea1*, respectively) under a fruit-specific promoter, resulted in the production of anthocyanins in fruits peel and flesh of tomato (Butelli et al., 2008). Studies have demonstrated that pathway engineering approaches implying the sole use of MYB factors belonging to the SG6 clade are sufficient to restore the biosynthesis of anthocyanins by promotion of the transcription of their bHLH partners and, therefore, by reconstituting the MBWW (Mehrtens et al., 2005; Takos et al., 2006; Zhang et al., 2019). The tomato *ANT1* gene encodes a MYB transcription factor belonging to the SG6 clade, highly homologous to the *Antirrhinum Rosea*. It has been demonstrated that ectopic expression of *ANT1* from a tomato wild relative (*S. chilense*), induces purple spotting on the epidermis of tomatoes (Mathews et al., 2003; Schreiber et al., 2012). The 35S promoter-driven expression of either the *Solanum lycopersicum ANT1* or *AN2* (another SG6 MYB), has been shown to induce anthocyanins production in the flesh and peel of the fruit and different organs of tomato plants (Kiferle et al., 2015). Upon overexpression of *SlAN2*, together with anthocyanins accumulation in fruits, flower organs, and vegetative parts, an enhancement of the emission of volatile molecules contributing to the aroma of fruits was found, as well (Jian et al., 2019). In addition, *SlAN2* has been related to the variation of levels of specialized metabolites other than anthocyanins, and of fruit softening (Meng et al., 2015). These findings seem to confirm that MYB transcription factors of the SG6 clade can regulate various, sometimes unrelated, processes in tomatoes, as well (Stracke et al., 2001; Zimmermann et al., 2004; Zhang et al., 2019). Therefore, a SG6 MYB-based approach may be considered suitable to affect multiple pathways in tomatoes.

The *Anthocyanin4* gene of *Petunia hybrida* (*PhAN4*) is a SG6 member of a small family of genes encoding very similar MYBs phylogenetically related to the snapdragon *AmROSEA*, the tomato *SlANT1*, and other anthocyanin-regulating MYBs from a multitude of plant species. All these petunia MYBs are involved in the induction of anthocyanins accumulation in different plant parts and response to different stimuli (Povero, 2011). In the present study, we performed *Agrobacterium rhizogenes*-mediated transfer of a construct for the expression of *PhAN4* into the miniature tomato genotype MicroTom to generate hairy root cultures (HRCs). HRCs were intended as a testbed for whole plant engineering strategies able to improve traits for space cultivation. We previously reported about improved *in vivo* response to space-mimicking conditions (i.e., static magnetic fields and X and gamma rays) of *PhAN4*-engineered HRC (Villani et al., 2017; Desiderio et al., 2019), confirming that this plant-based expression system, used over the last 30 years to produce various specialized metabolites and recombinant proteins of pharmaceutical value (Gutierrez-Valdes et al., 2020; Häkkinen et al., 2020), is useful in studies on the adaptation of plants to extraterrestrial conditions, as well. Recently, HRCs served in several plant species as handier and faster biotechnology tools, compared to whole plant transformation, to gain biological insights in gene function, spatial and temporal gene expression

studies, and signaling pathways in plant cell response to a changing environment (Ron et al., 2014).

Anthocyanin biosynthesis engineering in HRCs was reported in a few species (Sharma et al., 2013; Li et al., 2016; Thwe et al., 2016; Hou et al., 2017), and, to date, never in tomatoes. In this study, *PhAN4* gene expression resulted in anthocyanins accumulation in tomato HRCs. Transcript profiling showed that several genes encoding enzymes and transcription factors involved in anthocyanins biosynthesis were upregulated. Interestingly, also genes correlated to cell response to biotic and abiotic stress, including redox stimuli, resulted in transcriptionally upregulated.

In addition, we report about the antioxidant properties and diminished generation of ROS in HRCs expressing *PhAN4* exposed to ionizing gamma radiation. *PhAN4* HRCs were endowed with a ninefold enhanced antioxidant capacity *per se* compared to controls by 2,2-diphenyl-1-picrylhydrazyl (DPPH) assay. Furthermore, ROS accumulation was counteracted after gamma radiation, as shown by Electron Spin Resonance (ESR) Spectroscopy. Both UV-VIS spectra and photoluminescence analysis demonstrated that polyphenols content and stability of soluble protein folding were not significantly affected by high dose gamma irradiation in *PhAN4*-engineered HRCs compared to control.

In conclusion, MicroTom HRCs represented a simplified model that allowed to rapidly test *PhAN4* expression effects on tomato cells, possibly opening the way to the application of the strategy to the engineering of whole plants intended for cultivation in harsh environments like future space outposts.

MATERIALS AND METHODS

Gene and Constructs

Anthocyanin4 (*PhAN4*) complementary DNA (cDNA) from petals of *Petunia* × hybrida cultivar Violet 30 (GenBank: HQ428105.1) was amplified with primers containing AttB sites and recombined into pDONR221 (RU Ghent) to produce an entry clone. This was then recombined with pKGW,0 (RU Ghent) to produce the 35S:AN4 construct and in pK7FWG2 (RU Ghent) to yield the 35S:GFP-*PhAN4* construct (where the *GFP* gene fusion was adopted to possibly stabilize the PhAN4 transcription factor).

Hairy Root Cultures Generation

Solanum lycopersicum (cv. MicroTom) clonal hairy root lines were obtained from wild-type leaf explants by infection with *A. rhizogenes* A4 (ATCC, 43057^{TM}) harboring either the 35S:*PhAN4* or the 35S:GFP-*PhAN4* or no additional construct. Bacteria were grown in a YEB medium with 50 μg/ml rifampicin and 50 μg/ml kanamycin at 28°C and 220 rpm to OD600 = 0.6. Bacteria were centrifuged at 3,000 × *g* for 15 min and resuspended at OD_{600} = 1 in Murashige and Skoog medium (MS, Duchefa) with 30 g/l sucrose and 200 μM acetosyringone, pH 5.8. Leaves from 3-week-old MicroTom plants were harvested, sterilized in 0.1% (v/v) sodium hypochlorite solution for 15 min, and aseptically cut into explants of 1 cm × 1 cm. Explants were immersed in the recombinant *A. rhizogenes* suspension for 15 min, in a rotary shaker at the minimum speed, and in the dark. Explants were dried onto sterilized tissue paper and transferred on their adaxial side, on MS agar medium co-culture plates with 100 μM acetosyringone and incubated in the dark for 4 days. Explants were then blotted and transferred to MS medium supplemented with 250 μg/ml cefotaxime (Cef) at 25°C. Fresh growing hairy roots were obtained after 8–10 days. Emerging roots of 1 cm in length were excised and transferred to new plates. *A. rhizogenes* was eliminated with decreasing Cef concentrations (0.25, 0.125, and 0.05 μg/ml) until no antibiotic was added. HRCs were screened for pigmentation under a dissecting microscope. Growth was estimated by the increase in fresh weight at different time points after subculture over a 28-day culture period recorded for three biological replicates for chosen hairy root clones. Hairy root biomass harvested for analysis was carefully handled, pulverized in liquid nitrogen, and immediately stored at −80°C. For metabolite content and antioxidant properties analysis, HRCs were lyophilized in a freeze-dry system (FreeZone Labconco, Kansas City, MO, United States).

Polymerase Chain Reaction Assays

Standard polymerase chain reaction (PCR) assays were performed on genomic DNA of kanamycin-resistant hairy root clones (extracted with NucleoSpin Plant II Kit; Macherey-Nagel; Duren, Germany) with primers specific for *PhAN4*, *rol B, rol C*, *virC1*, respectively (**Supplementary Table 1**), to select hairy root lines carrying *PhAN4* transgene clean from *A. rhizogenes* in the tissue culture. In selected HRC clones, SYBR Green real-time PCR was used to determine the *PhAN4* copy number. The tomato actin 41 gene (NCBI Reference Sequence: NM_001330119.1) served as an endogenous gene reference. For qPCR (i-Cycler iQ detection system; BioRad Laboratories Inc., Milan, Italy) Kapa SYBR Fast 2× qPCR Master Mix (KAPA Biosystems, Milano, Italy) was used, according to the manufacturer's instructions. Samples were amplified at 95°C for 3 min, followed by 40 cycles of denaturation at 95°C for 15 s, annealing, and extension at 60°C for 30 s.

Total RNA was isolated using the RNeasy Plant Mini Kit (Qiagen; Valencia, CA, United States) and then treated with amplification grade DNaseI (Invitrogen, Cambridge, MA, United States). cDNA was synthesized using the iScript^{TM} cDNA Synthesis Kit (BioRad Laboratories Inc., Milan, Italy) and used as a template for real time-PCR analysis (Kapa SYBR Fast 2× qPCR Master Mix; KAPA Biosystems, Milan, Italy) in iCycler iQ detection system (BioRad Laboratories Inc., Milan, Italy). The actin 41 gene was used as the reference gene. Primers are listed in **Supplementary Table 1**. Relative gene expression levels were obtained using the $2^{-\Delta CT}$ formula (Livak and Schmittgen, 2001).

Phenylpropanoids Identification

Anthocyanin profile was carried out on representative *PhAN4* and GFP-*PhAN4* HRCs by liquid chromatography coupled to high-resolution mass spectrometry (LC-HRMS) as reported before (Diretto et al., 2019; Carmona et al., 2021) with slight

modifications. Briefly, 3 mg (dried weight) of ground hairy roots were re-suspended in 600 μl of 85:15 MeOH: 1N HCl, vortexed, shaken in Mixer Mill (MM) for 15′ at 20 Hz frequency and gently mixed at 4°C O.N. Samples were then centrifuged at 20,000 × *g* for 20 min, the supernatant recovered, completely dried and re-suspended in 600 μl of spiked (with 0.5 μg/ml formononetin, as internal standard) 75% MeOH + 0.1% formic acid. Samples were then centrifuged 10 min at 20,000 × *g* at RT, and the supernatant was transferred to HPLC vials for MS analysis with a Q-Exactive mass spectrometer (Thermo Fisher Scientific, Cambridge, MA, United States), coupled to a HPLC system equipped with a photodiode array detector (Dionex, Califiornia, United States). LC separation of anthocyanins was performed injecting 5 μl of sample on a C18 Luna reverse-phase column (100 × 2.1 mm, 2.5 μm; Phenomenex, Torrance, CA, United States), using as mobile phase water + 0.1% formic acid (A) and acetonitrile + 0.1% formic acid (B) at a total flow rate of 250 μl/min. The separation was developed using 5% B for 0.5 min, followed by a 24 min linear gradient to 75% B. The ionization was performed using heated electrospray ionization (HESI) source, with nitrogen used as sheath and auxiliary gas, and set to 35 and 10 units, respectively. The vaporizer temperature was 250°C, the capillary temperature was 30°C, the spray voltage was set to 3.5 kV, the probe heater temperature was 390°C, and the S-lens RF level was set at 50. The acquisition was performed in the mass range 110/1,600 m/z both in positive and in negative ion mode with the following parameters: resolution 70,000, microscan 1, AGC target 1e6, maximum injection time 50. UV-VIS detection was continuous from 220 to 700 nm. All solvents used were LC-MS grade (Merck Millipore, Burlington, MA, United States). Identification was achieved based on accurate masses and by comparison with authentic reference substances. The ion peak areas were normalized to the ion peak area of the internal standard (formononetin).

Total anthocyanins content was measured by spectrophotometric analysis, as described in the study of Brito et al. (2014), using the extinction coefficient of the most abundant anthocyanin (petunidin-3-(p-coumaroyl)-rutinoside-5-glucoside).

Determination of the Total Phenolics Accumulation Level

Total phenolic content of representative *PhAN4* and GFP-*PhAN4* MicroTom HRC was estimated by colorimetric assay with modified (Inglett et al., 2010) Folin–Ciocalteu reagent (Merk, Germany) (Şensoy et al., 2006). Briefly, 4.25 ml of de-ionized water was mixed with 0.25 ml of ethanolic extract diluted 1:5 with 80% (v/v) ethanol and 0.25 ml of Folin-Ciocalteu reagent. After 7 min incubation in the dark at room temperature, 0.5 ml of saturated sodium carbonate solution (20%) was added, and the mixture was incubated for 40 min in the dark at room temperature. Absorbance was measured at 725 nm using a UV-VIS spectrophotometer (PerkinElmer, Waltham, MA, United States). A standard curve was prepared with gallic acid, as the reference standard. Final values were obtained by interpolating the absorbance values recorded for tomato hairy root extracts with the gallic acid calibration curve. The total phenolic content was expressed as μg of gallic acid equivalents (GAE)/g of dry weight. Each analysis consisted of triplicate measurements of each sample and data were averaged over the three measurements.

1,1-Diphenyl-2-Picrylhydrazyl Radical Scavenging Activity Assay

Phenolic compounds accumulating in representative *PhAN4* and GFP-*PhAN4* HRCs were extracted (Morishita et al., 2007) to apply the DPPH free radical scavenging method in order to establish their antioxidant properties. Ground, freeze-dried tomato HRC (30 mg) were extracted with 0.6 ml EtOH 80% (v/v), shaken in a water bath at 80°C for 40 min, and then centrifuged at 3,000 rpm for 15 min. The recovered supernatant was filtered through polytetrafluoroethylene membrane (0.45 μm) and stored at −20°C. The antioxidant capacity of the ethanolic extracts was spectrophotometrically tested by DPPH (1,1-diphenyl-2-picrylhydrazyl) (Li et al., 2010), with some modifications. Briefly, 0.25 ml of diluted ethanolic extract was added to 2.9 ml of 0.06 mM DPPH working solution. The mixture was shaken and allowed to stand at room temperature, in the dark, for 30 min. Absorbance was measured at 515 nm using a UV-VIS spectrophotometer. Lower absorbance values of the reaction mixture indicated higher free radical scavenging activity. The inhibition of free radical DPPH was expressed as DPPH scavenging effect (% inhibition) I% = {(A0 − A1)/A0) × 100}, where A1 and A0 are the absorbance values of blank and of tested samples, respectively. Trolox (vitamin E equivalent antioxidant) was used as the reference standard. Each analysis consisted of triplicate measurements of each sample and data were averaged over the three measurements.

Complementary DNA *L*ibrary *C*onstruction and *S*equencing for *T*ranscriptomic *A*nalysis

Total RNA from wild type and *PhAN4*-1 HRC was extracted using the RNeasy Plant Mini Kit (Qiagen; Valencia, CA, United States). RNA was quantified using the Qubit® fluorometer (Thermo Fisher Scientific, Waltham, MA, United States) and assayed through Agilent 2100 Bioanalyzer® (Agilent Technologies, Santa Clara, CA, United States) for quality and Integrity Number (RIN) evaluation. Samples with $8 \leq \text{RIN} \leq 10$ were considered. For each sample, equal amounts of RNA (2 μg) extracted from three biological replicates were pooled for cDNA library construction. First, the poly-A mRNA in the total RNA was pulled down using poly-T oligo-attached magnetic beads. After purification, the mRNA was fragmented at 95°C for 2 min along with RT primer and first-strand buffer. The fragmented RNA was used for the synthesis of the first-strand cDNA by adding DTT, dNTPs, Rnase Inhibitor, and SMARTScribe. All chemicals were incubated for 2 h at 42°C. This was followed by second-strand cDNA synthesis using template-switching oligonucleotide and an additional 1 μl of SMARTScribe. Subsequently, the cDNAs were purified using

two rounds of AMPure beads. The samples were enriched by using PCR to create the final library. A final fragment size purification step was performed using the Blue Pippin system selecting fragments between 250 and 500 bp. The libraries were confirmed by electrophoresis on a 1% TAE agarose gel and the Agilent BioAnalyzer 2100® after purification by AMPure bead. The average read size was estimated at 250–350 bp. The libraries were sequenced at Novogene Corporation using two lanes of an Illumina HiSeq4000 system with a pair-end run of 2 × 150 bp (Illumina, San Diego, CA, United States).

Sequencing Read Mapping and Identification of Differentially Expressed Genes

Raw RNA-seq libraries were analyzed according to the bioinformatic in-house pipeline (University of Amsterdam, Netherlands)[1]. The raw reads (in FASTQ format) generated from sequencing were cleaned using Trimmomatic version 0.36 (Institut Pasteur, France) (Cock et al., 2009) by removing adaptor-polluted reads, reads with unknown sequences "N" accounting for more than 5% and low-quality reads (with a mass value less than 10 and proportion of a total number of bases in the reads greater than 20%). The clean reads were mapped to the *S. lycopersicum* reference genome sequence version ITAG4 (Consortium et al., 2012) downloaded from the Sol Genomics Network database (Fernandez-Pozo et al., 2015). Two programs were used for this purpose: Hisat2 version 2.1 (Institut Pasteur, France) (Kim et al., 2015) and STAR version 2.5.2b (Institut Pasteur, France) (Dobin et al., 2013). The mapping results were compared with the Picard Tools CollectAlignmentSummaryMetrics version 1.138 (Broad Institute, Cambridge, MA, United States)[2]. The STAR mapping results were selected for further analysis. BAM files were transformed to a subread matrix file using the Rsubread version 1.34.4 R package (Bioconductor, open source) (Liao et al., 2019). Differential expression analysis was performed with the DESeq2 R package version 1.22.2 (Bioconductor, open source) (Love et al., 2014). Genes with an adjusted *P*-value of $\leq$0.001 and a log2 fold change of $\geq$2 were defined as differentially expressed (Benjamini and Hochberg, 1995).

Functional Annotation and Enrichment Pathway Analysis of Differentially Expressed Genes and Identification of Tomato Genes

The list of DEGs (Cluster 1 – *PhAN4*/WT $<$ 1 and Cluster 2 – *PhAN4*/WT $>$ 1) was analyzed using the g:Profiler (Reimand et al., 2007) with the default parameters using Organism *Solanum lycopersicum*. No terms were statistically significant under the "Measure underrepresentation" option. The results were exported as CSV and uploaded into R Studio where they were plotted with ggplot2[3]. The gene functional annotation was performed by sequence homology search with different protein data sets using BLASTP and Protein domains search using InterPro Scan.

Measurements of Tomato Hairy Root Cultures pH

Measurement of both control and PhAN4 HRCs pH was accomplished as described by Verweij et al. (2008). Briefly, 10 mg of hairy root material were ground in 2 ml distilled water and immediately measured with a pH electrode (edge® Multiparameter pH Meter – Hanna Instruments, Italy).

Gamma Irradiation Tests

Irradiation tests were performed at the Calliope facility, a pool-type irradiation plant equipped with a ^{60}Co gamma source in a high volume (7 m × 6 m × 3.9 m) shielded cell at ENEA (Casaccia Research Centre, Rome, Italy). The source emits radiations consisting of two gamma photons with a mean energy of 1.25 MeV (Baccaro et al., 2019). Fricke dosimetric system was employed for the determination of the absorbed dose during the irradiation tests. HRCs-derived samples were irradiated at room temperature, at three different absorbed doses (0.5, 1, and 2 kGy), and a dose rate of 1.8 kGywater/h.

Electron Spin Resonance Spectroscopy Before and After Gamma Irradiation

The molecular species accumulating upon the ectopic expression of *PhAN4* were investigated for possible efficient maintenance of the ability to counteract the generation of reactive oxygen species upon strong ROS inducers such as ionizing radiations. Gamma rays were used to generate peroxyl radicals (which are proportional to the number of paramagnetic species present in the samples) in lyophilized HRC powder. We explored ROS formation before and after 0.5, 1, and 2 kGy absorbed dose in AN4-1 and control HRCs sample sets by ESR Spectroscopy measurements. Not irradiated sample sets were used as references. Each set consisted of two replicates. For each ESR analysis, 8 ± 0.1 mg of HRC lyophilized powder was split into two PT-Capillaries (NOX-A.8.1-PT NOXYGEN, Holland) that were then inserted in a conventional quartz sample tube (o.d./i.d. of 4/3 mm) closed by a plastic lid. Irradiated samples were analyzed straight after the end of irradiation and ESR signals and were normalized to the sample mass. ESR measurements were acquired using an ESR e-scan spectrometer (Bruker, Billerica, MA, United States) operating in the X-band frequency (9.4 GHz) with a field modulation frequency of 86 kHz and modulation amplitude of 5.152 G. The ESR spectra were recorded at a central magnetic field of 3466 Gauss with a sweep width of 160 G, microwave power of 0.14 mW, microwave frequency of 9.75 GHz. The ESR spectra reported in this work derived from the accumulation of four scans. Bruker WinEPR data processing software (Bruker, Billerica, MA, United States) was used for data elaboration.

[1]https://github.com/KoesGroup/Snakemake_hisat-DESeq

[2]http://broadinstitute.github.io/picard/

[3]https://ggplot2.tidyverse.org/

Ultraviolet-Visible Absorbance Spectra Analysis Before and After Gamma Irradiation

Ultraviolet-visible (UV-VIS) spectra were obtained from crude extracts of AN4-1 and control HRCs. Briefly, lyophilized HRCs were ground in liquid nitrogen and the resulting powder was finely homogenized using an Ultraturrax homogenizer (IKA, Germany) in water:HCl (100:1, v/v). Samples were incubated at 500 rpm for 1 h at R.T., clarified by centrifugation at 11,000 × *g* for 30 min. The resulting supernatants were examined at 280–600 nm, by a UV-spectrophotometer (Lambda 950, Perkin Elmer, Waltham, MA, United States) at R.T. with a slit width of 2 nm, using a 10 mm cell.

Photoluminescence Analysis Before and After Gamma Irradiation

Samples were finely ground in liquid nitrogen with mortar and pestle, resuspended, and homogenized in phosphate-buffered saline pH 7.2 (PBS, 1:3 w/v) containing a protease inhibitor cocktail (Complete^{TM}; Roche, Mannheim, Germany) to extract soluble proteins. Photoluminescence emission spectra of extracts were determined before and straight after 2 kGy absorbed dose in AN4-1 and control HRC dried biomass sample sets. Two replicates per set were poured into quartz cuvettes with an optical path length of 1 cm (104F-QS, Hellma, Germany). The emission spectra were recorded using the Edinburgh Instruments FS 5 spectrometer in the range 300–800 nm with 280 nm excitation wavelength. The recorded spectra were mass-normalized and corrected for background scattering (reference: extraction buffer).

Statistical Analysis

All data (HRCs growth, *PhAN4* gene expression, total phenolic content, DPPH antioxidant capacity, total anthocyanin content) were subjected to one-way ANOVA with Tukey's post-test to determine the differences in average of all tested parameters ± *SD*. A *p*-value less than 0.05 was considered statistically significant. GraphPad Prism version 8.0.2 for Windows (GraphPad Software, San Diego, CA, United States) was used for graphical and statistical data processing.

RESULTS

Hairy Roots Generation and Screening

Both 35S:*PhAN4* and 35S:GFP-*PhAN4* constructs were independently transferred into the miniature tomato genotype MicroTom to generate hairy root cultures. Control HRCs were obtained by transformation with *A. rhizogenes* not containing *PhAN4*. HRCs were collected from independent explants. While control HRCs grew as unpigmented organ cultures (**Figure 1A**, left), HRCs generated by 35S:*PhAN4* and 35S:GFP-*PhAN4* showed purple pigmentation (**Figure 1A**, right) that may vary among clones. Purple pigmentation was present on primary and secondary branches and was maintained on kanamycin selection (**Supplementary Figure 1**). HRCs showed typical abundant secondary branching. Three clones for each construct were selected and further analyzed. No statistical difference was found in the growth rate of PhAN4, GFP-PhAN4, and control HRCs (**Figure 1B**).

Polymerase chain reaction (PCR) screening showed amplification of the expected fragments from genomic DNA, confirming integration of the necessary root-inducing genes from *A. rhizogenes* and of the *PhAN4* transgene (**Supplementary Figure 2A**). No transgene loss was observed over time (**Supplementary Figure 2B**). Control HRCs were negative for *PhAN4* amplification, as expected. Integration of *PhAN4* was estimated at copy numbers ranging from 4 to 8 copies, depending on the selected clone analyzed (**Supplementary Figure 3**). *PhAN4* transcripts were detected in both HRCs harboring either 35S:*PhAN4* or 35S:GFP-*PhAN4* constructs, while they were absent in the control, as expected (**Supplementary Figure 3**).

Liquid Chromatography Coupled to High-Resolution Mass Spectrometry Analysis of Phenylpropanoids

Total anthocyanins content was measured. AN4-1 and AN4-4 HRCs showed the highest anthocyanins concentrations, equal to 37 and 36.6 $\mu g/g_{\ driedweight}$ (**Figure 2A**), respectively. The anthocyanins profile was determined by LC-HRMS and compared to control HRCs. Identification was achieved by m/z ion reconstruction starting with the aglycon (delphinidin, petunidin, pelargonidin, malvidin), followed by the recognition of all the conjugated sugar and phenolic moieties. Subsequently, absolute quantification was performed as previously described (Diretto et al., 2019; Carmona et al., 2021) and by interpolating anthocyanin signal intensities in the roots compared to the ones of external calibration curves of the Pelargonidin-3-glucoside and Delphinidin 3,5-*O*-diglucoside standards. In our experimental conditions, anthocyanins were virtually undetectable in control HRCs. Petunidin-3-(p-coumaroyl)-rutinoside-5-glucoside1 and Delphinidin 3,5-*O*-diglucoside were the most abundant anthocyanins in the *PhAN4* roots, followed by a second group including Petunidin-3-(p-coumaroyl)-rutinoside-5-glucoside2, Petunidin-3-feruloyl-rutinoside-5-glucoside and Delphinidin-3-(p-coumaroyl)-rutinoside-5-glucoside. Two additional anthocyanins, Pelargonidin-3-glucoside and Malvidin-3-*O*-(4'''coumaroyl)-rutinose-5-*O*-glucose, were detected, although at low levels (**Figure 2B**; Su et al., 2016). All lines show about the same relative amount of the different anthocyanin species.

To evaluate the effect of the accumulation of anthocyanins on their precursors and the final balance on flavonoids accumulation, a detailed analysis of phenylpropanoids was carried out by LC-HRMS on the engineered HRCs. A graphical representation of the accumulation levels of anthocyanins precursors is shown for the best anthocyanin-accumulating AN4-1 HRC (**Figures 3**, **4**) and the other engineered HRC (**Supplementary Files 1, 2**). A series of phenolic acids and their derivatives (e.g., dicaffeoylquinic, 5-caffeoyl-quinic, and 4-caffeoyl-quinic acids) were accumulated at a significantly lower level compared to control. This finding might be ascribed to the role of these compounds as flavanones and flavonols precursors

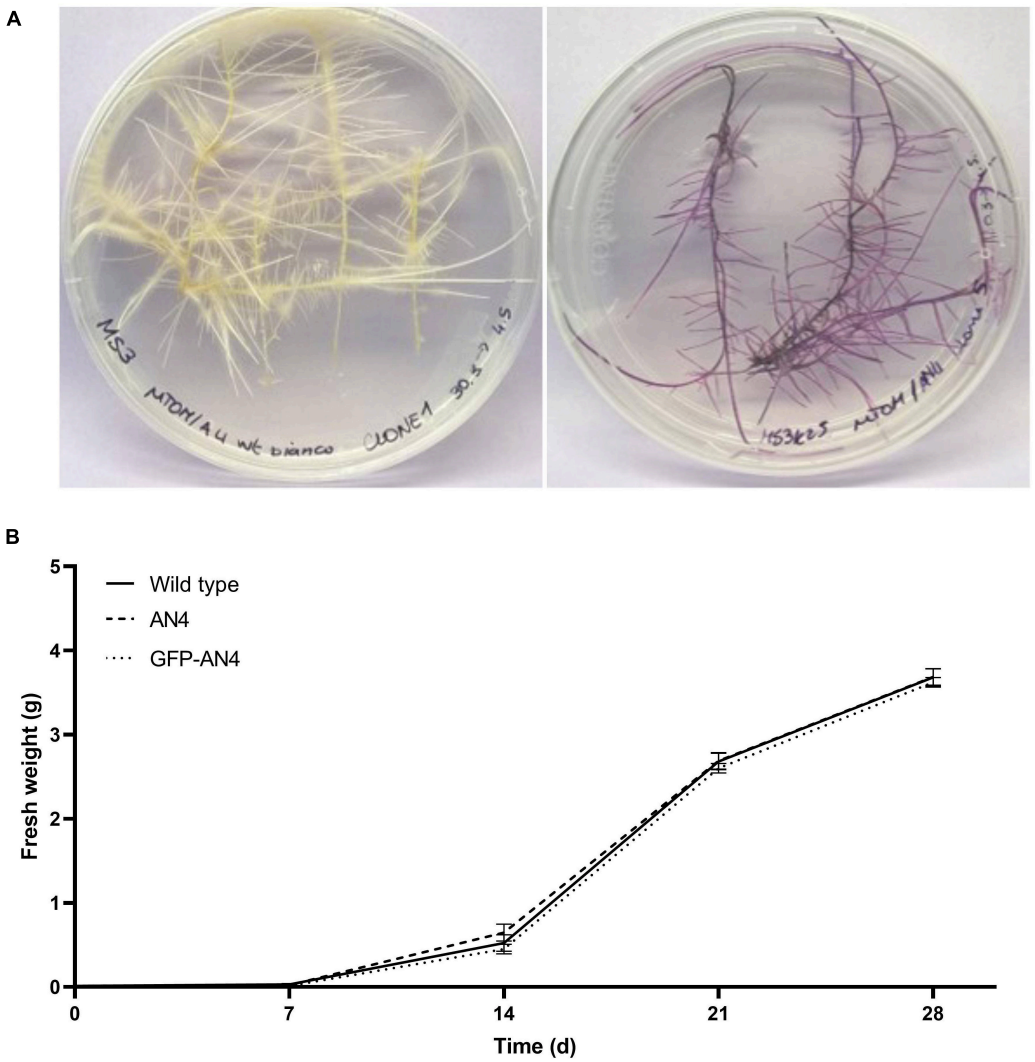

FIGURE 1 | Control (left) and transformed (35S:AN4, right) MicroTom hairy roots **(A)**. Hairy root culture (HRC) growth estimation by an increase in fresh weight along 28 days of cultures in MS medium (one-way ANOVA analysis of variance with Tukey's *post-hoc* test) by GraphPad Prism **(B)**.

of their sugar-decorated derivatives and of anthocyanins that, in turn, resulted to be enhanced in accumulation in engineered HRCs. As a consequence of the lower accumulation of phenolic acids, hydroxycinnamic acid accumulated at reduced levels in engineered HRCs, with respect to control. Interestingly, the hydroxybenzoic acid level was not significantly different. Significantly higher levels of other valuable phenolics such as coumaric acid and caffeic acid derivatives were found in AN4-1 HRC compared to control (**Figure 3**).

Accordingly, among flavonoids, both flavanones (i.e., naringenin chalcone and its sugar-decorated derivatives, naringenin, eriodictyol) and flavonols (i.e., dihydrokaempferol, sugar-decorated kaempferol, dihydroquercetin, quercetin derivatives, rutin, and myricetin) resulted in an overall significantly higher accumulation in engineered HRCs compared to control (**Figure 4** and **Supplementary File 2**). Notably, and coherently with phenolic acids precursor function, the observed fold change levels on most flavonoid groups (from naringenin and kaempferol derivatives to quercetin derivatives and rutin) displayed a much larger extent (192.82 ± 39.1 for naringenin dihexose I) compared to the phenolic acid precursor (0.623 ± 0.069 for 4-caffeoyl-quinic acids).

AN4-1 HRC was chosen as the candidate to perform the subsequent transcriptome analysis due to the higher content of the different anthocyanin and flavonoid species compared to the remaining clones.

Transcriptome Analysis of Tomato *PhAN4* Hairy Roots

The response to the constitutive expression of *PhAN4* in tomato HRCs were analyzed transcriptome-wide by RNAseq analysis and compared to control HRCs. AN4-1 showed a total of 442 differentially expressed genes (DEGs), of which 331

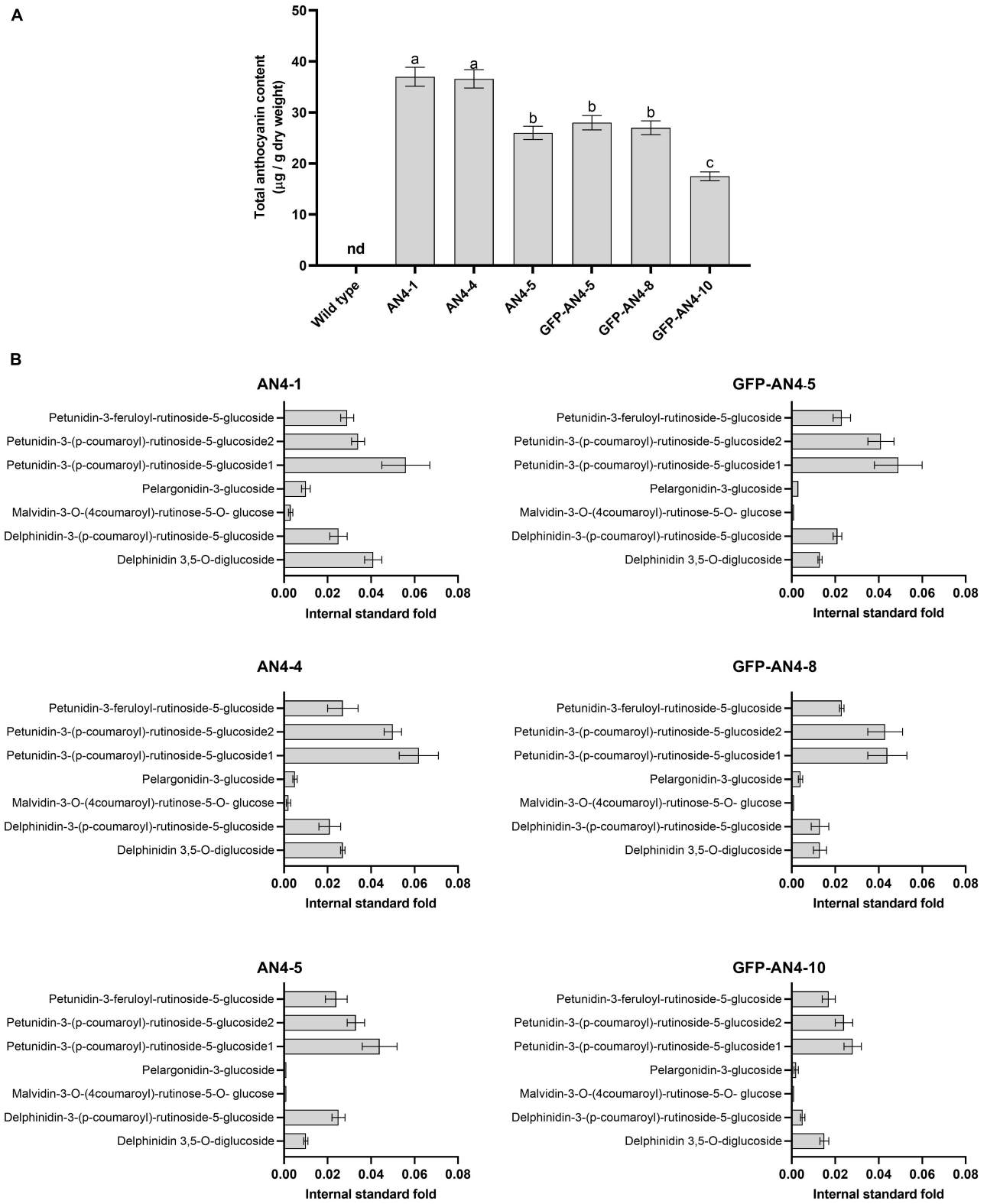

FIGURE 2 | Anthocyanins in PhAN4 HRC clones. Total anthocyanins content **(A)** and amount of specific anthocyanins **(B)** of six representative PhAN4-expressing hairy root clones. Columns report average values ± *SD* (*n* = 3).

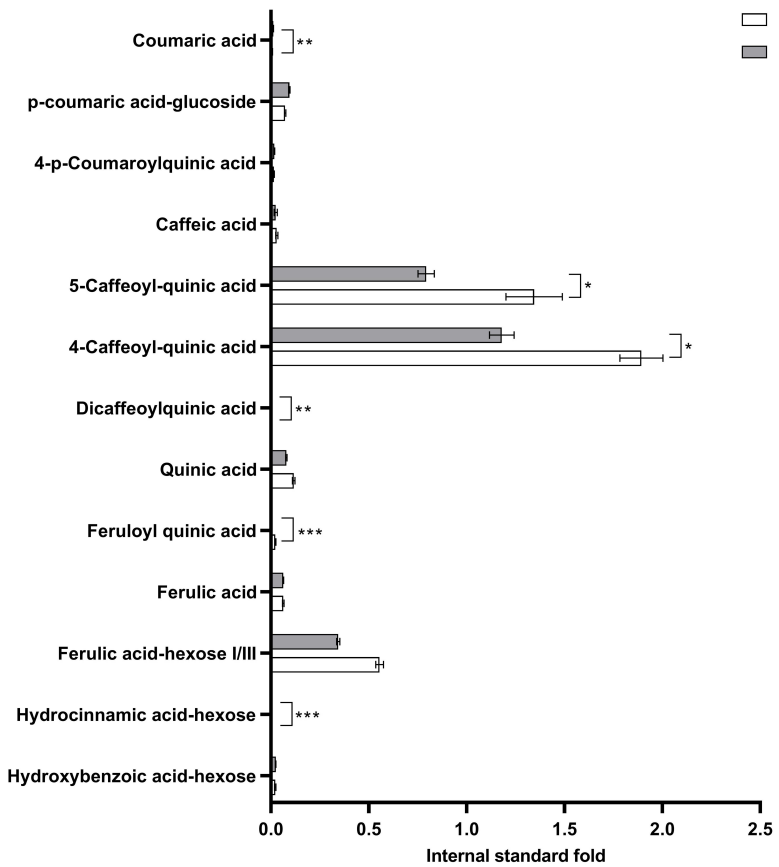

FIGURE 3 | Graph representing phenolic compounds and their derivatives expressed as internal standard (formononetin) fold of control and AN4-1 HRCs. Columns report average values ± *SD* (*n* = 3). **p*-value ≤ 0.05, ***p*-value ≤ 0.01 and ****p*-value ≤ 0.001.

were upregulated and 111 were downregulated (**Table 1** and **Supplementary File 3**). After Gene Ontology Enrichment (GOE) analysis, 38 upregulated and 8 downregulated genes were termed (**Supplementary File 4**). For upregulated DEGs, 3 GO categories were assigned: Molecular Function (MF), Biological Process (BP), and Cellular Component (CC) (**Figure 5**).

Gene Ontology Enrichment Analysis

Molecular function (MF) resulted in the most abundantly represented GO category, with 9 GO terms and an intersection size of 15 genes over a query size of 165 genes. The most enriched terms were related to 'enzyme inhibitory activity,' with nine upregulated DEGs, seven of which are classified as serine-type endopeptidase inhibitors in tomatoes. Among them, Solyc03g020080.3.1, Solyc03g020030.3.1, Solyc11g020960.2.1, Solyc08g080630.3.1, Solyc10g086090.2.1, Solyc10g086100.2.1 encode specific Pin-II type proteinase inhibitors or protease inhibitors that have been already demonstrated to be players of the defense against wounding, pathogens, and pests and of response to abiotic stress, especially UV, drought, and heat stress in tomato (Bergey et al., 1996; Conconi et al., 1996; Fan et al., 2020). Within MF also 'beta-glucosidase' and 'glucosidase activity' terms were represented with four upregulated DEGs. Among them, Solyc01g059965.1.1 has been demonstrated to be implicated in the defense of tomato plants against pathogens (Murata et al., 2019), and its expression has been found to be modulated in tomatoes upon infection with *Cladosporium fulvum* and *Phytophthora infestans* (van Kan et al., 1992; Fan et al., 2021). Upregulation of Solyc06g073760.3.1 has been correlated to increased softening of transgenic tomato overexpressing a MADS-box transcription factor, affecting fruit development and ripening (Huang et al., 2017).

Within the BP category, coherently with secondary metabolites analysis, the 'flavonoid biosynthetic process' term was found. In particular, GOE analysis highlighted the upregulation of four genes: Solyc05g053550.3.1, Solyc09g091510.3.1, Solyc02g083860.3.1, Solyc02g085020.3.1. Solyc09g091510.3.1, and Solyc05g053550.3.1 are tomato *chalcone synthase* (*CHS*) I and II, respectively, that are early pathway genes that determine the accumulation of the naringenin chalcone precursor of anthocyanins and other flavonoids (Zhang et al., 2019). Solyc02g083860.3.1 is tomato *Flavonoid-3-hydroxylase* (*F3H*) that leads to the accumulation of dihydromyricetin, dihydrokaempferol, and

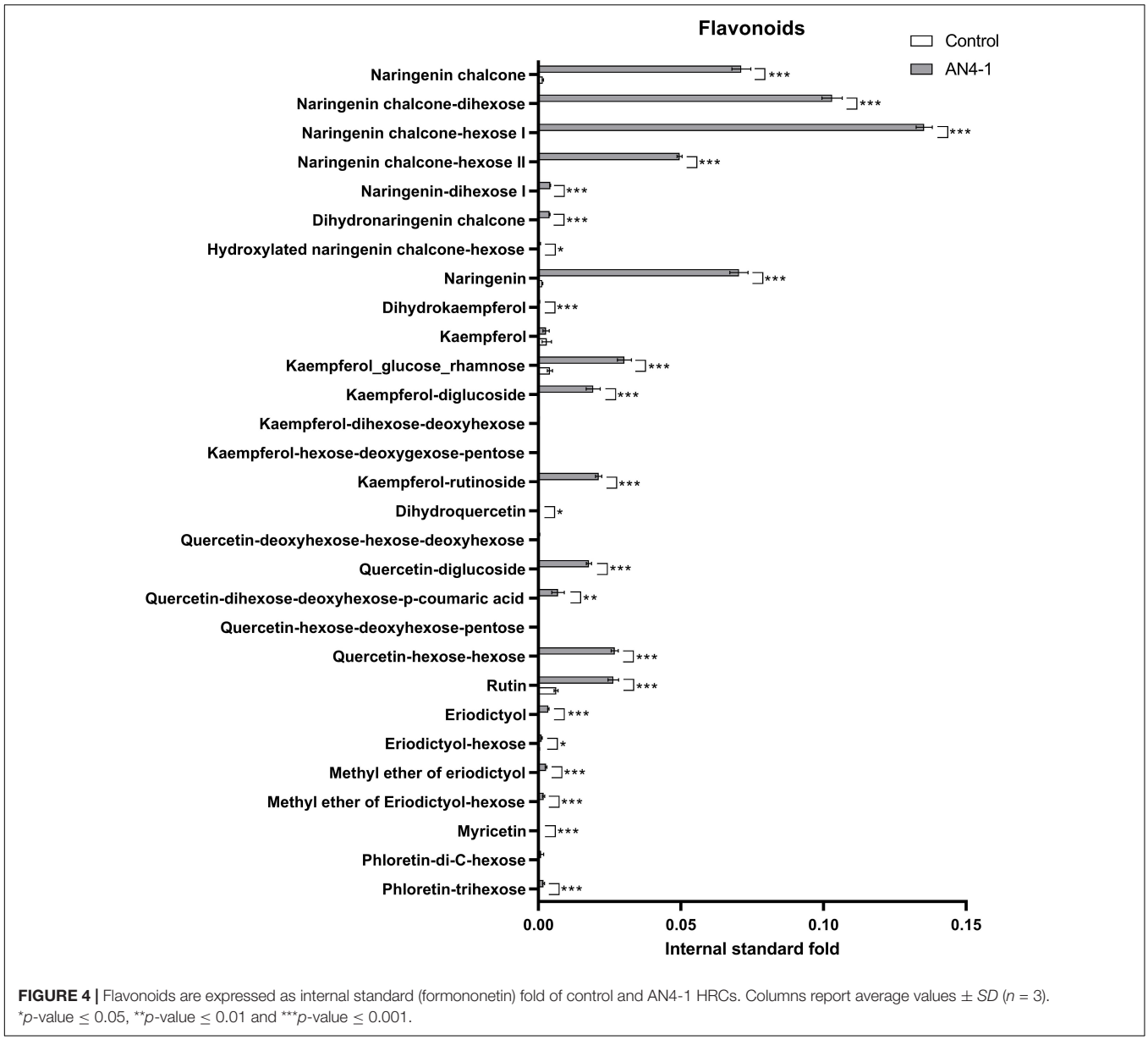

FIGURE 4 | Flavonoids are expressed as internal standard (formononetin) fold of control and AN4-1 HRCs. Columns report average values ± *SD* (*n* = 3). *p-value ≤ 0.05, **p-value ≤ 0.01 and ***p-value ≤ 0.001.

dihydroquercetin precursors of anthocyanins and of other flavonoids in tomatoes (Aoki et al., 2010; Zhang et al., 2019). Solyc02g085020.3.1 is tomato *dihydroflavonol reductase* (*DFR*) that leads to the accumulation of leucoanthocyanidins in tomatoes (Bongue-Bartelsman et al., 1994).

Within the CC GO category, 'Extracellular Region' and 'Casparian Strip' terms were categorized. Seventeen genes over a query size of 115, were found to be upregulated within these terms. These genes, in many cases, are specifically correlated to lignin biosynthesis, cell wall organization, and resistance to abiotic and biotic stress functions in tomatoes. In particular, Solyc05g052245.1.1 and Solyc09g010860.3.1 are the tomato expansins A8-like and EXPA4, involved in cell wall organization (Consortium et al., 2012). Solyc02g062510.3.1, which shares 86% homology with the *S. tuberosum* Peroxidase 72-like gene, and Solyc02g077300.2.1 (tomato Peroxidase 19) are involved in the phenylpropanoids biosynthesis (Mei et al., 2009). In addition, also Solyc04g080760.3.1 (tomato Peroxidase 9) plays a role in hypoxia tolerance and maintaining the iron balance in tomato (Safavi-Rizi et al., 2020). Peroxidase 9 was also demonstrated to be a pathogenesis-related protein upregulated upon *Tomato Mosaic Virus* infection (Andolfo et al., 2014). Solyc06g054320.1.1, Solyc10g055190.1.1, Solyc10g055200.1.1, and Solyc04g010270.1.1 represent tomato dirigent proteins that contribute to the dimerization of conyferil alcohol, a crucial step toward lignin biosynthesis, modulating cell wall metabolism during abiotic and biotic stress exposure in tomato (Paniagua et al., 2017). Solyc01g110110.3.1 and Solyc02g076710.3.1 are tomato cysteine proteinases. In particular, Solyc02g076710.3.1 shares 90% homology with *N. benthamiana* cathepsin B-like

cysteine proteases that are involved in the hypersensitive response (McLellan et al., 2009). Solyc08g080630.3.1, already highlighted as an upregulated DEG within the MF category GOE, is the tomato *SlPI31* protease inhibitor. This gene has been demonstrated to be upregulated under *Tomato Spotted Wilt Virus* infection in tomato roots and leaves and has been shown to be upregulated in drought-tolerant tomato lines and drought-sensitive varieties under drought conditions (Fan et al., 2020).

Gene ontology enrichment (GOE) analysis revealed only one downregulated DEG (**Supplementary File 4**) belonging to the Molecular Function term 'glycosyl transferase.' Solyc05g053890.2.1 represents the complete sequence of the tomato UDP-GT-like which is probably related to glycosylation of flavonoids prior to their transport to the vacuole (Solyc04g016200.1.1, Solyc04g016210.3.1, Solyc05g053890.2.1, Solyc01g095760.3.1 are incomplete sequences of tomato UDP-GT-like) (Fernandez-Moreno et al., 2016).

Differentially Expressed Genes Analysis

Despite no GOE being found in the Response to stimulus category, a relatively high number of DEGs was found that could be associated with response to abiotic and biotic stress response. Fifteen upregulated and seven downregulated DEGs were found to be correlated with such response. Among upregulated DEGs involved in early signals of defense responses against environmental cues, Solyc01g096560.2.1 (Log_2Fc = 4,10; *TomLOXD*; **Supplementary File 3**), was retrieved. *TomLOXD* encodes a lipoxygenase that has been demonstrated to elevate wound-induced jasmonate response, upregulation of wound-induced genes, and enhanced resistance to insects and necrotrophic pathogens in tomatoes (Yan et al., 2013). Solyc07g054840.3.1 (Log_2Fc = 3.34; tomato transcription factor 41) shares the best homology with Myb41 of *A. thaliana* where it functions as a Map-kinase involved in several signaling pathways that control plant development and salt stress tolerance (Hoang et al., 2012). Solyc03g095810.3.1 (Log_2Fc = 6.92; tomato Trichome birefringence-like protein) upregulation mediates xylan acetylation and has been demonstrated essential in tomatoes for invading microorganism resistance and against environmental stress like cold and drought (Zhang et al., 2020). Solyc10g007970.2.1 (Log_2Fc = 6.96; tomato WRKY transcription factor 77) has been demonstrated to be involved in the signaling to water deficit in tomatoes (Asins et al., 2021). Solyc07g043690.2.1 (Log_2Fc = 2.80; tomato *SlNPR1*) has been suggested to regulate tomato plant drought response (Li J. et al., 2019). Solyc03g096460.3.1 (Log_2Fc = 2.3) is a known modulator of wound signaling in tomatoes (Scranton et al., 2013). Solyc02g080790.3.1 (Log_2Fc = 3.31; tomato deoxypusine synthase *SlDHS*) has been shown to be upregulated during osmotic stress and chilling injury (Wang et al., 2001; Gupta et al., 2013). Solyc10g081300.1.1 (Log_2Fc = 2.56; *SlMC8*), encodes a metacaspase that is upregulated during apoptosis induction by pests and regulated by drought, cold, and salt in tomatoes (Liu et al., 2016). Solyc10g080690.2.1 (Log_2Fc = 2.3; tomato patatin defense protein) has been demonstrated to be upregulated upon soil flooding in tomatoes (de Ollas et al., 2021). Solyc06g073760.3.1 (Log_2Fc = 4.07; tomato β 1,3-glucanase 2 *BGL2*) has been found to be negatively correlated with the sugar/organic acid ratio of tomato fruits (Li et al., 2021). The simultaneous upregulation of *BGL2* and *PR1*, the marker genes of the salicylic acid (SA) pathway, is a hallmark of systemic resistance induced in tomato plants against different pathogens and can be followed by accumulation of SA at high levels (Peng et al., 2004; Fahim et al., 2016; Hanan et al., 2020). Solyc12g035225.1.1 (Log_2Fc = 9.26; tomato putative zinc-finger domain-containing protein) shares 75% homology with rice *RICESLEEPER1* that was found to be upregulated in *S. chilense* in relation to transcription factors for salt tolerance (Kashyap et al., 2020). Solyc12g010500.2.1 and Solyc12g010670.1.1 (Log_2Fc = 5.35 and 5.36, respectively) are categorized as E3 ubiquitin proteins that have been found to be upregulated in tomato genotypes resistant to *Xanthomonas perforans* (Shi and Panthee, 2020). Solyc12g009630.2.1 (Log_2Fc = 5.18; tomato calmodulin *SlCaM3*), encodes an important calcium-binding protein that has been found to be upregulated in tomato stem and roots upon *Botrytis cinerea* infection and mechanical wounding (Peng et al., 2014). In addition, it has been reported that *SlCaM3* is strongly expressed under salt and cold stress in tomatoes (Shi and Du, 2020). Solyc02g067750.3.1 (Log_2Fc = 6.91) shares 80% identity with *N. benthamiana CA1*. During drought stress CA1 proteins gradually diminish within the chloroplast and are accumulated in the cytosol, suggesting that they could be translocated from chloroplasts to the cytosol and act as a signal messenger from the chloroplast in tomato (Li P. et al., 2020). Importantly, in view of the possible improvement of resistance to abiotic stresses relevant to space, Solyc08g075705.1.1 (Log_2Fc = 4.25; tomato plastidial thioredoxin Y2, *pTRX y2*) was found to be upregulated. PTRX y2 together with pTRX y1 and x-type TRXs is mostly involved in ROS detoxification and takes part in the complex redox signaling network regulating tomato plant development (Serrato et al., 2013).

Among downregulated DEGs correlated with resistance functions, Solyc09g007190.3.1 ($Log2Fc$ = −2.21; tomato peroxiredoxin-like 2A PRXL2A) redox regulatory protein was found. Solyc03g098760.2.1 (Log_2Fc = −5.1; tomato proteinase inhibitor I3 Kunitz-type trypsin inhibitor) has been demonstrated to be upregulated upon the cell-content feeding mite *Tetranychus* species infection (Schimmel et al., 2018) and it is told to protect seeds from predators (Islam et al., 2015). Solyc09g089490.3.1 (Log_2Fc = −5.21; tomato SlPI40 protease inhibitor) can be induced by abiotic (drought and salt) and biotic (*Botrytis cinerea* and *Tomato Spotted Wilt Virus*) stress (Fan et al., 2020). Solyc06g008760.1.1 (Log_2Fc = −3.05; tomato *Glutaredoxin-C13-like*) has been demonstrated to be upregulated in ripening inhibitor (*rin*) mutants of *S. lycopersicum* (Kumar et al., 2016). Solyc07g055610.2.1 (Log_2Fc = −2.05); tomato Resistance protein R1) has been related to resistance to late blight (Bournival et al., 1989) and it has been shown to be linked to proteinase inhibitor I3 upon *Fusarium oxysporum* infection (Bournival et al., 1989; Pan et al., 2000). Solyc01g010480 (Log_2Fc = −2.2; tomato K+ channel KAT1) was demonstrated to be highly upregulated in low K tolerant tomato genotypes upon potassium deficiency (Zhao et al., 2018). Solyc01g102610.3.1

TABLE 1 | List of the more representative and significant DEGs obtained from the GOE and functional annotation analyses in relation to agrospace application.

Gene ID	Log_2Fc	Gene name	Function	References
Solyc03g020080.3.1	2.017930333	*SlPI11*	Pin-II type proteinase inhibitor/**biotic (herbivorous and insects resistance), abiotic (drought/heat)**	Fan et al., 2020
Solyc03g020030.3.1	10.72904412	*SlPI16*	Pin-II type proteinase inhibitor/**biotic (wound stress, insect resistance), abiotic (heat)**	Fan et al., 2020
Solyc11g020960.2.1	2.362943887	*SlPI51*	Proteinase inhibitor II/**biotic (wound stress)**	Fan et al., 2020
Solyc08g080630.3.1	2.33279266	*SlPI31*	Proteinase inhibitor 1/**biotic (TSWV infection), abiotic (drought)**	Fan et al., 2020
Solyc10g086090.2.1	2.247200225	*SlPI47*	Trypsin inhibitor 1/**abiotic (drought)**	Fan et al., 2020
Solyc10g086100.2.1	2.406338004	*SlPI48*	Proteinase inhibitor/**abiotic (heat)**	Fan et al., 2020
Solyc01g059965.1.1	3.476158885	*SlGluB*	Beta-1,3-glucanase/**biotic (defense against pathogens: *C. fulvum*, *P. infestans*)**	van Kan et al., 1992; Fan et al., 2021
Solyc09g091510.3.1	12.25514456	*CHS*	Chalcone synthase 1/**phenylpropanoids biosynthesis**	Zhang et al., 2019
Solyc05g053550.3.1	9.83030415	*CHS*	Chalcone synthase 2/**phenylpropanoids biosynthesis**	Kalt et al., 2020
Solyc02g083860.3.1	6.299607501	*F3H*	Flavonoid-3-hydroxylase/**phenylpropanoids biosynthesis**	Aoki et al., 2010; Zhang et al., 2019
Solyc02g085020.3.1	10.09460014	*DFR*	Dihydroflavonol reductase/**phenylpropanoids biosynthesis**	Bongue-Bartelsman et al., 1994
Solyc01g106650.3.1	3.003680242	–	Xyloglucan endotransglucosylase/**cell elongation**	Li P. et al., 2020
Solyc11g011210.2.1	2.189943987	*RSI-1*	RSI-1 precursor/**lateral root initiation**	Taylor and Scheuring, 1994
Solyc03g093390.3.1	2.390710296	*LeEXPB2*	Expansin-B15-like/**sexual reproduction**	Sundaresan et al., 2016
Solyc08g077910.3.1	3.227703527	–	Expansin-like B1/**sexual reproduction**	Nveawiah-Yoho et al., 2013
Solyc05g052245.1.1	2.186779111	–	Expansin A8-like/**cell wall organization**	–
Solyc09g010860.3.1	2.630126243	*EXPA4*	Expansin 4-like/**cell wall organization**	–
Solyc02g062510.3.1	2.392338587	–	Peroxidase 72-like/**phenylpropanoids biosynthesis**	Nveawiah-Yoho et al., 2013
Solyc04g080760.3.1	2.42913063	–	Peroxidase 9/**abiotic stress (hypoxia tolerance)**	Andolfo et al., 2014
Solyc02g077300.2.1	7.236518572	–	Peroxidase 19/**phenylpropanoids biosynthesis, biotic (ToMV infection)**	Andolfo et al., 2014; Safavi-Rizi et al., 2020
Solyc06g054320.1.1	2.690758759	–	Dirigent protein/**lignin biosynthesis**	Paniagua et al., 2017
Solyc10g055190.1.1	5.216357243	–	Dirigent protein/**lignin biosynthesis**	Paniagua et al., 2017
Solyc10g055200.1.1	2.06850204	–	Dirigent protein/**lignin biosynthesis**	Paniagua et al., 2017
Solyc04g010270.1.1	2.350516375	–	Dirigent protein/**lignin biosynthesis**	Paniagua et al., 2017
Solyc02g076710.3.1	2.307987898	*CathB*	Cathepsin B-like cysteine/**biotic (hypersensitive response)**	McLellan et al., 2009
Solyc05g053890.2.1	−2.032569214	–	UDP-GT-like/**flavonoids glycosylation**	Fernandez-Moreno et al., 2016
Solyc01g096560.2.1	4.109312617	*TomLOXD*	Subtilisin-like protease/**biotic (wound stress, resistance to insects and necrotrophic pathogens)**	Yan et al., 2013
Solyc07g054840.3.1	3.341226163	*AtMYB41*	Transcription factor 41/**abiotic (salt tolerance)**	Hoang et al., 2012
Solyc03g095810.3.1	6.923791313	–	Trichome birefringence-like/**xylan acetylation (resistance against micro-organisms, cold and drought)**	Zhang et al., 2020
Solyc10g007970.2.1	6.961895177	–	Transcription factor 77/**abiotic (water deficit)**	Asins et al., 2021
Solyc07g043690.2.1	2.800732902	*SlNPR1*	3-Hydroxyisobutyryl-CoA hydrolase/**abiotic (drought stress)**	Li J. et al., 2019
Solyc03g096460.3.1	2.302142017	–	**Wound signaling**	Scranton et al., 2013
Solyc02g080790.3.1	3.317661852	*SlDHS*	Deoxyhypusine synthase/osmotic stress and chilling injury	Wang et al., 2001; Gupta et al., 2013
Solyc10g081300.1.1	2.564715	*SlMC8*	Metacaspase 9/**biotic (apoptosis induction by pests), abiotic (drought, cold and salt)**	Liu et al., 2016
Solyc10g080690.2.1	2.304387313	–	Patatin/**abiotic (flooding)**	de Ollas et al., 2021
Solyc06g073760.3.1	4.071580028	*BGL2*	Beta-glucosidase/**sugar/organic acid ratio tomato fruits/resistance against different pathogens/softening**	Liu et al., 2016
Solyc12g035225.1.1	9.263765052	*RICESLEEPER1*	BED zinc-finger/**abiotic (salt tolerance)**	Kashyap et al., 2020
Solyc12g010500.2.1	5.358159809	–	E3 ubiquitin protein/**biotic (resistance to *X. perforans*)**	Shi and Panthee, 2020
Solyc12g010670.1.1	5.364030417	–	E3 ubiquitin protein/**biotic (resistance to *X. perforans*)**	Shi and Panthee, 2020
Solyc12g009630.2.1	5.183567126	*SlCaM3*	Calcium-binding protein/**biotic (*B. cinerea*), abiotic (mechanical wounding, salt and cold stress)**	Peng et al., 2014; Shi and Du, 2020

(Continued)

TABLE 1 | (Continued)

Gene ID	Log_2Fc	Gene name	Function	References
Solyc02g067750.3.1	6.915338794	*CA1*	Carbonic anhydrase/**abiotic (drought stress)**	Li X. et al., 2020
Solyc08g075705.1.1	4.258074963	*pTRX y2*	Thioredoxin Y2/**ROS detoxification, redox signaling network regulation**	Serrato et al., 2013
Solyc09g007190.3.1	−2.218315202	*PRXL2A*	Peroxiredoxin-like 2A/**redox regulatory protein**	–
Solyc03g098760.2.1	−5.109469505	–	I3 Kunitz-type trypsin inhibitor/**biotic (infection *Tetranychus* species infection)**	Islam et al., 2015; Schimmel et al., 2018
Solyc09g089490.3.1	−5.211378167	*SlPI40*	Proteinase inhibitor/**abiotic (drought, salt) biotic (*B. cinerea*, TSWV infection)**	Fan et al., 2020
Solyc06g008760.1.1	−3.056115855	–	Glutaredoxin-C13-like/**upregulated in tomato *rin* mutants**	Kumar et al., 2016
Solyc07g055610.2.1	−2.055605009	*PR1*	Resistance protein R1/**biotic (resistance to late blight and *F. oxysporum* infection)**	Bournival et al., 1989; Pan et al., 2000
Solyc01g010480.3.1	−2.123574853	*KAT1*	K+ channel KAT1/**abiotic (tolerance to potassium deficiency)**	Zhao et al., 2018
Solyc01g102610.3.1	−3.607916378	*FRO6*	Ferric reduction oxidase 6/**biotic (*P. solani* infection)**	Buoso et al., 2019
Solyc05g010320.3.1	4.308610241	*CHI*	Chalcone isomerase/**phenylpropanoids biosynthesis**	Morita et al., 2014; Li Z. et al., 2019
Solyc05g052240.3.1	8.452278685	*CHI*	Chalcone isomerase/**phenylpropanoids biosynthesis**	Ron et al., 2014; Hou et al., 2017
Solyc11g066580.2.1	16.35234434	*F3′5′H*	Flavonoid-3′,5′-hydroxylase/**phenylpropanoids biosynthesis**	Shi and Panthee, 2020
Solyc08g080040.3.1	8.861102345	*ANS*	Anthocyanin synthase/**phenylpropanoids biosynthesis**	Shi and Panthee, 2020
Solyc04g078140.3.1	8.35041607	*DilFl*	Cytochrome B5/**phenylpropanoids biosynthesis (essential for full activity of F3′5′H)**	de Vetten et al., 1999
Solyc09g082660.3.1	15.05027118	*OMT*	Caffeoyl-CoA-*O*-methyltransferase/**phenylpropanoids biosynthesis**	Roldan et al., 2014; Shi and Panthee, 2020
Solyc02g062975.1.1	7.081891304	*3UFGT*	UDP-glucose flavonoid 3-*O*-glucosyl transferases/**phenylpropanoids biosynthesis**	Hu et al., 2011; Tohge et al., 2020
Solyc10g083440.1.1	9.972475187	*3UFGT*	UDP-glucose flavonoid 3-*O*-glucosyl transferases/**phenylpropanoids biosynthesis**	Hu et al., 2011; Tohge et al., 2017
Solyc12g098590.2.1	16.55105848	*3UFGT*	UDP-glucose flavonoid 3-*O*-glucosyl transferases/**phenylpropanoids biosynthesis**	Hu et al., 2011; Tohge et al., 2020
Solyc09g059170.2.1	8.326262972	*3RT*	Anthocyanidin-3-*O*-glucoside rhamnosyltransferase/**phenylpropanoids biosynthesis**	Tohge et al., 2020
Solyc12g088170.2.1	13.21347105	*AAT*	Flavonoid-3-*O*-rutinoside-4"'-*O*-phenylacyltransferase/**phenylpropanoids biosynthesis**	Florio et al., 2021
Solyc03g025190.4.1	16.80814437	*MTP77*	Transparent testa 2-like/**toxic compound extrusion, regulation of cell turgescence**	dos Santos et al., 2017
Solyc10g006120.2.1	7.357873128	*LDOX*	Leucoanthocyanidin dioxygenase/**phenylpropanoids biosynthesis**	Pelletier et al., 1997
Solyc07g052490.3.1	7.173073383	*Atv*	Myb-like transcription factor Atv/**anthocyanin biosynthesis**	Cao et al., 2017
Solyc10g086290.2.1	8.651275639	*SlAN2*	AN2-like transcription factor/**anthocyanin biosynthesis**	Sun C. et al., 2019
Solyc12g005800.2.1	7.517786731	*SlMYBATV-like*	R3-MYB repressor/**anthocyanin biosynthesis**	Cao et al., 2017
Solyc09g065100.2.1	14.18672027	*AN1*	AN1-like transcription factor/**anthocyanin biosynthesis**	Qiu et al., 2016
Solyc10g084380.1.1	3.439413134	*PH3*	WRKY transcription factor/**anthocyanin biosynthesis**	Verweij et al., 2016
Solyc10g083900.2.1	3.542474125	*Myb27*	MYB transcription factor/**inhibitor of anthocyanin biosynthesis**	Albert et al., 2011, 2014
Solyc01g095640.2.1	4.928760848	*SlTRY*	Trichome initiation factor ECT3/**anthocyanin biosynthesis**	Tominaga-Wada et al., 2013; Kim et al., 2017
Solyc01g105880.4.1	3.469067651	*TPS4*	Monoterpenoid synthase/**terpene biosynthesis**	Velázquez-Márquez et al., 2021
Solyc09g092470.2.1	5.695783056	*TPS14*	Sesquiterpene synthase/**terpene biosynthesis, biotic (*F. oxysporum* resistance)**	Velázquez-Márquez et al., 2021
Solyc11g017240.2.1	3.78371117	*SlCM2*	Chorismate mutase/**volatile compounds biosynthesis, abiotic (drought stress)**	Tzin et al., 2015; Filiz et al., 2019
Solyc08g008630.3.1	−3.340796451	*Dwarf27*	Beta-carotene isomerase D27/**strigolactone and beta-carotene biosynthesis, biotic (psyllid resistance)**	Harrison et al., 2021
Solyc04g050930.3.1	−2.072953851	*VDE*	Violaxanthin de-epoxidase VDE/**carotenoid biosynthesis, biotic (*P. syringae* infection), abiotic (anoxia)**	Yang Y. X. et al., 2015
Solyc05g010180.3.1	−2.221215961	*CRTISO*	Carotenoid isomerase/**carotenoid biosynthesis**	Isaacson et al., 2002
Solyc12g006140.2.1	4.364619823	–	Chlorophyll a/b-binding protein/**fruits ripening**	Zouari et al., 2014
Solyc02g065220.3.1	−2.141082227	–	Cytochrome P450/**fruits ripening (extended shelf-life**	Gao et al., 2018

(Continued)

TABLE 1 | (Continued)

Gene ID	Log_2Fc	Gene name	Function	References
Solyc09g066150.1.1	−4.574546484	–	Cytochrome P450/**fruits ripening (extended shelf-life)**	Gao et al., 2018
Solyc07g006570.3.1	4.221848981	–	Ribonuclease 3-like/**RNA biogenesis**	Consortium et al., 2012
Solyc02g065230.3.1	3.170387722	*IMT7*	Cytochrome P450	–
Solyc02g091440.2.1	2.129583909	*bHLH83-like*	bHLH/**enhance root hair initiation, promote flowering in short day and maintain the iron balance**	Qian et al., 2021
Solyc12g088130.2.1	4.327213562	*bHLH93-like*	bHLH/**enhance root hair initiation, promote flowering in short day**	–
Solyc04g077780.3.1	2.019567752	–	LIM transcription factor/**cytoskeleton organization**	–
Solyc12g013850.2.1	−2.036803744	–	Glycosyltransferase/**regulates anther development and male-sterility**	Omidvar et al., 2015
Solyc02g081340.3.1	10.53476424	*GST*	Glutathione-*S*-transferase/**anthocyanin biosynthesis**	Alfenito et al., 1998
Solyc01g058030.2.1	8.08401203	–	Gibberellin 2-beta-dioxygenase/**determines dwarf phenotype with shorter internodes**	Sun X. et al., 2019
Solyc05g054360.3.1	6.837513657	–	Pectin methylesterase/**flower initiation**	Wen et al., 2020
Solyc12g010500.2.1	5.358159809	–	U-box protein/**biotic (resistance to *X. perforans***	Shi and Panthee, 2020

The function was provided by SolGenomics Network annotation and by specific literature (in bold).

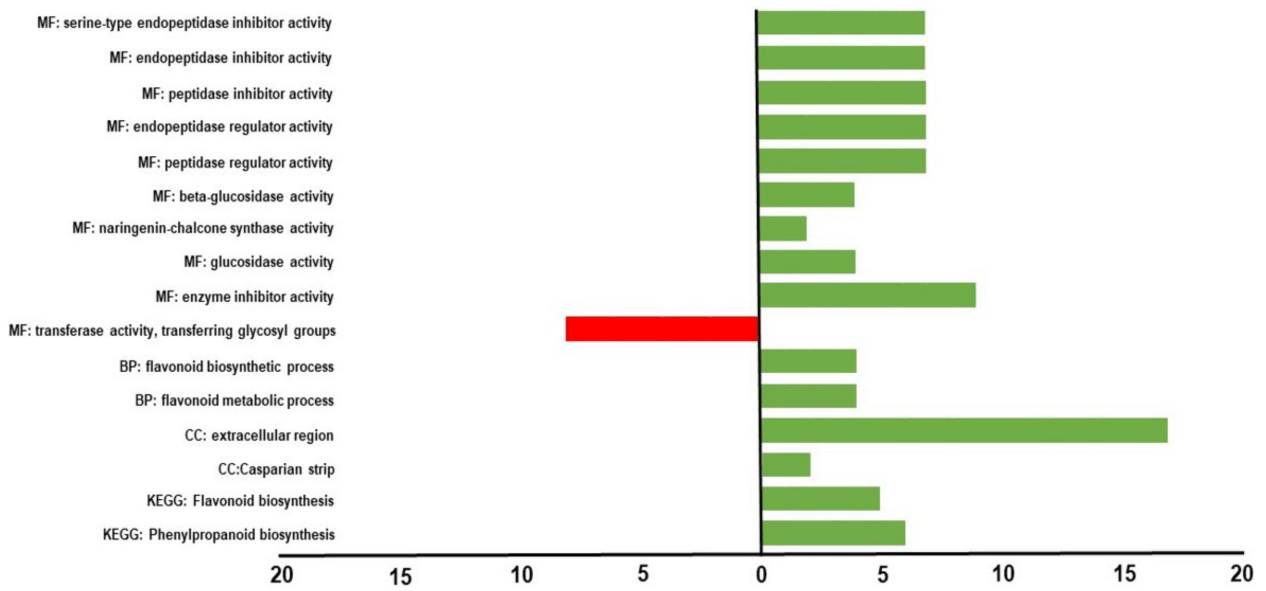

FIGURE 5 | GOs distribution of differentially expressed genes (DEGs). Gene Ontology (GO) terms associated with upregulated (green bars) and downregulated (red bars) genes in the PhAN4 HRCs compared to control HRCs, based on "Molecular Functions" (MF), "Biological Process" (BP), "Cellular Component" (CC) and KEGG ontological domain.

(Log2Fc = −3.60; tomato FRO6) is involved in nutrient transport in phloem and was observed to be downregulated under *Phytoplasma solani* infection of tomato (Buoso et al., 2019).

Despite GOE retrieving only four genes among the 'flavonoid biosynthetic process' term, many other upregulated DEGs resulted in the analysis that is associated with biosynthesis of anthocyanins and other specialized metabolites (**Figure 6**). Twelve additional structural genes and six transcription factors were identified as upregulated DEGs. In addition to *CHS*, *F3H* and *DFR*, DEGs analysis revealed also tomato naringenin-chalcone isomerase (*CHI*) (Solyc05g010320.3.1; Log_2Fc = 4.30 and Solyc05g052240.3.1; Log_2Fc = 8.45), tomato flavonoid-3′,5′-hydroxylase *F3′5′H* (Solyc11g066580.2.1; Log_2Fc = 16.35), tomato anthocyanin synthase *ANS* (Solyc08g080040.3.1, Log_2Fc = 8.86) were found. Interestingly, also Solyc04g078140.3.1, which shares the best homology with *Cytochrome b5* of *P. hybrida*, where it is essential for full activity of *F3′5′H*, was upregulated (Log_2Fc = 8.35) (de Vetten et al., 1999). In addition, tomato caffeoyl-CoA-*O*-methyltransferase Solyc09g082660.3.1; Log_2Fc = 15.0503), already identified as the prime candidate gene responsible for anthocyanin methylation in tomatoes due to significant correlation of expression with *ANS, DFR,* and *F3′5′H* in *Rosea1* and *Delila* fruits (Roldan et al., 2014), resulted upregulated. It shares the best homology with *P. hybrida O*-methyltransferase (*OMT*). Interestingly, it was found to have a significant correlation with abiotic stress in tomatoes (Shi and Panthee, 2020). Three tomato UDP-glucose flavonoid 3-*O*-glucosyl

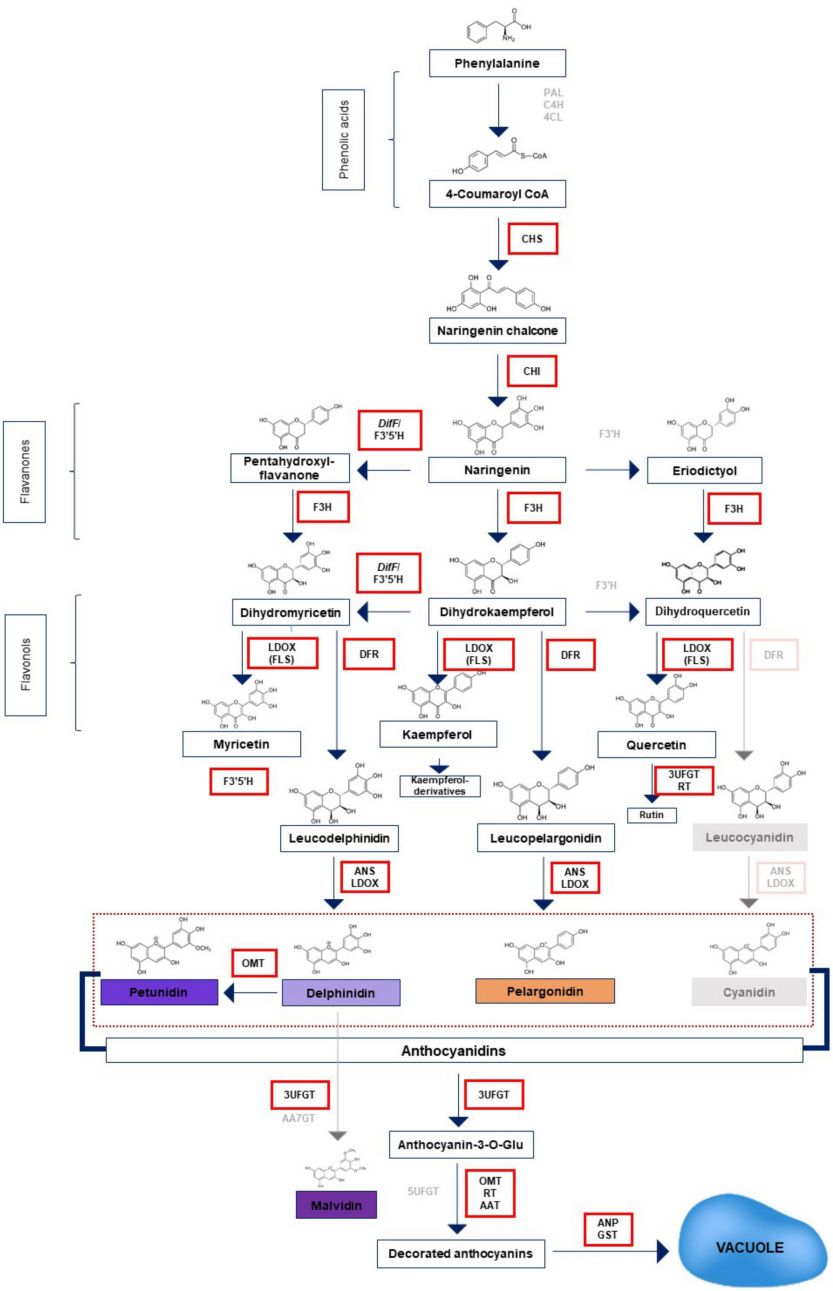

FIGURE 6 | Schematic diagram of the anthocyanin biosynthetic pathway. The structural genes upregulated by ectopic expression of *PhAN4* in MicroTom HRCs and leading to accumulation of compounds are in black and marked by red boxes. PAL, phenylalanine ammonia-lyase; C4H, cinnamate-4-hydroxylase; 4CL, 4-coumarate CoA ligase; CHS, chalcone synthase; CHI, chalcone isomerase; F3′H, flavonoid-3′-hydroxylase; F3′5′H, flavonoid-3′,5′-hydroxylase; DFR, dihydroflavonol reductase; ANS, anthocyanin synthase; OMT, O-methyltransferase; AAT, anthocyanin acyltransferase; RT, rhamnosyltransferase; UFGT, UDP-glucose flavonoid 3-*O*-glucosyl transferase; AA7GT, cyanidin-3-*O*-glucoside-7-*O*-glucosyltransferase; ANP, anthocyanin permease; GST, glutathione-*S*-transferase.

transferases (*3UFGT*) (Solyc02g062975.1.1, Log_2Fc = 7.08; Solyc10g083440.1.1, Log_2Fc = 9.97; Solyc12g098590.2.1, Log_2Fc = 16.55) catalyzing the transfer of the glucosyl moiety from UDP-glucose to the 3-hydroxyl group of anthocyanidins in tomato were found among upregulated DEGs, as well (Hu et al., 2011; Tohge et al., 2020). Furthermore, anthocyanidin-3-*O*-glucoside rhamnosyltransferase (*3RT*) (Solyc09g059170.2.1, Log_2Fc = 8.3262), which in tomato controls the conversion of anthocyanidin-3-glucosides to anthocyanidin-3-rutinosides by the UDP rhamnose, was found among upregulated DEGs (Tohge et al., 2020). Tomato anthocyanin acyltransferase (*AAT*, or Flavonoid-3-*O*-rutinoside-4‴-*O*-phenylacyltransferase; Solyc12g088170.2.1, Log_2Fc = 13.21) resulted upregulated, as well. Solyc02g081340.3.1 (Log_2Fc = 10.53) resulted among

upregulated DEGs. In tomato, it encodes a putative Glutathione S-Transferase that shares 84% homology with *P. hybrida GST* that is responsible for anthocyanin sequestration in the vacuole (Alfenito et al., 1998). Solyc03g025190.4.1 (Log_2Fc = 16.80; tomato *MTP77*) resulted highly upregulated among DEGs. This gene belongs to clade 1 of the multidrug and toxic compound extrusion (MATE) family member (*Transparent testa 2-like*), which in tomato has been associated with vacuolar chloride channels related to the regulation of cell turgescence. In Micro-Tom, many MATE belonging to clade 1 have been functionally related to the transport of secondary metabolites (dos Santos et al., 2017). Solyc10g006120.2.1 (Log_2Fc = 7) was found to be upregulated, as well. This gene shares 59% sequence identity with leucoanthocyanidin dioxygenase (*LDOX*) from *P. hybrida* and 61% with *S. tuberosum FLS* (Pelletier et al., 1997). LDOX has been demonstrated to be a bi-functional enzyme being able both to convert leucoanthocyanidins into anthocyanidins and to catalyze the *in planta* formation of flavonols in fls1-2 mutants of *A. thaliana* (Preuß et al., 2009).

Together with the regulation of structural genes, *PhAN4* positively modulated also transcription factors involved in anthocyanin biosynthesis. Solyc07g052490.3.1 (Log_2Fc = 7.17, tomato Myb-like transcription factor *Atv*) is involved in anthocyanin biosynthesis (Cao et al., 2017). Also, Solyc10g086290.2.1 (Log_2Fc = 8.65), which shares 83% homology with *Solanum tuberosum AN2-like*, is a R2R3Myb involved in anthocyanin biosynthesis, was found (Sun C. et al., 2019; Colanero et al., 2020; Yan et al., 2020). Solyc09g065100.2.1 (Log_2Fc = 14.18) maps the Hoffman's anthocyaninless (AH) locus and encodes a bHLH factor (SlAN1) that positively regulates anthocyanin biosynthesis in tomatoes (Qiu et al., 2016). No effects of *PhAN4* expression were found on another known regulator of anthocyanins biosynthesis, *AN11*. Additionally, Solyc10g084380.1.1 was upregulated (Log_2Fc = 3.43). In *Solanum lycopersicum,* this gene encodes a WRKY that shares 76% homology with *PH3* from *Petunia hybrida* where it regulates vacuolar acidification and boosts anthocyanin biosynthesis, as well (Verweij et al., 2016).

Among upregulated DEGs, putative repressors of anthocyanins biosynthesis were found. The upregulated Solyc12g005800.2.1 (Log_2Fc = 7.51) is the tomato SlMYBATV-like (Cao et al., 2017), a R3-MYB repressor. Solyc10g083900.2.1 (Log_2Fc = 3.54; tomato R2R3Myb transcription factor 27) shares the best homology with *Myb27* from *P. hybrida*, where it is a repressor of the synthesis of anthocyanins (Albert et al., 2011, 2014) and Solyc01g095640.2.1 (Log_2Fc = 4.92; tomato *ETC3* or *SlTRY*) orthologous in *A. thaliana* acts a repressor of anthocyanins accumulation, as well (Tominaga-Wada et al., 2013).

To complete the description related to the modulation of genes related to specialized metabolites, three DEGs resulted to be upregulated and three downregulated. Among upregulated DEGS, Solyc01g105880.4.1 and Solyc09g092470.2.1 (Log_2Fc = 3.46 and 5.69, respectively; tomato monoterpenoid synthases 2 *TPS4* and *TPS14*), are involved in the biosynthesis of monoterpenes and sesquiterpenes, respectively. *TPS4* has been found to be upregulated in tomato cultivars resistant to *Fusarium oxysporum* (Velázquez-Márquez et al., 2021). Solyc11g017240.2.1 (Log_2Fc = 3.78; tomato chorismate mutase 2 *SlCM2*), catalyzes the first step of the shikimate pathway from phenylalanine to the volatile compounds responsible for tomato fruit aroma and quality and defense from biotic and abiotic stress response (Tzin et al., 2015). In tomatoes, *SlCM2* has been also shown to be upregulated under drought stress (Filiz et al., 2019). Among downregulated genes, Solyc08g008630.3.1 (Log_2Fc = −3.34; tomato chloroplastic beta-carotene isomerase D27 *Dwarf27*) is involved in strigolactone and beta-carotene biosynthesis and has been found to be downregulated in psyllid-infested tomato plants (Harrison et al., 2021). Solyc04g050930.3.1 (Log_2Fc = −2.07; tomato violaxanthin de-epoxidase *VDE*) is involved in the carotenoid biosynthesis. Suppression of *VDE* can induce the photo-inhibition of the PSII and, at the same time, it results in an accumulation of fucoxanthin that functions as an efficient anti-oxidant in anoxia conditions (Tohge et al., 2020). Moreover, it has been shown that *VDE* is downregulated in tomato plants upon *Pseudomonas syringae* pv. tomato DC3000 infection (Yang Y. X. et al., 2015). Solyc05g010180.3.1 (Log_2Fc = −2.22; tomato carotenoid isomerase *CRTISO*) is involved in carotenoids biosynthesis. In MicroTom fruits, the downregulation of carotenoid isomerase has been demonstrated to induce an accumulation of zeta-carotene and *cis*-prolycopene (dos Santos et al., 2017; Florio et al., 2021), both elevating and modifying carotenoid profiles toward more bioavailable forms compared to wild-type (Pelletier et al., 1997).

To complete the description related to DEGs that were modulated upon expression of *PhAN4* and that are related to plant physiology, in addition to Solyc06g073760.3.1 (already described in GOE analysis in the MF category), Solyc12g006140.2.1 (Log_2Fc = 4.36; tomato chloroplastic light-harvesting chlorophyll a/b-binding protein 37) was found to be upregulated. Its upregulation was demonstrated to improve photosynthesis and in extending the shelf life in tomato plants (Zouari et al., 2014). Among downregulated DEGs, Solyc02g065220.3.1 (Log_2Fc = −2.14; tomato cytochrome P450) was shown to have significantly different transcript levels between purple and red sectors of VIGs *Del/Ros* tomatoes late ripening. Its downregulation has been associated with extended shelf life (Gao et al., 2018). Solyc09g066150.1.1 (Log_2Fc = −4.57; putative tomato cytochrome P450) suppression has been found in transgenic tomato plants unable to perform DNA methylation and its upregulation has been associated with fruit ripening (Zhao et al., 2018).

Phenolic Content and Antioxidant (2,2-Diphenyl-1-Picrylhydrazyl) Activity

To verify whether *PhAN4* expression was associated with increased antioxidant activity, *in vitro* scavenging activity of the hydroalcoholic soluble fraction of HRCs was assessed by non-enzymatic 2,2-diphenyl-1-picrylhydrazyl (DPPH) assay (de Torre et al., 2019). The total phenolic content (expressed as μg of gallic acid equivalents (GAE)/g of dry weight, DW) was found to be ninefold and eightfold compared to control (18.2 × 103 μg GAE/g DW in AN4-1 and 16.4 × 103 μg GAE/g DW AN4-GFP-8

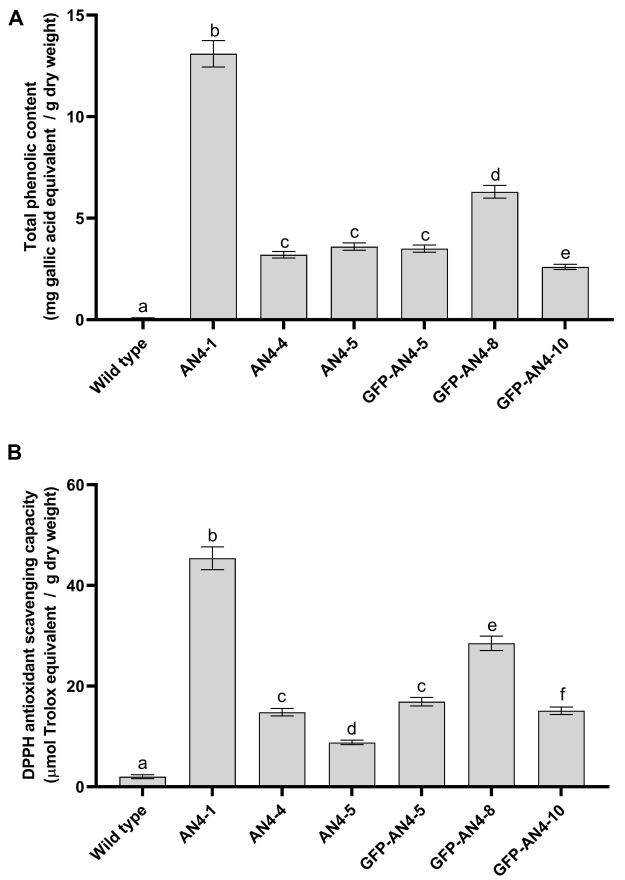

FIGURE 7 | Total phenolic content in MicroTom transgenic HRCs reported in mg of gallic acid equivalents/g of dry weight **(A)**. Analysis of antioxidant activity (DPPH) in MicroTom transgenic HRCs reported as µg Trolox equivalents/g dry weight (DW) **(B)**. Each analysis consisted of triplicate measurements of each sample and data were averaged over the three measurements. A univariate statistical analysis based on Student's *t*-test and one way-ANOVA ($P \leq 0.05$) was carried out.

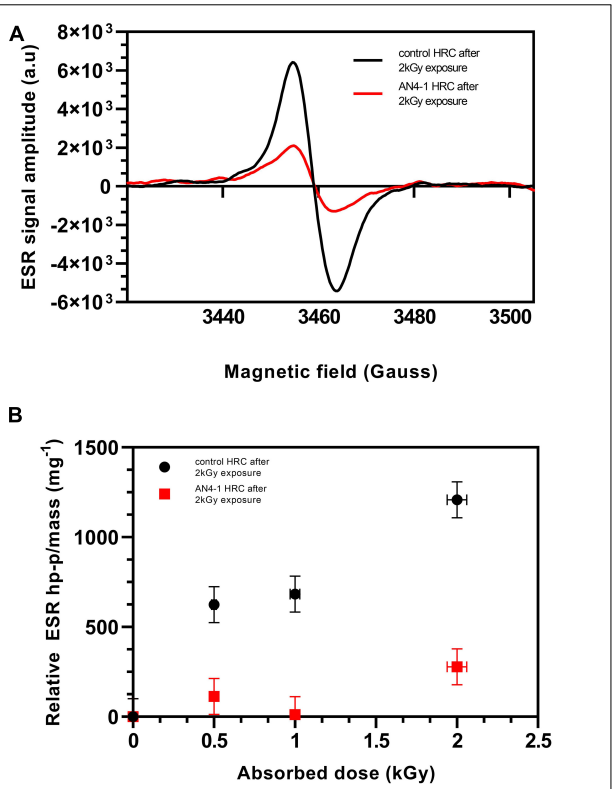

FIGURE 8 | ESR spectra of AN4-1 and control HRCs gamma-irradiated at 2 kGy absorbed dose (dose rate = 1.8) **(A)**. ESR kGy water/h signal intensity of white and purple HRCs gamma are reported as a function of the absorbed dose (up to 2 kGy absorbed dose; dose rate = 1.8 kGy water/h) **(B)**. The intensity of each signal is expressed as the peak-to-peak height normalized for mass units and by subtracting the intensities of the HRCs signals before irradiation.

HRCs (**Figure 7A**). The trolox equivalent antioxidant capacity of the hydroalcoholic soluble fraction (containing anthocyanins) in purple HRCs appears to be thirty (in the AN4-1 clone) and twenty (in the AN4-GFP-8 clone) times higher than in control HRCs (**Figure 7B**).

Electron Spin Resonance Analysis

To further characterize the effect of the ectopic expression of *PhAN4*, MicroTom HRC lyophilized material was investigated for its ability to counteract the generation of reactive oxygen species (ROS) and for the maintenance of this feature after high dose gamma radiation. The AN4-1 HRC was chosen as the best candidate to evaluate resistance to radiation by Electron Spin Resonance (ESR). This analysis assessed the amount of peroxyl radicals in lyophilized HRCs. The HRCs ESR signal is characterized by a singlet signal at 3454 Gauss, correspondent to peroxyl radicals induced by gamma irradiation (Andersen et al., 2000; Ichikawa et al., 2001; Nagata et al., 2003; Rossetto et al., 2007; Esatbeyoglu et al., 2014; Faure et al., 2014). Negligible satellite peaks below 3,440 and above 3,480 Gauss are present as well and are related to several different contributions (such as cellulose-like molecules and anthocyanins) (Andersen et al., 2000; Tuner and Korkmaz, 2007; Petrisor et al., 2008; Esatbeyoglu et al., 2014; Faure et al., 2014). Typical ESR spectra of HRCs irradiated at 2,000 Gy absorbed dose, are shown in **Figure 8A**.

The AN4-1 and control spectra before gamma radiation exposure do not show significant peaks (data not shown). After irradiation (0.5, 1, and 2 kGy), the control shows a signal intensity significantly higher than AN4-1 (**Figures 8A,B**). In particular, AN4-1 shows only a negligible signal increase after irradiation from the lowest to the highest absorbed dose. On the contrary, control HRC shows a constant and nearly linear increase of singlet intensity, already evident at low absorbed doses.

Ultraviolet-Visible Absorbance Spectra

We have used UV-VIS analysis of HRC extracts to characterize the resistance to gamma irradiation of the phenolic compounds accumulated in the AN4-1 line. Before irradiation, both control and AN4-1 acidic extracts revealed the main peak at 280 nm, followed by another peak at 315–320 nm (**Figure 9**).

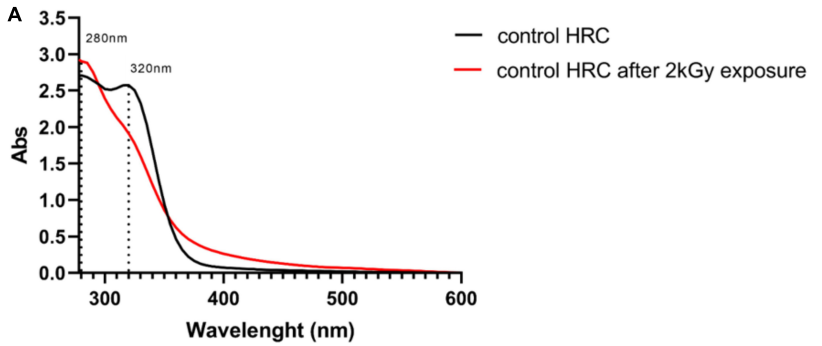

Wavelenght Bef. Irr.	Wavelenght After Irr.	Abs Bef. Irr.	Abs After Irr.	Δ Abs After – Before Irr.
280 nm	290 nm	2.70	2.90	+ 0.20
315-320 nm	325 nm	2.57	2.01	- 0.56

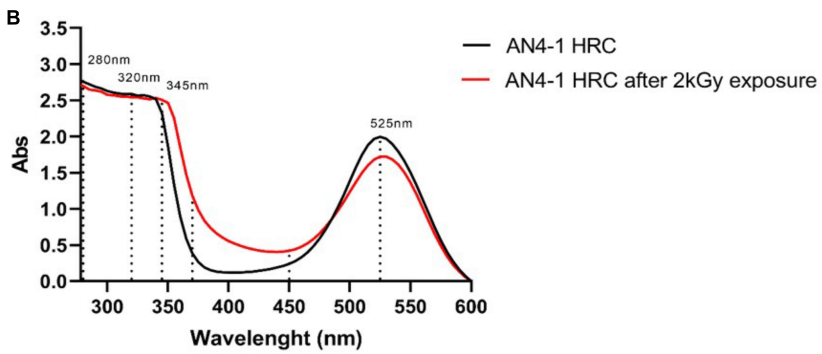

Wavelenght Bef. Irr.	Wavelenght After Irr.	Abs Bef. Irr.	Abs After Irr.	Δ Abs After – Before Irr
280 nm	285 nm	2.75	2.69	- 0.06
315-320 nm	320–325 nm	2.58	2.55	- 0.03
345 nm	350 nm	2.32	2.50	+ 0.18
525 nm	525-530	1.99	1.72	- 0.27

FIGURE 9 | UV-VIS spectra of MicroTom HRCs before and after 2 kGy absorbed dose. In control, peaks at 280 nm and 320 nm indicate the presence of flavonols, hydroxycinnamic acids, tannins, and flavanols **(A)**. In AN4-1, the additional peak at 345 nm completes the flavonols group profile compared to control, while the peak at 525 nm represents anthocyanins. The curve in the region between 400 and 450 nm refers to possible glycosylation, precipitation, complexation of anthocyanins **(B)**.

In accordance with metabolomic data, in the spectra obtained in absence of irradiation, peaks around 280 nm and 320 nm indicate the presence of flavonols, hydroxycinnamic acids, tannins, and flavanols (Solìs-Oviedo and de La Cruz Pech-Canul, 2019). The shoulder at 345 nm together with that at 280 nm further defines the UV-VIS spectra of the flavonols in AN4-1 (Saha et al., 2021). Anthocyanins and anthocyanins associated with phenolic acids also produce peaks around 280 nm and 320 nm, respectively (Solìs-Oviedo and de La Cruz Pech-Canul, 2019), contributing to the profile of AN4-1 HRCs in **Figure 7B**. Anthocyanins result in an additional characteristic peak at 525 nm (Vivar-Quintana et al., 2002; da Silva et al., 2007; Fedenko et al., 2017), which, as expected, is observed in AN4-1 and not in control HRCs. Gamma irradiation determined a slight absorbance increase at 280 nm and a significant decrease at 320 nm in controls. On the contrary, these peaks remained unchanged in AN4-1. In AN4-1, the absorbance at 400–450 nm is possibly an indication of glycosylation, precipitation, complexation with tannins of anthocyanins upon irradiation (Saha et al., 2021). Gamma irradiation determined a slight decrease of the absorbance at 525 nm in AN4-1, as confirmed by a slight discoloration of the root material after irradiation.

Photoluminescence Analysis

Photoluminescence emission spectra were analyzed to determine the resistance to misfolding and oxidation of MicroTom HRCs soluble proteins after gamma irradiation. Photoluminescence spectra of extracts containing soluble proteins from control (**Figure 10A**) and AN4-1 HRCs (**Figure 10B**) were produced. The mass-normalized emission spectra of not irradiated soluble

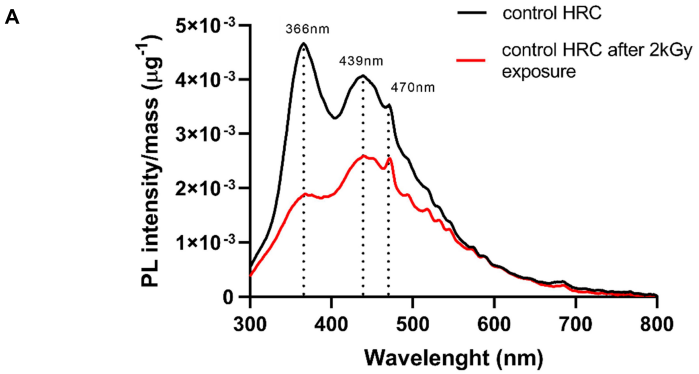

Wavelenght (nm)	PL intensity/mass (μg^{-1}) Before Irr.	PL intensity/mass (μg^{-1}) After Irr.	Δ % PL intensity/mass (μg^{-1}) After – Before Irr.
366 nm	0.0046	0.0018	-60.87%
439 nm	0.0040	0.0025	-37.5%
471 nm	0.0035	0.0025	-28.57%

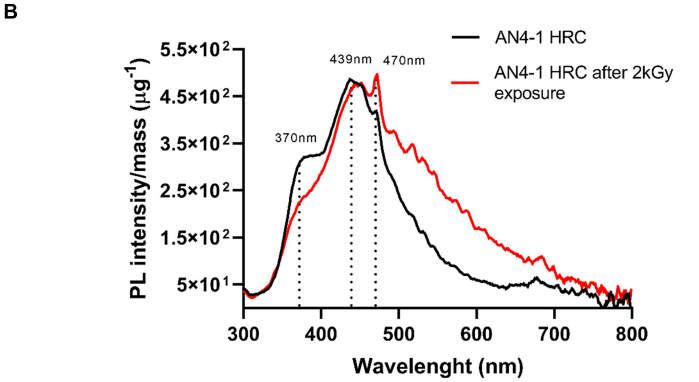

Wavelenght (nm)	PL intensity/mass (μg^{-1}) Before Irr.	PL intensity/mass (μg^{-1}) After Irr.	Δ % PL intensity/mass (μg^{-1}) After – Before Irr.
370 nm	300.96	217.76	-27.64%
437 nm	485.86	473.22	-2.60%
470 nm	418.38	496.08	+18.57%

FIGURE 10 | Photoluminescence spectra of control **(A)** and AN4-1 **(B)** HRCs and related mass-normalized emission intensities (tables) before and after 2 kGy gamma irradiation. Main peaks refer to tryptophan (370 nm), its degradation products kynurenine and 3-hydroxykynurenine (439 and 470 nm), and carbamate anion (470 nm).

protein samples are similar in controls and AN4-1 and are characterized by high peaks mainly corresponding to tryptophan (370 nm) (Yang H. et al., 2015; Hilaire et al., 2017) and its metabolic products such as kynurenine (470 nm) and 3-hydroxykynurenine (439 nm) (Lohmann et al., 1988; Daly et al., 2009; Gakamsky et al., 2017). In addition, a peak at 470 nm is indicative of the presence of carbamate anions (Pan et al., 2013). In control HRC, the 2 kGy absorbed dose caused a decrease of fluorescence emission intensity for all three peaks. In particular, the Δ% photoluminescence intensity after and before the irradiation shows that the peak at 370 nm is reduced by 67.87%, the peaks at 439 nm and 470 nm by 37.5%, and 28.57%, respectively (**Figure 8A**). In AN4-1 only the 370 nm peak decreased (−27.64%), while a slight increase (+18.57%) of the kynurenine peak (470 nm) was present. No significant modifications were observed at 439 nm (**Figure 10B**).

DISCUSSION

Anthocyanins are well known for their antioxidant and health-protection properties. Tomato has been already subjected to

genetic manipulation for improved levels and composition of these high-value compounds (Schauer et al., 2006; Klee and Tieman, 2013; Giovannoni, 2018; Wang et al., 2019). Nutraceutical improvement of tomato is expected to provide a nourishing food source for future long-term manned space missions such as NASA's "Artemis" lunar exploration program. The Artemis initiative includes sending a suite of new technology demonstrators to establish a sustained human presence by 2028 (DeZwart and Henderson, 2021). Low-power systems to grow plants will have the role to provide fresh and nutritious food to supplement astronauts' diet and provide psychological benefits. The experiments conducted in the VEGGIE module onboard the International Space Station over the last few years have pioneered this scenario (Wolff et al., 2014; Fu et al., 2016; Massa et al., 2016; Zabel et al., 2016; Imhof et al., 2018).

The space environment, totally unusual for plants, can affect their metabolic processes and, consequently, growth, due to high-energy ionizing radiation, microgravity, magnetic field, and ultra-vacuum (Williams et al., 2004; Lotito and Frei, 2006; Moghaddam et al., 2011; Thamaphat et al., 2015; van Hoeck et al., 2017). Among abiotic stresses that plants will have to cope with in extraterrestrial environments artificially adapted to space agriculture, pro-oxidant stimuli are, indeed, the most prominent, due to cosmic ionizing radiation. Acting directly and indirectly to delay oxidative damage, enzymatic players, and metabolites activating endogenous antioxidant defense systems may help plant growth in the space environment. ROS attack plant cells causing loss of their structure and function (Vandenhove et al., 2010; Moghaddam et al., 2011; Marcu et al., 2013a; Vardhan and Shukla, 2017; Gudkov et al., 2019), rapidly reacting with almost all structural and functional organic molecules in the plant cells and causing irreversible oxidative damage on DNA, lipids, and proteins (Scandalios, 2002; Sewelam et al., 2016). The issue of counteracting overproduction of free radicals generated by harmful ionizing radiation is crucial for human survival in space outposts, as well, and opens the way to the ideal 'anti-oxidant space fresh food.' Indeed, the oral intake of clinically tested chemical radioprotectants (i.e., thiols, aminothiols, thiadiazoles, and benzothiazoles) is limited due to toxicity (Copp et al., 2013). Therefore, there is great interest in the development of natural antioxidants possibly produced by plants and introduced with the diet (Gómez et al., 2021). Together with the above-mentioned abiotic 'macro-stresses,' plants intended for space agriculture will have to cope with a plethora of abiotic 'micro-stresses' related to the different cultivation environment/systems that will be adopted. Furthermore, plants will have to share with humans future crewed space habitats (spaceflights, planetary outposts, and life-support systems) where stringent microbial quality requirements may not be achieved (Amalfitano et al., 2020).

Plants have an intrinsic potential for adaptation as the heritage of ancestors that survived in the harsh initial terrestrial environments (de Vries and Archibald, 2018). The 'design' of plant ideotypes suitable to these environments may be achieved by further refinement of existing biochemical and physiological features, such as specialized metabolites, that plants use to survive stress. Novel genotypes boosting biosynthetic pathways for the production of specialized metabolites can be generated by manipulation of their regulators. Among regulators, there are MYB transcription factors, known for their contribution to the increased complexity of land plants and to be regulators of plant responses to the environment (Lloyd et al., 2017; Gao et al., 2018; Kashyap et al., 2020; Shi and Panthee, 2020). Members of this large family of regulators are key players in the modulation, among others, of the biosynthesis of flavonoids, like anthocyanins, in different plant parts and response to all kinds of stimuli (Ambawat et al., 2013; Liu et al., 2015; Roy, 2016). MicroTom is extremely compact, early yielding, and would be suitable for agriculture in the confined area of a crewed space module. Here, we described the ectopic expression of the anthocyanin R2R3-MYB regulator *PhAN4* from *Petunia hybrida* in MicroTom hairy roots as a testbed for future engineered whole plants. As known, anthocyanin production is regulated by R2R3-MYB, bHLH, WDR, and WRKY cooperation (MBWW transcriptional complex) (Spelt et al., 2000; Koes et al., 2005). In this complex, the R2R3-MYB transcription factor is probably the limiting factor, in that the WDR and bHLH proteins are thought to be constitutively expressed (Zhang et al., 2013, 2014). When specific MYB proteins are expressed in plants, this induces anthocyanin accumulation. Since some specific MYB transcription factors can function in regulating not only the biosynthesis of anthocyanins but also other traits (Meng et al., 2015; Vardhan and Shukla, 2017; Jian et al., 2019), we investigated if *PhAN4* may affect, together with accumulation of anthocyanins, features associated with improved traits related to survival in harsh and confined environments such as future space outposts.

Differently from the wealth of literature available on whole transgenic plants and cell culture systems, data concerning anthocyanins production are limited for hairy roots. To date, no data are available on anthocyanin accumulation in tomato hairy roots by metabolic engineering to make comparisons with our work. Although not comparable to levels achieved in transgenic plants (Butelli et al., 2008; Povero et al., 2011; Kiferle et al., 2015), accumulation of anthocyanins occurred in MicroTom HRCs upon *PhAN4* transformation, as expected due to the nature of the transgene. Importantly, no significant variation of transformed HRCs growth rates was found compared to controls. This gives a clue about the non-detrimental activity of *PhAN4* toward primary metabolism in this system.

In accordance with literature related to transgenic tomato plants (Butelli et al., 2008; Su et al., 2016; Jian et al., 2019), mass spectrometry allowed us to identify glycosylated and acylated delphinidin and petunidin as the most abundant anthocyanins in *PhAN4* HRCs. Interestingly, two additional anthocyanins, unusual in tomato, pelargonidin-3-glucoside, and malvidin-3-*O*-(4'''coumaroyl)-rutinose-5-*O*-glucose, were detected, as well. Malvidin and Pelargonidin derivatives have already been detected in *Del* and *Ros1* and *LC* and *C1* tomato plants, respectively (Bovy et al., 2002; Su et al., 2016). Interestingly, pelargonidin plays a major role in reducing genotoxic stress induced by environmental toxicants in plants (Khandelwal and Abraham, 2014). In addition, rather than other anthocyanins, pelargonidin-3-glucoside, that was accumulated in engineered MicroTom HRCs, has high bioavailability, being absorbed in an intact form into the gastrointestinal wall, undergoing first-pass metabolism and entering the systemic circulation as 4-hydroxybenzoic acid,

a stable metabolite that is considered one of the main players of the systemic health effects of anthocyanins (Fang, 2014). In order to achieve a better understanding of *PhAN4* in the tomato hairy root phenylpropanoid pathway, we measured 14 phenolic acids and derivatives and 29 flavonoids: notably, a reduction in the content of some members of the former, and a massive increase in most of the compounds in the latter were observed, thus proving *PhAN4* is able to trigger the metabolic flux at both flavonoid and anthocyanin levels.

Data on the accumulation of anthocyanins and phenylpropanoids obtained by mass spectrometry was supported by transcriptome-wide RNA-seq analysis. RNA-seq, in complex, depicted a reprogramming oriented not only to anthocyanin accumulation, as expected, but also to positive regulation of cell response to biotic and abiotic stress and, possibly, to fruit quality-related traits.

Expression of *PhAN4* increased the transcript levels of almost all of the genes encoding enzymes required for anthocyanin biosynthesis with the exception of *PAL, C4H, 4CL, F3′H,* and *5UFGT*. To facilitate comparisons, transcriptomic research on tomato plants for anthocyanins enrichment has been summarized in **Table 2**. *CHS* and *CHI* had been already found to be upregulated by overexpression of *SlAN2* in tomatoes, but not by ectopic expression of *Del/Ros* that, in turn, were able to upregulate *F3H* (Butelli et al., 2008; Jian et al., 2019). *DFR* had been already shown to be upregulated in the stem and leaf of tomato plants overexpressing *SlAN2* and *SlAN1* R2R3-MYBs (Kiferle et al., 2015). Interestingly, despite *FLS* was not found among upregulated DEGs in *PhAN4* HRCs, *LDOX*, a known bi-functional enzyme being able not only the conversion of leucoanthocyanidins in anthocyanidins but also to catalyze the formation of flavonols, resulted to be differentially upregulated in *PhAN4* HRCs. This may explain the accumulation of quercetin, kaempferol derivatives, and myricetin together with anthocyanidins. The flavonol biosynthetic activity of the upregulated *LDOX* is counterbalanced by the upregulated *DFR*. In tomatoes, DFR has a substantial preference for dihydromyricetin, which can be also derived by dihydrokaempferol and dihydroquercetin by F3′5′H activity. Interestingly, *DilFl* a tomato homolog of cytochrome b5 of *P. hybrida*, where it is essential for full activity of F3′5′H, was found to be upregulated in *PhAN4* HRCs. These findings may explain the differential accumulation of delphinidin and petunidin compared to pelargonidin, malvidin, and cyanidin (the latter was not detected at all). Among late biosynthetic genes, upregulation of *ANS* had been already shown upon *SlAN2* over-expression and *Del/Ros* expression in tomatoes. *OMT* and *AAT* transferases have already been described to be targets of a MYB in tomatoes, as well (Zhang et al., 2019). Their upregulation in *PhAN4* HRCs, together with that of *GST, PH3, OMT, 3UFGT, RT,* and *AAT* may explain the accumulation of the glycosylated and acylated forms of anthocyanidins. In particular, the function of the upregulated *PH3* (Solyc10g084380.1.1) in *PhAN4* HRC is rather to be associated with anthocyanin biosynthesis boosting than with acidification of pH, as tomato lacks *PH1* and *PH5* (i.e., the genes encoding the vacuolar P-ATPases which cooperate with PH3 and PH4 in determining flower color by hyperacidification of petal cell vacuoles in *Petunia*). Nevertheless, preliminary evaluation of pH of *PhAN4* and control HRC homogenates (Verweij et al., 2008) does not allow to exclude that the acidification function may occur (**Supplementary Figure 5**), given that pH differences between *PhAN4* and control HRC seem to be in accordance with variations recorded between vacuolar P-ATPases-defective mutants and wild type *Petunia hybrida* (Faraco et al., 2014). The upregulation of anthocyanin biosynthesis-relevant transcription factors further expands the influence of *PhAN4* MYB in tomato gene expression regulation. Among those, the upregulation of *SlAN1*, *SlAN2,* and *WD40* are coherent with already proposed models of anthocyanin biosynthesis regulation (Koes et al., 2005; Liu et al., 2018).

Interestingly, the *PhAN4*-related transcriptomic enhancement was found to involve more than 30 genes specifically related to response to biotic/abiotic and oxidative stress, as well. Indeed, GOE analysis was associated with proteinase inhibitors, beta-glucosidases, glucanases, glycosylases, xylan acetylases, resistance proteins, and other classes of enzymes that are players of defense against pathogens and pests and of response to abiotic stresses specifically associated with wounding, cold, heat, drought, hypoxia, and to UV exposure in tomato (Fan et al., 2020). Among those, the upregulated beta-glucosidases, together with the dirigent proteins and the monoterpenoid and sesquiterpenoid synthases that were found in the present work, are involved in the formation of required intermediates for cell wall lignification. The positive regulation of trichome birefringence-like protein mediating xylan acetylation also is another tool in possible protection against environmental stresses among which there is cold and excess of minerals in the soil. Acetylation of wall polymers is, indeed, vital for plant growth and adaptation to various environments, and is required for the structural integrity of the leaf surface exerting a global impact on plant stress responses (Gao et al., 2017). In relation to the positive regulation of beta-1,3-glucanases, beta-glucosidases, and xylan acetylases, together with expansions, it has to be added that these genes are related to fruit softening or improved emission of volatiles, as well (Tzin et al., 2015; Li P. et al., 2020). In this sense, the positive regulation of chlorophyll a/b binding protein (that is normally upregulated during fruit ripening) and of one gene related to volatile compounds biosynthesis (*chorismate mutase*) was found in *PhAN4* HRCs. At the same time, negative regulation of other genes, which down expression is involved in the extended shelf life of fruits, was found. The evaluation of these aspects might be important in view of the development/design of whole transgenic tomato plants in relation to the quality traits of fruits.

One player of ROS detoxification and regulator of the redox signaling network of tomato, plastidial thioredoxin Y2, was found to be highly upregulated, as well. Moreover, the analysis demonstrated the downregulation of violaxanthin de-epoxidase (*VDE*) and carotenoid isomerase (*CRTISO*), two genes involved in carotenoid biosynthesis. Despite being involved in the photo-inhibition of the PSII, suppression of VDE can induce, at the same time, an accumulation of fucoxanthin that functions as an efficient anti-oxidant in anoxia conditions (Mikami and Hosokawa, 2013). The downregulation of carotenoid isomerase was demonstrated to induce an accumulation of zeta-carotene

TABLE 2 | Summary of results from the main research on tomato plants enrichment with anthocyanins obtained by both conventional breeding and genetic engineering approaches.

Tomato line	Origin	Main overexpressed genes	Main anthocyanins detected	Anthocyanin concentration	References
V118	Breeding	–	Pet-3-(p-coumaryl)-rut-5-glc; Pet-3-caeoyl-rut-5-glc; Mal-3(p-coumaryl)-rut-5-glc	50.18 mg 100 g^{-1} DW 9.04 mg 100 g^{-1} DW 13.09 mg 100 g^{-1} DW	Li et al., 2011
Aft/Aft × *atv/atv*	Breeding	–	Pet-3-(p-coumaroyl)-rut-5-glc; Del-3-rut	Peel: 116.11 mg 100 g^{-1} FW	Mes et al., 2008
Sun Black (*Aft/Aft* × *atv/atv*)	Breeding	–	Pet-3-(*trans*-p-coumaroyl)-rut-5-glc; Mal-3-(*trans*-p-coumaroyl)-rut-5-glc	More than 1 mg g^{-1} DW	Mazzucato et al., 2013
Blue Japan Indigo tomato (*Aft/Aft* × *atv/atv*)	Breeding	—	Pet + p-coumaroyl + rut + glyc; Mal + p-coumaroyl + rut; Del	Peel: 17 mg g^{-1} DW Pulp: 0.1 mg g^{-1} DW	Ooe et al., 2016
Aft/Aft × *atv/atv* × *hp2/hp2*	Breeding	–	Pet-(p-coumaroyl)-rut-hex; Del-3-(p-coumaroyl)-rut-glyc; Pet-(p-coumaroyl)-rut-hex; Pet-3-(caffeoyl)-rut-5-glyc; Mal-3-(p-coumaroyl)-rut-5-glyc; Cya-3-*O*-rut;	Peel: 90.91 mg 100 g^{-1} FW	da Silva Souza et al., 2020
ANT1 from S. chilense	Genetic engineering	*CHS, DFR, 3-GT, 5-GT, GST, ANP*	Del-3-rut-5-glc; Del-3-(p-coumaroyl)-rut-glyc; Del-3-(caffeoyl)-rut-5-glyc; Pet-3-rut-5-glc; Pet-3-(p-coumaroyl)-rut-5-glyc; Pet-3-(caffeoyl)-rut-5-glyc; Mal-3-rut-5-glc; Mal-3-(p-coumaryl)-rut-5-glyc; Mal-3-(caffeoyl)-rut-5-glyc	3.574 mg g^{-1} FW	Mathews et al., 2003
Del/Ros1	Genetic engineering	*PAL, C3H, CHI, F3′5′H, DFR, ANS, 3-GT, 5-GT, RT, AAC, GST, ANP*	Pet-3-(*trans*-p-coumaroyl)-rut-5-glc; Del-3-(*trans*-p-coumaroyl)-rut-5-glc; Pet-3-(feruloyl)-rut-5-glc; Del-3-(feruloyl)-rut-5-glc	2.835 ± 0.456 mg g^{-1} FW	Butelli et al., 2008
Del/Ros1	Genetic engineering	–	Del-3-(*trans*-p-coumaroyl)-rut-5-glc; Pet-3-(*trans*-p-coumaroyl)-rut-5-glc; Mal-3-(p-coumaroyl)-rut-5-glc; Mal-3-(feruloyl)-rut-5-glc	Peel: 5.1 ± 0.5 g kg^{-1} DW Flesh: 5.8 ± 0.3 g kg^{-1} DW Whole fruit: 5.2 ± 0.5 g Peo-3-glc equivalent kg^{-1} DW, or 0.5% of DW	Su et al., 2016
ANT1 from S. lycopersicum	Genetic engineering	*CHI, F3H, DFR, ANS, 3-GT*	Pet Mal Del	–	Schreiber et al., 2012
SlANT1 and *SlAN2*	Genetic engineering	*SlAN2, SlANT1, SlAN1, SlAN11, SlJAF13, SlDFR*	–	–	Kiferle et al., 2015
Del/Ros1 × *AtMYB12*	Genetic engineering	*PAL, 4CL, CHS, CHI, F3H, FLS, DFR, ANP, 3-GT, C3H*	Del-3-(*trans*-p-coumaroyl)-rut-5-glc; Pet-3-(*trans*-p-coumaroyl)-rut-5-glc; Pet-3-(feruloyl)-rut-5-glc; Mal-3-(p-coumaroyl)-rut-5-glc	1.154 ± 0.011 mg g^{-1} FW 2.857 ± 0.218 mg g^{-1} FW 0.922 ± 0.102 mg g^{-1} FW 0.598 ± 0.011 mg g^{-1} FW	Zhang et al., 2015
SlMYB75	Genetic engineering	*PAL, CHI, CHS, AAC, ANS, 3-RT, LDOX*	–	∼2 mg g^{-1} FW	Jian et al., 2019
PhAN4	Genetic engineering (transformed tomato hairy root cultures)	*CHS, CHI, F3′5′H, F3H LDOX, DFR, ANS, 3-GT, RT, OMT, AAT, ANP, GST*	Pet-3-(feruloyl)-rut-5-glc; Pet-3-(p-coumaroyl)-rut-5-glc; Pel-3glc; Mal-3-(4-coumaroyl)-rut-5-glc; Del-3-(p-coumaroyl)-rut-5-glc; Del-3-5-glc	37 μg g^{-1} DW	

The main overexpressed genes and anthocyanins content are shown where available.
Del, delphinidin; Pet, petunidin; Mal, malvidin; Cya, cyanidin; Peo, peonidin; Pel, pelargonidin; rut, rutinoside; glc, glucoside; glyc, glycoside; hex, hexoside; FW, fresh weight; DW, dry weight.

and *cis*-prolycopene in tomato fruits (Isaacson et al., 2002; Pinheiro et al., 2019), both elevating and modifying carotenoid profiles toward more bioavailable forms compared to wild-type (Cooperstone et al., 2015). Therefore, the ROS counteracting potential of *PhAN4* HRC material may be related not only to anthocyanins but also to other accumulating anti-oxidant specialized metabolites.

In view of the future development of natural anti-oxidants produced by engineered plants and possibly administered with the diet, and to define whether the significantly higher DPPH

antioxidant capacity of specialized metabolites accumulating in *PhAN4* HRCs may be efficiently maintained after ionizing radiation, we exposed lyophilized biomass from AN4-1 HRC to high dose ^{60}Co gamma radiation. Gamma rays are a component of cosmic ionizing radiation and induce the formation of free radical species (i.e., paramagnetic species). When carried out in an air atmosphere, gamma rays induce the formation of ROS, such as superoxide, peroxide, and hydroxyl radicals, that are responsible for several oxidative processes in biological systems (Marcu et al., 2013b; Schreurs et al., 2016). Gamma rays are perfect ROS inducers both directly through water radiolysis, and indirectly *via* the activation of a broad range of signaling processes (e.g., damages to the mitochondria or cell microenvironment) (Riley, 1994; Azzam et al., 2012; Buttarelli et al., 2019). ESR Spectroscopy was used as a sensitive tool to identify the entity of the paramagnetic species generated in the HCRs samples after gamma irradiation (Aleksieva et al., 2009; Hawkins and Davies, 2014; D'Errico et al., 2018). ESR analyses revealed a significant difference in the overall amounts of radical species accumulated in the two HRC molecular backgrounds. At the same absorbed dose, control generates a very intense peroxyl radical signal, while a considerably lower level of the singlet intensity is generated in AN4-1. This result reveals that the molecular set formed upon *PhAN4* expression provides very effective free radical scavengers efficiently counteracting oxidative stress upon gamma radiation.

The UV-VIS analysis allowed us to confirm the results obtained by metabolomic data and to characterize the effect of ionizing radiation on the antioxidant compounds. Gamma irradiation, *via* releasing free radicals in solution, may alter these plant constituents (Lateef and Al-Nimer, 2009; Lalande et al., 2019). Compared to the substantially unchanged spectra of AN4-1, the absorbance decrease of the 320 nm peak (i.e., flavonols, hydroxycinnamic acids, tannins, flavonols, and anthocyanins associated to caffeic and coumaric acids) controls upon irradiation, suggests that the anthocyanins accumulated in *PhAN4* HRCs are particularly stable to gamma high absorbed dose and probably have protective effects on other biomolecules. Indirectly, this result shows that these molecules may give a major contribution to the ROS buffering capacity under radiation shown by ESR and to the overall antioxidant potential. As a confirmation of the possible significance of this result *in vivo*, it was reported that, even at higher absorbed doses than that used in this work, X rays (e.g., another type of ionizing radiation) leave the level of flavonoids in an aqueous solution unchanged due to the radiolysis-mediated formation of depsides that, in addition, maintain good anti-oxidant properties, as well (Kozlowski et al., 2007; Lateef and Al-Nimer, 2009).

For proteins to be functional within a cell requires coordinated folding processes to obtain a correct 3D shape. Disruptions to protein folding, that can occur in space due to ionizing radiation, can have profound biological implications for all organisms, including plant cells, leading to dysfunctions (Blanco et al., 2018; Lalande et al., 2019). For this reason, investigations were conducted through photoluminescence analysis on HRCs' total soluble protein extracts. When a protein is exposed to the wavelength of 280 nm, mainly the tryptophan and tyrosine residues get excited, which would reflect upon its tertiary structure (Yang H. et al., 2015). The maximum and emission peak position reflects upon secondary, tertiary, and quaternary structures (Hilaire et al., 2017). Moreover, the extent of protein oxidation is measured by determining the loss of specific tryptophan fluorescence. The emission spectra of HRCs showed an overall decrease in maximum emission intensities only in the case of irradiated controls, revealing that the structure of soluble proteins is partially lost upon irradiation in those samples. This result demonstrates a low capacity of proteins of control HRCs to counteract unfolding, binding to hydrophobic pockets, and aggregation, witnessed by the loss of fluorescence due to the burial of tryptophan residues after radiation. In particular, the Δ% photoluminescence intensity/mass units after and before irradiation indicated that soluble proteins from control undergo a doubled oxidative stress compared to AN4-1 samples. Being polyphenols emitting at 280 and 320 nm extracted by PBS together with total soluble proteins (anthocyanins are not efficiently extracted, **Supplementary Figure 4**), the contribution of these classes of molecules may be hypothesized in stabilizing proteins, as proofs of the interaction of anthocyanins with proteins seem to suggest (Sui et al., 2018). Possible additional contributions of enzymatic players to mitigation of misfolding and aggregation *in vivo* may be the object of future studies.

In conclusion, plant biotechnology methods may thus be exploited for the generation of plants capable of dealing with harsh conditions such as those typical of space outposts. MicroTom HRC allowed to rapidly test *PhAN4* expression effects on tomato cells, possibly opening the way to apply to the engineering of whole plants able to perform in a suitable and predictable manner in those environments.

DATA AVAILABILITY STATEMENT

The datasets presented in this study can be found in online repositories. The names of the repository/repositories and accession number(s) can be found below: https://dataview.ncbi.nlm.nih.gov/object/PRJNA794337?reviewer=estprpllasrt3f3libdoij8rco.

AUTHOR CONTRIBUTIONS

SM planned and designed the project, undertook tomato transformation experiments, PCR screening and maintenance of HRCs, and sample preparation for subsequent analysis, as well as wrote the manuscript. RP handled maintenance of HRCs, contributed to sample preparation and transcriptomic data retrieving and interpretation, and contributed to the writing of the manuscript and the preparation of figures. AB performed sequencing read mapping, identification of DEGs and functional annotation, and enrichment pathway analysis of DEGs. HP undertook cDNA library construction and sequencing for transcriptomic analysis. MB contributed to the identification of DEGs and functional annotation of genes. AC and IS performed gamma irradiation experiments, ESR, UV-VIS,

and photoluminescence analysis and contributed to writing the manuscript. GD and OD performed MS analysis, anthocyanin identification/quantification, and contributed to writing the manuscript. FP conducted the qPCR analysis. AD and PD performed the Trolox assay and the quantification of total polyphenol content and contributed to writing the manuscript. FQ, RK, and CS assembled and kindly provided the PhAN4 constructs used in this work. ElB contributed to the maintenance of HRCs. EuB reviewed and contributed to the writing of the manuscript. All authors contributed to the article and approved the submitted version.

FUNDING

This work was supported by the ENEA/ASI (Italian Space Agency) BIOExTREME and HORTSPACE Projects (ASI n. 2014-007-R.0, ASI n. 2017-11-H.0).

ACKNOWLEDGMENTS

We are deeply grateful to Stefania Baccaro (Fusion and Nuclear Safety Technologies Department, Casaccia Research Center, Rome, Italy) for enthusiastic support and for sharing precious advice concerning radiation experiments, although premature death did not allow her to see the end of the work. We thank Alessia Fiore (ENEA, BIOTEC) for help in the qualitative analysis of RNAs extracted from HRCs and Giulio Metelli (University of Viterbo/ENEA BIOTEC) for support in collecting data on HRCs growth.

SUPPLEMENTARY MATERIAL

The Supplementary Material for this article can be found online at: https://www.frontiersin.org/articles/10.3389/fpls.2022.830931/full#supplementary-material

Supplementary Table 1 | Primer identification (id.) as described in "Materials and Methods" for HRCs PCR screening (for, forward; rev, reverse).

Supplementary File 1 | List of figures representing the level of different phenolic compounds and their derivatives in control and *PhAN4* HRCs.

Supplementary File 2 | List of figures representing the level of different flavonoids in control and PhAN4 HRCs.

Supplementary File 3 | Complete list of DEGs.

Supplementary File 4 | GOE analysis results.

REFERENCES

Albert, N. W., Davies, K. M., Lewis, D. H., Zhang, H., Montefiori, M., Brendolise, C., et al. (2014). A conserved network of transcriptional activators and repressors regulates anthocyanin pigmentation in Eudicots. *Plant Cell* 26, 962–980. doi: 10.1105/tpc.113.122069

Albert, N. W., Lewis, D. H., Zhang, H., Schwinn, K. E., Jameson, P. E., and Davies, K. M. (2011). Members of an R2R3-MYB transcription factor family in Petunia are developmentally and environmentally regulated to control complex floral and vegetative pigmentation patterning. *Plant J.* 65, 771–784. doi: 10.1111/j.1365-313X.2010.04465.x

Aleksieva, K., Georgieva, L., Tzvetkova, E., and Yordanov, N. D. (2009). EPR study on tomatoes before and after gamma-irradiation. *Radiat. Phys. Chem.* 78, 823–825. doi: 10.1016/j.radphyschem.2009.05.013

Alfenito, M. R., Souer, E., Goodman, C. D., Buell, R., Mol, J., Koes, R., et al. (1998). Functional complementation of anthocyanin sequestration in the vacuole by widely divergent glutathione S-transferases. *Plant Cell* 10, 1135–1149. doi: 10.1105/tpc.10.7.1135

Amalfitano, S., Levantesi, C., Copetti, D., Stefani, F., Locantore, I., Guarnieri, V., et al. (2020). Water and microbial monitoring technologies towards the near future space exploration. *Water Res.* 177:115787. doi: 10.1016/j.watres.2020.115787

Ambawat, S., Sharma, P., Yadav, N. R., and Yadav, R. C. (2013). MYB transcription factor genes as regulators for plant responses: an overview. *Phys. Mol. Biol. Plants* 19, 307–321. doi: 10.1007/s12298-013-0179-1

Andersen, M. L., Outtrup, H., and Skibsted, L. H. (2000). Potential antioxidants in beer assessed by ESR spin trapping. *J. Agric. Food Chem.* 48, 3106–3111. doi: 10.1021/jf000354+

Andolfo, G., Ferriello, F., Tardella, L., Ferrarini, A., Sigillo, L., Frusciante, L., et al. (2014). Tomato genome-wide transcriptional responses to Fusarium wilt and Tomato Mosaic Virus. *PLoS One* 9:e94963. doi: 10.1371/journal.pone.0094963

Aoki, K., Yano, K., Suzuki, A., Kawamura, S., Sakurai, N., Suda, K., et al. (2010). Large-scale analysis of full-length cDNA from the tomato (Solanum lycopersicum) cultivar Micro-Tom, a reference system for the Solanaceae genomics. *BMC Genomics* 11:210. doi: 10.1186/1471-2164-11-210

Asins, M. J., Albacete, A., Martínez-Andújar, C., Celiktopuz, E., Solmaz, İ, Sarı, N., et al. (2021). Genetic analysis of root-to-shoot signaling and rootstock-mediated tolerance to water deficit in tomato. *Genes* 12, 1–25. doi: 10.3390/genes12010010

Azzam, E. I., Jay-Gerin, J.-P., and Pain, D. (2012). Ionizing radiation-induced metabolic oxidative stress and prolonged cell injury. *Cancer Lett.* 327, 48–60. doi: 10.1016/j.canlet.2011.12.012

Baccaro, S., Cemmi, A., and Sarcina, I. D. (2019). Calliope 60 Co gamma irradiation facility for space qualification at ENEA-Casaccia research centre. *Phys. Astron. Int. J.* 3, 94–100. doi: 10.15406/paij.2019.03.00164

Bendokas, V., Skemiene, K., Trumbeckaite, S., Stanys, V., Passamonti, S., Borutaite, V., et al. (2020). Anthocyanins: from plant pigments to health benefits at mitochondrial level. *Crit. Rev. Food Sci. Nutr.* 60, 3352–3365. doi: 10.1080/10408398.2019.1687421

Benjamini, Y., and Hochberg, Y. (1995). Controlling the False Discovery Rate: a Practical and Powerful Approach to Multiple Testing. *J. R. Statist. Soc. Ser. B* 57, 289–300. doi: 10.1111/j.2517-6161.1995.tb02031.x

Bergey, D. R., Howe, G. A., and Ryan, C. A. (1996). Polypeptide signaling for plant defensive genes exhibits analogies to defense signaling in animals. *Proc. Natl. Acad. Sci. U. S. A.* 93, 12053–12058. doi: 10.1073/pnas.93.22.12053

Bijlani, S., Stephens, E., Singh, N. K., Venkateswaran, K., and Wang, C. C. C. (2021). Advances in space microbiology. *Iscience* 24:102395. doi: 10.1016/j.isci.2021.102395

Blanco, Y., de Diego-Castilla, G., Viúdez-Moreiras, D., Cavalcante-Silva, E., Rodríguez-Manfredi, J. A., Davila, A. F., et al. (2018). Effects of Gamma and Electron Radiation on the Structural Integrity of Organic Molecules and Macromolecular Biomarkers Measured by Microarray Immunoassays and Their Astrobiological Implications. *Astrobiology* 18, 1497–1516. doi: 10.1089/ast.2016.1645

Blesso, C. N. (2019). Dietary Anthocyanins and Human Health. *Nutrients* 11, 10–13. doi: 10.3390/nu11092107

Bognar, E., Sarszegi, Z., Szabo, A., Debreceni, B., Kalman, N., Tucsek, Z., et al. (2013). Antioxidant and Anti-Inflammatory Effects in RAW264.7 Macrophages of Malvidin, a Major Red Wine Polyphenol. *PLoS One* 8:e65355. doi: 10.1371/journal.pone.0065355

Bongue-Bartelsman, M., O'Neill, S. D., Yusen, T., and Yoder, J. I. (1994). Characterization of the gene encoding dihydroflavonol 4-reductase in tomato. *Gene* 138, 153–157. doi: 10.1016/0378-1119(94)90799-4

Bournival, B. L., Scott, J. W., and Vallejos, C. E. (1989). An isozyme marker for resistance to race 3 of Fusarium oxysporum f. sp. lycopersici in tomato. *Theor. Appl. Genet.* 78, 489–494. doi: 10.1007/BF00290832

Bovy, A., de Vos, R., Kemper, M., Schijlen, E., Almenar Pertejo, M., Muir, S., et al. (2002). High-flavonol tomatoes resulting from the heterologous expression of the maize transcription factor genes LC and C1. *Plant Cell* 14, 2509–2526. doi: 10.1105/tpc.004218

Brito, A., Areche, C., Sepúlveda, B., Kennelly, E. J., and Simirgiotis, M. J. (2014). Anthocyanin characterization, total phenolic quantification and antioxidant features of some chilean edible berry extracts. *Molecules* 19, 10936–10955. doi: 10.3390/molecules190810936

Brunetti, C., di Ferdinando, M., Fini, A., Pollastri, S., and Tattini, M. (2013). Flavonoids as antioxidants and developmental regulators: relative significance in plants and humans. *Int. J. Mol. Sci.* 14, 3540–3555. doi: 10.3390/ijms14023540

Buoso, S., Pagliari, L., Musetti, R., Martini, M., Marroni, F., Schmidt, W., et al. (2019). "Candidatus phytoplasma solani" interferes with the distribution and uptake of iron in tomato. *BMC Genomics* 20:703. doi: 10.1186/s12864-019-6062-x

Butelli, E., Titta, L., Giorgio, M., Mock, H. P., Matros, A., Peterek, S., et al. (2008). Enrichment of tomato fruit with health-promoting anthocyanins by expression of select transcription factors. *Nat. Biotechnol.* 26, 1301–1308. doi: 10.1038/nbt.1506

Buttarelli, M., Babini, G., Raspaglio, G., Filippetti, F., Battaglia, A., Ciucci, A., et al. (2019). A combined ANXA2-NDRG1-STAT1 gene signature predicts response to chemoradiotherapy in cervical cancer. *J. Exp. Clin. Cancer Res.* 38:279.

Cao, X., Qiu, Z., Wang, X., van Giang, T., Liu, X., Wang, J., et al. (2017). A putative R3 MYB repressor is the candidate gene underlying atroviolacium, a locus for anthocyanin pigmentation in tomato fruit. *J. Exp. Bot.* 68, 5745–5758. doi: 10.1093/jxb/erx382

Carmona, L., Alquézar, B., Diretto, G., Sevi, F., Malara, T., Lafuente, M. T., et al. (2021). Curing and low-temperature combined post-harvest storage enhances anthocyanin biosynthesis in blood oranges. *Food Chem.* 342:128334. doi: 10.1016/j.foodchem.2020.128334

Cock, P. J. A., Fields, C. J., Goto, N., Heuer, M. L., and Rice, P. M. (2009). The Sanger FASTQ file format for sequences with quality scores, and the Solexa/Illumina FASTQ variants. *Nucleic Acids Res.* 38, 1767–1771. doi: 10.1093/nar/gkp1137

Colanero, S., Perata, P., and Gonzali, S. (2020). What's behind Purple Tomatoes? Insight into the Mechanisms of Anthocyanin Synthesis in Tomato Fruits. *Plant Physiol.* 182, 1841–1853. doi: 10.1104/pp.19.01530

Conconi, A., Smerdon, M. J., Howe, G. A., and Ryan, C. A. (1996). The octadecanoid signalling pathway in plants mediates Response To Ultraviolet Radiation. *Nature* 383, 826–829.

Consortium, T. T. G., Sato, S., Tabata, S., Hirakawa, H., Asamizu, E., Shirasawa, K., et al. (2012). The tomato genome sequence provides insights into fleshy fruit evolution. *Nature* 485:635. doi: 10.1038/nature11119

Cooperstone, J. L., Ralston, R. A., Riedl, K. M., Haufe, T. C., and Ralf, M. (2015). Enhanced bioavailability of lycopene when consumed as cis-isomers from tangerine compared to red tomato juice, a randomized, cross-over clinical trial. *Mol. Nutr. Food Res.* 59, 658–669. doi: 10.1002/mnfr.201400658

Copp, R. R., Peebles, D. D., Soref, C. M., and Fahl, W. E. (2013). Radioprotective efficacy and toxicity of a new family of aminothiol analogs. *Int. J. Radiat. Biol.* 89, 485–492. doi: 10.3109/09553002.2013.770579

da Silva, F. L., Escribano-Bailón, M. T., Pérez Alonso, J. J., Rivas-Gonzalo, J. C., and Santos-Buelga, C. (2007). Anthocyanin pigments in strawberry. *LWT Food Sci. Technol.* 40, 374–382. doi: 10.1016/j.lwt.2005.09.018

da Silva Souza, M. A., Peres, L. E. P., Freschi, J. R., Purgatto, E., Lajolo, F. M., and Hassimotto, N. M. A. (2020). Changes in flavonoid and carotenoid profiles alter volatile organic compounds in purple and orange cherry tomatoes obtained by allele introgression. *J. Sci. Food Agric.* 100, 1662–1670. doi: 10.1002/jsfa.10180

Daly, S., Bianchini, R., Polefka, T., Jumbelic, L., and Jachowicz, J. (2009). Fluorescence and coloration of grey hair. *Int. J. Cosmet. Sci.* 31, 347–359. doi: 10.1111/j.1468-2494.2009.00500.x

de Ollas, C., González-Guzmán, M., Pitarch, Z., Matus, J. T., Candela, H., Rambla, J. L., et al. (2021). Identification of ABA-Mediated Genetic and Metabolic Responses to Soil Flooding in Tomato (Solanum lycopersicum L. Mill). *Front. Plant Sci.* 12:613059. doi: 10.3389/fpls.2021.613059

de Torre, M. P., Cavero, R. Y., Calvo, M. I., and Vizmanos, J. L. W. (2019). A simple and a reliable method to quantify antioxidant activity *in vivo*. *Antioxidants* 8, 1–11. doi: 10.3390/antiox8050142

de Vetten, N., ter Horst, J., van Schaik, H. P., de Boer, A., Mol, J., and Koes, R. (1999). A cytochrome b5 is required for full activity of flavonoid 3′,5′-hydroxylase, a cytochrome P450 involved in the formation of blue flower colors. *Proc. Natl. Acad. Sci. U. S. A.* 96, 778–783. doi: 10.1073/pnas.96.2.778

de Vries, J., and Archibald, J. M. (2018). Plant evolution: landmarks on the path to terrestrial life. *New Phytol.* 217, 1428–1434. doi: 10.1111/nph.14975

D'Errico, G., Vitiello, G., de Tommaso, G., Abdel-Gawad, F. K., Brundo, M. V., Ferrante, M., et al. (2018). Electron Spin Resonance (ESR) for the study of Reactive Oxygen Species (ROS) on the isolated frog skin (Pelophylax bergeri): a non-invasive method for environmental monitoring. *Environ. Res.* 165, 11–18. doi: 10.1016/j.envres.2018.03.044

Desiderio, A., Salzano, A. M., Scaloni, A., Massa, S., Pimpinella, M., de Coste, V., et al. (2019). Effects of Simulated Space Radiations on the Tomato Root Proteome. *Front. Plant Sci.* 10:1334. doi: 10.3389/fpls.2019.01334

DeZwart, M., and Henderson, S. (2021). *Commercial and Military Uses of Outer Space*. Germany: Springer.

Diretto, G., Jin, X., Capell, T., Zhu, C., and Gomez-Gomez, L. (2019). Differential accumulation of pelargonidin glycosides in petals at three different developmental stages of the orange-flowered gentian (Gentiana lutea L. var. aurantiaca). *PLoS One* 14:e0212062. doi: 10.1371/journal.pone.0212062

Dobin, A., Davis, C. A., Schlesinger, F., Drenkow, J., Zaleski, C., Jha, S., et al. (2013). STAR: ultrafast universal RNA-seq aligner. *Bioinformatics* 29, 15–21. doi: 10.1093/bioinformatics/bts635

dos Santos, A. L., Chaves-Silva, S., Yang, L., Maia, L. G. S., Chalfun-Júnior, A., Sinharoy, S., et al. (2017). Global analysis of the MATE gene family of metabolite transporters in tomato. *BMC Plant Biol.* 17:185. doi: 10.1186/s12870-017-1115-2

Esatbeyoglu, T., Wagner, A. E., Motafakkerazad, R., Nakajima, Y., Matsugo, S., and Rimbach, G. (2014). Free radical scavenging and antioxidant activity of betanin: electron spin resonance spectroscopy studies and studies in cultured cells. *Food Chem. Toxicol.* 73, 119–126. doi: 10.1016/j.fct.2014.08.007

Fahim, S., Hussein, W., and Awad, H. (2016). Systemic Resistance Induction of Tomato Plants against ToMV Virus by Surfactin Produced from Bacillus subtilis BMG02. *Am. J. of Microbiol. Res.* 4, 153–158. doi: 10.12691/ajmr-4-5-5

Fan, K. T., Hsu, Y., Yeh, C. F., Chang, C. H., Chang, W. H., and Chen, Y. R. (2021). Quantitative proteomics reveals the dynamic regulation of the tomato proteome in response to phytophthora infestans. *Int. J. Mol. Sci.* 22:4174. doi: 10.3390/ijms22084174

Fan, Y., Yang, W., Yan, Q., Chen, C., and Li, J. (2020). Genome-Wide Identification and Expression Analysis. *Genes* 11:1.

Fang, J. (2014). Some anthocyanins could be efficiently absorbed across the gastrointestinal mucosa: extensive presystemic metabolism reduces apparent bioavailability. *J. Agric. Food Chem.* 62, 3904–3911. doi: 10.1021/jf405356b

Faraco, M., Spelt, C., Bliek, M., Verweij, W., Hoshino, A., Espen, L., et al. (2014). Hyperacidification of Vacuoles by the Combined Action of Two Different P-ATPases in the Tonoplast Determines Flower Color. *Cell Rep.* 6, 32–43. doi: 10.1016/j.celrep.2013.12.009

Faure, A. M., Sánchez-Ferrer, A., Zabara, A., Andersen, M. L., and Nyström, L. (2014). Modulating the structural properties of β-d-glucan degradation products by alternative reaction pathways. *Carbohydrate Polym.* 99, 679–686. doi: 10.1016/j.carbpol.2013.08.022

Fedenko, V. S., Shemet, S. A., and Landi, M. (2017). UV–vis spectroscopy and colorimetric models for detecting anthocyanin-metal complexes in plants: an overview of *in vitro* and *in vivo* techniques. *J. Plant Physiol.* 212, 13–28. doi: 10.1016/j.jplph.2017.02.001

Fernandez-Moreno, J.-P., Tzfadia, O., Forment, J., Presa, S., Rogachev, I., Meir, S., et al. (2016). Characterization of a New Pink-Fruited Tomato Mutant Results in the Identification of a Null Allele of the SlMYB12 Transcription Factor. *Plant Physiol.* 171, 1821–1836.

Fernandez-Pozo, N., Menda, N., Edwards, J. D., Saha, S., Tecle, I. Y., Strickler, S. R., et al. (2015). The Sol Genomics Network (SGN)-from genotype to phenotype to breeding. *Nucleic Acids Res.* 43, D1036–D1041. doi: 10.1093/nar/gku1195

Filiz, E., Cetin, D., and Akbudak, M. A. (2019). Aromatic amino acids biosynthesis genes identification and expression analysis under salt and drought stresses in Solanum lycopersicum L. *Sci. Hortic.* 250, 127–137. doi: 10.1016/j.scienta.2019.02.044

Florio, F. E., Gattolin, S., Toppino, L., Bassolino, L., Fibiani, M., and Scalzo, R. L., et al. (2021). A SmelAAT Acyltransferase Variant Causes a Major Difference in Eggplant (*Solanum melongena* L .) Peel Anthocyanin Composition. *Int. J. Mol. Sci.* 22:9174.

Fu, Y., Li, L., Xie, B., Dong, C., Wang, M., Jia, B., et al. (2016). How to establish a bioregenerative life support system for long-term crewed missions to the moon or mars. *Astrobiology* 16, 925–936. doi: 10.1089/ast.2016.1477

Gakamsky, A., Duncan, R. R., Howarth, N. M., Dhillon, B., Buttenschön, K. K., Daly, D. J., et al. (2017). Tryptophan and Non-Tryptophan Fluorescence of the Eye Lens Proteins Provides Diagnostics of Cataract at the Molecular Level. *Sci. Rep.* 7, 1–15. doi: 10.1038/srep40375

Gao, Y., He, C., Zhang, D., Liu, X., Xu, Z., Tian, Y., et al. (2017). Two trichome birefringence-like proteins mediate xylan acetylation, which is essential for leaf blight resistance in rice. *Plant Physiol.* 173, 470–481. doi: 10.1104/pp.16.01618

Gao, Y., Liu, J., Chen, Y., Tang, H., Wang, Y., He, Y., et al. (2018). Tomato SlAN11 regulates flavonoid biosynthesis and seed dormancy by interaction with bHLH proteins but not with MYB proteins. *Hortic. Res.* 5:27. doi: 10.1038/s41438-018-0032-3

Garg, M., Sharma, N., Sharma, S., Kapoor, P., Kumar, A., Chunduri, V., et al. (2018). Biofortified Crops Generated by Breeding, Agronomy, and Transgenic Approaches Are Improving Lives of Millions of People around the World. *Front. Nutr.* 5:12. doi: 10.3389/fnut.2018.00012

Gerszberg, A., Hnatuszko-Konka, K., Kowalczyk, T., and Kononowicz, A. K. (2015). Tomato (Solanum lycopersicum L.) in the service of biotechnology. *Plant Cell Tissue Organ Cult.* 120, 881–902. doi: 10.1007/s11240-014-0664-4

Giovannoni, J. (2018). Tomato Multiomics Reveals Consequences of Crop Domestication and Improvement. *Cell* 172, 6–8. doi: 10.1016/j.cell.2017.12.036

Gómez, X., Sanon, S., Zambrano, K., Asquel, S., Bassantes, M., Morales, J. E., et al. (2021). Key points for the development of antioxidant cocktails to prevent cellular stress and damage caused by reactive oxygen species (ROS) during manned space missions. *NPJ Microgravity* 7, 35. doi: 10.1038/s41526-021-00162-8

Gonzalez, A., Zhao, M., Leavitt, J. M., and Lloyd, A. M. (2008). Regulation of the anthocyanin biosynthetic pathway by the TTG1/bHLH/Myb transcriptional complex in Arabidopsis seedlings. *Plant J.* 53, 814–827. doi: 10.1111/j.1365-313X.2007.03373.x

Gonzali, S., Mazzucato, A., and Perata, P. (2009). Purple as a tomato: towards high anthocyanin tomatoes. *Trends Plant Sci.* 14, 237–241. doi: 10.1016/j.tplants.2009.02.001

Gudkov, S. V., Grinberg, M. A., Sukhov, V., and Vodeneev, V. (2019). Effect of ionizing radiation on physiological and molecular processes in plants. *J. Environ. Radioact.* 202, 8–24. doi: 10.1016/j.jenvrad.2019.02.001

Gupta, S., Shi, X., Lindquist, I. E., Devitt, N., Mudge, J., and Rashotte, A. M. (2013). Transcriptome profiling of cytokinin and auxin regulation in tomato root. *J. Exp. Bot.* 64, 695–704. doi: 10.1093/jxb/ers365

Gutierrez-Valdes, N., Häkkinen, S. T., Lemasson, C., Guillet, M., Oksman-Caldentey, K. M., Ritala, A., et al. (2020). Hairy Root Cultures—A Versatile Tool With Multiple Applications. *Front. Plant Sci.* 11:33. doi: 10.3389/fpls.2020.00033

Häkkinen, S. T., Nygren, H., Nohynek, L., Puupponen-Pimiä, R., Heiniö, R. L., Maiorova, N., et al. (2020). Plant cell cultures as food—aspects of sustainability and safety. *Plant Cell Rep.* 39, 1655–1668. doi: 10.1007/s00299-020-02592-2

Hanan, A., Basit, A., Nazir, T., Zeeshan Majeed, M., and Qiu, D. (2020). Anti-insect activity of a partially purified protein derived from the entomopathogenic fungus Lecanicillium lecanii (Zimmermann) and its putative role in a tomato defense mechanism against green peach aphid. *J. Inverteb. Pathol.* 11:574. doi: 10.1016/j.jip.2019.107282

Harrison, K., Mendoza-Herrera, A., Levy, J. G., and Tamborindeguy, C. (2021). Lasting consequences of psyllid (Bactericera cockerelli L.) infestation on tomato defense, gene expression, and growth. *BMC Plant Biol.* 21:114. doi: 10.1186/s12870-021-02876-z

Hawkins, C. L., and Davies, M. J. (2014). Detection and characterisation of radicals in biological materials using EPR methodology. *Biochim. Biophys. Acta* 1840, 708–721. doi: 10.1016/j.bbagen.2013.03.034

Hilaire, M. R., Ahmed, I. A., Lin, C. W., Jo, H., DeGrado, W. F., and Gai, F. (2017). Blue fluorescent amino acid for biological spectroscopy and microscopy. *Proc. Natl. Acad. Sci. U. S. A.* 114, 6005–6009. doi: 10.1073/pnas.1705586114

Hoang, M. H. T., Nguyen, X. C., Lee, K., Kwon, Y. S., Pham, H. T. T., Park, H. C., et al. (2012). Phosphorylation by AtMPK6 is required for the biological function of AtMYB41 in Arabidopsis. *Biochem. Biophys. Res. Commun.* 422, 181–186. doi: 10.1016/j.bbrc.2012.04.137

Hou, X. J., Li, J. M., Liu, B. L., and Wei, L. (2017). Co-expression of basic helix–loop–helix protein (bHLH) and transcriptional activator-Myb genes induced anthocyanin biosynthesis in hairy root culture of Nicotiana tabacum L and Ipomea tricolor. *Acta Physiol. Plantar.* 39, 1–7. doi: 10.1007/s11738-017-2362-4

Hu, C., Gong, Y., Jin, S., and Zhu, Q. (2011). Molecular analysis of a UDP-glucose: flavonoid 3-O-glucosyltransferase (UFGT) gene from purple potato (Solanum tuberosum). *Mol. Biol. Rep.* 38, 561–567. doi: 10.1007/s11033-010-0141-z

Huang, B., Routaboul, J. M., Liu, M., Deng, W., Maza, E., Mila, I., et al. (2017). Overexpression of the class D MADS-box gene Sl-AGL11 impacts fleshy tissue differentiation and structure in tomato fruits. *J. Exp. Bot.* 68, 4869–4884. doi: 10.1093/jxb/erx303

Ichikawa, H., Ichiyanagi, T., Xu, B., Yoshii, Y., Nakajima, M., and Konishi, T. (2001). Antioxidant activity of anthocyanin extract from purple black rice. *J. Med. Food* 4, 211–218. doi: 10.1089/10966200152744481

Imhof, B., Schlacht, I. L., Waclavicek, R., Schubert, D., Zeidler, C., Vrakking, V., et al. (2018). "Eden Iss – A Simulation Testbed To An Advanced Exploration Design Concept For A Greenhouse For Moon And Mars" in *69th International Astronautical Congress*. Germany: Institute of Space Systems. 1–5.

Inglett, G. E., Rose, D. J., Chen, D., Stevenson, D. G., and Biswas, A. (2010). Phenolic content and antioxidant activity of extracts from whole buckwheat (Fagopyrum esculentum Möench) with or without microwave irradiation. *Food Chem.* 119, 1216–1219. doi: 10.1016/j.foodchem.2009.07.041

Isaacson, T., Ronen, G., Zamir, D., and Hirschberg, J. (2002). Cloning of tangerine from tomato reveals a Carotenoid isomerase essential for the production of β-carotene and xanthophylls in plants. *Plant Cell* 14, 333–342. doi: 10.1105/tpc.010303

Islam, A., Mercer, C. F., Leung, S., Dijkwel, P. P., and McManus, M. T. (2015). Transcription of biotic stress associated genes in white clover (Trifolium repens L.) differs in response to cyst and root-knot nematode infection. *PLoS One* 10:e0137981. doi: 10.1371/journal.pone.0137981

Jian, W., Cao, H., Yuan, S., Liu, Y., Lu, J., Lu, W., et al. (2019). SlMYB75, an MYB-type transcription factor, promotes anthocyanin accumulation and enhances volatile aroma production in tomato fruits. *Hortic. Res.* 6:22. doi: 10.1038/s41438-018-0098-y

Kalt, W., Cassidy, A., Howard, L. R., Krikorian, R., Stull, A. J., Tremblay, F., et al. (2020). Recent Research on the Health Benefits of Blueberries and Their Anthocyanins. *Adv. Nutr.* 11, 224–236. doi: 10.1093/advances/nmz065

Kashyap, S. P., Prasanna, H. C., Kumari, N., Mishra, P., and Singh, B. (2020). Understanding salt tolerance mechanism using transcriptome profiling and de novo assembly of wild tomato Solanum chilense. *Sci. Rep.* 10, 1–20. doi: 10.1038/s41598-020-72474-w

Khandelwal, N., and Abraham, S. K. (2014). Intake of anthocyanidins pelargonidin and cyanidin reduces genotoxic stress in mice induced by diepoxybutane, urethane and endogenous nitrosation. *Environ. Toxicol. Pharmacol.* 37, 837–843. doi: 10.1016/j.etap.2014.02.012

Khodadad, C. L. M., Hummerick, M. E., Spencer, L. S. E., Dixit, A. R., Richards, J. T., Romeyn, M. W., et al. (2020). Microbiological and Nutritional Analysis of Lettuce Crops Grown on the International Space Station. *Front. Plant Sci.* 11:492. doi: 10.3389/fpls.2020.00199

Kiferle, C., Fantini, E., Bassolino, L., Povero, G., Spelt, C., Buti, S., et al. (2015). Tomato R2R3-MYB proteins SlANT1 and SlAN2: same protein activity, different roles. *PLoS One* 10:e0136365. doi: 10.1371/journal.pone.0136365

Kim, D., Langmead, B., and Salzberg, S. L. (2015). HISAT: a fast spliced aligner with low memory requirements Daehwan HHS Public Access. *Nat. Methods* 12, 357–360. doi: 10.1038/nmeth.3317.HISAT

Kim, S., Park, J., Yeom, S. I., Kim, Y. M., Seo, E., Kim, K. T., et al. (2017). New reference genome sequences of hot pepper reveal the massive evolution of plant disease-resistance genes by retroduplication. *Genome Biol.* 18, 1–11. doi: 10.1186/s13059-017-1341-9

Klee, H. J., and Tieman, D. M. (2013). Genetic challenges of flavor improvement in tomato. *Trends Genet.* 29, 257–262. doi: 10.1016/j.tig.2012.12.003

Koes, R., Verweij, W., and Quattrocchio, F. (2005). Flavonoids: a colorful model for the regulation and evolution of biochemical pathways. *Trends Plant Sci.* 10, 236–242. doi: 10.1016/j.tplants.2005.03.002

Kozlowski, D., Marsal, P., Steel, M., Mokrini, R., Duroux, J. L., Lazzaroni, R., et al. (2007). Theoretical investigation of the formation of a new series of antioxidant depsides from the radiolysis of flavonoid compounds. *Radiat. Res.* 168, 243–252. doi: 10.1667/RR0824.1

Krga, I., and Milenkovic, D. (2019). Anthocyanins: from Sources and Bioavailability to Cardiovascular-Health Benefits and Molecular Mechanisms of Action. *J. Agric. Food Chem.* 67, 1771–1783. doi: 10.1021/acs.jafc.8b06737

Kumar, V., Irfan, M., Ghosh, S., Chakraborty, N., Chakraborty, S., and Datta, A. (2016). Fruit ripening mutants reveal cell metabolism and redox state during ripening. *Protoplasma* 253, 581–594. doi: 10.1007/s00709-015-0836-z

Lalande, M., Schwob, L., Vizcaino, V., Chirot, F., Dugourd, P., Schlathölter, T., et al. (2019). Direct Radiation Effects on the Structure and Stability of Collagen and Other Proteins. *ChemBioChem* 20, 2972–2980. doi: 10.1002/cbic.201900202

Lateef, Z. W. A., and Al-Nimer, M. S. M. (2009). X-Rays Irradiation Produced Dual Effects on the Constituents of Medicinal Plants Extracts. *J. Biol. Sci.* 9, 872–877.

Li, D., Li, X., and Ding, X. (2010). Composition and antioxidative properties of the flavonoid-rich fractions from tartary buckwheat grains. *Food Sci. Biotechnol.* 19, 711–716. doi: 10.1007/s10068-010-0100-4

Li, H., Deng, Z., Liu, R., Young, J. C., Zhu, H., Loewen, S., et al. (2011). Characterization of Phytochemicals and Antioxidant Activities of a Purple Tomato (Solanum lycopersicum L.). *J. Agric. Food Chem.* 59, 11803–11811. doi: 10.1021/jf202364v

Li, J., Han, G., Sun, C., and Sui, N. (2019). Research advances of MYB transcription factors in plant stress resistance and breeding. *Plant Signal. Behav.* 14, 1–9. doi: 10.1080/15592324.2019.1613131

Li, Z., Vickrey, T. L., McNally, M. G., Sato, S. J., Clemente, T. E., and Mower, J. P. (2019). Assessing anthocyanin biosynthesis in solanaceae as a model pathway for secondary metabolism. *Genes* 10:559. doi: 10.3390/genes10080559

Li, N., Wang, J., Wang, B., Huang, S., Hu, J., Yang, T., et al. (2021). Identification of the Carbohydrate and Organic Acid Metabolism Genes Responsible for Brix in Tomato Fruit by Transcriptome and Metabolome Analysis. *Front. Genet.* 12:714942. doi: 10.3389/fgene.2021.714942

Li, P., Chen, B., Zhang, G., Chen, L., Dong, Q., Wen, J., et al. (2016). Regulation of anthocyanin and proanthocyanidin biosynthesis by Medicago truncatula bHLH transcription factor MtTT8. *New Phytol.* 210, 905–921. doi: 10.1111/nph.13816

Li, P., Liu, H., Yang, H., Pu, X., Li, C., Huo, H., et al. (2020). Translocation of Drought-Responsive Proteins from the Chloroplasts. *Cells* 9, 1–17. doi: 10.3390/cells9010259

Li, X., Tieman, D., Liu, Z., Chen, K., and Klee, H. J. (2020). Identification of a lipase gene with a role in tomato fruit short-chain fatty acid-derived flavor volatiles by genome-wide association. *Plant J.* 104, 631–644. doi: 10.1111/tpj.14951

Liao, Y., Smyth, G. K., and Shi, W. (2019). The R package Rsubread is easier, faster, cheaper and better for alignment and quantification of RNA sequencing reads. *Nucleic Acids Res.* 47:e47. doi: 10.1093/nar/gkz114

Liu, H., Liu, J., and Wei, Y. (2016). Identification and analysis of the metacaspase gene family in tomato. *Biochem. Biophys. Res. Commun.* 479, 523–529. doi: 10.1016/j.bbrc.2016.09.103

Liu, J., Osbourn, A., and Ma, P. (2015). MYB transcription factors as regulators of phenylpropanoid metabolism in plants. *Mol. Plant* 8, 689–708. doi: 10.1016/j.molp.2015.03.012

Liu, Y., Tikunov, Y., Schouten, R. E., Marcelis, L. F. M., Visser, R. G. F., and Bovy, A. (2018). Anthocyanin biosynthesis and degradation mechanisms in Solanaceous vegetables: a review. *Front. Chem.* 6:52. doi: 10.3389/fchem.2018.00052

Livak, K. J., and Schmittgen, T. D. (2001). Analysis of relative gene expression data using real-time quantitative PCR and the 2-ΔΔCT method. *Methods* 25, 402–408. doi: 10.1006/meth.2001.1262

Lloyd, A., Brockman, A., Aguirre, L., Campbell, A., Bean, A., Cantero, A., et al. (2017). Advances in the MYB-bHLH-WD Repeat (MBW) pigment regulatory model: addition of a WRKY factor and co-option of an anthocyanin MYB for betalain regulation. *Plant Cell Physiol* 58, 1431–1441. doi: 10.1093/pcp/pcx075

Lohmann, W., Lohmann, C., and Ibrahim, M. (1988). Fluorescence spectra of NADH/NAD, kynurenine, tryptophan, and tyrosine. *Naturwissenschaften* 75, 141–142. doi: 10.1007/BF00405305

Lotito, S. B., and Frei, B. (2006). Consumption of flavonoid-rich foods and increased plasma antioxidant capacity in humans: cause, consequence, or epiphenomenon? *Free Radic. Biol. Med.* 41, 1727–1746. doi: 10.1016/j.freeradbiomed.2006.04.033

Love, M. I., Huber, W., and Anders, S. (2014). Moderated estimation of fold change and dispersion for RNA-seq data with DESeq2. *Genome Biol.* 15, 1–21. doi: 10.1186/s13059-014-0550-8

Marcu, D., Cristea, V., and Daraban, L. (2013a). Dose-dependent effects of gamma radiation on lettuce (Lactuca sativa var. capitata) seedlings. *Int. J. Radiat. Biol.* 89, 219–223. doi: 10.3109/09553002.2013.734946

Marcu, D., Damian, G., and Cosma, C. (2013b). Gamma radiation effects on seed germination, growth and pigment content, and ESR study of induced free radicals in maize (Zea mays). *J. Biol. Phys.* 39, 625–634. doi: 10.1007/s10867-013-9322-z

Meng, X., Yang, D., Li, X., Zhao, S., Sui, N., and Meng, Q. (2015). Physiological changes in fruit ripening caused by overexpression of tomato SlAN2, an R2R3-MYB factor. *Plant Physiol. Biochem.* 89, 24–30. doi: 10.1016/j.plaphy.2015.02.005

Martí, R., Roselló, S., and Cebolla-Cornejo, J. (2016). Tomato as a source of carotenoids and polyphenols targeted to cancer prevention. *Cancers* 8, 1–28. doi: 10.3390/cancers8060058

Massa, G. D., Wheeler, R. M., Morrow, R. C., and Levine, H. G. (2016). Growth chambers on the International Space Station for large plants. *Acta Hortic.* 1134, 215–221. doi: 10.17660/ActaHortic.2016.1134.29

Mathews, H., Clendennen, S. K., Caldwell, C. G., Liu, X. L., Connors, K., Matheis, N., et al. (2003). Activation tagging in tomato identifies a transcriptional regulator of anthocyanin biosynthesis, modification, and transport. *Plant Cell* 15, 1689–1703. doi: 10.1105/tpc.012963

Mazzucato, A., Willems, D., Bernini, R., Picarella, M. E., Santangelo, E., Ruiu, F., et al. (2013). Novel phenotypes related to the breeding of purple-fruited tomatoes and effect of peel extracts on human cancer cell proliferation. *Plant Physiol. Biochem.* 72, 125–133. doi: 10.1016/J.PLAPHY.2013.05.012

McLellan, H., Gilroy, E. M., Yun, B. W., Birch, P. R. J., and Loake, G. J. (2009). Functional redundancy in the Arabidopsis Cathepsin B gene family contributes to basal defence, the hypersensitive response and senescence. *New Phytol.* 183, 408–418. doi: 10.1111/j.1469-8137.2009.02865.x

Mehrtens, F., Kranz, H., Bednarek, P., and Weisshaar, B. (2005). The Arabidopsis transcription factor MYB12 is a flavonol-specific regulator of phenylpropanoid biosynthesis. *Plant Physiol.* 138, 1083–1096. doi: 10.1104/pp.104.058032

Mei, W., Qin, Y., Song, W., Li, J., and Zhu, Y. (2009). Cotton GhPOX1 encoding plant class III peroxidase may be responsible for the high level of reactive oxygen species production that is related to cotton fiber elongation. *J. Genet. Genomics* 36, 141–150. doi: 10.1016/S1673-8527(08)60101-0

Mes, P. J., Boches, P., Myers, J. R., and Durst, R. (2008). Characterization of tomatoes expressing anthocyanin in the fruit. *J. Am. Soc. Hortic. Sci.* 133, 262–269. doi: 10.21273/jashs.133.2.262

Mikami, K., and Hosokawa, M. (2013). Biosynthetic pathway and health benefits of fucoxanthin, an algae-specific xanthophyll in brown seaweeds. *Int. J. Mol. Sci.* 14, 13763–13781. doi: 10.3390/ijms140713763

Moghaddam, S. S., Jaafar, H., Ibrahim, R., Rahmat, A., Aziz, M. A., and Philip, E. (2011). Effects of acute gamma irradiation on physiological traits and flavonoid accumulation of *Centella asiatica*. *Molecules* 16, 4994–5007. doi: 10.3390/molecules16064994

Morishita, T., Yamaguchi, H., and Degi, K. (2007). The contribution of polyphenols to antioxidative activity in common buckwheat and Tartary buckwheat grain. *Plant Prod. Sci.* 10, 99–104. doi: 10.1626/pps.10.99

Morita, Y., Takagi, K., Fukuchi-Mizutani, M., Ishiguro, K., Tanaka, Y., Nitasaka, E., et al. (2014). A chalcone isomerase-like protein enhances flavonoid production and flower pigmentation. *Plant J.* 78, 294–304. doi: 10.1111/tpj.12469

Murata, M., Nakai, Y., Kawazu, K., Ishizaka, M., Kajiwara, H., Ab, H., et al. (2019). Loliolide, a carotenoid metabolite, is a potential endogenous inducer of herbivore resistance. *Plant Physiol.* 179, 1822–1833. doi: 10.1104/pp.18.00837

Nagata, T., Todoriki, S., Masumizu, T., Suda, I., Furuta, S., Du, Z., et al. (2003). Levels of active oxygen species are controlled by ascorbic acid and anthocyanin in Arabidopsis. *J. Agric. Food Chem.* 51, 2992–2999. doi: 10.1021/jf026179+

Nveawiah-Yoho, P., Zhou, J., Palmer, M., Sauve, R., Zhou, S., Howe, K. J., et al. (2013). Identification of Proteins for Salt Tolerance Using a Comparative Proteomics Analysis of Tomato Accessions with Contrasting Salt Tolerance. *J. Am. Soc. Hortic. Sci.* 138:13. doi: 10.21273/jashs.138.5.382

Omidvar, V., Mohorianu, I., Dalmay, T., and Fellner, M. (2015). Identification of miRNAs with potential roles in regulation of anther development and male-sterility in 7B-1 male-sterile tomato mutant. *BMC Genomics* 16:878. doi: 10.1186/s12864-015-2077-0

Ooe, E., Ogawa, K., Horiuchi, T., Tada, H., Murase, H., Tsuruma, K., et al. (2016). Analysis and characterization of anthocyanins and carotenoids in Japanese blue tomato. *Biosci. Biotechnol. Biochem.* 80, 341–349. doi: 10.1080/09168451.2015.1091715

Pan, Q., Liu, Y. S., Budai-Hadrian, O., Sela, M., Carmel-Goren, L., Zamir, D., et al. (2000). Comparative genetics of nucleotide binding site-leucine rich repeat resistance gene homologues in the genomes of two dicotyledons: tomato and arabidopsis. *Genetics* 155, 309–322. doi: 10.1093/genetics/155.1.309

Pan, X., Wang, G., Lay, C. L., Tan, B. H., He, C., and Liu, Y. (2013). Photoluminescence from Amino-Containing Polymer in the Presence of CO 2: carbamato Anion Formed as a Fluorophore. *Sci. Rep.* 3, 1–6. doi: 10.1038/srep02763

Paniagua, C., Bilkova, A., Jackson, P., Dabravolski, S., Riber, W., Didi, V., et al. (2017). Dirigent proteins in plants: modulating cell wall metabolism during abiotic and biotic stress exposure. *J. Exp. Bot.* 68, 3287–3301. doi: 10.1093/jxb/erx141

Pelletier, K., Murrell, J. R., and Shirley, B. W. (1997). Characterization of flavonol synthase and leucoanthocyanidin dioxygenase genes in Arabidopsis. Further evidence for differential regulation of "early" and "late" genes. *Plant Physiol.* 113, 1437–1445. doi: 10.1104/pp.113.4.1437

Peng, H., Yang, T., and Jurick, W. M. (2014). Calmodulin gene expression in response to mechanical wounding and Botrytis cinerea infection in tomato fruit. *Plants* 3, 427–441. doi: 10.3390/plants3030427

Peng, J., Deng, X., Huang, J., Jia, S., Miao, X., and Huang, Y. (2004). Role of salicylic acid in tomato defense against cotton bollworm, Helicoverpa armigera Hubner. *Z. Naturforsch. C J. Biosci.* 59, 856–862. doi: 10.1515/znc-2004-11-1215

Petrisor, D., Damian, G., Simon, S., Hosu, A., and Miclaus, V. (2008). Antioxidant activity of some types of white wines and juices investigated by EPR spectroscopy. *Mod. Phys. Lett. B* 22, 2689–2698. doi: 10.1142/S0217984908017175

Pinheiro, T. T., Peres, L. E. P., Purgatto, E., Latado, R. R., Maniero, R. A., Martins, M. M., et al. (2019). Citrus carotenoid isomerase gene characterization by complementation of the "Micro-Tom" tangerine mutant. *Plant Cell Rep.* 38, 623–636. doi: 10.1007/s00299-019-02393-2

Povero, G. (2011). *Physiological and Genetic Control of Anthocyanin Pigmentation in Different Species*. Netherlands: Vrije Universiteit Amsterdam.

Povero, G., Gonzali, S., Bassolino, L., Mazzucato, A., and Perata, P. (2011). Transcriptional analysis in high-anthocyanin tomatoes reveals synergistic effect of Aft and atv genes. *J. Plant Physiol.* 168, 270–279. doi: 10.1016/j.jplph.2010.07.022

Preuß, A., Stracke, R., Weisshaar, B., Hillebrecht, A., Matern, U., and Martens, S. (2009). Arabidopsis thaliana expresses a second functional flavonol synthase. *FEBS Lett.* 583, 1981–1986. doi: 10.1016/j.febslet.2009.05.006

Qian, Y., Zhang, T., Yu, Y., Gou, L., Yang, J., Xu, J., et al. (2021). Regulatory Mechanisms of bHLH Transcription Factors in Plant Adaptive Responses to Various Abiotic Stresses. *Front. Plant Sci.* 12:677611. doi: 10.3389/fpls.2021.677611

Qiu, Z., Wang, X., Gao, J., Guo, Y., Huang, Z., and Du, Y. (2016). The Tomato Hoffman's Anthocyaninless Gene Encodes a bHLH Transcription Factor Involved in Anthocyanin Biosynthesis That Is Developmentally Regulated and Induced by Low Temperatures. *PLoS One* 11:e0151067. doi: 10.1371/journal.pone.0151067

Ramsay, N. A., and Glover, B. J. (2005). MYB-bHLH-WD40 protein complex and the evolution of cellular diversity. *Trends Plant Sci.* 10, 63–70. doi: 10.1016/j.tplants.2004.12.011

Reimand, J., Kull, M., Peterson, H., Hansen, J., and Vilo, J. (2007). G:Profiler-a web-based toolset for functional profiling of gene lists from large-scale experiments. *Nucleic Acids Res.* 35, 193–200. doi: 10.1093/nar/gkm226

Riley, P. A. (1994). Free Radicals in Biology: oxidative Stress and the Effects of Ionizing Radiation. *Int. J. Radiat. Biol.* 65, 27–33.

Roldan, M. V. G., Outchkourov, N., van Houwelingen, A., Lammers, M., de La Fuente, I. R., Ziklo, N., et al. (2014). An O-methyltransferase modifies accumulation of methylated anthocyanins in seedlings of tomato. *Plant J.* 80, 695–708. doi: 10.1111/tpj.12664

Ron, M., Kajala, K., Pauluzzi, G., Wang, D., Reynoso, M. A., Zumstein, K., et al. (2014). Hairy root transformation using Agrobacterium rhizogenes as a tool for exploring cell type-specific gene expression and function using tomato as a model. *Plant Physiol.* 166, 455–469. doi: 10.1104/pp.114.239392

Rossetto, M., Vanzani, P., Lunelli, M., Scarpa, M., Mattivi, F., and Rigo, A. (2007). Peroxyl radical trapping activity of anthocyanins and generation of free radical intermediates. *Free Radic. Res.* 41, 854–859. doi: 10.1080/10715760701261533

Roy, S. (2016). Function of MYB domain transcription factors in abiotic stress and epigenetic control of stress response in plant genome. *Plant Signal. Behav.* 11:e1117723. doi: 10.1080/15592324.2015.1117723

Safavi-Rizi, V., Herde, M., and Stöhr, C. (2020). Identification of nitric oxide (NO)-responsive genes under hypoxia in tomato (Solanum lycopersicum L.) root. *Sci. Rep.* 10, 1–20. doi: 10.1038/s41598-020-73613-z

Saha, S., Singh, J., Paul, A., Sarkar, R., Khan, Z., and Banerjee, K. (2021). Anthocyanin profiling using UV-vis spectroscopy and liquid chromatography mass spectrometry. *J. AOAC Int.* 103, 23–39. doi: 10.5740/jaoacint.19-0201

Scandalios, J. G. (2002). Oxidative stress responses - What have genome-scale studies taught us? *Genome Biol.* 3, 1–6. doi: 10.1186/gb-2002-3-7-reviews1019

Schauer, N., Semel, Y., Roessner, U., Gur, A., Balbo, I., Carrari, F., et al. (2006). Comprehensive metabolic profiling and phenotyping of interspecific introgression lines for tomato improvement. *Nat. Biotechnol.* 24, 447–454. doi: 10.1038/nbt1192

Schimmel, B. C. J., Alba, J. M., Wybouw, N., Glas, J. J., Meijer, T. T., Schuurink, R. C., et al. (2018). Distinct signatures of host defense suppression by plant-feeding mites. *Int. J. Mol. Sci.* 19:3265. doi: 10.3390/ijms19103265

Schreiber, G., Reuveni, M., Evenor, D., Oren-Shamir, M., Ovadia, R., Sapir-Mir, M., et al. (2012). ANTHOCYANIN1 from Solanum chilense is more efficient in accumulating anthocyanin metabolites than its Solanum lycopersicum counterpart in association with the ANTHOCYANIN FRUIT phenotype of tomato. *Theor. Appl. Genet.* 124, 295–307. doi: 10.1007/s00122-011-1705-6

Schreurs, A. S., Shirazi-Fard, Y., Shahnazari, M., Alwood, J. S., Truong, T. A., Tahimic, C. G. T., et al. (2016). Dried plum diet protects from bone loss caused by ionizing radiation. *Sci. Rep.* 6, 1–11. doi: 10.1038/srep21343

Scranton, M. A., Fowler, J. H., Girke, T., and Walling, L. L. (2013). Microarray Analysis of Tomato's Early and Late Wound Response Reveals New Regulatory Targets for Leucine Aminopeptidase A. *PLoS One* 8:e77889. doi: 10.1371/journal.pone.0077889

Şensoy, Í, Rosen, R. T., Ho, C. T., and Karwe, M. V. (2006). Effect of processing on buckwheat phenolics and antioxidant activity. *Food Chem.* 99, 388–393. doi: 10.1016/j.foodchem.2005.08.007

Serrato, A. J., Fernández-Trijueque, J., Barajas-López, J., de, D., Chueca, A., and Sahrawy, M. (2013). Plastid thioredoxins: a "one-for-all" redox-signaling system in plants. *Front. Plant Sci.* 4:463. doi: 10.3389/fpls.2013.00463

Sewelam, N., Kazan, K., and Schenk, P. M. (2016). Global plant stress signaling: reactive oxygen species at the cross-road. *Front. Plant Sci.* 7:187. doi: 10.3389/fpls.2016.00187

Sharma, P., Padh, H., and Shrivastava, N. (2013). Hairy root cultures: a suitable biological system for studying secondary metabolic pathways in plants. *Eng. Life Sci.* 13, 62–75. doi: 10.1002/elsc.201200030

Shi, J., and Du, X. (2020). Identification, characterization and expression analysis of calmodulin and calmodulin-like proteins in Solanum pennellii. *Sci. Rep.* 10, 1–17. doi: 10.1038/s41598-020-64178-y

Shi, R., and Panthee, D. R. (2020). Transcriptome-based analysis of tomato genotypes resistant to bacterial spot (Xanthomonas perforans) race t4. *Int. J. Mol. Sci.* 21, 1–31. doi: 10.3390/ijms21114070

Solìs-Oviedo, R. L., and de La Cruz Pech-Canul, Á (2019). *Frontiers and New Trends in the Science of Fermented Food and Beverages*. London: IntechOpen. doi: 10.5772/intechopen.73404

Spelt, C., Quattrocchio, F., Mol, J. N. M., and Koes, R. (2000). anthocyanin1 of Petunia Encodes a Basic Helix-Loop-Helix Protein That Directly Activates Transcription of Structural Anthocyanin Genes. *Plant Cell* 12:1619. doi: 10.2307/3871178

Stracke, R., Werber, M., and Weisshaar, B. (2001). The R2R3-MYB gene family in Arabidopsis thaliana. *Curr. Opin. Plant Biol.* 4, 447–456. doi: 10.1016/S1369-5266(00)00199-0

Su, X., Xu, J., Rhodes, D., Shen, Y., Song, W., Katz, B., et al. (2016). Identification and quantification of anthocyanins in transgenic purple tomato. *Food Chem.* 202, 184–188. doi: 10.1016/j.foodchem.2016.01.128

Sui, X., Sun, H., Qi, B., Zhang, M., Li, Y., and Jiang, L. (2018). Functional and conformational changes to soy proteins accompanying anthocyanins: focus on covalent and non-covalent interactions. *Food Chem.* 245, 871–878. doi: 10.1016/j.foodchem.2017.11.090

Sun, C., Deng, L., Du, M., Zhao, J., Chen, Q., Huang, T., et al. (2019). A Transcriptional Network Promotes Anthocyanin Biosynthesis in Tomato Flesh. *Mol. Plant* 13, 42–58. doi: 10.1016/j.molp.2019.10.010

Sun, X., Shu, J., Mohamed, A. M. A., Deng, X., Zhi, X., Bai, J., et al. (2019). Identification and characterization of EI (elongated internode) gene in tomato (solanum lycopersicum). *Int. J. Mol. Sci.* 20, 1–18. doi: 10.3390/ijms20092204

Sundaresan, S., Philosoph-Hadas, S., Riov, J., Mugasimangalam, R., Kuravadi, N. A., Kochanek, B., et al. (2016). De novo transcriptome sequencing and development of abscission zone-specific microarray as a new molecular tool for analysis of tomato organ abscission. *Front. Plant Sci.* 6:1258. doi: 10.3389/fpls.2015.01258

Takos, A. M., Jaffé, F. W., Jacob, S. R., Bogs, J., Robinson, S. P., and Walker, A. R. (2006). Light-induced expression of a MYB gene regulates anthocyanin biosynthesis in red apples. *Plant Physiol.* 142, 1216–1232. doi: 10.1104/pp.106.088104

Taylor, B. H., and Scheuring, C. F. (1994). A molecular marker for lateral root initiation: the RSI-1 gene of tomato (Lycopersicon esculentum Mill) is activated in early lateral root primordia. *Mol. Gener. Genet.* 243, 148–157. doi: 10.1007/BF00280311

Thamaphat, K., Goodman, B. A., Limsuwan, P., and Smith, S. M. (2015). Rapid screening for anthocyanins in cane sugars using ESR spectroscopy. *Food Chem.* 171, 123–127. doi: 10.1016/j.foodchem.2014.08.126

Thwe, A., Arasu, M. V., Li, X., Park, C. H., Kim, S. J., Al-Dhabi, N. A., et al. (2016). Effect of different Agrobacterium rhizogenes strains on hairy root induction and phenylpropanoid biosynthesis in tartary buckwheat (Fagopyrum tataricum Gaertn). *Front. Microbiol.* 7:318. doi: 10.3389/fmicb.2016.00318

Tian, L., Tan, Y., Chen, G., Wang, G., Sun, J., Ou, S., et al. (2019). Metabolism of anthocyanins and consequent effects on the gut microbiota. *Crit. Rev. Food Sci. Nutr.* 59, 982–991. doi: 10.1080/10408398.2018.1533517

Tohge, T., de Souza, L. P., and Fernie, A. R. (2017). Current understanding of the pathways of flavonoid biosynthesis in model and crop plants. *J. Exp. Bot.* 68, 4013–4028. doi: 10.1093/jxb/erx177

Tohge, T., Scossa, F., Wendenburg, R., Frasse, P., Balbo, I., Watanabe, M., et al. (2020). Exploiting Natural Variation in Tomato to Define Pathway Structure and Metabolic Regulation of Fruit Polyphenolics in the Lycopersicum Complex. *Mol. Plant* 13, 1027–1046. doi: 10.1016/j.molp.2020.04.004

Tominaga-Wada, R., Nukumizu, Y., and Wada, T. (2013). Tomato (Solanum lycopersicum) homologs of TRIPTYCHON (SLTRY) and GLABRA3 (SLGL3) are involved in anthocyanin accumulation. *Plant Signal. Behav.* 8, 8–10. doi: 10.4161/psb.24575

Tuner, H., and Korkmaz, M. (2007). Radiostability of butylated hydroxytoluene (BHT): an ESR study. *Nuclear Instr. Methods Phys. Res. B Beam Interact. Mater. Atoms* 258, 388–394. doi: 10.1016/j.nimb.2007.02.098

Tzin, V., Rogachev, I., Meir, S., Moyal Ben Zvi, M., Masci, T., Vainstein, A., et al. (2015). Altered Levels of Aroma and Volatiles by Metabolic Engineering of Shikimate Pathway Genes in Tomato Fruits. *AIMS Bioeng.* 2, 75–92. doi: 10.3934/bioeng.2015.2.75

van Hoeck, A., Horemans, N., Nauts, R., van Hees, M., Vandenhove, H., and Blust, R. (2017). Lemna minor plants chronically exposed to ionising radiation: rNA-seq analysis indicates a dose rate dependent shift from acclimation to survival strategies. *Plant Sci.* 257, 84–95. doi: 10.1016/j.plantsci.2017.01.010

van Kan, J. A. L., Joosten, M. H. A. J., Wagemakers, C. A. M., van den Berg-Velthuis, G. C. M., and de Wit, P. J. G. M. (1992). Differential accumulation of mRNAs encoding extracellular and intracellular PR proteins in tomato induced by virulent and avirulent races of Cladosporium fulvum. *Plant Mol. Biol.* 20, 513–527. doi: 10.1007/BF00040610

Vandenhove, H., Vanhoudt, N., Cuypers, A., van Hees, M., Wannijn, J., and Horemans, N. (2010). Life-cycle chronic gamma exposure of Arabidopsis thaliana induces growth effects but no discernable effects on oxidative stress pathways. *Plant Physiol. Biochem.* 48, 778–786. doi: 10.1016/j.plaphy.2010.06.006

Vardhan, P. V., and Shukla, L. I. (2017). Gamma irradiation of medicinally important plants and the enhancement of secondary metabolite production. *Int. J. Radiat. Biol.* 93, 967–979. doi: 10.1080/09553002.2017.1344788

Velázquez-Márquez, S., De-La-Cruz, I. M., Tapia-López, R., and Núñez-Farfán, J. (2021). Tropane alkaloids and terpenes synthase genes of Datura stramonium (Solanaceae). *PeerJ.* 9:e11466. doi: 10.7717/peerj.11466

Verweij, W., Spelt, C., Di Sansebastiano, G. P., Vermeer, J., Reale, L., Ferranti, F., et al. (2008). An H+ P-ATPase on the tonoplast determines vacuolar pH and flower colour. *Nat. Cell Biol.* 10, 1456–1462. doi: 10.1038/ncb1805

Verweij, W., Spelt, C. E., Bliek, M., de Vries, M., Wit, N., Faraco, M., et al. (2016). Functionally similar WRKY proteins regulate vacuolar acidification in petunia and hair development in arabidopsis. *Plant Cell* 28, 786–803. doi: 10.1105/tpc.15.00608

Villani, M. E., Massa, S., Lopresto, V., Pinto, R., Salzano, A. M., Scaloni, A., et al. (2017). Effects of high-intensity static magnetic fields on a root-based bioreactor system for space applications. *Life Sci. Space Res.* 15, 79–87. doi: 10.1016/j.lssr.2017.09.002

Vivar-Quintana, A. M., Santos-Buelga, C., and Rivas-Gonzalo, J. C. (2002). Anthocyanin-derived pigments and colour of red wines. *Anal. Chim. Acta* 458, 147–155. doi: 10.1016/S0003-2670(01)01619-1

Wang, T., Zhang, H., and Zhu, H. (2019). CRISPR technology is revolutionizing the improvement of tomato and other fruit crops. *Hortic. Res.* 6:77. doi: 10.1038/s41438-019-0159-x

Wang, T. W., Lu, L., Wang, D., and Thompson, J. E. (2001). Isolation and Characterization of Senescence-induced cDNAs Encoding Deoxyhypusine Synthase and Eucaryotic Translation Initiation Factor 5A from Tomato. *J. Biol. Chem.* 276, 17541–17549. doi: 10.1074/jbc.M008544200

Wen, B., Zhang, F., Wu, X., and Li, H. (2020). Characterization of the Tomato (Solanum lycopersicum) Pectin Methylesterases: evolution, Activity of Isoforms and Expression During Fruit Ripening. *Front. Plant Sci.* 11:238. doi: 10.3389/fpls.2020.00238

Williams, R. J., Spencer, J. P. E., and Rice-Evans, C. (2004). Flavonoids: antioxidants or signalling molecules? *Free Radic. Biol. Med.* 36, 838–849. doi: 10.1016/j.freeradbiomed.2004.01.001

Wolff, S. A., Coelho, L. H., Karoliussen, I., and Jost, A. I. K. (2014). Effects of the extraterrestrial environment on plants: recommendations for future space experiments for the MELiSSA higher plant compartment. *Life* 4, 189–204. doi: 10.3390/life4020189

Yan, L., Zhai, Q., Wei, J., Li, S., Wang, B., Huang, T., et al. (2013). Role of Tomato Lipoxygenase D in Wound-Induced Jasmonate Biosynthesis and Plant Immunity to Insect Herbivores. *PLoS Genet.* 9:e1003964. doi: 10.1371/journal.pgen.1003964

Yan, S., Chen, N., Huang, Z., Li, D., Zhi, J., Yu, B., et al. (2020). Anthocyanin Fruit encodes an R2R3-MYB transcription factor, SlAN2-like, activating the transcription of SlMYBATV to fine-tune anthocyanin content in tomato fruit. *New Phytol.* 225, 2048–2063. .

Yang, H., Xiao, X., Zhao, X., and Wu, Y. (2015). "Intrinsic Fluorescence Spectra of Tryptophan. Tyrosine and Phenyloalanine" in *Proceedings of the 5th International Conference on Advanced Design and Manufacturing Engineering*. (Netherlands: Atlantis Press). 224–233. doi: 10.2991/icadme-15.2015.46

Yang, Y. X., Wang, M. M., Yin, Y. L., Onac, E., Zhou, G. F., Peng, S., et al. (2015). RNA-seq analysis reveals the role of red light in resistance against *Pseudomonas* syringae pv. tomato DC3000 in tomato plants. *BMC Genomics* 16:120. doi: 10.1186/s12864-015-1228-7

Zabel, P., Bamsey, M., Schubert, D., and Tajmar, M. (2016). Review and analysis of over 40 years of space plant growth systems. *Life Sci. Space Res.* 10, 1–16. doi: 10.1016/j.lssr.2016.06.004

Zabel, P., Bamsey, M., Zeidler, C., Vrakking, V., Johannes, B., and Rettberg, P. (2015). "Introducing EDEN ISS - A European project on advancing plant cultivation technologies and operations," in *45th International Conference on Environmental Systems*.

Zhang, H., Koes, R., Shang, H., Fu, Z., Wang, L., Dong, X., et al. (2019). Identification and functional analysis of three new anthocyanin R2R3-MYB genes in Petunia. *Plant Dir* 3, 1–13. doi: 10.1002/pld3.114

Zhang, Y., Butelli, E., Alseekh, S., Tohge, T., Rallapalli, G., Luo, J., et al. (2015). Multi-level engineering facilitates the production of phenylpropanoid compounds in tomato. *Nat. Commun* 6, 1–11. doi: 10.1038/ncomms 9635

Zhang, Y., Butelli, E., de Stefano, R., Schoonbeek, H. J., Magusin, A., Pagliarani, C., et al. (2013). Anthocyanins double the shelf life of tomatoes by delaying overripening and reducing susceptibility to gray mold. *Curr. Biol.* 23, 1094–1100. doi: 10.1016/j.cub.2013.04.072

Zhang, Y., Butelli, E., and Martin, C. (2014). Engineering anthocyanin biosynthesis in plants. *Curr. Opin. Plant Biol.* 19, 81–90. doi: 10.1016/j.pbi.2014.05.011

Zhang, Y., Song, H., Wang, X., Zhou, X., Zhang, K., Chen, X., et al. (2020). The roles of different types of trichomes in tomato resistance to cold, drought, whiteflies, and botrytis. *Agronomy* 10:411. doi: 10.3390/agronomy10030411

Zhao, X., Liu, Y., Liu, X., and Jiang, J. (2018). Comparative transcriptome profiling of two tomato genotypes in response to potassium-deficiency stress. *Int. J. Mol. Sci.* 19:2402. doi: 10.3390/ijms19082402

Zimmermann, I. M., Heim, M. A., Weisshaar, B., and Uhrig, J. F. (2004). Comprehensive identification of Arabidopsis thaliana MYB transcription factors interacting with R/B-like BHLH proteins. *Plant J.* 40, 22–34. doi: 10.1111/j.1365-313X.2004.02183.x

Zouari, I., Salvioli, A., Chialva, M., Novero, M., Miozzi, L., Tenore, G. C., et al. (2014). From root to fruit: rNA-Seq analysis shows that arbuscular mycorrhizal symbiosis may affect tomato fruit metabolism. *BMC Genomics* 15:221. doi: 10.1186/1471-2164-15-221

Conflict of Interest: The authors declare that the research was conducted in the absence of any commercial or financial relationships that could be construed as a potential conflict of interest.

Publisher's Note: All claims expressed in this article are solely those of the authors and do not necessarily represent those of their affiliated organizations, or those of the publisher, the editors and the reviewers. Any product that may be evaluated in this article, or claim that may be made by its manufacturer, is not guaranteed or endorsed by the publisher.

frontiers | Frontiers in Plant Science

ORIGINAL RESEARCH
published: 25 April 2022
doi: 10.3389/fpls.2022.878677

The B1 Domain of Streptococcal Protein G Serves as a Multi-Functional Tag for Recombinant Protein Production in Plants

*Shi-Jian Song†, Hai-Ping Diao†, Byeongho Moon, Areum Yun and Inhwan Hwang**

Department of Life Science, Pohang University of Science and Technology, Pohang, South Korea

Plants have long been considered a cost-effective platform for recombinant production. A recently recognized additional advantage includes the low risk of contamination of human pathogens, such as viruses and bacterial endotoxins. Indeed, a great advance has been made in developing plants as a "factory" to produce recombinant proteins to use for biopharmaceutical purposes. However, there is still a need to develop new tools for recombinant protein production in plants. In this study, we provide data showing that the B1 domain of Streptococcal protein G (GB1) can be a multi-functional domain of recombinant proteins in plants. N-terminal fusion of the GB1 domain increased the expression level of various target proteins ranging from 1.3- to 3.1-fold at the protein level depending on the target proteins. GB1 fusion led to the stabilization of the fusion proteins. Furthermore, the direct detection of GB1-fusion proteins by the secondary anti-IgG antibody eliminated the use of the primary antibody for western blot analysis. Based on these data, we propose that the small GB1 domain can be used as a versatile tag for recombinant protein production in plants.

Keywords: plant-based molecular pharming, *Nicotiana benthamiana*, biopharmaceutical proteins, GB1, protein folding

OPEN ACCESS

Edited by:
Domenico De Martinis, Italian National Agency for New Technologies, Energy and Sustainable Economic Development (ENEA), Italy

Reviewed by:
Johan Nilvebrant, Royal Institute of Technology, Sweden
Johannes Felix Buyel, Fraunhofer Society (FHG), Germany

***Correspondence:**
Inhwan Hwang
ihhwang@postech.ac.kr

†These authors have contributed equally to this work

Specialty section:
This article was submitted to Plant Biotechnology, a section of the journal Frontiers in Plant Science

Received: *18 February 2022*
Accepted: *21 March 2022*
Published: *25 April 2022*

Citation:
Song S-J, Diao H-P, Moon B, Yun A and Hwang I (2022) The B1 Domain of Streptococcal Protein G Serves as a Multi-Functional Tag for Recombinant Protein Production in Plants. Front. Plant Sci. 13:878677. doi: 10.3389/fpls.2022.878677

INTRODUCTION

Advances in life science have led to the production of recombinant proteins that can be used for various purposes. The first recombinant protein, insulin, was produced for use in humans as a protein drug (Dingermann, 2008). Now, a large number of recombinant proteins, such as antibodies and vaccines, and enzymes are being used as pharmaceuticals (Soler and Houdebine, 2007; Oliveira et al., 2011; Frenzel et al., 2013). Moreover, the area to which these recombinant proteins can be used continues to expand. Thus, the demand to produce more diverse recombinant proteins is increasing. Recombinant proteins can be produced in all kinds of living organisms. Animal cells are largely used for therapeutic proteins (Wurm, 2004; Grillberger et al., 2009). Bacteria and fungi are also convenient systems for recombinant protein production (Specht et al., 2010; Chen, 2012; García-Fruitós, 2012). As a recombinant protein production platform, plants are a more recently developed system (Sainsbury, 2020). These systems have specific advantages and disadvantages.

Compared to animal and bacterial systems, the plant system was introduced most recently (Buyel, 2019; Chung et al., 2021; Schillberg and Finnern, 2021). Thus, the plant system is still in need of improvement in various aspects. In developing plants as a recombinant production platform, the main focus has been to increase the protein production level (Schillberg et al., 2019). Various approaches have been used to increase the expression levels of recombinant proteins. In animal cells, the most powerful approach to increase the expression level is to use drug-induced gene amplification (Hunter et al., 2019). However, the same approach has not been developed in plants. Instead, a similar effect was obtained by using RNA or DNA virus-based vectors that rely on amplification of the target at the level of mRNA or DNA, respectively (Mardanova et al., 2017; Abrahamian et al., 2020). Another powerful approach has been to use the integration of the target gene into plastid chromosomes, leading to a great increase in the level of recombinant proteins in transgenic plants (Adem et al., 2017; Dyo and Purton, 2018). For instance, human somatotropin (hST) recombinant proteins accumulated to the level of more than 7% total soluble protein through the transplastomic transformation approach, which was more than 300-fold higher than the nuclear transgenic approach with a similar gene (Staub et al., 2000). In addition, there have been various approaches to increasing efficiency at the translational level. One approach to increase the expression level in plants was to insert a small domain with multiple *N*-glycosylation sites (Kang et al., 2018). Additionally, various 5' untranslated sequences were shown to increase the expression level (Kim et al., 2014).

In general, these approaches were successful in increasing protein production levels in plants. However, despite these advances, there is still a big challenge in recombinant protein production, namely the great degree of variation in yield depending on the type of target protein (Hammarström et al., 2006). This is a problem not only in the plant platform but also in other platforms as well (Mancia et al., 2004; Thoring et al., 2017). The causes underlying the variation in protein yield are not fully understood. Yield variation may be due to the intrinsic properties of target genes or target proteins caused at many different levels or by many different mechanisms depending on individual target genes or proteins. One simple approach to address this problem is to optimize codon usage according to the platform. Indeed, the optimization of heterologous genes to the expression host greatly improves the expression level. Another problem may be caused by the folding of the target proteins. The coexpression of chaperons leads to an increase in the protein level (Hammond et al., 1994; Hebert et al., 1995). Furthermore, CRT (calreticulin) of humans leads to an increase in the expression of HIV envelope glycoproteins in plants (Margolin et al., 2020). The stability of recombinant proteins in a foreign environment can cause limitations in the increase in production levels. The fusion of soluble tags to recombinant proteins is a promising strategy that has been used in the production of bioactive proteins (Esposito and Chatterjee, 2006; Hung et al., 2014). The fusion of foreign domains can lead to an increase in production yield. This was thought to have resulted from enhanced folding or stability. These include GST, MBP, SUMO, and GB1 domains, which have been shown to increase protein solubility. In *Escherichia coli*, the GB1 domain of Streptococcal protein G, an antibody binding protein, leads to an increase in the expression level when it is fused to a target protein. GB1, consisting of 56 aa residues, can be divided into two motifs, N- and C-terminal motifs containing 40 and 16 aa residues, respectively. The GB1 domain forms a compact fold that enhances solubility. The increase in the expression level of GB1 fusion proteins was thought to occur *via* the enhancement of protein folding.

In this study, we explored the possibility of using the GB1 domain to enhance protein production in plants. Here, we provide evidence that the fusion of GB1 to the *N*-terminus of various proteins leads to an increase in the production level by enhancing transcription, translation, and stability. Moreover, we showed that the GB1 domain can also serve as an epitope tag that can be detected by western blot analysis using only the secondary anti-IgG antibody.

RESULTS

The N-Terminal Fusion of GB1 to GFP Significantly Improves the Expression of GFP in *Nicotiana benthamiana*

To examine whether the GB1 domain has any beneficial effect on the production of recombinant proteins in plants, we fused it to the N-terminus of a target protein, green fluorescent protein (GFP), as a model protein, thereby yielding *GB1-GFP*. GFP has been widely used as a model protein (Leuzinger et al., 2013; Yamamoto et al., 2018). In plants, the ER and chloroplasts are the two main places for storing recombinant proteins. Thus, the leader sequence of BiP or the transit peptide of RbcS was fused to the N-terminus of GB1-GFP to yield *BiP-GB1-GFP* or *RbcS(tp)-GB1-GFP*, respectively. In addition, we generated two constructs, BiP-GFP and RbcS(tp)-GFP, as controls (**Figures 1A,B**). These recombinant constructs, together with the cytosolic localized reporter construct *GB1-GFP* and *GFP* alone (**Figure 1C**), were expressed in *Nicotiana benthamiana via Agrobacterium*-mediated infiltration. The expression of GFP was examined at various time points after infiltration. First, the expression level was examined using the signal intensity of green fluorescence. The signal was captured by LAS3000 under 488 nm excitation. The GB1-fused GFP showed a significantly higher fluorescence signal than GFP without GB1 at 3 days post-infiltration (DPI), regardless of the three subcellular localizations, the ER, chloroplasts, and cytosol (**Figures 1D–F**). In addition, at five and seven DPI, the GB1-fused GFP gave a higher signal intensity than GFP alone (**Supplementary Figures 1A,C,E**). These results indicate that the N-terminal fusion of the GB1 domain leads to a higher expression of the fusion protein. To quantify the GB1-mediated increase in the expression level, we calculated the ratio of fluorescence signals between GB1-GFP and GFP at three time points. The ratios for the ER-, chloroplast-, and cytosol-localized proteins were 2.5, 2.5, and 1.7, respectively (**Supplementary Figures 1A,C,E**), confirming that GB1 fusion leads to dramatic increases in the expression level.

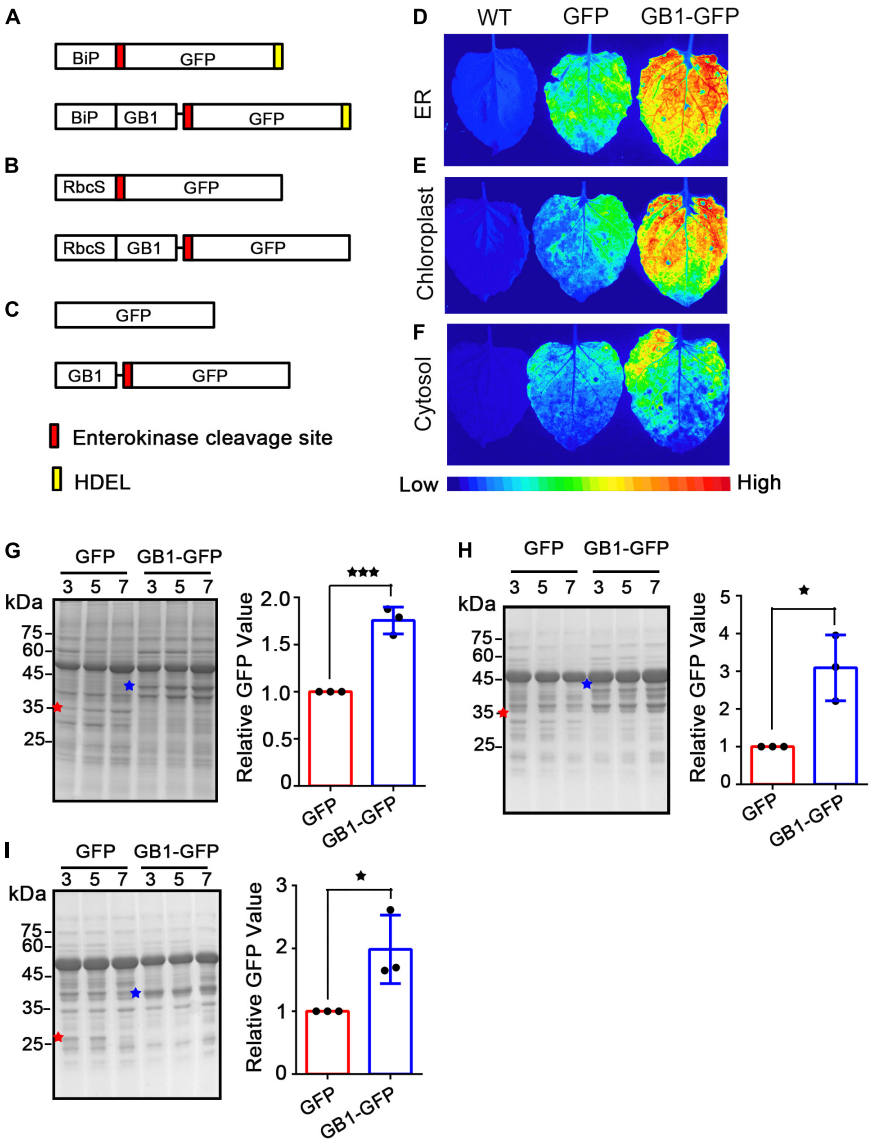

FIGURE 1 | GB1 dramatically increases the expression level of GFP in the leaves of *Nicotiana benthamiana*. **(A–C)** Schematic representation of constructs. *BiP-EK-GFP-HDEL* and *BiP-GB1- EK-GFP-HDEL* **(A)**, *RbcS*$_{tp}$*-EK-GFP-HDEL* and *RbcS*$_{tp}$*-GB1-EK-GFP-HDEL* **(B)**, and *GFP-HDEL* and *GB1-EK-GFP-HDEL* **(C)**. BiP, the leader sequence of BiP; RbcS$_{tp}$, transit peptide of the rubisco complex small subunit. **(D–F)** Images of GFP fluorescence. GFP fluorescent signals of the constructs targeted to ER **(D)**, chloroplasts **(E)**, and cytosol **(F)** were measured from infiltrated leaves at 3 days post infiltration (dpi). **(G–I)** Coomassie brilliant blue (CBB)-stained GFP bands. Total protein extracts from infiltrated *N. benthamiana* leaves at 3, 5, and 7 dpi were separated by SDS-PAGE and stained with Coomassie brilliant blue. ER **(G)**, chloroplast **(H)**, and cytosol **(I)**-localized GFP (red asterisks) and GB1-GFP (blue asterisks). Band intensity was quantified and represented as a relative value to the GFP alone. Three independent experiments were carried out to quantify the signal intensity. Results in panels **(G,I)** are the mean ± SD (n = 3). Asterisks indicate a significant difference (Student's t-test; one asterisk and three asterisks indicate $P < 0.05$ and $P < 0.001$, respectively).

To corroborate this finding, we analyzed the expression levels by western blot analysis using an anti-GFP antibody. Again, the expression level of GB1-GFP was significantly higher than GFP alone in all three locations, the ER, chloroplast, and cytosol (**Supplementary Figures 1B,D,F**). However, the GB1 domain is derived from protein G, the antibody-binding protein. The GB1 domain alone has the ability to bind to the Fc domain of IgG, indicating that the GB1 domain can be detected by the secondary antibody during western blot analysis. Thus, western blot analysis cannot be used for the quantification of proteins. Hence, instead of western blot analysis employing antibodies, we separated the total protein extracts from *N. benthamiana* by SDS-PAGE and stained them with Coomassie brilliant blue (CBB). We were able to detect GFP and GB1-GFP by CBB staining. Furthermore, the levels of GB1-GFP were increased by 1. 7-, 3. 1-, and 2.0-fold compared to the GFP alone in the ER, chloroplasts, and cytosol, respectively (**Figures 1G–I**), confirming that the GB1 domain leads to an increase in the expression level of fusion proteins.

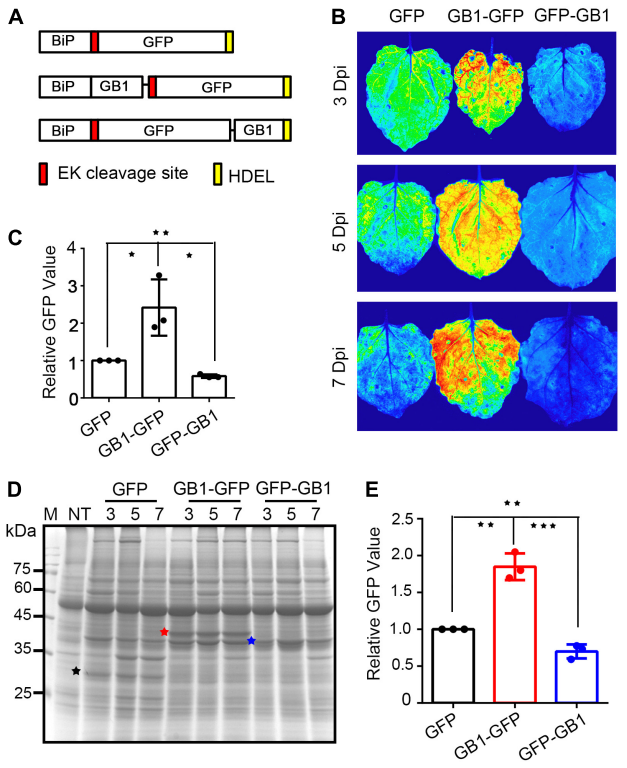

FIGURE 2 | C-terminal fusion of GB1 does not enhance the expression level of GFP in the ER of *Nicotiana benthamiana*. **(A)** Schematic representation of constructs. *BiP-EK-GFP-HDEL* (top), *BiP-GB1-EK-GFP-HDEL* (middle), and *BiP-EK-GFP-GB1-HDEL* (bottom). **(B)** Images of GFP fluorescence. The indicated constructs were expressed in leaf tissues of *N. benthamiana via* agroinfiltration, and images were taken at 3, 5, and 7 DPI. GFP (top), GB1-GFP (middle), and GFP-GB1 (bottom). **(C)** Quantification of GFP fluorescent signals. Signal intensity was quantified using three DPI samples. Three independent experiments were carried out. **(D)** GFP level by CBB staining. Total protein extracts from leaves harvested at 3, 5, and 7 DPI were separated by SDS-PAGE and stained with CBB. GFP band intensity was quantified from the CBB-stained gel after SDS-PAGE. **(E)** Quantification of GFP levels. The GFP bands in Figure **(D)** were quantified and represented as relative values.Results for panels **(C,E)** are the mean ± SD (n = 3). Asterisks indicate a significant difference (Student's t-test; one, two, and three asterisks indicate $P < 0.05$, $0.001 < P < 0.05$, and $P < 0.001$, respectively).

Next, we asked whether the location of the GB1 domain had any effect on the expression of fusion proteins. The GB1 domain was fused to the C-terminus of BiP-GFP to yield BiP-GFP-GB1. Three constructs, BiP-GFP, BiP-GB1-GFP, and BiP-GFP-GB1, were introduced into the leaf tissues of *N. benthamiana via Agrobacterium*-mediated infiltration. The expression levels of GFP were examined by fluorescence imaging. In contrast to the N-terminally fused construct BiP-GB1-GFP, the C-terminally fused construct BiP-GFP-GB1 did not show any increase in expression level (**Figure 2**). In fact, the signal intensity of BiP-GFP-GB1 was even lower than that of BiP-GFP. Together, these results indicate that the location of the GB1 domain in the fusion protein is critical for the effect on the protein expression level.

N-Terminal GB1 Enhances the Expression of Recombinant Biopharmaceutical Proteins in *Nicotiana benthamiana*

The effect of the GB1 domain on the expression level of GFP prompted us to examine its effect on various target proteins. GFP is well-known to have good solubility and expression in plants. To further test the functionality of the GB1 domain in increasing the expression levels of recombinant proteins, we selected two proteins, human interleukin 6 (hIL-6) (Islam et al., 2019) and hemagglutinin (HA) of H9N2 (Song et al., 2021). The recombinant constructs, BiP-MP-CBM3-SUMO-hIL6-HDEL (hIL6 in short) and BiP-HA^{H9N2}-mCor1-LysM-His-HDEL (HA^{H9N2} in short) were tested in *N. benthamiana*, and they showed good expression. To test the effect of the GB1 domain on the expression of hIL6 and HA^{H9N2}, the GB1 domain was fused to the BiP leader sequence to yield BiP-GB1-MP-CBM3-SUMO-hIL6-HDEL (GB1-hIL6 in short) and BiP-GB1-HA^{H9N2}-mCor1-LysM-His-HDEL (GB1-HA^{H9N2} in short), respectively. These constructs, with or without the GB1 domain, were transiently expressed in leaf tissues of *N. benthamiana via Agrobacterium*-mediated infiltration. First, the expression of these constructs was examined by western blot analysis using anti-CBM3 and anti-His antibodies for the GB1-hIL6 and GB1-HA^{H9N2} recombinant proteins, respectively. Both hIL6 and HA^{H9N2} recombinant proteins with and without the GB1 domain were expressed in *N. benthamiana* (**Supplementary Figures 2A,B**). Those with the GB1 domain showed a much stronger signal intensity. However, the signal intensity of western blot can be biased toward those with the GB1 domain. Thus, to quantify the expression level, we purified both GB1-hIL6 and hIL6 from 0.1 g of infiltrated tissues of each using microcrystalline cellulose (MCC) beads *via* the MCC-binding affinity of the CBM3 domain of the recombinant proteins. The proteins bound to the MCC beads were released by boiling in SDS buffer and separated by SDS-PAGE (**Figure 3A**). The gels were stained with CBB, and the signal intensity of bands was quantified. The level of GB1-hIL6 was higher by 28% compared to that of hIL6 (**Figure 3D**). Next, we purified HA^{H9N2} and GB1-HA^{H9N2} from infiltrated tissues of each by using Ni^{2+}-NTA beads, followed by SDS-PAGE analysis (**Figure 3B**). The level of GB1-HA^{H9N2} was higher by 48% compared to that of HA^{H9N2} (**Figure 3E**). Both two recombinant proteins have been quantified in the previous studies. The yield of purified hIL6 was approximately 18.5 μg/g FW leaf tissues at near homogeneity (Islam et al., 2019), and the expression level of trimeric HA^{H9N2} was 150 μg/g FW leaf tissues (Song et al., 2021). We estimated that the expression level of GB1-hIL6 and GB1-HA^{H9N2} is approximately 23.7 μg/g FW and 222 μg/g fresh weight, respectively, according to the relative ratio with hIL6 and HA^{H9N2}.

To further expand our findings, we tested the effect of the GB1 domain on the expression of the cholera toxin B subunit (CTB), a natural homopentamer protein, without any other translational enhancing domains. When CTB as recombinant construct *BiP-CTB-His-HDEL* (CTB in short) was expressed in *N. benthamiana*,

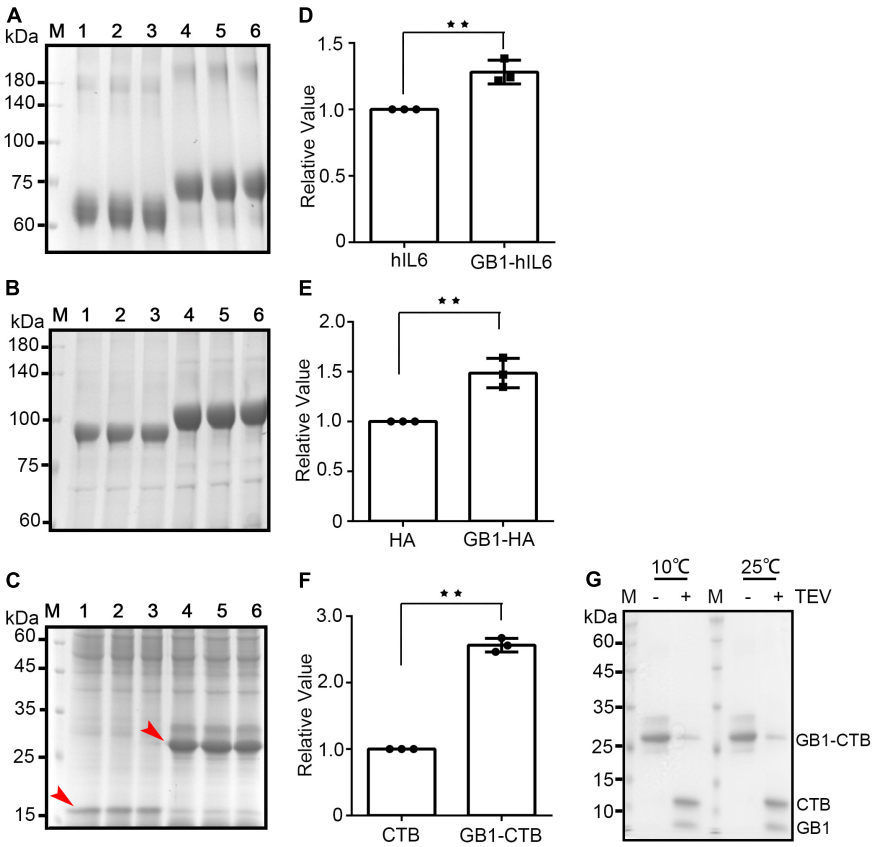

FIGURE 3 | GB1 enhances the expression of various target proteins in *Nicotiana benthamiana*. **(A–C)** SDS-PAGE analysis of target protein levels. The indicated target proteins were transiently expressed in *Nicotiana benthamiana*. These proteins from 0.1 g infiltrated tissues for each sample were purified using Ni^{2+}-NTA affinity column chromatography and separated by SDS-PAGE. The gels were stained with CBB. **(A)** Lanes 1–3, purified hIL6; lanes 4–6, GB1-hIL6. **(B)** Lanes 1–3, purified HA; lanes 4–6, GB1-HA. **(C)** Lanes 1–3, purified CTB; lanes 4–6, GB1-CTB. Red arrows indicate the target proteins. **(D–F)** Quantification of signal intensity. The signal intensity of target protein bands in Figures **(A–C)** was quantified and represented in panels **(D–F)**, respectively, as relative values. Results in panels **(D–F)** are the mean ± SD ($n = 3$). Asterisks indicate a significant difference (Student's *t*-test; two asterisks indicate $0.001 < P < 0.05$). **(G)** SDS-PAGE (15%) analysis of GB1-CTB cleaved by TEV protease at 10 and 25°C overnight.

it was expressed at low levels. The GB1 domain was fused next to BiP to yield BiP-GB1-CTB-His-HDEL (GB1-CTB in short) (**Supplementary Figure 2C**). These two constructs, *CTB* and *GB1-CTB*, were transiently expressed in *N. benthamiana via Agrobacterium*-mediated infiltration. First, their expression was examined by western blot using an anti-His antibody, confirming their expression (**Supplementary Figure 2F**). Next, to quantify the expression levels of these two recombinant proteins, both CTB and GB1-CTB were purified from 0.1 g infiltrated tissues using Ni^{2+}-NTA affinity column chromatography. The purified proteins were separated by SDS-PAGE, and the gel was stained with CBB (**Figure 3C**). The GB1 domain led to an increase of CTB recombinant protein level by 2.6-fold (**Figure 3F**). The GB1-mediated increase in expression was higher with CTB than with other target proteins. Together, these results showed that the N-terminal GB1 broadly enhanced the expression of recombinant proteins in plants. GB1 is a domain that increased the expression level of recombinant proteins in plants and also can be used as an epitope tag for detection during western blot analysis. However, in a certain case, it is desirable to remove the GB1 tag. We tested the possibility of removal of the GB1 domain from GB1-containing fusion proteins, GB1-CTB that had a tobacco etch virus (TEV) potease cleavage site in between GB1-CTB. GB1-CTB was purified using Ni^{2+}-NTA affinity column chromatography and treated with TEV protease at 10 or 25°C overnight. Most of GB1-CTB recombinant protein was successfully cleaved by TEV at both conditions (**Figure 3G**). CTB released from GB1-CTB by TEV was slightly smaller in size than BiP-CTB-His, likely due to BiP leader sequence.

The GB1 Domain Enhances Both Transcriptional and Translational Efficiency

The previous study suggested that GB1 is a soluble-promoting tag that can enhance the solubility of target protein for better folding and, in turn, enhance the final yield in an *E. coli* expression system (Zheng et al., 2016). To understand the mechanism by which the GB1 domain led to high expression of fusion proteins in *N. benthamiana*, we first examined the effect of GB1

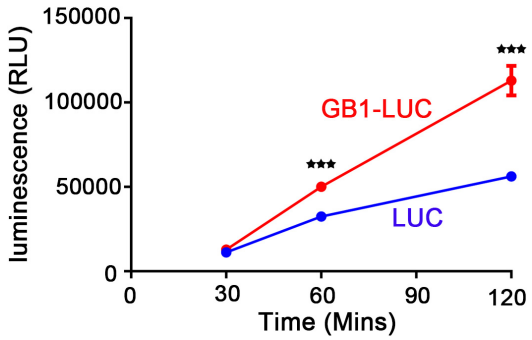

FIGURE 4 | GB1 fusion leads to an enhanced translation rate *in vitro*. LUC and GB1-LUC were transcribed and translated *in vitro* in wheat germ extracts. During the reaction, 5 μl were taken from the 50 μl reaction volume at 30, 60, and 120 min and diluted 24-fold. The RLUC activity was measured using the Renilla Luciferase Assay System. Three independent translation reactions were carried out. The error bar is the mean ± SD (n = 3). Asterisks indicate a significant difference (Student's t-test; three asterisks, $P < 0.001$).

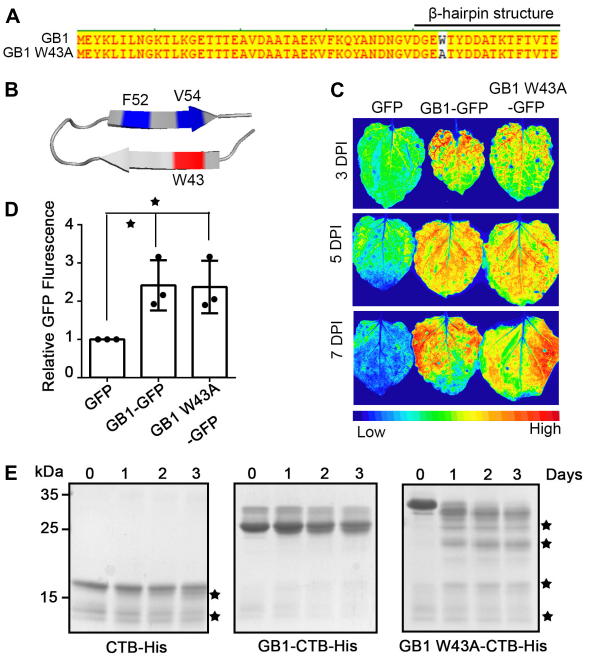

FIGURE 5 | The β-hairpin structure of GB1 is critical for the thermal stability of CTB but has no contribution to the increase in protein expression. **(A)** Protein sequences of GB1 and GB1[W43A]. **(B)** The β-hairpin structure of GB1. **(C)** Images of GFP fluorescence. The indicated constructs were expressed in *Nicotiana benthamiana* leaves, and images were taken at three DPI. **(D)** Quantification of GFP signals. GFP signals in Figure **(C)** were quantified and represented as relative values. The error bar is the mean ± SD (n = 3). Single Asterisks indicate a significant difference (Student's t-test, $P < 0.05$). **(E)** Thermal stability of GB1 and GB1[W43A]-fused CTB. The indicated constructs were expressed in *N. benthamiana via Agrobacterium*-mediated infiltration. Proteins were purified using Ni^{2+}-NTA affinity column chromatography. Purified proteins (2 μg) were incubated at 60°C for 1, 2, and 3 days and separated by SDS-PAGE. The gel was stained with CBB. Black asterisks indicate protein breakdown products.

on translational efficiency. We generated LUC and GB1-LUC constructs, and the translation rate was examined in wheat germ extracts *in vitro* by measuring the bioluminescence. The signal intensity of luminescence was almost the same at the 30 min time point. However, luminescence signals of GB1-LUC were increased by 1.6- and 2.0-fold to that of LUC alone at 60 and 120 min time points, respectively (**Figure 4**), indicating that GB1 enhances translation of the fusion protein.

Next, we examined whether the GB1 domain had any effect on transcriptional efficiency. We performed qRT-PCR analysis of the target genes. GFP and GB1-GFP were transiently expressed in *N. benthamiana* leaves *via Agrobacterium*-mediated infiltration. Total RNA was used for qRT-PCR analysis. The transcript level of GB1-GFP was increased by 1.7-fold compared to that of GFP alone (**Supplementary Figure 3A**). To corroborate this finding, we tested the effect of GB1 on another target, CTB. The transcript levels of GB1-CTB and CTB were examined by qRT-PCR (**Supplementary Figure 3B**). Again, the transcript level of GB1-CTB was higher than that of CTB, although the increment was smaller compared to that of GFP. These results suggest that GB1 can also increase the transcription efficiency of fusion genes.

The Hydrophobic Cluster of GB1 Enhances the Thermal Stability of Recombinant Cholera Toxin B Subunit but Does Not Affect the High Expression

Recombinant proteins that have been used as biopharmaceuticals are generally thermal stable (Huus et al., 2005; Wakankar et al., 2010; Mulinacci et al., 2011). However, certain recombinant proteins that are under development as protein drugs have a problem of poor stability (Willuda et al., 1999; Arndt et al., 2003). The 16-residue hairpin of GB1 exhibits many basic features involved in protein folding, including stabilization by both hydrogen bonding and hydrophobic interactions (Muñoz et al., 1997). In GB1, W43 interacts with F52 and V54, forming a hydrophobic cluster that has been proven to play a key role in the stabilization of the GB1 structure, which, in turn, contributes to stabilizing the GB1 fusion protein (**Figure 5B**; Muñoz et al., 1997). We examined whether the stabilization effect of the GB1 β-hairpin on GB1 fusion proteins contributes to the high expression of the GB1 fusion protein. We introduced the W43A (**Figure 5A**) point mutation to GB1 to abolish the hydrophobic bond of GB1. GB1[W43A] was fused to GFP to give GB1[W43A]-GFP, and the resulting construct together with *GB1-GFP* was transiently expressed in *N. benthamiana*. The expression level was examined by GFP fluorescence in the leaves. The expression levels of GB1-GFP and GB1[W43A]-GFP were similar to each other (**Figures 5C,D**), indicating that the W43A mutation does not affect the enhancement of protein expression. Next, we examined that whether the β-hairpin structure can enhance the stability of GB1-fused recombinant proteins. Here, we fused GB1[W43A] to cholera toxin B subunit (CTB) and tested its effect on thermal stability. GB1-CTB and GB1[W43A]-CTB were purified using Ni^{2+}-NTA affinity column chromatography and incubated at 60°C for 3 days. Proteins were

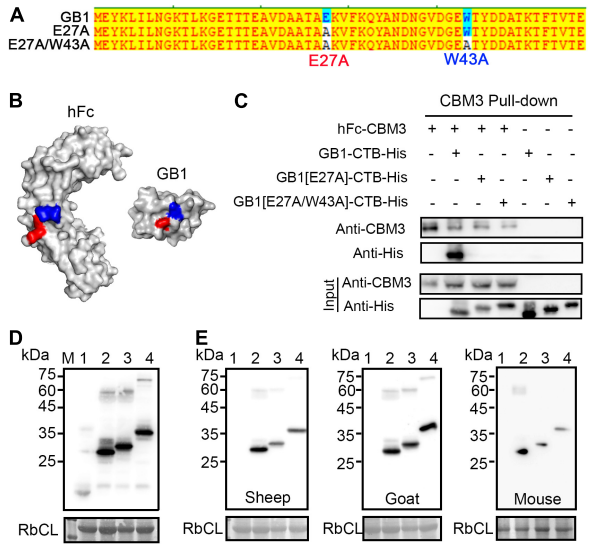

FIGURE 6 | GB1 is directly detected by IgG from various animals. **(A)** Protein sequences of GB1, GB1[E27A], and GB1[E27A/W43A]. Asterisks indicate mutations. **(B)** The 3-D structures of human Fc and GB1. These structures were obtained from the public database. Human Fc, PBD: 1aj7; GB1, PBD: 2gi9. The red color at the GB1 structure indicates E27, which functions as a knob for the hole of Fc (H433 and N434, red); the blue color at the GB1 structure indicates W43, which functions as a hole for the knob of Fc (I253 and S254, blue). **(C)** Strong binding of hFc to GB1 but not GB1 mutants. The indicated constructs were expressed in *Nicotiana benthamiana*, and total protein extracts were subjected to MCC beads-based protein pull-down. The proteins bound to the MCC beads were analyzed by western blotting using anti-CBM3 and anti-His antibodies. **(D)** Western blot analysis. Total protein extracts from *N. benthamiana* expressing the indicated constructs were analyzed by western blotting using the anti-His antibody. RbcL stained with CBB was used as a loading control. **(E)** Binding of various IgGs to GB1. Protein extracts used in Figure **(D)** were separated by SDS-PAGE and analyzed by western blotting using sheep anti-Mouse IgG (Sheep), goat anti-Human IgG (Goat), and mouse anti-Goat IgG (Mouse) without primary anti-His antibody. CTB, lane 1; GB1-CTB, lane 2; GB1[E27A]-CTB, lane 3; GB1[W43A]-CTB, lane 4. All constructs contain a His-tag at the C-terminus but are omitted to simplify the description.

analyzed by SDS-PAGE. CTB alone showed a gradual increase in protein degradation over time, whereas GB1-CTB was intact even during the 3 days of incubation. In contrast, GB1[W43A]-CTB showed clear degradation even 1 day after incubation (**Figure 5E**), indicating that W43 plays a role in the stability of the GB1 fusion protein. These results strongly suggest that the hydrophobic cluster of GB1 confers the thermal stability to the GB1-fused recombinant CTB but does not affect the high expression. However, it is not clear whether the thermal stability conferred by GB1 is specific to CTB or is a general phenomenon to other proteins.

GB1 Can Be Detected by Various Secondary Antibodies Due to Its Affinity for the Fc Domain

Protein G shows the binding affinity to various types of IgG derived from most of the organisms with different binding strengths (Björck and Kronvall, 1984) by its affinity for the Fc, Fab, scFv, and Dab domains (Akerström and Björck, 1986; Choe et al., 2016). Thus, it is possible that the GB1 domain can also bind to IgG from various animals. Indeed, the GB1 binding site on the Fc fragment of human IgG has been dissected in a previous study (**Figure 6B**; Sloan and Hellinga, 1999). Thus, we first examined the interaction between GB1 and Fc by protein pull-down experiments. We generated a fusion construct, hFc-CBM3, and used it for the pull-down experiments. *hFc-CBD* was co-expressed with *GB1-CTB-His*, *GB1[E27A]-CTB-His*, or *GB1[E27A/W43A]-CTB-His* (**Figure 6A**) in *N. benthamiana via Agrobacterium*-mediated infiltration. Total protein extracts were prepared and used for protein pull-down experiments with microcrystalline cellulose (MCC) beads. The proteins bound to MCC beads were analyzed by western blotting using both anti-CBM3 and anti-His antibodies. GB1-CTB-His, but not GB1[E27A]-CTB-His and GB1[E27A/W43A]-CTB-His, was detected in the MCC beads-bound proteins by the anti-His antibody (**Figure 6C**). However, after long-term exposure, GB1[W43A]-CTB-His was also detected (**Supplementary Figure 5**). The results suggest that both mutations E27A and W43A affect the binding to hFc, and the E27A was more detrimental to the binding affinity than the W43A mutation.

The interaction between GB1 and hFc raises the possibility that GB1 can be used as a liner epitope that could be directly detected by associated paratopes of secondary antibodies in western blot analysis. To test this idea, we performed western blot analysis of CTB, GB1-CTB, GB1[E27A]-CTB, and GB1[W43A]-CTB. These recombinant proteins were tagged with the small epitope His (His6). Thus, these proteins were analyzed by western blotting using anti-His antibody (1,000×), followed by anti-mouse IgG as a secondary antibody, or secondary IgG alone from various sources, namely mouse, goat, and sheep without the anti-His antibody, as the primary antibody. As in the case of inclusion of the anti-His antibody as the primary antibody, when we used various secondary IgGs alone, they all detected these GB1 fusion proteins (**Figures 6D,E**). Wild-type GB1 showed a stronger signal, indicating that the mutations affected the binding affinity to IgG. Both GB1[E27A]-CTB and GB1[W43A]-CTB showed an increased size in SDS-PAGE compared to GB1-CTB. A similar effect was observed when they were fused to GFP, indicating that slower migration is caused by the structural changes caused by the mutations (**Supplementary Figure 4**). These results confirm that the GB1 domain can be used for western blot analysis as an epitope tag that can be detected using only the secondary IgG of various animals.

DISCUSSION

In this study, we provide evidence that the fusion of a small domain GB1 leads to significant enhancement of protein yield in plants and gains high stability to the recombinant proteins. The fusion of tags to increase the solubility of aggregation-prone proteins has been widely used in the production of recombinant proteins in *E. coli* (Bao et al., 2006; Peti and Page, 2007; Sugase et al., 2008). One of them is the B1 domain of streptococcal

protein G (56 aa), which forms a compact fold with high solubility, which can contribute to enhanced solubility to the GB1 fused target protein in *E. coli* (Bauer et al., 2009; Hung et al., 2014). GB1 contains two separable domains: N-terminal (1–40 aa) and C-terminal (41–56 aa) domains. The C-terminal domain tends to form a β-hairpin structure that makes it one of the smallest known peptides to fold into a defined structure (Muñoz et al., 1997; Du et al., 2004). The β-hairpin structure has been studied and contributes to much of the basic physics of protein folding, including stabilization by hydrogen bonding and hydrophobic interactions.

In this study, we explored the possibility of the GB1 domain as a tag for the purpose of increasing the protein production yield in plants. We reasoned that the mechanism by which GB1 leads to the high-level production of GB1 fusion proteins recombinant proteins is likely attributed to better folding *via* its solubility-enhancing activity. Various GB1 fusion constructs, when expressed in *N. benthamiana*, showed an increase in the level of GB1-fused target proteins with a certain degree of variation compared to untagged versions. This result suggests that the GB1 domain can be used in many different proteins for high-level production in plants. However, the effect of GB1 on the increase in the protein level was strictly dependent on its N-terminal localization. The reason for localization dependency is not clearly understood. One possible explanation is that the N-terminal localized GB1 can contribute to the folding of newly translated proteins. In contrast, *C*-terminal tagged GB1 may not have much chance of contributing to the fold. Indeed, this finding is consistent with the notion of the effect of GB1 on fusion proteins in *E. coli* (Bao et al., 2006; Peti and Page, 2007; Sugase et al., 2008). In addition, the effect of the GB1 domain on an increase in the expression level did not show any dependency in the subcellular localization of proteins, indicating that the GB1 domain can be used in many different types of proteins without any restriction on the localization.

We examined the mechanism by which GB1 enhances protein production levels in plants. As mentioned above, it is possible that GB1-mediated folding enhancement is the mechanism underlying high-level protein production in plants as well. However, unexpectedly, the GB1 domain also contributed to the increase in the transcript levels of GB1-fused target genes. Currently, this is not fully understood, since it is part of the coding region but not the promoter or terminator of fusion genes. However, often the nucleotide sequence of the coding region also contributes to the level of transcripts by affecting the transcription efficiency or stability of mRNA. Currently, we have not further addressed these points in this study. Thus, the mechanism underlying the GB1-mediated increase in the level of mRNA is still not fully understood. Another mechanism we examined was translation efficiency *in vitro*. Indeed, GB1-fused LUC was translated at a much higher level compared to LUC alone *in vitro*. Again, this can be attributed to the enhanced folding of GB1-fused LUC compared to LUC alone. However, we cannot rule out the possibility of a higher translation rate of *GB1-LUC* mRNA than of *LUC* mRNA. Together, these results suggest that GB1 positively contributes to the expression of GB1-fused genes at both the transcriptional and translational levels.

Protein G is widely used as a purification resin of antibodies, owing to its ability to bind to the Fc and Fab regions. We found that the GB1 domain alone could bind to hFc. We explored the possibility of using the GB1 domain as an epitope tag for western blot analysis. Many small epitopes, such as His, FLAG, and HA, have been used as epitope tags for western blot analysis. However, these tags require the use of a primary antibody that can specifically detect tags. Subsequently, the primary antibody was detected by the secondary anti-IgG antibody fused to horseradish peroxidase. Most of these primary antibodies are expensive. Additionally, using both primary and secondary antibodies requires a fairly long period of experimental time. GB1-fused CTB was successfully detected by anti-IgG antibodies from various animals without using any primary antibodies. Even though GB1 can be used as a multi-functional tag in the study of molecular farming, its removal should be concerned in the final application of proteins for use as biopharmaceuticals, similar to other tags. The tags are usually removed using specific proteases. The released target proteins without the tag should be further purified, which results in increase in production cost and yield loss. Approaches to reduce cost has been proposed that include the self-cleaving intein tag (Coolbaugh et al., 2017) and a sequence-specific chemical protein cleavage tag (Dang et al., 2019).

In summary, we showed that the small GB1 domain can be a versatile tag for recombinant protein production in plants. First, GB1-fused proteins can be highly expressed and well-folded. Second, GB1-fused recombinant proteins can be detected by the secondary antibody in a cost-effective and time-saving manner. Finally, the GB1 tag can potentially be used for Fc resin-mediated purification, which can be developed in the future.

MATERIALS AND METHODS

Construction of Recombinant Genes

DNA fragments encoding GFP together with an N-terminal enterokinase site (EK) were N-terminally fused with the ER leader peptide of Arabidopsis BiP1 or the transit peptide of Arabidopsis RbcS ($RbcS_{tp}$) to yield BiP-EK-GFP-HDEL or $RbcS_{tp}$-EK-GFP. The B1 domain (amino acid positions from 1st to 56th) of *Streptococcal* protein G (GB1) was inserted after the ER leader sequence or $RbcS_{tp}$ of BiP-EK-GFP or $RbcS_{tp}$-EK-GFP to yield BiP-GB1-EK-GFP-HDEL, or C-terminally fused to BiP-EK-GFP to yield BiP-EK-GFP-GB1. The DNA fragments encoding hIL6 and HA^{H9N2} were prepared from recombinant constructs *BiP-MP-CBM3-SUMO-hIL6-HDEL* and *BiP-*HA^{H9N2}*-mCor1-LysM-His-HDEL*, respectively (Islam et al., 2019; Song et al., 2021), by digesting with *Bam*HI and *Xho*I, and ligated into BiP-GB1-EK-GFP-HDEL digested with *Bam*HI and *Xho*I to yield *BiP-GB1- MP-CBM3-SUMO-hIL6-HDEL* and *BiP-GB1-*HA^{H9N2}*-mCor1-LysM-His-HDEL,* respectively. *CTB* with *Bam*HI and *Xho*I restriction sites at N- and C-terminal ends, respectively, was chemically synthesized (Gene Universal, Inc., Newark, United States). All the constructs were placed under the MacT promoter

(Song et al., 2021) and accompanied by RD29B Terminator of Arabidopsis *RD29b*. Primers used in this study are shown in **Supplementary Table 1**.

Production of Transient Transgenic Plants

Expression vectors were introduced into *Agrobacterium* strain GV3101 by electroporation. A single colony of *Agrobacterium* harboring expression vectors was inoculated to LB Broth (LPS Solution, Cat. LBL-05) and cultured in an incubator at 28°C overnight. Four–five week-old *N. benthamiana* plants grown in a greenhouse at 25^{o}C with a 16 h light/8 h dark cycle were used for Agroinfiltration by syringe. The infiltrated leaves were harvested at 3, 5, and 7 days post infiltration (DPI) to examine the expression level.

SDS-PAGE and Western Blot Analysis

Infiltrated leaves were ground and homogenized in protein extraction buffer [PBS buffer containing 1 mM EDTA, 0.5% Triton X-100(v/v), 1 X protease inhibitor cocktail]. The total protein extracts or purified proteins were separated by 7.5–12% SDS-PAGE. Western blot analysis was performed using the mouse anti-His antibody (1: 1,000 dilution, Novus, AD1.1.10), mouse anti-GFP antibody (1: 1,000 dilution, Clontech, Cat. number: 632381), and mouse anti-HA antibody (1: 1,000 dilution, Sigma, H3663). The secondary antibodies used in this study were goat anti-Human IgG conjugated HRP, sheep anti-Mouse IgG conjugated HRP (1: 5,000 dilution, Bethyl Laboratories), and mouse anti-Goat IgG conjugated HRP (1: 5,000 dilution, Santa Cruz Biotechnology, Inc.). Immunoblots were developed with the enhanced chemiluminescence kit (Amersham Pharmacia Biotech, Piscataway, NJ, United States), and images were captured using the LAS3000 system (Fujifilm, Tokyo, Japan).

Green Fluorescent Protein Fluorescence Acquisition and Quantification

Infiltrated leaves expressing *GFP* or *GB1-GFP* were harvested at 3, 5, and 7 DPI. The GFP fluorescence image of leaves was captured using the LAS3000 system (Fujifilm, Tokyo, Japan). The density of GFP fluorescence from the whole infiltrated leaves was measured by the official software of LAS3000 system (Fujifilm, Tokyo, Japan).

Ni^{2+}-NTA and Microcrystalline Cellulose Beads-Based Affinity Purification

Total protein extracts were prepared from 0.1 g leaf tissues infiltrated with *Agrobacterium* harboring HA^{H9N2}, *GB1-*HA^{H9N2}, *CTB,* or *GB1-CTB* using extraction buffer (50 mM Tris-HCl, pH 7.5, 150 mM NaCl, 1 mM DTT, 0.1% [v/v] Triton X-100, 10 mM imidazole, and protease inhibitor cocktail), and incubated with Ni^{2+}-NTA agarose beads (Qiagen, Valenica, CA, United States) on a shaker in a cold room for 30 min. Ni^{2+}-NTA agarose beads with bound proteins were washed using extraction buffer supplemented with 20 mM imidazole. Target proteins were eluted with 400 mM imidazole in the extract buffer. For MCC bead-based protein purification, total extracts were prepared from 0.1 g of leaf tissues expressing *hIL6* or *GB1-hIL6* using extraction buffer (50 mM Tris-HCl, pH 7.5, 150 mM NaCl, 1 mM DTT, 0.1% [v/v] Triton X-100, and protease inhibitor cocktail) and incubated with MCC beads (Sigma-Aldrich, St. Louis, MO, United States, CAS Number 9004-34-6) on a shaker for 30 min. MCC beads with bound proteins were washed with extraction buffer and boiled in the extract buffer for 10 min to release proteins from MCC beads.

Coomassie Brilliant Blue Staining and Statistics Analysis

The protein bands separated by SDS-PAGE were stained in Coomassie brilliant blue dyes, Coomassie brilliant blue 0.025% (m/v), methanol 50% (v/v), acetic acid 10% (v/v), ddH_2O 30%(v/v). The bands in the PAGE were imaging captured by LAS3000 system (Fujifilm, Tokyo, Japan) after de-staining. The bands' density was measured by using its official software. All the values of western band density or GFP fluorescence density were analyzed using the Student t-test or using the software, GraphPad Prism 6.02. *P*-values ≤ 0.05 were considered statistically significant.

TEV Cleavage

GB1-CTB proteins (2 μg) purified from the plant extracts were mixed with 0.2 U AcTEV^{TM} Protease (Invitrogen, Cat. 2575015) and 2 μL 20 x TEV buffer, by adding ddH_2O up to 40 μL. The mixtures with or without TEV protease were incubated at 10 or 25°C overnight, followed by SDS-PAGE analysis.

RNA Extraction and qRT-PCR

Leaf tissues were collected at 3 DPI and ground using stainless steel beads that had been precooled by liquid nitrogen. The total RNA was purified by using GeneJET plant RNA purification kit (Thermo Scientific, Waltham, MA, United States), following the protocol provided by the manufacturer. The final RNA concentration was measured by NanoDrop^{TM} 2000/2000c Spectrophotometer (Thermo Scientific, Waltham, MA, United States). Total RNA (2 μg) was reverse-transcribed to cDNA by MutiScribe Reverse Transcriptase (Thermo Fisher Scientific, REF 4368813) for qRT-PCR. The cDNA (50 ng), primers, and SYBR Green mix (Thermo Fisher Scientific, REF A25742) were mixed for qRT-PCR under the condition of 15 s denaturation at 95°C and 20 s annealing at 60°C and 30 s extension at 70°C with 40 cycles. The primers used in qRT-PCR were shown in **Supplementary Table 1**.

Protein Pull-Down Experiments Microcrystalline Cellulose Beads

hFC-CBM3 was infiltrated into the *N. benthamiana* leaf tissues together with *GB1-GFP-His*, GB1[E27A]-CTB-His, GB1[E27A/W43A]-CTB-His, or GB1[W43A]-CTB-His. Total protein extracts from leaf tissues of these infiltrated plants were incubated with MCC beads followed by washing three times with TBS buffer. The proteins pulled down by MCC beads were released by boiling and analyzed by western blotting using anti-CBM3 or anti-His antibodies.

In vitro Translation and Transcription

Both *BiP-LUC* and *BiP-GB1-LUC* were ligated into the pCS2++(modified from pCS2+) vector digested with *Xba*I and *Pst*I restriction endonucleases. DNA templates in the pCS2++vector were linearized by PCR using two primers covering the SP6 promoter and terminator. Capped mRNA was transcribed in the presence of a cap analog m7G[5′]ppp[5′]G using the mMESSAGE mMACHINE TM SP6 kit (Invitrogen, Cat. AM1340). The *in vitro* transcription was carried out at 37°C for 2 h in the mixture containing 5 mM ATP, 5 mM CTP, 5 mM UTP, 1 mM GTP, 4 mM cap analog m7G[5′]ppp[5′]G. The *in vitro* translation reaction mixture of wheat germ extracts (Promega, Cat. L4130) contained 10 mM creatine phosphate, 50 μg/ml creatine phosphokinase, 5 mM DTT, 2.1 mM magnesium acetate, 53 mM potassium acetate, 0.5 mM spermidine, 1.2 mM ATP, 0.1 mM GTP, 40 μM methionine, 40 μM leucine, 80 μM other amino acids and 40 units RNasin Ribonuclease Inhibitor. *In vitro* synthesized mRNA (8 fmol/μl) was quantified by a NanoDrop^{TM} 2000/2000c Spectrophotometer (Thermo Scientific, Waltham, MA, United States) and added to the reaction mixture and the translation reaction was performed at 25°C for 2 h in a 50 μl total reaction volume. 5 μl from the 50 μl reaction volume were collected at 30, 60, and 120 min points, diluted to 24-fold, and frozen using liquid nitrogen. RLUC activity of samples was measured using the Renilla Luciferase Assay System kit (Promega, E2710). Primers used in this study are shown in **Supplementary Table 1**.

DATA AVAILABILITY STATEMENT

The datasets presented in this study can be found in online repositories. The names of the repository/repositories and accession number(s) can be found in the article/ **Supplementary Material**.

AUTHOR CONTRIBUTIONS

IH and S-JS contributed to the conception of the study and wrote the manuscript. S-JS and H-PD made the constructs and contributed significantly to analysis and experiments. BM and AY contributed to the *in vitro* translation and vector construction, respectively. All authors contributed to the article and approved the submitted version.

FUNDING

This work was carried out with the support of Cooperative Research Program for Agriculture Science and Technology Development (Project No. PJ015701012021), Rural Development Administration, South Korea, and also a grant of the Korea Health Technology R&D Project through the Korea Health Industry Development Institute (KHIDI), funded by the Ministry of Health (HV20C0156), South Korea.

SUPPLEMENTARY MATERIAL

The Supplementary Material for this article can be found online at: https://www.frontiersin.org/articles/10.3389/fpls.2022.878677/full#supplementary-material

Supplementary Figure 1 | GB1 dramatically increases the expression of soluble GFP in leaf tissues of *Nicotiana benthamiana*. **(A,C,E)** Images of GFP fluorescence for the ER **(A)**, chloroplast **(C)**, and cytosol **(E)**-localized GFP constructs. Images were taken at 5 and 7 dpi. The GFP signals were quantified at three DPI from three different samples. **(B,D,F)** Western blot analysis. Total protein extracts from leaf tissues harvested at 3, 5, and 7 DPI were analyzed by western blot analysis using the anti-GFP antibody. ER **(B)**, chloroplast **(D)**, and cytosol **(F)**-localized GFP and GB1-GFP at three time points. Lanes 1, 3, and 5 indicate GFP at 3, 5, and 7 DPI, respectively. RbcL stained with CBB was used as a loading control. Lanes 2, 4, and 6 indicate GB1-GFP at 3, 5, and 7 DPI, respectively. Results in panels **(A,C,E)** mean ± SD ($n = 3$). Asterisks indicate a significant difference (Student's *t*-test; two asterisks, $0.001 < P < 0.05$).

Supplementary Figure 2 | Western blot analysis of the expression of various target genes in *Nicotiana benthamiana*. **(A–C)** Schematic representation of constructs. **(D–F)** Western blot analysis for the expression of various recombinant proteins. *Nicotiana benthamiana* leaf tissues were infiltrated with Agrobacterium harboring MCS-hIL6-HDEL(hIL6) or GB1- MCS-hIL6-HDEL(GB1-hIL6) **(D)**, HA^{H9N2}-mCor1-LysM-His-HDEL or GB1- HA^{H9N2}-mCor1-LysM-His-HDEL **(E)**, or CTB-His-HDEL(CTB) and GB1-CTB-His-HDEL (GB1-CTB) **(F)**. Total protein extracts from leaf tissues of *N. benthamiana* harvested from 3, 5, and 7 DPI were analyzed by western blotting using anti-CBM3 **(D)** or anti-His **(E,F)** antibodies. RbcL stained with CBB was used as a loading control. Lanes 1, 3, and 5 indicate target proteins without GB1 fusion, and lanes 2, 4, and 6 indicate GB1-fused target proteins.

Supplementary Figure 3 | Fusion of GB1 leads to an increase in transcript levels of target genes. The indicated constructs were transiently expressed in *Nicotiana benthamiana via Agrobacterium*-mediated infiltration. Total RNA was prepared from leaf tissues at 3 dpi and used for qRT-PCR. *ACT3* was used as an internal control for qRT-PCR. **(A)** GFP and GB1-GFP. **(B)** CTB and GB1-CTB. GB1-GFP and GB1-CTB levels were represented relative to the levels of GFP and CTB, respectively. Results in panels **(A,B)** are the mean ± SE ($n = 3$). Single asterisks indicate a significant difference (Student's *t*-test; asterisk, $P < 0.05$).

Supplementary Figure 4 | Expression of GB1 mutant forms in *Nicotiana benthamiana*. Total protein extracts prepared from leaf tissues harvested at 3, 5, and 7 DPI were analyzed by western blot analysis using anti-GFP antibody. RbcL stained with CBB was used as a loading control. Lanes 1, 2, 3, and 4 indicate GFP, GB1-GFP, GB1[E27A], and GB1[E27A/W43A], respectively.

Supplementary Figure 5 | Human Fc weakly interacts with GB1[W43A]. Protein extracts from *Nicotiana benthamiana* expressing the indicated constructs were used for the pull-down experiments using microcrystalline cellulose (MCC) beads. The pull-down proteins were analyzed by immunoblotting with anti-CBM3 or anti-His antibodies.

REFERENCES

Abrahamian, P., Hammond, R. W., and Hammond, J. (2020). Plant virus-derived vectors: applications in agricultural and medical biotechnology. *Annu. Rev. Virol.* 7, 513–535.

Adem, M., Beyene, D., and Feyissa, T. (2017). Recent achievements obtained by chloroplast transformation. *Plant Methods* 13:30.

Akerström, B., and Björck, L. (1986). A physicochemical study of protein G, a molecule with unique immunoglobulin G-binding properties. *J. Biol. Chem.* 261, 10240–10247.

Arndt, M. A. E., Krauss, J., Schwarzenbacher, R., Vu, B. K., Greene, S., and Rybak, S. M. (2003). Generation of a highly stable, internalizing anti-CD22 single-chain Fv fragment for targeting non-Hodgkin's lymphoma. *Int. J. Cancer* 107, 822–829. doi: 10.1002/ijc.11451

Bao, W.-J., Gao, Y.-G., Chang, Y.-G., Zhang, T.-Y., Lin, X.-J., Yan, X.-Z., et al. (2006). Highly efficient expression and purification system of small-size protein domains in *Escherichia coli* for biochemical characterization. *Protein Exp. Purificat.* 47, 599–606. doi: 10.1016/j.pep.2005.11.021

Bauer, M., Xue, W.-F., and Linse, S. (2009). Protein GB1 folding and assembly from structural elements. *IJMS* 10, 1552–1566. doi: 10.3390/ijms10041552

Björck, L., and Kronvall, G. (1984). Purification and some properties of streptococcal protein G, a novel IgG-binding reagent. *J. Immunol.* 133, 969–974.

Buyel, J. F. (2019). Plant molecular farming - integration and exploitation of side streams to achieve sustainable biomanufacturing. *Front. Plant Sci.* 9:1893. doi: 10.3389/fpls.2018.01893

Chen, R. (2012). Bacterial expression systems for recombinant protein production: *E. coli* and beyond. *Biotechnol. Adv.* 30, 1102–1107. doi: 10.1016/j.biotechadv.2011.09.013

Choe, W., Durgannavar, T., and Chung, S. (2016). Fc-Binding ligands of immunoglobulin G: an overview of high affinity proteins and peptides. *Materials* 9:994. doi: 10.3390/ma9120994

Chung, Y. H., Church, D., Koellhoffer, E. C., Osota, E., Shukla, S., Rybicki, E. P., et al. (2021). Integrating plant molecular farming and materials research for next-generation vaccines. *Nat. Rev. Mater.* Online ahead of print. doi: 10.1038/s41578-021-00399-395

Coolbaugh, M. J., Shakalli Tang, M. J., and Wood, D. W. (2017). High-throughput purification of recombinant proteins using self-cleaving intein tags. *Anal. Biochem.* 516, 65–74. doi: 10.1016/j.ab.2016.10.016

Dang, B., Mravic, M., Hu, H., Schmidt, N., Mensa, B., and DeGrado, W. F. (2019). SNAC-tag for sequence-specific chemical protein cleavage. *Nat. Methods* 16, 319–322. doi: 10.1038/s41592-019-0357-353

Dingermann, T. (2008). Recombinant therapeutic proteins: production platforms and challenges. *Biotechnol. J.* 3, 90–97. doi: 10.1002/biot.200700214

Du, D., Zhu, Y., Huang, C.-Y., and Gai, F. (2004). Understanding the key factors that control the rate of -hairpin folding. *Proc. Natl. Acad. Sci. U S A.* 101, 15915–15920. doi: 10.1073/pnas.0405904101

Dyo, Y. M., and Purton, S. (2018). The algal chloroplast as a synthetic biology platform for production of therapeutic proteins. *Microbiology* 164, 113–121. doi: 10.1099/mic.0.000599

Esposito, D., and Chatterjee, D. K. (2006). Enhancement of soluble protein expression through the use of fusion tags. *Curr. Opin. Biotechnol.* 17, 353–358. doi: 10.1016/j.copbio.2006.06.003

Frenzel, A., Hust, M., and Schirrmann, T. (2013). Expression of recombinant antibodies. *Front. Immunol.* 4:217. doi: 10.3389/fimmu.2013.00217

García-Fruitós, E. (2012). Lactic acid bacteria: a promising alternative for recombinant protein production. *Microb Cell Fact.* 11:157. doi: 10.1186/1475-2859-11-157

Grillberger, L., Kreil, T. R., Nasr, S., and Reiter, M. (2009). Emerging trends in plasma-free manufacturing of recombinant protein therapeutics expressed in mammalian cells. *Biotechnol. J.* 4, 186–201. doi: 10.1002/biot.200800241

Hammarström, M., Woestenenk, E. A., Hellgren, N., Härd, T., and Berglund, H. (2006). Effect of N-terminal solubility enhancing fusion proteins on yield of purified target protein. *J. Struct. Funct. Genomics* 7, 1–14. doi: 10.1007/s10969-005-9003-9007

Hammond, C., Braakman, I., and Helenius, A. (1994). Role of N-linked oligosaccharide recognition, glucose trimming, and calnexin in glycoprotein folding and quality control. *Proc. Natl. Acad. Sci. U S A.* 91, 913–917. doi: 10.1073/pnas.91.3.913

Hebert, D. N., Foellmer, B., and Helenius, A. (1995). Glucose trimming and reglucosylation determine glycoprotein association with calnexin in the endoplasmic reticulum. *Cell* 81, 425–433. doi: 10.1016/0092-8674(95)90395-X

Hung, Y.-F., Valdau, O., Schünke, S., Stern, O., Koenig, B. W., Willbold, D., et al. (2014). Recombinant production of the amino terminal cytoplasmic region of dengue virus non-structural protein 4A for structural studies. *PLoS One* 9:e86482. doi: 10.1371/journal.pone.0086482

Hunter, M., Yuan, P., Vavilala, D., and Fox, M. (2019). Optimization of protein expression in mammalian cells. *Curr. Protocols Protein Sci.* 95:e77. doi: 10.1002/cpps.77

Huus, K., Havelund, S., Olsen, H. B., van de Weert, M., and Frokjaer, S. (2005). Thermal dissociation and unfolding of insulin. *Biochemistry* 44, 11171–11177. doi: 10.1021/bi0507940

Islam, M. R., Kwak, J., Lee, J., Hong, S., Khan, M. R. I., Lee, Y., et al. (2019). Cost-effective production of tag-less recombinant protein in *Nicotiana benthamiana*. *Plant Biotechnol. J.* 17, 1094–1105. doi: 10.1111/pbi.13040

Kang, H., Park, Y., Lee, Y., Yoo, Y.-J., and Hwang, I. (2018). Fusion of a highly N-glycosylated polypeptide increases the expression of ER-localized proteins in plants. *Sci. Rep.* 8:4612. doi: 10.1038/s41598-018-22860-22862

Kim, Y., Lee, G., Jeon, E., Sohn, E. J., Lee, Y., Kang, H., et al. (2014). The immediate upstream region of the 5'-UTR from the AUG start codon has a pronounced effect on the translational efficiency in *Arabidopsis thaliana*. *Nucleic Acids Res.* 42, 485–498. doi: 10.1093/nar/gkt864

Leuzinger, K., Dent, M., Hurtado, J., Stahnke, J., Lai, H., Zhou, X., et al. (2013). Efficient agroinfiltration of plants for high-level transient expression of recombinant proteins. *JoVE* 77, e50521. doi: 10.3791/50521

Mancia, F., Patel, S. D., Rajala, M. W., Scherer, P. E., Nemes, A., Schieren, I., et al. (2004). Optimization of protein production in mammalian cells with a coexpressed fluorescent marker. *Structure* 12, 1355–1360. doi: 10.1016/j.str.2004.06.012

Mardanova, E. S., Blokhina, E. A., Tsybalova, L. M., Peyret, H., Lomonossoff, G. P., and Ravin, N. V. (2017). Efficient transient expression of recombinant proteins in plants by the novel pEff vector based on the genome of potato virus X. *Front. Plant Sci.* 8:247. doi: 10.3389/fpls.2017.00247

Margolin, E., Oh, Y. J., Verbeek, M., Naude, J., Ponndorf, D., Meshcheriakova, Y. A., et al. (2020). Co-expression of human calreticulin significantly improves the production of HIV gp140 and other viral glycoproteins in plants. *Plant Biotechnol. J.* 18, 2109–2117. doi: 10.1111/pbi.13369

Mulinacci, F., Capelle, M. A. H., Gurny, R., Drake, A. F., and Arvinte, T. (2011). Stability of human growth hormone: influence of methionine oxidation on thermal folding. *J. Pharm. Sci.* 100, 451–463. doi: 10.1002/jps.22293

Muñoz, V., Thompson, P. A., Hofrichter, J., and Eaton, W. A. (1997). Folding dynamics and mechanism of β-hairpin formation. *Nature* 390, 196–199. doi: 10.1038/36626

Oliveira, C., Guimarães, P. M. R., and Domingues, L. (2011). Recombinant microbial systems for improved β-galactosidase production and biotechnological applications. *Biotechnol. Adv.* 29, 600–609. doi: 10.1016/j.biotechadv.2011.03.008

Peti, W., and Page, R. (2007). Strategies to maximize heterologous protein expression in *Escherichia coli* with minimal cost. *Protein Exp. Purificat.* 51, 1–10. doi: 10.1016/j.pep.2006.06.024

Sainsbury, F. (2020). Innovation in plant-based transient protein expression for infectious disease prevention and preparedness. *Curr. Opin. Biotechnol.* 61, 110–115. doi: 10.1016/j.copbio.2019.11.002

Schillberg, S., and Finnern, R. (2021). Plant molecular farming for the production of valuable proteins - critical evaluation of achievements and future challenges. *J. Plant Physiol.* 25:153359. doi: 10.1016/j.jplph.2020.153359

Schillberg, S., Raven, N., Spiegel, H., Rasche, S., and Buntru, M. (2019). Critical analysis of the commercial potential of plants for the production of recombinant proteins. *Front. Plant Sci.* 10:720. doi: 10.3389/fpls.2019.00720

Sloan, D. J., and Hellinga, H. W. (1999). Dissection of the protein G B1 domain binding site for human IgG Fc fragment. *Protein Sci.* 8, 1643–1648. doi: 10.1110/ps.8.8.1643

Soler, E., and Houdebine, L.-M. (2007). Preparation of recombinant vaccines. *Biotechnol. Ann. Rev.* 13, 65–94.

Song, S., Shin, G., Noh, J., Lee, J., Kim, D., Ryu, G., et al. (2021). Plant-based, adjuvant-free, potent multivalent vaccines for avian influenza virus *via Lactococcus surface* display. *J. Integr. Plant Biol.* 63, 1505–1520. doi: 10.1111/jipb.13141

Specht, E., Miyake-Stoner, S., and Mayfield, S. (2010). Micro-algae come of age as a platform for recombinant protein production. *Biotechnol. Lett.* 32, 1373–1383. doi: 10.1007/s10529-010-0326-325

Staub, J. M., Garcia, B., Graves, J., Hajdukiewicz, P. T. J., Hunter, P., Nehra, N., et al. (2000). High-yield production of a human therapeutic protein in tobacco chloroplasts. *Nat. Biotechnol.* 18, 333–338. doi: 10.1038/73796

Sugase, K., Landes, M. A., Wright, P. E., and Martinez-Yamout, M. (2008). Overexpression of post-translationally modified peptides in *Escherichia coli* by co-expression with modifying enzymes. *Protein Exp. Purification* 57, 108–115. doi: 10.1016/j.pep.2007.10.018

Thoring, L., Dondapati, S. K., Stech, M., Wüstenhagen, D. A., and Kubick, S. (2017). High-yield production of "difficult-to-express" proteins in a continuous exchange cell-free system based on CHO cell lysates. *Sci. Rep.* 7:11710. doi: 10.1038/s41598-017-12188-12188

Wakankar, A. A., Feeney, M. B., Rivera, J., Chen, Y., Kim, M., Sharma, V. K., et al. (2010). Physicochemical stability of the antibody-drug conjugate Trastuzumab-DM1: changes due to modification and conjugation processes. *Bioconjugate Chem.* 21, 1588–1595. doi: 10.1021/bc900434c

Willuda, J., Honegger, A., Waibel, R. J., Schubiger, P. A., Stahel, R., Zangemeister-Wittke, U., et al. (1999). High thermal stability is essential for tumor targeting of antibody fragments: engineering of a humanized anti-epithelial glycoprotein-2 (epithelial cell adhesion molecule) single-chain Fv fragment. *Cancer Res.* 59, 5758–5767.

Wurm, F. M. (2004). Production of recombinant protein therapeutics in cultivated mammalian cells. *Nat. Biotechnol.* 22, 1393–1398. doi: 10.1038/nbt1026

Yamamoto, T., Hoshikawa, K., Ezura, K., Okazawa, R., Fujita, S., Takaoka, M., et al. (2018). Improvement of the transient expression system for production of recombinant proteins in plants. *Sci. Rep.* 8:4755. doi: 10.1038/s41598-018-23024-y

Zheng, X., Wu, X., Fu, X., Dai, D., and Wang, F. (2016). Expression and purification of human epidermal growth factor (hEGF) fused with GB1. *Biotechnol. Biotechnol. Equipment* 30, 813–818. doi: 10.1080/13102818.2016.1166984

Conflict of Interest: The authors declare that the research was conducted in the absence of any commercial or financial relationships that could be construed as a potential conflict of interest.

Publisher's Note: All claims expressed in this article are solely those of the authors and do not necessarily represent those of their affiliated organizations, or those of the publisher, the editors and the reviewers. Any product that may be evaluated in this article, or claim that may be made by its manufacturer, is not guaranteed or endorsed by the publisher.

Advantages of publishing in Frontiers

OPEN ACCESS
Articles are free to read for greatest visibility and readership

FAST PUBLICATION
Around 90 days from submission to decision

HIGH QUALITY PEER-REVIEW
Rigorous, collaborative, and constructive peer-review

TRANSPARENT PEER-REVIEW
Editors and reviewers acknowledged by name on published articles

Frontiers
Avenue du Tribunal-Fédéral 34
1005 Lausanne | Switzerland

Visit us: www.frontiersin.org
Contact us: frontiersin.org/about/contact

REPRODUCIBILITY OF RESEARCH
Support open data and methods to enhance research reproducibility

DIGITAL PUBLISHING
Articles designed for optimal readership across devices

FOLLOW US
@frontiersin

IMPACT METRICS
Advanced article metrics track visibility across digital media

EXTENSIVE PROMOTION
Marketing and promotion of impactful research

LOOP RESEARCH NETWORK
Our network increases your article's readership